

Государственное образовательное учреждение
высшего профессионального образования
**«Томский государственный университет
систем управления и радиоэлектроники»**

ТЕМАТИЧЕСКИЙ РЕФЕРАТИВНЫЙ СБОРНИК № 4-2/4

**“Radar Remote Sensing”
(«Дистанционное зондирование в радиолокации»)**

Публикации в трудах конференций

Источник: *Digital Library IEEEExplore*

Язык: *английский*

Глубина поиска: *2003 – 2004 гг.*

Дата формирования: *март 2011 г.*

Составитель: *В.И. Карнышев*

Томск – 2011

ТЕМАТИЧЕСКИЙ РЕФЕРАТИВНЫЙ СБОРНИК № 4-2/4

"Radar Remote Sensing"

(«Дистанционное зондирование в радиолокации»)

Публикации в трудах конференций

"A study of rough surface thermal emission and reflection using Voronovich's small slope approximation"

Monte Carlo simulations are used to compute average direct surface thermal emission and reflected atmospheric radiation using the "active" small slope approximation of Voronovich. The surface used are realizations of an ocean-like spectrum, and contain features ranging from 64 to 0.5 electromagnetic wavelengths. The parallel computing approach used in these simulations is described, and results are compared with predictions from the commonly applied "two-scale" theory of sea emission. Results show a reasonable level of agreement in a small height surface case, which degrades as the surface height is increased [C4491]

"Experimental investigation of radar backscatter from plunging breakers using an ultrawideband radar and visible/infrared cameras"

Interim results of a laboratory investigation of the low-grazing angle radar backscatter generated by plunging breakers are presented. A primary objective of this investigation is to experimentally verify a scattering mechanism through which the horizontally-polarized backscatter generated by the breaker can exceed that at vertical polarization, without involving multipath propagation between the front face of the wave and its crest. The experiments were conducted at the University of Maryland-College Park wave tank, and involved the deployment of a dual-polarized, ultrawideband radar, multiple high-speed visible cameras, and an ultra-sensitive infrared camera. All instruments were deployed simultaneously on a moving carriage, located above the wave tank channel, that followed the breakers as they evolved in space and time. Representative ultrawideband radar data and optical images are presented in this paper [C4492]

"Forward scattering phenomena at low grazing"

A series of low angle radar measurements was conducted over a large wave pool capable of producing a wide range of scaled sea conditions. The X-band measurements observed the forward scattering from a 1D, 1/10th scale Pierson-Moskowitz surface at sea states. The experiment observed several interesting phenomena at low grazing angles including the Lloyd mirror rotation effect and channeling phenomenon. The Lloyd mirror rotation effect is a shift in the interference pattern due to shadowing. The channeling phenomenon is a type of forward scattering that occasionally occurs when a well-formed sea wave briefly reflects or focuses the out-of-plane energy towards the receiver, yielding a higher than expected, broad-band power gain. Observations for both phenomena are summarized and physical explanations are provided [C4493]

"Correlation time analysis of delay-Doppler waveforms generated from ocean-scattered GPS signals"

The ocean-scattered Global Positioning System (GPS) signal can be used, in a bistatic radar configuration, for estimating the ocean surface roughness. This requires fitting a scattering model to the distribution of reflected power in delay and Doppler. The delay-Doppler map, or waveform, is generated through the cross-correlation of a local copy of the pseudorandom noise (PRN) code assigned to each GPS satellite with the reflected signal over increments in Doppler frequency equal to the pre-detection bandwidth. The correlation time of the reflected signal voltage sets an upper limit on the pre-detection integration time. Correlation time was estimated from experimental data through fitting a model Gaussian function to the magnitude of the complex autocorrelation of the time series of the waveform. Range bins were taken 1.1 chips prior to the averaged waveform peak in the leading edge and 2.5 chips after the averaged waveform peak in the trailing edge. Doppler bins were set at -500, 0, and +500 Hz relative to the Doppler frequency of the corresponding direct GPS signal. The direct GPS signal was tracked using a frequency locked loop (FLL). Results showed that maximum correlation time occurs approximately 0.72 code chips prior to the averaged waveform peak. The correlation time was found to vary with the elevation angle of the satellite, with lower elevation satellites showing longer correlation time. Some experimental results were compared with model predictions. A good comparison was usually found for delay bins

near the specular point and both the model and experiment showed a decrease in the correlation time for longer delays. In the higher range bins the model tended to predict longer correlation times than those observed in the experimental data [C4494]

"A simple approximation of transmitted wavefront shape from point sources above lossy half spaces"

Many subsurface sensing problems require knowledge of the shape of a wavefront in a half-space originating from a point source above the half-space. Impulse ground penetrating radar and air-coupled acoustic underground sensing systems usually have their emitters in air, transmitting waves through a quasi-planar interface into soil or water. The waves radiated by the emitter can be approximated as circular, but once they enter the half-space, they propagate with wavefront shape that resembles a hyperbola. The objective of this paper is to derive the exact shape and show that it is well approximated by a hyperbola with specific parameters depending on the dielectric constant of the half-space $\epsilon' (=n^2)$ the height of the source h , and the propagation time from source to wavefront multiplied by the wave velocity in the half space p . In addition, a correction formula is provided to reduce the error between the approximate hyperbola and the exact shape [C4495]

"Microwave scattering from 3-D breaking water wave crests"

An MLFMA numerical electromagnetics code has been used to find the microwave backscattering from 3D surface profiles approximating the crests of intermediate-scale breaking water waves. The test surfaces were synthesized by azimuthally aligning numerically generated 2D crests that represent the wave in various stages of breaking. The results show that the cancellation of vertically polarized backscatter (VV) that was previously predicted with 2D targets appears with the 3D crests when specular reflection points on both the breaker jet and the cavity under the jet are visible. Horizontally polarized backscatter (HH) undergoes constructive interference in this case, leading to strong super events where the HH radar cross-section exceeds that at VV [C4496]

"Applying a common allometric equation to convert forest height from Pol-InSAR data to forest biomass"

Forest biomass (wood volume) is the most integrative forest structural parameter. Since no remote sensing technique can measure wood volume or biomass directly, a direct biomass determination from air- or spaceborne images always has a regression character. A different approach is to estimate forest biomass indirectly from a forest parameter that can be extracted more accurately than biomass, of which forest height is the closest related one. This makes it possible to utilize remote sensing methods that extract forest heights for biomass assessments: stereoscopic aerial photography, Lidar and Pol-InSAR. In this paper, forest heights were extracted from polarimetric interferometric SAR data (Pol-InSAR) over the spruce dominated test site 'Fichtelgebirge'. The extracted heights proved a good correlation with the upper canopy height (h_{100} , top height), and could be converted into forest biomass by means of height-biomass allometry. On this basis, the potential of Pol-InSAR systems for forest biomass estimation is critically discussed, and directions towards a performance optimisation are pointed out [C4497]

"Microwave remote sensing: a perspective from the last few field experiments"

There have been numerous field experiments which have tested the effectiveness of microwave remote sensing, both active and passive under varied land surface conditions. The Southern Great Plains Experiment 1999 (SGP99) was held in Chickasha Oklahoma where winter wheat and rangeland was the predominant land surface type whereas at the Soil Moisture Experiment 2002 (SMEX02) in Walnut River watershed in Ames Iowa it was a mixture of corn, and soybeans. In the SMEX03 (Soil Moisture Experiment in 2003) in Little River Watershed, the land surface was a mixture of peanuts, vegetables, cotton and pasture and for SMEX04 (Soil Moisture Experiment in 2004) in Walnut Gulch, Arizona, the land surface cover is primarily brush and grass covered rangeland vegetation. Given that microwaves have low sensitivity to soil moisture in the presence of vegetation, these field experiments offer an opportunity to examine observations of sensitivity in the presence of varied (and varying with time) vegetation densities. In addition, in each of these experiments, there were different instruments on aircrafts and satellite sensors that were deployed. In SGP99, we had observations from the PALS (Passive Active L and S band Radar and Radiometer), PSR (Polarimetric Scanning Radiometer) from the C130 aircraft and the TMI (TRMM Microwave Imager) and SSM/I (Special Sensor Microwave Imager) from space. In SMEX02, we had PALS, PSR, AIRSAR (Airborne Synthetic Aperture Radar) from the aircraft platforms and in SMEX03 PSR only. Satellite sensors in SMEX02 and SMEX03 included AMSR (Advanced Microwave Scanning Radiometer), TMI, and SSM/I. In the recently concluded SMEX04, PSR was used from the aircraft and AMSR, TMI and SSM/I satellite observations were available. We will use these sensors and observations in the microwave channel in conjunction with ground observations of vegetation characteristics and soil moisture to

study the sensitivity of microwaves to soil moisture under varied land surface conditions. [C4498]

"Comparison of soil moisture retrieval algorithms using simulated HYDROS brightness temperatures"

The HYDROS mission objective is to collect global scale measurements of the Earth's soil moisture and land surface freeze/thaw conditions, using a combined L band radiometer and radar system operating at 1.41 and 1.26 GHz, respectively. In order to examine how HYDROS soil moisture retrieval will be performed and how the retrieval accuracy will be impacted by vegetation water content and surface heterogeneity, an observing system simulation experiment (OSSE) was conducted using a modeled geophysical domain in the south-central United States centered on the Arkansas-Red River basin for a one-month period in 1994. Three separate radiometer retrieval algorithms were evaluated: (1) a single-channel algorithm (H polarization), (2) a two-channel iterative algorithm, and (3) a two-channel reflectivity ratio algorithm. Analysis indicates that the HYDROS accuracy goal of 4% volumetric soil moisture can be met anywhere in the test basin except woodland areas. Nonlinear scaling of higher resolution ancillary vegetation data can adversely affect algorithm retrieval accuracies, especially in heavy tree areas on the east side of the basin [C4499]

"Optimum polarimetric analysis of backscattering from rough sea surface"

Using SIR-C/X-SAR that provided simultaneously images of Southern-China Sea at three microwave wavelengths, L-band quad-polarization, C-band quad-polarization and X-band with VV polarization, the present paper calculate and analyze the optimum polarization of the backscattering from the rough sea surface. The utmost applications of radar remote sensing of ocean come down to quantitative derivation of some oceanographic parameters instead of simple interpretation of patterns on the SAR image itself of ocean surface. Accordingly, we concern mainly the polarimetric parameters of return signals from sea surfaces relate some physical oceanographic variables. Since the backscattering matrix contains the backscattering information of moving sea surface, concentration should be on understanding the properties of this matrix alone. Meanwhile, polarization is a key to aim this goal. A physical approach is to study polarization optimization. The optimization result shows that an optimum polarization changes with position of sea surface. And as a heuristic derivation, we prove that there exist optimum polarimetric responses with orientations at all sea-wind conditions. [C4500]

"Homomorphic wavelet transform and new subband statistics models for SAR image compression"

In the framework of wavelet based SAR compression techniques, this paper proposes a new approach to model subband coefficients marginal distributions. The decomposition scheme involves homomorphic wavelet transform and "second kind statistics" characterization models. Our method has been successfully tested on real data experiments [C4501]

"Windsat validation using seawinds, windrad and polscat measurements"

Global mapping of near surface ocean wind vectors is crucial for many oceanographic and atmospheric studies. The US Navy together with the National Polar Orbiting Environmental Satellite System (NPOESS) launched the WindSat with multifrequency polarimetric radiometers in January 2003 to demonstrate the passive polarimetry for large spatial coverage of ocean surface wind vector measurements from space. We derived the geophysical model function (GMF) for Windsat polarimetric brightness temperature measurements using six months of matchup dataset. The Windsat GMF was compared with the aircraft radiometer and radar measurements and the SeaWinds scatterometer winds with good agreement up to about 20 m/s wind speed [C4502]

"Design and implementation of a miniaturized water vapor profiling radiometer"

At present, the vast majority of ground-based and airborne microwave remote sensing instrumentation is produced using waveguide-based or connectorized discrete microwave components, which are high in cost and large in volume. Recent maturation of monolithic microwave and millimeter-wave integrated circuit (MMIC) technologies developed for the wireless communications and defense industries is expected to enable development of a new generation of radiometers. This work describes the design of a prototype miniaturized water vapor profiler for the 3D measurement of tropospheric water vapor using a four-sensor network, including the fabrication and initial performance evaluation of its RF and IF sections. [C4503]

"Data fusion techniques of heterogeneous sensor images for debris hazard assessments"

A new data fusion method, which combines all-weather monitoring ability of SAR imagery and multispectral and 3D mapping abilities of high-resolution optical imagery, were proposed to monitor the debris hazard in mountain area. In this study, the large hazard caused by slope failures in Taiwan on September 2001 was studied using

the data fusion method of RADARSAT1 SAR images and SPOT5 optical images. The slope failure area was detected and the failure volume (i.e. elevation change) was measured. Our results were compared with the ground truth data obtained from the photo-interpretation and the ground measurement, and were in good agreement with those truth data. This study indicated that the fusion techniques of recent satellite technologies are highly suitable and efficient for hazard monitorings [C4504]

"Multiple-model multiscale data fusion regulated by a mixture-of-experts network"

Multiscale Kalman smoothers (MKS) have been traditionally employed for data fusion applications and estimation of topography. The standard MKS algorithm embedded with a single stochastic model has been found to give suboptimal performance in estimating nonstationary topographic variations, particularly when there are sudden changes in the terrain. In this work, multiple models are regulated by a mixture-of-experts (MOE) network to adaptively fuse the estimates. Though MOE has been widely applied to one-dimensional data, its extension to multiscale estimation is new [C4505]

"Forward and backscattering measurements of rainfall using the NASA Microwave Link"

This paper studies the feasibility of making backscatter measurements from rainfall with the NASA/Microwave Link system at Wallops Island, VA. The research entails the implementation of an FMCW radar at the Link frequencies to enable simultaneous forward and backscatter measurements from rain. The backscatter measurements will be used in conjunction with the forward measurements and the measurements from a ground-based network of disdrometers and rain gauges located under the propagation path to develop new microwave retrieval techniques, and to test established single-frequency and dual-frequency radar retrieval-algorithms relevant to the ongoing TRMM and up coming GPM missions [C4506]

"Performance simulation of spaceborne P-band SAR for global biomass retrieval"

This paper evaluates the use of a spaceborne low-frequency synthetic aperture radar (SAR) for forest biomass retrieval. Airborne radar data are used as input to a SAR simulator in which SAR system parameters of the assumed spaceborne system and propagation effects in the ionosphere (primarily scintillation and Faraday rotation) are modelled. The simulations are performed for different ionospheric perturbation states. Some simulated spaceborne low-frequency SAR images over boreal forest are shown and their usefulness for forest biomass retrieval are studied and discussed. The results indicate that it is possible to separate boreal forest into three classes assuming a moderate distorted ionosphere [C4507]

"The GBFM radar mosaic of the Eurasian Taiga: selected topics on geo-location and preliminary thematic products"

In the context of the Global Boreal Forest Mapping project (GBFM), an initiative of the Japan Aerospace Exploration Agency (JAXA), a continental scale radar mosaic of the Eurasian Taiga was compiled. The mosaic is composed of some 520 strip-images (typically covering 80 km by 2500 km each) acquired in 1997-98 by the L-band SAR aboard the JERS-1 spacecraft. The mosaic was assembled in two phases. Coverage in the first stage included the area between the Ural Mountains in the west, Bering Strait in the east, Arctic Ocean in the north and the Korean Peninsula in the south. In the second phase an extended version was produced that comprises the European part of the Boreal ecosystems west of the Ural Mountain and up to the European Union region. Pixel spacing of the high resolution final products is 100 m and map projection is Albers equal-area conical. In this paper selected topics are presented related to a revision of the mosaic geometry. This step was called for to improve the internal consistency and assure proper absolute geo-location of the mosaics with respect to reference data sets. It consists of: i) a data representation (virtual frames) for handling the strip-images in smaller units that are more effective for dealing with local distortions; and ii) inclusion of control points derived from the Landsat GeoCover data sets. Results characterizing the mosaic geometric accuracy in terms of root mean square residuals are reported. Finally, we present, as a first thematic result, a vegetation map at coarse resolution (900 m) derived by a combination of the Global Land Cover 2000 map and the GBFM radar mosaic [C4508]

"Analysis of the virtual baseline of cluster SAR satellites"

The change of the virtual baseline (equivalent baseline or projection of baseline) of cluster SAR satellites is analyzed when the constellation is circling around the Earth and at the same time the satellites are rotating around the center. This paper provides the assessment of baseline error, which influence on the precision of height measurement in the across-track interferometric mode. The relevant mathematical model is built and simulation analysis as well as the curve of height error is presented. Numerical results confirm theoretical analysis and quantitatively show that the virtual baseline is varying periodically with the latitude of the nadir of

the "virtual" satellite, the constellation circling angle, the linear velocity of the Earth surface, and the angle between the projection of satellite orbit on the Earth surface and latitude circle, etc. The baseline error must be taken into account in the process of InSAR imaging and can be compensated by using the formulae derived in this paper to recover digital elevation models (DEM's) accurately [C4509]

"SAR interferometric baseline calibration without need of phase unwrapping"

Baseline calibration is a needed step in all applications of SAR interferometry and differential interferometry. A new approach for baseline calibration is proposed, based on the idea of maximizing the correlation between the original complex interferogram and reference values of it obtained from ground control points. The main advantage with respect to traditional techniques is that the method does not require the phase to be unwrapped in advance, and therefore the results are not affected by possible unwrap errors. In addition, successive phase unwrap is facilitated by the better phase flattening possible after baseline calibration. The method is computationally more demanding than traditional techniques, though the requested computational time is comparable with that of other processing steps of SAR interferometry. Tests performed on real ERS SAR images confirm the validity of the proposed approach [C4510]

"On the influence of the surface fractal dimension on the IFSAR baseline decorrelation"

Coherence is the key factor in Synthetic Aperture Radar Interferometry. We study the baseline decorrelation due to antenna spatial diversity in order to take into account the effect of the surface statistic roughness in a more general case. As a model of surface roughness we use the fractional Brownian motion [C4511]

"Texture classification using optimized support vector machines"

Support vector machines (SVMs) have been developed during the last two decades and recently acknowledged as very effective methods for general purpose pattern recognition. The important key in using a SVM is to select the appropriate parameters of its kernel function. In this paper, we present techniques on adjusting kernel parameters of SVMs to improve their performances with two remote sensing texture classification problems. [C4512]

"Incorporating texture information into polarimetric radar classification using neural networks"

Most of the recent research on polarimetric SAR classification focused on pixel-based techniques using the covariance matrix representation. Since multiple channels are inherently provided in polarimetric data, conventional techniques for increasing the dimensionality of the observation, such as texture feature extraction, were ignored. In this paper, we have demonstrated the potential of texture classification through gray level cooccurrence probabilities (GLCP), and proposed an unsupervised scheme using the self-organizing map (SOM) neural network. The increase in separability of the feature space is shown via the Fisher criterion and also verified by increased classification performance. Compared to the Wishart classifier, promising classification results are obtained from the Flevoland data set. [C4513]

"Automatic segmentation of multiple VHF-band SAR images to improve stem volume retrieval"

Ground slope effects have been identified as a limiting factor for stem volume retrieval from VHF-band SAR images since the ground-trunk dihedral scattering, which dominates the measured signal, is highly affected by surface relief and slope. To mitigate this problem coregistered SAR images from different flight headings have been acquired. These images are segmented to find regions with homogenous backscatter amplitude that are used with additional topography data to correct for the ground slope [C4514]

"Biomass estimation from polarimetric SAR interferometry over heterogeneous forest terrain"

Polarimetric SAR interferometry (Pol-InSAR) permits an accurate forest height extraction by inverting the SAR data with the Random Volume over Ground-model (RVoG). These forest heights were subsequently converted to forest biomass through forest height-biomass relation (allometry). Both the height extraction (L-band) and the allometric biomass conversion proved a good performance over dense forest stands. In open forests and stands of variable canopy height (here referred to as heterogeneous stands), the behaviour of the height extracting algorithm is unknown, and height-biomass allometry cannot easily be applied. To facilitate a direct biomass comparison of the Pol-InSAR-height extraction with ground measurements, the effective height heff was introduced as a direct biomass equivalent. Examples from spruce dominated sites of variable stand densities showed a sensitivity of the height extraction to the stand density, though not in correlation with the heff. It might be promising to exploit additional information from the shape of the extracted heights-histogram for an accurate biomass estimation even over dense and heterogeneous forests [C4515]

"Evaluation of JERS-1 L-band SAR backscatter for stem volume retrieval in boreal forest"

To assess the possibility of using L-band synthetic aperture radar (SAR) backscatter for forest stem volume mapping in the boreal zone, a comparative analysis was carried out at test sites located in Sweden, Finland and Central Siberia from which an extensive set of Japanese Earth Resources Satellite (JERS-1) images and ground data was available. The backscatter showed clear seasonal dynamics, increasing by 3-4 dB in dense forests and 1-2 dB in sparse forests when going from frozen to unfrozen conditions. To retrieve stem volume a simple L-band Water Cloud-related scattering model was used. Model training performed well in all cases, the model parameters estimates being affected by weather conditions at acquisition and test site-specific forest stand structure. At each test site the retrieval performed best under unfrozen conditions and worst under frozen conditions. The highest retrieval accuracy was achieved at the small and intensively managed test site of Kattbole in Sweden with a 25% relative RMS error. For the other test sites the much larger retrieval error could be explained as a consequence of heterogeneities in the forest stand structure, as well as differences in the ground dielectric properties and inaccuracy in the ground data [C4516]

"Use of backscatter differential phase in weather surveillance radars"

The polarimetric technique consists of simultaneous transmission and reception of Horizontally and Vertically polarized waves. Thus, transmitted polarization will be elliptical with equal horizontal and vertical components and arbitrary phase between the two. This scheme has been tested at NSSL on the NOAA research and development WSR-88D radar. Here reports on backscatter differential phase measurements with this radar. The radar also has a mode of transmitting horizontal polarization and receiving both the strong H and the weak V component (for short we refer to this mode as Linear Depolarization Ratio mode, LDR). Backscatter differential phase is considered a secondary polarimetric variable of lesser value for precipitation measurements than (the forward) specific differential phase or differential reflectivity. This is because backscatter differential phase is seldom significant. At 10 cm wavelength the only precipitation that can cause appreciable backscatter differential phase is hail. But it turns out that backscatter differential phase from other scatters provides two benefits. (1) it is suitable for discrimination between nonmeteorological scatters and precipitation and (2) it offers a way to calibrate (measure) the system differential phase. Of relevant and special importance is that, for some scatters, the measured total differential phase in the SHV scheme can differ from the value obtained in the sequential H, V scheme. The radar system contributes two distinct phases to the total differential phase. One is the differential phase in the transmission channel, the other is the differential phase in the receiver channel [C4517]

"A Bayesian technique for terrain mapping using multi-frequency ground based interferometric SAR systems"

In this paper we present some preliminary results of the application on real data of a statistical method to solve the height estimation problem in Interferometric Synthetic Aperture Radar (InSAR). The method is based on maximum a posteriori (MAP) estimation and Markov Random Fields (MRF) image modeling, and makes use of multifrequency/baseline SAR raw data. The real data set is acquired by a Ground-Based SAR (GB-SAR) interferometer based on the LiSA technology [C4518]

"Radar radial velocity variance measurements to decipher mountain-influenced Kelvin-Helmholtz waves, slope flows, and rotors"

The variance of the radial velocity in a cloud radar's signature is an underused parameter. The parameter represents a combination of the effects of convective turbulence and mechanical mixing from wind shear. It's usefulness in deciphering laminar, sheared, and turbulent mountain-influenced airflows within clouds is demonstrated in this paper [C4519]

"Retrieval of reflectivity in a networked radar environment"

This paper describes a methodology for reflectivity and attenuation retrieval in a networked radar environment. Electromagnetic waves backscattered from a common volume are attenuated differently along the different paths. Solution of the specific attenuation distribution is proposed by solving the integral equation for reflectivity, in a manner similar to that used with a differential phase constraint. The set of governing integral equations describing the backscatter and propagation of common resolution volume are solved simultaneously with constraints on observed total path attenuation. The algorithms developed are evaluated on simulated X-band radar observations in rain obtained from S-band measurements by CSU-CHILL radar. Retrieved reflectivity and specific attenuation using the iterative method show good agreement with intrinsic reflectivity and specific attenuation [C4520]

"Spatial rainfall rate estimation through combined use of radar reflectivity and raingauge data"

In this work we propose a procedure for the estimation of the spatial distribution of the rainfall rate in the observation time T over an area covered by a meteorological radar and a raingauge network. T can be the whole duration of a rainfall phenomenon or a part of it. The procedure is applied to a data set composed by PPI scans of absolute reflectivity gathered by a weather radar and by point rainfall measurement as provided by a raingauge network over the area monitored by the radar. The procedure was applied and tested on a experimental dataset related to a one-day precipitation phenomenon observed in Tuscany (Italy) on 29 October 1999, along the Arno river basin. The performance of the proposed procedure has been evaluated assuming a subset of the raingauge network as "true" rainfall rate reference [C4521]

"Mitigation of tropospheric InSAR phase artifacts through differential multisquint processing"

We propose a technique for mitigating tropospheric phase errors in repeat-pass interferometric synthetic aperture radar (InSAR). The mitigation technique is based upon the acquisition of multisquint InSAR data. On each satellite pass over a target area, the radar instrument will acquire images from multiple squint (azimuth) angles, from which multiple interferograms can be formed. The diversity of viewing angles associated with the multisquint acquisition can be used to solve for two components of the 3D surface displacement vector as well as for the differential tropospheric phase. We describe a model for the performance of the multisquint technique, and we present an assessment of the performance expected [C4522]

"Advanced InSAR coregistration using point clusters"

In this study, we introduce a refined algorithm for the fine InSAR image coregistration which could be used in highly decorrelated scenes. The refinement is introduced at the point of selection of points necessary for the estimation of the offset vectors between master and slave image. A new approach for point selection based on the Harris corner detector algorithm is presented. The new point selection algorithm results with the clusters of point candidates for the offset vectors over a scene. Consequently, the number of points and their spatial distribution are improved, which results in a better global quality of the coregistration model [C4523]

"Height retrieval by using a pseudo-differential approach in SAR interferometry preliminary results with actual SAR data"

In SAR interferometry a new approach to height retrieval has been defined, with the aim to obtain the elevation of selected targets in the scene without performing phase unwrapping procedures in the space domain. Following our preliminary simulations, in the paper the results of a first experimentation of this approach with actual SAR data will be introduced [C4524]

"Repeat pass SAR interferometry of the Pi-SAR (L) for DEM generation"

This paper describes generation of the digital elevation model (DEM) using the L band repeat pass airborne polarimetric Interferometric SAR (Pi-SAR) system, which is jointly developed by Japan Aerospace Exploration Agency (JAXA) and National Institute for Communication Technology (NICT). An image pair acquired over the Tottori calibration site in 2000 had a baseline of less than hundred meters and was used for this interferometric data analysis. Although the quantitative evaluation has not been conducted, the result shows that the detailed feature of the topography in the target area was well obtained [C4525]

"Avoiding phase unwrapping in DEM generation by fusing multi frequency ascending and descending interferograms"

This paper presents an approach to fuse an ensemble of interferograms of different wavelengths and viewing geometries to one common digital elevation model (DEM). Phase unwrapping and geocoding are performed "on the fly" and the different interferograms support each other. Propagation of phase unwrapping errors to large areas can no more occur which makes this method especially suitable for rugged mountains. The method is explained and a fusion of SRTM ascending and descending data with data with different wavelengths is demonstrated. The limits and possibilities are demonstrated by varying the number of interferograms and the viewing conditions. Furthermore a performance measure is given and compared with reference data [C4526]

"Comparing and combining the capability of detecting earthquake damages in urban areas using SAR and optical data"

The prompt detection, mapping and assessment of urban damages due to earthquakes is a key point, particularly in remote areas or where the infrastructures are not well developed to ensure the necessary

communication exchanges or where their operability has strongly decreased as a consequence of the event. The combination of Synthetic Aperture Radar (SAR) data and optical images is a promising and suitable approach. We propose two test cases, the 1999 Izmit (Turkey) and the 2003 Bam (Iran) earthquakes where we investigate the capability to detect urban changes and classify them. Moreover, a comparison with ground based data is also shown. [C4527]

"Study on land subsidence evolvement tendency by means of "integrated DInSAR""

In this paper, SAR interferometry with JERS SAR data and ERS SAR data was applied to investigate the land subsidence evolvement tendency in Wuan, China from 1993 to 1998. The subsidence was caused not only by coal mining but also by iron mining, and the investigated region is covered with some vegetation. The investigation shows that in a plain area, as long as the image pairs' time interval is short even if the perpendicular baseline exceeds 1100 m, it is possible to obtain a good interferometry effect with JERS SAR data. [C4528]

"Wind vector inversion from RADARSAT SAR images: a new algorithm"

Wind speed and direction are estimated from backscatter σ^0 measurements at two adjacent subscenes of RADARSAT-1 synthetic aperture radar (SAR) images, each subscene with slightly different incidence angles. Resultant wind vectors are validated using in situ buoy measurements, and compared with SAR-derived wind vectors obtained by using the wind directions determined from a spectral analysis of SAR images and colocated QuikSCAT measurements, as inputs to a hybrid model wind retrieval model. The implemented hybrid model consists CMOD-IFR2 (applicable to C-band, VV polarization) and the C-band copolarization ratio for Kirchhoff scattering. The new algorithm displays improved skill in wind vector estimation from RADARSAT-1 SAR data. [C4529]

"Evaluation of an operational SAR wind field retrieval algorithm for ENVISAT ASAR"

The operational algorithm WiSAR is introduced, which enables to extract high-resolution ocean surface wind fields from satellite borne synthetic aperture radars (SARs) on a fully operational basis. WiSAR can be applied to SAR data acquired in C-band at either vertical (VV) or horizontal (HH) polarization in transmit and receive from the European satellites ERS-1/2 and ENVISAT as well as the Canadian satellite RADARSAT-1. SAR wind field retrieval is a two step process. In the first step wind directions are extracted from wind induced streaks that are visible in the SAR images at scales above 200 m and that are assumed to be approximately in line with the mean surface wind direction. The orientations of these streaks are derived by a method based on investigation of local gradients of the SAR intensity image. The SAR retrieved wind directions are used in the second step, where wind speeds are derived from the normalized radar cross sections of the SAR data under consideration of the wind direction and local SAR imaging geometry. Therefore, the empirical model CMOD4, is used, which was developed for the C-band VV polarized scatterometer aboard ERS-1/2. CMOD4 has been extended to HH polarization considering the polarization ratio and its dependency on incidence angle. To show WiSARs applicability it is applied to a set of 32 ENVISAT ASAR data from the North Sea. The resulting wind fields are compared to the results of the operational numerical model of the German Weather Service. [C4530]

"Validation of ocean surface wind vector sensing using combined active and passive microwave measurements"

A new ocean surface wind vector measurement has been developed using combined active and passive microwave measurements from the TRMM satellite. In this method, collocated ocean normalized radar backscatter from the Precipitation Radar (PR) and retrieved wind speeds from the TRMM Microwave Imager (TMI) are used to derive ocean wind direction. Since PR provides only a single azimuth look, multiple wind direction solutions exists; but we compare the "closest" retrieved wind direction with near-simultaneous surface truth from three ocean buoy networks, namely; National Data Buoy Center (NDBC), Tropical Atmosphere Ocean (TAO), and Pilot Research moored Array in the Tropical Atlantic (PIRATA). Comparisons are also presented for QuikSCAT wind vector retrievals. [C4531]

"Sea SAR image analysis by fractal data fusion"

SAR images from space-borne platforms have proved to be helpful data for identification of oil spills and other surface anomalies, such as low wind areas, man-made targets, and natural films. The use of fractal dimension, which is related to the concept of surface "roughness", as a feature for classification, improves the detection of anomalies, since enhances texture discrimination. In the particular case of oil slicks, the surface tension of seawater is increased and the surface wave motion is significantly depressed. This effect relatively reduces the sea surface roughness, decreases the radar backscattered energy and enables oil slicks to be discernible from

the radar image. Several algorithms may be applied for local fractal dimension estimation, but most solutions are tailored for specific applications and are characterized by estimation accuracies depending on the adopted image model and also on the value being estimated. This paper describes a decision-based fusion approach for local fractal dimension estimation of SAR images of the sea surface. Three different estimation algorithms are considered and the three resulting fractal maps are fused by means of a weighted average. The weights are calculated from the performance characteristics of the three algorithms measured on synthetic fractal surfaces. The experimental results carried out on ERS-2 SAR images prove the effectiveness of the proposed decision-based fusion approach [C4532]

"Different fusion strategies to detect geographical objects by active contours in multitemporal SAR images"

When a geophysicist has to make a visual interpretation in multitemporal SAR images, it may be long and repetitive. To avoid this, an automatic object detection using multitemporal active contours is proposed in this paper. The information brought by the different images can be fused at different levels: either at the data level, the feature level or a level close to the decision level. On two data-sets, both located in French Guyana, two different strategies will be tested depending on the knowledge of the object, whether it is temporally stable or moving. [C4533]

"Merging of SAR and optical features for 3D reconstruction in a radargrammetric framework"

The aim of this paper is to propose a framework for the use of both SAR and optical data in a 3D reconstruction process. The SAR data provide height information either by interferometric or radargrammetric process and the optical data provides building shapes. The method is based on a Markov random field defined on a region adjacency graph. The regions are obtained using a segmentation of the optical image. The graph is then fed by the height information (either interferometric or radargrammetric) computed with the SAR data. The Markovian regularization takes height discontinuities into account thanks to an implicit edge process. [C4534]

"Landslide risk analysis by means of remote sensing techniques: results from the ESA/SLAM project"

In the framework of the SLAM (Service for Landslides Monitoring) project funded by the European Space Agency, the Permanent Scatterers (PS) processing and the analysis of high resolution images (e.g. SPOT5 and aerial-photos) have been performed at a basin scale, on the whole territory of the Arno River basin (Central Italy). About 350 SAR images have been interferometrically processed by means of the PS technique, detecting about 650,000 PS. The processing of SPOT5 images and aerial-photos, still in progress, have been performed for the extraction of features related to the landslide presence, useful for the geomorphological analysis and, as a consequence in order to give a spatial meaning to the punctual information provided by the PS. This procedure has been coupled with a intense geological interpretation phase characterized by the analysis of traditional in situ monitoring data, ancillary data and the performing of field surveys. The final results will impact on the current instruments used by the Arno Basin Authority for the landslide risk management (e.g. Hydrogeological Management Plan-Piano per l'Assetto Idrogeologico-PAI). [C4535]

"Pipeline encroachment monitoring using polarimetric SAR imagery"

Mechanical damage incurred from unauthorized third party activities remains a leading cause of onshore oil and gas pipeline failure, indicating the need for effective strategies to monitor encroachment over extensive sections of pipeline right-of-way (ROW). In this paper, the use of polarimetric SAR imagery (as will be available from RADARSAT-2) for pipeline monitoring of encroachment activities is explored. Experimental data were acquired of a test area near the shores of Lake Simcoe (north of Toronto, Ontario) in September 2001 by the C-SAR on board the Convair-580. The vehicle deployments and ground truthing were conducted by C-CORE with processing from signal data (including calibration) and analysis performed at the Canada Centre for Remote Sensing [C4536]

"IGARSS 2004. 2004 IEEE International Geoscience and Remote Sensing (IEEE Cat. No.04CH37612)"

{no data available} [C4537]

"Environmental monitoring with remote sensing data from Chinese spacecraft"

Five spacecrafts named in the Shenzhou series (SZ in abbreviation) have been launched during 1999 to 2003 in

China. Earth observation is a major scientific mission of the SZ spacecrafts. SZ-3 carried a 34-band medium resolution spectrometer, and SZ-4 was equipped with multimode microwave sensors composing a microwave scatterometer, radiometer, and radar altimeter. Our research group made "spacecraft-aircraft-ground" synchronous measurements. This paper presents the review of the mission of SZ spacecrafts, and gives the results of data processing and environment and geoscience applications. [C4538]

"An improved method of Doppler centroid estimation in SAR"

Successful processing of Synthetic Aperture Radar (SAR) requires that the Doppler centroid frequency (fdc) be accurately estimated. The energy balancing method is one of the methods to estimate the fdc, though it has some shortcomings. The paper brings forward an improved method which estimates the fdc more effectively. This paper finally shows the new method's results by processing raw data and analyzes its performance. A conclusion is drawn that the results of the improved method are precise; furthermore, the improved method can compute the fdc without iterative computations, so it is more suitable for real time processing on DSP and has higher efficiency. [C4539]

"Implementation of a co/decoding method in SAR processing based on time domain correlation"

Applications which could benefit from the use of an artificial device capable of encoding the SAR signal have been recently presented in literature. In this paper an implementation of a processing algorithm suitable to exploit such a device is described. Two general purpose figures of merit are proposed for the algorithm and the preliminary results of their theoretical and experimental evaluation are presented. [C4540]

"A new method for Total Zero Doppler Steering"

This paper describes a new method to perform zero Doppler steering, namely Total Zero Doppler Steering. It is developed for spaceborne synthetic aperture radar (SAR) systems. This new method combines the yaw-steering with an additional pitch-steering, resulting in a Doppler centroid of theoretically zero Hertz over the whole desired range of incidence angles for the whole orbit and simultaneously for left and right looking geometry. [C4541]

"3-D hurricane boundary layer wind retrieval algorithm for airborne Doppler radar measurements"

This paper presents a 3D boundary layer wind retrieval algorithm for airborne Doppler radar measurements of precipitation inside hurricanes. The data was collected, inside Hurricane Lili during NOAA's 2002 Atlantic Hurricane Ocean Winds Field Experiment with University of Massachusetts's newly developed Imaging Wind and Rain Airborne Profiler. Two forms of Kalman filters for 3D wind retrieval are analyzed for accuracy using simulations. Preliminary results of the actual 3D wind estimates using the chosen algorithm were obtained and compared with simultaneous and independent wind vector measurements by GPS dropwindsondes, surface wind speed measurements by a microwave radiometer and flight level wind vector measurements [C4542]

"Comparison of high-resolution wind maps from SAR imagery with in situ measurements from the ONR CBLAST experiments"

Each summer during the years 2001-2003, we have obtained SAR imagery over the Mid-Atlantic Bight area off the US east coast to complement ground-truth and airborne measurements collected as part of an ONR-sponsored CBLAST directed research initiative. This imagery has been converted to high-resolution wind maps of the CBLAST experimental area and compared with the extensive in situ and airborne measurements as well with concurrent and coincident SST estimates from AVHRR collected during the CBLAST experimental campaigns. These comparisons show good agreement that furthers our confidence in the SAR wind-mapping technique. Because of the relatively dense sampling of the CBLAST experimental area by our SAR overpasses, we believe the resulting SAR wind maps can provide important constraints on the various modeling studies of the marine boundary layer and ultimately the final conclusions of CBLAST. [C4543]

"C- and Ku-band ocean backscatter measurements under extreme wind conditions"

During the 2002 and 2003 ONR CBLAST Hurricane Program Field (HPF) and the NOAA/NESDIS Hurricane Ocean Winds and Rain Experiment, the University of Massachusetts (UMass) installed IWRAP, a conically scanning dual-band (C- and Ku-band), dual-polarized pencil-beam airborne Doppler radar that profiles the volume backscatter and Doppler velocity from rain and the backscatter from the ocean surface simultaneously at four incidence angles covering incidence angles from 25 to 55 degrees. From the measurements acquired during missions flown through hurricanes Gustav, Isadore, and Lili (2002) and Fabian and Isabel (2003), high wind regime Geophysical Model Functions have been derived at both frequencies and polarizations. Concrete

saturation effects in the NRCS are presented, and sensitivity in the wind direction at high wind speed is discussed through the analysis of the second harmonic of the NRCS. [C4544]

"Correcting SeaWinds measurements for rain effects"

Correcting SeaWinds scatterometer data for rain using radiometer rain rates is possible at moderate rates when the antenna footprint is fully-filled with rain. We address use of the "slice" sub-footprints to correct for partially filled footprints. Using the number of slices containing heavy rain, we propose adjusting the rate reported by the radiometer to a value near that if the heavy rain filled the footprint and applying this value to empirical formulas to calculate backscatter from and attenuation through the rain. Simulations show the errors are not very sensitive to the estimate of raining area. [C4545]

"High quality wind retrievals for hurricanes Isabel and Fabian using the SeaWinds scatterometer"

Hurricanes Isabel and Fabian offer an unprecedented look at tropical cyclones. With the availability of two identical instruments, temporal sampling was as frequent as 6-12 hours. Utilizing the SeaWinds scatterometers' ability to make simultaneous active and passive measurements, high quality wind and rain retrievals were performed for 8 storm passes. Passive rain estimates are used to quantify both the attenuating and scattering effects of precipitation, which can then be used to correct the active wind measurements. The high resolution of the retrievals allows for feature identification, while a binary rain mask removes pixels too contaminated for wind speed retrieval. Wind results compare well with surface models produced by the Hurricane Research Division of NOAA, and rain rates show great spatial similarity to SSM/I F13 and F15 data sets. [C4546]

"Polarimetric SAR image classification-exploiting optimal variables derived from multiple-image datasets"

Polarimetric SAR image classification remains an important research area. Various methods continue to be developed for specific applications. Instead of focusing upon one specific problem, we have developed nonlinear dimensionality reduction techniques that extract information from inherently high dimensional datasets. We present computationally tractable, suboptimal extensions of the full nonlinear dimensionality reduction techniques. We apply these suboptimal techniques to polarimetric SAR image classification. Comparisons will be made between optimal and suboptimal techniques, and, as a reference, to standard statistical Wishart classifiers. [C4547]

"Statistical assessment of eigenvector-based target decomposition theorems in radar polarimetry"

This paper concerns the analytical study of the eigen decomposition of hermitian, positive semidefinite matrices applied to PolSAR data analysis. Based on the Gaussian scattering assumption for multidimensional SAR data, the joint distribution of the sample eigenvalues of the coherency, or covariance, matrices is derived for a general case. The distribution is particularized for PolSAR data, and the moments of the sample eigenvalues, the entropy (H), and the anisotropy (A) are analyzed [C4548]

"Improvement of polarimetric SAR calibration based on the Quegan algorithm"

The polarimetric cross-talk calibration algorithm proposed by Quegan, which is more general than the one proposed by van Zyl, is modified to improve polarimetric SAR calibration. L-band polarimetric SAR data acquired by the JAXA/NICT airborne Pi-SAR, including a variety of natural and artificial targets, are calibrated introducing noise imbalance of cross-polarized channels into the Quegan algorithm and deriving the cross-talk parameters from areas with low correlation between like and cross-polarized observed echoes. The achieved enhancement in stability of cross-talk parameter estimation and removal over is demonstrated in terms of CR response analysis and polarimetric classification result [C4549]

"Application and extension of a quasioperational approach to wind speed measurement from spaceborne synthetic aperture radar"

Over the past several years, a consensus has been firmly established that it is possible to make high-resolution (sub-kilometer) marine wind speed measurements from space using synthetic aperture radars (SARs) [F.M. Monaldo, et al., 2003]. Conventionally, the wind field is measured from space using active microwave scatterometry or passive microwave measurements. For example, the SeaWinds scatterometer on the QuikSCAT satellite uses microwave backscatter to measure ocean surface wind vectors. The special sensor microwave/imager aboard the defense meteorological satellite program satellites makes passive microwave measurements of wind speed. These instruments are best suited for global measurements, so their 25-km resolution misses important high-spatial-frequency phenomena, particularly in coastal areas. Since 1999, we

have operated a near-real time processing scheme that converts quick-look processed RADARSAT-1 SAR imagery into high-resolution estimates of wind speed. This software and processing protocols have matured and evolved into the APL/NOAA SAR wind speed retrieval system (ANSWRS). ANSWRS has been upgraded recently to process ENVISAT SAR imagery as well. This paper is a brief description of this system. [C4550]

"SAR-derived winds in coastal Alaska waters"

High-resolution winds derived from RADARSAT-1 synthetic aperture radar (SAR) images have been produced for the waters around Alaska since 1999. Wind speed images show useful details of many meteorological phenomena of interest in weather analysis and forecasting. These include wakes, gap flows, lee waves, atmospheric fronts, cyclones, and barrier jets [C4551]

"Polarimetric analysis of scatterometer data for ocean surface wind measurement"

An experiment using a polarimetric scatterometer (POLSCAT) has been conducted by JPL for ocean surface wind measurement. It shows that sigma0 values for HH, VV, HV, and VH have the property of even symmetry with respect to the upwind direction, and correlation coefficients between co- and cross-polarizations have the odd symmetry property. In this paper, the symmetry properties will be further examined using polarimetric analysis to investigate the depolarization effect, the scattering mechanism, and the polarization orientation angle. Theoretical results based on a two scale model are used to verify the derived experiment results. The newly derived symmetry property has the potential to solve the 180deg ambiguity in wind direction, and to enhance the accuracy of wind vector measurements [C4552]

"Spiral eddy detection using surfactant slick patterns and polarimetric SAR image decomposition techniques"

Surfactant slicks are widely dispersed throughout the oceans. Current driven features, such as spiral eddies, can be made visible by associated slick patterns. In this study a combined algorithm using the Cloude-Pottier decomposition and the Wishart classifier is presented to produce accurate maps of slick patterns. The study then uses the classified slick patterns to detect spiral eddies. The competing background wave-field is eliminated. Satellite SAR instruments performing wave spectral measurements, or operating as wind scatterometers, regard the slicks as a measurement error-term. The maps produced by the algorithm facilitate the flagging of slick contaminated pixels within the image [C4553]

"Knowledge-based sea ice classification by polarimetric SAR"

Polarimetric SAR images acquired at C- and L-band over sea ice in the Greenland Sea, Baltic Sea, and Beaufort Sea have been analysed with respect to their potential for ice type classification. The polarimetric data were gathered by the Danish EMISAR and the US AIRSAR which both are airborne systems. A hierarchical classification scheme was chosen for sea ice because our knowledge about magnitudes, variations, and dependences of sea ice signatures can be directly considered. The optimal sequence of classification rules and the rules themselves depend on the ice conditions/regimes. The use of the polarimetric phase information improves the classification only in the case of thin ice types but is not necessary for thicker ice (above about 30 cm thickness) [C4554]

"Matching-pursuit based analysis of fluctuating scatterers in polarimetric SAR images"

This paper addresses the problem of moving and nonstationary objects analysis in SAR images. A method, based on Matching Pursuit (MP) algorithm is proposed to decompose the SAR signal into a set of chirplets. Chirplets parameters can be related to physical characteristics of the SAR scene constituents and used to produce a multidimensional polarimetric bright point model of the object of an observed object [C4555]

"Characterization of the electromagnetic response of maize crops with polarimetric backscatter profiles"

An exhaustive analysis of the electromagnetic response from a maize sample, measured in laboratory conditions, is presented. Fully polarimetric wide-band radar data have been collected in order to compute backscatter profiles (i.e. 1D images) as a function of height. First results consist on backscatter images expressed in Pauli and linear basis. These plots demonstrate that the extinction coefficient is higher for vertical polarization than for horizontal polarization due to the predominant vertical orientations of the components of the corn plants (mainly the stems). In addition, the crosspolar backscattered power decreases importantly as the frequency increases, and it is always lower than the copolar returns, again as a result of the oriented morphology, which produces a very low depolarization of the signal. On the other hand, the second kind of results is based on the polarimetric

target decomposition proposed by Cloude and Pottier. Height profiles of alpha, entropy and anisotropy have been calculated. These parameters have been carefully analyzed in order to extract information to be used in the application of parameters inversion algorithms [C4556]

"Iceberg and ship discrimination with ENVISAT multipolarization ASAR"

Spaceborne synthetic aperture radar (SAR) can provide wide area and all-weather surveillance for iceberg and ship targets. However, the discrimination between icebergs and ships in SAR imagery, especially in the single polarization imagery that has been available over the past decade, is not always reliable. This is especially true when vessel and iceberg size are on the order of the pixel spacing. Present requirements for ocean surveillance with SAR data include a high detection and classification accuracy due to the necessity of comparable performance with other reconnaissance methods, such as aerial. ENVISAT advanced SAR (ASAR) data offers a potential solution to the iceberg-ship discrimination problem. ASAR data has comparable swath and resolution to other operational SAR systems and in addition offers an alternating polarization (AP) mode. AP targets offer more information than single polarization with respect to radar scattering mechanisms. The AP ship and iceberg targets in this study were observed to have considerably different polarization responses. In particular, ship targets in the HH and HV channels were comparable. In contrast, iceberg targets had at best, weak HV responses compared to the HH channel. Two methods for target discrimination were investigated: a multipolarized area ratio and HV signal-to-clutter ratio (SCR). [C4557]

"Melt detection in Antarctic ice-sheets using spaceborne scatterometers and radiometers"

Backscatter measurements from the Sea Winds on QuikSCAT scatterometer are used to determine periods of surface freeze and melt on Antarctic ice-shelves. A maximum likelihood method is used to infer the daily ice-surface conditions for various study points located on the Ronne, Ross, Larsen, Fimbul, Amery, and Shackleton ice-shelves. Criteria for determining the dates of melt-onset and freeze-up for each Austral summer are presented. Validation of the ice-state and melt-onset date estimates is performed by analyzing the corresponding brightness temperature (Tb) measurements from special sensor microwave/imager (SSM/I) radiometers. QuikSCAT σ° measurements from 1999 through 2003 are analyzed and found to be very useful for determining periods of melt in Antarctic ice-sheets and provide high temporal and spatial resolution ice-state estimates. [C4558]

"Design, fabrication, and evaluation of a mobile robot for polar environments"

This paper describes the design, fabrication, and evaluation of a mobile robot as part of a radar system for measuring ice characteristics in Greenland and Antarctica. The robot can survive the polar environments, navigate the terrains, is capable of carrying the necessary radar equipment while providing power, can tow an antenna, and can provide precise positioning for the bistatic synthetic aperture radar (SAR). [C4559]

"A Bayesian network for autonomous sensor control during polar ice sheet measurements"

The PRISM (Polar Radar for Ice Sheet Measurements) project at the University of Kansas is developing intelligent radar sensors for the measurement and study of the mass balance of the polar ice sheets. An important component of PRISM is intelligent, autonomous synthetic aperture radar that can reason about its operating mode (monostatic vs. bistatic) and frequency, based on a variety of environmental and sensor-related factors. The PRISM sensors are placed on autonomous robotic vehicles ("rovers") that use the sensor and environmental information to decide about what paths to traverse, how to traverse them, and at what speeds. In our work, we have implemented the reasoning component of the autonomous radar and the rovers, using intelligent agents and Bayesian networks. This implementation is the first ever of a dynamically modifying adaptive radar and mobile data collection system based on autonomous rovers for accurate polar ice sheet measurements. [C4560]

"A wideband radar depth sounder for measuring the thickness of glacial ice"

We developed a wideband coherent radar depth sounder (WCORDS) system developed to measure glacial ice thickness and map internal layers with high resolution. The radar operates over a frequency range of 50-200 MHz, providing a resolution of about 1 m in ice. A high-speed arbitrary waveform generator (AWG) is used to generate a chirp from 50-200 MHz over a very small pulse width to obtain high sensitivity needed to sound 5-km thick cold ice and map internal layers high resolution. It also consists of a two-channel receiver to obtain very high dynamic range. The low-gain channel is used to map the shallow internal layers and the high-gain channel provides ice sheet thickness and bedrock properties up to a depth of 5000 m. The gain in both the channels can be adjusted to obtain optimum performance. A high-speed data acquisition system is used to digitize and perform necessary real time processing on the data before transferring it to the storage device. The radar and

data-acquisition systems have been significantly miniaturized using the latest RF and fabrication technologies. The entire system is designed to fit into multiple compact-PCI cards. Laboratory tests show that the radar system has the required sensitivity to map 5000-m-thick ice. Considerable improvement in sidelobe performance was achieved. The radar system will be tested during the summer 2004 field experiment at the Summit Camp, Greenland. [C4561]

"Multiband multistatic synthetic aperture radar for measuring ice sheet basal conditions"

Ice sheet models are necessary to understand ice sheet dynamics and to predict their behavior. Of the primary inputs to these models, basal conditions are the least understood. By observing the forward and backscatter across a wide frequency range (over two octaves) the basal conditions can be established with a high level of confidence. For this purpose, we developed a multistatic synthetic aperture radar system that operates on three frequency bands (75-85 MHz, 140-160 MHz, and 330-370 MHz). The radar system is designed to use pulse compression techniques and coherent integration to obtain high loop sensitivity (203 dB) necessary to overcome radio frequency losses in ice. The system will be tested at Summit, Greenland (72deg34'N, 38deg29'W) during July 2004 [C4562]

"Synthetic aperture radar and high-resolution MM5 simulations of barrier jets in coastal Alaska"

The mesoscale atmospheric flow near coastlines with prominent terrain has a tremendous impact on those who live and work in the coastal environment. One of the most common of these terrain-induced flows, the barrier jet, creates especially dangerous weather conditions, particularly in southeast Alaska and the Pacific Northwest. The resulting severe winds pose a threat to life, property and economic activities. They play a major role in safety at sea for the fishery and oil industries. Barrier jets occur when stable onshore flow interacts with a mountain barrier. In classical barrier jet theory, the barrier normal flow is blocked when the Froude number is much less than 1. In these situations, the onshore flow is too stable to rise over the barrier. The dynamic response is for the ascending air to cool and generate a hydrostatic positive pressure perturbation which forces a turning of the wind to the left along the barrier in the Northern Hemisphere. The Gulf of Alaska is uniquely suited to studying barrier jets of both the classical and hybrid types. This is because of the frequency of onshore flow events associated with landfalling synoptic cyclones, the mountain ranges with complex dimensional terrain (including gaps) that occur along large sections of the coast, and the orientation of the coast line (particularly along the SE coast of the Gulf). In addition, the fact that much of the Gulf lies at high latitudes ensures excellent coverage from polar orbiting satellites such as the scatterometer aboard QuikSCAT and the synthetic aperture radars aboard the ENVISAT and RADARSAT-1 satellites. [C4563]

"A compact high-resolution radar for determining snow accumulation rates"

Rising sea level has important humanitarian and economic implications. Scientists are rigorously investigating the contribution of glacial ice sheets to sea-level rise. Knowledge of the mass balance of the ice sheets is important in understanding their dynamics. The accumulation rate of snow on ice sheets is an important variable in determining this mass balance. The accumulation rate is currently determined using ice cores and pits. This is a tedious method to obtain coverage over the entire ice sheet due to the limited number of samples that can be acquired. The only practical means of obtaining coverage over a large area would be by means of remote sensing. We have developed a wideband radar to map the isochronous layers in the ice sheet. This will help reduce the uncertainty associated with sparse sampling of the ice sheet. We built a compact FM-CW radar that operates from 500 to 2000 MHz with range resolution of about 10 cm. Both the transmitter and receiver were housed in a single Compact PCI chassis. We used a YIG oscillator to generate the FM signal. The performance of an FM-CW is usually degraded by the nonlinearity of the source. We linearized the sweep of the YIG oscillator by means of a phase-locked loop (PLL). We have successfully tested the radar in the lab and we will be performing tests during the 2004 summer field experiments at the Summit camp in Greenland. We successfully tested a connectorized version of this radar during the 2003 field experiments at the North Greenland Ice Core Project (NGRIP) camp. We were able to map the internal layers up to a depth of about 150 m over a 5-km transect. We also conducted detailed snow pit studies at several spots over the transect for correlating the visually determined layers with the radar determined layers. We will present the radar design, laboratory test results of its performance, results from the experiments at Summit and a comparison of the radar data with information derived from ice cores and snow pits. [C4564]

"Validation of synthetic aperture radar for iceberg detection in sea ice"

SAR satellites can detect icebergs over very large areas in all weather, regardless of ambient conditions like darkness, rain, and fog. As a result, SAR satellites are currently being used on the Grand Banks to enhance iceberg surveillance. During the iceberg season, the Grand Banks region is also frequented by sea ice, which is

known to degrade radar performance. To quantify this performance, a validation of the iceberg detection capabilities of satellite radar in sea ice conditions was conducted. The satellite radars used in this validation process were RADARSAT-1 synthetic aperture radar (SAR) and ENVISAT advanced synthetic aperture radar (ASAR). Several sources have documented average radar signature backscatter values for various sea ice types in microwave radar imagery. As part of the validation effort discussed here, sea ice backscatter values were extracted from RADARSAT-1 SAR and ENVISAT ASAR data and validated against these documented values. Iceberg data for various iceberg sizes have also been extracted from data for both satellites. Using the sea ice backscatter values and the iceberg data information, probability of detection (POD) curves were generated for small, medium and large sized icebergs in multiyear ice, first-year ice, thin lead ice and typical ice conditions found on the Grand Banks. This work was performed with the support of the European Space Agency (ESA), the Canadian Ice Service (CIS) and a consortium of oil and gas companies off the east coast of Newfoundland [C4565]

"Virtual PRISM-on the ice via the web with the polar radar for ice sheet measurements project"

The PRISM project at the University of Kansas has developed the necessary tools and infrastructure to bring the daily activities of polar ice sheet research to students and the general public via the Web. PRISM is developing advanced intelligent remote sensing technology to measure key ice sheet characteristics, and PRISM investigators travel to remote ice sheet sites annually. We have developed "Virtual PRISM" as part of the PRISM web page, to allow the public to follow the field activities of the PRISM team in Greenland. "Virtual PRISM" includes a daily field log, digital images, video clips, access to weather data on the ice sheet, and a Java-based applet called the "Virtual Dashboard" that simulates sitting in the driver's seat of the PRISM robotic rover. [C4566]

"Data fusion: remote sensing for target detection and tracking"

As part of an ongoing research program in data fusion applied to the multisensor environment for iceberg detection on the east coast of Canada, this paper describes the efforts to use modeling of iceberg movement to perform iceberg detection data fusion. Data fusion and sensor combination are integral parts of a cost effective ice management regime for safe offshore oil and gas recovery programs. This paper addresses data fusion in the form of associations of detections to create tracks from multiple sensor sweeps of an area. The Coupled Ice Ocean (CIO) Model of Iceberg Kinematics from the Canadian Ice Services (CIS) is used as a maneuvering model to the tracking process. The fusion system was tested using iceberg detections from the 2003 ice season. All data were collected in the Grand Banks area of Newfoundland, Canada. [C4567]

"Fusion of low resolution optical and high resolution SAR data for land cover classification"

A set of ERS SAR and optical MODIS-images were classified to land cover and tree species classes. Different methods for pixel and decision based data fusion were tested. Classifications of featuresets were carried out using Bayes rule for minimum error. The results were not very successful, the classification accuracies of land cover classes varied from 43% to 75%, depending on the used features and classes. The decision based data fusion method, where the a posteriori probabilities representing the proportions of different land cover classes of low resolution classification are used as a priori probabilities in high resolution classification looks promising. Using this method, the increase of overall and classwise accuracies can be more than 10 and 25 %-units, respectively. [C4568]

"Effect of texture measures to separability of land cover classes using ERS SAR images"

Texture features based on Haralick's co-occurrence matrix were compared for land cover and forestry classification purposes. According to these results, the best texture features were Angular Second Moment, Mean and Entropy, the worst Correlation and Standard Deviation. The best SAR-images were taken during wet snow or ground. Usually, the larger the window used to construct the co-occurrence matrix, the better the results. The suitable length of the spatial step depended on texture feature and classes. The directionless texture features performed usually well. The results of the performed classification experiment were disappointing. [C4569]

"A novel hybrid method to unwrapping interferometric phase"

Phase unwrapping is the most difficult and unavoidable problem in the interferometric synthetic aperture radar (InSAR) processing procedures. Intensive researches have been done and the methods proposed were summarized into two categories: path following and minimum norm. Unwrapping result by path following is congruent with wrapped phase and require less time and memory. While minimum norm method usually could not obtain congruent result directly and take more computing resource. Weighting could improve phase

unwrapping result very much if the suspicious region could be correctively separated out by weighting function. However, common used weighting such as coherence or phase gradient could not serve this purpose very well. In this paper, we proposed a novel method to unwrap phase, which combined the advantages of both categories, and set weight based on phase unwrapping consistence. We demonstrated the method with real InSAR phase. The unwrapping result showed the novel method could recover the dynamic range of phase than least square method while keep correct trend. [C4570]

"InSAR technology processing and result analysis"

InSAR (synthetic aperture radar interferometry) is currently a hot topic that is rapidly evolving thanks to the spectacular results achieved in various fields, especially in the construction of digital elevation models (DEMs) of the Earth's surface. This paper goes deep into the interference imagery mechanism, and from the application requirement of surveying and mapping, stresses solving InSAR key technology. A phase unwrapping method based on the principle of mean field annealing (MFA) is put forward. Finally, we testing this algorithm on some InSAR data, the result shows that this algorithm can obtain DEM correctly and efficiently. Then we analysis the result and display it through 3D. The display effect looks better. [C4571]

"A simple class-set based vegetation classification of a South Pacific volcanic island (Moorea Island, French Polynesia) using both AirSAR and MASTER data"

This paper addresses the vegetation mapping and land use of Opunohu Valley (Moorea Island, French Polynesia) using JPL-AirSAR and MASTER (MODIS/ASTER simulator) images. We first define an original set of classes based on the relative canopy-height of vegetation, out of a well-suited RGB SAR-composite image that visually discriminates our vegetation classes. An interesting "pineapple fields" class (an important economic resource in Moorea island) proves to discriminate particularly from the height-related "Low Vegetation" class. Two supervised maximum likelihood classification maps have been processed on both the AirSAR and the MASTER images, using aerial photographs as a ground truth training set. The vegetal species included in each class as well as the classification results are discussed. Comparison of the MASTER and AirSAR based classification results leads us to propose a fusion of AirSAR and MASTER classification maps keeping the best of both worlds in order to improve the overall accuracy of the AirSAR classification. [C4572]

"Temporal analysis of RADARS AT-1 imagery from Delaware Bay"

The objective of this study is to identify, catalog, and relate surface phenomena observed in SAR imagery of the Delaware Bay with concurrent environmental conditions (tides, winds, currents, river discharge, etc). To accomplish this objective, we examined a sequence of RADARSAT-1 SAR containing approximately 176 standard mode scenes collected over the Delaware Bay and adjacent coastal waters between May 1997 and February 2004. In this paper we report on 58 standard mode-2 scenes collected during ascending orbits. Unique to this RADARSAT image time sequence is the contemporaneous set of in situ meteorological and oceanographic observations that were collected from shipboard platforms and fixed stations throughout the Delaware Bay during the image acquisition period. [C4573]

"Use of a global wave model to correct altimeter sea level estimates"

The study reports an assessment of global ocean wave model (Wavewatch III) outputs using altimeter algorithms wave statistics at global and regional scales. The focus is upon the sensitivity if the modeled wave moments to two distinct types of wind forcing fields, one from the NCEP atmospheric model analysis and the other from a blended product combining NCEP with scatterometer winds (QuickSCAT). [C4574]

"FCM and HCA performance analysis for crop type classification of SAR imagery"

In this study, we investigate the classification performance of two clustering algorithms, the fuzzy C-means (FCM) and hierarchical clustering analysis (HCA) algorithms applied to crop type classification of high-resolution airborne synthetic aperture radar (SAR) imagery based on Haralick and autocorrelation textural features. The contribution of the different polarization channels toward the overall classification of different cluster regions are also analyzed as well as the influence in the election of the optimum parameters for wavelet image enhancement. [C4575]

"Cross-validation of Jason-1 and QuikSCAT wind speeds"

Observing near-surface ocean winds is important to the understanding of global weather patterns. Wind speed information can be retrieved from σ^0 measurements made by Jason-1 and SeaWinds on QuikSCAT. Though co-located measurements from the two satellites generally agree, significant differences between the co-located

measurements are occasionally observed, particularly associated with rain events. Co-located data from TRMM PR 2A25 and ECMWF is used to study the effects of rain on Jason-1. Key observations are discussed. [C4576]

"Spectral filtering for radar interferometry: position analysis of filtering"

This paper discusses spectral filtering for radar interferometry, especial the impact of the filters' position in the processing procedure. After analysis, we get the best filtering process for interferometry which contains one time of azimuth filtering and two times of range filtering. Using this process, we can improve the coherence between image pairs greatly and get an interferogram with high quality. [C4577]

"Development of a Radarsat-1 interferometric baseline catalog"

With the improved orbit maintenance of the Radarsat-1 satellite, there has been an increased interest in the interferometric SAR (InSAR) processing of Radarsat data. One of the most vital parameters in the selection process for InSAR processing is the baseline. The baseline indicates whether an interferometric image pair is suitable for a certain application. As interferometric baselines cannot be part of the regular metadata that are attached to a single data set, there is a need to provide this kind of essential information for SAR interferometric processing to user community in searchable and easily accessible form. This paper describes the development of an interferometric baseline catalog for the Radarsat-1 satellite at the Alaska Satellite Facility. The baselines are calculated from metadata information in the archive. Based on the orbit information in form of state vectors, the Doppler centroid and the slant range, a baseline can be estimated on a frame basis. The baselines for all existing image pairs in the archive are stored in a database that serves as backbone of a Web interface. [C4578]

"Stochastic modeling of time series radar interferometry"

Quality description and evaluation of InSAR results is hampered by the fact that the model to derive parameters from the observations is usually underdetermined. Only using strong, often rather qualitative, assumptions it is possible to reach unique solutions. One of the most prominent assumptions is that phase ambiguity resolution can be treated as a deterministic problem. In this study, a model formulation is presented that captures the majority of the assumptions in a mathematical sense, allowing for adjustment, testing procedures and formal error propagation. The influence of stochastic ambiguity resolution to the probability distribution of the estimated parameters is shown. [C4579]

"Rapid object recognition from high resolution SAR image supported by geo-database"

The objective of this paper is to present a basic study of rapid object recognition in full scene of high resolution SAR image. In this paper the recognition is viewed as a recipient of information from two sources: a scene containing the object to be recognized and a geo-database indicating the location of the objects to be recognized with feature class. Using the prior information offered by geo-database and SAR imaging model, the efficiency of object recognition is improved rapidly. [C4580]

"Multi-channel along track interferometry"

In this paper we introduce an algorithm for velocity estimation of a ground moving point target using a multi-channel along-track interferometry (MC-ATI) system. The presented results are relative to a multi frequency system, but the algorithm can be used also for a multi-baseline one. The performance of the system is evaluated by presenting also the probabilities of detection. [C4581]

"Interferometric point target analysis of RADARSAT-1 data for deformation monitoring at the Belridge/Lost Hills oil fields"

Interferometric point target analysis using Gamma Remote Sensing's IPTA module has been applied to two interferometric stacks of RADARSAT-1 FINE mode data over the Belridge/Lost Hills oil fields in California. The stacks (30 images each) are both from descending orbits and span the same 2 year time period (2002/02-2004/02) but incidence angles are different (F1 vs. F3F). An IPTA analysis is carried out on each stack separately and results are then compared in terms of achieved density of the scatterers and residual errors of the motion analysis. We verify the accuracy of our methods indirectly by studying the subtle difference in line-of-sight motion caused by the different incidence angles of the data stacks (38.4 vs. 43.1 degrees at the study site). [C4582]

"New methods of the filtering the phase noise in the interferometric SAR"

Because of the existence of the noise in the fringe, it influences the computing efficiency and precision of the algorithms of the unwrapping, and then influences the precision of the generation of digital elevation models. This paper firstly analyzes the sources of the phase noise in the fringe. Then introduces several methods used to filter the phase noise in the fringe. For the phase jump in the fringe, it proposes a method of sine & cosine transformation to solve the problem of phase jump. At the basic of the method of sine & cosine transformation, it puts forward two new methods-sine & cosine mean filter (SCMeanF) and sine & cosine median filter (SCMedianF). Lastly, we carried out the contrast test. [C4583]

"The improvement of the conventional GMTI method with single-channel SAR"

SAR/GMTI (synthetic aperture radar/ground moving target indicator) can detect targets with low velocities and provide images of the area covered by a scanning antenna with high revisit rates. By the conventional GMTI method, the estimated velocity of the moving target is not accurate. The authors improve it by a new idea which uses a series of moving windows. This paper shows the new method's results by processing raw radar data and analyzes its performance finally. A conclusion is drawn that the improved method is more effective and accurate for GMTI. [C4584]

"Preprocessing to improve the quality of SAR interferogram"

In this paper, the preprocessing method for improving the quality of interferograms is described. The method consists of three processing steps-azimuth filtering, range filtering and oversampling. It is shown that the first two steps are effective to eliminate the decorrelation caused by spectrum misalignment in azimuth and range and the oversampling can eliminate the error introduced by the aliasing because of convolution in frequency domain. The validity of the proposed method is verified by ERS SLC data. [C4585]

"Motion error analysis and compensation for airborne formation flying InSAR"

Because the stability of plane platform is not good, airborne SAR can not acquire the precise orbit parallelism and velocity as spaceborne SAR. Motion error problem for airborne formation flying InSAR is analyzed here. The plane interval changes (across track baseline changes) can be discussed in three situations: interval increasing, interval decreasing, interval changing according to sine curve. Phase changes with baseline changes are deduced quantitatively. The simulation result of plane interval changes is given out. It can be concluded that across track baseline changes lead to azimuth slope. The digital relation between across-track baseline error and phase error, height error is concluded by simulation experiment result. The paper presents the method of azimuth slope elimination. Azimuth slope eliminating is adopted in simulation terrain. Two control points are set in topographic area to compensate the phase error of baseline changes. This algorithm can improve the DEM precision for whole area. Even if the plane track is curve, the method in this paper can still compensate most of the motion error. [C4586]

"Multi-frequency polarimetric snow discrimination in Alpine areas"

This paper presents a new method to map dry snow in Alpine areas. A supervised discrimination algorithm, based on polarimetric contrast, is proposed to enhance multi-temporal and/or multi-frequency polarimetric behavior variations over snow-covered areas. This technique is shown to be more robust with respect to topography and underlying media diversity than classical contrast enhancement approaches. The effectiveness of the proposed method is demonstrated using SIR-C L and C-band polarimetric data sets [C4587]

"Modeling of snow wetness inversion using multi-polarization SAR at C-Band"

Radar backscattering response has the potential of retrieving desired snow parameters, such as snow water equivalence, snow depth, liquid water content which are important factors in hydrological investigation. The objective of this study is to develop an algorithm which can decompose the scattering of wet snow and also develop new description of surface scattering. There are two scattering sources-the volume scattering component from snow pack and the air-snow surface scattering component-for radar backscattering while observing wet snow. Depending upon which scattering component is dominant and then controls the response to snow wetness, an algorithm can be developed to quantitatively describe the relationship between this two scattering sources and snow wetness. We have established a model-simulated at C-band at a base by using two scattering components. The database covers the most possible wet snow physical properties and surface roughness conditions. Using this data-base, an inversion algorithm can be developed for using C-band multi-polarization measurements. The newly developed algorithm mainly involved two steps: 1) decomposes the surface and volume scattering signals, and 2) then use each scattering component to estimate snow wetness [C4588]

"Bistatic parasitic SAR processor evaluation"

Bistatic radar systems will play a great role in the coming decade since a large number of radar missions are being foreseen. Using existing transmitters, formations of small passive receivers will enhance our capability to gather backscatter information from Earth. A bistatic SAR system operates with separated transmitting and receiving antenna and both antennas can follow independent trajectories. In this paper, the recently developed imaging algorithm for the case where the transmitting antenna follows a rectilinear trajectory while the receiver remains in a fixed position and orientation will be evaluated. This new imaging algorithm is based on a projecting the bistatic geometry onto the chirp scaling algorithm which results on a scaling factor in the azimuth compression function. This scaling factor is derived from the bistatic configurations and assumes a flat topography. The main purpose of this paper is to determine the accuracy of the algorithm when used with real case simulated scenarios such as the airborne case where the transmitter is onboard an airplane while the receiver will be installed in the top of a high tower [C4589]

"Estimation of snow pack characteristics and snow covered area in boreal forests from ERS-2 SAR and Envisat ASAR data"

Estimation of snow moisture (total liquid water content) and the fraction of snow covered area (SCA) are investigated by applying multi-year ERS-2 SAR and Envisat ASAR data sets. An inversion approach for the moisture retrieval is introduced. The results suggest that C-band radar is operationally feasible for both applications [C4590]

"Snow thickness estimation using correlation functions at C-band"

An accurate measurement of snow-layer thickness on the ground is a critical process for estimating the equivalent water content of snow. Previous studies were mainly based on the analysis of the backscattering cross-section of two co-polarized signals at different frequencies. The snow thickness was inferred by comparison with the analytical model. Recently, we have applied the angular and frequency correlation functions (ACF/FCF) for the estimation of sea-ice thickness. One of the advantages of the ACF/FCF method is suppression of the interfering volume scattering, which results in better accuracy and reliability of thickness estimation. We apply a simplified 1D three-layer model for the analysis. The layers are air, snow, and ground. The interfaces between layers are modeled as rough surfaces. Within the layers, there are small inclusions which introduce the volume scattering. Rough surfaces are modeled by the Kirchhoff approximation methods. The volume scattering is calculated using the quasi-crystalline approximation with coherent potential approximation (QCA-CP) for small particles. The ACF/FCF works by correlating two signals with different frequencies and/or incident angles. Using this model, we can determine the behavior of ACF/FCF and use it for snow thickness retrieval [C4591]

"SAR image segmentation by 2-D fussy entropy"

In the process of SAR (synthetic aperture radar) ATR (automatic target recognition), segmentation is the core procedure. In this paper, analyzing the characteristics of SAR images, we introduced a new method for segmenting SAR images. The method is based on 2D c-partition fussy entropy and adaptive genetic algorithm. 2D fussy entropy is used as the fitness function, and adaptive genetic algorithm is used for optimizing thresholds. The results of the segmentation procedure are presented in this paper and it shows a promising output [C4592]

"Road network extraction in high resolution SAR images"

The application of high-resolution synthetic aperture radar (SAR) images from aerial and satellite sensors challenges the researchers for new and effective interpretation tools. Although most of the main axes in the road network may be detected by a skilled human observer looking for dark or bright linear structures, automatic detection remains a difficult task. In this paper, we proposed a new simple approach to extract main road network in high-resolution SAR images automatically. The approach is based on three steps. The first step is pre-filtering the initial SAR images by using a two-way thresholding process in order to discard uninteresting parts of image. In the second step, the results of the first step are input and use the Hough transform to identify the roads respectively. The last step is based on a feature fusion technique. The road networks detected are combined with the fusion operators. We show the improved results from some examples. It is proved that this approach is effective for the straight highways in high-resolution images [C4593]

"A data fusion approach for distributed orbit estimation"

To achieve good on-board SAR processing results a precise knowledge of the position of the concerned

satellites is essential. For this reason we develop real-time orbit estimation and calibration algorithms which in spite of the small time frame improve the position estimates in an efficient way. Considering future satellite cluster missions (e.g. Cartwheel, Pendulum, Techsat 21, ...), it will be possible to reduce the computing time by splitting of the processing load onto several algorithms that can be implemented in the individual satellites' hardware. The satellites can be considered as a distributed sensor network, which individual (sensor-) nodes have local processors that are used to calculate state estimates using all available data (we want to combine GPS derived and intersatellite distance measurements). A node to node communication is necessary to ensure that no information is lost in order to yield the best possible estimates. The paper specifies advantages and disadvantages of decentralized estimation and compares computational burden and estimation accuracy of decentralized and standard Kalman filter approaches and also analyzes the communication overhead [C4594]

"Creating a geographic footprint from LIDAR data in ArcGIS"

LIDAR (Light Detection and Ranging), like radar, is an active remote sensing system. This technology involves the use of pulses of laser light directed toward the ground and measures the time of pulse return. The return time for each pulse, back to the sensor is processed to calculate the variable distance between the sensors and the various surfaces present on the ground. The project is to create a geographic footprint from LIDAR data, using Microsoft Visual Basic for Application (VBA) and ArcGIS. VBA is an across product language that allows users to create complex and fully functional applications. The problem at hand was to find the line beginning and the line end of each scan line and mark those points to extract the polygon outline. The maximum and minimum points, which will declare the left or right outermost points of the sample image, were found. These x and y connecting points cannot have openings or dangling lines when being shaped into a polygon. In order to avoid unwanted shapes, the programs used to arrange points to draw a polygon of the selected data were written. VBA was used to write the program codes and then the codes were integrated with ArcGIS software. This paper demonstrates specific examples regarding the creation of geographic footprint from LIDAR data in ArcGIS. The end product of the project can be useful for anyone working with LIDAR data [C4595]

"Design considerations for bistatic radar probing of winds in clear air conditions"

A bistatic radar system for measurement of clear-air winds is considered. The proposed system exploits bistatic Bragg scattering from refractive index turbulence which is visible to short wavelength radars (e.g. C-band and higher frequencies) for particular scattering geometries. Beam-limited scattering volume is considered, and the relative influences of Bragg scattering and Rayleigh scattering from particulate tracers are compared, as well as their influences on retrieved wind estimates. Provided system design constraints can be addressed, systems with relatively low power (e.g. hundreds of watts) are feasible. [C4596]

"A joint analysis of microwave radiometer and scatterometer data to characterize meso-scale structures in the Mediterranean Sea"

An analysis of a large set of data, collected from the Special Sensor Microwave/Imager (SSM/I) radiometer and from the NASA SeaWinds scatterometer over the Mediterranean Sea is presented, with the aim of studying the mean behavior of various geophysical parameters, such as water vapor, surface rain rate, wind speed and Ekman pumping for the years 2000 and 2001. This paper presents the results of the study of two different meteorological situations occurring in the Mediterranean basin. Moreover, ability of these instruments for analyzing extreme events is shown through examples. [C4597]

"The scattering fields of 2-D sea fractal surface with finite conductivity illuminated by ellipse polarization wave. Part One. Scattering fields in Cartesian coordinates"

Recently, many analytical expressions of scattering fields of sea fractal surface with infinite conductivity were derived. In order to simulate multi-polarization SAR imaging of sea surface and consider the effects of polarization on remote sensing of sea surface, we derive the scattering fields from 2D sea fractal surface with finite conductivity illuminated by ellipse polarization wave at Kirchhoff approximation. Then we present the scattering matrix of this model and numerically simulate the bistatic radar cross section (RCS) of 2D sea fractal surface. It shows that the result of applying our model coincides with that of relevant literatures. Our work is divided into two parts. In the first part, we derive the scattering fields in Cartesian coordinates. And in the second part, we evaluate the scattering matrix of this model and then give the numerical results and discuss them. [C4598]

"RADARSAT-1: Canadian Space Agency Hurricane Watch program"

Since 1999 the Canadian Space Agency (CSA) has undertaken a joint project, called Hurricane Watch (HW),

with the Canada Centre for Remote Sensing (CCRS), the U.S. National Oceanic and Atmospheric Administration/Atlantic Oceanographic and Meteorological Laboratory (NOAA/AOML), and more recently the Canadian Department of Fisheries and Oceans (DFO). This project has evolved from archival data searches to storm monitoring and dedicated planning. Program focus in recent years has been an effort to plan RADARSAT-1 coverage with coincident NOAA aircraft penetration flights. In this paper, we will describe the CSA Mission Planning Center, the RADARSAT-1 planning timeline and guidelines, which form the basis for all planning, and activities related to storm tracking and request submission to support the HW program. The CSA maintains responsibilities for the overall management of issues related to data acquisition for the program, which involve: (1) monitoring active and potential hurricanes and tropical storms; (2) determining possible RADARSAT-1 coverage and generating requests; (3) submission of requests; (4) planning requests through routine operations and standard procedures; (5) monitoring status of submissions; (6) communication with project partners, and (7) acting as a liaison for project partners. We will discuss the challenges of hurricane imaging due to sometimes unpredictable storm trajectories coupled with imaging geometry, coverage and planning constraints. Finally, 2003 post-season results will be presented to demonstrate the contribution of RADARSAT-1 data in the study of hurricanes. [C4599]

"Simulation of X-band radar observation of precipitation from S-band measurements"

Monitoring of precipitation using high frequency radar systems such as X-band is becoming increasingly popular due to their lower cost compared to their counterpart at S-band. Meteorological radar systems operating at S-band frequencies are not affected by attenuation due to precipitation. The S-band radar systems are typically expensive with large antennas, and high power transmitters. Recently, network of meteorological radar systems at higher frequencies such as X band are being pursued, especially for low cost and targeted applications, such as coverage over a city or a small basin. Attenuation correction of the signal returns from these radars is important for quantitative applications. In order to design the radar systems as well as evaluate algorithm development, it is useful to have simultaneous X-band observation with and without the impact of path attenuation. The only way to collect such data is from dual frequency radar system with matched beams. This paper presents a methodology to generate realistic range profiles of radar observations at attenuating frequencies, such as X band, for rain medium. Fundamental microphysical properties of precipitation, namely size and shape distribution information are used to generate realistic profiles of X-band starting with S-band observation. Conditioning the simulation from S-band maintains the natural distribution of rainfall microphysical parameters. Data from the Colorado State University CHILL radar and the National Center for Atmospheric Research S-POL radar are used to simulate X-band radar observations. The two procedures and sample applications are presented. [C4600]

"The scattering fields of 2-D sea fractal surface with finite conductivity illuminated by ellipse polarization wave. Part two. Scattering matrix and numerical results"

The scattering fields of 2D sea fractal surface with finite conductivity illuminated by ellipse polarization wave in Cartesian coordinate system have been evaluated in part one. We derive here the relation expression between scattering fields and d illumination fields with 343 matrix in local coordinate system. The radar cross section (RCS) on different polarization is obtained and numerically simulated. It shows that the results of our scattering model are in agreement with those of other literatures for some special case. We get some conclusions: (1) valued of radar cross sections of cross polarization (VH and HV) are less than those of co-polarization (VV and HH) but cannot be neglected; (2) when the incidence angle θ_1 , and the scattering angle θ_2 are determined, the angle of the scattering plane out of the illuminating plane θ_3 varies from 0° to 180° , different relations among θ_1 , θ_2 and θ_3 in different relationships between $\sigma_{vs}, \sigma_{vt}, \sigma_{h\delta}, \sigma_{h\delta}, \sigma_{v\delta}, \sigma_{h\delta}, \sigma_{v\delta}, \sigma_{h\delta}$ are derived, we can use these inequalities to predict the critical angle θ_3 where the relation between RCS of VV and HH, VH and HV polarization will exchange, respectively; (3) the effects of depolarization can be neglected though we derived the expressions for them. [C4601]

"Characteristics of permanent scatterer in coastal area"

We have succeeded in estimating tide height in the coastal area with an r.m.s. error of 5.7 cm by exploiting interferometric phase and image intensity of JERS-1 SAR data in our previous work. We used an array of oyster farming frames, composed of two vertical poles and one horizontal pole for each frame, as permanent scatterers. In this paper, we investigate the backscattering characteristics of the structure using AIRSAR data and results of experiment in laboratory. AIRSAR polarimetric images show L-band HH- and VV-polarization produce strong returns from the target structures. Classification of L-band polarimetric AIRSAR data confirms the double-bounce scatter is dominant scattering mechanism. Odd-number scatter is, however, not negligible. The ratio of single-bounce to double-bounce scattering depends of the relative radar look direction to the target array and sea surface conditions. Laboratory experiments were carried out using Ku-band according to the target

scale. The results of the experiments can be summarized as: i) the structures produce a mixed signal of double-bounce and odd-bounce scatter; ii) the backscattering from horizontal pole is very sensitive to radar look direction; iii) the signals from vertical poles are stronger than that from horizontal pole. From the results, it is concluded that water level change can be most effectively estimated when vertical poles in the water are observed by L-band HH- or VV-polarization [C4602]

"Synthetic aperture radar simulations from an idealized tidal channel"

To gain insight into the effects of currents in tidal channels on SAR imaging, a series of hydrodynamic and SAR simulations were conducted using an idealized tidal channel. Preliminary results from the hydrodynamic and SAR modeling reveal the following: (1) peak modulations lie over mid-channel during flood and over the channel banks during ebb, (2) there is little, if any, change in these positions during respective tidal phases; only during transition is peak migration evident, and (3) there are distinct relationships between NRCS and along-channel current velocity and between NRCS and tide height. [C4603]

"Combination of passive and active microwave data for soil moisture estimates"

Various remote sensing techniques have been evaluated and proven to be a valuable source of information for different hydrological applications. For example, with the actual Earth observation satellites, we can observe the entire river basin in rather than sparse points and provide unique information about properties of the surface or shallow layers of the Earth. Furthermore, the actual remote sensing sensors offer the potential of measuring new hydrologic variables not generally possible with traditional techniques such as soil moisture, snow status, land cover parameters etc. Previous researches in microwave remote sensing technology indicate that surface soil moisture can be inferred with remote sensing systems operating in the microwave region of the electromagnetic spectrum. The ability to estimate soil moisture in the upper surface layer by microwave remote sensing (active and passive) has been demonstrated under a variety of the topographic and land-cover conditions. The primary intent of this project is to produce a spatial estimation of soil moisture from active microwave data with sufficient spatial and temporal resolution using neural networks. The derived soil moisture was analyzed in conjunction with vegetation data to understand the effect of land cover on the soil moisture variation. This paper describes the first steps in evaluating the performance of the neural network classification and presents some of the early results. [C4604]

"Polarimetric, L-band, combined radiometer and short pulse scatterometer system"

In this paper L-band, polarimetric, combined, short pulse scatterometer-radiometer system is described, for short distance remote sensing application, under laboratory and field-control conditions. Developed system allows to carry out polarimetric (vv, vh, hv, hh), simultaneous and spatially coincident microwave active-passive measurements of observed surface (soil, soil vegetation, snow and water surface) microwave reflective and emissive characteristics at angles of incidence from the while of 0-80°. [C4605]

"The HYDROS radiometer/radar instrument"

The science objectives of the Hydrosphere State Mission (HYDROS) are to provide frequent, global measurements of surface soil moisture and surface freeze/thaw state. In order to adequately measure these geophysical quantities, the key instrument requirements were determined by the HYDROS science team to be: (1) Dual-polarization L-Band radiometer measurements at 40 km resolution, (2) Dual-polarization L-Band radar measurements at 3 km resolution, and (3) A wide swath to insure global three-day refresh time for these measurements (1000 km swath at the selected orbit altitude of 670 km). As an optimal solution to this set of instrument requirements, a relatively large, 6-meter, conically-scanning reflector antenna architecture was selected for the instrument design. The deployable mesh antenna is shared by both the radiometer and radar instruments by using a single L-Band feed. [C4606]

"Determination of polarimetric calibration parameters of L band SAR using uniform forest data"

Proposes a new method to calibrate L band polarimetric SAR using the forest data. Model based covariance matrix containing the distortion matrices and the scattering components from the forest were solved using the Pi-SAR data over the Japan uniform forest of Tomakomai, Hokkaido. The result showed that the distortion matrices depend on the function of the incidence angle and the operation timings. [C4607]

"NASA's L-Band Imaging Scatterometer"

The L-Band Imaging Scatterometer (LIS) is an airborne radar developed at NASA Goddard Space Flight Center which combines electronic beam steering and digital beamforming allowing the implementation of different

scanning techniques. The LIS efforts are part of the RadSTAR initiative intended to develop the technology that will enable a combined radar/radiometer system that jointly uses a single, dual frequency antenna with cross-track scanning capabilities, but no moving parts. The new technology will enable single aperture measurements of important Earth Science Enterprise climate applications such as ocean salinity, soil moisture, sea ice, and surface water among others. The LIS instrument will be flown along with existing NASA Synthetic Thinned Array Radiometers (STAR) in order to prove the concept of coregistered data and to provide a prototype for a spaceborne, single aperture radar/radiometer system. [C4608]

"Digital beamforming developments for the joint NASA/Air Force Space Based Radar"

The Space Based Radar (SBR) program includes a joint technology demonstration between NASA and the Air Force to design a low-earth orbiting, 2450 m L-band (1.26 GHz) radar system for Earth science and intelligence-related observations. A key subsystem aboard SBR is the electronically-steerable digital beamformer (DBF) network that interfaces between 32 smaller subantenna panels in the array and the on-board processing electronics for Synthetic Aperture Radar (SAR) and Moving Target Indication (MTI). In this paper, we describe the development of a field-programmable gate array (FPGA) based DBF processor for handling the computationally intensive inner-product operations for wideband, coherent beamforming across the 50 m length of the array. The core functions of the DBF-the CORDIC (Coordinate Rotation Digital Computer) phase shifters and combiners-have been designed in the Verilog HDL (hardware description language) and implemented onto a high-density Xilinx Virtex II FPGA. This design achieves real-time processing at an input data rate of 25.6 Gbit/s. Tests with an antenna array simulator demonstrate that the beamformer performance metrics (0.07° rms phase precision per channel, -35.2 dB peak sidelobe level) will meet the system-level requirements for SAR and MTI operating modes. [C4609]

"A study on extraction of urban areas from polarimetric Synthetic Aperture Radar image"

This paper discusses the polarimetric correlation coefficient to extract the urban areas from polarimetric Synthetic Aperture Radar (POLSAR) image. For classification of POLSAR image, several methods have been proposed to extract polarimetric feature, such as Polarimetric Entropy-Alpha, three-component scattering model, Huynen parameters and so on. However, there is a possibility that the polarimetric correlation coefficient has a potential for the objective of this paper, too. In order to verify the capability of polarimetric correlation coefficient, we examine the behavior of this coefficient between the urban areas and the natural distributed areas with respect to the several polarimetric scattering models and the difference of polarization basis. Moreover, we apply the polarimetric correlation coefficient to the actual polarimetric SAR data acquired by Pi-SAR/X-SAR. [C4610]

"Initialization of Markov Random Field clustering of large polarimetric SAR images"

Markov Random Field clustering, utilizing both spectral and spatial inter-pixel dependency information, often provides higher accuracy for remote sensing images, such as polarimetric SAR images. However, it is heavily sensitive to initial conditions, i.e. the initialization of parameters and the choice of the number of clusters. In this paper, an initialization scheme for MRF clustering approaches for polarimetric SAR images is suggested. The method takes into account spatial relations between pixels and provides a guideline to the choice of the number of clusters using Pseudolikelihood Information Criterion (PLIC) criterion. A well-known polarimetric SAR image of Flevoland in the Netherlands is given as an example, showing that this approach gives very good performance. [C4611]

"Monitoring for 2003 Huai River flood in China using multisource SAR data"

In the summer of 2003, the most serious flood since 1991 occurred in the catchments of Huai River in central of China. Many of areas were inundated. The Chinese Ku-band airborne radar system and Canadian RADARSAT were used for flood monitoring and damage assessment. Based on the analysis of the SAR data and related database, the area of flood inundation is more than 3800 km². The land types of flood inundation includes in farmland, residential site, woodland/grassland, fishpond, and bottomland. Further, the extent and distribution of flood and damage assessment were indicated, and the suggestions on flood prevention and control were provided. [C4612]

"Physical interpretation on eigen-analysis of the polarimetric coherency matrix for microwave scattering from vegetation"

The potential of using the eigen-analysis of the coherency matrix is discussed for improved understanding of microwave interaction mechanism in vegetated areas. Using a nonsymmetric vegetation scattering model, a theoretical target matrix is generated to compare the eigen-parameters of the coherency matrix with vegetated scattering mechanisms. [C4613]

"A wavelet multiresolution technique for polarimetric texture analysis and segmentation of SAR images"

A technique is presented for multiscale texture analysis and segmentation of polarimetric SAR images. Textural features are extracted using a multiscale wavelet decomposition based on a wavelet frame. The feature vector is composed of local variance estimates of the smooth image and of the wavelet coefficients. The decomposition is performed at two scales and using images derived by polarimetric power synthesis at a set of polarization configurations. This set is chosen based on a priori-knowledge of the texturally optimal polarization states. Alternatively a complete and nonredundant representation of the full polarimetric information consisting of nine backscatter intensities is used. Feature reduction is achieved by an approximate solution of the Multiple Discriminant Analysis (MDA) transform. A set of controlled experiments, based on Monte Carlo simulations, is set up to assess the performance of the technique with respect to texture segmentation problems. One case is reported concerning the simulation of a fragmented forest, where two vegetation classes with different structural characteristics are mixed. Finally, as an example of the application of the technique to real SAR data, texture segmentation of a high resolution image acquired by the DLR E-SAR sensor at L-band is illustrated. [C4614]

"An overview of NASA's Laser Risk Reduction Program"

Over the years, lasers have proven themselves to be invaluable to a variety of remote sensing applications. LIDAR techniques have been used to measure atmospheric aerosols and a variety of trace species, profile winds, and develop high resolution topographical maps. In many cases, it would be of great advantage to make these measurements from an orbiting satellite. Unfortunately, the space environment is a challenging one for the high power lasers that would enable many LIDAR missions. Optical mounts must maintain precision alignment during and after launch. Outgassing materials in the vacuum of space lead to contamination of laser optics. Electronic components and optical materials must survive the space environment, including a vacuum atmosphere, thermal cycling, and radiation exposure. Laser designs must be lightweight, compact, and energy efficient. Many LIDAR applications require frequency conversion systems that have never been designed or tested for use in space. The National Aeronautical and Space Administration (NASA) has undertaken a program specifically directed at addressing the durability and long term reliability issues that face space-borne lasers. The effort is shared between NASA Goddard Space Flight Center in Greenbelt, Maryland, and NASA Langley Research Center in Hampton, Virginia. We will give an overview of the issues facing space-borne lasers and the efforts that these two centers are pursuing to address them. [C4615]

"SAR interferometry from satellite and ground-based system for monitoring deformations on the Stromboli volcano"

After the collapse of a landslide of 20 million m³ from the NE slope of the Stromboli volcano and the subsequent tsunami at the end of December 2002, a ground-based InSAR system (interferometric synthetic aperture radar) was installed on the flank of the Sciara del Fuoco, a collapse depression formed 5 million BP. Through the radar measurement it has been possible to assess the deformation field over a large portion of the target area and to differentiate different processes. Twelve months of radar monitoring have permitted to follow the temporal and spatial evolution of the mass movement in the Sciara. The landslide showed wide fluctuations in the displacement rate, between 0.6 and 10 mm/h, with acceleration phases coinciding with episodes of more intense effusive activity. The dynamic of the volcano has been also studied through the use of DInSAR from satellite platform. Different images acquired from the ERS2 satellite before and after the collapse of the landslide have been interferometrically processed in order to extract information about the ground deformation occurred on the island due to the volcanic activity. [C4616]

"Deformation of the Aniakchak caldera, Alaska, mapped by InSAR"

The deformation of Aniakchak volcano is investigated using 19 ERS-1/2 interferometric synthetic aperture radar (InSAR) data from 1992 through 2002. InSAR images from the different time intervals, reveal that the 10-km-wide caldera has been subsiding during the time of investigation. The pattern of subsidence does not following the pyroclastic flows from the last eruption of the caldera in 1931. The maximum subsidence is near the center of the caldera, with a rate of up to 13 mm/yr. Deformation outside the caldera is insignificant. Least squares inversion of the multitemporal deformation maps indicates that the subsidence rate has been relatively constant. Field observations have identified numerous fumaroles inside the caldera. In 1973, temperatures of 80° C were measured at a depth of 15 cm in loose volcanic rubble adjacent to the small cinder cone (about 1.5 km northeast of the vent of the 1931 eruption), whereas springs near a caldera lake had a temperature of 25° C in July 1993. Therefore, we suggest the observed subsidence at Aniakchak caldera is most likely caused by the reduction of pore fluid pressure of a hydrothermal system located a few kilometers beneath the caldera. [C4617]

"Neural image fusion of remotely sensed electro-optical and synthetic aperture radar data for forest classification"

Although the processing of electro-optical imagery from Earth observation satellites has been effectively used for classification of many types of land cover, forest classification has been generally limited to broad categories such as deciduous or coniferous. Recent studies suggest that the combination of imagery from satellites with different spectral, spatial, and temporal information may improve classification performance. This paper discusses the results of new fusion research aimed at extracting additional information from the combination of multisensor imagery to improve forest classification performance. For this investigation multiseason LANDSAT and RADARSAT imagery was combined using a new biologically-based opponent-color image fusion and data mining technique, in conjunction with visual texture enhancement, and the Fuzzy ARTMAP neural classifier [A. M. Waxman et al. (2002)]. This approach is shown to quickly learn individual forest classes from a small number of training examples and enable added-value assessment of different sensor modalities. [C4618]

"Identifying SAR permeability zones on groundwater recharge areas"

High-resolution multirate SAR spring images with similar incidence angles were used to update permeability maps over recharge areas on glacial aquifers. From a difference image produced from two dates in early spring we interpreted high medium and low permeability zones. These SAR permeability zones are related to the distribution and behavior of soil moisture on different surficial deposits and slopes. Permeability thematic maps will be useful to identify nutrient infiltration patterns and accumulation on farmed recharge areas. [C4619]

"The geology, landforms and topography of sub-Antarctic Macquarie Island, Australia, as revealed by AIRSAR"

Enhancements of AIRSAR data are revealing an extraordinary amount of land-surface and geological information relevant to the island's genesis at a midocean ridge, ongoing uplift and subsequent shaping of the surface by extensive faulting, wave action and active processes including freeze/thawing, wind and rain. Overlaying these enhancements on the TOPSAR DEM enables this active landscape to be analyzed in three dimensions. The level of detail indicates that the radar signals are penetrating the snow cover and being backscattered by the underlying surface of rock, lag gravels and vegetation. Drainage patterns, dammed lakes, levels of incision, fault structures, raised beach deposits and terraces, and possible evidence of glacial action can all be recognized in various enhancements of the AIRSAR data. [C4620]

"Initial validation and results of Geoscience Laser Altimeter System optical properties retrievals"

In this presentation, we will show results from intercomparison case studies of Cloud Physics Lidar under-flights of GLAS orbit tracks during the GLAS Validation Experiment in October 2003. Compared products include Rayleigh backscatter profiles, calibrated attenuated backscatter, layer identification, optical depth, extinction, and backscatter cross section. We will show examples of GLAS operational optical data products. [C4621]

"Simultaneous laser and radar altimeter measurements over land and sea ice"

Elevation data derived from space-based altimeter measurements over land and sea-ice are key to understanding the Earth's ice mass balance. This importance is recognized by both NASA, as expressed in the laser altimeter GLAS on ICESat, and ESA, as expressed in the radar altimeter SIRAL on CryoSat. The JHU/APL Delay-Doppler Phase-monopulse (D2P) radar altimeter has shown its value as a scientific/calibration/validation instrument, and has participated in two airborne field campaigns sponsored by NASA and ESA to collect simultaneous radar and laser altimeter measurements over land and sea ice. These measurements are unique; they provide colocated, cross-calibrated, and high-precision altimetry data over a variety of geophysical ice conditions in two very different frequency regimes. In this paper, we give an overview of the CryoVEx field campaign in 2003 including basic system parameters, flight tracks, and sample waveforms from the airborne experiment. [C4622]

"CryoSat payload calibration and characterization"

The CryoSat Earth Explorer Opportunity Mission will allow an accurate determination of the marine and land ice mass fluxes at a global scale. This paper gives a brief overview on the CryoSat payload calibration. Special attention is given to the calibration of the interferometric baseline attitude, which is a novelty with respect to conventional radar altimeter calibration. [C4623]

"SIRAL the radar altimeter for the CryoSat mission, pre-launch performances"

The development phase of the SAR Interferometer Radar Altimeter (SIRAL) is in the final stage in Alcatel Space and during year 2004 the Engineering and the Flight Models is tested before delivery to the Mission Prime ASTRIUM GmbH. This ESA mission will be used to estimate-on a global scale-the fluctuations in mass of sea-ice and land-ice. This paper gives a detailed presentation of the microwave and processing units developed, followed by a survey of the pre-launch performances. [C4624]

"Synthetic aperture radar for search and rescue: polarimetry and interferometry"

The use of synthetic aperture radar (SAR) provides an opportunity to assist search and rescue in the location of downed airplanes in particular in the northern areas of Canada. This paper presents results of examining the detection of crashed aircraft targets using airborne SAR data. Considerations for decreasing the number of "false targets" using a combined polarimetric and interferometric analysis have been tested with results indicating a promising approach for target detection using these SAR techniques. [C4625]

"Analysis of the limitations of coherent polarimetric decompositions on vessel classification using simulated images"

This paper presents a study performed with high resolution simulated SAR data that outline the limitations of polarimetric coherent decompositions on vessel classification. In these days, these theorems have been set up as the most advisable alternative for this application but an evident lack of real data avoids know their true usefulness. In this way, this study overcomes this limitation opening the doors to other alternatives, which would provide better performances in this research line. [C4626]

"CryoSat Ground Segment: PDS-IPF infrastructure design overview"

CryoSat is the first ESA Earth Explorer Opportunity mission. It is designed to remotely sense the Earth's ice-covered surfaces using a new concept of radar altimeter instrument. It will use synthetic aperture radar and radar interferometry techniques in addition to conventional nadir looking pulse limited technique to provide superior measurements of surface elevation over both the continental ice sheets and sea ice. In the frame of a European tender competition, Advanced Computer Systems SpA has been awarded by ESA in 2001 for the design and development of the Payload Data Segment (PDS) and of the Instrument Processing Facility (IPF) infrastructures for the CryoSat Ground Segment. With more than twenty years of experience in design, developing and delivery of Earth Observation Data processing systems, Advanced Computer Systems SpA (ACS), based in Rome, Italy, is a leading firm in this field. More than one hundred operational systems are today in operation in 25 countries, within and outside Europe, mostly running 24 hours a day, ingesting and processing many of the available EO satellites like Landsat, SPOT, ERS, JERS, SRTM, Radarsat, Envisat. The aim of this paper is to provide an overview of the developed infrastructure. [C4627]

"Relating polarimetric SAR image texture to the scattering entropy"

In our previous paper, an extension of the polarimetric product model to explain polarimetric variation of texture in high-resolution synthetic aperture radar (SAR) images has been proposed. The extended model suggests that existence of multiple scattering mechanisms provides the polarimetric texture diversity. In this paper, the polarimetric target decomposition theorem is utilized to validate the model. The entropy derived from the target decomposition is a useful sign of scattering randomness. The results of data analyses reveal that there is significant correlation between the variation of the K-distribution's order parameters and the entropy value. [C4628]

"Target scattering decomposition of one-look and multi-look SAR data using a new coherent scattering model: the TSVM"

A new model, the target scattering vector model (TSVM), is introduced for decomposition of coherent scattering. The model that is inspired from Kennaugh and Huynen [1965] con-diagonalization method, Cameron and the SSCM coherent scattering decomposition [1996] represents coherent scattering of symmetric and non-symmetric targets in term of five independents parameters; the target orientation angle and four orientation invariant target parameters. The TSVM is integrated in Cloude's incoherent decomposition method to derive a general scattering decomposition method, the TSVM-coherency characteristic decomposition, which can be applied to both single and multi-look SAR data for characterization of point and distributed targets. The conditions requested for a successful application of the TSVM-coherency characteristic decomposition are discussed. [C4629]

"Fusion of optical and microwave remote sensing data for snow cover mapping"

Optical remote sensing data and microwave remote sensing data are complementary to each other and hence

the fusion of these data would help in improving the classification accuracy. In this paper IRS LISS-III data and Radarsat-1 SAR data are fused using Bayesian formulation of data fusion. For this purpose SAR image is modeled using multiplicative autoregressive random field model. The synthesized SAR image is fused with IRS LISS-III image using a model, which incorporates transition probability to give allowance for temporal ambiguity. Fusion technique is used to improve the classification accuracy of snow related features in Himalayan region, India. [C4630]

"Residential area information extraction by combining China airborne SAR and optical images"

Residential area extraction from remote sensing data plays an important role for map updating. In this paper, a fused method is proposed to extract residential area information originating from China airborne SAR and optical data. First, the airborne SAR and optical images are registered. Then texture analysis, using gray level co-occurrence matrix (GLCM) texture features, is applied to the SAR image. According to those texture features, with a proper threshold, the silhouette of building area can be obtained. With the optical multispectral image, vegetation plots in residential area are extracted. The logic OR is applied to fuse the processed results of the SAR and optical images. Finally, the coverage of residential areas is overlaid on the optical image to check the effectiveness of this method. [C4631]

"A new polarization state conformation and its application to coherence optimization in PolInSAR"

A new coherence optimization algorithm is proposed for PolInSAR applications by using the polarization state conformation (PSC) algorithm based on the polarimetric basis transformation along with the polarization signatures. After this algorithm applied the resemblance between the scattering mechanisms of the same invariant target in both images is maximized. Then, coherence maps between the multistate POLSAR images, before and after the algorithm has been applied, are generated. As a result, the coherence, after the PSC algorithm has been applied, gives the best coherence or optimized coherence between the multistate POLSAR images. The effects predicted by the theory are confirmed by the POLSAR data acquired by the Jet Propulsion Laboratory SIR-C mission. [C4632]

"A multi-frequency polarimetric scattering model for subsurface structure detection"

In this work an attempt is made to extract information about the subsurface soil layers by means of multi-frequency fully polarimetric SAR data. The model of scattering from two-layer structure is proposed and analysis of experimental SAR data at L- and P-band is carried out. [C4633]

"Development of ASIRAS (Airborne SAR/Interferometric Altimeter System)"

ASIRAS is an airborne system designed for sea-ice and ice sheet monitoring. It has been developed by ESA under a Technology Research Program contract. The main sensor of this system is a high resolution Ku-band radar altimeter with 1GHz bandwidth. The observation concept is based on a scaled configuration of SIRAL sensor on board CryoSat. The principle of the measurements is based on a combination of ranging, SAR and Interferometric techniques. The development and the validation of ASIRAS are now completed. The system will be extensively used during the Calibration and Validation campaigns of CryoSat mission. This paper describes the key design drivers and the main features of the system. The key operational parameters of the instrument are discussed, with particular focus on the link between the space-based and the airborne configuration. Finally, the performance of the instrument is presented, based on the results obtained from technical flights and a validation campaign. [C4634]

"Estimation of forest stem volume using optical SPOT-5 satellite and laser data in combination"

In this paper, the accuracy of forest stem volume estimation using a combination of optical SPOT-5 satellite and TopEye laser scanner data is investigated, at stand level. It is anticipated that the accuracy will be improved for the combined stem volume estimate compared to using SPOT-5 data only. The test site is located in the south of Sweden and consists mainly of coniferous forest. The stem volume for the selected stands was in the range of 30-620 m³ha⁻¹ with an average stem volume of 288 m³ha⁻¹ and an average size of 2.9 ha. Regression analysis has been used to develop stem volume functions for each sensor and for the combination. In the combined stem volume function the horizontal forest structure is captured by the optical satellite data whereas the vertical structure is represented by the laser derived tree height data. The accuracy in terms of relative root mean square error was 30.8% of the average stem volume for SPOT-5 and 15.7% for the combination. Thus, compared to using only SPOT-5 data the improvement was found to be 49%. The result implies that the combination of multi-spectral optical satellite and laser derived tree height data can be used for standwise stem volume estimation in forestry applications. [C4635]

"Combining CARABAS-II VHF SAR and Landsat TM satellite data for estimation of forest stem volume"

The accuracy of forest stem volume estimation at stand level using a combination of airborne synthetic aperture radar (SAR) and optical satellite data is investigated in this paper. It is anticipated that the accuracy will be improved for the combined stem volume estimate compared to using single sensor data. The test site is located in the south of Sweden and consists mainly of coniferous forest. The stem volume for the selected stands was in the range of 15-585 m³ha⁻¹ with an average stem volume of 266 m³ha⁻¹ and an average size of 3.5 ha. Remotely sensed data have been collected with the airborne CARABAS-II VHF SAR sensor and the multi-spectral optical Landsat TM satellite sensor. Regression analysis has been used to develop stem volume functions for each sensor and for the combination. The accuracy in terms of root mean square error was 49 m³ha⁻¹ (corresponding to a relative error of 18.5% of the average stem volume) for CARABAS-II, 66 m³ha⁻¹ (24.8%) for Landsat TM, and 38 m³ha⁻¹ (14.3%) for the combination. Thus, compared to using only CARABAS-II data the improvement was found to be 23% and using only Landsat TM data 42%. For high stem volumes CARABAS-II gave the best result, while for lower stem volumes Landsat TM was more accurate. Hence, the combination of the two techniques provided significantly better results over the full range of stem volumes. The result implies that the combination of low-frequency SAR data and multi-spectral optical satellite data can be used for standwise stem volume estimation in forestry applications. [C4636]

"Near real-time monitoring of river ice in support of flood forecasting in eastern Canada: towards the integration of Earth observation technology in flood hazard mitigation"

The development of ice covers on large rivers can result in ice jamming and flooding of large areas. The seventy and economic impact of floods related to ice jams is exacerbated by the danger of post-flooding freeze-up. This study is the first step towards the integration of satellite SAR imagery into operational flood forecasting of river ice on the Exploits River near the Town of Badger, Newfoundland and Labrador, Canada. Due to the location of the current area of interest within the monitoring mask of the Canadian Ice Service, this study utilized RADARSAT-1 Scan SAR imagery. The images were analyzed in near real-time, geometrically corrected to a base map in UTM coordinates and subjected to a visual interpretation. In addition to the location of the ice front, four interpretative ice classes were identified and extracted from the image data. This information was subsequently compared to a predictive model used to forecast the development of the ice cover and the progression of the ice front on the Exploits River. [C4637]

"Assessing the efforts of the flood diversion and storage in the drainage area of Huaihe River using remote sensing"

Flood is one of the most severe natural disasters that do great harm to Chinese economic and social development. In July 2003, the drainage area of the Huaihe River suffered from the most serious flood disaster since 1981. Some areas had been damaged severely. Using remote sensing, we monitored the whole developing process of the flood disaster, from the very beginning of the flood to the recovering after the disaster. The monitored area covered the middle and lower reaches of the Huaihe River. We used remote sensing data to monitor the flood in two modes: the MODIS data were used to monitor the whole area flood situation; higher resolution radar data were used in the areas that seriously suffered from the flood. We produced 23 reports of the monitoring results from three different types of remote sensing data sources. Combining the remote sensing data with a resource and environment database and a social economic database, we performed analysis and evaluation on the flood disaster. Based on the monitoring results, we evaluated the efforts of the flood diversion and storage in the study area. [C4638]

"Study on the forest observation in Kushiro wetland by using dual-frequency and fully polarimetric airborne SAR (Pi-SAR) data"

We chose the Kushiro wetland in Hokkaido, Japan, as a test site to monitor wetland areas. Synthetic aperture radar (SAR) can carry out continuous observation in any weather conditions, and can therefore be used to observe high humidity areas such as wetlands. We applied multi-parameter SAR data (dual-frequency, multi-polarization, and multi-incidence angle) to monitoring the wetland forest. To find the optimum incidence angle and polarization for monitoring the wetland biomass, a simple backscattering model of wetland vegetation was developed and applied to estimate backscattering coefficients for different biomass and surface conditions. [C4639]

"Generation of multi-temporal JERS-1 SAR mosaics over the Manaus-Coari-Urucu Region, Western Amazonia, Brazil"

Studies conducted by Petrobras (the Brazilian national oil company) in Western Amazonia indicate a high demand for petroleum in the region. This fact encouraged Petrobras to build a pipeline that transports 60 thousand barrels of oil per day from the Urucu oil and gas province to the Solimoes terminal north of the city of Coari. This oil is then shipped to another terminal in Manaus. The water level changes between dry and wet seasons attain a difference up to 14 meters in the surroundings of Coari city. The strong seasonal character of the Amazonian climate gives rise to four distinct scenarios in the annual hydrological cycle: low water, high water, receding water, and rising water. These scenarios constitute the main reference for the definition of oil spill response planning by Petrobras. The systematic coverage of JERS-1 SAR images obtained in Western and Central Amazonia between October 1995 and November 1996 allowed the construction of mosaics contemplating these four seasonal scenarios, and therefore improving information about oil spill environmental sensitivity. Twenty-two (22) images per seasonal scenario were used to build the mosaics, which were then classified using the unsupervised semivariogram textural classifier (USTC). Cover types identified using USTC included flooded forest, upland forest and water. These four seasonal mosaics were manipulated using GIS technology to: (1) serve as a spatial framework to environmental studies, such as genetics and distribution offish species, malaria, social-economics, macrophyte distribution, water chemistry, among others; (2) design Petrobras' contingency plans and guide simulated oil spill exercises in the fluvial environment; (3) model water hydrodynamics over the flooded forest; (4) define the route of the Coari-Manaus pipeline avoiding oil sensitive and environmentally protected areas. The information derived from JERS-1 SAR data is straightforward to interpret and constitutes an operational representation in the cartographic space of oil spill sensitivity classes conceived by Petrobras.

[C4640]

"Forest height estimation from X-band SAR"

Forest stand height is an important indicator of standing biomass for management purposes as well as for the assessment of carbon storage. In this paper we assess Intermap Star-3i X-band SAR interferometry products for forest height estimation. DEM data sets are initially assessed for accuracy, and are then used to estimate forest height. Height is underestimated by 22.65%. Regression analysis is used to predict height to within 12.5%. Reasons for errors are investigated through the use of a simple interferometric model. [C4641]

"A comparison of forest canopy height estimates derived from SRTM and TOPSAR in the Sierra Nevada of California"

A study was conducted to determine the extent to which data from the 2000 Shuttle Radar Topography Mission (SRTM) could be used to estimate vegetation canopy height in conjunction with an existing bald-Earth DEM provided by the National Elevation Dataset (NED). A densely forested study site with maximum canopy heights reaching 70+ m in the central Sierra Nevada of California was identified based on the availability of suitable field data from within the general mission timeframe. Preliminary work has been conducted to compare C-band SRTM and TOPSAR digital elevation products with canopy height estimates obtained from ground measurements. Results indicate that SRTM data can be successfully correlated via linear regression modeling with ground-measured metrics of vegetation canopy height including median, mean, and maximum height. Maximum canopy height was predicted from SRTM data with an RMSE of 4.9 meters when a minimum of 50 SRTM pixels was available for averaging. This study confirms previous findings, which suggest that after averaging a minimum of 20 SRTM-NED difference pixels to reduce phase noise errors, stable estimates of interferometric mean scattering phase center height can be extracted. [C4642]

"Tight correlations between forest parameters and backscattering coefficient derived by the L-band airborne SAR (PiSAR)"

We examined relationship between forest parameters and σ_0 derived by airborne multi-polarization SAR (PiSAR). PiSAR observations and field measurements were simultaneously performed on November 2002 and August 2003. One data set was taken from stands with pure pine (*Picea glehnii* Masters) forest. More than 70% of the trees in biomass are *Picea glehnii* Masters in the data set with same stand age. The other data set was taken from the stands where mixture of species is proceeding in some degree. The former data set shows more tight correlations compared to the other and correlation coefficient reaches 0.98. We conclude that (1) the mixture of the species and stand age are two of the major reasons of data scattering between forest parameters and σ_0 , and (2) the above ground biomass saturation level is about 150 tons/ha for L-band σ_{HH0} and σ_{HV0} and 70 tons/ha for σ_{VV0} in this *akaezomatsu* site, using a biomass expansion factor of 1.36 to convert from the trunk biomass to the above-ground biomass. [C4643]

"Motion compensation of squinted airborne SAR raw data: role of processing geometry"

We discuss the role of processing geometry and the problem of motion compensation for non zero squint in

airborne SAR processing. [C4644]

"UV Rayleigh lidar for measuring atmospheric temperature profiles of the troposphere"

A new scheme of UV Rayleigh scattering lidar has been developed for profiling daytime temperature distribution of the troposphere with a compact system. Measurement accuracy of 1-K was obtained at 2-km in daytime. [C4645]

"High-performance 1.5 μm coherent Doppler LIDAR for wind-field measurement"

Recent technical progress of fiber-optics and nonlinear wavelength conversion improves the performance of 1.5 μm coherent Doppler LIDAR (CDL) dramatically. Our new development of the 1.5 μm CDL with all-fiber type transmitter/receiver circuit and optical parametric amplifier is briefly described. [C4646]

"Anomaly subspace detection based on a multi-scale Markov random field model"

We introduce a multi-scale Gaussian Markov random field (GMRF) model and a corresponding anomaly subspace detection algorithm. The proposed model is based on a multiscale wavelet representation of the image, independent components analysis (ICA), and modeling each independent component as a GMRF. The anomaly detection is subsequently carried out by applying a matched subspace detector (MSD) to the innovations process of the GMRF, incorporating a priori information about the targets. The robustness of the proposed approach is demonstrated with application to automatic detection of airplanes on synthetic cloudy sky backgrounds. [C4647]

"Probing the atmosphere using a femtosecond terawatt lidar"

We present applications of the nonlinear propagation of ultra-short ultra-intense laser pulses in air for multicomponent remote sensing, aerosol detection by in-situ nonlinear processes, as well as anomalous transmission through clouds. [C4648]

"Photonics technology development for optical fuzing"

The paper reports on the development of a robust and compact photonic proximity sensor for munition applications. The technologies exploited in the optical fuze design are vertical cavity surface emitting lasers (VCSELs), integrated resonant cavity photodetectors (RCPD) and diffractive micro-optics. This work will culminate in a robust, fully integrated, component design suitable for proximity fuzing applications. [C4649]

"EMI in orbiting sounding radar from ripple in solar arrays"

Electromagnetic compatibility (EMC) of DC/DC converters is discussed in the specific context of satellite missions for remote sensing, where low-frequency radar are used to characterise subsurface layering in planetary bodies like Mars, Venus, Europa. The operating frequency range of these instruments extends down to 100 kHz, and may include switching frequency of the power conversion units aboard spacecraft. So, relevant conducted electromagnetic interference (EMI) may be produced when electromagnetic fields associated to the current fluctuations in solar arrays, related to operation of the switching DC/DC converters, are coupled to radar antennas. In this work we discuss the low-frequency EMI phenomenon, in terms of the related reduction of dynamic range in spaceborne radar systems. We also discuss the effectiveness of some filtering approaches to be used in order to attenuate radio-frequency (RF) signals in the solar array power lines is also discussed in the specific context, taking into account the trade-offs involved with weight and volume constraints, typical of space applications. [C4650]

"Design and demonstration of an interference suppressing microwave radiometer"

Microwave radiometers operating outside the protected portions of the frequency spectrum can be adversely impacted by radiofrequency interference. We describe a new radiometer which coherently samples 100 MHz of spectrum and applies real-time RFI mitigation techniques using FPGAs. A field test of an interim version of this design in a radioastronomy observation corrupted by radar pulses is described. Experiments currently in progress to demonstrate the system in ground-based remote sensing are also detailed. [C4651]

"Femtosecond white-light filaments: A new tool in atmospheric research"

The extraordinary physical properties of femtosecond white-light filaments open fascinating perspectives for the investigation of the atmosphere. In this presentation, the following aspects are also discussed: conventional air

monitoring methods and their limits; principle of femtosecond LIDAR; formation and propagation of plasma channels in air; absorption measurements on atmospheric trace gases; electrical properties; and aerosol measurements. [C4652]

"Iterative DCT algorithm for digital elevation model reconstruction from isogram maps"

The problems of digital elevation model (DEM) reconstruction from isogram maps and the arising problems are considered. An iterative algorithm based on discrete cosine transform with taking into account several nonlinear constraints is proposed. The algorithm efficiency and accuracy analysis for test and real data are performed and compared to Delaunay triangulation based method. The advantages of the proposed technique are shown. [C4653]

"0.5 J frequency stabilized diode pumped solid state laser for a next generation lidar system"

A pulsed diode pumped Nd:YAG rod-laser system has been frequency stabilized with a modified Pound-Drever-Hall scheme. It delivers 35 ns pulses in up to 0.5 J at 1064 nm with $M^2=1.5$ and 0.25 J at 532 nm at 100 Hz rep.-rate. [C4654]

"Introduction to special session on electromagnetics in communications"

This paper presents the MELECON 2004 special session conference entitled 'Electromagnetics in Communications'. Six papers are selected as representative examples of the newest research trends in electromagnetics related to communication technologies. The first paper deals with modeling of propagation for mobile communications in urban environment. The second paper is about the rectangular waveguide filled with uniaxial negative permeability meta-materials that can make arbitrary thinner than a half of the wavelength. The third paper presents the design of the multiband miniaturized microstrip antenna. The fourth paper is about spherical antenna arrays, a valuable contribution to the very new field in antenna theory. The fifth paper is based on the modeling the human body as the linear antenna. And the last paper deals with application of radar remote sensing to detection of oil-spills in ocean. [C4655]

"Radar remote sensing for oil spill classification (optimization for enhanced classification)"

Oil spills are a major factor in the ocean pollution. The complications involved in detecting oil spills are due to varying wind and sea surface conditions. The main aim of this paper is to find the best combination of transmit and receive polarizations for optimal detection of oil spills which can extend the tolerance and validity ranges of single and dual polarization spaceborne missions. The optimization has to be handled in a careful way for the oil spill detection because the backscattering is very low from the oil spilled region due to high Fresnel reflection. This paper deals with an improved optimization technique for the detection and classification scheme using the spaceborne imaging radar (SIR) data sets of the oil spilled regions. Both the theory and the experimental results obtained are discussed. [C4656]

"Influence of multiplicative noise variance evaluation accuracy of mm-band SLAR image filtering efficiency"

Image filtering is a stage commonly implied in remote sensing data processing in order to remove noise. In this paper we pay attention to filtering the images formed by millimeter (Ka) band side look aperture radars (SLARs) that can serve as imaging subsystems of multipurpose airborne remote sensing complexes. For SLAR images the dominant factor degrading their quality is multiplicative noise that is characterized by probability density function close to Gaussian and relative variance. The goal of this paper is to study how the errors in multiplicative noise variance evaluation influence the performance of different filters with application to Ka-band SLAR image processing. We have considered two test images, one containing a lot of texture and details, and the other image has many homogeneous regions. If the test image contains a lot of details and texture, the optimal value is commonly less than for test image that contains a large percentage of homogeneous regions. The error of variance evaluation more strongly influences the performance of the modified sigma filter than the performance of the local statistic Lee and DCT-based filters. The performance of filters greatly depends upon considered test image, noise statistical characteristics, setting the filter parameters. The numerical simulation data presented serve as good background and motivation for the design of locally adaptive filters that perform hard or soft switching of several different filter outputs in order to make use of the advantages of these filters and to avoid their drawbacks. [C4657]

"Orthomode transducer for mm-wave range"

The orthogonal polarized signals are widely used in millimeter-wave applications such as in radar,

communications, remote sensing and radiometry. The diplexing (i.e., combination or separation) of the orthogonal signals is imposed on the components, which are usually called as "orthomode transducers" (OMTs). In general, the OMT has three physical ports, though it exhibits properties of a four-port device, because the common port, usually with a square or circular cross section, provides two electrical ports that correspond to the independent orthogonal polarized signals. In modern systems, requirements to the OMT are a high cross-polarization discrimination between the orthogonal signals and a good match of all electrical ports. In the millimeter-wave range, it is a difficult problem to design and produce OMT meeting to the required specification, because of dimensions of the components are very small. Therefore, the development of a new OMTs design suitable for mm band is an important task. In the present report we consider a narrowband OMT design that suits most applications in radar and radio-relay link systems. [C4658]

"Analysis of 2-D correlation properties of sea surface backscattered signal"

New radar technology applications need more and more advanced signal processing algorithms. In order to design processing algorithms it is necessary to dispose sufficiently accurate signal model. In this paper the 2-D correlation properties of sea surface radar return are analysed. The data for the analysis are real registered radar signals. The results show the dependence of correlation coefficients and correlation distances on range. Some parameters of power spectral density are introduced and analysed too. The conclusions formulated can be useful for modelling, simulation and segmentation of 2-D radar signals (images). [C4659]

"Cloud and aerosol lidar channel design and performance of the Geoscience Laser Altimeter System on the ICESat mission"

The design of the 532 and 1064 nm wavelength atmosphere lidar channels of the Geoscience Laser Altimeter System on the ICESat spacecraft is described. The lidar channel performance per on orbit measurements data will be presented. [C4660]

"Surface-structure identification using THz radar techniques with spatial beam filtering and out-of-focus detection"

We propose two terahertz reflectometry modalities, optimized to be sensitive to the curvature of surface features. A dark-field approach yields higher sensitivity whilst the out-of-focus technique allows one to distinguish between convex and concave shapes. [C4661]

"From airborne via drones to space-borne polarimetric-interferometric SAR environmental stress-change monitoring-comparative assessment of applications"

Very decisive progress was made in advancing fundamental POL-IN-SAR theory and algorithm development during the past decade. This was accomplished with the aid of airborne and shuttle platforms supporting single-to-multi-band multi-modal POL-SAR and also some POL-IN-SAR sensor systems, which are compared and assessed with the aim of establishing the hitherto not completed but required missions such as tomographic and holographic imaging. Because the operation of airborne test-beds is extremely expensive, aircraft platforms are not suited for routine monitoring missions which is better accomplished with the use of drones or UAVs. Such unmanned aerial vehicles were developed for defense applications, however lacking the sophistication of implementing advanced forefront POL-IN-SAR technology. This shortcoming is thoroughly-scrutinized resulting in the finding that we do now need to develop the most rapid POL-IN-SAR drone-platform technology especially for environmental stress-change monitoring with a great variance of applications beginning with flood, bush/forest-fire to tectonic-stress (earth-quake to volcanic eruptions) for real-short-time hazard mitigation. However, for routine global monitoring purposes of the terrestrial covers neither airborne sensor implementation-aircraft and/or drones-are sufficient; and therefore multi-modal and multi-band space-borne POL-IN-SAR space-shuttle and satellite sensor technology needs to be further advanced at a much more rapid phase. The existing ENVISAT with the forthcoming ALOS-PALSAR, RADARSAT-2, and the TERRASAT are compared, demonstrating that at this phase of development the fully polarimetric and polarimetric-interferometric modes of operation must be viewed and treated as preliminary algorithm verification support modes and at this phase of development, they are still not to be viewed as routine modes. [C4662]

"Recent advances in the development of polarimetric interferometric SAR imaging in microwave remote sensing of the terrestrial covers: need for developing multi-band single and multiple pass POLinSAR monitoring platforms in air and space"

In this overview, reasons are provided on why we do need to place multi-modal, multi-band single and multiple pass POLinSAR monitoring platforms into air and space. The questions "on what POLinSAR monitoring can

provide that POL-SAR and IN-SAR by themselves cannot accomplish" is assessed; whereupon facts and justifications on placing POL-IN-BISAR satellite clusters into space are presented. Reasons for this technology becoming a basic requirement for current, near-future and much more so for future all-day & night year around monitoring of the terrestrial covers are analyzed in view of the un-abating and uncontrollable terrestrial population explosion, which has, does and for ever will result in unavoidable conflicts deteriorating unfortunately at times into terrorism. The pertinent questions on how to reduce the exorbitant cost for initiating this "home-globe security protection" technology are therefore also broached, and the expected benefits are laid out. The pertinent National and International airborne and space borne multi-modal, multi-band SAR remote sensing and security conflict surveillance support agencies are herewith invited for co-sponsoring our proposal, which is timely and fleets of orbiting multi-band space-borne POLinSAR platforms are urgently required. [C4663]

"Corrections to the seawinds scatterometer wind vectors by removing the effects of rain from the NRCS"

A method of correcting the errors caused by rain, to the normalized radar cross section measured by spaceborne scatterometers is presented. The simultaneous, collocated measurements of the vertical precipitation profile by the TRMM and AMSR passive radiometers are converted into reflectivity and attenuation to develop a method for removing the effects of rain backscatter and signal attenuation from the total signal received at the satellite. A mathematical model has been developed, which represents the principal electromagnetic mechanisms of Ku-band attenuation and scattering, using the polarization and illumination details for this scatterometer. The rain-impact NRCS is also considered. The amount of correction to the L2A data product values depends on the wind speed, rainrate and polarization [C4664]

"Evaluation of ocean surface vector winds observed by QuikSCAT/seawinds and ADEOS-II/seawind"

Ocean surface vector winds observed by QuikSCAT/SeaWinds and ADEOS-II/SeaWinds are evaluated by comparison with wind and wave data from the NDBC (National Data Buoy Center), TAO (Tropical Atmosphere and Ocean)/TRITON (Triangle Trans-Ocean buoy Network), PIRATA (Pilot Research Moored Array in the Tropical Atlantic), and JMA (Japan Meteorological Agency) buoys in the Atlantic and Pacific Oceans, Gulf of Mexico, and seas around Japan. Only buoys located offshore and in deep water were analyzed. The temporal and spatial separations between the scatterometer and buoy observations were limited to less than 10 min and 12.5 km. The buoy wind speeds were converted to equivalent neutral winds at a height of 10 m above the sea surface. The comparisons show that the wind speeds and directions observed by the two Sea Winds sensors agree well with the buoy data. The typical root-mean-squared differences of the wind speed and direction are 1 m/s and 20 deg, respectively, while no significant dependences on the wind speed are discernible. The collocated data set is also used to explore differences of wind speed and direction against oceanic and atmospheric parameters and footprint positions. Residuals of the wind speed and direction show slight dependence on the cross-track cell locations, which correspond to combination of the azimuth observation angles. The wind speed residuals exhibit no significant dependences on the oceanic and atmospheric parameters, such as the sea surface temperature, air-sea temperature difference, and sea state [C4665]

"End to end performances of a short baseline interferometric radar altimeter for ocean mesoscale topography"

The swath radar altimeter concept has been revisited-in the framework of an ESA study-with the objective of defining an optimal functioning point with respect to mission performance while keeping the instrument complexity as low as possible. We show that a swath altimeter concept, with a shorter interferometric baseline than WSOA and moderate power can meet the requirements of mesoscale topography mapping. The paper presents a complete sea surface height (SSH) error budget for the mission [C4666]

"The L-band SAR pre-development"

This paper outlines the development status of an L-band synthetic aperture radar (SAR) antenna demonstrator undertaken by an industrial consortium under contract to the European Space Agency (ESA). Its aim is to verify the technology and the satisfactory performance of the SAR active antenna in advance of the development of the full L-band SAR instrument [C4667]

"Impact of ocean currents on scatterometer winds in the tropical Pacific Ocean"

The SeaWinds scatterometer on QuikSCAT has been measuring wind vectors globally since mid-July, 1999. The scatterometer signal is generated by backscatter from centimeter-scale wind-generated waves. When the wind

blows against (with) the surface currents, the scatterometer will measure higher (lower) winds than the absolute wind measured by an anemometer at a buoy. We estimate time-varying surface currents by differencing the scatterometer and buoy winds from the Tropical Atmosphere-Ocean array. We compare the wind differences with climatological and actual currents derived from drifters at 15-m depth, acoustic Doppler current profiles (ADCP) at 25-m depth and the TOPEX/Poseidon altimeter. We find the zonal wind differences in good agreement with the zonal currents, particularly with the geostrophic zonal currents from the altimeter. Climatological current estimators that include an annual and semiannual component as well as a linear dependence on the Southern Oscillation Index (SOI) show good skill in predicting the zonal wind differences. The meridional wind differences have magnitudes as large as the zonal differences; however, the meridional wind differences are not well predicted by the estimators. Previous studies of the meridional currents also show less predictability in the meridional component than in the zonal component. The relative motion winds from the scatterometer are precisely what are needed in bulk algorithms for air-sea fluxes. Therefore, ignoring the effect of ocean currents will contribute to errors in the flux fields. Comparisons of flux fields derived using QuikSCAT winds with those derived using NCEP Reanalysis winds show that, while the current effect can be quite large, other NCEP model errors exceed those from currents [C4668]

"Comparison of two inversion methods for retrieval of soil moisture and surface roughness from polarimetric radar observation of soil surfaces"

This paper presents comparison of the direct inversion method (DIM) and the genetic algorithm-based inversion method (GAIM) for retrieval of soil moisture and surface roughness from polarimetric radar observation of soil surfaces. Those inversion methods are based on the polarimetric semiempirical model (PSEM), which was developed empirically to estimate the backscattering coefficients from the volumetric soil moisture content and the surface roughness parameters k_s and k_l , where $k = 2\pi if/c$, s is the rms height and l is the correlation length. The copolarized ratio p and the vh -polarized backscattering coefficient of the semiempirical model have been inverted directly to retrieve the soil parameters in the DIM. The cross-polarized ratio q can additionally be used to improve the inversion results in the DIM. A good agreement between the values of k_s estimated by the inversion method and those measured in situ for $k_s < 3.5$, with a correlation coefficient of 0.822. The genetic algorithm (GA) is applied for an inversion method to retrieve both the volumetric soil moisture contents and the rms surface heights from multipolarized radar observations of bare soil surfaces. The cost function for each chromosome is evaluated using the semiempirical scattering model. Good agreement was found between the values of the rms height and the soil moisture content estimated by the inversion technique and those measured in situ. It was also found that the GAIM shows higher accuracy than the DIM in the estimation of the surface parameters from the radar observations [C4669]

"A two parameter backscattering model for bare soil surfaces: from theory to application"

To make use of the multiple imaging capabilities of ENVISAT ASAR, theoretical backscattering models can help to improve surface parameter inversion. The surface roughness characterization is crucial in this context. Commonly used surface roughness descriptors are the rms height and autocorrelation length. Empirical comparisons with SAR imagery show that these descriptors result in an ambiguous surface roughness parameterisation. A theoretical, two parameter surface backscattering model based on IEM simulations is proposed, where the surface roughness is described by a single static parameter. It will be shown that the surface roughness can be inverted using multitemporal ENVISAT ASAR imagery. Finally the accuracy of the proposed model is validated and the applicability of the model will be outlined [C4670]

"Vegetation effects on soil moisture estimation"

Several successful algorithms have been developed to estimate soil moisture of bare surfaces. We previously reported a new algorithm using the tilted Bragg approximation. However, these algorithms are only applicable to bare surfaces. When vegetation is present, soil moisture is typically underestimated by bare surface algorithms. In order to derive soil moisture under vegetation, we have to understand the complex scattering process due to vegetation. Our main interest is to retrieve the global soil moisture information using Hydros L-band polarimetric radar data. The Hydros mission will provide the first global view of land soil moisture using L-band radar and radiometer. The unique characteristics of the Hydros data are the availability of the low resolution soil moisture information from radiometer data and the continuous time series radar data collected at the same incidence angle. In this paper, we will examine a potential inversion algorithm to retrieve soil moisture under vegetation canopies using Hydros L-band polarimetric radar data [C4671]

"A modified empirical model for soil moisture estimation in vegetated areas using SAR data"

Among the major models developed for soil moisture retrieval, the empirical model developed by Dubois et al. in

1995 proves to be a good choice, because of its accuracy and simplicity of implementation. The model provides quite good results for the estimation in bare soil areas. However, it does not explicitly incorporate vegetation backscatter effects and does not provide good results for vegetated areas with a cross-polarization ratio greater than -11dB. A modified empirical model is developed to address this concern. The water-cloud model is used to introduce vegetation effects into the VV backscatter coefficient, which is further used in the inversion model. The modified model is applied to the Washita 1994 SIR-C data and a correlation of 0.81 is obtained between the ground based measurements and the soil moisture estimated from radar data [C4672]

"Forward model and sensitivity study of uplink large array calibration using in-orbit targets"

In this paper an uplink large array calibration technique using in-orbit targets is proposed and a forward model is developed to simulate the calibration scenario. A sensitivity study on the performance of such technique due to array phase uncertainties is conducted and the results are presented [C4673]

"Endmember-based in-scene atmospheric retrieval (EMISAR)"

The Aerospace Corp. in-scene atmospheric compensation (ISAC) algorithm offers the ability to remove the effects of the atmosphere on long wave infrared (LWIR) hyperspectral data using only the image data itself. The ISAC algorithm attempts to find blackbody pixels in the data and then uses the known spectral signature of a blackbody to correct the data. The most common examples of blackbodies in LWIR data are vegetation and water. While it has been applied successfully to a wide variety of data, the ISAC algorithm can fail when there is little or no vegetation or water in the scene. In this case, the algorithm will find some other material as a blackbody and this can result in an error in the correction process. The EMISAR algorithm is based on the ISAC method but offers an alternative approach that allows the use of other known materials. The data is first transformed to apparent emissivity, and then the spectral endmembers are found in the scene. This approach has the advantage of finding the true blackbodies in the scene (vegetation and water pixels with high fractional abundances), and can do it autonomously. It also can be used with scenes without vegetation, if the spectrum of some scene material is known. [C4674]

"Measuring the performance of track-to-track fusion systems"

An effort is ongoing to develop a multi-source integration (MSI) system for the E-2C Hawkeye aircraft. The objective of this system development is to merge track information from a variety of dissimilar sources and present to the operator a useful and uncluttered real-time picture of the battlespace to support the current suite of missions being performed by the aircrew onboard the E-2C. In other words, the operator's display should have "one track for one piece of metal" and this process should be automatic and accurate. The inputs to the MSI system are tracks from several different sources that arrive at different times and with varying and sometimes unknown accuracies. Thus, the MSI system is a track-to-track fusion system. In order to evaluate the effectiveness of the MSI system in the E-2C operating environment we needed to develop a set of scenarios to run the MSI system against and to define a set of metrics that will quantify the performance of the MSI system with these scenarios. The metrics assume ground truth is known. This work focuses on the development of the metrics that will eventually be used to evaluate the performance of the MSI system. One of the key and unique aspects of these metrics is that they deal with the fact that the track data given to the MSI system is often incorrect or impure. Ideally, each track should be updated with reports from exactly the same platform each time. But since the E-2C operates in environments with large numbers of platforms, it is likely that many of the tracks contain updates from more than one platform. These types of tracks are called impure source tracks. In defining our metrics, we needed to generalize them so that they could deal with both pure and impure source tracks. This work discusses what metrics were defined, how they are computed, and how the metrics were extended to deal with impure tracks. [C4675]

"The HYDROS mission: requirements and system design"

The HYDROS mission is under development by NASA as part of its Earth System Science Pathfinder (ESSP) program. HYDROS is designed to provide global maps of the Earth's soil moisture and freeze/thaw state every 2-3 days, for weather and climate prediction, water, energy and carbon cycle studies, natural hazards monitoring, and national security applications. HYDROS uses a unique active and passive L-band microwave system that optimizes measurement accuracy, spatial resolution, and coverage. It provides measurements in nearly all weather conditions, regardless of solar illumination. The design of the radar and radiometer electronics, antenna feed system, reflector and science data system, are driven by specific mission and science objectives. These objectives impose requirements on the frequencies, polarizations, sampling, spatial resolution, and accuracy of the system. We describe the HYDROS mission requirements, baseline design, and measurement capabilities. [C4676]

"Multi-use, low SWaP, ultra-sensitive photoreceiver arrays for ladar & remote sensing"

A monolithic photoreceiver is described, which combines a vertical cavity optical amplifier (VCSEL) optical preamplifier (VCSOA) with an RTBT optical converter in a totally monolithic approach, thus enabling low SWaP and multi-use capabilities. The optical amplifier is capable of optical gain as high as 15 dB and noise figure as low as 4-6 dB. The optical converter has sensitivities of -32.5 dBm at 2.5 Gb/s and BER of 10⁻⁹, that are comparable to or better than APD and PIN diode photoreceivers. The monolithic photoreceiver, resulting from integrating the optical amplifier and optical converter, is capable of sensitivities approaching -47 dBm at a BER of 10⁻⁹ and a bit rate of 2.5 Gb/s. The monolithic photoreceiver can be applied to imaging ladar and remote sensing for maximum ranges as high as 220 km and resolution as low as 25 cm. [C4677]

"An assessment of multi-static radar remote sensor networks"

Bistatic radar has been considered for many years as an element of ground based air defense systems to counter against low observable airframes. To achieve these benefits, it is necessary to deploy the network of bistatic radar elements across an area where a large proportion of the reflected energy is anticipated. For security and vulnerability reasons this network is typically deployed within safe, protected areas. This requirement limits the range of applications to which bistatic and multi-static radar can be applied. The recent emergence of unattended ground sensors (UGS) and uninhabited air vehicle (UAV), systems shows that these platforms are sufficiently mature for consideration as remote receiver/transmitter sites. However for this to be realized it is essential that the cost, capability and vulnerability of these sensors is considered. Within This work a multi-static radar tool which is used to compare a range of multi-static radar network distributions is described. This tool is used to assess detection capability and hence indicate comparative costs for two geometric targets frying a linear path. [C4678]

"Landcover attributes from ICESat GLAS data in Central Siberia"

NASA's ICESat Geoscience Laser Altimeter System (GLAS) was launched in January 2003 and collected lidar data during February and September of that year. Lidar is a laser altimeter that measures the distance from the instrument to the surface by measuring the time elapsed between the pulse emission and the reflected return. The returned signal may identify multiple returns originating from trees, buildings and other objects and permits the calculation of their height. Sampling the returns at discrete time intervals enables backscatter profiles to be constructed. Lidar data can provide estimates of other structural parameters such as biomass, stand volume and leaf area. This study used GLAS data acquired over our study sites in central Siberia to examine the signal as a source of information of forest stand characteristics. Example lidar profiles are presented and preliminary analysis is described. The results indicate that GLAS profile information may be useful for understanding MODIS landcover classes [C4679]

"A solid state L to X-band flexible ground-based SAR system for continuous monitoring applications"

Continuous terrain fast changes monitoring is difficult to implement via airborne/satellite SAR systems, mainly due to the lack of flexibility and low revisiting times. Other SAR approaches based on small and simple ground-based systems, easy to deploy wherever are needed, must be considered. Transportability, low cost, and ruggedized structure are the main constrains, but the required resolution and performances have to be preserved. An experimental, short to medium range, ground-based, with optional polarimetric capability, Synthetic Aperture Radar (SAR) will be presented. First results of an experimental X-band SAR with a 100 MHz bandwidth, with 20 dBm of radiated power in differential interferometry operation will be shown [C4680]

"Reconfigurable computing as an enabling technology for single-photon-counting laser altimetry"

Single-photon-counting laser altimetry is a new measurement technique offering significant advantages in vertical resolution, reducing instrument size, mass, and power, and reducing laser complexity as compared to analog or threshold detection laser altimetry techniques. However, these improvements come at the cost of a dramatically increased requirement for on-board real-time data processing. Reconfigurable computing has been shown to offer considerable performance advantages in performing this processing. These advantages have been demonstrated on the multi-kilohertz micro-laser altimeter (MMLA), an aircraft based single-photon-counting laser altimeter developed by NASA Goddard Space Flight Center with several potential spaceflight applications. This paper describes how reconfigurable computing technology was employed to perform MMLA data processing in real-time under realistic operating constraints, along with the results observed. This paper also expands on these prior results to identify concepts for using reconfigurable computing to enable spaceflight single-photon-counting laser altimeter instruments. [C4681]

"ENVISAT-1 data for urban area detection and characterization"

In this paper we investigate the use of SAR and multispectral sensors on board of the ENVISAT-1 satellite for urban remote sensing applications. We are interested mainly on the mapping capabilities of these two sensors and provide results for urban land use extraction using ASAR data and urban area definition using MERIS bands [C4682]

"Spaceborne spotlight SAR processing using the frequency-scaling algorithm"

In this paper, the frequency scaling algorithm (FSA) has been introduced for the first time to spaceborne spotlight SAR. According to the characteristics that the range time extension of the observed scene is smaller than the width of the transmitted pulse, FSA applied in airborne spotlight SAR dechirps on received echoes and reduces the sampling rate to release the computational burden. However, in spaceborne SAR, the range extension is much larger and the bandwidth after dechirping increases instead so that the existing FSA cannot be adopted. To solve this problem, a method to perform directly frequency scaling on chirps in the range direction has been proposed. And azimuth compression has also been applied to reduce the pulse repetition frequency in the azimuth direction. Finally, simulation results of point targets are given to demonstrate the validity and efficiency of the proposed algorithm. [C4683]

"Travel time and intensity statistics of the pulsed signals backscattered by a rough surface [Cgeophysical remote-sensing applications]"

Two-way travel times of waves scattered at a rough surface contain important information about the physical properties of the scattering boundaries and the intervening medium. Precise measurements of the travel times, and especially those of the first (i.e. earliest) arrivals, underlie a number of geophysical remote-sensing techniques that employ GPS signals, radars, and lidars as well as acoustic and seismic waves. In this paper, we address, in the geometrical optics limit, the challenging problem of the statistical properties of the travel times and intensity of the first and second arrivals. [C4684]

"An L-band SAR for repeat pass deformation measurements on a UAV platform"

We are proposing to develop a miniaturized polarimetric L-band synthetic aperture radar (SAR) for repeat-pass differential interferometric measurements of deformation for rapidly deforming surfaces of geophysical interest such as volcanoes or earthquakes that is to be flown on an unmanned aerial vehicle (UAV) or minimally piloted vehicle (MPV). To support the repeat pass deformation capability it is necessary to control flight track capability of the aircraft to be within a specified 10 m tube with a goal of 1 m. This requires real-time GPS control of the autopilot to achieve these objectives that has not been demonstrated on these aircraft. Based on the Proteus and ALTAIR's altitude of 13.7 km (45,000 ft), we are designing a fully polarimetric L-band radar with 80 MHz bandwidth and a 16 km range swath. The radar has an active electronic beam steering antenna to achieve a Doppler centroid stability that is necessary for repeat-pass interferometry. This paper presents the radar configuration along with some of the trade studies for the platform and instrument. [C4685]

"MATLAB-based ERS SAR data acquisition and processing software for classroom use"

The paper provides a review into the steps involved in acquiring and processing synthetic aperture radar (SAR) data transmitted by the European remote sensing (ERS) satellites. The paper reports on a simple MATLAB-based SAR processing system, that reads the image out of the complex SAR data files and that is suitable for use in the classroom to demonstrate one of the procedures used in SAR data processing. The paper can also help a beginner in the field of SAR signal processing to get information and understand the basics that are necessary to acquire and process a SAR image. The data, provided by the Alaskan Satellite Facility (ASF), is categorized into different levels and the paper describes the process of obtaining the level-1 basic image from the level-0 raw data file provided by ASF. [C4686]

"On indirect method of RCS calculation of conducting targets in random media"

One of the random medium effects is the enhancement in radar cross-section (RCS) of targets, and it can be explained by the coherent addition of doubly scattered waves. In several earlier studies (Tateiba, M. and Tomita, E., 1992; El-Ocla, H. and Tateiba, 2001, 2002, 2003), we have proved that the spatial coherence length (SCL) of waves around the target in a random medium, together with the target configuration, affects the RCS and backscattering enhancement, apart from the polarization of the incident waves. This conclusion is important in radar detection and remote sensing applications. These results need a lot of computation time if we use our method directly. We propose an indirect estimate for the RCS by using a beam wave incident on a conducting target in free space. This method presents an approximate solution to the scattering problem in a random

medium. This indirect estimate reduces the processing time that is so important in radar detection, especially in real time applications. H-wave scattering is quite different from E-wave scattering, especially in the resonance region, because of waves creeping along objects. Therefore, we need to analyze the scattering for both polarizations. The time factor is assumed and suppressed. This method is applicable for low and high frequency ranges. [C4687]

"DCT and DWT based image compression in remote sensing images"

With the improvement of synthetic aperture radar technology, larger areas are being imaged and the resolution of the images has increased. Larger images have to be transmitted and stored. Due to the limited storage and downlink capacity on the airplane or satellite, the volume of data must be reduced. This makes compression of SAR images with minimal loss of information important. This study aims to compare the best-known compression techniques, namely discrete cosine transform and discrete wavelet transform. It investigates RADARSAT and SPOT images of different regions of different characteristics. The regions investigated are sea areas, forest areas, and residential and industrial areas which define different patterns of urban land use. The studies showed that compression ratios changed according to the pixel classification. The second purpose of this study is to compare the two compression algorithms. The DWT based algorithm gave the minimum mean square error compared to the DCT based compression algorithm. The results changed according to the quantization process and the transform-coding algorithm. [C4688]

"Optimal pulse penetration in Rocard-Powles-Debye model dielectrics using the Brillouin precursor"

When an ultrawideband electromagnetic pulse penetrates into a causally dispersive dielectric, the interrelated effects of phase dispersion and frequency dependent attenuation alter the pulse in a fundamental way that results in the appearance of precursor fields. For a dielectric described by the Rocard-Powles extension of the Debye model, the dynamical field evolution is dominated by the Brillouin precursor as the propagation depth typically exceeds a single penetration depth evaluated at the carrier frequency of the input pulse. This is because the peak amplitude in the Brillouin precursor decays only as the square root of the inverse of the propagation distance. Because of its unique nonexponential peak decay, the Brillouin precursor has direct application to foliage and ground penetrating radar, remote sensing and wireless communications in adverse environments. Of equal importance is the frequency structure of the Brillouin precursor which exhibits a complicated dependence on both the material dispersion and the input pulse characteristics. A Brillouin pulse is then defined and shown to possess near optimal (if not indeed optimal) material penetration. [C4689]

"IEEE Antennas and Propagation Society Symposium (IEEE Cat. No.04CH37529)"

{no data available} [C4690]

"Simulation of radar scattering from electrically large objects under tree canopies"

A model is developed to investigate the scattering behavior of hard targets embedded inside a forest canopy, at high frequencies. Wave penetration through, and scattering from, a forest canopy is calculated, using a coherent scattering model which makes use of realistic tree structures (Yi-Cheng Lin and Sarabandi, K., IEEE Trans. Geosci. Remote Sensing, vol.37, p.440-51, 1999). A physical optics (PO) approximation is used to estimate the equivalent current on an electrically large, perfectly electrically conducting (PEC) object, located above a ground plane and under a tree canopy. In this model, the reciprocity theorem is used effectively in order to derive the backscattering from the target above the ground plane, and also to calculate the interaction of the target scattered field with the foliage. [C4691]

"Advanced geostationary radar for hurricane monitoring and studies"

The current geostationary operational environmental satellites (GOES) are equipped to make cloud top measurements only. In contrast, a millimeter-wave radar allows 3D measurements of precipitation associated with hurricanes and other convective systems. It also provide important inputs for numerical weather prediction models for improving the accuracy of weather nowcasting and forecasting. Recently, a novel instrument concept and the associated critical technologies are being developed for a 35 GHz Doppler radar for detailed monitoring of hurricanes and severe storms from a geostationary orbit. This instrument is designed to be capable of producing rainfall rate at 13-km horizontal resolution and 300-m vertical resolution, and the line-of-sight Doppler velocity at 0.3 m/s precision, of the 3D hurricane structure once per hour throughout its life cycle. [C4692]

"Neural network-based signal processing for enhancing the multi-sensor remote sensing imagery"

We intend to fill the methodological-level gaps which exist in the theory of imaging radar (IR) for remote sensing

(RS) systems by addressing a novel look at RS imaging as an ill-conditioned inverse problem with model uncertainties. We extend the theory presented in previous studies by developing the fused Bayesian-regularization method for RS image formation subject to the projection-type regularization constraints imposed on the solution. Next, we propose to employ neural network-based-processing for efficient implementation of the developed radar image enhancing algorithms and include some simulation examples to illustrate the overall performances of the proposed approach. Our study is intended to establish the foundation to assist in understanding the basic theoretical aspects of the multi-level (Bayesian-regularization-neural-network-computing) optimization of signal processing techniques for enhancing RS imagery. [C4693]

"Spots segmentation in SAR images for remote sensing of environment"

The paper proposes an algorithm to segment spots in synthetic aperture radar (SAR) images in order to support environmental remote monitoring. This approach consists of isolating dark areas that may have originated from oil pollution, thus achieving the aim of our investigation. The proposed algorithm combines a region growing approach and a multiscale analysis employed by an undecimated wavelet transform to localize dark areas in the sea. The undecimated wavelet applied to SAR images smooths the speckle noise while enhancing edges, thus providing a better result for the proposed segmentation algorithm that is achieved by a modified region growing approach. The minmax scheme is used to provide post processing of the segmented image. The algorithms were tested on real SAR images of oil spills. [C4694]

"A problem solving environment for remote sensing data processing"

A huge quantity of Earth observation and geospatial data is produced daily by numerous satellites launched by several worldwide space agencies. The processing of remote sensing data requires several steps, some of which are computationally intensive. The extraction of prominent information from remote sensing data requires a coordinated use of many applications and algorithms. Sharing computational resources among different scientists represents the sole way to approach the problem in order to achieve good performance. We describe a problem solving environment for remote sensing data processing layered on grid technologies. The proposed architecture allows sharing resources among different organizations taking into account each access policy defined by the owner of the resource. [C4695]

"The fused Bayesian maximum entropy-variational analysis method for computer reconstruction of remote sensing imagery"

We address the aggregated Bayesian maximum entropy-variational analysis (BMEVA)-based algorithm for high resolution radar image enhancement and denoising. The use of the variational analysis (VA) approach is formalized by imposing the metrics structures in the corresponding signal spaces. A new formalism for combining the Bayesian maximum entropy (BME) strategy with the VA paradigm is developed. The advantages in image enhancement and denoising achieved using the proposed BMEVA method is illustrated through numerical simulations. [C4696]

"Unsupervised classification of polarimetric SAR images using neural nets"

Classification of earth terrain components using fully polarimetric SAR images is one of many important application of radar polarimetry. In this paper, we are interested in unsupervised classification method because of their rapidity, automatic criterion and their independency on the images to be classified. [C4697]

"On-board processor for direct distribution of change detection data products [Cradar imaging]"

We are developing an on-board imaging radar data processor for repeat-pass change detection and hazard management. This is the enabling technology for NASA ESE to utilize imaging radars. This processor enables the observation and use of surface deformation data over rapidly evolving natural hazards, both as an aid to scientific understanding and to provide timely data to agencies responsible for the management and mitigation of natural disasters. Many hazards occur over periods of hours to days, and need to be sampled quickly. The new technology has the potential to save many lives and millions of dollars by putting critical information in the hands of disaster management agencies in time to be of use. The processor architecture integrates two key technologies by combining a field programmable gate array (FPGA) front-end with a reconfigurable computing back-end. A searchable on-board data archive stores the reference data sets needed for the change detection processing. In this paper, we present an overview of the change detection processing algorithm and the preliminary hardware architecture. [C4698]

"Developments in repeat pass interferometric radar for Earth and planetary sciences"

Repeat pass radar interferometry has developed into a wide ranging geodetic and change mapping tool from space. For large areas of the Earth, and for numerous applications that demand more persistent monitoring, the true potential of the repeat pass technique remains largely untapped. While the research community has made enormous strides in extracting as much information as possible from existing data sets, fundamentally new observing systems are needed for breakthroughs in a number of areas. Repeat pass interferometry techniques applied on missions to the terrestrial planets, Earth's Moon and the icy moons of Jupiter can reveal new insights in to the history of the surface and near subsurface. [C4699]

"Analyzing satellite image with blind separation of sources, knowledge based system and fusion of multisource images"

In this paper, an intelligent satellite image analysis is proposed from blind source separation (BSS) method, knowledge based system and fusion of multisource images. The experimental results demonstrate that the proposed hybrid method provides an effective intelligent technique for remotely sensed images classification. This approach is validated on optical images of the satellite SPOT4 and radar images of the satellite ERS2 acquiring on the central Tunisian region for five classes of land. [C4700]

"A sensitivity analysis of radar backscattering coefficient to multiscale roughness description and radar parameters using the small perturbation model"

In this paper, we study the impact of multiscale description of rough surface on the radar backscattering using the small perturbations model which is used when the surface height standard deviation is much smaller than wavelength and the rms slope s is not high. This sensitivity analysis gets an inverse model of the backscattering model in order to retrieve the roughness and soil moisture parameters. [C4701]

"Optimisation of the spatial attitude of the bistatic and multistatic synthetic aperture radar"

In this paper the advantages of the multiposition synthetic aperture radar (SAR) system are discussed. Usage of SAR requires careful positioning of receivers and transmitters. This positioning as well as the transmitted signal determines the quality of the estimation through the space ambiguity functions which strongly depend on relative positions of the transmitter and receiver. Bistatic and multistatic synthetic aperture radar system has advantages over the single position remote sensing system. Special regard must be paid to the fact that spatial resolution as well as intervals of the ambiguous measurements strongly depend on spatial attitude of the receiver and transmitter in the bistatic and multistatic SAR. Spatial attitude optimisation therefore must be made with the following scheme: analysis of the equal distance lines and its gradients. Then spatial attitude optimisation must also be made for analysis of the equal Doppler frequency lines. Each bistatic pair is modelled for the side looking and forward side looking SAR with the same space attitude and velocity. [C4702]

"Characteristics of a signal backscattered from a rough water surface at small incidence angles"

This paper presents the results of the experiment devoted to the study of the properties of the backscattered microwave signal at small incidence angles. Measurements have been carried out by the 3-sm Doppler radar mounted at the bridges across the Oka river in Nizhny Novgorod (the height of bridge is approximately 40 meters). During the measurements, two antennas are used: the knife-like antenna ($\delta x_2=1, 5^\circ$; $\delta y_2= 24, 5^\circ$) and the parabolic one ($\delta x_2= 2, 4^\circ$; $\delta y_2= 2, 4^\circ$). Cycles of measurement are carried out separately for each antenna. Thus the developed model may be applied for the determination of the characteristics of the scattering surface using the parameters of the reflected signal. From the experimental measurements the theoretical calculations of power, shift and width of Doppler spectrum is obtained. [C4703]

"High-resolution mapping of near-surface internal snow layers with a wideband radar"

First Page of the Article [C4704]

"Doppler-polarimetric method of turbulence intensity retrieving in rain using remote sensing with microwave radar"

The developed procedure for turbulence contribution retrieval to the total Doppler Spectrum width can be successfully used for measuring intensity of turbulence in rain by Doppler weather radar. Further improvement of the method can be achieved by increasing the accuracy of median drop diameter estimation. This can be done, for example, by using polarization diversity. Measuring ZDR gives good possibility for this, especially by airborne radar with horizontal sounding. Spectral differential reflectivity gives independent parameter for turbulence in rain characterization that can be used additionally to Doppler spectrum width. Further researches should be aimed to develop Doppler-polarimetric algorithm for real time signal processing. [C4705]

"Passive multichannels millimeter-waves imaging system"

32-channels passive imaging system is developed in the frequency range 33...38 GHz. The system contains multibeam quasi-optical scanning antenna with an array of low noise direct detection receivers. New type of scanning mechanism on the base of asynchronous three-phase motor is used. The software-hardware complex has been created to control scanning mechanism and to process the receiving information. Simultaneous receiving of signals from different parts of scene allows to form a good quality image on the monitor screen in 3 seconds. The developed imaging system can be used to provide navigation on the ground or at sea, especially at short distances where surface radar clutter is high, for remote sensing in space and air investigations, for all-weather surveillance, for objects discovering, and many other commercial applications. [C4706]

"Wind influence on sea radar backscattering intensity"

This paper presents the wind influence on sea radar backscattering intensity. The remote radar methods are widely applied to the oceanographic investigations for the estimation of the state of surface and near-surface layer over scattered signal characteristics. The main characteristic of scattered signal is the intensity, which is characterized by normalized radar cross-section (RCS). The normalized RCS also essentially depends on the wavelength and polarization of the radar signal as well as on the angle of sea surface irradiation. The estimation for normalized sea RCS have been obtained for sounding signal wavelength from 2 to 200 mm, near-surface wind velocities from 5 to 40 m/s and incidence angles from 30 to 85°. The dependence of the backscattering intensity from the operating wavelength is practically absent. The normalized RCS changes on less than 10 dB for wavelength changing by a factor of 25 in a wind velocity range from 5 to 40 m/s. This is explained by a selected model of the spatial spectrum. [C4707]

"Optimal and quasioptimal processing algorithms in the multisatellite SAR in terms of the stochastic vector fields"

This paper represents description and analysis method of the multisatellite/ multiposition/ multichannel synthetic aperture radars in terms of the stochastic vector fields and operational analysis. Due to this method electrodynamic model of the surface, scattered and received signal models are considered as operators in the function space. This allows to generalise existing methods of the description and analyse multiposition systems. [C4708]

"The arrival angle performances for signals scattered by the targets and sea surface and their usage for detection efficiency improvement"

The target angular noise is used for detection reliability improvement or as a criterion for pattern recognition. The experimental research of angular fluctuations is conducted using the impulse 8 millimeter-wave radar. Results have shown that the small surface target signals are characterised by a much smaller range of azimuth fluctuations in comparison to that of from the sea surface. While the average value of the surface target bearing coincides with right direction and has a rather small variance of fluctuations, the marine surface is characterised by arrival angle roaming in the limits of the whole highlighted area. Application of the angular noise for target detection is based on its statistical performance modification, when the compact reflector (surface target) appears on the background of spatially distributed sea surface reflections. [C4709]

"Dual-polarization determination of soil parameters: theory and experimental data comparison"

In this paper the problem of electromagnetic wave scattering from rough surface has been studied. Theoretical models are based on methods of solving the problem of scattering by a statistically rough surface. Time integral equation method permits to determine the scattering intensity from soil without vegetation at great values of roughness mean square (rms) height. In the models of rough surface scattering the normalised RCS of surface characterising the intensity of scattered field is a product of two functions. The first function called dielectric function, characterizes the dielectric properties of the scattering medium and depends on polarization, the angle of incidence and dielectric constant. The second function takes into account the surface roughness influence on normalised RCS. Drawbacks of theoretical models cause the development of empirical models based on experimental results. Empirical model analysis of Oh has shown that for comparatively smooth surfaces, sufficiently fast growth of polarization ratios is observed. There exist best coincidence calculations for the empirical model and experimental values of the normalised RCS. Here, for comparing, the results of the normalised RCS calculations are shown by perturbation and integral equation methods. [C4710]

"GPR measurement of crop canopies and soil water dynamics- implications for radar remote

sensing"

First Page of the Article [\[C4711\]](#)

"Automatic detecting system for ship wakes in SAR images"

An automatic system based on localized Radon transform was proposed for detecting ship wakes in SAR images. Ship pixels in SAR image were masked out during pre-process in order to eliminate their own disturbance. Then localized Radon transform windows around ship targets were selected. At last, normalized line integrals were calculated within the localized Radon transform windows and the extremum in Radon transform space was the corresponding ship wake coordinates. This automatic system can detect ship wakes in SAR images accurately and quickly. So, the algorithm efficiency is very high. [\[C4712\]](#)

"GPR 2004 Conference is organized"

First Page of the Article [\[C4713\]](#)

"A novel feed system for soil moisture spaceborne radar: dual-frequency dual-polarized stacked patch microstrip array"

This paper describes the development and performance of a dual-frequency and dual-linear polarization microstrip antenna to be used in a synthetic aperture radar (SAR) for remote-sensing applications. The synthetic aperture radar (SAR) UHF/VHF design is used to deliver data for estimation of soil moisture. Two operating frequencies of 137.5 MHz and 435 MHz have been chosen to separate the effects of vegetation and soil and polarimetry at each frequency is needed to sufficiently characterize vegetation and soil. The planned parabolic reflector antenna has two different antenna widths of 30 m by 2.8 m at UHF and 30 m by 11 m at VHF by subilluminating a 30 m parabolic reflector antenna with a dual-frequency stacked microstrip array feed. [\[C4714\]](#)

"Multiscale segmentation of remotely sensed images using pairwise Markov chains"

Among the statistical approaches to image modeling, Markov random fields have recently gained significant attention, especially in texture segmentation. Different from Markov random fields, in pairwise Markov chains, the class field is not necessarily a Markov field, an advantage in the segmentation of texture images without any model approximation. Supervised texture segmentation of a multiscale image is introduced in a pairwise Markov chain tree model using the wavelet domain. The essence of this tree-structured probabilistic graph is based on capturing the statistical properties of the wavelet transforms and the intrinsic characters of textural regions of any multispectral image. [\[C4715\]](#)

"Modelling and migration of two dimensional GPR images"

First Page of the Article [\[C4716\]](#)

"GPR 2004 conference is organised in cooperation with"

First Page of the Article [\[C4717\]](#)

"GPR investigations of a prehistoric native american village site, lower snake river Floodplain, Idaho, USA"

First Page of the Article [\[C4718\]](#)

"System survey of deep penetrating radar"

First Page of the Article [\[C4719\]](#)

"Design and simulation of a GPR system for deep probing"

First Page of the Article [\[C4720\]](#)

"Estimation of soil moisture with I-band multi-polarization radar"

Through analyses of the model simulated database, we developed a technique to estimate surface soil moisture under HYDROS radar sensor (L-band multipolarizations and 40deg incidence) configuration. This technique includes two steps. First, it decomposes the total backscattering signals into two components-the surface

scattering components (the bare surface backscattering signals attenuated by the overlaying vegetation layer) and the sum of the direct volume scattering components and surface-volume interaction components at different polarizations. From the model simulated data-base, our decomposition technique works quit well in estimation of the surface scattering components with RMSEs of 0.12, 0.25, and 0.55 dB for VV, HH, and VH polarizations, respectively. Then, we use the decomposed surface backscattering signals to estimate the soil moisture and the combined surface roughness and vegetation attenuation correction factors with all three polarizations [C4721]

"RADARSAT-1 image quality evolution to the extended mission"

RADARSAT-1, the first Canadian SAR remote sensing satellite has successfully completed its design lifetime of five and a quarter years. It is currently in extended mission operation meeting customer demands. The Image Quality Control program is kept fully operational, and measured results indicate image quality performance is maintained better than system specification. This paper briefly describes image quality results and recalibration work [C4722]

"Pol-InSAR for agricultural vegetation parameter estimation"

The quantitative bio/geo physical agricultural and land-use parameter estimation has attained significant prominence as it is a challenge to quantify complex and fast changing media in terms of geometry and material properties. In this work the behavior of agricultural vegetation in terms of polarimetric interferometric SAR (Pol-InSAR) observables is investigated. For this a two layer model, the Oriented Volume over Ground (OVog) model, is discussed and validated against experimental data [C4723]

"Atmospheric dynamics mission: Aeolus"

The Atmospheric Dynamics Mission (ADM-Aeolus) represents the second Earth Explorer core mission within ESA's 'Living Planet Programme'. Following launch in 2007 the spacecraft would be injected into a sun-synchronous, polar orbit and provide global observations of atmospheric wind profiles throughout the troposphere and the lower part of the stratosphere. Due to its excellent sampling capabilities, combined with a systematic processing and dissemination of key data products in near-real-time (i.e., within 3 hours after sensing) Aeolus would enable major advances in operational short- and medium-range weather forecast systems. The ALADIN payload on board Aeolus is a direct detection Doppler Lidar system, equipped with a pulse laser operating in the ultraviolet) and a dual-channel receiver system. The spectrometer assembly would allow independent recording of the Mie (aerosol) and Rayleigh (molecular) components of the atmospheric backscatter signal, covering an overall height range from ground up to approximately 25 km. The Aeolus mission concept foresees systematic processing and dissemination of various data products over the envisaged mission lifetime of three years. This includes both the generation and delivery of Level 1B data (calibrated Doppler wind observations) to meteorological service centers in near-real-time and the off-line distribution of higher level products, serving a variety of scientific applications [C4724]

"High resolution SAR micro-satellite based on passive reflectors"

In a study proposed by CNES, EADS ASTRIUM has analysed the feasibility and the design of Synthetic Aperture Radars within the stringent envelope of micro satellites. The primary mission objective is high resolution (2 metres for -17 dB.m²/m² sensitivity) for a 5 km swath width, in X band. Two options have been analysed for this study. The first one was based on a passive reflector. Platform agility is required to achieve steering of the SAR beams in elevation. The second option was based on an active reflector antenna designed by THALES which detailed performances are currently studied under a Research and Technology study with CNES. This paper presents the definition and performances of a micro-satellite based on passive reflector antenna. This satellite design is compatible of a launch of up to three satellites at a time on low earth orbit, and offers Stripmap and ScanSAR modes capabilities. Finally, this short overview identifies the technological developments required to achieve the SAR on a micro satellite concept in the mid term [C4725]

"Retrieval of height and topography of corn fields by polarimetric SAR interferometry"

Polarimetric SAR interferometry (Pol-InSAR) has been applied successfully to retrieve biophysical parameters from forest areas. This technique employs a scene model composed of a random volume over the ground. However, that model is based on the assumption that the wave propagation through the vegetation canopy is independent of polarization, which is not valid for agricultural crops because the medium shows a strong anisotropic behavior. In this work we have studied the implications of the polarization dependence of the extinction coefficients, and a redefinition of the line fit inversion model is proposed and validated with indoor measurements. As we will show, provided that agricultural vegetation is short, the influence of the different extinction coefficient is minor. Consequently, it is demonstrated that an accurate inversion of the vegetation

height and the underlying topography is still possible. However, it is also shown that the model is not sensitive to changes in the extinction coefficient, so this parameter is not well estimated. Implications about the necessity of fully or partially polarimetric data have been also analyzed [C4726]

"Spaceborne 3D SAR tomography: experiments with ers data"

This paper presents the first results of a multibaseline SAR experiments for the reconstruction of the 3D back-scattering properties of ground scenes by using ERS data [C4727]

"Parameter inversion of "reduced" SAR flight-tracks: first results over forest"

In this paper, inversion of synthetic aperture radar data is dealt with and, in particular, the problem of reconstructing forest height is addressed. The forest is modelled as a random volume of particles over a rough ground. Under this model, the forest height turns out to be related to the bandwidth of the scattered field. The inversion is cast as an optimization one. Preliminary results using DLR-ESAR experimental SAR data are shown [C4728]

"Full maximum likelihood inversion of polinsar scattering models"

We expand upon the maximum likelihood inversion approach presented in Flynn, Tabb, and Carande ["Direct estimation of vegetation parameters from covariance data in polarimetric SAR interferometry", IGARSS 2002], and show how to optimally combine the polarimetric channels to form a bare earth estimate for the case of single layer ground scattering. In addition, for the two layer randomly oriented volume over ground (RV+G) scattering model, we show how to optimally recover the canopy structural parameters (bare earth and tree height) as well as the ground and volume backscatter polarimetric covariance matrices. This approach outperforms other techniques in terms of both estimation accuracy and computational complexity [C4729]

"Local orientation analysis of spatial texture from polarimetric SAR data"

In this paper we present two methods to estimate the local orientation of spatial texture in polarimetric SAR data. The first approach is based on an original spatial parametric modelling of the 2D autocorrelation function, and was introduced in a previous paper. The second method is based on orientation interpolation between a reduced set of basis functions called steerable filters. Both are applied to measured polarimetric SAR data [C4730]

"RADARSAT-2 program update"

RADARSAT-2 would be the next Canadian commercial Synthetic Aperture Radar (SAR) satellite. The construction of the spacecraft and the development of the ground segment are progressing well. This paper presents an overview of the mission, some featured innovations, imaging capabilities and data distribution aspects [C4731]

"Mapping of tidal currents with SAR along track interferometry"

An update of the status of SAR Along Track Interferometry (ATI) is given and examples from X-SAR/SRTM for the waters around the Orkney Islands are provided. A special InSAR "Ocean-Processor" is described. The derived SRTM "velocity maps" demonstrate how valuable this method can be for a world-wide mapping of tidal ocean currents and for the detection of promising sites for hydropower installations [C4732]

"Microwave radar remote sensing of surface currents in the nearshore region"

We present observations of microwave radar backscattered power in the nearshore region, and results of a surface current estimation algorithm using microwave radar data. In low wind and wave conditions, patches of increased backscatter are observed in radar images. Animations of the images show these patches advected by nearshore flows such as wave induced cell circulations and longshore currents [C4733]

"Glacier flow estimation by SAR image correlation"

The Shirase Glacier is the largest in the Lutzow Holm Bay and is well known as the fastest-flowing ice stream in Antarctica. Although several attempts have been made to measure ice flow velocities of the glacier using ground measurements and remotely sensed data, continuous measurement over a long period has been impossible due to severe environmental conditions and the lack of datasets from continuous observation. This report of our preliminary ice-flow estimations of the Shirase Glacier correlates the amplitude images with the available synthetic aperture radar (SAR) data. We propose to determine ice-flow velocities using this image correlation.

We apply our technique to the SAR data obtained by observing the Shirase Glacier to determine and analyze the ice flow velocities in the summary [C4734]

"Decadal mass balance of the antarctic ice sheet and its contribution to global sea level rise"

We analyzed Antarctic ice sheet elevation change (dH/dt) from 1992-2002 using nearly 307 million elevation change measurements from ERS-1 and ERS-2 satellite radar altimeter data covering an area of about 8.5 million km². Ten-year elevation change time series were constructed for 1,500 local regions, 22 drainage basins, East and West Antarctica, and the continent as a whole (north of 81.6degS). Almost all basins in East Antarctica were found to have long-term dH/dt trends that fell within ± 3 cm/yr. In West Antarctica the long-term dH/dt trends varied from -9 cm/yr to +22 cm/yr occur over basin scales. Despite these significant spatial variations, both the East and West Antarctic ice sheets, and the continent as a whole are very close to a state of overall mass balance. The average elevation change for the Antarctic continent from 1992-2002 was found to be 1.4 ± 0.2 cm/yr. Considering decadal accumulation variability, this translates to a net sink of fresh water of 42 ± 23 Gt/yr. The Antarctic continent's decadal contribution to global sea level change is estimated to be -0.12 ± 0.07 mm/yr, which is very close to zero. The ± 0.07 mm/yr error is a three-fold reduction in uncertainty compared to the most recent best estimate for the Antarctic ice sheet [C4735]

"UHF riversonde observations of cowlitz river flow velocity at Castle Rock, Washington"

A UHF RiverSonde system, operating at a frequency of approximately 350 MHz, has been in operation on the Cowlitz River at Castle Rock, Washington since October 2003. The system uses SeaSonde electronics developed over many years for measuring ocean surface currents in salt water at HF. A three-Yagi antenna system designed using a genetic algorithm optimization procedure replaces the conventional crossed-loop HF array. The antennas, located on one bank of the river, are directed across the river at three different azimuths and are separated by approximately one-half wavelength, allowing both amplitude and phase differences to be used for MUSIC direction finding. Scattering from the fresh water surface is dominated by Bragg scattering as it is at HF, but the data processing algorithms are modified to accommodate flow velocities which can be several times the deep-water phase velocity of the Bragg waves. Data are processed in real time on a portable laptop computer and are available through a dial-up modem. The radar data provide hourly estimates of mean flow and cross-channel variations in the flow. Mean values of the radar flow profile track very closely continuous in situ stage height measurements. River flow velocities of 0.8-3.5 m s⁻¹ were observed in the first five months of the experiment, with a nearly linear relationship between radar-inferred flow velocity and stage height of 9-14 m. The radar velocity also appears to have a weak correlation with the local wind and several tidal frequencies. The strong correlation between surface velocity and stage height suggests that with refinement surface velocity could replace stage height in river gaging, as well as offering additional flow information [C4736]

"Observation of the Soya warm current using HF ocean radar"

Three HF ocean radar stations were installed at the Soya/La Perouse Strait in the Sea of Okhotsk in order to monitor the Soya Warm Current. Frequency of the HF radar is 13.9 MHz, and range and azimuth resolutions are 3 km and 5 deg., respectively. It covers a range of about 70 km from the coast. Surface current velocity observed by the radars is compared with data from drifting buoys and shipboard ADCPs (Acoustic Doppler Current Profilers). The current velocity derived from the HF radars shows good agreement with that observed by the drifting buoys. The rms (root-mean-squared) differences are about 15 cm/s for the zonal and meridional components. The observed current velocity also exhibits a reasonable agreement with the shipboard ADCP data. It is shown that the HF radars clearly capture seasonal and short-term variations of the Soya Warm Current. The velocity of Soya Warm Current reaches its maximum, which is about 1 m/s, in summer, and becomes weak in winter. The current axis is located at a distance from 20 to 30 km from the coast, and the width is about 40 km. The surface transport across the strait shows a significant correlation with the sea level difference along the strait derived from coastal tide gauge records [C4737]

"Accuracy of surface current velocity measurements obtained from HF radar in Corpus Christi Bay, Texas"

Surface current mapping by means of high frequency radar is an operational oceanographic tool. Researchers have identified the basic sources of error associated with this technology. Further research evaluating errors relating to the HF radar system and corresponding algorithms can facilitate coastal environment data assimilation. Uncertainty due to two sources of error is studied to obtain a more complete accuracy of the HF radar-measured total surface current velocity vectors. The error sources include geometry of the two station HF radar system and limits of the deep-water wave assumption of the algorithm that calculates current velocity from the HF radar signal. The latter is of particular interest to our work in a shallow environment such as Corpus

Christi Bay. Water depths in portions of this and other Texas bays will push the limits of the deep-water assumption for the wavelengths of interest. A map of Corpus Christi Bay illustrating quantified GDOP for each point on the radar grid and an applicable matrix transformation that accounts for error due to the deep water wave assumption. The deep water assumption error is quantified and shown to be minimal for depths as shallow as one meter [C4738]

"Using multifrequency HF radar to estimate ocean wind fields"

HF radar has become an important tool for mapping surface currents in the coastal ocean and has been used to determine wind direction. Here the author investigate further the ability of multifrequency HF radar to measure the vector wind field and the impact that such measurements have on the measurement of coastal wind fields over both the land and sea. In this study the author use data collected over Monterey Bay, California from Jan. to Aug. 2001. Their multifrequency coastal radars (MCR's) operated at 4.8, 6.8, 13.4 and 21.8 MHz, measuring currents at effective depths of about 2.5, 1.8, 0.9 and 0.6 m respectively. Here, the author move beyond their preliminary reports by examining the durability of their HF wind vector measurements over a seven-month data set. The results over this longer time span indicate standard errors of prediction (SEP's) of 1.2 and 1.1 m/s for the U and V wind speed components respectively with biases less than 0.15 m/s. The author also investigate a Kalman filtering modification to their partial least squares algorithm. Further, the author demonstrate the beneficial impact of multifrequency HF radar, wind field measurements, on estimation of the coastal wind field over both land and sea [C4739]

"Anomaly detection in VHF radar measurements"

The present work develops a new aspect in the use of HF radar as a tool for real time operational oceanography. We propose to implement new algorithms for detecting anomalies (outliers) on VHF radar data. Perspectives of such work are to detect changes in sea surface, such as ship or oil pollution. In this preliminary work, no information are given about the anomalies. We propose to study new detection methods based on Support Vector expansion to perform a binary separation between observations. This technique is well adapted to HF radar observations that are never statistically representative but give a good temporal resolution [C4740]

"An approach to unsupervised change detection in multitemporal SAR images based on the Generalized Gaussian distribution"

This paper presents a novel approach to unsupervised change detection in multitemporal SAR images. This approach is based on three main steps: (1) controlled preprocessing based on adaptive filtering (despeckling); (2) comparison between multitemporal images according to a proper operator; (3) automatic thresholding of the log-ratio image. The first step aims at reducing the speckle noise in a controlled way in order to maximize the separability between changed and unchanged classes. The second step is devoted to compare the two filtered images in order to generate a log-ratio image. Finally, the third step deals with the identification of changes by thresholding the log-ratio image according to a novel technique. Such a technique is based on the double thresholding Kittler & Illingworth (K&I) algorithm, which is reformulated under the Generalized Gaussian (GG) assumption for the changed and unchanged classes. Experimental results obtained on a multitemporal SAR data set confirm the effectiveness of the proposed approach. [C4741]

"Techniques for seismic damages assessment by using remotely sensed images"

This paper discusses the methods of seismic damages assessment by utilizing remotely sensed data. Classical Change Detection (CD) algorithms are effective when the author can acquire both pre and post-event images in a very short period of time. For images those have large temporal difference, edge detection and neighborhood operations and occurrence calculations are used to enhance the texture information and detect the displacement of outlines of ground objects. When there is only post-quake image, the Direct Recognition from Single Image (DRSI) method is used. But automated DRSI is difficult because the pattern of houses is very complex and varies greatly in different geographical areas. Experiments were carried out for 2003 Jiashi-Bachu Ms 6.8, 1999 Taiwan Jiji Ms 7.2 and 1998 Zhangbei Ms 6.2 quakes. SPOT, ERS-2 SAR and airborne images were obtained. The results were in agreement with field surveys. [C4742]

"Oil spill detection by means of neural networks algorithms: a sensitivity analysis"

Synthetic Aperture Radar (SAR) images provided by satellite missions may provide a significant support for oil spill detection over the sea. In particular neural networks algorithms have recently demonstrated their potentialities for discrimination between oil spills and objects which resemble oil spills (called "look-alikes"). The main steps of the classification procedure are the identification of dark spots over the sea, the computing of a set of parameters (features) for each dark spot and the classification of the oil spill candidate using a trained

neural network, where the network input is a vector containing the values of the features extracted. The features so far mainly consist of physical-geometrical characteristics of the dark spot. This study presents a new neural network algorithm for the oil spill detection. The results also report a sensitivity analysis of the classification performance on the quantities that are given as input to the neural network. Among the considered inputs the value of the local wind speed has been also included. [C4743]

"Remote measurements of snowfalls in Wakasa Bay, Japan with Airborne Millimeter-wave Imaging Radiometer and Cloud Radar"

Results of concurrent airborne measurements of snowfalls with the Millimeter-wave Imaging Radiometer (MIR) and the Airborne Cloud Radar (ACR) are reported in this paper. The measurements were obtained during January-February 2003 in a field experiment in Wakasa Bay, Japan. The MIR is an imaging radiometer that measures radiation at seven channels between 89 GHz and 340 GHz. The ACR operates at 94 GHz and provides nadir-viewing radar reflectivity profiles with very good accuracy. Three days of snowfall events were observed during this field deployment. It was found that the MIR brightness temperature depressions at the frequencies of 183.3 ± 1 , 183.3 ± 3 , 183.3 ± 7 , and 340 GHz strongly correlate with the ACR reflectivity profiles during these snow events. Radiometric signatures from the remaining less opaque channels of the MIR (89, 150 and 220 GHz) showed ambiguity in snowfall detection due to variation in surface emissivities. An attempt to retrieve the ice water path and the median mass equivalent sphere diameter of the snowfalls would be described and results discussed. [C4744]

"Radar signatures of road vehicles"

Development and modeling of the road vehicle detection algorithms for SAR images requires the knowledge of the radar cross section of these targets. The radar signatures of the parked cars were derived experimentally from airborne E-SAR image data collected during two flight campaigns. First examples of the catalogue of radar signatures for road vehicles are presented. [C4745]

"Finite mixture models and stochastic expectation-maximization for SAR amplitude probability density function estimation based on a dictionary of parametric families"

In remotely sensed data analysis, a crucial problem is represented by the need to develop accurate models for the statistics of the pixel intensities. This paper deals with the problem of parametric probability density function (PDF) estimation in the context of Synthetic Aperture Radar (SAR) amplitude data analysis. Several theoretical and heuristic models for the PDFs of SAR data have been proposed in the literature, that have been proved to be effective for different land-cover typologies, thus making the choice of a single optimal SAR parametric PDF a hard task. In this paper, an innovative estimation algorithm is described, that faces such a problem by adopting a finite mixture model (FMM) for the amplitude PDF, with mixture components belonging to a given dictionary of SAR-specific PDFs. The method automatically integrates the procedures of selection of the optimal model for each component, of parameter estimation, and of optimization of the number of components by combining the Stochastic Expectation Maximization (SEM) iterative methodology with the recently developed "method-of-log-cumulants" (MoLC) for parametric PDF estimation. Experimental results on several real SAR images are reported, showing that the proposed method accurately models the statistics of SAR amplitude data. [C4746]

"Next generation on-board SAR processor for compact airborne systems"

A new generation of on-board SAR processors for compact airborne systems is presented, which is currently under development at the Laboratorium für Informationstechnologie (Lfi), Universität Hannover. The processor uses the ωk -algorithm (also known as the wavenumber domain algorithm) and features region of interest support and source coding of the SAR images for further reduction of the output data rate. This is important for data transmission via radio data links. The hardware architecture of the SAR processor is based on the HiBRID-SoC, a new signal processor with three fully programmable cores. This SoC allows the mapping of the whole SAR processing chain to a single chip. This reduces the number of hardware components, which is important for the realization of compact and power efficient hardware design. [C4747]

"The feasibility of traffic monitoring with TerraSAR-X-analyses and consequences"

This paper analyzes the potential of the upcoming German satellite mission TerraSAR-X to monitor traffic from space. As it is well-known, an object moving with a velocity deviating from the assumptions incorporated in the focusing process will generally appear both displaced and blurred in azimuth direction. To study the impact of these (and related) distortions in focused SAR images, the analytic relations between an arbitrary moving point scatterer and its conjugate in the SAR image have been derived and adapted to the TerraSAR-X specifications.

To be able to monitor traffic under these boundary conditions in real-life situations, a specific detection strategy is proposed. This strategy makes use of knowledge derived from external sources, as e.g. GIS and semantic models for traffic flow. [C4748]

"Airborne scan mode ISAR imagery of ships using high resolution spectral methods and particle filter"

The basic principle of Inverse Synthetic Aperture Radar (ISAR) imaging consists of performing a Doppler analysis of the signal returned by the target. In the context of maritime surveillance mission, the Doppler analysis, which is usually performed via FFT-based methods, enables to form a profile view of the ship. We propose to form the ISAR image while antenna is scanning via high resolution spectral estimation methods. The goal of using superresolution algorithms instead of Fourier methods is to improve resolution and to remove sidelobe, especially in our context where the rotation of the antenna implies a shorter dimension of the processed signals. We present in this article results of the application of such methods on both synthetic and real data. Next, this paper considers the possibility to track the scattering centers of the ISAR image along the different antenna scans. This technique will allow a better estimation of discriminating parameters in an additional classification step. We propose to use particle filter methods to perform tracking because they are more adapted to the context than Kalman filtering which imposes a linear state-space modelling and a necessarily white Gaussian noise. Preliminary results of these methods will be presented in this paper. [C4749]

"Sea slicks and oil spills-the chemical structure and morphology determines the remote sensing signals"

The different morphology of palmitic acid methyl ester (PME) slicks spread from n-hexane or ethanol was studied by 'Brewster Angle Microscopy' [BAM]. In the latter case, already at large areas per molecule a foam-like structure is being formed on the water surface, i.e., a two-dimensional network which appears to be comparable with the morphological structure of biogenic sea slicks. In line with this assumption, both the magnitudes of the radar backscatter damping ratios and the characteristics of the damping ratio/wavenumber curves were comparable for the PME slick spread from ethanol and for the biogenic slicks, while in the presence of the PME slick spread from n-hexane lower damping ratios were determined. Furthermore, the relaxation of alkanic acid esters, which are often being found in biogenic sea slicks, was investigated by 'Infrared Reflection-Absorption Spectroscopy' [IRR4S]. It turned out that the ester group is continuously hydrated and dehydrated during compression and dilation on an undulating water wave field. It can be safely assumed that the strong water wave damping induced by these chemical compounds is centrally related to this phenomenon. [C4750]

"On the assimilation of C-band radar data into CERES-wheat model"

Based on recent experimental studies which have found a strong correlation between a multitemporal series of C-band HH/W backscatter ratios acquired at 40deg incidence angle and wheat biomass, this work investigates the effect of the assimilation of the radar retrieved information into CERES-Wheat crop model. A sensitivity analysis has shown that an inaccurate knowledge of some model inputs, concerning soil properties and crop management, can lead to erroneous predictions. However adopting a reinitialisation assimilation strategy, significant improvements in the model estimations have been obtained [C4751]

"Planting date estimation in semi-arid environments based on Ku-band radar scatterometer data"

A method to determine planting dates in semi-arid regions is presented, based on Ku-band spaceborne scatterometer data. The planting date analysis was performed for Mali, a region with a broad range of vegetation cover with tropical forest in the south and desert in the north. The Ku-band data was acquired by the Sea Winds scatterometer onboard the QuikSCAT satellite during the time from January 2000 to December 2003. Climate data from meteorological stations was compared with scatterometer time series of data colocated from a circular area of a specific size. The comparison shows that the evolution of the backscatter signal is highly correlated with the vegetation cycle triggered in turn by the rain season. An accurate date for the onset of the growing season and therefore a basic planting date can be determined from noise-filtered backscatter time series using a simple threshold method. The temporal variations of the backscatter time series are mainly caused by vegetation growth and changes of surface soil moisture. An increased backscatter signal indicates therefore more and more sufficient growing conditions. For the estimation of the contribution of surface soil moisture, the backscatter was additionally compared with in situ data from test sites within the Duero basin in Spain, covered by the soil moisture measurement network of the University of Salamanca. The comparison showed a significant influence of surface soil moisture on the microwave backscatter [C4752]

"3-D broadband ground-based polarimetric SAR data processing for the monitoring of vegetation"

growth variations"

SAR is usually used for airborne or space borne remote sensing. It can also advantageously be exploited in a ground-based radar imaging system named Ground-based SAR (GB-SAR). We extended earlier approaches and developed an ultrawideband, ground-based, fully polarimetric SAR (Pol-GB-SAR) system for the monitoring of vegetation growth variations. Measurements on three type trees in different conditions were carried out by the developed SAR system. We proposed effective 3D broadband Pol-GB-SAR data processing algorithms in the paper. In situ polarimetric calibration obviously improved the features of the system. 3D images were reconstructed from the acquired data by a series of signal processing procedures based on a variety of wave equation migration methods. By implementing methods of radar polarimetry, the broadband GB-SAR system has possibility for monitoring changes in tree structure characteristics due to seasonal variations. Interpreted results demonstrated the target scattering characteristics in different vegetation growth situations showed good agreement with the ground truth [C4753]

"Simultaneous retrieval of surface wind speed and rain rate using radar and radiometer measurements"

A retrieval algorithm has been developed which simultaneously estimates the over ocean near-surface wind speed and rain rate profile using data from a 10.7 GHz microwave radiometer and a dual-frequency Doppler radar. The algorithm uses the radar backscatter measurements to estimate two parameters of the gamma drop size distribution (GDSD) at each range gate. The parameterized GDSD can be integrated to determine the rain rate profile. The wind speed is estimated from the 10.7 GHz brightness temperatures (TBs) by removing the contribution from the atmosphere and isolating the contribution from the surface wind speed. The atmospheric optical depth at 10.7 GHz is estimated by integrating the extinction coefficient determined at each radar range gate using the parameterized GDSD and Mie theory. Results of wind speed and rain rate retrievals are presented from a field campaign in June of 2003 in which several precipitation overflights were made with a NASA DC-8 equipped with the PR-2 radar and the LRR-X microwave radiometer [C4754]

"Estimating subpixel surface roughness using remotely sensed stereoscopic data"

Surface roughness at the 10-2-101m scale is estimated using the ratio between the reflectances of the surface measured from two view angles. As reflectance is dependant on surface roughness at these scales, this ratio provides us with a proxy for relative surface roughness within a single image that is largely independent of surface composition. Roughness estimates using stereoscopic data with 15-m spatial resolution from the Advanced Spaceborne Thermal Emission and Reflection Radiometer (ASTER) in Death Valley, California and ground based stereoscopic measurements at the 1-m scale were both found to be in good agreement with observed surface roughnesses. [C4755]

"Influence from polarized galactic background noise on L-band measurements of the sea surface salinity"

The polarimetric EMIRAD radiometer, based on novel digital down conversion and detection techniques, has been installed on a C-130 aircraft from the Royal Danish. Air Force during the L-band Ocean Salinity Airborne Campaign (LOSAC) in 2001 and 2003. Full 360° circle flight patterns around the same target area as well as clover leaf patterns have been measured, and both provide an azimuth signature of the ocean at a constant incidence angle. The resulting azimuth signatures show significant variations in all the three first Stokes parameters, and a correlation is found between the downwelling galactic background signal and the measured results. The measured 3rdStokes parameter has variations of the same order of magnitude as the two linear polarizations, and to verify this result, an experiment for direct observation of the sky over long time is set up. This experiment confirms the presence of a polarized galactic background signal, and conclusions are made with respect to the necessity for polarimetric corrections in future measurements over the sea at L-band. [C4756]

"Microwave remote sensing modeling of ocean surface salinity and winds using an empirical sea surface spectrum"

Active and passive microwave remote techniques have been investigated for the remote sensing of ocean surface wind and salinity. We revised an ocean surface spectrum using the CMOD-5 geophysical model function (GMF) for the European Remote Sensing (ERS) C-band scatterometer and the Ku-band GMF for the NASA SeaWinds scatterometer. The predictions of microwave brightness temperatures from this model agree well with satellite, aircraft and tower-based microwave radiometer data. This suggests that the impact of surface roughness on microwave brightness temperatures and radar scattering coefficients of sea surfaces can be consistently characterized by a roughness spectrum, providing physical basis for using combined active and passive remote sensing techniques for ocean surface wind and salinity remote sensing. [C4757]

"Observations of Arctic environmental change"

This overview paper presents recent observations of anomalous change in Arctic environment using satellite scatterometer data together with in-situ and field measurements over land, snow, sea ice, and Greenland ice sheet. [C4758]

"Performance evaluation of microwave radiometer carried by Shenzhou IV for land surface parameters retrieval"

The multiple model microwave remote sensor is an important part of the payload carried by Shenzhou IV spacecraft launched on 30 December 2002 and is also China's first experimental microwave remote sensing system operating in space. The system includes three kinds of microwave remote sensors, namely microwave radiometer, radar altimeter and radar scatterometer. The radiometer instrument provides global passive microwave measurements of terrestrial, oceanic, and atmospheric variables for the investigation of water and energy cycles. Here we discussed the retrieval of land surface parameters by using the Shenzhou IV brightness data aimed at evaluating the performance of this microwave radiometer. The results shows that the microwave radiometer observations of Shenzhou IV can be used to study seasonal and interannual changes of land surface parameters. Although compared with other satellite passive microwave sensor, the radiometer of Shenzhou IV has it's limitation. [C4759]

"SOM of space borne precipitation radar rain profiles on global scale"

The Precipitation Radar (PR) from the Tropical Rainfall Measuring Mission (TRMM) produces high resolution vertical profiles of precipitation. Extensive information about the type of storm is contained in its vertical structure. This paper develops classification methodology precipitation radar profiles using self organizing maps. Reflectivity observation of vertical rain profile on global scale obtained from TRMM PR is classified with Self-Organizing Maps. The methodology is demonstrated by computing a SOM for a month of TRMM radar data around the globe. A sample application of the methodology is provided to study the difference between east and west Pacific Ocean. [C4760]

"Space borne GPM dual-frequency radar simulation from high resolution ground radar observations"

The global precipitation measurement (GPM) mission is dedicated to improving the understanding of the global water cycle by measuring and mapping precipitation throughout the globe. The core GPM satellite will incorporate two separate precipitation radars: one operating at Ku-band (13.6 GHz) and the other at Ka band (35.6 GHz). Each radar beam will be steered such that they both point to the same location in the atmosphere. The main purpose of the dual-frequency radar system is to resolve the DSD in precipitation as well as discriminate between rain and ice. With the two beams collocated on the same precipitation volume, new algorithms are being developed to reliably estimate attenuation and rain rate. Any algorithm is based on models of precipitation. In addition, the GPM system assumes collocated beams and matched resolution volumes. Electromagnetic and microphysical models have been developed based on ground-based dual-frequency radar data at S-band to simulate Ku- and Ka-band results for comparison with the new GPM algorithms. This paper evaluates the dual-frequency inversion algorithm with synthesized S-band and known perfect data and presents results. Results show the expected performance of the new dual-precipitation radar algorithms with the potential for guiding algorithm and system improvements. [C4761]

"Measurement of global precipitation"

The Global Precipitation Measurement (GPM) Program is an international cooperative effort whose objectives are to (a) obtain increased understanding of clouds and rainfall processes, and (b) make frequent rainfall measurements on a global basis. The National Aeronautics and Space Administration and the Japanese Aviation Exploration Agency have entered into a cooperative agreement for the formulation and development of GPM. This agreement is a continuation of the partnership that developed the highly successful Tropical Rainfall Measuring Mission (TRMM). NASA has taken lead responsibility for the planning and formulation of GPM. Key elements of the program are discussed in this paper. [C4762]

"Preparations for Global Precipitation Measurement (GPM) ground validation"

The Global Precipitation Measurement (GPM) program is an international partnership led by the National Aeronautics and Space Administration (NASA) and the Japan Aerospace Exploration Agency (JAXA). GPM will improve climate, weather, and hydrometeorological forecasts through more frequent and more accurate

measurement of precipitation across the globe. This paper describes the concept and the preparations for ground validation within the GPM program. Ground validation (GV) plays a critical role in the program by investigating and quantitatively assessing the errors within the satellite retrievals. These quantitative estimates of retrieval errors will assist the scientific community by bounding the errors within their research products. The two fundamental requirements of the GPM ground validation program are: (1) error characterization of the precipitation retrievals and (2) continual improvement of the satellite retrieval algorithms. These two driving requirements determine the measurements, instrumentation, and location for ground observations. This paper describes GV plans for estimating the systematic and random components of retrieval error and for characterizing the spatial and temporal structure of the error. This paper describes the GPM program for algorithm improvement in which error models are developed and experimentally explored to uncover the physical causes of errors within the retrievals. GPM will ensure that information gained through ground validation is applied to future improvements in the space-borne retrieval algorithms. This paper discusses the potential locations for validation measurement and research, the anticipated contributions of GPM's international partners, and the interaction of ground validation with other GPM program elements. [C4763]

"Suppression of surface clutter interference with precipitation measurement from space by the Dual frequency Precipitation Radar"

A new method to suppress the surface clutter interference with precipitation measurement from space by the Dual frequency Precipitation Radar (DPR, 13.8 GHz and 35.5 GHz) is introduced for the Global Precipitation Measurement (GPM) mission, which is planned in succession to the Tropical Rainfall Measuring Mission (TRMM). The DPR has very high sensitivity and its minimum detectable rain rate is designed to be 0.3mm/h(attained by the 35.5 GHz radar) at the rain top. In this study, the radiation pattern of the slotted wave guide planar phased array antenna was calculated by considering the Taylor distribution with random errors in excitation current. The signal (S) to clutter (C) power ratio (S/C ratio) was evaluated for the antenna pattern given by the Taylor distribution (designed peak side lobe level=-35 dB, $n=6$, ; these values are same as the TRMM PR), where the S means received power from rain scattering volume, and the C means the backscattered power from sea/land surface. A uniform rain rate of 0.3 mm/h was assumed for the calculation of signal S at 35.5 GHz and 0.5 mm/h for S at 13.6 GHz. A side lobe clutter interferes the rain echo severely when the strong side lobe illuminates the nadir direction, where the specular component of the scattering coefficient of sea/land surface is dominant. The introduced method to suppress the side lobe clutter is to tilt the antenna beam a few degrees in coordinate plane determined by the satellite flight direction and the nadir direction. The radiation pattern of the phased array antenna is characteristic in that the region of the strong side lobe arises in crisscross. By tilting the antenna beam, the strong side lobe illuminates the off nadir direction. So that makes it possible to suppress the side lobe clutter. Calculation results show that the surface clutter interference is suppressed well at the main beam tilt angle 2 degrees. [C4764]

"ERS-ENVISAT Permanent Scatterers"

The phase time series of a perfect point-wise Permanent Scatterer (PS) would show a phase jump passing from ERS to ENVISAT SAR images. A PS analysis has been carried out on a dataset including both ERS and ENVISAT images. For each PS, elevation, LOS velocity and phase jump have been jointly estimated and removed, allowing the identification of the atmospheric phase screen. The PS population so found represents the intersection of ERS and ENVISAT PS populations. The probability of natural targets to behave as PS both in ERS and ENVISAT has been analyzed as a function of their Radar Cross-Section, acquisition geometry and amplitude. Distributed targets with a narrow backscattering lobe pointed towards the first sensor (ERS) are not coherently observed by the second one (ENVISAT), whereas point-wise targets (e.g. natural corner reflectors, dihedrals and small mirrors) will remain coherent in both cases. Experimental results have been carried out on a data set of 69 ERS images and 7 ENVISAT images (ERS-like mode) on Milano over a 20 km side area. [C4765]

"Combination of point and extended target based interferometric techniques"

The objective of this paper is to present an approach that combines the interferometric point target analysis (IPTA) and the extended target based interferometric techniques (InSAR). The improvements achieved are most obvious in cases where the individual techniques result in complementary coverage in the information retrieved. [C4766]

"Initial vector velocity estimates from the UMass Dual Beam Interferometer"

The Dual Beam Interferometer consists of two interferometric SARs, one squinted at 20 degrees forward of broadside, and the other 20 degrees aft, to allow estimation of vector surface velocity with only a single aircraft pass. It was developed by the University of Massachusetts and is operated in collaboration with the Naval

Research Laboratory. The paper presents initial estimates of surface velocity vectors in the coastal region during high tidal flow. The data were gathered over the barrier islands west of Ft. Myers, Florida, as part of March 2004 deployment. While no attempt has been made at this stage to correct for Doppler contributions from surface waves, the retrieved velocity field clearly follows the expected outflow pattern, and velocity magnitudes agree well with in-situ data. [C4767]

"Split band interferometry versus absolute ranging with wideband SAR systems"

Estimation of differential shift of image elements between two SAR images is the basis for many applications, like DEM generation or ground motion mapping. The shift measurement can be done nonambiguously on the macro scale at the accuracy of the range resolution of the system or on the micro scale by employing interferometric methods. The latter suffers from phase cycle ambiguities and requires phase unwrapping. Modern wideband high resolution SAR systems boast resolutions as small as a few tens of a wavelength. If sufficiently many samples are used for shift estimation, the accuracy can be increased to a small fraction of a resolution cell and even in the order of a wavelength. Then accurate absolute ranging becomes precise enough to support phase unwrapping or even make it obsolete. The paper gives equations and simulation results for the achievable shift estimation accuracy for several algorithms: coherent speckle correlation, incoherent speckle correlation, split band interferometry, and correlation of point scatterers in clutter. It is shown that the performance of split band interferometry is close to the one of optimum MLE. Special Δk systems are proposed to best take advantage of the available bandwidth. [C4768]

"Selected analyses of TRMM instantaneous rainfall data"

Distributions of Tropical Rainfall Measuring Mission (TRMM) Version 5 (V5) and Version 6 (V6) data are presented. The fraction of pixels determined by the Precipitation Radar (PR) to be convective has increased by 5% from V5 to V6. In V6, PR contributes more rain in medium (4 to 20 mm/hr) but less in heavy (>20 mm/hr) rainfall rates than the TRMM Microwave Imager (TMI). Joint probability distributions show the V6 TRMM Combined Instrument rainfall more strongly related to PR than to TMI. [C4769]

"Comparison of two methods for extracting surface soil moisture from C-band radar imagery"

The integral equation method (IEM) model and a newly defined delta index were used to estimate near surface soil moisture from C-band radar satellite imagery in a semiarid rangeland in southern Arizona, USA. Model results were validated against soil moisture measurements made in the field at the time of satellite overpass. The IEM model performed poorly in this environment possibly due to abundant near-surface rock fragments which were not considered in the model. The delta index performed better than the IEM model and was shown to work with both ERS and Radarsat imagery. Additionally the index was simple to implement and implicitly accounted for both rock fragments and surface roughness [C4770]

"Estimation of snowfall over the sea of Japan using AMSR-E passive microwave remote sensing observation"

Snowfall is an important geophysical parameter and the observation of the spatial and temporal distribution of snowfall can provide valuable information for a wide range of applications including climate change studies and atmospheric modelling. This paper investigates the feasibility to estimate the amount of solid precipitation and the cloud liquid water content over the ocean using AMSR-E passive microwave brightness temperature observations. The parameters are retrieved by minimizing the difference between the observed and modeled brightness temperature. The radiative transfer in the atmosphere is solved using the discrete ordinate method (4 streams) and the Henyey-Greenstein phase function. The scattering effect of the snow particles is calculated using Mie theory and the liquid-equivalent size of the ice particle. Except for the snowfall and the cloud liquid water content, most parameters, which influence the observation are derived from other data sources. The Newton-Raphson method is used to solve the iteration process using observed brightness temperatures at 89 GHz vertical polarization and 36.5 GHz horizontal polarization. The algorithm was applied using data from the Wakasa Bay Experiment 2003 in Japan and the results are compared to snowfall observation derived using a Z-R relationship and data from the Mikuni Doppler radar. Good agreement was achieved for different atmospheric conditions [C4771]

"Soil properties estimates from SAR data by using a bayesian approach combined with IEM"

An experiment aimed at investigating the potential of ENVISAT/ASAR in measuring soil moisture is described in this paper. Two test areas were chosen as test sites: Montespertoli and Alessandria, in Central and Northern Italy, respectively. After a preliminary analysis of the direct relationship between the backscattering coefficient at C-band and the soil moisture content of individual fields, a Bayesian approach was attempted for retrieving soil

moisture. To obtain a statistically significant data set, simulations performed with the integral equation model were added to experimental data. Moreover, an artificial neural network was tested on Alessandria area [C4772]

"Two novel surface model based inversion algorithms using multi-frequency polSAR data"

The aim of this paper is to present two novel surface model based inversion algorithms using multifrequency and polSAR data. The first part of this work introduces a polarimetric scattering model using the integral equation model (IEM) with a transition model for the reflection coefficient. Polarimetric descriptors: the entropy (H), the anisotropy (A), and the mean alpha angle obtained from the Cloude/Pottier polarimetric decomposition theorem are employed for surface characterization. A new polarimetric parameter: the eigenvalue relative difference (ERD) is developed to overcome the anisotropy limitations in case of rough surfaces. Built on relevant polarimetric descriptors: H, alpha1 and ERD, two novel surface model based inversion algorithms using multifrequency polSAR data are presented. The first algorithm is built up in a "low frequency" (P to S band)-"high frequency" (C to K band) scheme. This algorithm retrieves the soil parameters by using multifrequency least-square fit [C4773]

"How much seawinds wind direction data improve AMSR SST"

Accuracies of sea surface temperature (SST) retrieved from the Advanced Microwave Scanning Radiometer (AMSR) aboard the Advanced Earth Observing Satellite-II (ADEOS-II) are compared between two methods of removing wind direction effects; one is using only AMSR data, and the other is using the SeaWinds aboard ADEOS-II. The result is that rms of SST difference between AMSR and buoy is 0.626 degC from the method of using only AMSR, and is 0.660 degC from the one of using SeaWinds [C4774]

"Millimeter-wave measurement of frozen hydrometeors during the 2003 Wakasa bay field experiment"

Snowfall is an important component of the Earth's precipitation and hydrological cycle. Remote measurements of frozen hydrometeor properties have been limited because coincident measurements of microphysical and electromagnetic properties of snowfall have not been available. Snowfall measurement from space has been suggested as a solution to overcome this limitation. The precipitating clouds contain a sufficient density of ice water equivalent from snow crystals, graupel, or both, when brightness temperature is at 85 GHz. The NOAA Advanced Microwave Sounding Unit (AMSU) has been used to derive snowfall over land using millimeter-wave radiometry. This study analyzes the millimeter-wave radiometric measurements of frozen hydrometeors during the field experiment that was held in Wakasa bay of Japan in January 29, 2003. It was found that a lognormal distribution represents the snow PSD during the field experiments. The MM5 cloud simulation is employed to provide temperature and humidity profiles for the radiative transfer calculations. This study seeks to derive characteristics of snow whose electromagnetic properties are consistent with microwave brightness temperature at several frequencies provided by the MIR sensors and the radar reflectivity measured by PR-2 (Precipitation Radar) and ACR (Airborne Cloud Radar). [C4775]

"The characteristics of system noise of TRMM/PR and their application to the rain detection algorithm"

The characteristics of the system noise sampled by the precipitation radar (PR) onboard the Tropical Rainfall Measuring Mission (TRMM) satellite are investigated in this study. The long term trend of the system noise shows a periodical change relating to the temperature of the PR. This change is corresponding to the changes in the solar beta angle which is the angle between the satellite orbit plane and the direction to the sun. The amplitude of the fluctuation of the system noise by the solar illumination to the PR is about 0.15 dB. The fluctuation of the noise caused by surface emission over ocean is examined by averaging the system noise of no-rain condition for a long time (e.g. one month) in order to remove the effect of the temperature fluctuation relating to the change of solar illumination and fading effect. The resulting amplitude is about 0.05 dB and the spatial distribution almost corresponds to the pattern of the sea surface temperature (SST). These results indicate that the system noise of the PR is quite stable so that the fluctuation of the sampled system noise is mainly caused by the fading effect. The characteristics of the system noise in three rain categories, rain certain, rain possible and no rain, are examined by taking a histogram assuming that the PR's system noise distribution is caused by the fading effect. The histogram of rain certain and no rain cases show a Gaussian shape with a few tenths of decibel difference caused by the emission from rain drops. On the other hands, rain possible case shows two-peak pattern with a large count peak existing at lower system noise. Since the rain detection algorithm compares the difference between the system noise and the received power with a threshold of about 1 decibel, this algorithm allows categorizing as "rain possible" the combination of the low system noise and high received power, both of which are caused by the fading effect, even under no-rain condition. [C4776]

"Simulation of SAR images of a forested area based on a 3-D full-wave model of wave scattering"

A coherent 3D model of wave scattering by a forested area is used to produce the data necessary to construct SAR images of the given field. Based on a domain integral representation of the scattered field, the model is applied, in VHF band, to a configuration where the separation between the trees is such that the coupling between the latters is weak. The computed backscattered field is used as an input to classical algorithms of SAR image reconstruction [C4777]

"Combined tree growth, l-system, and radar backscatter modeling"

In this study, a forest stand was assembled according to the results from forest growth model. The L-system was used to generate the realistic geometry of trees. The 3D model of the assembled forest stand then was used as input to 3D radar backscatter model. As the first step, larch forest stands at ages of 10, 30 and 80 years, that correspond to the young, mid-age, and mature forests commonly used in forest management practice in Northeastern China, were simulated. The simulation results were compared with SAR images [C4778]

"Building damage detection using satellite SAR intensity images for the 2003 Algeria and Iran earthquakes"

An earthquake occurred in the coast of Algeria on May 21, 2003. The cities of Boumerdes and Zemmouri were the most extensively damaged areas. Canadian SAR satellite, RADARSAT, observed Boumerdes area by the fine-beam mode, on 4 days after the event. European SAR satellite, ERS, also observed the same area on June 7, 2003. On December 26, 2003, another strong earthquake occurred beneath the city of Bam, Iran. Severely damaged areas were found widely being distributed in the city from high-resolution optical satellite images obtained after the event. ENVISAT also captured the hard-hit areas on January 7, 2004. In this paper, we investigated the characteristics of damaged areas in these SAR images by visual interpretation and clarified the effect of spatial resolution for the detection of damaged buildings. Then, we applied our automated damages detection technique, which was developed based on the data set of the 1995 Kobe earthquake, to the SAR images of Algeria and Iran [C4779]

"On the real capabilities of remote sensing for disaster management-feedback from real cases"

One of the applications where remote sensing could be very useful is the management of major disasters. While remote sensing has shown its interest for recovery and inventory tasks after the crisis period, an assessment of its usefulness during the crisis period is needed. Periodic image acquisitions over any point of the Earth surface, with improved resolutions available today seem to fulfill the required specifications of a global monitoring system. Earth Observation satellites in orbit today were not designed for such a purpose. However, several initiatives have been proposed in order to use them in this kind of applications, as for instance, the International Charter Space and Major Disasters, or the CEOS Disaster Management Support Group. In this paper we discuss, based on past experiences, what are the real capabilities of present and near future satellites, which are their drawbacks and how they could be used at best for real cases of crisis management. A list of recommendations with regards to what could be improved at the system level (sensor, acquisition scheduling, ground segment data production) and the techniques for information extraction (image processing, sensor fusion), is given [C4780]

"Automated texture recognition system based on 2D minimum variance spectral estimation"

The primary feature of any image texture is the spatial frequency content. This paper proposed the use of a 2D minimum variance spectral estimation (MVSE) method for recognizing target multispectral image textures. The power spectral density of the target texture is estimated via MVSE. This estimate is then used as a feature to discriminate between target and nontarget textures. A remotely sensed multispectral image of a row crop agricultural field is analyzed and, the corresponding results are presented to illustrate the applicability of the proposed technique. [C4781]

"Polarimetric feature of small urban area measured with SIR-C"

We analyzed the polarimetric backscattering characteristics of a small urban area measured with SIR-C using a target decomposition method and polarimetric entropy method. Relative contribution of cross scattering as well as polarimetric entropy increase as a function of building density. This result may suggest that the probability of scattering becomes large as the number of surfaces (roofs and walls) increases. [C4782]

"Swiss alpine airborne sar experiment (SASARE) part I: multi-baseline polarimetric SAR interferometry studies at L- and P-band"

In the frame of the Swiss Alpine Airborne SAR Experiment 2003 (SASARE) multitemporal/-baseline Pol-InSAR (polarimetric SAR interferometry) data sets were acquired with the German E-SAR (Experimental SAR) platform at L- (1.3 GHz) and P-band (350 MHz) in the region of the Great Aletsch glacier in Switzerland. For SASARE, several sub test sites had been selected below and significantly above the equilibrium line. One of the two campaigns was designed as a joint venture experiment and therefore also includes measurements of the Swedish CARABAS UWB (Coherent All Radio Band Sensing, ultra wide-band) sensor operating in the VHF frequency range (20-90 MHz). We provide first results from analysis of multitemporal/-baseline Pol-InSAR Land P-band measurements of the polarisation-dependent complex interferometric coherence of different glaciological surface types of an Alpine glacier [C4783]

"SAR interferometry for DEM generation and movement of Indian glaciers"

Two famous glaciers viz. Gangotri and Siachen were studied for DEM generation and movement using ERS-1&2 tandem data. While surrounding areas along the glaciers showed more decorrelation, glacier area showed a very good correlation between two image acquisitions. Contours obtained using ERS-1&2 SAR tandem data closely match with topographic maps of the area. Two-pass differential method was used along with SRTM DEM to study the movement of the glaciers. According to the differential interferogram over Gangotri, 3 fringes equivalent to 8.4 cm displacement in the radar look direction were observed, whereas for Siachen the fringes were about 8 which is equivalent to 22 cm. The estimated DEMs and movements are to be verified using GPS measurements [C4784]

"Velocities field of mountain glacier obtained by synthetic aperture radar interferometry. comparison of insar and surveyed velocities"

The Mer de Glace and Argentière glaciers are located in the Mont Blanc region, French Alps. They are temperate glaciers and their velocity flow is about one hundred meters a year (~270 mm a day). This paper presents a use of synthetic-aperture radar (SAR) interferogram obtained from the two European Remote-Sensing satellites (ERS1-2) to measure the motion of Mer de Glace and Argentière glaciers. We investigate whether the interferometric data are quantitatively consistent with terrestrial velocity measurements along two transverse profiles and two longitudinal profiles. Interferometric and terrestrial velocity are in agreement if a (terrestrially measured) surface-normal velocity component is properly accounted for. This suggests that both the interferometric velocities and the conversions of terrestrial data to the winter period are reliable. Finally we show that the application of repeat-pass SAR interferometry to the glaciers enables precise mapping of ice flow dynamics at a much higher level than usually obtained [C4785]

"Swiss alpine airborne sar experiment (SASARE) part II-imaging of high alpine glaciers at the VHF-band"

For part I see *ibid.*, (2004). This paper describes first results from a low frequency sensor campaign in the high Alpine region of Switzerland. Several parallel tracks were flown with the Swedish radio wave sensor CARABAS-II in late autumn 2003. We rate the geometric quality of the automatic processing of the ultra-wideband (UWB) radar data, discuss its most characteristic features, as well as problems caused by highly variable topographic gradients. The relatively long wavelengths used should theoretically allow penetration into cold ice bodies. The first results did not show obvious evidence of subsurface echoes [C4786]

"SAR firn line detection and correlation to glacial mass balance; Svartisen Glacier, northern Norway"

The glacial firn line of the Svartisen Glacier has been detected using ERS II SAR and ENVISAT ASAR data from 1995 and up to today. The firn line is detected by first correcting the image backscatter intensity for topographic and geometric contributions using the Muhleman backscattering model. Then we discriminate between firn and ice facies based on the backscatter intensity since frozen firn has a much higher backscatter than ice. Transects across different areas of the glacier were chosen based on requirements of smoothness of topography, precipitation zones, as well as the availability of field data for validation and comparison. From having quite stable conditions during the nineties we have observed a substantial retreat of the firn line over the last few years. The equilibrium line derived from field measurements shows a similar trend as the firn line changes, but has a much larger year to year variability. This indicates that the firn line may be a better indicator of climate change than the equilibrium line due to the smaller variance [C4787]

"A comparison on texture classification algorithms for remote sensing data"

Ground penetrating radar (GPR) systems are widely used to inspect underground structures. We have collected

GPR images to detect and identify structures beneath rail tracks. Several approaches, including a statistical edge detector and machine learning methods, have been applied to analyze the images. Our results show that the edge detector efficiently enhance the layer boundaries that separate ballast, subballast, and clay. The machine learning approaches are promising means to detect these layers automatically. [C4788]

"TanDEM-X: a TerraSAR-X add-on satellite for single-pass SAR interferometry"

TanDEM-X is a mission proposal for a TerraSAR-X add-on satellite for high-resolution single-pass SAR interferometry. This mission proposal has been selected for a Phase A study within the scope of a Call for Proposals for a next German Earth Observation Mission to be launched in 2008/2009. The mission has the goal of generating a global Digital Elevation Model (DEM) with an accuracy corresponding to the DTED-3 specifications (12 m posting, 2 m relative height accuracy for flat terrain). This goal will be achieved by means of a second, TerraSAR-X like satellite (TanDEM-X) flying in a close orbit configuration with TerraSAR-X. This paper describes the mission concept and requirements, including several innovative aspects like operation modes, orbit selection and maintenance as well as PRF and phase synchronization. Results from a detailed performance estimation show the achievable DEM accuracy. Finally, an overview of the potential of the TanDEM-X mission for several scientific applications is presented. [C4789]

"Interferometric coherence of SAR signals backscattered by a building"

In this paper we analytically evaluate the correlation coefficient between the signals backscattered towards two spatially separated antennas by a building modelled as a parallelepiped over a possibly rough terrain. We consider both single and multiple scattering contributions. [C4790]

"Efficient detection and correction of residual motion errors in airborne SAR interferometry"

This paper discusses the detection and correction of residual motion errors in airborne SAR interferograms. They usually appear due to the lack of precision in the navigation system. Two techniques existing in the literature to detect such errors are presented, highlighting differences and similarities. The effects of residual motion errors in the final interferogram are mainly two: azimuth phase undulations and azimuth registration errors. A new correction approach is proposed, which corrects both effects in one step, avoiding the use of interpolations. Additionally, the spectral diversity technique, used to estimate registration errors, is critically analyzed. Airborne L-band repeat-pass interferometric data of the German Aerospace Center (DLR) experimental airborne SAR (E-SAR) is used to validate the method. [C4791]

"Combining multitemporal SAR differential interferograms: a curvature based method"

Given a series of SAR acquisitions, when a sufficient number of differential interferograms between different dates are computed and the phases unwrapped, the phases of each possible time interval can be obtained through a linear combination of the computed ones, i.e. by the solution of a determined linear system of equations. Usually (e.g. with ERS data), not all the interferograms necessary to obtain a determined system can be computed, unless one accepts that only few pixels (corresponding to stable point-like scatterers) remain coherent. In fact, spatial and temporal baselines can be very large. Previous works proposed to solve the under-determination of this system by singular value decomposition, i.e., by assuming that the solution (i.e. the terrain displacement) has minimum velocity. In this work, a different assumption is exploited in order to find a determined solution to the problem of combining SAR multitemporal differential interferometric measurements. The proposed approach is based on the idea that the solution should have minimum curvature. Tests performed on simulated and ERS SAR real data confirm the validity of the method. [C4792]

"Monitoring of soil moisture and vegetation water content variations in boreal forest from C-band SAR data"

The response of ERS-2 SAR to changes in soil and forest canopy moisture is investigated at a boreal forest test region in Finland. An inversion approach to estimate moisture characteristics from SAR data is applied. The method requires that a priori information on forest biomass (stem volume) and soil type distribution is available. The inversion technique provides estimates that are here, in addition to backscattering signatures, directly compared with daily in situ moisture values. The results indicate that time-series of C-band radar observations can be used for the monitoring of boreal forest moisture variations. Especially, the detection of the driest and the wettest conditions on mineral soil sites appears to be a feasible application even for single channel radar. The obtained SAR-based soil moisture estimates showed an RMSE level of 6% units against the in situ data for pine-dominated mineral soil sites. [C4793]

"Investigations on ARD monitoring in Siberian forest using spaceborne SAR"

Nation-wide monitoring of afforestation, reforestation and deforestation (ARD) activities is explicitly addressed in the Kyoto Protocol. This paper investigates the feasibility of ARD mapping using spaceborne synthetic aperture radar (SAR) and interferometric SAR (InSAR) data from the European Remote Sensing (ERS) satellite, the ENVISAT satellite and the Japanese Earth Resources Satellite (JERS). As test site the forest enterprise of Bolshe-Murtinsky, Central Siberia, was chosen since relatively long time series of ERS-ENVISAT and JERS SAR data were available spanning 1996-2004 and 1994-1997 respectively. The ERS-2 SAR and ASAR Image Mode (IM) backscatter acquired during winter under frozen conditions decreased by 1-2 dB following stand-wise logging, whereas reforestation in young stands could not be detected. The JERS SAR backscatter commonly showed stronger forest/nonforest contrast, between 2 and 4 dB depending on the weather conditions at image acquisition, whereas the repeat-pass JERS coherence was characterized by a 0.3-0.4 difference before and after deforestation activities. None of these two signatures was found to provide information on reforestation, mainly because of the too short time series with respect to the forest growth rate. To assess the possibility of using ERS-ENVISAT- and JERS-type of data for reforestation, a first-order approach has been developed. Preliminary results show that young stands can be distinguished from nonforested areas not earlier than approximately 25 years using JERS repeat-pass coherence and 30 years using ERS-ENVISAT SAR backscatter.

[C4794]

"An overview of the JERS-1 SAR Global Boreal Forest Mapping (GBFM) project"

Boreal ecosystems play an essential role in global climate regulation. Forests constitute pools of terrestrial carbon and are generally considered as global sinks of atmospheric CO₂, contributing to attenuating the greenhouse effect. Large amounts of carbon are also stored in boreal lakes, bogs and wetlands, partially released as CH₄ and other trace gases to the atmosphere during the spring and summer months. Human activities in the forest zone are however reducing the size of the carbon pool and climate change is triggering shorter winters and earlier thaw onset, changing the natural equilibrium. Given its global importance, there is a need to map and monitor the boreal zone, and as the changes occur on all from local, regional to global scales, fine resolution information over vast areas is required. The Global Boreal Forest Mapping (GBFM) project is an international collaborative undertaking initiated by NASDA in 1996, as a follow-on to the tropical-focused Global Rain Forest Mapping (GRFM) project [A. Rosenqvist et al., (2000)]. Utilising the L-band Synthetic Aperture Radar (SAR) on the Japanese Earth Resources Satellite (JERS-1), one of the main objectives of the GBFM project is the generation of extensive, pan-boreal SAR image mosaics, to provide snap-shots of the forest wetland and open water status in the mid-1990's. Mosaics over Canada, Alaska, Siberia and Europe have been generated, available on the Internet and on DVD free of charge for research and educational purposes. The GBFM project also entails research activities in North America, Siberia and northern Europe, aimed at advancing scientific applications of L-band SAR data in the boreal zone. [C4795]

"Biophysical parameter retrieval in production forest stands using C-band polarimetric radar"

A 40-km strip of polarimetric AIRSAR imagery over New Zealand's Kaingaroa Forest was analysed for retrieval of biophysical parameters. The imagery was collected in November 2000 as part of the PACRIM-2 mission. Only the C-band data were analysed, as we are most interested in the potential of applications using future C-band satellite imagery. A series of regressions between stand age and radar information are reported where the level of radar complexity or use of additional covariate input is increased for each regression. The results show that stand age cannot be predicted using any single C-band polarisation. Promising results are found for dual-polarisation data, which will be available from future satellites. A regression using full-polarisation information yielded an adjusted R² of 82.3%. However, many of the common decomposition indices were found to be of little significance in this regression. The result is an improvement on methods based on backscatter intensity alone, and has important implications for inventory monitoring of commercial forestry stands. [C4796]

"Backscattering simulation for nonuniform forest canopies using multilayer MIMICS"

In this paper, we introduce a multilayer MIMICS for nonuniform forest canopies and present the model applications. The Michigan Microwave Canopy Scattering model (MIMICS) has been developed to simulate microwave backscattering from tree canopies. However, the crown-trunk canopy model is too restrictive for nonuniform canopy coverage. Multilayer MIMICS is developed to remove the two-layer canopy restriction. The model is a simulation solution to an array of radiative transfer equations and it includes the layer interactions between overlapping layers. This paper is focused on the model validation and application of multilayer MIMICS. Our collaborators have supplied us with extensive ground truth data from a 220,000 ha woodland and forest study areas within central Queensland, Australia. The field measurement is at the individual tree level. We can simulate the polarimetric backscattering for the ground measurement. AIRSAR data of the same area are obtained to validate the model simulation. The results show good agreement between the model simulation and

SAR measurements. Analyzing an individual layer's contribution offers better understanding of canopy composition effects on backscattering. The multilayer canopy configuration improves the estimate accuracy over that from a crown-trunk layer model, as in the older version of MIMICS. [C4797]

"Feasibility and design of the surface penetrating radar for lunar lander"

This presentation describes some issues about the surface penetrating radar for lunar rover. The radar is proposed for the China's lunar landing program, which is to be conducted after the launch of the lunar satellite. [C4798]

"Clutter statistical analysis for high resolution SAR data"

The ONERA RAMSES system (Radar Aeroporte Multi-spectral d'Etude des Signatures) is a flexible SAR system in constant evolution developed mainly as a test bench for new technologies and to provide specific data for TDMI (Target Detection, Recognition and Identification) algorithm evaluation. It is flown on a Transall C160 platform operated by the CEV (Centre d'Essais en Vol). Recently, the system was upgraded to include a very high resolution mode in X, Ku and Ka bands. The resolution cell is then only a few wavelength wide and the usual hypothesis underlying the speckle phenomena, i.e., a large number of scatterers per resolution cell, is not verified. This work presents the analysis made on the clutter statistical behavior and contrasts the change of behavior observed when shifting from medium resolution to high resolution to very high resolution. It is based on actual radar data acquired with the RAMSES radar system. A new parameter identifying the largest spatial resolution for which the natural surface can no longer be considered homogeneous (in a speckle based criteria) is proposed. This parameter characterizes the scale of the contributing scatterers. [C4799]

"Simulation of distributed Spotlight raw data from X-SAR/SRTM Stripmap data"

This paper describes the simulation of Staring Spotlight as well as Sliding Spotlight distributed target raw data sets from Stripmap raw data, using a time variant bandpass filter. Examples of simulated raw data generated from X-SAR/SRTM Stripmap raw data, are shown for both, Staring as well as Sliding Spotlight modes. The simulated raw data are processed using the TerraSAR-X Spotlight processor. The focused data are compared to the results of the operational X-SAR/SRTM Stripmap processor. Quality analyses of a point target contained within the data, demonstrate the applicability of both, the simulation approach and the TerraSAR-X Spotlight processor [C4800]

"Raw signal simulation for very high resolution SAR based on polarimetric scattering theory"

A method for raw signal simulation for extended SAR scenes with very high resolution is described. This simulator can handle resolution better than 1 m, squinted geometry, elliptical orbit motion and use a polarimetric reflectivity matrix. Classical polarimetric scattering theory is based on electromagnetic harmonic fields using Maxwell's equations, Green's function, Huygens' principle and Kirchhoff's approximation. Here, the scattering theory is modified for a chirp field. Calculated expressions for the scattered chirp field or the reflectivity matrix are presented. Such a reflectivity matrix can then be input to the inverse-EETF4 for raw data generation [C4801]

"Structure extraction from high resolution SAR data on urban areas"

This article handles with the problem of man-made structure extraction in high resolution Synthetic Aperture Radar (SAR) data. The ability of new sensors to provide fine resolution imagery of the Earth surface leads to new remote sensing applications. As a matter of fact, the extraction and recognition of smaller and smaller structures in crowded environment is now possible: in dense urban areas the detection of structures from building to car is expected. In this article, a chain of structure extraction in urban areas is proposed: the problem is split into different levels, detecting at each level smaller and smaller structures. In this framework, road extraction is considered and two algorithms based on dynamic programming and Hough transform are proposed and merged. [C4802]

"Improving coherence estimation for high-resolution polarimetric SAR interferometry"

This work presents a new method for filtering the coherence map issued from Synthetic Aperture Radar (SAR) polarimetric interferometric data. For each pixel of the interferogram, an adaptive neighborhood is determined by a region growing technique driven by the amplitude image information. Then, pixels in the derived adaptive neighborhood are complex averaged to yield the filtered value of the coherence, after performing a phase compensation step. The proposed method has been applied on airborne high-resolution polarimetric interferometric SAR images. Both subjective and objective performance analysis, including coherence edge detection, shows that the proposed method provides better results than the standard phase-compensated fixed

multi-look filter and a linear adaptive coherence filter proposed by Lee et al. [C4803]

"Improved ship detection using polarimetric SAR data"

The improvements in ship detection performance that can be obtained by using polarimetric synthetic aperture radar (SAR) data as compared to single-channel SAR data are investigated. Statistical decision theory is used to define decision variables that quantify the trade-off between the probability of missed detection and the probability of false alarm; performance is characterized by calculating receiver operating characteristics from single-channel and polarimetric SAR data by using likelihood ratio tests with the Neyman-Pearson criterion. It is shown that improvements in detection performance can be obtained with polarimetric SAR data as compared to single channel SAR data. We evaluate the results of these algorithms applied to single channel, dual channel amplitude only, dual channel with amplitude and phase, and fully polarimetric SAR data of known ships. In this way, the relative improvement in ship detection performance that is realized by introducing polarimetric information is quantified [C4804]

"Retrieval of building shapes from shadows in high resolution SAR interferometric images"

Discontinuous objects, such as buildings, produce shadows in SAR images. Shadows are striking features which greatly help in the image understanding. Due to the high density of buildings in urban areas, shadows cover a large part of the image and provide a major hint to build a map of the city. A straightforward use of the shadows is to determine the building height from the shadow dimensions. We propose another approach here which makes use of the shadow to help in detecting the building itself when a high resolution interferogram is available. Starting from an amplitude image with very high definition and the corresponding interferogram, we model the building detection problem as an energy minimization where the interaction between a building and its shadow is taken into account. The method allows to obtain excellent detections especially for high or isolated building, despite the important noise level. [C4805]

"Potential of coherent decompositions in SAR polarimetry and interferometry"

A comparative study has indicated that coherent decompositions may have high potential in applications using fully polarimetric and interferometric SAR data, as an alternative or supplement to standard non-coherent techniques developed during the last decade. One important reason for this seems to be that the coherent techniques are better able to benefit from the coherent nature of the underlying data and scattering mechanisms. By avoiding averaging at the first processing stage, the coherent techniques can extract target features that may otherwise be lost in the early averaging process. On the other hand, averaging is indeed important in most cases for obtaining stable and reliable end results. [C4806]

"Efficient hybrid stripmap/spotlight SAR raw signal simulation"

Recently, a new operating mode for Synthetic Aperture Radar (SAR) system, referred to as hybrid stripmap/spotlight mode, has been presented. In the hybrid acquisition mode the radar antenna beam is steered about a point farther away from the radar than the area being illuminated, thus generating microwave images with an azimuth resolution better than that achieved in the stripmap configuration, and a ground coverage better than the one of the spotlight configuration. The subject of design, processing and data interpretation for the hybrid SAR mode is gaining an increasing interest in the remote sensing scientific community. Consequently, a hybrid SAR raw signal simulator is strongly required, especially when real raw data are not available yet, to test processing algorithms and to help mission planning. In addition, to analyse the effects of processing errors and to verify the impact of different system design choices on the final image for different kinds of imaged scenes, an extended scene SAR raw signal simulator is very useful: it is what we present in This work. After showing that in this case a 2D Fourier domain approach is not viable, we demonstrate that a 1D range Fourier domain approach, followed by 1D azimuth time domain integration, is possible when some approximations, usually valid in the actual cases, are accepted. [C4807]

"Radiometric resolution optimization for future SAR systems"

This paper presents a radiometric resolution optimization strategy which can be used in new generation of Synthetic Aperture Radar (SAR) systems. An expression, which allows optimization depending on application, has been developed for this purpose. In particular, special effort has been made for improving the radiometric resolution keeping the geometric resolution constant. Optimization examples have been carried out with realistic parameters taken from TerraSAR-X. The objective is to provide an effective and realistic way to tradeoff the instrument parameters for optimal exploitation of SAR images. Furthermore, a precise SNR formulation has been derived including processing gain and noise distribution [C4808]

"Near nadir scattering properties at W-band frequency for the sea surface"

The sea surface is considered a useful natural calibration target for satelliteborne cloud profiling radar with a narrow antenna beam. However, the normalized radar cross section (NRCS) of the sea surface at W-band frequency is not well known. It is known that the NRCS depends on the wind speed and direction over ocean. We made experiments to measure sea surface NRCS under various conditions using NICT's W-band airborne cloud profiling radar (SPIDER). The sea surface properties measured in this experiment are similar to these measured with microwave scatterometers at other frequencies [C4809]

"Robust radiometric terrain correction for SAR image comparisons"

We demonstrate a robust technique for radiometric terrain correction, whereby terrain-induced modulations of the radiometry of SAR imagery are modelled and corrected. The resulting normalized images may be more easily compared with other data sets acquired at different incidence angles, even opposing look directions. We begin by reviewing the radar equation, pointing out simplifications often made to reduce the complexity of calculating the backscatter coefficient, normalized either by ground area (σ_0), or illuminated area projected into the look direction (γ_0). The integral over the illuminated area is often approximated by a scale factor modelling a simple planar slope, departing only slightly from "ideal" flat terrain: for γ_0 , the radar brightness (β_0) is normalized via modulation with the tangent of the local incidence angle. We quantify the radiometric errors introduced by ignoring terrain variations, comparing results based on (a) a robust radar image simulation-based approach properly modelling variations in local illuminated area, and (b) an ellipsoidal Earth assumption. A second simplification often made in solving for backscatter using the radar equation is the assumption that the local antenna gain does not vary significantly from a simple model draping the antenna gain pattern (AGP) across an Earth ellipsoid, returning the local antenna gain as a function of slant range alone. In reality, the AGP is draped across the Earth's rolling terrain retrieval of properly calibrated backscatter values should model these variations and compensate for them: although smaller than the errors caused by not properly modelling variations in local illuminated area, they can be significant. We use well-calibrated and annotated ENVISAT ASAR images acquired over Switzerland to show how robust radiometric terrain correction, incorporating models for the variations of local illuminated area with terrain enables calibrated mixture of imagery acquired at differing incidence angles. Only robust retrieval of backscatter values enables such inter-mode comparisons—a capability that significantly reduces the required revisit time for monitoring changes to the radar backscatter. In conclusion, we describe a technique for combining a set of terrain-geocoded and radiometrically calibrated images derived from ascending and descending passes and multiple incidence angles to create composite radar backscatter maps. At each point, the contribution of each image to the composite is weighted according to its local resolution. The resulting composite image manifests relatively uniform high ground resolution, even in highly mountainous terrain [C4810]

"Azimuth phase coding for range ambiguity suppression in SAR"

A novel ambiguity suppression technique is proposed. Range ambiguities in synthetic aperture radar (SAR) images are eliminated with an azimuth filter after having applied an azimuth phase modulation to the transmitted pulses and a corresponding demodulation to the received pulses. The technique excels by actually eliminating the ambiguities rather than just defocusing them as most other techniques do. This makes the proposed technique applicable to distributed targets. The range ambiguity suppression permits the pulse repetition frequency (PRF) to exceed the upper limit otherwise defined by the antenna elevation dimension. The fundamental antenna area constraint still applies, but the PRF can be chosen with more freedom. In addition to ambiguity suppression, potential applications include nadir return elimination and signal-to-noise ratio improvement [C4811]

"A polarization-rotating Van Atta array reflector and its application to polarimetric radar calibration"

This paper presents the principle, design, and measured characteristics of a 90-degree polarization-rotating Van Atta array reflector with suppressed scattered field as a reference target for polarimetric radar calibration. A polarimetric calibration method that uses a trihedral and the present reflector needs no assumptions on scene characteristics and statistics and no independent phase calibration [C4812]

"New aspects of bistatic SAR: processing and experiments"

The interest in bistatic synthetic aperture radar, using separated transmitter and receiver flying on different platforms, has been increasing rapidly over the last years. The reason for this is specific advantages, like the reduced vulnerability in military systems, forward looking SAR imaging, additional information about the target, or increased RCS. Nevertheless, besides technical problems-like the synchronisation of the oscillators, the involved

adjustment of transmit pulse versus receive gate timing, antenna pointing, flight coordination, double trajectory measurement and motion compensation-the processing of bistatic radar data is still not sufficiently solved. Some of the possibilities and problems discussed. The second part of This work deals with a bistatic experiment performed in November 2003: two SAR systems of FGAN have been flown on two different airplanes, the AER-II system has been used as a transmitter and the PAMIR system as a receiver. Different spatially invariant flight geometries have been tested. High resolution bistatic SAR images were generated successfully. [C4813]

"SAR signal reconstruction from non-uniform displaced phase centre sampling"

The displaced phase centre (DPC) technique enables a wide swath SAR with high azimuth resolution. In a classic DPC system, the PRF has to be chosen such that the SAR carrier moves just one half of its antenna length between subsequent radar pulses. Any deviation from this PRF results in a non-uniform sampling of the synthetic aperture. This paper shows that an unambiguous reconstruction of the SAR signal is also possible in case of such a non-optimum PRF. For this, an innovative reconstruction algorithm is derived, which enables a recovery of the unambiguous Doppler spectrum also in case of a non-uniform sampling of the synthetic aperture. This algorithm also has a great potential for multistatic satellite constellations as well as the dual receive antennas in Radarsat II and TerraSAR-X [C4814]

"Synchronisation of bistatic radar systems"

Bistatic radar is gaining more and more interest over the last years. It offers more freedom to deploy the transmitter and the receiver, e.g. in a way to enhance the signature of stealthy targets. Furthermore, the bi- or multistatic system can be realized without using expensive transmit/receive-modules. An additional feature of bistatic radar is that continuous wave signals can be used. A crucial problem associated with bi- and multistatic systems is the synchronisation of time and frequency at the transmitters and receivers for coherent signal processing and range measurement. Modern communications satellites and world wide accessible GPS signals allow to synchronise the time easily over a long period with a time difference of less than 1 ns. The required frequency stability depends on the baseline and may vary with application. Image generation with bistatic SAR systems requires a frequency coherence for at least the coherent integration time. For interferometric SAR systems this coherence has to be expanded over the whole processing time. The paper concentrates on the problem of time and frequency synchronisation between a bistatic transmitter and receiver pair. Possible solutions for attaining the requirements of bistatic radar systems are discussed. [C4815]

"Impact of ambiguities in multistatic SAR: some specificities of an L-band interferometric cartwheel"

An important question with respect to the performance of the interferometric cartwheel and similar bistatic SAR systems, is whether the ambiguities combine coherently and introduce artifacts in the resulting interferograms. We here review the theoretical behavior of range and azimuth ambiguities and extend the description to the case of non-zero Doppler processing. Simulation results confirm that ambiguities cannot significantly degrade the performance of an L-band interferometric cartwheel [C4816]

"Algorithms for ship detection and tracking using satellite imagery"

Ship detection and tracking are important to maintain a Recognized Maritime Picture (RMP). Satellite surveillance provides wide area coverage but is often limited by revisit times and by the time taken to process the imagery, analyze it and send messages in an appropriate format to update the RMP. The paper describes the development of a new ship detection and tracking program that is designed to analyze processed imagery rapidly and inexpensively and to deliver messages automatically by email in the OTH Gold format. The message can include ship position, length, heading and speed. The program structure is designed to be versatile, flexible and extendable and a RADARSAT image can be loaded and analyzed and a message sent typically in less than one minute [C4817]

"Retrieval of ocean surface wave fields using marine radar-image sequences"

This paper describes and validates an empirical method for inversion of marine radar-image sequences to time series of ocean surface wave fields without calibration. External sensors are not required. The radar system can measure as a stand-alone device. The method has been developed within the framework of the European project "MaxWave" and is based on a local description of the RCS in space and time, whereby the ocean surface is subdivided into local facets. A local transfer function between local RCS and ocean surface is determined for each facet. The inversion scheme is applied to radar-image sequences acquired by a marine X-band radar, operating at grazing incidence and horizontal polarization in transmit and receive. The system is mounted aboard an offshore platform in the North Sea. The ocean-surface image sequences are validated by comparison of the calculated significant wave heights with values from co-located wave records of three in-situ

sensors. It is shown that the accuracy of the radar-retrieved significant wave height is within the accuracy of the in-situ sensors [C4818]

"A new historic ERS wave mode data set for oceanographic applications"

Since 1991, the ERS satellites have collected high resolution SAR data over the oceans on a global and continuous basis. Operating in wave mode the ERS SAR yields a patchy coverage of the oceans with about 1500 images of 10 by 5 km size each day. These data have recently been shown to be able to deliver wind speed and wave spectra as well as information on individual waves. In the scope of the ESA AO WaveAtlas, the ERS-2 raw data acquired in 1999 and 2000 are reprocessed to single look complex imageries. This paper describes the necessary steps for the reprocessing of historic wave mode data including an assessment of the effort required to reprocess all available ERS wave mode raw data archived at ESA. Furthermore the paper demonstrates the potential of these data for different oceanographic applications. Special emphasis is put on wind, wave and sea ice measurements. In addition atmospheric features can be analyzed. The data in particular enable the estimation of two-dimensional sea surface elevation fields which are of high practical relevance for ship design or offshore operations. Mean wave parameters like the mean period derived from SAR wave mode data can be used for the assimilation of numerical wave models thus helping to improve wave forecast. Global maps of mean and individual wave parameters are presented. The reprocessing of wave mode data is planned to be extended to the full lifetime of ERS-1 and ERS-2, which is at least 1991-2004. This allows the derivation of wave climatologies on a decadal basis in particular enabling the analysis of climate trends. As wave mode data are also available from the ENVISAT mission a consistent update of these climatologies is possible [C4819]

"A simple algorithm for spatial disaggregation of radiometer derived soil moisture using higher resolution radar observations"

The SMEX02 experiments held in June-July 2002, at Iowa demonstrated the potential of an L band radiometer (PALS) in estimation of near surface soil moisture under dense vegetation canopy conditions. The L band radar was also shown to be sufficiently sensitive to near surface soil moisture. However, the spatial resolution of a typical satellite mounted L band radiometer is of the order of 10's of kilometers which is not sufficient to serve the science needs of land surface hydrology and weather modeling applications. Disaggregation schemes for deriving sub pixel estimates of soil moisture from radiometer data using higher resolution radar observations hold the promise of making global soil moisture observations at much finer scale available. The HYDROS instrument is proposed to have an L band radiometer and L band radar onboard. The passive instrument has spatial resolution of the order of tens of kilometers and operates along with the active instrument that takes observations at a resolution of tens of meters. This paper presents a simple approach for disaggregation of coarser resolution radiometer estimates of soil moisture using higher resolution radar backscatter measurements. The algorithm has been applied to a coincident PALS radar/radiometer and AIRSAR dataset acquired during the SMEX02 campaign [C4820]

"Extreme wave statistics from radar data sets"

The objective of this paper is the identification of areas of extreme wave events, in which rogue waves of exceptional height and shape do occur. These extreme waves are dangerous for navigation safety, as well as the operability on board offshore platforms. An explanation for the existence of groups of high waves based on the superposition of wave systems that form a solution of the linear wave equation is given. Synthetic Aperture Radar wave mode images from the ERS and ENVISAT satellites are investigated. These images are acquired every 200 to 100 km along the satellite orbit and thus yield global coverage. For ERS these images had to be specially reprocessed from radar raw data, for ENVISAT the imageries are now available as a standard ESA product. High wave groups were found in situations of storm systems moving with the group speed of the ocean waves. The highest waves occurred near the center of the lows in the region of high wind speed [C4821]

"Investigation of typhoons using ERS-2 SAR wave mode data"

It is well known that typhoons are hard to forecast because of their complicated dynamical behaviour. In this study a new global data set of reprocessed ERS-2 wave mode data is used to study typhoons assessing the potential of these data for improving typhoon forecast. Operating in wave mode the ERS SAR acquires high resolution images of 10 by 5 km size every 200 km along the track yielding a patchy coverage of the global oceans with about 1500 scenes taken each day. The images contain information on both ocean waves and near surface wind. The typhoon TRINING in November 1999 is analyzed. Local wind speeds are estimated from the SAR image intensity. Results are compared with collocated ERS-2 altimeter measurements of wave height and wind speed as well QuikScat wind vectors. The potential of the high resolution SAR information with regard to the analysis of rain cells and atmospheric turbulence is discussed. SST measurements obtained from spaceborne

radiometers are used as complementary information. The combined use of altimeter wind speeds and radar cross sections obtained from SAR to estimate wind vectors is investigated [C4822]

"Ocean surface winds retrieved from marine radar-image sequences"

A new method for wind-field retrieval with spatially and temporally high-resolution using marine radar-image sequences is presented. The method is based on analyzing the movement of wind gusts, which become visible in radar image sequences after filtering. In contrast to previous methods, this new technique requires no calibration phase of the radar system. The retrieved wind directions are compared to wind directions of the recently developed method, where wind directions are extracted from wind induced streaks that are orientated in wind direction. Wind speeds are derived from the backscatter of temporal integrated radar-image sequences using an empirical model function, which was parameterized by training a Neural Network. The different methods are applied to radar image sequences acquired by a marine X-band radar mounted aboard an offshore platform in the North Sea. The radar derived winds from more than 1300 radar-image sequences are compared to in-situ wind data measured at the platform. In contrast to traditional offshore wind sensors, the retrieval of the wind field from the backscatter of the ocean surface makes the system independent of the sensors motion and installation height and reduces the effects due to platform induced blockage and turbulence effects [C4823]

"A strip adaptive processing approach for the SMOS space mission"

This article is concerned with the apodization windows to be applied to brightness temperature maps reconstructed from complex visibilities provided by the MIRAS (Microwave Imaging Radiometer with Aperture Synthesis) instrument on board the SMOS (Soil Moisture and Ocean Salinity space mission) spacecraft in order to achieve a close to uniform pixel at the Earth's surface level [C4824]

"Observations of near-inertial internal waves in the East (Japan) Sea by Synthetic Aperture Radar"

Propagation of near-inertial (18 hours) internal waves were observed on the western part of East (Japan) Sea during May 18 and 19, 2004 from C-band Synthetic Aperture Radar (SAR) image data. Current and temperature measurements carried out during the field experiment from 10 May to 9 June, 2004 (IWXS2004, Internal Wave Experiment in the East Sea), were analyzed to study why near-inertial internal wave can be seen in SAR image and how it evolves. The spatial distributions of horizontal wavelength and the phase speed estimated from the successively acquired two SAR images, are consistent with those inferred from water temperature and current measurements obtained during the field experiment. Based on these two independent observations (SAR and IWXS2004) we report that the observed wave patterns in the SAR images during IWXS2004 are near-inertial internal waves propagating into the east coast of Korea with phase speed of about 0.3 m/s [C4825]

"Analysis of island wakes and katabatic winds imaged by RADARSAT-1 synthetic aperture radar"

In this study, the sea surface imprints of strong mountain katabatic winds and gap winds are observed on RADARSAT-1 synthetic aperture radar (SAR) ScanSAR wide images off the west coast of the U.S. and in the Gulf of Alaska. Two case studies are presented. In the first case study, a RADARSAT-1 SAR scene taken at 14:25:30 UTC on January 21, 2003 shows a finger-like wind pattern that mirrors the coastal mountain height. In the second case, the SAR image was taken at 4:41:45 UTC on December 22, 1999. It shows a strong gap wind and vortex streets through the Aleutian Islands. In order to understand the dynamics of these wind patterns observed in the SAR images, we simulated the low level atmospheric circulation using the fifth-generation Pennsylvania State University (PSU)-National Center for Atmospheric Research (NCAR) Mesoscale Model, MM5. A triple nested-grid (9/3/1 km) technique is employed to achieve a multi-scale simulation. In general the MM5 model captures the wind pattern very well and reveals the dynamics of these meso-scale atmospheric phenomena. However, the MM5 did not resolve the vortex shedding due to the model resolution and the complex nature of this phenomenon [C4826]

"Assimilation of remotely sensed soil moisture into a hydrologic model"

We discuss the assimilation of remotely sensed soil brightness temperature into a runoff prediction model. Data used in this study was acquired during the 2002 Soil Moisture Experiments (SMEX02) near Ames, IA. The Passive and Active L- and S-band (PALS) instrument was flown for six days of the study before and after a major rain event in the region. We combine a radiative transfer model and observed PALS brightness temperatures to estimate soil moisture within the top five centimeters over watershed. These estimates are assimilated into the active soil layer in a distributed runoff model. Runoff estimates are compared to observed stream gauge measurements within the watershed [C4827]

"Calibration and validation plans of ALOS optical sensors"

This paper introduces the updated plans for sensor calibration and product validation of the two optical sensors i.e., the Panchromatic Remote-sensing Instrument for Stereo Mapping (PRISM) and the Advanced Visible and Near Infrared Radiometer type-2 (AVNIR-2), which are to fly on the Advanced Land Observing Satellite (ALOS). PRISM consists of three panchromatic radiometers, and is used to derive Digital Elevation Models (DEMs) with very high spatial resolution, which is also one of the objectives of the ALOS mission. The geometric calibration is important in generating a highly accurate DEM by using PRISM's triplet images. Highly accurate ground control points (GCPs) are necessary to calibrate the geometric accuracy and validate the generated DEM. The geometric calibration of AVNIR-2 can be done using the calibrated PRISM product. In this paper, we describe the current plans for calibrating and validating PRISM and AVNIR-2. In particular, preparation status of GCPs with evaluation items for geometric calibration, including expected problem effects regarding geometric accuracy, orbit and observation simulations to determine pointing accuracy, and preliminary investigation of nighttime GCP using current available satellite images [C4828]

"On the use of symmetric scatterers for calibration and validation of PALSAR polarimetric modes"

PALSAR L-band SAR is affected by Faraday rotation. In this study, PALSAR system is briefly described, and Freeman's method is considered for the calibration of PALSAR. Unless channel imbalances are measured abroad, a reference point target has to be deployed for each scene to be calibrated. For practical reasons, the use of symmetric targets is investigated for calibration and validation of polarimetric PALSAR data [C4829]

"High resolution InSAR "Builtscapе" improvement using LIDAR as ancillary data"

In this paper, we analyze a multiple sensor data set corresponding to three-dimensional data coming from interferometric radar (InSAR) or laser ranging (LIDAR) measurements. LIDAR and InSAR are now mature technologies, and there are examples of their usefulness for urban area characterization. Unfortunately InSAR measurements show a serious disadvantage in describing built areas, due to problems derived from radar ranging. As a matter of fact, the possibility to have in the same area LIDAR data can reliably help in correcting all these effects. The advantage of LIDAR and InSAR joint use resides in exploiting the higher resolution offered by laser data and comes from the fact that LIDAR data is more expensive, and usually at the same cost we may obtain InSAR data on a much wider area than the one obtainable with a laser scanning survey [C4830]

"Comparison of ocean surface vector winds observed by SeaWinds on ADEOS-II with ocean buoy data"

Wind vectors observed by SeaWinds on ADEOS-II are compared with wind and wave data from offshore moored buoys. The wind data were collocated with buoy observations operated by the National Data Buoy Center (NDBC), Tropical Atmosphere Ocean (TAO), and Pilot Research Moored Array in the Tropical Atlantic (PIRATA) projects. Only buoys located offshore and in deep water were selected. Temporal difference and spatial separation between the ADEOS-II/SeaWinds and buoy observations were limited to less than 10 min. and 12.5 km. Wind speeds measured by the buoys at various height above the sea surface were corrected to equivalent neutral winds at a height of 10 m. Wind speeds and directions observed by ADEOS-II/SeaWinds agree well with the buoy data. Root-mean-squared differences of the wind speed and direction are 0.93 m/s and 20.7 deg., respectively. Dependences of the residuals of wind speed and direction on the wind speed and cross-track cell locations are investigated. Dependences of wind speed residuals on oceanographic and atmospheric parameters observed by buoys are also examined using the collocated data. No significant dependences on the sea surface temperature, atmospheric stability, and sea state are discernible [C4831]

"Snow covered area retrieval using Envisat ASAR widesswath in mountainous areas"

It has previously been shown that wet snow can be detected using ERS SAR repeat pass imagery where a reference image is captured during cold dry snow conditions and subtracted from the image one want to classify. We have extended and validated this technique for retrieving snow covered area (SCA) using Envisat ASAR wide swath data (500 by 500 km swath coverage, 100 meter resolution), covering the mountainous regions of Southern Norway. The algorithm has also been extended to postulate dry snow above areas with wet snow, thus giving a total snow covered area that is comparable to SCA from optical sensors. A sliding window technique has been applied to facilitate the dry snow classification. The method has been implemented in a near-real time environment and has been run pre-operationally in Norway in 2004. The relatively large coverage allows SAR to become an operational tool for snow monitoring, as opposed to standard modes used in previous works. In order to improve snow classification we have used air temperature data from the Norwegian meteorological station network to create high-resolution surface air temperature maps. These maps are used to filter wet snow from reference images and prevent incorrect classification of dry snow. Snow covered area maps for South Norway

has been derived for the spring melt season with a one-week temporal resolution. The results are validated against optical sensor retrievals (MODIS, ASTER) and high accuracy field measurements. [C4832]

"Assessment of wetland ecosystems and flooding in the Tonle Sap Basin, Cambodia, using AIRSAR"

AIRSAR data were collected over the Tonle Sap and Angkor regions of Cambodia during the NASA-Australia sponsored PACRIM2 Mission flown in September 2000. This imagery was interrogated to produce a flood map of the western end of the TSGL against which subsequent seasonal changes in the extent and duration of flooding can be made using other radar and optical datasets acquired from spaceborne sensors. In addition, the multi-parameter capabilities of AIRSAR were used to classify and map the structure, composition and extent of wetland vegetation communities present at the time of data capture [C4833]

"InSAR-based hydrology of the Everglades, South Florida"

New space-based observations of South Florida reveal spatially detailed, quantitative images of water levels in the Everglades, the focus of the largest wetlands restoration project yet attempted. The new data capture dynamic water level topography, providing the first three-dimensional regional-scale picture of wetland sheet flow. We observe localized radial sheet flow in addition to well-known southward unidirectional sheet flow. Our study shows that space-based hydrological observations can provide critical information for monitoring, understanding and managing wetland sheet flow, and contribute to wetland restoration [C4834]

"Retrieval of snow characteristics from spaceborne scatterometer data"

We study the feasibility of using space borne scatterometer (QuikScat onboard SeaWinds) data for retrieval of snow parameters in Finland: onset of snow melt, end of snow melt, and fraction of snow-covered area during the seasonal snow melting period. The results are based on satellite and ground truth data for 21 test sites in Finland covering the winters of 1999-2000, 2000-2001 and 2001-2002. Radar-derived time series of snowmelt are produced and compared with corresponding snow products based on optical MODIS spectrometer data. [C4835]

"Recent anomalies in Great Lakes ice cover based on statistical analysis and observation"

In this work, the anomalous change in ice cover on the Great Lakes was observed and recorded during our GLAWEX1997, GLAWAEX2002 and GLAWEX2003 field experiments on the upper Great Lakes. The objective of the experiments is to develop algorithms to map and classify ice using satellite synthetic aperture radar (SAR) and scatterometer data. Moreover, the large spatial and high temporal coverage of satellite scatterometer measurements with its all-weather, day/night sensing capabilities make it well suited to map and monitor Great Lakes ice cover to extend the historical climatological record that was largely developed using aircraft observations [C4836]

"Range and velocity ambiguity mitigation techniques for the WSR-88D weather radar"

Several mechanisms are currently provided to alleviate effects of range overlaid echoes and velocity aliasing in the Weather Surveillance Radar-1988 Doppler (WSR-88D). However, due to limitations in these techniques, observation of severe weather phenomena is significantly impaired. This paper presents results from a multi-year study at the National Severe Storms Laboratory dealing with methods to mitigate the effects of range and velocity ambiguities in the WSR-88D [C4837]

"Analysis of nonlinear ocean wave features in synthetic aperture radar imagery"

Spaceborne Synthetic Aperture Radar (SAR) is a reliable tool to analyze sea states in the open ocean on a global scale. The sea state information obtained from SAR systems is mainly based on two different approaches. The first approach considers the spectral description of a sea state in terms of the so-called directional wave spectrum. The second more recent approach provides estimations of the wave elevation fields in two dimensions, which permits to detect individual wave heights. Both approaches consider a linear wave field (i.e. a linear superposition of single monochromatic wave components). Although the linear wave theory is sufficient to explain most of the mean statistical features of sea states, it is not able to describe properly some wave phenomena, such as the asymmetries between wave crests and troughs, which are of special interest for off-shore platform and ship designers. This work analyses the effects of nonlinear wave field features in the SAR imaging mechanisms in order to detect these phenomena on the SAR images of the open ocean. [C4838]

"Passive microwave detection of bubble wakes"

Microwave detection of ocean (sub)surface bubble populations including patches, patterns, flows, and wakes is considered. The physical principles are based on specific electromagnetic properties of the air-bubble-water media that produce strong anomalies in ocean thermal microwave emission, especially at X- C-, S- and L-bands (e.g., at wavelengths of 4, 6, 8, 18, and 21 cm). Related model estimations are presented. [C4839]

"Lightweight linear broadband antennas enabling small UAV wing systems and space flight nanosat concept"

The RadSTAR initiative merges an interferometric radiometer with a digital beam forming scatterometer, providing Earth surface backscatter and emission measurements. Heretofore these instrument developments have been designed for low flying brown platforms such as the NASA P-3. Commercial-off-the-shelf design materials can be used to inexpensively build antennas that approximate free-space permittivity, enabling remote sensing of soil moisture levels locally using small Unmanned Aerial Vehicles (UAVs). A foam/free-space sandwich can be used to minimize the weight of the dielectric backing structure. This technique enables rapid prototyping with space-grade materials. A low-mass 3-element antenna array of this design is already baselined for a University nano-satellite mission. A light-weighted version of the L-band Imaging Scatterometer (US) radar electronics is being developed for a Small Business Innovative Research (SBIR) program. This lightweight wing antenna has a large potential payoff to NASA. For example, it may enable an active/passive hydrology mission using a fleet of low cost small UAVs. A mesh ground plane can further reduce the overall mass and stowability of the very large antennas required for spaceborne observations at L-Band. The cross track scan success criterion was met at L-Band frequencies for radar and radiometry. That is, we designed and prototyped a wideband antenna patch tunable in this range and additional work is being earned out to improve the cross polarization isolation. Making the present broadband design into arrays will be limited to one dimension due to array spacing and the aspect ratio of the patch elements. A fore and aft Doppler beam synthesis and the US cross-track beam forming concept will be considered for potential application to surface hydrology measurements using these arrays [C4840]

"Marine radar imaging of nearshore bar structure: biases due to tidal and RMS wave height variations"

We present results of an experiment using a marine radar to image the surface roughness patterns due to wave breaking and energy dissipation over coastal offshore sand bars. Data were collected at the US Army Coastal Engineer Field Research Facility research pier, Duck, NC. The experiment was designed to compare marine radar and video imaging mechanisms of wave breaking and dissipation that is responsible for surface expression of the bar using the two methods. The approach uses half-hourly averages of a sixty-second sequence of thirty-two images of wave propagating onshore. This averaging causes individual wave patterns to smear out to a weak background level, and the region of enhanced wave breaking and dissipation over the bar to stand out in the image. The experiment studies the bar location shore-normal biases associated with the effects of local mean tide height and rms wave height in their role of determining the location of wave breaking and dissipation relative to the bar position. In this work we show examples of the analysis used, with comparisons made between video imaging and the radar imaging approaches. Quantitative comparisons of offshore bias are presented at the conference [C4841]

"Laboratory study of fine structure of the short surface waves due to breaking: two-directional wave propagation"

This study was stimulated by the need to identify the influence of breaking on the evolution on the short surface wave field, responsible for microwave scattering. Laboratory measurements of the fine space-time structure of short gravity-capillary waves and Ku-band scattering at grazing and moderate incidence by spilling and plunging breaking waves in a laboratory wave channel are presented. Unsteady breaking waves are generated by focusing wave groups in space-time domains. A line-scanning laser slope gauge was used for measuring capillary-gravity waves from 2 mm to 20 cm wavelengths and frequency ranges up to 150 Hz. A dual polarized (VV, HH) coherent pulsed Ku-band scatterometer with temporal resolution of 3 ns was used to obtain simultaneously Doppler spectra of the scattered signals from the breaking area for grazing angles from 6 to 25 degrees. Two-dimensional filtering in the wave number-frequency plane, as well as plus/minus Doppler spectra was used to separate the direction of propagation of the surface waves within the breaking region. It was found that the breaking splash is the main source of the surface wave generation. The short surface wave slope fields produced by breaking could be separated into short (4-8 mm wavelength) fast waves, having a phase velocity equal to the velocity of the crest of the breaking dominant 1 Hz waves, and free gravity-capillary waves. Both types of waves were found to co-and counter-propagate relative to the dominant wave propagation

direction. The Doppler spectrograms reveal the presence of high frequency waves at the moment of breaking that can be associated with short fast waves. The low frequency part of the Doppler spectrogram is consistent with the appearance of free gravity waves. [C4842]

"Environmental sensitivity mapping for oil spill in the Amazon coast using remote sensing and GIS technology"

Accidental oil spills may impact sensitive wetlands in the Amazon coast. To generate an environmental sensitivity index (ESI) maps were used: (1) JERS-1 SAR data; (2) RADARSAT-1 data in the W1 beam mode; (3) X-band mosaics of the RADAM Project; and (4) SRTM digital elevation models. As result was identified artificial structures (break water and peers) and nineteen coastal features and environments subject to oil spill. The lowest ESI was assigned to cliffs (ESI 1) and the highest to mangroves and fresh wetland zones (ESI 10a and 10b). An annual monitoring of both natural and human-induced changes would provide invaluable information for the construction of multitemporal sensitivity index maps to oil spills in different seasons and tidal cycles [C4843]

"Detection of surface mines using hyperspectral sensors"

Hyperspectral imaging is an important technology for the detection of surface and buried land mines from an airborne platform. For this reason, hyperspectral was included in the two experiments that were executed by the Army RDECOM Night Vision and Electronic Sensors Directorate (NVESD) in Fall 2002 and in Spring 2003. The purpose of these experiments was to bring together a wide variety of airborne sensors for the detection of mines, with well ground-truthed targets. The hyperspectral sensors included the Airborne Hyperspectral Imager (AHI), a University of Hawaii LWIR HSI sensor and the Compact Airborne Spectral Sensor (COMPASS), an NVESD VNIR/SWIR sensor. These experiments were carried out at sites where an extensive array of buried and surface mines were deployed. At the first experiment called Forest Fusion I, the mines were deployed against several different backgrounds ranging from bare dirt to long grass. For the second experiment, called Desert Fusion, the mines were placed on backgrounds ranging from loose sand to mixed sand and vegetation. The COMPASS and AHI sensors were both placed on the Twin Otter aircraft, and data was collected with the airplane at a variety of altitudes. In this paper, the data collected on surface mines are reviewed, and specific examples from each background type presented. Spectral detection algorithms are applied to the data and the results of the algorithm processing are presented [C4844]

"Optimal polarization for the observation of ocean features with SAR"

Fully polarimetric synthetic aperture radar (SAR) data collected by AIRSAR and SIR-C/X-SAR are used to analyze radar signatures of ocean features such as ocean waves, oil slicks, ship wakes, ocean fronts and submarine topography in the China Seas. The optimal polarization (OP) for the observation of these features with SAR is given based on the analyses. [C4845]

"Analysis of scatterometer observations of Saharan ergs using a simple rough facet model"

The Sahara desert includes large expanses of sand dunes called ergs. These dunes are formed and constantly reshaped by prevailing winds. Previous study shows that Saharan ergs exhibit significant radar backscatter (sigmadeg) modulation with azimuth angle (Phi). We use sigmadeg measurements observed at various incidence angles (thetas) and Phi from the NASA scatterometer (NSCAT), the Seawinds scatterometer aboard QuikSCAT (QS-CAT), the ERS scatterometer (ESCAT) and the Tropical Rain Monitoring Mission's Precipitation Radar (TRMM-PR) to model the sigmadeg response from sand dunes. Sand dunes are modeled as a composite of tilted rough facets and small ripples. The dune fields are modeled as composed of many simple dunes. The sigmadeg measured by the scatterometer from (thetas, Phi) look direction is the sum of the returns from all the rough facets in the footprint. The model is applied to linear and transverse dunes with rough facets and Gaussian tilt distributions. The model results in a sigmadeg response similar to the NSCAT and ESCAT observations over areas of known dune types in the Sahara. This analysis gives a unique insight into scattering by large scale sand bedforms [C4846]

"Introduction, overview, and status of the Microwave Autonomous Copter System (MACS)"

Unmanned Aerial Vehicle (UAV) capabilities are evolving rapidly, from technical, regulatory and operational standpoints. It is likely that these platforms will begin to offer new alternatives for agricultural and other applications needing high spatial resolution data and delivered in near real-time. This paper presents an overview of the Microwave Autonomous Copter System (MACS) currently under development at the Center for Hydrology, Soil Climatology and Remote Sensing (HSCaRS), Alabama A & M University. An L-band (1.4-GHz), horizontal polarization, radiometer is one of the sensors that has been proposed for MACS. The UAV helicopter

system will be used for monitoring the temporal changes of soil moisture as a function of depth, even in the presence of vegetative covers. These measurements could greatly improve our understanding of soil moisture under vegetation covers that are necessary for completing algorithms of global energy and water balance products for examining variations in weather and climate. The paper describes the UAV helicopter, the microwave system and current status of the development [C4847]

"Application of QuikSCAT radiometer rain rates to near-real-time global precipitation estimates: a global precipitation mission pathfinder"

The SeaWinds scatterometer onboard the QuikSCAT satellite simultaneously measures the polarized microwave brightness temperature of the ocean/atmosphere. QuikSCAT Radiometer (QRad) brightness temperatures are used to infer instantaneous oceanic rain rates using a statistical retrieval algorithm that has been developed using collocated QRad brightness temperatures with TRMM Microwave Imager (TMI) rain rate measurements. The algorithm produces earth-located instantaneous rain rate binned in 0.5 hour universal time windows and produced on a 50-km earth grid. The orbit of QuikSCAT allows independent rain temporal sampling that can be used to improve the estimation of global rainfall in 3 hour windows, which is a goal of the future Global Precipitation Mission (GPM). In this work, QRad retrieved rain rate examples are presented and comparisons are made with the TRMM 3B42RT near real time product. Results demonstrate that QRad rain measurements agree well with these independent microwave rain observations and superior to the visible/infrared rain estimates, which demonstrates the utility of adding QRad to the 3B42RT product. [C4848]

"Parameterizations of single scattering properties of frozen hydrometeors at millimeter-wave frequencies"

Physical approaches in microwave remote sensing to measure nonspherical frozen hydrometeors are frequently parameterized as spherical particles, assuming either dielectric mixing approximation or equivalent spheres, to make Mie-theory applicable. However, the applicability of those simplified approximations in millimeter-wave radar and radiometric remote sensing of frozen hydrometeors need to be evaluated. To seek a parameterization to represent the electromagnetic (EM) properties of frozen hydrometeors at millimeter-wave frequencies, this study analyzes the Discrete Dipole Approximation (DDA) method calculated single scattering from nonspherical snow crystals at millimeter-wave frequencies (95, 140, 183, 220, and 340 GHz). Sizes, shapes, density, and refractive indices for five snow crystal models (hexagonal column, hexagonal plate, sector plate, planar rosette, and spatial rosette) employed in this study are described in Kim et al. (2004). The results shown in this study assume that all particles are randomly oriented. By comparing with the DDA calculated single scattering properties, this study evaluates fast parameterization methods to represent the EM properties of snow at millimeter-wave frequencies. Dielectric mixing theory, which is widely used by the microwave remote sensing community, and the equivalent sphere approach, which is commonly used by infrared (IR) and ultraviolet (UV) remote sensing community are considered. In addition, equivalent cylinders and equivalent ellipsoids are also tested to examine how much the single scattering properties depend on the detailed shapes of ice crystals. [C4849]

"Soil moisture measurement and retrieval using Envisat ASAR imagery"

High resolution data of the ASAR sensor aboard ESA's Envisat satellite offers the opportunity for monitoring surface soil moisture at high spatial resolution with multi-polarization and multi-incidence capabilities. Using Integral Equation Model (IEM), we simulated the backscattering coefficients of C band SAR backscatter at different incidence angles and the alternating polarization mode, and analyzed the sensitivity to soil moisture. The algorithm of inferring surface soil moisture from radar backscatter is developed according to semi-empirical model from the results of simulation and sensitivity analysis. The soil moisture map are retrieved from ASAR backscatter measurements in Hetian, Xinjinag (37°15'N, 79°48'E) area, where are the arid and semi-arid area of west China. Accuracy in the retrieval of the surface moisture content from ASAR is compared to the spatially distributed ground truth. The results demonstrate the effects of soil moisture monitoring using multi-polarization multi-incidence ASAR data. [C4850]

"Prediction of locust outbreaks from RADARSAT-1 multi-angle data"

Locust infestations of semiarid areas are preceded by well defined soil moisture conditions. Therefore the potential of outbreaks can be partially predicted by accurate mapping of soil moisture on the field-scale (100 m). In this manner, Radarsat International has run a successful locust outbreak prediction campaign in Kazakhstan (LIMIS). This was based on Radarsat-1 backscatter images combined with simultaneous soil moisture ground truth. Although, as shown by LIMIS, soil moisture maps can be successfully derived from RADARSAT-1 imagery using high quality ground measurements, this method has disadvantages. The main

problem is the high cost and difficulty associated with collecting sufficient ground measurements. To overcome this problem, soil moisture maps can be derived without the use of ground measurements from multiple RADARSAT-1 images, each with a different incidence angle. This work presents encouraging research results towards an automated ground-measurement free system based on multi-angle SAR data inversion. [C4851]

"Computation of electromagnetic characteristics of frozen hydrometeors at millimeter-wave frequencies"

The development of physical model to retrieve snowfall from millimeter-wave measurements require the calculation of scattering and emission properties which can generate brightness temperatures (Tbs) and/or radar reflectivities that are consistent with observations. Frozen hydrometeors have various sizes, shapes, orientations, phase, and density so that it is difficult to parameterize their electromagnetic (EM) properties. For many physical approaches in remote sensing, non-spherical frozen hydrometeors are parameterized as spherical particles and Mie-theory is employed because it is faster than more rigorous analyses of scattering by nonspherical particles. However, the applicability of those simplified approximations in millimeter-wave radar and radiometer remote sensing of frozen hydrometeors has not yet been proved. To seek a parameterization to represent the EM properties of frozen hydrometeors at millimeter-wave frequencies, this study employs the Discrete Dipole Approximation (DDA) method Drain and Flatau (2003) and analyzes the calculated single scattering from nonspherical snow crystals at millimeter-wave frequencies (95, 140, 183, 220, and 340 GHz). Various assumptions, which were made in previous studies, for the snow microphysical properties, such as density, dimension, and particle size distribution are applied to these comparisons. The uncertainty range of EM property caused by various snow habits, density, and particle size distribution are presented [C4852]

"Development of the spaceborne Dual-frequency Precipitation Radar for the Global Precipitation Measurement mission"

The Dual-frequency Precipitation Radar (DPR) installed on the Global Precipitation Measurement (GPM) core satellite is being developed by JAXA and NICT. This paper describes the mission objectives, the precipitation measurement method and techniques, and the construction of the DPR [C4853]

"Classification of precipitation type from space borne precipitation radar data and 2D wavelet analysis"

Classification of precipitation into convective and stratiform type is an important product of Tropical Rainfall Measuring Mission (TRMM) data set. This work presents the results of a new algorithm, used to classify precipitation into convective and stratiform types, developed using two dimensional wavelet transform. The methodology analyzes the three dimensional radar profile of precipitation in both horizontal and vertical directions (with respect to the surface of the earth). The rain type is determined by analyzing the wavelet coefficients of the horizontal and vertical details of each plane. The data structure used in each plane is rebuilt using the suitable wavelet coefficients to extract the proper signal components at the selected plane. Data from TRMM-PR are analyzed to produce precipitation type classification. The results are compared against ground validation inferences. [C4854]

"Mass and mean size dual-frequency radar relations for frozen hydrometeors"

Airborne in situ frozen particle size distribution data from the TRMM field campaigns is used to develop mass and mean size dual-frequency radar relations [C4855]

"Examination of surface cross section statistics over ocean and land"

Weather radars that operate at frequencies higher than about 3 GHz can be affected adversely by rain attenuation. However, for spaceborne applications, where the size and mass of the antenna are limited, adequate spatial resolution can be obtained only by increasing the frequency. For the Tropical Rainfall Measuring Mission (TRMM) precipitation radar (PR), the use of 13.8-GHz frequency with a 2-m antenna size represents a compromise between the desire to minimize the antenna size and rain attenuation and maximize the spatial resolution. As demonstrated by Hitschfeld and Bordan (1954) in their classic study, estimates of rain rate from a single-attenuating wavelength radar are unstable when the path attenuation is large, unless the radar constant and the drop size distribution are known to a high degree of accuracy. Because these conditions are seldom met, an alternative strategy is needed to complement the Hitschfeld-Bordan method for moderate and high rain rates. One of the proposed ways of estimating attenuation is the surface reference technique (SRT). In this work, the data from TRMM PR is used to study the statistical characteristics of the surface return (s_0) as a function of the surface type (ocean/land) and incident angles during rain and rain-free times, this analysis is

further used to study the effectiveness of using surface return as the reference. [C4856]

"Multi-sensor and algorithm fusion with the Choquet integral: applications to landmine detection"

We discuss the application of Choquet integrals to multi-algorithm and multi-sensor fusion in landmine detection. Choquet integrals are defined. Specific classes of measures, the full and Sugeno measures, are described. Full measures are optimized via quadratic programming. A steepest descent algorithm for optimizing Sugeno measures is derived by applying implicit differentiation. Multiple detection algorithms are applied to hyper-spectral and synthetic aperture radar imagery. In addition, a LWIR vegetation index is computed using statistics of apparent emissivity. The detection algorithms are combined using an OR operator and Choquet integrals with respect to full and Sugeno measures. The Choquet integral with respect to the full measure achieves lower false alarm rates [C4857]

"Design and demonstration of an interference suppressing microwave radiometer"

Microwave radiometers operating outside protected portions of the frequency spectrum can be adversely impacted by radio frequency interference. In this paper, we describe a new radiometer which coherently samples 100 MHz of spectrum and applies real-time RFI mitigation techniques using FPGAs. Experiments currently in progress to demonstrate the system are also detailed [C4858]

"Airborne radio frequency interference studies at C-band using a digital receiver"

An airborne system for observing radio frequency interference at C-band is described. The digital receiver included has the capability of providing high temporal and spectral resolution of interference, as well as implementing simple mitigation strategies. Plans for observations with the system are discussed. [C4859]

"A diurnal difference indicator for freeze-thaw monitoring from Ku band scatterometer applied within the Siberia II project"

We present and assess a diurnal difference indicator that is related directly to the seasonal freeze-thaw effects, focusing, in this paper, primarily on the onset of snowmelt and terrestrial thawing. In order to be able to provide a level of certainty with the indicator our approach is based upon the development, and application, of a noise model that accounts for instrument noise, speckle, spatial heterogeneity, "environmental" noise and the influence of azimuth angle at which the measurement was acquired [C4860]

"Simulation and measurement of 24 GHz Short Range Radar (SRR) Interference"

The automotive industry is currently considering the introduction of Short Range Radars operating near 24 GHz for improving road traffic safety. Short Range Radars are intended to observe the full azimuthal space cover around a vehicle using up to eight sensors. The sensors would operate in an ultra wideband (UWB) mode, occupying 3 to 5 GHz of bandwidth. Interference from SRR transmitters with passive microwave remote sensing satellites could occur as the result of several coupling mechanisms, including direct coupling via the transmit antenna beam and scattering and diffraction of the transmitted signals from leading vehicles, buildings, and other nearby objects. In this study, we estimate the amount of coupling anticipated to occur from SRRs, including the direct and scattered contributions. The calculations are based on bistatic scattering measurements at of a typical automobile and ray optical simulations of reflection and propagation in an urban environment. [C4861]

"Requirements for a space mission for DInSAR and PS analysis based on past and present missions"

The aim of this paper is to highlight some important issues that should be taken into account when designing and planning a SAR mission dedicated to differential SAR interferometry (DInSAR) and Permanent Scatterers (PS) analysis. Special attention is paid to the impact of different design parameters on the information that can be retrieved, namely: (1) different wavelengths; (2) repeat cycle; (3) polarization modes; (4) platform stability; (5) state vectors accuracy. The impact of satellite dead band at different frequencies is discussed as well, taking into account DEM estimation issues and the problem of atmospheric effects. It is shown how very small baselines are not always the best design solution at least for PS analysis. PS results obtained processing 3 multi-temporal data sets acquired by JERS, ERS and Radarsat over Tokyo are presented and discussed [C4862]

"Intelligent matchmaking for Polar Ice Sheet Data collection and delivery"

The PRISM (Polar Radar for Ice Sheet Measurement) project is developing mobile, autonomous sensors for the measurement and study of the mass balance of the polar ice sheets. These sensors consist of intelligent radars

integrated into robotic vehicles. They autonomously decide where and how to measure by examining a variety of information including onboard sensor data and collections of a priori knowledge. These data include the health and status of the rover, health and status of the sensors themselves, the state of the environment as measured by the sensors, satellite measurements of the area indicating expected ice sheet motion, and so on. All of this information is used to direct the data collection process by allowing for the dynamic configuration of sensors and the motion of the rovers that carry them. The PRISM intelligent sensor and rover control system is built upon a multiagent collaborative architecture that involves a number of distinct data collection and data dissemination agents functioning continuously and autonomously in a distributed computing framework. A critical component of this system is an agent service called the Matchmaker. The Matchmaker coordinates requests for information and services within the agent community and allows decision-making agents to locate and communicate with the data source-agents that can fulfill these requests [C4863]

"Errors due to the reflectivity of calibration targets"

For a microwave total-power radiometer, we consider the error introduced by neglecting the difference in the antenna reflection coefficient between when it views a distant scene and when it views a nearby calibration target. An approximate expression is presented for the error, and measurement results are presented that enable one to estimate the resulting uncertainty in the measured brightness temperature. This uncertainty ranges from about 0.1 K to several kelvins for the representative cases considered [C4864]

"Scientific use of TerraSAR-X"

TerraSAR-X is a new German radar satellite to be launched in April 2006. The expected lifetime is 5 years. It carries a high frequency X-band SAR sensor that can be operated in different modes and polarization. The Spotlight-, Stripmap- and ScanSAR-modes provide high resolution SAR images for detailed analysis as well as wide swath data whenever a larger coverage is required. Imaging is possible in single, dual and quad-polarization. TerraSAR-X is an operational SAR-system for scientific and commercial applications that equally shares the satellite tasking time. DLR is responsible for the scientific use while the Astrium GmbH has the exclusive commercial exploitation rights. The status "scientific use" needs to be gained via a selection process. An announcement of opportunity (AO) is to be released one year before the launch. TerraSAR-X data can be provided for the costs of fulfilling the user request [C4865]

"The radar altimeter and scatterometer of China's HY-2 satellite"

This presentation describes the specifications and parameters of the radar altimeter and scatterometer for China's Oceanic Dynamic Environment Mission (ODEM) (HY-2, Haiyang-2. "Haiyang" means ocean in Chinese). Some details about the design of these two instruments are also presented. The instrument on-board HY-2 includes a microwave imager (MWI), a dual-band radar altimeter (RA) and Ku-band radar scatterometer (SCAT). [C4866]

"Multi-sensor and time-series approaches for monitoring of snow parameters"

Frequent mapping of snow parameters, like snow cover area (SCA) and snow surface wetness (SSW), is important for applications in hydrology, meteorology and climatology. In this study, we have developed a few general multi-sensor/time-series approaches for such monitoring. The objective is to analyze, on a daily basis, a time series of optical and Synthetic Aperture Radar (SAR) data together producing sensor-independent products. A few algorithms for multi-sensor/time-series processing have been developed and are compared in this study. A typical approach is to analyze each image individually and combine them into a day product. How each image contributes to the day products is controlled by a pixel-by-pixel confidence value that is computed for each image analyzed. The confidence algorithm may take into account information about the local observation angle/IFOV size, probability of clouds, prior information about snow state, etc. The time series of day products are then combined into a multi-sensor/multi-temporal product. The combination of products is done on a pixel-by-pixel basis and controlled by each individual product/pixel's confidence and a decay function of time. The "multi product" should then represent the most likely status of the monitored variable. The sensors applied in this algorithm study are MODIS for optical data and ENVISAT ASAR for SAR data. The study area is South Norway, and the study focuses on the snowmelt seasons in 2003 and 2004 [C4867]

"Improving landmine detection using frequency domain features from ground penetrating radar"

Landmine detection is an important and yet challenging problem remains to be solved. Ground penetrating radar (GPR) is an effective sensor to detect landmines that are made of plastic or have low metal content. Most GPR signal processing algorithms apply processing in the time (depth) domain. This paper proposes to use the frequency domain features from the GPR signal to improve the detection of weak plastic mines and to reduce the

number false alarms due to clutter objects. The motivation comes from the fact that the energy density spectrum may be different between mine targets and clutter objects, although both may have strong GPR signal return in the time domain. Experimental results based on clutter lane data collected at a test site corroborate the effectiveness of the proposed spectral features to increase the accuracy for landmine detection [C4868]

"Application of texture feature classification methods to landmine/clutter discrimination in off-lane GPR data"

Recent advances in ground penetrating radar (GPR) fabrication and algorithm development have yielded significant performance improvements for anti-tank landmine detection in government sponsored blind tests. However, these blind tests are typically conducted over well-maintained homogeneous testing lanes specifically designed to test landmine detection performance in low-clutter population situations. New GPR data collections over targets emplaced in un-maintained off-lane soils have much higher GPR anomaly populations and provide more stringent tests of landmine detection algorithms. In this work, we focus on the application of feature-based class separation techniques to lower false alarm rates in heterogeneous off-road soils. In particular, we explore the application of texture feature coding methods (TFCM), which have previously shown promise in fields like tumor detection [C4869]

"An experimental complex for multi-frequency, short distance, coincident, microwave active-passive and in-situ combined measurements of soil and snow moistures"

An experimental polygon is represented, equipped by a complex of polarimetric (dual polarization), combined, short pulse scatterometer-radiometer systems of L-, C-, and X-band of frequencies, for bare soil, soil vegetation and land snow cover microwave reflective and emissive characteristics simultaneous and spatially coincident measurements. The polygon equipped as well by facilities for microwave devices absolute calibration, by spatially distributed sensors for in-situ measurements of soil moisture, and has local meaning small weather station. This paper has an aim to attract attentions of researchers engaged in such kind of measurements and to interest them to perform their own or joint measurements using available facilities [C4870]

"Combined seismic, radar, and induction sensor for landmine detection"

An experimental system to collect co-located ground penetrating radar (GPR), electromagnetic induction (EMI), and seismic data was developed to investigate the possibility of using the sensors in a cooperative manner and to investigate the benefits of the fusion of the sensors. These sensors were chosen because they can sense a wide range of physical properties. The seismic sensor is sensitive to the differences between the mechanical properties of a landmine and the soil while the GPR is sensitive to the dielectric properties, and the EMI sensor is sensitive to the conductivity [C4871]

"A national inventory of land management practices: estimating soil conservation practices using optical and radar imagery"

Agriculture and Agri-Food Canada is developing a national land use and agricultural management practices inventory. This inventory is envisioned as a representative, statistical database of land use and management information. Considering the magnitude of this project, the use of remotely sensed earth observation data is a key source of information. This project is exploring the use of optical imagery for crop residue mapping and the use of SAR data for establishing changes in surface roughness, which occur as a result of tillage. It is anticipated that land management classes can be determined through the integration of the crop residue and surface roughness products. This paper discusses the project, summarizes the data acquisition and analysis plan and provides some preliminary results [C4872]

"Estimation of snow water equivalence with two Ku-band dual polarization radar"

Snow water equivalence is an important parameter for studies of the natural sciences, particularly in hydrology and climatology. This study demonstrates a concept of estimating snow water equivalence under the consideration of a dual frequency Ku band (13.4 GHz and 17 GHz) and a dual polarization system [C4873]

"Analysis of soil roughness measurements using a 25 m laser profiler and a 4 m wide meshboard"

The currently available backscatter inversion models often do not yield satisfactory results when applied to natural surfaces due to an inaccurate characterization of the soil roughness properties. This is caused by inadequacy of the applied soil roughness measuring techniques and by the high variation on soil roughness parameters within one agricultural field. From a theoretical study it was found that long profiles are necessary to obtain an accurate estimation of the roughness parameters. Short profiles, which are generally measured, tend

to underestimate the roughness parameters. Soil roughness data were collected over three different tillages with the ESA laser profiler, which allows measurements of profiles up to 25 m, and a 4 m wide meshboard. This research compares the two measuring techniques and studies the possibility of compensating for the underestimation of short profiles. Analysis of the 25 m laser profiles confirmed the theoretical study that the rms height and the correlation length increase as profile length increases. The rms height reached a constant value for all three tillages whereas the correlation length only reached a constant value for the roughest tillages. The dependency on profile length of both rms height and correlation length could be quite accurately modeled which allowed the extrapolation from short profile data to rms height and correlation length values at higher profile lengths. Additionally, it was found that it is possible to convert the less accurate meshboard derived rms values to those obtained from the laser profiler. This conversion greatly improves when the parameter values of at least six, 4 m profiles are averaged. For the correlation length this conversion is not possible due to the high variance on this parameter [C4874]

"Measuring spatial variability of crops and soils at sub-paddock scale using remote sensing technologies"

Certain ground-based, airborne and space-borne sensors provide useful information to capture paddock scale variability. The combination of these sensors forms a suite of rapid mapping tools of crop and soil variability. The study exemplifies a dryland agricultural system of southern Australia, which is important for crops and animal production. This paper addresses the two key issues of precision farming: (1) Seasonal crop variability, and (2) Soil variability as contributor to crop variability. Crop yield has been derived from multi-temporal and multi-spectral Landsat data. The soil properties have been mapped using ground-based gamma ray spectrometers and the electrical conductivity measures. The results of image-derived yield were tested against the available yield data sets from the crop harvester. An existing algorithm of paddock zoning has been tested and modified to adequately map the seasonal crop variability and identify zones. This paper sets the scenario to explore how much seasonal yield variability can be attributed to the known soil properties so that the influence of other factors including, weather and management practices, can be studied further [C4875]

"Evaluating spaceborne passive microwave snow water equivalent retrievals across the Canadian northern boreal-tundra ecotone"

Time series analysis of the spaceborne passive microwave data record (1978-present) has identified an interannually consistent zone of high snow water equivalent (SWE) retrievals across the northern boreal forest of Western Canada. Because of potentially significant hydrological and climatological implications, and the sparse conventional observing network across this region, a dedicated field sampling campaign was conducted to verify the existence of this pattern. Snow measurements were made along an approximately 500 km transect across Northern Manitoba, Canada, during late November 2003 and early March 2004. Both snow surveys revealed strong agreement between Special Sensor Microwave/Imager (SSM/I) derived passive microwave SWE retrievals (using the Meteorological Service of Canada algorithm suite) and in situ measurements across the northern boreal forest: a gradient of increasing SWE between Thompson and Gillam was evident, as was a well defined zone of high SWE values to the north and east of Gillam. Further to the north, SSM/I derived SWE retrievals over the open tundra were anomalously low. These findings suggest that development of a tundra-specific SWE retrieval algorithm is necessary, given the unique snow pack properties, and high fraction of surface water (frozen lakes) [C4876]

"An examination of U.S. plans for meeting operational ocean observation needs with radar altimetry"

The proven performance of space-based radar altimeter observations for accurate, systematic, quantifiable, and ubiquitous measurements of sea surface height has led to broad adoption of this technique as a means for satisfying existing and future observation needs. Associated requirements to meet U.S. user needs-from basic research to current operations-have been articulated by a broad cross section of stakeholders. The NPOESS IPO IORD-II represents a coordinated Federal strategy for operational environmental remote sensing from low Earth orbit and is the single existing source of U.S. approved operational requirements for observations using radar altimetry. Due to the projected availability of resources and the difficulty in translating user needs to system specifications, the ability of the NPOESS Program to address beyond-baseline improvements to meet the complete spectrum of user needs of U.S. national interest-in particular precise, continuous, and unbiased measurements of low frequency, large scale climatic signals critical to the unambiguous determination of global climate change-will be challenged without reliance on data sources external to the program. Existing altimeter sensor technologies necessitate multiple platforms in dissimilar orbits to meet requirements across the scales of interest. Emerging technologies and exploitation techniques have the capacity to provide increased efficiencies in performance and cost [C4877]

"An integrated approach of remote sensing and geophysics for investigating geological structure in the East Vietnam Sea"

The East Vietnam Sea (South China Sea) is a large area with the diversely complicated conditions of geological structure. In spite of over the past many years of investigation, many marine places have remained poorly understood because of a thick seawater layer as well as of the sensitive conflicts among the countries in the region. Fortunately, satellite altimeter technology is allowing the enhancement of marine investigation in any area. The spatial variation of the ocean surface topography can be measured by a very accurate radar altimeter mounted on a satellite. The ocean surface is an equipotential surface of the Earth's gravity field. Therefore it can be converted into marine satellite-derived gravity by using the mathematical model. The detailed satellite-derived gravity anomaly and its variants are essential for understanding geological structure and marine geophysics. They provide a reliable opportunity to geologists and geophysicists for studying the geological features beneath the oceanfloor. Also satellite altimeter data is perfect for planning the more detailed shipboard surveys. The satellite altimeter data is collected by the Geosat, ERS-frac12 altimeters. In this paper, the authors emphasize the application of satellite-derived data for investigating of geological structure in the East Vietnam Sea. The satellite data is compared and combined with the shipboard data and has resulted in a significant improvement on its accuracy and resolution. It is constrained by shipboard data using the finite difference, minimum curvature methods. The satellite-derived gravity along with the geophysical advanced methods such as finite difference, gravity gradient, gravity derivative, residual isostatic gravity etc, have brought out an unambiguous picture on the geological structure in the area. Many geological features, such as seafloor spreading ridges, fault systems, volcanic chains, seamounts and shear zones are revealed on the satellite-derived gravity maps as-well as on its variants. Especially, it is more meaningful in the remote or sparsely surveyed areas. The achieved results are checked and confirmed by the shipboard and seismic data [C4878]

"Nonlinear internal wave study during ASIAEX"

In recent Asian Seas International Acoustics Experiment (ASIAEX), extensive moorings have been deployed around the continental shelf break area in the northeast of South China Sea in May 2001. Simultaneous RADARSAT SAR images have been collected during the field test to integrate with the in situ measurements from moorings, ship-board sensors, and CTD castings. Besides providing synoptic information, satellite imagery is very useful for tracking the internal waves, and locating surface fronts and mesoscale features. During ASIAEX in May 2001, many large internal waves were observed at the test area and were the major oceanic features for acoustic volume interaction. Based on the internal wave distribution maps compiled from satellite data, the wave crest can be as long as 200 km with an amplitude of 100 m. Environmental parameters have been calculated based on extensive CTD casts data near the ASIAEX area. Nonlinear internal wave models have been applied to integrate and assimilate both SAR and mooring data. The shoaling, turning, and dissipation of large internal waves on the shelf break, elevation solitons, and wave-wave interaction have been studied and are very important issues for acoustic propagation. The internal wave effects on acoustic modal coupling has been implicated and discussed. [C4879]

"Design of an operation control and remote monitoring system of small unmanned ship for close-range observations"

A small-unmanned observation ship (UOV) that automatically surveys various information of ocean environment in the close range around the large mother ship, has been designed. Two main support systems are needed to perform the observation in the unmanned ship. Firstly, the unmanned automatic operation system that follows a planned route and avoids obstacles is needed. Secondly, the remote monitoring system that acquires the ocean information and sends it to the station is also essential. In this study, we design the two support systems as follows. Firstly, for the unmanned automatic operation system, we develop an autopilot algorithm using DGPS and a fuzzy algorithm to calculate the collision risk with obstacles in real-time on a basis of radar and AIS. Secondly, we design a data acquisition and monitoring system that is in three-step communication type, that is, wireless LAN network, UHF/VHF communication and satellite communication. Therefore, we can design more stable monitoring system in network. To evaluate the developed algorithms for our UOV, we conducted several simulations and model tests in a lake. In this paper, we describe the main features of our UOV and discuss about the results of simulations and model tests. [C4880]

"Airborne polarimetric SAR monitoring for ships and coastal seas"

Airborne polarimetric and interferometric synthetic aperture radar (PiSAR) images are analyzed for monitoring ships and coastal seas especially for estimating sea surface wind speed and direction. Though in situ ships data through AIS (Automatic Identification System) were not available by the time of analysis, PiSAR's X band images

showed the potential to map coastal wind vectors with high spatial resolution of 2.5 m [C4881]

"Nondestructive and noncontact dielectric measurement methods for low-loss liquids using free space microwave measurement system in 8-12.5 GHz frequency range"

Nondestructive, noncontact and real time evaluation of dielectric properties of low-loss liquids is important for applications such as service-aged transformer oil, biomedical, remote sensing and design of radar absorbing material. Free-space methods (which are nondestructive and noncontact) were developed for accurate measurement of dielectric properties of low-loss liquids at microwave frequencies. Two methods, namely, transmission only method and metal-back method are developed for measurements using a free space microwave measurement system (FSMM). The FSMM system consists of spot focusing horn lens antennas, mode transitions, coaxial cables and vector network analyzer (VNA). Dielectric constants and loss factors were measured for low-loss liquids such as dioxane, benzene and new transformer oil. It is observed that both the transmission only method and metal-back method are suitable for dielectric measurement of low-loss liquids. [C4882]

"2004 4th International Conference on Microwave and Millimeter Wave Technology Proceedings (IEEE Cat. No.04EX827)"

{no data available} [C4883]

"Survey report of offshore wind conditions in prospect of offshore wind energy conversion systems in Japan"

Wind energy is viewed as a promising new energy resource in its pure, clean, and inexhaustible nature. Because of less disturbed, stable and strong wind conditions, coastal areas are considered to be suitable for constructing wind energy systems. Moreover, it is said that offshore wind conditions are better than inshore wind conditions for power generation. However, actual measured reports of offshore wind are very few. This report describes the applicability of laser radar system to offshore wind measurement [C4884]

"Nondestructive and noncontact dielectric measurement method for high-loss liquids using free space microwave measurement system in 8-12.5 GHz frequency range"

Nondestructive, noncontact and real time evaluation of dielectric properties of liquids is important for applications such as biomedical, remote sensing and design of radar absorbing material. Free-space methods (which are nondestructive and noncontact) were developed for accurate measurement of dielectric properties of high-loss liquids at microwave frequencies. The free space microwave measurement system (FSMM) consists of spot focusing horn lens antennas, mode transitions, coaxial cables and vector network analyzer (VNA). For high-loss liquids, namely, methanol, ethanol, ethylene glycol and N-propyl alcohol, dielectric constants and loss factors were measured using the reflection-transmission method. It is observed that the reflection-transmission method is suitable for accurate measurement of dielectric properties of high-loss liquids. [C4885]

"Seeing beyond the perimeter: the Advanced Exterior Sensor (AES)"

The system design of the Advanced Exterior Sensor (AES), test data and Sandia National Laboratories' current work on the AES is described. The AES integrates three sensor technologies (thermal infrared waveband, visible waveband, and microwave radar) in a Remote Sensor Module communicating with three motion detection target trackers and a sensor fusion software module in the Data Processor Module to achieve higher performance than single technology devices. Wide areas are covered by continuously scanning the three sensors 360 degrees in about one second. The images from the infrared and visible detector sets and the radar range data are updated as the sensors rotate each second. The radar provides range data with approximately one-meter resolution. Panoramic imagery is generated for immediate visual assessment of alarms using the Display Control Module. There is great potential for site security enhancement using the AES, which was designed for low-cost, easy use and rapid deployment to cover wide areas beyond typical perimeters, possibly in place of typical perimeter sensors, and for tactical applications around fixed or temporary high-value assets. Commercial-off-the-shelf (COTS) systems have neither the three sensor technologies nor the imaging sensor resolution. Cost and performance will be discussed for different scenarios. [C4886]

"Radar development at the technical University Delft after world war II"

First Page of the Article [C4887]

"Detection of objects with non-reciprocal properties by polarization radar"

First Page of the Article [C4888]

"Introduction to the 1st European Radar Conference 2004"

First Page of the Article [C4889]

"EuRAD 2004 sessions"

First Page of the Article [C4890]

"The using SICH-1/SICH-1M side-looking radar data for ecological environment monitoring"

First Page of the Article [C4891]

"Compression of tactical real-valued SAR imagery in the complex SAR phase history domain"

This paper introduces a technique that exploits the statistical properties of complex synthetic aperture radar (SAR) data to effectively compress the information required to produce tactical real-valued SAR imagery. Performing the compression on the complex data as opposed to the real-valued image enables the inherent sinusoidal structure of the radar returns to be modeled. The compression technique also takes advantage of the fact that the phase information in the complex SAR data is discarded in the image formation process. This enables a vocoding technique where white noise is passed through the source model to effectively recreate the frequencies required to reconstruct the SAR image. Line spectral pairs are used to quantized the model parameters and a 45:1 compression ratio is achieved with very little loss in perceptual image quality compared to the JPEG standard. [C4892]

"The growth of the New Jersey Shelf Observing System for monitoring plumes and blooms on the Mid-Atlantic continental shelf"

To study changes occurring within the Mid-Atlantic Bight (MAB), we have constructed a shelf-wide ocean observatory. While initial efforts focused on using an undersea cable, our experience during a series of coastal predictive skill experiments demonstrated that spatial data were the most highly valued commodity. Because of this we have focused on developing a subsurface capability to mirror the existing satellite and HF radar capabilities. Currently in situ spatial data are collected with a fleet of autonomous underwater Slocum Gliders to collect physical and biooptical data throughout the year. Our scientific efforts have focused on understanding biogeochemical dynamics on the MAB. Topographic steering of currents and its impact on material transport on the MAB plays a central role in transporting material from the nearshore to offshore slope waters. Additionally hypoxia and anoxia dynamics in the coastal MAB appear related to offshore dynamics. Gliders provide ideal platforms for tackling those problems. [C4893]

"Conference Record of the Thirty-Eighth Asilomar Conference on Signals, Systems and Computers (IEEE Cat. No.04CH37592)"

{no data available} [C4894]

"Session MA1b Radar and Remote Sensing"

{no data available} [C4895]

"An automatic method of coarse registration between multi-source satellite images"

The paper gives an automatic registration method for coarsely aligning multi-source satellite images. The contributions of the presented method lie in its novel feature matching strategy. Area features are depicted by a shape matrix and principle component analysis (PCA). By fusing the constraints of shape similarity and object orientation consistency of corresponding area objects, the ambiguity of feature matching can be effectively avoided. The registration results for SAR-optical satellite images demonstrate the robustness and efficiency of the given method. [C4896]

"A study of signal-processing about wind and temperature profiler radars in the troposphere"

The accurate acquisition of atmospheric parameters is important in practice. There are a lot of disadvantages in the old detecting methods. A new method of remotely measuring wind and atmospheric temperature is given in

the paper by combining the acoustic and radar techniques. The theory of this method is discussed in detail. An advanced PMC interface and DSP technologies is used in developing the whole digit measurement platform. In the end, the signal processing technique is set forth correspondingly. [C4897]

"Unsupervised segmentation of the POL-SAR image using similarity parameters in sequential projection pursuit model"

A sequential projection pursuit model (SPPM) for unsupervised segmentation of the polarimetric synthetic aperture radar (POL-SAR) image is proposed in this paper. The features of the high dimension data are extracted out via orthogonal projection and the classification is accomplished by the Bayesian decision rule. Also the similarity parameters of POL-data are expressed as the characters of a target and form new target data. The SPPM utilizes new target data to classify the target into various subclasses. Good-segmented results have been obtained for the POL-SAR image processing. The segmented results using the SPPM are better than that of using entropy-alpha plane. [C4898]

"Development of a low-power high-sensitivity cloud profiling FM-CW radar at 95 GHz"

We developed a low-power and high-sensitivity cloud profiling radar transmitting frequency-modulated continuous waves (FM-CW) at 95 GHz for ground-based observations. Millimeter waves at 95 GHz are used to realize high sensitivity to small cloud particles. An FM-CW type radar realizes similar sensitivity with much smaller output power than a pulse type radar. Two 1 m-diameter parabolic antennas, separated by 1.4 m from each other, are used for transmitting and receiving the wave. The direction of the antennas is fixed at the zenith. The radar is designed to observe clouds between 0.3 km and 15 km in height with a resolution of 15 m. Using the facility, test observations and long term campaign observations have been done. Results of observations show that the system can observe clouds of -30 dBZ at a distance of around 5 km, which is sensitive enough to observe various kinds of clouds. [C4899]

"Restore of broadband radar pulse distorted by the Martian ionosphere"

The signal distortion and restoration of Gauss pulse and rectangle pulses when they propagate through the ionosphere of the Mars are presented. A modified matched filter is proposed for the restoration of Gauss pulses. The restoration of rectangle pulse can be done by measuring the total electron content using the I-Q channels. [C4900]

"A real-time compressing method for complex SAR images"

Complex image compression is widely used in diverse remote sensing applications in order to reduce the costs of data storage and release the burden of data transmission on limited data transmission channels. However, the huge amount of data makes it difficult to compress in real-time. A novel real-time compressing method for complex SAR images is presented in this paper. The system uses a fixed-point DSP of TI SM320c6416 with IGB SDRAM (synchronous dynamic random access memory). After removing the redundancy of complex image in frequency domain, arithmetic codec is applied for statistical redundancy, further. With the least data regress limes, good performance is achieved. The results show that compressing a complex image of 8192*2048 needs only 4315 ms in an acceptable distortion with compression ratio of 16.214:1. So, the method is highly suitable for real-time (or low delay) applications. [C4901]

"DDC design by using FPGA in HF OSMAR system"

A new design for digital down conversion (DDC) in Ocean State Measuring and Analyzing Radar (OSMAR) is presented. Some examples are given, and the result can prove the validity. All parameters can be adjusted freely according to our needs, and the new system can be adapted to the next generation HF system OSMAR. [C4902]

"Multiresolution wavelet decomposition to merge Landsat TM and SPOT panchromatic data"

A new algorithm is developed to merge a high-resolution panchromatic image and a low-resolution multi-spectral image based on the combination of multi-resolution wavelet decomposition and the IHS (intensity-hue-saturation) transform. The high-resolution panchromatic image is firstly decomposed to the wavelet planes, then the region is divided by edge information from the wavelet planes and the intensity component from the multispectral image is merged by a fusion operator in different regions. The proposed method is compared with the IHS and the MWT (multiresolution wavelet transform) methods. The experimental results show that the proposed method can achieve better fusion performance in combining and preserving spectral-spatial information. [C4903]

"External calibration of the CRS-1 satellite"

CRS-1 is a SAR satellite in L-Band comprising a phased array antenna. In a cooperation by the Beijing Remote Sensing Institute (BRSI), China, and Radar Systemtechnik AG (RST) in Rorschacherberg, Switzerland, calibration of the CRS-1 active phased array antenna was studied. Both partners were working towards a high performance SAR image product made from the CRS-1 SAR raw data. The paper shows the complexity of calibration under the umbrella of a high performance active on-board array SAR antenna. The calibration uses a new development of an active radar target (ARC) that was specially developed for the purpose. [C4904]

"L-Band SAR-processor for the Chinese SAR satellite"

The SAR processor was developed for fast delivery of high-resolution images from the Chinese CRS-1 satellite based on Pentium IV technology. Through testing, all the following requirements were met at an acceptable hardware and software cost: fast delivery time; high resolution; high precision. The development of the SAR processor was a joint project between BRSI (Beijing Remote Sensing Institute), China, and RST (Radar Systemtechnik AG), Switzerland. The paper contains an overview of the architecture used by the SAR processor. Due to the complexity of the SCAN-SAR algorithm, it is described in detail. In strip mode, the standard range of the Doppler algorithm was optimised to meet the SCAN-SAR requirements. The results using a simulated point target are given. [C4905]

"A method for characterizing a target in polarimetric radar remote sensing"

A method for characterizing a target is proposed in this paper, based on the eigenvalue decomposition of a scattering matrix. From this method, a set of parameters is derived. The parameters are not only independent of the spans of the scattering matrices, but also independent of the target orientation angles. With these parameters, we enhance the contrast between the road and forest of a SAR image, demonstrating the effectiveness of the proposed parameters. [C4906]

"Novel infrared phototransistors for atmospheric CO₂ profiling at 2 μ m wavelength"

Two-micron detectors are critical for atmospheric carbon dioxide profiling using the lidar technique. The characterization results of a novel infrared AlGaAsSb/ InGaAsSb phototransistor are reported. Emitter dark current variation with the collector-emitter voltage at different temperatures is acquired to examine the gain mechanism. Spectral response measurements resulted in responsivity as high as 2650 AAV at 2.05 μ m wavelength. Bias voltage and temperature effects on the device responsivity are presented. The detectivity of this device is compared to InGaAs and HgCdTe devices. [C4907]

"A feasibility study on a novel method of visual obstacle detection"

We discuss potential applications of a novel visual sensing method that is particularly suitable for obstacle detection and/or path planning, in this method, scenes are illuminated by short laser pulses and images are captured by a gated camera. By controlling the pulse width and the gating time, it is possible to get images that contain only objects within a predefined distance from the camera. The rest of the scene remains invisible. The presented experimental results confirm that the method can be prospectively used to create very fast, robust and reliable systems for vision-based navigation. Many significant constraints of the existing algorithms are overcome. [C4908]

"Design of a portable potentiostat for electrochemical sensors"

In this paper, we propose a portable and wireless data transmission potentiostat and further exert the amperometric morphine sensing and the potentiometric pH sensing to verify its performance. The proposed potentiostat has the ability to process the long-term electrochemical signals in both the amperometric and potentiometric modes at a remote site. Based on the popular General Packet Radio Service (GPRS) communication systems, we adopt a personal digital assistant (PDA) cellular telephone, rather than a personal computer (PC), to control and collect data. The sensed data collected by PDA cellular telephone is transmitted to a telecommunication server. In addition, the data stored in the telecommunication server can be retrieved by a PDA cellular telephone or by a remote PC through the Internet at any time and any place. Our experimental results show that the proposed potentiostat has the merits of moderate accuracy, low cost, and long-distance wireless data communication capability. [C4909]

"2004 International Conference on Image Processing (ICIP) (IEEE Cat. No.04CH37580)"

{no data available} [C4910]

"Opportunities for NRL WARLOC radar validation and calibration of NASA Earth Observing Space Missions"

The NRL WARLOC radar is a high average power, coherent W-band (94 GHz) radar now operating at the NRL Chesapeake Bay Detachment (CBD) site in Maryland. Developed by the Navy as a research radar for imaging and tracking applications, WARLOC also brings unprecedented sensitivity to the measurement of cloud parameters (including phase, morphology, and particle size and motion) at spatial resolutions unparalleled by contemporary radar systems. The NASA CloudSat satellite, planned for launch in early 2005, features a nadir pointing non-coherent W-band cloud profiling radar (CPR). As part of the "A-Train" constellation (a series of five low-earth-orbiting satellites in formation flight with the EOS Aqua platform), CloudSat provides the first space-based cloud vertical profile information on a global scale. This paper discusses opportunities for the use of WARLOC for atmospheric physics studies in general, and potential for quantifying the instrument performance and science limitations of the CloudSat CPR. [C4911]

"The design of frequency synthesizer for the ocean state measuring and analyzing radar"

The design and realization of a synthesizer for high frequency radar, OSMAR2003 (ocean state measuring and analyzing radar), is proposed. To provide a 47.5 MHz local signal and 7 MHz transmitting signal, two kinds of frequency synthesizer architectures are presented, and their advantages and disadvantages are compared. The preferred synthesizer is based on an architecture supporting a flexible combination of direct synthesizer and DDS (direct digital synthesizer) techniques with a low frequency reference crystal oscillator. The benefit of this architecture is the generation of signals with low phase noise and low spurious level. The measured output spectrum and field experiments undertaken in Zhujiajian Island demonstrate successful frequency synthesis operation. [C4912]

"The effect of phase noise on the remote sensing of ocean surface currents"

This paper studied the phase noise effect on the range spectrum and Doppler spectrum measured by high frequency (HF) radar which was used for remote sensing of sea surface state parameters. The presence of phase noise in the master oscillator caused a widening of the range spectrum and clutter velocity spectrum, degrading the range and velocity resolution. In this paper, a practical phase noise model is presented, and based on it, the relationship between the phase noise power spectrum density (PSD) and cumulative phase noise is investigated. Then, the basic minimum requirements for the PSD are calculated to maintain radar performance. The results show that a commercial off the shelf oscillator can meet the phase noise requirements. [C4913]

"2004 Asia-Pacific Radio Science Conference Proceedings (IEEE Cat. No.04EX825)"

{no data available} [C4914]

"Polarimetric EM scattering and information retrieval in SAR remote sensing"

The advance of polarimetric SAR imagery technology, such as SIR-C and RADARSAT-2 has promoted extensive study and applications for information retrieval from polarimetric scattering measurements. This paper briefly reports our research on three issues: (1) solutions of the Mueller matrix, the eigenvalues of the coherency matrix and information entropy to directly relate with measurements of the co-polarized and cross-polarized scattering in SAR imagery; (2) an inversion approach for digital elevation mapping (DEM) by using a single pass instead of two-pass or interferometric SAR (INSAR), of polarimetric SAR data; (3) an algorithm of two-threshold EM (expectation maximisation) and MRF (Markov random field) for automatic analysis of the context change detection in the urban area from multi-year SAR observations. [C4915]

"FPGA implementation of a phased array DBF using polyphase filters"

Efficient digital phased array beams require a high resolution timing vector. The timing coefficients cause speed bottleneck in FPGA implementation of such systems in the HF frequency range. We present polyphase structures to overcome the speed limitation for an ionospheric radar. The radar requires a constant phasing vector to steer the beam over a specified region of the ionosphere. Sixteen digital beams are derived from the vector with beam resolution of approximately three degrees. The phasing weights can be employed either in the time domain or in the frequency domain. Comparison of phase delay and time delay methods is presented for broadband frequencies of the radar. Performance of the proposed DBF system is discussed using clock efficiency and beam resolution. [C4916]

"Fast imaging of a target in inhomogeneous media for pulse radar systems"

Many works have been done to develop efficient imaging algorithms for ground penetrating radars. We have developed a new imaging algorithm SEABED for homogeneous media and confirmed its performance. This algorithm has an advantage that the calculation time is quite short because it is based on a reversible transform. However, its performance for inhomogeneous media has not studied yet. In this paper, we examine the performance of SEABED for inhomogeneous media [C4917]

"Analysis on uncertainty in the MODIS retrieved land surface temperature using field measurements and high resolution images"

In this paper, a generalized split-window method to derive land surface temperature (LST) from MODIS (Moderate Resolution Imaging Spectroradiometer) data is applied. A major problem in land surface temperature inversion is that there are too many unknown variables, especially for MODIS data which is in low resolution, one pixel is a mixture of several cover types. To analysis the uncertainties of the LST retrieval algorithm based on MODIS images, the field measurements, together with fine resolution images, AMTIS (the airborne multi-angle TIR/VNIR imaging system) data and ASTER (Advanced Spaceborne Thermal Emission and Reflection Radiometer) data have been used [C4918]

"Space-based observations in the International Polar Year: educational opportunities to strengthen the STEM pipeline"

Data from current and planned satellite missions can play an important role in providing synoptic atmospheric, terrestrial and oceanic environmental data from space. These data promotes multidisciplinary research in the circumpolar regions and can be instrumental in furthering our understanding of the Earth as a System. The International Polar Year in 2007 (IPY-4) presents unprecedented opportunities for integrated circumpolar research and for education outreach to a wide audience ranging from preschoolers through high end researchers, defined by NASA as the "pipeline". We foresee a world-wide participation which improve science competence and citizen awareness of the importance of the Polar Regions. Opportunities for integrating native knowledge of the indigenous residents of the Arctic is an essential component of IPY programs. Acquisition of reliable ground truth data in support of remote sensing of geophysical and geochemical variables are essential, especially with broad long-term coverage in the Polar Regions. In the United States NASA has developed a strategy for long-term monitoring of some key parameters needed to bring us closer to the answers we need regarding climate change and its relation to social systems. This technology consists of a group of six satellites that can make a suite of earth observations referred to as the "A-Train". Data from this group of polar orbiting satellites, as well as from the Orbital Carbon Observatory (OCO), and older Quikscat and new Seawinds radar missions, provide focus for an education program based not only on the acquisition of polar data but also on how these data correlate with global observations. This work presents strategies and recommendations for streamlining an effective educational outreach program in the IPY-4. It presents a concept of disseminating data, models and research results to a variety of audience and integrating several traditional aspects in building a strong educational component to IPY-4. [C4919]

"The impact of forest heterogeneity on the height retrieval using X-band interferometry"

This paper assesses factors, which affect tree height retrieval using SAR phase coherence due to the heterogeneity within the forest stand. Factors such as edge effects, density, crown shape, slope, and emergent trees are assessed using a Polarimetric Radar Interferometry Simulator (PRIS). Results from the model simulation are compared to actual retrieved height from X-band Intermap data over pine plantations [C4920]

"Electromagnetic wave attenuation for propagation through a forest belt"

Some theoretical and experimental results on the attenuation of electromagnetic wave propagating through a forest belt are presented. A theoretical model proposed for evaluating the wave field amplitude is based on the Kirchhoff-Fresnel principle. It concerns with both the horizontal and vertical polarizations, relevant wave diffraction problems being solved in the two-dimensional approximation. An experimental study was carried out at the frequency of 0.6 GHz. The transmitter was located in front of the belt edge at the distance of 25 m, being positioned at the heights of 5, 11, and 16 m above the ground, while the receiver, placed at the height of 2 m, was being moved through the forest belt and further on to the point located at the distance of 60-120 m from the rear edge of the forest belt. The latter had about 100 m in width, and was situated 150 km to the northwest from the city of Ulan-Ude near Baikal lake, being consisted mostly of the birch and cedar trees. The height and diameter of trees varied from 10 to 15 m and from 0.15 to 0.25 m, respectively, with the average density of those being of 0.3 trees/m². All measurements were conducted in August 2003. The magnitude of wave field was

found to attenuate with the distance from transmitter as an exponential function. In the case of vertical polarization, the rates of attenuation were measured of 0.2-0.5 dB/m and of 0.05-0.08 dB/m, as related to the wave paths located inside the forest belt and behind it, respectively. As expected, the rate of attenuation for the wave with horizontal polarization was found 0.1-0.15 dB/m below that relating to the vertical polarization. Finally, the relative contributions of specific partial components to the total amplitude of wave field were analyzed, using the theoretical model proposed [C4921]

"ENVISAT ASAR AP data for operational sea ice monitoring"

The information content of ENVISAT ASAR alternating polarization data is evaluated with respect to operations at the Canadian Ice Service. A data set covering an entire ice season is shown to have a higher information content compared to single polarization data. The potential for automated information extraction is also investigated, in particular problems caused by system noise and its variation over the swath. [C4922]

"Landfast sea ice extent and variability in the Alaskan Arctic derived from SAR imagery"

Landfast sea ice is a seasonal phenomena in the Alaskan Arctic and throughout its annual existence, between formation in late fall and break-up in late spring, it is shaped by a range of thermodynamic and dynamic forces. The results of a manual and an automated technique to derive positions of the seaward landfast ice edge (SLIE) as it changes over time from synthetic aperture radar (SAR) data covering the Alaskan Arctic coast and nearshore waters from east of Point Lay, Alaska to the Mackenzie delta. Observing the variability in the position of the SLIE for a large study area over the course of the year identifies the occurrences of significant change including the timing of freeze-up and break-up and episodic events in between. It is also possible to identify the maximum stable extent of the landfast ice for a given period, which should prove valuable for all nearshore activity in the Arctic. We can give a greater understanding of the factors controlling the SLIE position by calculating the standard deviation in landfast ice width along the coast. This analysis identifies stable nodes along the SLIE where variability is small and processes, as of yet unidentified, helps to stabilize the landfast ice edge [C4923]

"Temporal soil moisture estimates from Radarsat-1 and Envisat ASAR for flood forecasting"

Estimating the amount of water stored in a soil profile is essential in most water management projects and for assessing the hydrologic state of a basin. It determines infiltration during a rainfall event and controls evapotranspiration between storms. Rarely, however, are soil moisture data available for model input. In many cases, particularly watershed scale monitoring or modelling, soil moisture is inferred from more easily obtainable hydrologic variables such as rainfall, runoff and temperature. As such, there is a strong need for procedures to estimate soil moisture in a watershed independently from the models. These procedures must provide not only basin average estimates but also the spatial distribution within a basin in order to meet the requirements of emerging distributed models. Active and passive microwave imagery are both candidate sources for these data. Active SAR imagery, with its high resolution, is particularly attractive for use in areas of mixed land cover. This paper addresses the potential of Radarsat and Envisat ASAR Synthetic Aperture Radar (SAR) data to extract information on soil moisture at the watershed scale. Multiple Radarsat and Envisat data acquisitions collected over the Roseau River watershed, located in Manitoba, for the period of September 2002 through June 2003 were analyzed in relation to ground observations and meteorological conditions. A method was then developed to produce soil moisture maps for input to a hydrological model for flood forecasting [C4924]

"Dependence between spatial statistics and distance for C-band backscattering signatures of the Baltic Sea ice"

We have studied using C-band one-dimensional helicopter scatterometer data dependence between distance l and standard deviation (std) and correlation length L for the Baltic Sea ice backscattering coefficient (sigmadeg). The results indicate strong linear dependence between l and L and between $\ln(l)$ and $\ln(\text{std}(\text{sigmadeg}))$ at least up to distance of few kilometers. This suggests fractal-like behavior for the variation of the Baltic Sea ice sigmadeg as a function of l . The regression coefficients describing the dependencies of l vs. L and $\ln(l)$ vs. $\ln(\text{std}(\text{sigmadeg}))$ do not discriminate various ice types better than just mean and standard deviation of sigmadeg [C4925]

"Public policymaking and climate change: The essential but little known contribution of earth science remote sensing data and products"

This paper traces the evolution of space-derived remote sensing data and data products from their initial dissemination to their eventual impact on the nature and outcome of public policy addressing climate change

issues. We focus on two examples, renewable energy and public health and ecosystem assessment, in tracing US policy debate and the influence of science results on that debate. The research seeks to answer the question posed by Congress, NASA administrators, and other decision makers about what has been the contribution of space-derived earth science in "making a difference" in societal well being. We find that even though policymakers themselves can be unaware of the role of earth science, much of their debate is informed (or not) depending on the extent to which science results have been appropriately translated and communicated for the purposes of improving the quality of debate. The usual "route" of influence is by way of "decision support systems", or the collection of tools, methods, and data that enable researchers to use earth science in scenarios that ask "what it" or "what causes". Research results are increasingly being carried forward to policy debate including but not limited to public and ecosystem health, carbon management, and energy issues [C4926]

"Monitoring mining induced surface deformation"

There exists a significant demand for the monitoring of mining induced surface deformation for legal obligation safety, and environmental reasons. In recent years land surface deformation monitoring with SAR data reached some maturity. Nevertheless, there remain important limitations to the availability of the EO based information. Reasons include incomplete spatial coverage with information gaps for low coherence areas, problems in resolving high phase gradients, and unavailability of the required SAR data. The objective of our contribution is to show that important improvements to these limitations are still possible. In vegetated areas and for fast deformations L-band INSAR was found to be more robust with a wider applicability than C-band INSAR. In some low coherence areas point-like scatterers can be identified which permit to fill important information gaps. Furthermore, pairs with long baselines can be included in the interferometric analysis, supporting a more complete use of the available SAR acquisitions and to improve the temporal sampling [C4927]

"Use of ICESat GLAS data for forest disturbance studies in central Siberia"

Lidar is a laser altimeter that determines the distance from the instrument to the physical surface by measuring the time elapsed between the pulse emission and the reflected return. The returned signal may identify multiple returns originating from trees, building and other objects and permits the calculation of their height. Studies using field data have shown that lidar data can provide estimates of structural parameters such as biomass, stand volume and leaf area index. NASA's ICESat Geoscience Laser Altimeter System (GLAS) was launched in January 2003 and collected data during February and September of that year. This study used GLAS data acquired over our study sites in central Siberia to examine the returned signal as a source of information about fire and insect damaged forest stands [C4928]

"Impact of solar radiation on sea surface salinity remote sensing by spaceborne synthetic aperture imaging radiometers"

Since the Sun is a very bright radiation source at L-band, reception of direct and Earth-reflected solar radiations by downward-looking radiometers raises a significant challenge for the remote sensing of ocean surface salinity. For a given spaceborne mission concept, the impact of the Sun radiations depends on the sensor antenna properties, the location of the Sun relative to both the spacecraft and the reflecting surface, as well as on the surface scattering properties of the observed Earth scene. Effects on interferometric data, (i.e. visibilities), provided by Synthetic Aperture Imaging Radiometers (SAIR) need to be accounted for; the affected area, determined through both geometrical and geophysical considerations, have to be either masked or flagged, or submitted to specific correction procedures, for correct sea surface salinity retrieval. Focusing on the future ESA Soil Moisture and Ocean Salinity (SMOS) space mission, we provide quantitative and qualitative estimates for measurements contamination by Sun as expected for the period 2007-2010, and we derive methods that can serve to develop a consistent correction strategy [C4929]

"Comparison of measured galactic background radiation at L-band with model"

Radiation from the celestial sky in the spectral window at 1.413 GHz is strong and an accurate accounting of this background radiation is needed for calibration and retrieval algorithms. Modern radio astronomy measurements in this window have been converted into a brightness temperature map of the celestial sky at L-band suitable for such applications. This work presents a comparison of the background predicted by this map with the measurements of several modern L-band remote sensing radiometers. [C4930]

"Spaceborne lidar aerosol retrieval approaches based on aerosol model constraints"

In the absence of auxiliary optical depth or transmittance information, or self-determination of same for specialized observing situations, aerosol backscatter and extinction profiles cannot be retrieved from lidar observations along a single direction without an assumption linking aerosol extinction and backscatter (i.e., the

aerosol extinction-to-backscatter ratio, or aerosol lidar ratio, S_a). Aerosol retrievals at 532 nm for the current GLAS and upcoming CALIPSO satellite lidar missions employ/can employ a look-up table approach to select climatologically based Samodel values for these retrievals when alternate, less uncertain methods for either defining S or providing the needed auxiliary information are unavailable. This paper addresses a revised table look-up approach that incorporates two notable revisions for improved Saselection which, as a consequence, enable more bounded aerosol retrievals. One is a refined, more bounded set of S values, both for 532 nm and 1064 nm, representative of a definitive set of aerosol types/models determined from an extensive analysis of the global aerosol solar radiometer network, AERONET, data base. The other is an accompanying set of key spectral ratio parameters (i.e., dual wavelength, 532 nm to 1064 nm, ratios of backscatter, extinction and S_a) also derived from the AERONET data which offer additional ways to bound the lidar aerosol retrievals. Thus, aerosol retrievals can be obtained subject to the constraints that the lidar data yield retrievals with spectral ratio parameters consistent with a given aerosol model (or models), to confirm the model choice and better bound the retrievals. Examples of retrievals make subject to these constraints are included as a part of the paper [C4931]

"Spectral ratio biospheric lidar"

A new active vegetation index measurement technique has been developed and demonstrated using low power laser diodes to make horizontal-path lidar measurements of nearby deciduous foliage. The two wavelength laser transmitter operates within and adjacent to the 680 nm absorption feature exhibited by all chlorophyll containing vegetation. Measurements from early October through late November 2003 are presented and the results are discussed [C4932]

"Laser-based system for ground-based measurement of backscatter surface reflectance"

The on-orbit verification of spaceborne lidar systems relies on several approaches including those based on measuring the returned signal from the surface. This returned signal depends on both the atmospheric transmittance and the surface reflectance in the backscattered direction. Thus, knowledge of the surface reflectance is critical to such approaches. The Remote Sensing Group at the University of Arizona has developed a laser-based system to measure the backscatter surface reflectance at the ground for use in vicarious calibration of lidar systems. The device relies on a beam expander and fold mirror system to illuminate the ground. A detector is placed behind an aperture cut into the fold mirror to allow the backscattered signal to be measured. This work describes the results from the use of this system for the ground-based validation of GLAS using data from White Sands Missile Range in New Mexico. Measurements from a field-portable, passive spectrometer are also shown for comparison [C4933]

"1.5 microns: the future of unattended aerosol lidar?"

Unattended lidars for clouds and aerosols are currently deployed at tens of locations in the U.S. and in other countries. These lidars operate in the mid-visible region. The micro-pulse lidar known as MPL is a very successful instrument in terms of numbers deployed, and it is also very sophisticated, because its operating wavelength of 523 nm combines two challenges: it is at the peak of the eye's sensitivity, so eye safety can only be achieved with very low pulse energy (on the order of 10 μ J); and it is at the peak of the solar spectrum, so minimizing sky background radiation is a major problem. In order to operate during daytime, micro-pulse lidars must have an extremely narrow field of view (FOV) and a very small optical bandpass. They are consequently not inexpensive, they tend to suffer from mechanical instability, and they are not field serviceable when certain types of failures occur. In order to establish the optimum wavelength region for an unattended aerosol lidar, the spectral dependencies of eye safety standards, sky radiance, laser availability, detector performance, atmospheric optical properties, and optical materials are presented. In particular, eye safety standards allow a fluence of 1 J/cm² at 1.5 micron, which is 107 times the fluence allowed in the mid-visible. Pulse energies on the order of 10 mJ are sufficient to make daytime operation easy and low-cost. A conventional bistatic lidar configuration can then be used with a field of view on the order of milliradians, which eliminates the problem of mechanical instability, and the optical bandpass can be limited with an inexpensive interference filter. In addition, the InGaAs detectors used at 1.5 microns are much less susceptible to optical damage than the Geiger-mode Silicon APDs used in visible-light lidars [C4934]

"Diode laser transmitter for water vapor DIAL measurements"

The design and performance of two diode laser based transmitters for differential absorption LIDAR (DIAL) are presented. The first laser transmitter uses a tunable external cavity diode laser (ECDL) in the Littman-Metcalf cavity configuration to injection seed a flared amplifier. Water vapor absorption measurements are demonstrated with this laser transmitter operating in a continuous wave mode. The second diode based laser transmitter uses an ECDL in the Littrow cavity configuration and angle-angle semiconductor optical amplifiers to produce

amplified laser pulses. Both designs are easily adaptable to wavelengths in the visible to the near infrared spectral region. [C4935]

"The secret of the Svalbard sea ice barrier"

An elongated sea ice feature called the Svalbard sea ice barrier rapidly formed over an area in the Barents Sea to the east of Svalbard posing a significant navigational hazard. The secret of this sea ice formation lies in the bottom bathymetry, which governs the distribution of cold Arctic waters masses and sea ice growth [C4936]

"Application of the audio interface for ground penetrating radar data representation and interpretation"

The present article offers a description of software complex, which supports reception and preliminary processing of ground penetrating radar (GPR) information, development of flag description, generation of radar displays and synthesis of their audio representation in the tasks of underground sounding data interpretation. A method of image-to-sound conversion is described, with the storage of image information at the level of attainable resolution. Technical feasibility of the replacement of visual perception with acoustic perception has been substantiated. Practical limitations of the parameters of conversion have been defined, and the conformity of the coded values with the level of perception of audio information has been verified. [C4937]

"Some aspects of usage of the pseudo noise sequences in the radiolocation systems"

Pseudo noise sequences (Barker's codes, M sequences etc.) widely use in communication and navigation systems. But for nowadays this kind of signals almost has no application in the radiolocation systems. This work investigates aspects of usage of pseudo noise sequences (PNS) in the radiolocation systems, some aspects of generating and processing of the input processes. Main emphasis was made on signal-to-noise ratio behaviour in the systems with pseudonoise signals in comparison with classic radiolocators. [C4938]

"The analysis of the matching opportunity of the parameters of the wideband through ionosphere signals with real dispersion radio line"

Concept of active mastering and constructive use of dispersive deforming properties of the transmitting environment which are limiting accuracy, carrying and resolution of broadband radio-electronic systems, for example, communication, location, navigation (including global) are first worked out in This work. [C4939]

"Signal processing in UWB radars of small distance"

In the paper, the methods of signal processing with reference to ultrawide band (UWB) radars designed for detection and remote measuring parameters of moving objects at short ranges (tens of centimeters-several meters) are considered. It is shown that the relative changes of an oscillation frequency filling an outgoing pulse and duration of these pulses originating at reflection from a moving target are very small; that makes impossible their practical measurement. Therefore, for detection of signals reflected from a moving target the phase method is chosen. [C4940]

"Advantages of the wideband and ultra wideband signals in the remote sensing"

Some aspects of the wideband and ultrawideband signals usage considered. Essential aspects of the processing techniques as well as models of the input process represented and discussed. The term efficiency bandwidth and principle of the waveform selection represented. Concept of the wideband signals in the synthetic aperture radar presented. Results which show advantages of these signals are shown. [C4941]

"The eigenvector-based identification of shallow buried targets in ground penetrating radar"

A new approach to the super-resolution eigenvector method implementation, in step-frequency ground penetrating radar (GPR), is proposed. The pseudospectrum determination, fulfilled by the eigenvector algorithm, is followed by a procedure of more precise signal parameter estimation. Accordingly, the distance to the object obtained by the eigenvector algorithm is considered more reliable. Then, complex amplitudes of the determined signal components are calculated, which allows distinguishing different types of buried objects. [C4942]

"FPGA implementation of digital upconversion using distributed arithmetic FIR filters"

Distributed arithmetic (DA) is a high speed multiplication technique used for implementation of digital filters and signal upconversions. The DA is bit serial word parallel approach where throughput rate does not depend on

filter length or data size. In this work a serial DA method is employed for FPGA implementation of digital component of the TIGER transmitter. A prototype has been synthesized and mapped using Xilinx Virtex II. The design with fourteen bit 100 tap FIR filter and upsampling ratio of eight takes only 18% of the device. Performance of the DA modulator is discussed with variable filter length and precision level. [C4943]

"The automatic determination of soil permittivity using the response from a subsurface local object"

The method for determining permittivity of soil containing a local object is proposed. The method based on the Hough transform is one of effective means to detect hyperbolic reflections from such objects on the GPR profile image. On the basis of the same method the iterative algorithm, which allows automatic determination of exact value of permittivity of ground using the results of subsurface radiolocation, has been developed. Its efficiency is shown using the simulated GPR profile example. [C4944]

"GPR-based adaptive sensing: GPR manipulation according to terrain configurations"

In this paper, we introduce an adaptive sensing method to a landform using a ground reflection of a ground penetrating radar (GPR). When GPR scans a ground surface, an antenna of GPR should be put on a ground as an ideal condition. The farther an antenna is put away from a ground, the shallower the sensing depth becomes, because a ground surface reflects most of the electromagnetic wave radiated by the antenna. Practically an antenna should be manipulated, keeping a small distance from a ground in order to avoid a collision with a ground. Besides, the distance should be controlled so as to observe the ground reflection at a constant position in B-scan image, which is eliminated by a simple algorithm. There are many sensors to measure a ground configuration, but we propose an adaptive sensing which does not require any additional sensors such as laser range finder. In addition, the ground reflection in B-scan image is precisely eliminated by manipulating the sensor head according to GPR sensor information. We show some experimental results to confirm its effectiveness and its performance. [C4945]

"A few examples of interferometry applications in space-related active and passive remote sensing"

The paper describes only a few examples of interferometry applications for space related active and passive remote sensing scenarios. Pulses with defined bandwidths as needed in a total system picture are applied (active remote sensing). Several accurate radar remote-sensing satellites have been produced under ESA's technical management. Work continues (www.esa.inQ) and new missions are developed. Also, such activities are ongoing at the level of National Space Agencies (Italy, Germany, etc.). Stability in instrumentation and related signal settings permits to make further advances and interferometry applications are advancing strongly. Some examples are shown, from which one observes, that accuracy is a very important factor. Ultra stabile reference clock signals are needed in interferometry applications with as an extreme example an experiment to perform Very Long Baseline Interferometry (VLBI) tracking of a weak transmission signal at Saturn's distance. Clock stability, using masers with 10^{-14} to 10^{-15} sec accuracy is needed here. [C4946]

"Aerosol optical properties derived from lidar observations using cluster analysis"

We present the distributions of the lidar observable optical properties for dust, continental pollution and marine aerosols using the Cloud Physics Lidar (CPL, ef.) measurements. This study uses CPL measurements during CRYSTAL-FACE off the coast of Florida to extract probability distribution functions (PDFs) of the lidar depolarization ratios (δ), and the ratio of the backscatter at 1064 nm to 532 nm (χ , referred to as the color ratio) for dust, continental pollution, and marine aerosols. The aerosol types are identified using a clustering algorithm. In this study, cluster analysis by partitioning is used to categorize the CPL data set based on the backscatter and depolarization ratio. The cluster results for clouds and aerosols are compared to the other classification schemes and observations. The results of the aerosol clusters are verified using in situ measurements where these are available [C4947]

"A multi-frequency microwave aperture synthesis radiometer for high-resolution imaging"

Many geophysical parameters can be determined with the aid of a passive microwave sensor. To achieve a high spatial resolution in passive microwave imaging the method of aperture synthesis can be applied. Narrowband radiometric measurements within a wide frequency range allow extracting more surface information on observed objects or materials and it is possible to obtain depth information on layered structures. Furthermore, the advantages of using a range of different center frequencies, i.e., a higher spatial resolution with increasing frequency and a higher penetrating capability at lower frequencies, can be combined in many cases to enhance the overall imaging capabilities. Thus our recent interest is focused on the development of an experimental system offering those features but keeping the costs affordable. In this paper the basic system concept is

outlined [C4948]

"An evaluation of SeaWinds/QuikSCAT data for the estimation of the decay status of first-year sea ice"

This analysis evaluates the temporal evolution of the microwave backscatter coefficient (sigmadeg) and VV/HH sigmadeg co-polarization ratio from Qscat for estimating sea ice thermodynamics. Qscat sigmadeg were compared against RADARSAT-1 SAR sigmadeg and in situ data from the Collaborative Interdisciplinary Cryospheric Experiment (C-ICE) for 2000, 2001, and 2002 were used as validation. Results indicate that the temporal evolution of sigmadeg from Qscat is analogous to RADARSAT-1. The Qscat sigmadeg temporal evolution has the ability to identify Winter, Snow Melt, and Ponding thermodynamic states. Moreover, the co-polarization VV/HH ratio of Qscat provides a more robust estimate of the Ponding state and identifies the Drainage state that is difficult to detect by single polarization SAR [C4949]

"Observations of aerosols using the Micro-Pulse Lidar NETwork (MPLNET)"

MPLNET is a network of lidar systems that provide long term observations of aerosol and cloud properties at multiple sites around the globe. Each site in the network uses an elastic-scattering lidar co-located with a sunphotometer to provide data products of aerosol optical and physical properties. Expansion of the network is based on partnering with research groups interested in joining MPLNET. Results have contributed to a variety of studies including aerosol transport processes and satellite calibration and validation efforts [C4950]

"Point target angular resolution in near field for Ka-band interferometric synthetic aperture radiometer with sub-Y-type array configuration"

This article evaluates the performance of interferometric synthetic aperture radiometer using sub-Y-type array proposed by our research group, SSL at GIST, Korea. The proposed array type has an improved resolution than the conventional Y-type known as optimal array configuration in the design of 2-D interferometric radiometer. To evaluate it, the interferometric synthetic aperture radiometer with 40 antenna array is developed at 37 GHz and two target noise sources were used for performance test. Through the experiments, the performance evaluation shows 23% improvement of angular resolution than the conventional Y-type [C4951]

"2004 Second International Workshop Ultrawideband and Ultrashort Impulse Signals (IEEE Cat. No.04EX925)"

{no data available} [C4952]

"Wideband radar remote sensing of the atmosphere: a data interpretation problem"

Wideband radar application for the remote sensing of the atmosphere is considered. Features of distributed targets as objects of wideband radar observations are shown. The difficulties of the retrieval meteorological information from the returns are discussed. Prospect of UWB radar for remote sensing is reviewed. [C4953]

"Signal deconvolution with successive filterings"

Image filtering by Richardson-Lucy algorithm shows an iterative solution for monodimensional signal deconvolution. In this paper the performance of this algorithm will be verified when lidar (light detection and ranging) signals are pre-filtered by an adaptive low-pass filter followed by a couple of ner/nerd filters. Most interesting results, for real-time deconvolution and filtering of lidar signal, will be also showed. [C4954]

"Discontinuous Non-Rigid Motion Analysis of Sea Ice using C-Band Synthetic Aperture Radar Satellite Imagery"

Sea-ice motion consists of complex non-rigid motions involving continuous, piece-wise continuous and discrete particle motion. Techniques for estimating non-rigid motion of sea ice from pairs of satellite images (generally spaced three days apart) are still in the developmental stages. For interior Arctic and Antarctic pack ice, the continuum assumption begins to fail below the 5 km scale with evidence of discontinuities already revealed in models and remote sensing products in the form of abrupt changes in magnitude and direction of the differential velocity. Using a hierarchical multi-scale phase-correlation method and profiting from known limitations of cross correlation methods, we incorporate the identification of discontinuities into our motion estimation algorithm, thereby descending below the continuum threshold to examine the phenomenon of discontinuous non-rigid sea-ice motion. [C4955]

"Retrieving soil moisture over bare soil from ERS wind scatterometer data"

The ERS-1/2 wind scatterometer (WSC) has a resolution cell of about 50 km but provides a high repetition rate (less than four days) and makes measurements at multiple incidence angles. In order to estimate effective surface reflectivity (related to soil moisture content) over bare soil using this instrument, an original methodology based on the integral equation model (IEM) is presented that takes advantage of multiple view angular observations which means two independent observations at the same resolution cell and same time. The possibility of applying the inversion procedure to retrieve soil moisture is investigated using a set of data collected from the Intensive Observation Period (IOP '98) field campaign in 1998 of the Global Energy and Water Experiment (GEWEX) Asian Monsoon Experiment Tibet (GAME/Tibet). The retrieved values obtained for the bare surface are consistent with ground measurements collected in these areas [C4956]

"Estimate LAI of crops using airborne multi-angular data"

Usually we use multi-channel image data, such as TM, and empirical relationship, such as NDVI-LAI relation or SR-LAI relation, to estimate LAI. Multi-angular remote sensing data provide more information for canopy structure. This paper presents a method to estimate LAI using multi-angular data and model inversion method. The airborne multi-angular data were acquired by AMTIS (Airborne Multi-angle TIR/VNIR Imaging System), which was a prototype sensor designed by the Institute of Remote Sensing Applications of Chinese Academy of Science. Our study is based on two datasets: one was acquired in Beijing Shunyi in April 11, and the major crop is sparse winter wheat; another was acquired in Haerbin in August 24, and major crops are dense corn and soybean. Both datasets have been geometrically atmospherically corrected. Ground based measurements were carried out during the flight experiment. SAIL model is chosen to predict reflected radiance of a presumed LAI. Various view angles relate to the different components ratio in view field, and the reflected radiance is different accordingly. Hence, a certain LAI value was given, SAIL model predicts a set of reflected radiances of various angles. We compare the model predict radiance with the radiance viewed by an multi-angular sensor, to find the optimized LAI which can make the radiance predicted by the model be closest to the viewed radiance, then take this LAI value as the right value [C4957]

"L-band active-passive and L-C-X-bands passive data for soil moisture retrieval, two different approaches in comparison"

In the context of the project HYDRO-POL, a study was carried out to test the efficiency of two different approaches: the use of L band active and passive data or the use of L-C-X bands passive data to retrieve soil moisture of bare soils. Simulated data are generated implementing classical superficial scattering models: IEM model for active L-band and L-C-band passive data, GO model for X-band passive data. Data are simulated considering different roughness conditions and moisture content. As the inversion problem is very complex, artificial feedforward backpropagation neural networks (NN) were employed. The best performing NNs are chosen to simulate a retrieval with a dataset artificially added with noise. In each case, the best retrieved parameter is the real part of the dielectric constant, while roughness parameters, especially autocorrelation length, is not very well retrieved. In many cases, retrieved values are out of range, so that the simulated values and targets appear unrelated. Applying a very generic filter that eliminates values very far from the proper range, correlation coefficients grow up. This filter cleans up the resulting data removing a small part of them. After this filtration, correlation coefficients relative to the real part of the dielectric constant surpass 0.82. In spite of the filtering process, roughness parameters retrieval is of inferior quality. On smooth soil, the three considered configurations work in an equivalent way, excellently retrieving the real part of the dielectric constant, without a need for filtration. On medium and rough soil, inversion results generally more difficult, so that performance gets worse. Active-passive approach results more efficient than the L-C-X one [C4958]

"Validation of raindrop size distribution retrieval from spaceborne radar using ground polarimetric radar observations"

The cumulative attenuation (A) along TRMM PR path given by the surface reference technique (SRT) can be distributed along the radar range using a power law relation between the specific attenuation (k) and reflectivity factor (z) written as, $k = \alpha z^\beta$. A commonly used approximation is that β is constant and α changes according to the raindrop size distribution (DSD). More recently physical interpretation of α has been provided with the normalized drop size distributions. This paper evaluates the method to estimate the DSD parameters from TRMM PR observations. Coincident data collected with polarimetric radar on the ground during the TRMM field campaigns was used to compare the estimates of DSD retrieved from TRMM PR. This paper also introduces a new methodology for comparing DSD estimates from widely varying sampling volumes. The cross validation shows fairly good agreement, thereby validating the DSD retrieval process [C4959]

"High resolution radar imaging using GPOF based data extrapolation"

A new data extrapolation technique which utilizes pole extraction based GPOF method is proposed to fit the scattering characteristics of an object. The proposed data extrapolation method is very efficient for data extrapolation when applied to the ISAR data. Modeling the data as the superposition of complex exponential signals, GPOF and Prony methods do not guarantee a stable prediction filter like the MCM method, while Burg ensures. Meanwhile, the performance of GPOF decreases with the increasing number of scattering centers but the radar images obtained using this extrapolated data is still more accurate than those obtained using the extrapolated data generated by other methods [C4960]

"Vegetation height derivation from Shuttle Radar Topography Mission data in southeast Georgia, USA"

A study was conducted to determine the extent to which data from the 2000 Shuttle Radar Topography Mission (SRTM) can be used to estimate vegetation canopy height in conjunction with an existing bald Earth DEM as provided by the National Elevation Dataset (NED). Intensively managed slash pine stands with canopy heights ranging from 11 to 21 m were biometrically surveyed within the general mission timeframe in early 2000. Results indicate that SRTM data can be successfully correlated via linear regression modeling with ground-measured mean vegetation canopy height at the stand level when mean SRTM-NED height difference measures are extracted by averaging pixels within the stands. Regression analysis using 20 and 50 pixels as stand size thresholds yielded adjusted r^2 values of 0.79 and 0.86 with rms errors of 1.1 m and 1.0 m respectively. Thus a minimum SRTM mapping unit of approximately 1.8 hectares can be postulated which allows vegetation canopy height retrieval at the stand scale [C4961]

"Comparison of DEMs derived from SRTM/X- and C-band"

In February 2000, the Shuttle Radar Topography Mission (SRTM) successfully mapped the entire landmass between 60deg N and 54deg S using an Interferometric Synthetic Aperture Radar (InSAR). The data were acquired in Cand X-band and were independently processed to Digital Elevation Models (DEM) by NASA-JPL (C-band) and DLR (X-band). A commonly used source was the Position and Attitude Determination Record (PADR) generated by the Attitude Orbit Determination Avionics (AODA) system. The PADR file provides the orbit and baseline information. All C- and X-band data were systematically processed to 1 arc-second resolution DEMs. The X-band DEMs are globally available at DLRs German Remote Sensing Data Center (DFD). USGS provides the C-band derived elevation data in 1 arc-second for the US and globally a reduced version with 3 arc-second spacing. The presentation compares the X- and C-band derived elevation models. Starting from the individual verification results the correspondence of the SRTM DEMs with respect to height and location accuracy is investigated. Potential global and local discrepancies are discussed. Both datasets are compared to the Altimetry Corrected Elevations global DEM (ACE) [C4962]

"TerraSAR-L SAR parameter simulation"

The TerraSAR-L system, currently being designed in a Phase B definition study, provides ESA with its most powerful radar-imaging programme to date. The platform, based on a Snapdragon configuration, is optimized for and built around the 11 m times 2.9 m active phased array antenna of the L-band Synthetic Aperture Radar (L-SAR). The L-SAR features, on top of standard Stripmap and ScanSAR operations, full polarimetric capabilities, repeat-pass ScanSAR interferometry and a Wave Mode. The TerraSAR-L spacecraft flies in a near-polar sun-synchronous low Earth orbit. An attitude steering operation to reduce the Doppler frequency caused by the Earth's rotation is foreseen. The knowledge of the relative distance between the spacecraft in orbit and a point scatterer on Earth during the radar illumination time, the so-called slant range history, is a crucial input for SAR focusing. Usually, this trajectory is approximated by an appropriate function. The validity of the approximation within the required accuracy margins has to be ensured. The applied attitude steering is a major driver for the Doppler parameters and thus the allowed approximations. This paper introduces the major TerraSAR-L orbit parameters and imaging configurations. Based on the nominal Kepler reference orbit, the round-orbit Doppler characteristics for TerraSAR-L are derived. The DLR developed Total Zero Doppler Steering is investigated as a suitable candidate for the TerraSAR-L attitude steering. A range trajectory approximation is investigated [C4963]

"The TerraSAR-L mission and system"

The TerraSAR-L system, currently in Phase B definition carried out by a European/Canadian consortium lead by EADS Astrium Ltd., provides ESA with its most powerful radar imaging programme to date. Key mission characteristics are a 5-year mission lifetime, global coverage from a 14-day repeat 635-km orbit, more than 20 minutes per orbit of SAR data acquisition in L-band, in both right-looking (nominal) and left-looking

configurations, and a launch in late 2008. TerraSAR-L first mission priority is serving commercial applications focused on agriculture, forestry and marine applications. Joint products from TerraSAR-L and the German national programme TerraSAR-X use the complementary properties of the backscattering in L and X bands for high levels of classification performance necessary for crop monitoring, forest inventory and cartographic maps of different thematic content and scale. Scientific and institutional applications are defined focused on solid Earth monitoring relying on differential interferometry. L-band penetration of vegetation cover facilitates these applications also over vegetated surfaces. The high coherence of L-band assists the monitoring of ice sheet and glacier dynamics. Sea ice classification is supported with full polarimetric measurements. Large-scale land cover change detection, global forest biomass estimation, permafrost monitoring, wetland inventory, soil moisture retrieval and flood monitoring are also supported. A dedicated Wave Mode provides measurements of directional ocean surface wave spectra. Additionally for single-pass interferometry and generation of a global DEM, a complementary cartwheel system with different micro satellite constellations flying in close formation with TerraSAR-L has been investigated. The spacecraft is built around an active phased array antenna and provides full polarimetric capabilities, maximum bandwidth within the 85 MHz allocation for Earth observation in L-band, and repeat-pass ScanSAR interferometry.- The platform is based on a novel Snapdragon configuration. The TerraSAR-L Ground Segment provides the operational link between the spacecraft, the TerraSAR Exploitation and Service Infrastructure and the users. A high-performance modular architecture is designed to fulfil the high requirements on throughput, quality and accessibility of data, as well as the reuse of existing infrastructure elements and the interoperability with other missions, especially with the companion TerraSAR-X Ground Segment [C4964]

"Implementation of systematic data observation strategies for ALOS PALSAR, PRISM and AVNIR-2"

The Advanced Land Observing Satellite (ALOS) is scheduled for launch by the Japan Aerospace Exploration Agency (JAXA) in 2005, and it carries three remote sensing instruments: an L-band polarimetric Synthetic Aperture Radar (PALSAR), an along-track 2.5 metre panchromatic resolution stereo mapper (PRISM) and a 10-metre multi-spectral scanner (AVNIR-2). The successor of the JERS-1 satellite (1992-1998), ALOS not only provides enhanced sensor performance, but also feature an entirely new acquisition concept. Abandoning traditional, local-focused instrument operations, JAXA is implementing a comprehensive acquisition strategy, in which geographical region, sensor mode, acquisition timing and repetition frequency, are fixed in advance, to achieve spatially and temporally consistent, global coverage on a repetitive basis, at the same time as reducing programming and user conflicts [C4965]

"Study on the sea ice thickness observation in the Sea of Okhotsk by using dual-frequency and fully polarimetric airborne SAR (Pi-SAR) data"

The Sea of Okhotsk is located in the most southerly region of the Northern Hemisphere in which sea ice exists during winter. Since the area and volume of the sea ice in this region are related to climate change locally as well as globally, it is important to develop methods for monitoring sea ice parameters around this region. Since Synthetic Aperture Radar (SAR) can observe continuously in any weather conditions, it is useful for observing the sea ice covered region. In order to investigate the possibilities of dual frequency and polarimetric SAR to monitor the sea ice, we derived the relation between backscattering coefficients each polarization and sea ice physical parameters, and then we proposed a sea ice classification using a polarimetric decomposition and a sea ice thickness estimation using the backscatter ratio [C4966]

"An effective algorithm in radar image processing"

The memory organization of Radix-4 FFT is considered. The new memory addressing assignment allows simultaneously access to all the data needed for butterfly calculation. The advantage of this memory addressing lies in the fact that it reduces the delay of address generation to one fourth of the existed [C4967]

"A simple boundary process technique for empirical mode decomposition"

The empirical mode decomposition (EMD) proposed by Huang et al. in 1998 shows remarkably effective in analyzing nonlinear signals. It adaptively represents nonstationary signals as sums of zero-mean amplitude modulation-frequency modulation (AM-FM) components by iteratively conducting the sifting process. How to determine the boundary conditions of the cubic spline when constructing the envelopes of data is the critical issue of the sifting process. A simple bound hit process technique is presented in this paper which constructs two periodic series from the original data by even and odd extension and then builds the envelopes using cubic spline with periodic boundary condition. The EMD is conducted fluently without any assumptions of the processed data by this approach. An example is presented to pick out the weak modulation of internal waves

from an Envisat ASAR image by EMD with the boundary process technique [C4968]

"Use of the multiresolution capability of wavelets for ship detection in SAR imagery"

Carrying out an effective control of fishing activities is essential to guarantee a sustainable exploitation of sea resources. As the regulated areas are extended, satellite-based synthetic aperture radar (SAR) provides a powerful surveillance capability allowing the observation of broad expanses, independently from weather effects and from the day/night cycle. This paper proposes a novel approach for ship detection based on the analysis of oceanic SAR images by means of the wavelet transform. The analysis of the detection performance over both simulated and real RADARSAT SAR images confirms the robustness of the proposed method: ships, undetectable with other conventional techniques are noticeably sharpened, whereas background noise is drastically reduced [C4969]

"High resolution DBS imaging and the moving target trajectory forming with raw SAR/GMTI Data"

DBS (Doppler beam sharpening) technique is widely used in military. In this paper, the basic theory of DBS imaging is introduced at first, and a conclusion is reached by analysis that range cell migration correction technique and azimuth dechirping technique can improve image quality effectively on SAR/GMTI (synthetic aperture radar/ground moving target indication) mode. And it is possible to form the moving target trajectory on the image because of the high resolution. Lastly, some satisfactory results based on the raw radar data are presented [C4970]

"A wavelet transform method to detect boundaries between land and water in SAR image"

Edge detection is important and key to image segmentation, information extraction, mapping etc. It is more difficult with SAR images than optical images, because of speckle. The aim of the paper is to show how boundaries between land and water can be detected from SAR images by using wavelet transform method, block-tracing algorithm and snake algorithm. The Ku-Band SAR image was obtained on 14 July 2003. The test area is near Huai River, located in city of Fuyang, Anhui Province. This SAR is made by Institute of Electronics, Chinese Academy of Sciences. Its azimuth resolution is 1.25 m and its range resolution is 1.2 m. To detect water edge, we apply a wavelet transform method to obtain the low-resolution image of the original image and suppress the speckle. Then we use a block-tracing algorithm to determine the coarse boundary between land and water and obtain a continuous edge. In the end, we use the snake algorithm to obtain the accurate edge. The result proves our method is a good method [C4971]

"Radar backscatter of rice fields from ASAR data and modeling"

Rice is one of the agricultural crops most suited to monitoring with the SAR instruments. Backscatter response measured by SAR is correlated with rice conditions, including height, density, biomass and structure, which are variable at different growing stages. In this paper, multi-date Envisat ASAR Alternating Polarization Mode (APMode) imageries were acquired during the rice crop growing cycle. At the same time, the rice parameters were measured in field. A continuous canopy model was used to compute the backscatter from rice fields during the growth cycle. The simulated backscattering coefficients were compared with the ASAR image data, and the relationship of rice parameters and radar backscattering coefficients from both ASAR and modeling were analyzed. It was found that simulated radar backscatter has similar trends as ASAR data, and that the HV polarization data is more suitable for rice parameters estimation. This will be meaningful for the further research of rice parameters estimation from ASAR data [C4972]

"Open water detection from Baltic sea ice SAR imagery"

The algorithm for separating Baltic Sea Ice and open water from our operational SAR data are presented. The algorithm is based on segment wise autocorrelation with some simple additional rules to improve the classification. The algorithm results are compared to the open water and sea ice separation available in daily digitized ice charts and the algorithm performance is also compared to open water detection by pixel-wise autocorrelation thresholding [C4973]

"Measurement of scattering coefficient dependence on soil moisture content and surface roughness by 35 GHz polarimetric scatterometer"

Polarimetric measurements of scattering coefficient σ_0 of a bare soil were performed changing a roughness of a soil surface and a soil moisture content using the 35 GHz polarimetric scatterometer. At Ka band, a few experimental results of σ_0 data are available. One of the purpose of this experiment is to obtain the surface backscattering characteristics to evaluate surface clutter interference with precipitation measurement from space

using the Dual frequency Precipitation Radar (DPR, 13.8 GHz and 35.5 GHz), which is planned to be onboard the Global Precipitation Measurement (GPM) Mission core satellite to observe precipitation globally. In evaluation of surface clutter interference, σ^0 data for various surface conditions are needed, especially σ^0 dependence on soil moisture content and surface roughness. Another purpose of this experiment is to apply the measured σ^0 data to estimate a soil moisture content globally after the launch of the GPM core satellite. An angular scan range of the DPR is from nadir direction though the incidence angle of 8.4 degrees (with the 35.5 GHz radar) or 17 degrees (with 13.6 GHz radar), so the measured data by the DPR is useful to observe the earth surface condition globally. In this study, the roughness of the soil surface was measured with a laser profile meter to determine the roughness dependence of the scattering coefficient. A soil moisture content was measured comparing the weight of the soil before and after the heating of the soil. The soil was heated enough to contain no water. To increase the number of the independent samples for each experimental conditions (soil moisture content/surface roughness/incidence angle), azimuthal angle is changed like clockwork using the turntable of 2 m diameter. The system of the scatterometer is network analyzer based polarimeter [C4974]

"Application of bistatic MIMICS to forest canopies"

A bistatic version of the Michigan Microwave Canopy Scattering model (MIMICS) is developed to simulate bistatic scattering from forest canopies. We present the applications of bistatic MIMICS in This work. By simulating the forest canopy scattering from multiple viewpoints, we can observe how a forest's structure, orientation and density affect the canopy scattering. We show that the bistatic scattering is more sensitive to forest biomass changes than backscattering. Analyzing the scattering contributions from different parts of the canopy gives us better knowledge of the microwave's interaction with the tree components. The ground effects can also be studied. The simulation results of the model offer credible results for the research and design of future bistatic radar systems. [C4975]

"The TerraSAR-L basic product tree"

The TerraSAR-L system, currently being designed in a Phase B definition study, provides ESA with its most powerful radar-imaging programme to date. The platform is optimized for and built around the 11 m times 2.9 m active phased array antenna of the L-band Synthetic Aperture Radar (L-SAR). The L-SAR features, on top of standard Stripmap and ScanSAR operations, full polarimetric capabilities, repeat-pass ScanSAR interferometry and a Wave Mode. Specification of the L-SAR has been guided by a careful analysis of the product requirements resulting in a robust baseline design with considerable margins. Besides, a major contribution to applications in areas of climate change and oceanography, the TerraSAR-L design responds specifically to requirements from interferometric applications. One key element of the TerraSAR-L operations strategy is a long-term systematic and repetitive acquisition scenario to ensure consistent data archives and to maximize the scientific and commercial exploitation of this SAR system. The other important factor is a systematic processing of all acquired data to Single-look Slant-range Complex (SSC) products to facilitate higher level product generation and services based on these products. This paper describes the TerraSAR-L basic product tree and explains the rationale behind. The nominal TerraSAR-L imaging modes are introduced and their performance characteristics are described. The generation concept of multi-look detected products based consistently on complex products-generated either at an intermediate stage during ground segment processing or serving as input product into a stand-alone tool-is introduced. A modular SAR processor design using the same complex product generation algorithms as far as possible independent of the underlying imaging mode is addressed [C4976]

"Eddy detection using RADARSAT-1 synthetic aperture radar"

Two projects undertaken by the National Oceanic and Atmospheric Administration (NOAA) National Environmental Satellite, Data, and Information Service (NESDIS) have shown success in using spaceborne synthetic aperture radar (SAR) to identify oceanic eddies and current boundaries. In addition to detecting the frontal area and change in slick patterns, the SAR imagery may also pick up a change in the low-level wind structure as a result of the sea surface temperature (SST) gradient between the eddy and its surroundings affecting the marine atmospheric boundary layer (MABL) stability. This wind fluctuation modulates the sea surface roughness, allowing the eddy boundaries to be imaged by SAR. Two examples, one of an eddy in the Gulf of Alaska, and the second of the Loop Current boundary in the Gulf of Mexico, are analyzed to show the correlation between the SST and surface wind gradients across their boundaries [C4977]

"Application of multi-band and full-polarization SAR in shallow sea bottom topography measurement"

Based on the imaging mechanics of synthetic aperture radar (SAR) mapping shallow sea bottom topography, a new method was proposed using multi-band and full-polarization SAR. If this method was used, it should need fewer in-situ data in multi-band and full-polarization SAR than single-band and single-polarization SAR for bottom topography measurement. It should be much more accurate [C4978]

"Applications of CBERS-2 image data in flood disaster remote sensing monitoring"

This study aimed at investigating the potential applications of the China Brazil Earth Resource Satellite 2(CBERS-2) image data in flood disaster remote sensing monitoring and assessing. We selected the area of Lixiahe situated in the north of Jiangsu province, China, as the study area, which is part of the drainage area of Huaihe River. In the summer of 2003, this area seriously suffered from flood disaster. CBERS-2 image data from Nov. 16th, 2003 was used. We also used RADARSAT image, high-resolution airborne radar image and Landsat-5 TM image data in this study. Based on the detailed analysis of satellite images by visual interpretation and comparison, combined with field validation, the applicability of CBERS-2 image data in flood disaster monitoring and assessment was evaluated in the following 3 aspects: 1) analyzing and assessing the disaster situation; 2) producing data of normal water extent; and 3) producing orthographic maps for flood disaster monitoring [C4979]

"A FARIMA based analysis for wind falls and oil slicks discrimination in sea SAR imagery"

The aim of this paper is to define an analysis technique, which uses the fractionally integrated autoregressive-moving average (FARIMA) model, for discriminating wind falls from oil slick areas in sea SAR imagery. The method deals with the estimation of the fractional differencing and ARMA parameters for the sea SAR images mean radial PSD and is applied to some ERS-1 and ERS-2 images of the Mediterranean sea, North sea and Atlantic (Galicia) ocean containing only oil slick or only wind falls, or wind falls and oil slick anomalies [C4980]

"Applicability of the K distribution to RADARSAT maritime imagery"

Estimators of K distribution parameters are reviewed. On the basis of a χ^2 -test, 12 RADARSAT images (Standard, Wide and ScanSAR) are found to be rather well described by a K distribution; however, their false alarm rate is an order too high. The impact of 8 bit storage is discussed [C4981]

"Oil slick detection by SAR imagery: algorithms comparison"

C-band SAR is well adapted to detect ocean pollution because backscatter is reduced by oil slicks. They appear as dark patches on the image as the increase of viscosity due to the presence of oil damps gravity-capillarity waves. In order to detect these dark patches, we use algorithms based on filters, gradients, and morphological mathematics, and a new approach based on ocean surface characterization. We have tested these methods on ERS and ENVISAT images acquired during Prestige tanker wreckage and the results are compared with aircraft surveys. We conclude that slicks with high contrast and simple shape are easily detected using basic algorithms, but most of the time, other methods are needed. The ocean characterization method is a way to follow for improving oil slick detection and providing decision aids for classification step [C4982]

"SAR ocean wave measurements based on an empirical imaging model"

Spaceborne Synthetic Aperture radar is still the only instrument providing continuous wave measurements on a global basis. For more than a decade, the European satellites ERS-1 and ERS-2 have acquired about 1500 globally distributed SAR images daily. It is well known however that strong uncertainties exist in the SAR ocean wave imaging models used so far, which are either purely theoretical or semi-empirical. In this study, a new empirical model for the SAR ocean wave imaging process is proposed. The empirical model is derived based on a global data set of ERS-2 wave mode spectra and collocated two-dimensional ocean wave spectra from the numerical ocean wave model WAM. A quasi-linear model function is fitted using a least-square minimization approach to calculate an optimal estimate of the ocean to SAR transfer function. The empirical transfer function is compared to the theoretical expression used in the literature. The quality of the empirical model is tested by comparison of simulated and observed SAR spectra. Furthermore, the model is used to estimate significant wave heights based on a quasi-linear inversion approach. Statistics as well as global maps of wave parameters are presented. The study is a contribution to the optimization of the operational use of global SAR data for the assimilation of numerical wave forecast models [C4983]

"An improved CFAR model for ship detection in SAR imagery"

This paper presents an improved constant false alarm rate (CFAR) model for ship detection in synthetic aperture radar (SAR) imagery. The model includes the probabilistic neural networks, CFAR technique, golden section method and area growth method. It is compared with other ship detection methods. The results show that the

improved CFAR model performs well [C4984]

"Sea surface ship detection in SAR images"

Algorithm for sea surface ship detection is described. The algorithm is designed for ship detection in SAR images. Morphological filter is introduced to decrease false alarms. Scan line based seed cluster algorithm is used during ship pixel clustering. Ship parameters can be estimated finally [C4985]

"Mapping of flooding in the Alessandria area with ERS"

We demonstrate a fully automatic flood detector for non-forested areas on an ERS SAR image of the 1994 flooding incident in Alessandria, Italy. The flood detector is capable of detecting the majority of the flooded area. However, there are some undetected flooded areas which exhibit high backscatter caused by double bouncing from flooded vegetation [C4986]

"Dualband-TerraSAR simulation/campaign results for L-band configuration"

The objectives of the TerraSAR-SIM campaign were to quantify the impact of the time intervals between SAR acquisitions at different wavelengths on agricultural applications. In 2 flight campaigns in 5 similar flight programs suitable multipolarised L-, X- and C-band radar data were acquired in a test site in Barrax. The different processing qualities of the level 1b data were analysed with different evaluation methods such as separability analysis, scatter plots, histogram analysis, biomass correlation, classification. Particularly the separability analysis was used in order to assess the influence and quality of the different radar wavelength, polarisations, acquisition dates/time lags and of level 1B processing parameters on the quality of agricultural and land use applications and retrieval algorithms. Campaign and analysis results are presented in the following paper [C4987]

"Land surface observation using multi-polarization ENVISAT ASAR data"

Multi-polarized space borne SAR data can be used to detect changes in land cover. The ENVISAT ASAR has the ability to acquire images using two polarizations simultaneously. This paper discusses the capability of detecting land surface characteristics using ENVISAT ASAR dual polarization data. The applicability of image mode and alternative polarization mode data are investigated, and backscattering coefficients for images with different polarizations are compared. Optical images and GIS data are used as reference data. Two types of land cover in Japan are examined: forest on an active volcano (Miyakejima, a volcanic island that erupted in 2000), and an urban area (central Tokyo). Differences were evident between bare land and forest areas in the HH and HV polarized data sets. City street patterns exhibit differences in backscattering characteristics between like- and crosspolarized SAR images: cross-polarization backscattering is increased for streets that are inclined to the radar irradiation direction [C4988]

"A description of the data-driven SAR data workflow in the TerraSAR-X Payload Ground Segment"

TerraSAR-X is a national German satellite providing a high-resolution X-Band SAR instrumentation featuring StripMap, ScanSAR and SpotLight imaging modes in various polarizations. The experimental full polarization mode is carried out using a dual receive antenna capability. An active lifetime of five years is anticipated, the launch is expected in 2006. The TerraSAR-X mission serves both commercial and scientific needs. It is implemented in the frame of a public-private partnership between EADS Astrium GmbH (providing the TerraSAR-X Space Segment) and the German Aerospace Center DLR (providing the TerraSAR-X Ground Segment). The commercial product exploitation rights are with Infoterra GmbH, the scientific ones remain at DLR. The Infoterra business concept foresees the inclusion of a Direct Access Service through which TerraSAR-X data may be directly received by stations either for the sole purpose to produce geo-information products for their own and private applications or to generate and distribute commercial products. Essential tasks of the TerraSAR-X Payload Ground Segment developed (and later operated) by DLR are the SAR payload data reception, their archiving and processing, and the distribution of the generated SAR products to users. This paper summarizes the TerraSAR-X Payload Ground Segment design. It describes the SAR data workflow ranging from the payload data reception at the Neustrelitz Ground Station to the long-term data archiving in the multi-mission Product Library at the German Remote Sensing Data Center. Supplementary data as provided by the TerraSAR-X Mission Operation Segment and used during the data-driven generation of the SAR level 0 products are described together with their dissemination concept. The adaptability of the chosen approach for the operation of a Direct Access Station is addressed [C4989]

"High resolution DEM generation from ALOS PRISM data-simulation and evaluation"

The Advanced Land Observing Satellite (ALOS) has been developed to contribute to the fields of mapping,

precise land coverage observation, disaster monitoring, and resource surveying. The Panchromatic Remote-sensing Instrument for Stereo Mapping (PRISM), carried on ALOS satellite is expected to generate worldwide Digital Maps in respects of its high resolution and stereoscopic observation. The development and evaluation of the software for generating Digital Elevation Model (DEM), based on this aim of ALOS operation, is now undertaking for the purpose of equipping the system which producing DEM semi-routinely in the Earth Observation Research and application Center (EORC). In this paper, the software's outline of functions, the algorithm and the current status of its development and evaluation are described. PRISM consists of three panchromatic radiometers for forward, nadir, and backward views and acquires each image in the same orbit at almost the same time. It enables to generate more precision DEM frequently than usual stereoscopic observations. For this specific stereo image configuration, the triplet images matching algorithm is applied for the DEM generation. To evaluate the algorithm, Three Line Scanner (TLS) data is used as the PRISM simulation data and the Lidar DEM is used as the reference data. The absolute accuracy of generated DEM is estimated in this simulation [C4990]

"Biophysical properties of wetlands vegetation retrieved from satellite images"

The investigation carried out at wetlands in Biebrza Basin, the biggest area of the marshes and swamps in Central Europe, aimed at finding the best biophysical properties of wetlands vegetation to characterise marshland habitats. The various soil-vegetation indices on the basis of all considered spectral bands of satellites as Landsat +ETM, SPOT, ERS-2, NOAA, ENVISAT have been calculated. The GEMI and EVI index calculated from SPOT VEGETATION was the best for distinguishing vegetation classes. Significant correlation between LAI measured at the ground and the indices was with GEMI and EVI index. Soil moisture values calculated from ERS-2 and ENVISAT microwave data well characterise marshland humidity classes. For the retrieval of the biophysical parameters as LAI (Leaf Area Index), vegetation moisture (VM) and soil moisture (SM), ERS-2.SAR and ENVISAT ASAR data acquired at VV, HV, VH and HH polarisations at two different viewing angles (IS2, IS4) have been applied. Evapotranspiration was assessed using NOAA AVHRR and meteorological data. ERS-2 and ENVISAT images have been obtained from ESA for AO-ID122 project [C4991]

"The estimation of distribution in field scale of surface aerodynamic roughness using remote sensing data"

This paper presents a new way to calculate the aerodynamic roughness using the surface geometric roughness retrieved from SAR (Synthetic Aperture Radar) and TM thermal infrared image data. On the one hand, the SPM (Small Perturbation Model) was used as a theoretical SAR backscattering model to describe the relationship between the SAR backscattering coefficient and the surface geometric roughness and its dielectric constant retrieved from the physical model between the soil thermal inertia and the soil moisture with the simultaneous TM thermal infrared image data and the ground microclimate data. On the basis of the SAR image matching with the TM image, the non-volume scattering surface geometric information was obtained from the SPM model at the TM image pixel scale, and the ground pixel surface's equivalent geometric roughness-height standard RMS (Root Mean Square) was achieved from the geometric information by the transformation of the typical topographic factors. The vegetation (wheat, tree) height retrieved from spectrum model was also transferred into its equivalent geometric roughness. A complete two-dimensional distribution map of the equivalent geometric roughness over the experimental area was produced by the data mosaic technique. On the other hand, according to the atmosphere eddy currents theory, the aerodynamic surface roughness was iterated out with the atmosphere stability correction method using the wind and the temperature profiles data measured at several typical fields such as bare soil field and vegetation field. After having analyzed the effect of surface equivalent geometric roughness together with dynamic and thermodynamic factors on the aerodynamic surface roughness within the working area. The final result retrieved from above series of models was validated by the in-situ measured data [C4992]

"Soil parameters retrieval from remotely sensed data: efficiency of neural network and Bayesian approaches"

Six remote sensing experiments are analyzed in order to study the feasibility of soil parameters extraction from active and passive microwave data. The inversion process has been carried out through two methodologies: a Bayesian and a neural network approach. Two different sets of data have been analyzed: one experiment with active and passive data on a smooth soil and five experiments carried out with a C-band scatterometer on rough and smooth soils at different polarizations and incidence angles. In the case of active and passive data, using a Bayesian algorithm, the correlation coefficients between the extracted and the measured values of soil moisture are $R=0.83$, $R=0.84$ and 0.72 for the three analyzed data configurations. In the neural network approach, the correlation coefficients are $R=0.72$, $R=0.83$ and 0.79 . The best performance is achieved when two different frequencies, 4.6 GHz for active data and 2.5 GHz for passive data are employed where the neural networks

produce the lowest errors in the estimates. For the second group of data, the neural network makes fewer mistakes and overestimates only the values of ϵ_{SIV} that originated from backscattering coefficients acquired on the rougher field. The Bayesian approach tends to overestimate the values of ϵ_{SIV} with an average bias of 5% [C4993]

"Monitoring the Siberian boreal forest using ENVISAT/ASAR data: first analysis results"

This paper investigates the use of EVISAT/ASAR data for deriving forest information over Central Siberia. Temporal series of alternating polarisation data (HH and HV) at low and high incidence angles acquired at the Bolshemurstinsky test area are analysed. The backscattering coefficient of different forest types and land cover is analysed as a function of time, polarisation and incident angle using a GIS forest database available within the Siberia-II project. The results of the analysis indicate that HV data are adapted to forest/non forest mapping and both HH and HV are sensitive to low biomass values up to 50 m³ /ha [C4994]

"Temporal snow cover variation and terrain characteristics of Peary caribou habitats in the Canadian arctic using optical and InSAR data"

Interferometric synthetic aperture radar (InSAR) data from RADARSAT-1 have been examined to assess their potential for mapping terrain and changes in snow cover characteristics, relative to the limiting effects of snow on foraging by endangered Peary caribou (*Rangifer tarandus*). Radar is one of the few observational tools that can provide information on the changing snow pack during the dark winter months. The goal of this research is to characterize the general ensemble of terrain characteristics that may affect winter foraging patterns of Peary caribou and the inter-annual consistency of snow cover patterns within our specific study area [C4995]

"Analysis on noise reduction method for interferometric SAR image"

Noise in SAR interferogram brings much trouble in phase unwrapping. It will also influence the accuracy of digital elevation models. Based on realization of complex mean filtering, pivoting mean filtering, pivoting median filtering three noise reduction algorithms, their computations are analyzed and the effect of noise reduction is given out. In order to get the most optimized balance between computation and effect of noise reduction, a new noise reduction idea-second-time or multiple combined noise reduction is proposed. The algorithm can comprehend the merits of several noise reduction methods. It can preserve edge information well and decrease phase noise dramatically at the cost of adding a little computation. Based on computer simulation, certain terrain is set and the effect of noise reduction of new method is verified. The variance of before and after combined noise reduction is given out. The effect of three-time or more combined noise reduction is not obvious because noise has been reduced by second-time noise reduction. We do not recommend 4 or more-time combined noise reduction for its large computation. ERS-frac12 real data are also used to verify the validity of the new algorithm [C4996]

"Agent communication based SAR image parallel processing"

Airborne SAR remote sensing image has the characteristic of large data volume and computation burden, so the processing needs very large computer memory and stronger computation ability. Based on the introduction of the SAR image processing procedure, this paper studies the SAR image processing using computer parallel computation technology. The parallel processing mechanism is based on the parallel computer cluster operation and the large virtual shared memory technology. In the Client/Server architecture based SAR image parallel system, agent based network communication plays an important role in the computer performance monitor and burden distribution. In the end, the application of the SAR image parallel processing system in the disaster monitor and assessment system is introduced. The application result illustrates the high efficiency of the system and the feasibility of our research [C4997]

"SAR automatic range-migration correction"

A new idea is presented to correct range migration in SAR imaging. In the range-Doppler domain, all the samples at a given Doppler frequency constitute a Doppler slice. Different Doppler slices are found to have similar envelopes. According to this similarity, the Doppler slices are shifted in range to correct range migration. This technique applies even without the prior information about the relative motion between the radar and the target [C4998]

"Joint despeckling and edge detection of SAR images based on the Mumford-Shah functional"

In this paper, we propose a joint despeckling and edge detection algorithm based on the Mumford-Shah functional, which accomplishes the image filtering and segmentation as a result of an analytical variational

problem. This approach turns out to be well suited to jointly despeckle and segment SAR image data; the experimental results demonstrate that the proposed technique yields high quality despeckling without impairing critical image features and with the additional advantage to provide a detailed edge map [C4999]

"Geometric distortion correction in the subaperture processing for high squint airborne SAR imaging"

Basic subaperture processing for synthetic aperture radar (SAR) imaging consists of generating a set of low-resolution images and adding them coherently to form the final high resolution image. For an airborne high squint imaging mode SAR, the coherent addition processing suffers from the geometric distortion in the subaperture images caused by range-Doppler interaction and the irregularities in aircraft motion. This paper presents a method to compensate these effects based on the geographical coordinate transform, which is used as a middle processing prior to the coherent summation of the subaperture images. It mainly involves coordinates calculations between the focus target plane and the image display plane under the flat-Earth model, and then a 2D interpolation is carried out in the image domain. A quantitative evaluation using point-target simulations of the coherent subaperture imaging algorithm for a squint angle of 60deg is also provided. Its performance successfully demonstrates the validity of the proposed method. The further advantage of implementing this approach is that the crucial step of compensating the spatially-variant residual phase error can be done at the same time, and the resultant images with constant sample spacing are ready to be mosaiced to produce the full-strip image [C5000]

"Squint-spotlight SAR imaging by subband combination and range-walk removal"

A new algorithm for spotlight SAR imaging under squint mode is proposed in this paper. The structure of the algorithm is rather simple and can be divided into two parts: the sub-aperture imaging with range-walk removal and sub-band combination, which are relatively independent [C5001]

"Realization of SAR real-time processor by FPGA"

This paper designs and realizes a Synthetic Aperture Radar (SAR) real-time processor by FPGA chip EP1S25F672C6, analyses the performance advantages of using FPGA, and present the processing result of a frame of airborne SAR original data [C5002]

"Calibration of portable FM-CW Doppler radar profilers with an artificial target"

Two portable mono-static FM-CW Doppler radar profiler systems have been calibrated using a continuously rotating corner reflector. The front-ends of both radars apply semiconductors for the generation of the transmitted power. The portable 24 GHz profiler's aim is to record and investigate precipitation close to the ground. The 94 GHz profiler was developed for cloud investigation from the ground and from a research aircraft. The calibrations showed that the 24 GHz rain profiler is sensitive enough to fulfill its purpose. The 94 GHz profiler lacks the required sensitivity to date. Both radar systems will undergo major design revisions to gain higher system sensitivities. [C5003]

"Study on airborne ISAR imaging of ship targets"

Inverse Synthetic Aperture Radar (ISAR) is used to image noncooperative moving targets such as aircrafts, ships and celestial objects. The target rotation relative to the radar is the source for obtaining cross-range resolution in ISAR imaging. In airborne ISAR imaging of ships, the composition of the relative motion is more complicated than in other cases. One component is produced by the relative movement between the radar and the target. The other comes from the ship sway (roll, pitch and yaw). Furthermore, the practical sea-state changes frequently, and is also unpredictable. All of these increase the difficulty in image formation. In this paper, the airborne ISAR imaging of ship targets is substantially discussed, and we design a simulation software kit applicable to practical sea-state and arbitrary flight path. By using the simulated data, the effects of the various relative rotations between the radar and the target on the ISAR image are clearly demonstrated, and this simulation work provides good experiences for further study. Finally, some imaging results under certain simulation conditions are presented [C5004]

"Automatic extraction of vertical obstruction information from interferometric SAR elevation data"

Vertical obstructions (VOs) such as radio towers, power pylons, and windmills present a hazard to low-flying aircraft. We describe an automated VO detection scheme that processes digital surface models (DSMs) provided by interferometric SAR (InSAR) systems to produce heights and locations of VOs. By using only the height data from the InSAR, the resulting techniques can be applied to other DSM sources, such as lidar. Innovative

morphological filtering algorithms are described, which optimize detection performance against various DSM resolutions over smooth or rough terrain. The height and position estimates of the detected VOs are computed, and they compare favorably to ground truth. Software that implements these algorithms has been packaged as an add-on module to ERDAS IMAGINE®. [C5005]

"A novel theory of SAR image restoration and enhancement with ICA"

Active radar sensing is an important method of obtaining inventory information about remote and cloud-covered areas of the world. However, automatic interpretation of SAR images is often difficult due to speckle noise. Appearing as a random granular pattern, speckles seriously degrade the image quality and affect the task of human interpretation and scene analysis. For this kind of speckle removal problem, one of the difficulties is to overcome the tradeoff between noise reduction and preserving significant image details. In this paper, a novel theory of SAR image restoration and enhancement with independent component analysis (ICA) is proposed. We assume that the speckle noise in SAR images comes from a different signal source, which accompanies but is independent (their statistical characteristics are not same.) of the "true signal source" (image details). Thus the speckle removal problem can also be described as "signal source separation" problem. Then in order to enhance the "true signal source", we classify the basis images and span them into two different signal subspaces, namely "true signal subspace" and "speckle subspace". Finally we build different nonlinear estimators in each signal subspace to recover the original image. In our experiments, the SAR images consist of nine channels of images. We compare our method with two other well known speckle reduction approaches (Kuan filter and Lee filter). The results show that with our method the speckle noise is efficiently removed while at the same time important details (edges in particular) are retained without introducing artificial structures. We further calculate the ratio of standard deviation to mean (SD/Mean) for each image and use it as a criterion for image quality and find that the improvement with our method is more evident for images with "high level speckle noise" [C5006]

"An adaptive multiscale filter for segmenting vegetation in ALSM data"

A multiscale filter designed for segmenting ground from nonground points in ALSM data is extended to be adaptive by analytically determining admission thresholds based on prescribed error rates. The filter performs well on simulated and actual ALSM data [C5007]

"Automatic registration of synthetic aperture radar (SAR) images"

The huge amount of incoming synthetic aperture radar (SAR) data nowadays demands the need for automatic image registration. Due to the presence of speckle noise and the huge size of SAR images, registering SAR images is more difficult than traditional image registration methods. In this paper we present an automatic hierarchical registration method, based on polar block matching, that can handle the registration of SAR images efficiently. Results show us that our proposed registration method outperforms the manual registration and that our method is very robust against speckle noise. An additional advantage of our registration method is that there is no need for a despeckling preprocessing step [C5008]

"The effect of some internal neural network parameters on SAR texture classification performance"

Artificial neural networks have been successfully applied to image processing, and have shown a great potential in the classification of a wide range of remote sensing data. The major advantages of neural network algorithm over traditional classifiers are its nonparametric nature and its easy adaptation to different types of data format from multiple sources. However, a successful application of neural networks in remote sensing data classification requires a good comprehension of the effect of some internal parameters related to the neural network structure and training process. In this work we report the application of backpropagation neural network in classifying natural wetlands vegetation using SAR data. The effect of some parameters related to the architecture and the training process on classification performance was investigated and new techniques for ameliorating this performance are discussed. The results showed that the variations of the number of hidden layers and the number of nodes by layer have not a substantial effect on classification accuracy but affect only the training time. However, other parameters related to the neural algorithm computation (such as the threshold value) affect significantly the overall classification. It is concluded that, although the neural network method has a great potential in remote sensing data classification, a rigorous choice of the threshold value is still necessary to optimize the ratio of the incorrectly and the correctly classified pixels [C5009]

"Change detection in SAR images: spatial accuracy analysis"

In this work, the positional error components are studied in the process of registering SAR image data to vector data. We study the case in which only imprecise knowledge of a terrain model is available, affecting the achievable accuracy of the final registration. The available information is used to draw a spatial quality map

which aids in determining the local spatial change which can reliably be measured in parts of the image. [C5010]

"Vector reconstruction and mosaicing from multiple Doppler weather radar velocity data"

Radial velocity data from two or more Doppler weather radars are commonly combined to obtain the vector or true velocity of winds at a given location. This paper proposes a novel scheme for combining scalar and vector data from multiple radars. The number of overlapping radars at a point is automatically determined. The data combining algorithm (2D, 3D, or least-squares) is automatically determined from the number of overlapping radars. The use of latitude-longitude grid results in a universal grid presentation. A variable (user-definable) box-averaging method of vector representation is adopted and vector fields are depicted as fields of arrows. A novel method is adopted for handling boxes lying on boundaries of overlapping radar zones [C5011]

"Use of geo-referenced images for the surveillance of transmission lines right-of-way"

CTEEP transmission system is a government dependent company operating in the State of Sao Paulo (Brazil). Its aim is to provide power to this State which happens to be the most industrialized within Brazil. In some developing countries the continuous growing population trend to build their houses over corridors pertaining to transmission lines right-of-way. For this reason, the transmission companies have a continuous supervising task over these corridors, so that proper juridical actions are taken once such invasions occur. Satellite images, photogrammetry images and laser-based images generated are now available in the market. Due to the accuracy these technologies present (spatial resolution), they may become and constitute good tools with high applicability when used for this purpose. A methodology for the inspection of transmission lines right-of-way, making use of the previously mentioned images, is proposed. Along with the afore mentioned tools, it is also generated an information system (database) in which transmission towers, properties and land invasions are recorded under a geo-referenced juridical/civil aspect, and whose coordinates result in key information for the company. [C5012]

"Signatures of vessels in ENVISAT AP-mode imagery"

A series of ENVISAT AP mode data has been collected over the Nome field off the coast of central Norway. An oil production vessel has been imaged with different ASAR beams and polarisations to study how its signature changes with varying imaging parameters. Cross-polarised data gives better contrast for automated detection compared to co-polarised data, when the incidence angle is small. [C5013]

"SAR image change detection using distance between distributions of classes"

The problem of detecting abrupt changes in a set of synthetic aperture radar (SAR) images is carried out by comparing the results of segmentation between images with different modalities acquired before and after a disaster. Individual segmentations are not considered by themselves since they yield surface map characterization while the goal is to detect a temporal evolution of soil characteristics. Hence, we propose to use the modification of class statistics in the images in order to characterize potential changes and to prevent from false alarms that may be induced by the specific modality of each SAR acquisition. The change detection process is divided in two steps; 1) segmentation of the observations in order to have an estimation of the marginal probability distribution function (pdf) of each class; 2) comparison of the pdf from different images to detect changes by means of evidential and paradoxical reasoning. This two-stages process has been applied on Radarsat images (F2 and F5) of the Nyiragongo volcano, DR Congo, erupted on January 2002. The results obtained outperform simple strategies based on image differencing/ratioing [C5014]

"Assessment of multitemporal DInSAR stepwise processing"

We present an assessment of stepwise co-registration procedures applied to multitemporal SAR datasets. Images are connected in pairs through a minimum spanning tree structure, obtained by adopting a distance measure which is a function of the expected co-registration quality. Experiments have been performed on a test dataset by a) directly estimating the (a posteriori) co-registration quality over all possible image combinations, b) using an a priori model inspired by similar models for the multitemporal InSAR coherence, with parameters obtained experimentally, c) using the same a priori model with first-guess parameters. Performances were evaluated by analyzing the amplitude inverse coefficient of variation distribution over the co-registered image stacks obtained by the three procedures above. Results show that, although the best coupling strategy depends on the particular dataset and is thus difficult to model via general rules, a nonnegligible improvement in the performance of persistent scatterers interferometry techniques can be obtained by adopting stepwise approaches based on a priori models for the expected co-registration quality, rather than using a single acquisition as master [C5015]

"Aerosol and cloud measurements at 532 and 1064 nm by the GLAS polar orbiting lidar instrument"

The first polar orbiting satellite lidar instrument, the Geoscience Laser Altimeter System (GLAS), was launched in 2003 and is approaching six months of data operations. As part of the NASA Earth Observing System (EOS) project, the GLAS instrument is intended as a laser sensor fulfilling complementary requirements for several Earth science disciplines including atmospheric and surface applications on the Ice, Cloud and Land Elevation Satellite. In this paper we present examples of atmospheric measurement results and explain data products now accessible for the science community [C5016]

"Benchmarking operational SAR ship detection"

The performances of eight satellite SAR ship detection systems (most of them operational) are compared, by running a benchmark test on RADARSAT images of various modes. No single system is best under all circumstances [C5017]

"An edge detection method using 2-D autoregressive lattice prediction filters for remotely sensed images"

Edges characterize boundaries and are therefore a problem of fundamental importance in image processing. Edge detecting an image significantly reduces the amount of data and filters out useless information, while preserving the important structural properties in an image. Edge detection is useful for segmentation, registration, and identification of objects in remote sensing images. Two dimensional lattice filters have been shown to be useful in many applications such as multidimensional spectral estimation, image data compression, high-resolution radar imaging, and removal of correlated clutter to enhance the detection ability of small objects in images. In this work, lattice filters are used for detecting the edges in remote sensing images. Lattice filter can be used to predict the correlated parts in an image and the resulting error (the output of the filter) will be edges. Edge detection results have been compared with other conventional edge detection methods as well as wavelet based methods. Results show that the proposed method is a good candidate for edge detection problem in remotely sensed images [C5018]

"Extraction mechanism of alteration zones using ASTER imagery"

Remote sensing plays an important role in the mineral exploration. One of the common applications is to locate alteration zones related to gold deposits. Many studies based on landsat thematic mapper (TM) imagery have been carried out and several methods have been developed. However, the advanced spaceborne thermal emission and reflection radiometer (ASTER) imagery, which has better spectral resolution (14 bands) and spatial resolution (15 m in VNIR bands), was not widely used in this application field. This article indicates the ASTER imagery application in locating alteration zones in Laizhou area of Shandong Province. First, we studied the geological information and main alteration minerals' spectral features of the study area. Based on the above work, we calculated some band ratios (b_4/b_1 , b_4/b_6 , b_3/b_2) to enhance spectral response of some mineral materials and vegetations. Then, a principal component analysis was applied to these band ratios. After applying PCA, the eigenvector matrix was analyzed to identify which PC (principal component) contained more useful information of alteration minerals. We chose the PC that enhanced the response of alteration minerals and reduced the response of vegetations, from which we could discriminate the alteration rocks. The satisfactory result shows that ASTER imagery works well in the exploration of alteration zones [C5019]

"An MRF based technique for speckle reduction in SAR images"

SAR images are affected by speckle that affects radiometric resolution and class discrimination capabilities. Recently, different speckle reduction techniques based on maximum a posteriori (MAP) estimation have been proven to have very good performances. These techniques are based on the introduction of an a priori statistical model of the speckle free image to be estimated. We propose a MAP method using more than one sub-band filtered intensity images and a Markov random field (MRF) a priori model. The method has been experimented on simulated and real images [C5020]

"Extraction of ground control points (GCPs) from synthetic aperture radar image using DEM"

Synthetic aperture radar (SAR) data have serious geometric distortions caused by inherent side looking geometry and are usually corrupted by speckle noises so that it is difficult to identify ground control points (GCPs). The location of the pixel in a given SAR image can be derived from the knowledge of sensor position and velocity. We propose a GCP extraction algorithm that has an improved capability. The algorithm is based on

the geocoding process of the radar image and requires precise orbit information. Whereas conventional geolocation algorithms depend on the knowledge of the target height relative to an assumed Earth ellipsoid model, more precise positioning can be achieved if utilizing an available digital elevation model (e.g. USGS GTOPO-30 DEM, SRTM DEM, etc.). The ERS SAR data with precise Delft orbit information and the national digital elevation model (DEM) were used. We analyze the accuracy of the results from our algorithm by using digital map. In case of using SRTM DEM, the mean values of the planimetric distance error are 9.1 m and 14.7 m with standard deviations of 6.4 m and 9.3 m in northing and easting direction, respectively. The errors in northing direction depend mainly on the imaging pulse time, and those in easting direction are related to the accuracy of used digital elevation model. The GCPs extracted were used for georectification of optical images as well as SAR data. [C5021]

"Combined wavelet and curvelet denoising of SAR images"

Synthetic aperture radar (SAR) images are corrupted by speckle noise due to random interference of electromagnetic waves. The speckle degrades the quality of the images and makes interpretations, analysis and classifications of SAR images harder. Therefore, some speckle reduction is necessary prior to the processing of SAR images. The speckle noise can be modeled as multiplicative i.i.d. Rayleigh noise. Logarithmic transformation of SAR images convert the multiplicative noise models to additive noise. In this paper, two combinations of time invariant wavelet and curvelet transforms will be used for denoising of SAR images. The first one is called the combined filtering algorithm (CFA). This method is based on a constrained optimization problem, both in the wavelet and curvelet domains. The second method is called the adaptive combined method (ACM) which uses the wavelet transform to denoise homogeneous areas and the curvelet transform to denoise areas with edges [C5022]

"A study on rice field edge extraction in Radarsat SAR images"

In order to make an accurate estimation of how much rice has been planted, it is essential to calculate the area of rice fields as precise as possible. Therefore, to delineate the edge of rice fields and remove the area occupied by the widened ditch roads around the rice fields caused by corner reflector effect in SAR images, have become a critical topic in rice monitoring and yield estimation using SAR images. To detect the linear features of rice fields for rice monitoring, this paper introduces an edge detection and extraction scheme in Radarsat SAR images by applying a two-dimensional (2D) filter in eight directions. To reduce the isolated speckle noise on SAR images, an sigma-filter is performed firstly and then the two-dimensional filter in eight directions can be selected and applied to detect edges. Finally, a nonlinear operator is used to threshold its magnitude and produces the edge maps of Radarsat SAR images. The proposed scheme achieves positive results of extracting linear features, reducing the speckle noise effectively, and meeting the need of practical radar remote sensing application in rice monitoring and yield estimation [C5023]

"DEM generation from stereo SAR images based on polynomial rectification and height displacement"

This work introduces the algorithm on DEM generation from stereo SAR images based on polynomial rectification and height displacement, and experiments according to the algorithm on RADARSAT and airborne SAR images in mountain area. To generate DEM from stereo SAR image, there are three kinds of models mostly to be used: 1) the model of range and Doppler equations, 2) the equivalent line central projection model based on the photogrammetry theory, 3) the parallax and elevation relation model which uses the relation between parallax and elevation to calculate elevation difference and then getting the plane coordinates. The model used in This work can be one of the third ones. In our model, image distortion caused by factors other than elevation is corrected by polynomial rectification, and elevation is decided by the difference of height displacement in the pair of the stereo SAR images. As the first step, a certain elevation, for instance the mean elevation of the image pair, is given to the point in process. Secondly, the height displacement in the left image can be corrected, and then the plane coordinates can be gotten by polynomial rectification functions of the left image. Thirdly, by polynomial rectification functions of the right image, the image coordinates of the "same name point" in the right image are available. Finally, from the difference between the coordinates and the actual ones, a new elevation can be gotten by the model of the height displacement of the right image. These steps can be repeated until the new elevation is very close to the old one. According to the above algorithm, programme has been designed. And then, experiment has been down on RADARSAT image in a mountain area in China (Dali, Yunnan). The accuracy is about 3 pixels. For airborne SAR images, some experiments have been down in another mountain area of China (Zhengzhou, Henan) with 1 meter resolution SAR images, and the results are similar to that of the first experiment. So, the new algorithm on DEM created from SAR image pairs introduced by This work is efficient and practicable. After modification, this method can also be used for mixed pair of SAR and optical images. [C5024]

"Implementation of a SAR image mapping module using the OGC grid coverage"

In the view of geometry, a SAR image is very different from the general optical image by the radar sensor and unique geometric characteristics. So, to combine or analyze with the other image, it must correct the slant range images into the geo-referenced images. This paper describes the SAR geocoding module, which is the sub-module of an IRIHS (Integrated RS s/w for High resolution satellite Images): package of "Development of High Resolution Satellite Image Processing Technique" project in Electronics and Telecommunications Research Institute (ETRI). In this paper, we briefly describe the algorithm that is adopted to the functions, and component architecture [C5025]

"Determination and implications of the rock physical parameter in the Maergaichaka fault, Tibet, China, using remote sensing data"

Synthetic aperture radar interferometry was used to study the Maergaichaka fault where Manyi earthquake occurred on Nov. 8, 1997 in Tibet, China. With a more appropriate base line, we present the coseismic interferometric fringe. With the prior knowledge of strike-slip movements, the decomposition of the displacement vector in the direction of the fault strike indicates that the horizontal displacement amount to 5.03 meters near the epicenter of the Manyi earthquake, which is more consistent with the field observation (4.5 meters) than the previous work (Peltzer et al., 1999; Shan Xinjian et al., 2002). We also modeled the rock physical parameter using Okada elastic model of half space, which was characterized by a high Poisson ratio. The high Poisson ratio of the upper crust indicate the structural back grounding that it is more possible that the interior crustal shortening play an more important role in the development of Tibet plateau than the doubling the continental crust by replacement of the Tibetan upper mantle by underthrust of Indian continental crust [C5026]

"Synergy of multitemporal Radarsat SAR and Landsat ETM data for extracting agricultural crops structure"

In China, crop structure adjustment policy has brought great change of different breed's planting area in different years. Government managers of agricultural industry need timely crop structure information to monitor the performance of the crop structure adjustment policy. The objective of this research was to evaluate the synergistic effects of multitemporal RADAR SAT synthetic aperture radar (SAR) and Land sat ETM+ data for extracting agricultural crops structure using an object-oriented classification approach. This paper instructs and analyses the crop structure near the Kaifeng city area in 2002. Four crop types were extracted: corn, soybean, cotton, and peanut. With the object-oriented classification approach, the overall accuracy of crop structure extracting from two-date F5 mode's SAR data (mid- to last-season) and two-date Land sat ETM+ is over 90% [C5027]

"Use of airborne hyperspectral image data to assess winter wheat yield"

PHI (pushbroom hyperspectral imager) is a hyperspectral imaging sensor which was developed by Chinese Academy of Science. From April to May of 2002, three airborne PHI images were obtained over a winter wheat field near Beijing. In this paper, wheat yield prediction models are established using PHI spectrum information and after-harvest grain yields data. Within-field yield variability was mapped for entire wheat field based on the models. A yield map was produced from the combine harvest yield data to evaluate those models. The analysis results indicates that (1) hyperspectral remote sensing data could be used to estimate yields in winter wheat yield, (2) new and more effective indicators are needed to capture more of the factor's that affect crop yield, and such parameters should be extracted from remote sensing data [C5028]

"Analysis of surrogate indicators for evidence of subsurface preferential flow pathways: impact of subsurface preferential flow on variability of NDVI"

Watershed-scale processes governing chemical fluxes to adjacent ecosystems are so poorly understood that effective strategies for mitigating chemical contamination cannot be formulated. Characterization of hydrologic processes and chemical behavior at the watershed scale is critical to the development of sustainable agricultural practices. Identifying locations for monitoring hydrologic processes like subsurface preferential flow is difficult because conventional sampling methods are inadequate for measuring this highly variable, yet critical process. A method for detecting and mapping subsurface preferential flow pathways based primarily on ground-penetrating radar (GPR) data and digital elevation maps (DEM) was developed. This procedure was confirmed for a Maryland cornfield using real-time soil moisture data, maps of within-field grain yield, and remotely sensed imagery. Unfortunately, it is economically unfeasible and logistically impractical for producers to use the GPR-DEM procedures to map subsurface preferential flow pathways for all crop fields. It may, however, be possible to use remotely sensed imagery, grain yield maps, and a DEM as surrogate indicators of subsurface preferential

flow pathways occurring at or near crop rooting depth. The normalized difference vegetation index (NDVI) shows an increase with distance from primary, secondary and tertiary preferential flow pathways during above-normal rainfall growing seasons. There appears to be a decrease of NDVI with distance from preferential flow pathways for a dry/drought year. Imagery collected during drought conditions appears especially useful as only within-field locations with subsurface irrigation from preferential flow pathways maintain vigor. Maps of vegetative productivity derived from remotely sensed imagery may be more useful than within-field grain yield maps for detecting and delineating locations of subsurface preferential flow pathways. The ability to delineate field locations with a high probability of subsurface preferential flow pathways will allow producers to better manage crop production, and mitigate losses of agricultural chemical inputs to neighboring ecosystems and waterways. [C5029]

"Bi-dimensional soil roughness measurement by photogrammetry for SAR modelling of agricultural surfaces"

In the description of soil roughness for SAR monitoring, the hypothesis of surface isotropy was currently admitted and in-situ roughness measurements were recorded along linear profiles. However, this paper showed for agricultural soil surfaces this hypothesis is not valid and anisotropic surface must be assumed. Stereoscopic pairs of vertical photographs were acquired to produce digital elevation models (DEM) for the soil roughness description. This paper presents a measurements method to describe the bi-dimensional soil roughness and discuss 3 advantages of the photogrammetric method compared to the linear measurements, (i) a high variability of the roughness parameters estimated by linear profiles was observed. Using the DEM, a high number of profiles were drawn for a given direction. A more accurate estimation of rms and correlation length was obtained averaging several profiles, (ii) the anisotropy were measured and represented by a directional variograms. (iii) The anisotropic roughness were decomposed in 2 models: the isotropic random roughness and the anisotropy induced by the sowing rows [C5030]

"Application of a SAR image archive to climatological analysis of coastal wind storms"

This study uses the high-resolution all-weather surface wind field mapping capability of SAR to detect and quantitatively describe the strong mountain-parallel, low-level mesoscale wind maxima, commonly called barrier jets that occur along the synoptically windward slopes of Alaska's coastal mountain ranges. SAR reveals that there are two classes of this phenomenon: pure barrier jets caused by terrain blocking of on-shore (i.e. upslope) flow and hybrid jets resulting from the cyclonic turning of off-shore gap flow until it becomes shore-parallel. This paper includes a five-year study from May 1998 through April 2003 of coastal barrier and hybrid jet occurrence in the Gulf of Alaska. Temporal and spatial distributions of banner jet and hybrid occurrence highlight the favored seasons and locations for jet formation and explanations for shape of each distribution are given. The climatological values of structural characteristics of barrier and hybrid jets including strength and width are also computed [C5031]

"Penetrating radar study of the collapse features in a Nantou earth slide, Central Taiwan"

This paper shows that ground-penetrating radar is an indispensable tool to study the internal configuration of a slide mass. The georadar facies and sliding surface are easily recognizable on the GPR profiles. The study area in this paper had undergone at least two earth slides. The internal configuration of the slide mass details the mechanism of this mass movement. Ten georadar facies were observed on the GRP profiles. They are chaotic, contorted, disrupted, hummocky, lenticular, oblique, onlap, overlap, subparallel, and reflection-free. At the head or crown part of the slide mass, chaotic, contorted, disrupted, oblique, and onlap facies are dominant. At the toe part, contorted, oblique, onlap, and reflection-free facies are most common. In the main body of the slide mass, chaotic, contorted, disrupted, hummocky, lenticular, overlap, and subparallel facies dominate. Chaotic, contorted, and disrupted facies exist throughout the slide mass. Chaotic facies indicates severe movement, including rotation. Contorted facies results from a checked gravity sliding, whether checked by friction or blockade. Disrupted facies is caused by extension from gravity sliding. Similar studies can be extended to other areas prone to earth slide, so preventive measures can be adopted to abate the landslide hazards [C5032]

"Detection of systematic error areas on a DTM by comparison with a high resolution LIDAR DTM"

This article aims at studying the spatial repartition and the impacts of the errors on a DTM. We show that some errors are recurrent whichever interpolation method is chosen [C5033]

"Exploration assessment in a petroleum frontier area offshore the Amazon River mouth using RADARSAT-1 images"

The study discusses the use of RADARSAT-1 images to identify oil seepage in the Foz do Amazonas Basin, an

oil and gas exploration frontier in the Brazilian Equatorial margin. An unsupervised semivariogram textural classifier algorithm was used to enhance areas of smooth texture and low radar backscatter, indicative of these targets. Complementary information related to cloud top temperature, wind velocity, and modelling for the tidal regime (all obtained as close as possible to the RADARSAT-1 images acquisition) was used to support image interpretation and to exclude false-targets. Together with previously discovered sub-commercial shallow water oil accumulations, the detection of seepage slicks an additional evidence of oil generation in the study area. Results also indicate that radar remote sensing can be used as a tool to reduce risks in the exploration of frontier areas like the Foz do Amazonas Basin [C5034]

"Use of genetic algorithm to identify the source point of seepage slick clusters interpreted from Radarsat-1 images in the Gulf of Mexico"

A large multitemporal set of RADARSAT-1 ScanSAR Narrow 1 images obtained in offshore regions of the Gulf of Mexico enabled the identification of a seepage slick cluster, which is considered to share a common geologic origin. The existence of seepage slick clusters is a positive indicator of present-day hydrocarbon generation and migration. Therefore, their correct location reduces the risk of acquiring piston cores with oil at the sea floor for further geochemical studies. A cluster is interpreted as a group of seepage slick polygons which share the same source point in geographic space. The source point can be tentatively defined as the intersection of overlaying polygons or as the intersection of the forward prolongation of closely spaced and converging polygons. The present study aims to identify quantitatively the origin of a seepage slick cluster at the sea surface using a genetic algorithms (GA). The model employ the Euclidian or the Mahalanobis distance function in order to determine the minimum distance among points within one seepage slick cluster and a population of points randomly generated. We used points in UTM coordinates system generated within a grid cell (x,y) of fifty meters defined in the seepage slick polygons that constitute a cluster In addition, one hundred points are generated randomly as the initial population. The fitness function provides the 10 best ranked points in UTM coordinates system that represent the candidates source point of the seepage slick cluster. The best source point identified using GA (considering both the Euclidian and Mahalanobis distance functions) coincided with a salt dome and fault seismically identified at the sea floor. The methodology have been tested elsewhere in the Gulf of Mexico, in order to identify with enhanced precision possible source points of seepage slick clusters detected using RADARSAT-1 images [C5035]

"On the extension of the SBAS algorithm for the generation of ERS/ENVISAT deformation time-series"

We present a differential synthetic aperture radar interferometry (DIFSAR) technique for generating displacement maps and deformation time-series by exploiting data acquired by the ERS and ENVISAT/ASAR systems. The proposed solution is focused on investigating large scale displacements with a relatively low spatial resolution (of about 100 Ч 100 m). Since the two radar sensors operate at different carrier radar frequencies, the easy computation of cross-platform interferograms is prevented, thus leading to independent subsets of interferograms. An easy and efficient way to combine ERS/ERS and ENVISAT/ENVISAT multilook interferograms is represented by the application of the Small BAseline SubSet (SBAS) strategy. This solution guarantees the continuity in the monitoring of the Earth's surface by benefiting of the present and future availability of ASAR data, preserving the archived ERS data. The presented results, obtained on a descending ERS and ENVISAT SAR data set, spanning the time interval from 1992 until October 2003, are relevant to the Napoli Bay area (Italy) and clearly demonstrate the effectiveness of the proposed extension of the SBAS technique. [C5036]

"A quantitative analysis of the SBAS algorithm performance"

The Small BAseline SubSet (SBAS) approach is a differential synthetic aperture radar interferometry (DIFSAR) technique that allows analyzing deformation phenomena affecting both extended area and localized structures, by exploiting the phase difference of SAR image pairs characterized by small baselines. In this work we process a large set of ERS-1/2 data, acquired from ascending and descending orbits, at both small and large scale resolution and extend the obtained time series with available ENVISAT acquisitions. The results, relevant to the Napoli Bay area (Italy), are compared with geodetic and GPS data in order to achieve a quantitative analysis of the SABS algorithm performances [C5037]

"TerraSAR-X for oceanography mission overview"

TerraSAR-X is a new generation, high resolution radar satellite, which is planned for launch in 2006. The mission is setup to produce operational remote sensing products for commercial and scientific use from a spaceborne X-Band synthetic aperture radar (SAR) system. After a 5 month in-orbit commissioning phase TerraSAR-X will be operational for an active lifetime of 5 years. TerraSAR-X is Germany's first Earth

Observation space project based on public-private partnership of the German Aerospace Center and the ASTRJUM GmbH. The TerraSAR-X mission was designed to serve two main objectives: 1) provide the scientific community with high-quality, X-band SAR-data for research and application purposes; 2) support the establishment of an Earth Observation market; and 3) and develop a sustainable Earth Observation service in Europe, based on TerraSAR-X derived products. The broad spectrum of TerraSAR-X applications, include: Hydrology, Geology, Climatology, Oceanography, Environmental- and Disaster Monitoring as well as Cartography. The scientific potential of TerraSAR-X is based on a combination of unprecedented features of the SAR instrument, which will for the first time be operational in space. The features of TerraSAR-X offer new and promising applications for oceanography. In this work some promising applications concerning wind, wave and current measurements as well as monitoring of morphodynamic changes are introduced. [C5038]

"Combination of multiple interferograms for monitoring temporal evolution of ground deformation"

SAR and differential SAR interferometry are operational tools for monitoring surface deformation and topographic profile reconstruction. However, they still have limitations due to temporal and geometric decorrelation. These disturbances strongly compromise the accuracy of the results, but reliable measurements can be obtained over a large multitemporal population of interferograms. In this paper we propose a new algorithm for monitoring temporal evolution of ground surface using several interferograms covering ground movements over a long period of time. It is based on a statistical approach with hypothesis test. The objective of multiple interferograms elevation retrieval is to deal with noisy data. Another important advantage of the multiple image processing is that all baselines (small or large) are considered. The method described in this paper can be applied in both SAR and differential SAR interferometry context. We chose to study the SAR interferometry case [C5039]

"Gulf Stream observations obtained with the UMass Dual Beam Interferometer and an infrared camera"

The Dual Beam Interferometer (DBI) developed by University of Massachusetts (UMass) and an infrared camera operated by the Naval Research Laboratory (NRL) were jointly deployed during a March 2004 flight campaign off the east coast of Florida. Data collected produced simultaneous observations of features over the Gulf Stream's western boundary by both instruments. Use of instruments with different imaging capabilities enabled extraction of wind direction as well as current velocity measurement. [C5040]

"Feasibility study of along-track SAR interferometry with the COSMO-SkyMed satellite system"

Currently, particular interest is growing on spaceborne along-track synthetic aperture radar interferometry (ATI-SAR). In this work, we investigate the possibility of applying the ATI-SAR technique to the Italian COSMO-SkyMed satellite system with the latest hardware concept of split antenna mode. A preliminary study on the possible achievable accuracy on current velocity and coherence time estimation, as a function of environmental and radar parameters, is developed, based on Cramer-Rao lower bound analysis and physical signal models. Possible multibaseline ATI configurations are included in the study. First results are presented about the choice of the optimal split configuration [C5041]

"Experiments of interferometric layover solution with the three-antenna airborne AER-II SAR system"

Interest is recently growing in exploiting the advanced multibaseline operation of synthetic aperture radar interferometry (InSAR) to solve layover effects, that can degrade conventional SAR and InSAR imagery. In this work we report about: experiments of the functionality of "layover-free" or "higher-order" interferometry with the dual-baseline single-pass SAR interferometer AER-II. Non-parametric, parametric and hybrid spatial spectral estimators are applied to process the three-antenna non uniform array data. Calibration issues, first real data results and impact of order selection are discussed for a bridge over the valley scene [C5042]

"Airborne differential interferometry: X-Band experiments"

In this work we present the results of an airborne differential interferometry experiment carried out by using the ORBISAR X-band system. Use of a high track measurement accuracy allowed us to fulfill the requirements of Fornaro et al. (2003), where repeat pass phase accuracy has been quantified in terms of position measurement errors. The presented experiment can be considered a first step towards the development of operative airborne differential interferometry for accurate ground deformation monitoring. [C5043]

"Monitoring city subsidence by D-InSAR in Tianjin area"

D-InSAR technique has been widely adopted to monitor land subsidence caused by withdrawal of water, oil, gas,

and other minerals. Though many cities in China have seriously suffered from land subsidence caused by ground water over-extracting, few of them have enough money to do the leveling control of the subsidence. Compared with leveling and GPS surveying, D-InSAR is more cost-efficient and precise. As Tianjin city has scores of ERS-1/2 SAR data, thousands of valuable leveling data, smooth topography and severe subsidence, it is an ideal place to test and analyze D-InSAR technique. However, D-InSAR is liable to be contaminated by atmosphere delay, temporal decorrelation and baseline errors. As these errors cannot be removed by SAR data processing, some auxiliary data such as leveling data and DEM data have been introduced into D-InSAR data processing. Therefore, This work accurately analyzes the features of atmosphere delay and temporal decorrelation with the auxiliary data in Tianjin urban area. The results demonstrate that D-InSAR can detect subsidence within three months. Further actions will be undertaken to improve the D-InSAR subsidence monitoring system, such as using Envisat data, gathering GPS zenith delay data to eliminate the atmosphere delay, and so on. The ultimate interest of our research is to establish a robust, cost efficient city subsidence monitoring system by using D-InSAR technique and other measurement. [C5044]

"AVTIS-a dual-mode imaging millimetre wave radar/radiometer for volcanological surveying"

We present the design and preliminary results for an advanced mm-wave remote sensing instrument. AVTIS (AH Weather Volcano Topography Imaging Sensor) is a dual-mode passive imager and active radar operating at 94 GHz, designed to yield topographic and thermal maps of volcanic lava domes. The mechanically scanned imager uses a 0.5m Cassegrain antenna mounted on a pan & tilt gimbal. The radiometer is of the total power heterodyne type, and the radar operates in an FMCW mode. When images are collected from multiple viewpoints, it will be possible to construct a thermo-spatial 3D map of the lava dome. The project volcanologists will use this data to enhance the modeling of the growth and collapse mechanisms in lava domes, which may ultimately lead to improved hazard warning. [C5045]

"The operational impact of QuikSCAT winds at the National Oceanic and Atmospheric Administration Ocean Prediction Center"

The primary responsibility of National Oceanic and Atmospheric Administration's (NOAA) Ocean Prediction Center (OPC) is to issue marine warnings and forecasts of winds and seas for the high seas and offshore waters of the Atlantic and Pacific Oceans. This covers vast open ocean areas from the subtropics to the near arctic. Accurate and timely surface data are necessary to make these warning decisions. Although conventional observations from buoys and ships of opportunity are very useful to marine forecasters, their distribution is sparse, often being limited to trade routes or continental waters. Over the past twelve years, forecasters have come to rely more and more on remotely sensed data. Special sensor microwave/imager (SSM/I) winds have been used to help fill in the gaps between conventional observations. However the SSM/I retrievals are not available in areas of liquid cloud and precipitation and are restricted to the lowest wind warning category (GALE). Wind retrievals from various scatterometers flown onboard satellites have been available to OPC forecasters over the last ten years and were used with some success. QuikSCAT winds are now fully integrated into OPC operations and have proven to be invaluable. The wide swath width and all weather capabilities have enabled OPC forecasters to use these winds routinely to determine the extent and magnitude of strong winds, the location of fronts and pressure systems, and wind gradients associated with oceanographic thermal features. Since the inclusion of QuikSCAT into OPC operations the marine forecaster's ability to accurately assess wind conditions over the open oceans has never been better [C5046]

"Validation of wind vector retrieval from ENVISAT ASAR images"

Ocean wind speeds and wind directions are estimated simultaneously using the normalized radar cross sections corresponding to two neighboring images, having slightly different incidence angles. The wind direction ambiguity is removed by using the direction closest to that given by the buoy or some other determination. To validate this method, some ENVISAT ASAR images of the Gulf of Mexico and coastal waters of the North Atlantic are used to estimate wind vectors, compared with wind measurements from buoy data. Moreover, ASAR can also provide dual-polarization SAR images. Therefore, we derived an empirical polarization ratio as a function of the radar incidence angle. Wind vector fields are retrieved from RADARSAT-1 SAR HH-polarization images based upon this empirical ratio and compared with buoy measurements and QuikSCAT data [C5047]

"Wind retrieval over the China Seas using satellite synthetic aperture radar"

The high spatial resolution and large coverage of synthetic aperture radar (SAR) offers a good opportunity to retrieve detailed wind vector information over the oceans, especially in the coast areas. In the work presented here, the wind speeds estimate is based on the data from ScanSAR aboard the Canadian satellite RADARSAT, operating at C-band with horizontal polarization, and the empirically derived CMOD4 model. Because the

CMOD4 model was originally developed for the C-band, W-polarized scatterometer data, polarization ratio should be applied to process RADARSAT ScanSAR data. In order to get an estimate of a suitable polarization ratio, wind directions from the collocated QuikSCAT data in the China Seas were taken as input to CMOD4 model for wind speeds retrieval from RADARSAT ScanSAR data, the results of the comparison of wind speeds from QuikSCAT versus the RADARSAT ScanSAR derived wind speeds indicate that Kirchhoff polarization ratio is suitable for wind speeds retrieval using horizontal polarization RADARSAT ScanSAR data. The corresponding mean bias and standard deviation is 0.37m/s and 1.54m/s, respectively [C5048]

"Laboratory measurements of wave-turbulence interaction for scatterometry application"

Measurements of the space-time structure of short gravity-capillary waves in the presence of turbulence in a laboratory wave channel are presented. This study was stimulated by the need to investigate the influence of turbulence on the scattering surface, which contributes to a microwave scattering at grazing and moderate incidence. Mechanically generated periodic (4 to 10 Hz) waves and multijet manifold were used as sources of surface waves and subsurface turbulence. A laser slope gauge (LSG) and an imaging slope gauge (ISG) were used to measure short waves of length 2-10 cm and frequencies up to 150 Hz. A dual polarized (VV, HH) coherent CW X-band scatterometer was used to obtain Doppler spectra of the scattered signals for grazing angles from 30 to 60 degrees. Simultaneous time series of wave slopes and microwave scattering and their frequency spectra permitted a comparison of these parameters both with and without turbulence. Both scattering and decaying of the surface waves by turbulence were observed. A presence of turbulence had a pronounced distortion effect on the short waves due to scattering by submerged turbulence. Interaction with turbulence caused decrease of the energy of short waves and broadened the directional spectra of their propagation. Measurements of the Doppler frequency shift and amplitude of the scattered microwave signal are consistent with this changing in the wave field and reveal Bragg scattering by the short waves [C5049]

"In situ soil moisture network for validation of remotely sensed data"

An automated soil moisture network for continuous measurement of soil moisture in the top 30 cm of the soil over an 8000 km² region has been established. The network consists of 32 stations encompassing a diversity of soil types. The measurements are being used to improve drought, flood, and agronomic production forecasts. In addition, the data are being used to examine the accuracy of remotely sensed measurements of soil moisture and the degree to which they represent natural variability across the landscape. The data were used to evaluate soil moisture conditions during the SMEX03 experiment. The data are being used to support testing of AMSR, AMSR-E, PSR, and synthetic aperture radar (SAR) observations. Gravimetric samples were collected for the period from June 23, 2003 to July 2, 2003 for comparison to both the in situ network and the remotely sensed data. During the experiment, daily in situ soil moisture measurements were taken and plant and soil samples collected for oven drying and determination of moisture content. The automated network provided continuous in situ soil moisture measurements throughout the coverage area. A wide variation in soil moisture was observed both over the time period and from site to site [C5050]

"Radiometric calibration and preliminary results of airborne 2003 FASA Campaign"

During July 2003 a new airborne system named FASA was tested on Italian volcanoes. FASA that stands for Fire Airborne Spectral Analyzer, is a system devoted to high temperature events study. The payload on the airborne consisted of an imager (ABAS) and an high resolution Michelson interferometer with rotating retroreflector MIROR operating in the nominal infrared 2.5-18 μ m range. MIROR was developed by DLR and adapted for airborne measurement by INGV that provided an opto-mechanical interface and a calibration unit software control. By using three black body sources at different temperature is possible to compute instrumental transfer function and reduce instrumental noise. In this study we describe pre-flight test and the in flight calibration results. Preliminary results of radiance spectra on the Mount Etna surface and emissivity are shown. [C5051]

"Spatial averaging techniques for pulse compression of spaceborne meteorological radar"

In order to achieve very low range side-lobe ([C5052]

"Rainfall and snowfall observations by the airborne dual-frequency precipitation radar during the Wakasa Bay Experiment"

Radar data obtained through the NASA/JPL Airborne Precipitation Radar APR-2 during the Wakasa Bay Experiment in January/February 2003 were processed to obtain calibrated reflectivity measurements, rainfall/snowfall velocity measurements, classification of the surface type and detection of the boundaries of the melting layer of precipitation. In this paper the processing approach is described together with an overview of the

resulting data quality and known issues [C5053]

"Assimilation of the Aqua/AMSR-E data to numerical weather predictions"

An application of satellite information to numerical weather predictions (NWP) is one of the most expected achievements in satellite remote sensing. In some meteorological agencies, the data of the space-borne microwave radiometers (MWRs) have been used in their operational weather forecasts. The Japan Meteorological Agency (JMA) introduced the assimilation system of rain rate (RR) and total column precipitable water (TCPW) derived from Special Sensor Microwave/Imager (SSM/I) and TRMM microwave imager (TMI) for the operational mesoscale model in October 2003 and we are trying some observation system experiments about TCPW assimilation using the global model. These water-related data are very useful to detect tropical and extratropical cyclones over ocean. The advanced microwave scanning radiometer (AMSR) for EOS (AMSR-E) on board the Aqua satellite was launched in May 2002. The AMSR-E measures several parameters related to global water circulation at 1:30 a.m./p.m. in local time in which no MWR observation is implemented so far. The MWR constellation composed of AMSR-E, SSM/I, and TMI is satisfactory for global observation at six-hour refresh rate. The refresh rate is essential to give homogeneous initial field for the Global Model and to detect and assimilate the signal of severe weather phenomena with short lifetime such as heavy rain for the mesoscale model. We are investigating the impacts of the retrieved TCPW and RR by the MWR constellation with the JMA NWP systems. In the global model experiments, the homogeneous data distribution with the constellation improves the performance of the data assimilation and the forecast. In the mesoscale model experiments, the frequent observation with the constellation succeeds in detecting the signal of heavy rain and improving the short-range rainfall forecast for disaster prevention. [C5054]

"On the suitability of a TerraSAR-L Interferometric Cartwheel for ocean current measurements"

The main idea behind the French "Interferometric Cartwheel" and similar other concepts is to put some small satellites with synthetic aperture radar (SAR) receivers into slightly different orbits behind a bigger master satellite in such a way that sufficient baselines for cross-track interferometry between at least two satellites are always available. In a recent study for ESA, the potential of such configurations in combination with the upcoming ESA satellite TerraSAR-L was investigated. Favorable cross-track baselines for land applications would be on the order of several kilometers. We discuss the suitability of such configurations for ocean current measurements by along-track interferometry. The main parameter to be considered is the time lag between pairs of satellites, which may be changing continuously. We find that reasonable current measurements can be expected for a long-track satellite spacings of about 10 to 1000 m. This wide range of suitable baselines should permit the design of a satellite configuration with continuously good performance for topographic measurements and current measurements. [C5055]

"Accuracy assessment for HUT snow covered area estimation method"

The statistical accuracy of HUT Snow Covered Area (SCA) estimation method is assessed. The HUT SCA method is a two step procedure for estimating Snow Covered Area for boreal forest regions. The analysis of the method is conducted with 24 ERS-2 SAR intensity images for 14 boreal forest dominated sub-drainage basins in Northern Finland. The accuracy analysis is carried out for several statistical variables and the statistical interpretation is done with respect to several affecting parameters. The accuracy analysis shows a high correlation coefficient between the SCA estimates and the reference data and RMSE values of 0.213 for open areas and 0.179 for forested areas. [C5056]

"Soil moisture analysis using RADARSAT satellite image in the Choke Canyon Reservoir Watershed, South Texas"

The surface soil moisture is very difficult to measure on a river basin scale due to versatile soil types and their associated textures. Consistency of measuring in-situ soil moisture on site is barely obtainable even on a local scale. Recent advances in remote sensing technology have demonstrated that soil moisture can be measured systematically by many optical techniques, such as microwave technology of Synthetic Aperture Radar (SAR). It has the ability to quantitatively measure soil moisture under a variety of topographic and vegetation cover conditions from a satellite system. RADARSAT-1 is a space borne SAR imagery satellite. With its all-weather capability, the RADARSAT-1 is a promising tool for measuring the surface soil moisture. This research focuses on relations made to soil moisture variability within RADARSAT-1 footprints and on the use of SAR images to develop models of surface soil moisture profile. The case study in the Choke Canyon Reservoir Watershed, South Texas reflects soil moisture spatial distribution patterns in the summer that can be viewed as an extreme situation of water resources management within a semi-arid coastal watershed in 2003. [C5057]

"Satellite observation of the Zhejiang-Fujian coastal front in the East China Sea"

The Zhejiang-Fujian coastal front in the East China Sea has been studied using an 12-year time series (1991-2002) of Advanced Very High Resolution Radiometer (AVHRR) images. Satellite observation has shown that the front exists all year round and has a length scale of about 597 km. The strength and width of the front vary with average values of 0.14 degC/km and 14 km respectively. The front is characterized by the presence along its edges of rings which have a time scale of 1-7 days and a length of 30-90 km [C5058]

"RADARSAT based surface soil moisture retrieval on agricultural catchments of Navarre (Spain)"

The present paper reports the first results of an ongoing research whose main objective is the development of a simple methodology for initialising and updating the soil moisture component of distributed hydrological models using SAR data. Five RADARSAT-1 images acquired between 27 February 2003 and 2 April 2003 over the Navarre region (Northern Spain) have been processed. Soil moisture, surface roughness and crop parameters have been monitored coinciding with image acquisition dates over La Tejeria experimental watershed (Navarre). Calculated backscattering values have been compared to soil moisture and surface roughness ground measurements fitting empirical linear regression models. In the case of vegetated fields a semi-empirical water cloud model has been applied to account for vegetation effects on the observed backscattering values. Acceptable correlation has been observed between calculated backscattering values and ground measured soil moisture at field and watershed scale, although variability was high between fields belonging to the same vegetation and roughness classes. The physically based Integral Equation Method (IEM) model has been applied seeking for a more consistent approach. IEM reflected observed backscattering trends. However, dispersion was high probably due to an inadequate characterisation of surface roughness variability [C5059]

"Estimation of the change of soil moisture in vegetated surface with multi-temporal AirSAR data"

The ability to estimate soil moisture in the surface layer by microwave remote sensing has been demonstrated. But its application to hydrological and agricultural sciences has been hampered by the complexity of the vegetation canopy and surface roughness which significantly affect the sensitivity of radar backscattering to soil moisture. In this study, we used a simple vegetation model to estimate soil moisture and evaluated the results using multi-temporal L-band AirSAR data [C5060]

"Preliminary results on soil moisture mapping in Alessandria area (Northern Italy) using Envisat ASAR"

This work presents some experimental campaigns aiming to assess the potential of monitoring soil moisture by ENVISAT ASAR (Advanced Synthetic Aperture Radar). Soil moisture measurements were carried out on November 2003 and June 2004 close to Alessandria (Northern Italy) by using a TDR probe simultaneously to ENVISAT overpasses. In situ measurements had been collected in agricultural fields that were subsequently identified on ENVISAT ASAR images by means of a geo-coding process. Pixels of each area have been averaged in order to compute the mean backscattering coefficient. Results have been derived concerning the sensitivity of the backscattering coefficient to soil-moisture compared to what is predicted by a semi-empirical scattering model. [C5061]

"Backscattering of electromagnetic waves from layered rough surfaces and its application in estimating deep soil moisture"

An analytical method to calculate the scattering coefficients of a three-layer 3D rough surface is introduced. The two rough interfaces are assumed to be distinct. The waves in each region are represented as a superposition of an infinite number of up- and down-going spectral wave components, whose amplitudes are found by applying the boundary conditions. A small-perturbation formulation is used in the process and the scattering coefficients are derived to the first order. The formulation is validated against known solutions for special cases of flat interfaces as well as the single rough surfaces. Results are then generated for several cases of the three-layer rough interface medium, to be used for modeling of the backscattered signals from a tower-based radar system and subsequent estimation of multilayered soil properties such as moisture content and subsurface layer height [C5062]

"Derivation of hydrological parameters from ENVISAT ASAR wide swath data"

Spatially distributed information about the current state of the land surface can be obtained from remote sensing measurements. These may be used with great benefit for the understanding of hydrological processes on the landscape level, where in situ measurements must fail due to lacking spatial coverage. The potential to quantify

soil moisture conditions of the top soil layer, as well as the derivation of snow parameters by means of active microwave imagery has been successfully demonstrated in numerous studies. In contrast to earlier and rather experimental research efforts, data acquired from the ENVISAT ASAR sensor firstly enables to continuously monitor large areas with high temporal frequency and high spatial resolution. The different operation modes of ASAR allow the derivation of soil moisture maps on both, the field and the regional scale. The paper presents new methods to derive soil moisture and snow covered area information from ASAR wide swath (WSM) datasets. The presented approaches allocate a robust, yet practicable and reliable technique to derive near-surface soil moisture and snow patterns, being the key prerequisite for an operational application in hydrologic modelling.

[C5063]

"On the accuracy of soil moisture content retrieved at pixel, segment or field scale, from advanced-SAR data: a simulation study"

In this work, the effects of SAR measurement errors as well as direct model errors on soil moisture retrieval from SAR data are investigated. In particular, the attention is focused on understanding under which conditions it is more convenient: a) feed the retrieval algorithm with accurate backscattering values (i.e. estimated at "field scale") then retrieve soil moisture estimate directly at "field" scale; b) use relatively noisy backscattering values, estimated at smaller scales (i.e. "segment scale"), to retrieve soil moisture estimates at "segment" scale and subsequently average the obtained soil moisture estimates at "field" scale. The adopted soil moisture retrieval algorithm is based on a regularized Neural Networks appropriately trained by IEM model. The SAR synthetic data simulates SAR data acquired by ERS and ENVISAT satellites. The performance of the inversion method is given as a function of the SAR configuration and noise level. [C5064]

"A comparison of satellite and cruise chlorophyll-a measurements in the Scotia Sea, Antarctica"

We compared both SeaWiFS (Sea-viewing Wide Field-of-View Sensor) and MODIS (Moderate-resolution Imaging Spectroradiometer) chlorophyll-a (chl-a) measurements with simultaneous ship based data obtained during a 2003 British Antarctic Survey (BAS) research cruise. This cruise provided in situ data from a large area of the Scotia Sea containing areas of extreme contrasts in terms of chl-a concentration. We present the results of correlation analysis between the in situ ship based chl-a measurements and the satellite chl-a products (SeaWiFS, and from MODIS the semi-analytic, SeaWiFS analog OC3M, HPLC empirical algorithms). The results confirm the good correlation between SeaWiFS and in situ chl-a measurements. The results indicate Terra MODIS chl-a measurements show reduced correlation to in situ values when compared to SeaWiFS. In addition, we compared chl-a averages from the various algorithms, over wider geographical regions of greater ecological relevance than point measurements. Over an area of $3^{\circ} \times 3^{\circ}$, SeaWiFS estimates could be as much as 2 times higher than estimates from MODIS. [C5065]

"LIDAR-based change detection of buildings in dense urban areas"

An automatic method for LIDAR-based (Light Detection And Ranging) change detection is proposed. Highly dense LIDAR point clouds are recommended as the most suitable gathered data for dense urban areas. The main goal is to develop an up-to-date building inventory database, which is in great demand for the earthquake-prone areas like Japan, using LIDAR as primary data. Two LIDAR surveying flights in 1999 and 2004 provide the test data over Roppongi, Tokyo, Japan. Detected results are visual evaluation using orthophoto produced by LIDAR surveying flights. The highly automated processing proved the efficiency of using LIDAR for a quick and reliable updating. Moreover, it also implies the feasibility for detection of damaged buildings due to earthquake.

[C5066]

"Scattering analysis using fractional Fourier with applications in mine detection"

This paper uses the fractional Fourier transform to identify dispersive scatterers in a GPR signature. The motive is that certain dispersive scatterers that uniquely define an object can be better localized in the fractional Fourier spectrum. These scattering features that are extracted via the fraction Fourier transform are then presented to a nonparametric landmine detection scheme. The motive is to detect landmines based on specific scattering mechanisms thus avoiding the use of the significant ground return as a primary feature [C5067]

"IFSAR: an airborne interferometric SAR simulator"

The IFSAR is an airborne SAR simulator for extended targets developed by INTA. This tool generates simulated signal data of an artificial three-dimensional scene as collected by an interferometric SAR with a fully configurable system oriented to airborne applications. Scene is made of points and triangular extended targets, over a selected ellipsoid, and it can be drawn using common CAD software. GPS motion records of plane and moving point targets, extended targets, associated scattering patterns, chirp signal, antenna patterns and TxRx

diagram can be simulated too. Experimental results comparing interferograms from real and simulated missions shows that the tool is extremely accurate and requires few computer resources. It is used to calibrate of MOCO algorithms and interferometric processors, to probe new techniques and solve problems in real acquisitions of interferometric airborne SAR data [C5068]

"InSAR coherence estimation"

For interferometric SAR processing (InSAR), the quality of the interferogram is affected by many factors such as Doppler centroid difference, baseline, atmospheric effect. It can be measured by the estimation of the coherence of the data. It has been shown that the coherence image can be used to do the classification in the area such as water, soil, plants, city or something else. But the coherence estimation is always biased somehow. To find an asymptotically unbiased coherence estimation method is therefore challenging and important for InSAR processing. In this paper, several different coherence estimators are introduced. An accurate coherence computation method using an existing DEM is proposed and illustrated [C5069]

"Measurement and simulation of L-band emission for a larch forest stand"

In this work, there was tested a possibility to establish quantitative relationship between the moisture of forest stand, as a system of the trees, litter, and soil layers, and the radiometer antenna temperature. The radio brightnesses of radiometer antenna at L-band was measured as a function of viewing angle for both the V and H polarizations, with the antenna being directed at the larch forest stand. The radiometer was mounted on the tower at the height of 21.5 m, with the viewing angle being changed from close to the nadir to the horizon. The larch forest stand of 100 Ч 100 m², used as an object of study, was located 50 km to the north from the city of Krasnoyarsk, Russia, with the average tree height, diameter, and density of trees being of 13.8 m, 0.1 m, and 0.38 trees/m². All data were recorded in August 2001. In the theoretical model developed for predicting the radiometer antenna temperature, the forest canopy was considered as a three layers medium with each layer having its own complex dielectric permittivity. The latter was calculated using the refractive mixing dielectric model with its parameters being determined experimentally in L-band through the laboratory measurements using the data collected in situ at the site of measurement. As a result, there have been proved the possibility of using comprehensive radiobrightness and dielectric models as a physical basis in developing processing algorithms for radiometric remote sensing of moisture, on the forested territories. [C5070]

"Bound water spectroscopy for the soils with varying mineralogy"

A technique for estimating the data obtained on spectral dielectric properties of the soil bound water (BSW) as a function of the mineral composition are presented. The Debye spectroscopic parameters related to the BSW were derived with the use of the general refractive mixing dielectric model (GRMDM). The static dielectric constant (DC) of SBW was found to depend to a large extend on the content of humus. The static DC of the SBW present in the natrium humate sample ($\epsilon_0 = 22.3$), which is one of the components of the soil humus matter, appeared to have the least static DC as compared to those for the natural humus soil ($\epsilon_0 = 31.9$), clay soil with low humus content ($\epsilon_0 = 46.7$), and coal ashes collected from the filter of energy power station is ($\epsilon_0 = 64.9$). At the same time, the relaxation times related to the all soil types considered were shown to be higher than that of the water out of soil, which does not interact with the soil mineral substance. The data obtained can be used for developing the moist soil spectroscopic dielectric data bases, which are used in the radar and radiometry remote sensing algorithms. [C5071]

"Sea surface brightness temperature at L-band: impact of surface currents"

Drastically different sea states result for a growing, decaying, or a fully-developed sea due to the presence of a wind field. In addition, the sea state is altered by the superposition of oceanic currents on the wave field created by the wind. This study presents a numerical analysis of the change in the sea surface brightness temperature at L-band computed using the SSA model and a modified Kitaigorodskii-Pierson-Moskowitz sea surface spectrum to account for the presence of surface water currents. Their impact on the brightness temperature variations is evaluated and compared to the brightness temperature fluctuations observed from a tower-based field experiment. The consequences for salinity retrievals from space using L-band radiometry are discussed [C5072]

"Measured spectrum and polarization of wideband radar signal from forest stand"

We report on an experiment regarding the spectra of super-wide band radar (SWBR) backscatter amplitude generated by forest canopy. The larch forest stand of 100 Ч 100 m², used as an object of study, was located 50 km to the north from the city of Krasnoyarsk, Russia, with the average tree height, diameter, and density of trees being of 14.2 m, 0.116 m, and 0.38 trees/m². All data were recorded in August 2003. The SWBR, radiating pulses with duration of 1.5 ns and 0.15 ns, was mounted on the tower at the height of 21.5 m, the range and

viewing angle being of from 3 to 100 m and from 50° to 75°, respectively. The backscatter was recorded as a function of distance. Noticeable correlation was found between the positions of peaks of the backscatter signal and those of single trees. This suggests similarity in spatial structure of the radar signal and inhomogeneities inside the forest canopy. Subsequently the record of backscatter was turned into the analytical signal. Finally, the module of analytical signal was processed to evaluate its spatial spectrum. Thus attained spectra were shown to follow a combination of the power laws, with two exponents being distinguished at the low and high frequencies. This type of spectra remained for vertical, horizontal, and cross polarizations. The discovered features of the backscatter spectra were proposed to be applied for the classification of forests, using SWBR technique. [C5073]

"Spectral dielectric properties of moist soils in the microwave band"

In this work, the spectral dielectric properties of moist soils in the microwave band were analyzed, using the generalized refractive mixing dielectric model (GRMDM). First, for different types of soil, all available data on dielectric constant (DC) and loss factor (LF) at zero volumetric moisture, maximum bound water fraction (MBWF) values, relating to these types of soil, as well as the static dielectric constants, relaxation times, and conductivities of both the bound soil water (BSW) and free soil water FSW were systematized in the form of a spectroscopic data base for moist soils. Second, using such a data base, the spectroscopic parameters relating to BSW and FSW were analyzed in terms of their dependence on the type of soil. In addition, for each individual soil, the dielectric spectra of both types of soil water were calculated with the use of GRMDM, in order to demonstrate the variability of those as a function of soil type. Finally, the soil water dielectric spectra together with the other parameters of the moist soil dielectric data base were applied to evaluate the dependence of moist soil emissivity on the type of soil, in the whole microwave band. From this point of view, the study conducted can be considered as a new approach, that opens perspective for carrying out both the feasibility studies and developing data processing algorithms in radiometry or radar remote sensing, using an appropriate spectroscopic data base for moist soils. [C5074]

"Wind fields from hurricane Isabel"

IWRAP, the imaging wind and rain airborne profiler, is the first high-resolution dual-hand airborne Doppler radar designed for studying the inner core of tropical cyclones (TCs). The system is designed to provide high-resolution, dual-polarized C and Ku-Band reflectivity and Doppler profiles of precipitation volume backscatter and ocean surface backscatter within the inner core precipitation bands of tropical cyclones (TCs). SFMR is a C-band nadir viewing radiometer used operationally to provide continuous estimates of the surface wind speed and title column average rain rate. Both IWRAP and SFMR arc operated from a National Oceanic and Atmospheric Administration (NOAA) WP-3D aircraft during missions through TCs and severe ocean storms. In this paper, we present wind and reflectivity profiles of the atmospheric boundary layer within the inner-core of hurricane Isabel (2003) from IWRAP measurements. These profiles are the highest resolution measurements of the ABL winds of a hurricane ever obtained. The profiles are compared to coincident surface wind speed measurements provided by SFMR, flight level wind measurements and GPS dropsonde winds [C5075]

"Integration of digital elevation data scanning 3D and interferometric SAR systems"

This work concerns the surface 'change detection' by means of differential digital elevation model (D_DEM) techniques, based on laser scanning 3D data. The laser scanning 3D technology allows to generate an high precision DEM, that can be used to calculate the morphological ground surface variations at different acquisition time intervals. The basic operation has been to acquire several DEMs in the test area: through the subtraction of different DEMs we can obtain the temporal decorrelation of two geometrical parameters: volume and elevation vector. The validation is performed by the comparison with the GPS data. The integration with differential interferometric SAR systems will allow to investigate wide areas. So, when the alarm event has been individuated, the laser scanning 3D is used to generate a precision DEM reconstruction. The results show that with such technique it is possible to calculate the volume and elevation variations with a standard deviation less than a centimetre. [C5076]

"Validation of DEMs derived from radar interferometry, airborne laser scanning and photogrammetry by using GPS-RTK"

A high resolution digital elevation model (DEM) enables easy derivation of subsequent information for various applications. This work uses real-time kinematic (RTK) GPS to examine the quality of some DEMs generated by such means as radar interferometry (InSAR), airborne laser scanning (ALS) and photogrammetry. The preliminary results show that a DEM generated from ALS has the highest accuracy with a RMS error of 0.09 0.3 m. The RMS errors of DEMs derived by photogrammetric and radar interferometric techniques are 1.03 3.75m and 4.26 27.81 m respectively. [C5077]

"Algorithms for oil spill detection in Radarsat and ENVISAT SAR images"

We present algorithms for detection of oil spills in Radarsat and ENVISAT SAR images. The algorithms are trained on 60-100 images from each sensor from European water (mainly the North Sea and the Baltic Sea). Results show that they perform very well when applied to benchmark data sets, but in some cases additional information is needed to discriminate between oil slicks and algae, particularly in the Baltic Sea [C5078]

"Effect of precipitation on ocean wind scatterometry"

This paper presents preliminary results of precipitation effect on microwave scatterometry wind estimates at C and Ku band. The results show that microwave scatterometer underestimates the wind speed by up to 10 m/s for rain rate condition of 15 mm/hr and wind speed condition of 25 to 30 m/s for both frequency bands [C5079]

"Spaceborne P-band radar for ice-sheet sounding: design and performances"

The Antarctic ice sheet is one of the most prominent physical features on our planet. It represents an area of about 14 millions km². The average ice thickness being around 2200 m (and up to 4500 m), the Antarctic ice sheet contains a 30 million km³ ice volume corresponding to about 70 m of sea level. However, this huge reservoir of water is still partially unknown and due to its large extent, only observations from space can give some global insight into the structure of the ice sheet. The Antarctic ice sheet is an exceptional archive of the past climates and a major actor of the Earth water cycle. Each ice layer corresponding to one period of time keeps its own chemical characteristics linked to past atmospheric events. The typical temporal scale involved allow for a description of past climate over a few climatic cycles, or a few 100000-year events. A dedicated mission has been proposed to European Space Agency as a candidate for an Earth Explorer Opportunity mission. This mission is based on a P-band radar instrument with a nadir-looking geometry, working at 435 MHz with a bandwidth of 6 MHz (imposed by ITU regulation), allowing to sound the vertical structure of the ice from the surface down to the bedrock. A feasibility study of the mission was done in Alcatel Space under ESA contract with an emphasis on the radar instrument. For coherent reflection and deep sounding (corresponding to the so-called Fresnel zone), the useful signal coming from any ice layer or from the bedrock overlap with lateral incoherent surface scattering. The surface clutter is reduced by the antenna pattern in the across-track direction (typical aperture is lower than 5°) and by Doppler filtering in the along-track direction. These beam requirements impose to have a very long antenna in the across-track direction. The typical dimension of the antenna is 10 m \times 1 m. This work summarizes the principle of the instrument, and the associated antenna solution. Main performances are also presented. [C5080]

"An algorithm to acquire the average height of land surface"

For an airborne altimeter, an algorithm to acquire the average height of the land surface is suggested based on the return waveform. Through the origin analysis about each point of return, scattering from assured distance reflects the corresponding information of incident scope. In the difficult situation of how to decide the single characteristic point, the technique built in the theory can be handled easily in practice. Otherwise, we validate our model by simulation in a good way. [C5081]

"Seismic source parameters from InSAR data through neural networks [Through reads through]"

In the recent years InSAR (Synthetic Aperture Radar Interferometry) technique showed its wide potentialities to detect the surface displacement field due to an earthquake. Of great interest and usefulness in this context is the solution of the inverse problem that means to recover the source parameters from the knowledge of InSAR surface displacement field. In this work a novel approach for the solution of such a problem is presented. [C5082]

"High resolution airborne SAR triangulation application supported by sparse-GCPs"

At present, a great deal of western area in China has still lacked of corresponding relief maps. Because of the cloudy or soupy mountainous conditions in these districts, the high resolution airborne SAR imagery has often been chose as the irreplaceable data resource, while remote sensing cartography technique is being performed. At the same time, the mission that how to acquire enough accuracy and quantity of ground control points (GCPs), which are difficult to be measured in practical, has become an urgent demand for mapping tasks. This work analyzes the practical conditions, and divides it into two instances, that is, which with and without navigation data provided from GPS/INS system. It discusses the aerial triangulation theory from airborne SAR images, with which only sparse GCPs around the mapping area could be provided, puts forward the corresponding mathematical model, and sequent technique flow, according of which we can obtain the coordinates of the required GCPs for cartography. Lastly, the airborne SAR imagery of 1m-resolution, in the

area of Zhengzhou, in China, has been taken as an experiment data to validate the model, and a corresponding accuracy analysis derived from the developed software has been presented. [C5083]

"The effects of scale on fractal dimension of topography: a case study from Sudbury, Ontario, Canada"

An issue of concern when analyzing remotely sensed data is the impact of data resolution on the results of the analysis and on the conclusions that are subsequently drawn. In this paper, we investigate the effects of spatial resolution on fractal dimension of digital elevation models (DEMs) generated at various spatial resolutions. The DEMs used in this study were created from three sources: 2-m resolution derived from LiDAR altimetry data, 20-m resolution derived from 1:20000-scale topographic maps, and 100-m resolution derived from National Topographic Series (NTS) maps of Canada at 1:250000 scale. Directional variograms were used to determine the fractal characteristics of the study area for each scale. In addition, the 2-m LiDAR data, which show detailed lithological and structural textures, were resampled to simulate lower resolutions of 50-m and 100-m. The results of the study indicate that, while the three data sources display a multifractal surface, the fractal dimension (D) at range-scale shows a consistent decrease with increasing cell size. The lower resolution, therefore, appears to cause a smoothing of the topographic surface, thereby reducing the fractal dimension in all directions. In contrast, the results from the resampled LiDAR data are less consistent. This suggests that the detailed lithological information present in the high-resolution LiDAR data is sufficiently retained, even at degraded resolutions, to influence the fractal characteristics [C5084]

"Measuring lake water level using multi-source remote sensing images combined with hydrological statistical data"

The Poyang Lake, as one of the most frequently flooded area, is the largest freshwater lake in China. It is very significant to monitor the water level and water regime accurately and in real-time during flooding. To provide an operational method to measure shape parameters, such as water level, water regime area, and water distribution of Poyang Lake using remote sensing images, we carried out the study. In the paper, using the hydrological statistical data of Poyang Lake through many years, we fit a mathematic model of water regime area varied with water level. Meanwhile, water regime distribution is extracted from Radarsat SAR and Terra Modis remote sensing images, and then its area can be calculated. Comparisons between model results and remote-sensing-image-based measuring results are carried out and the absolute error is less than 0.70%. Then we revise the fitted mathematic model using remotely sensed data and finally build a high precision ($R^2 > 0.99$) and practical mathematical model of water level versus water distribution of Poyang Lake main regime. It is a great contribution to the prevention, monitoring and mitigation of great flood disaster around the Poyang Lake district [C5085]

"Remote Internet-based lidar experimentation and education"

Remote sensing projects typically require the collaboration and expertise of professionals from multiple disciplines. In order to motivate and train undergraduate students for future careers and/or education in the field of remote sensing, they should be exposed to remote sensing technologies and concepts throughout their undergraduate studies within their selected majors. This paper describes the design and development of a laboratory and Internet-based systems environment that facilitates remote sensing education and research based on cross-institutional resource sharing of lidar instrumentation [C5086]

"Solving the strip adjustment problem of 3D airborne lidar data"

This paper proposes a contribution to the adjustment problem of airborne laser scanner strips. Based the comparison of each laser strips with a photogrammetric derived Digital Surface Model (DSM), and on the modeling of the discrepancies between these two data sets, the algorithm produces an homogeneous 3D deformation field. The measurements of these deformations is performed using a modified Hough transform and we search for the maximum of the accumulator whereupon we assign a probability of correctness. Depending of this probability, we estimate a global affine transform over the cloud of points. For transitivity properties, all strips are registered with regard to this DSM and therefore they all perfectly fit on overlapping areas. This fine registration is of importance for many applications, especially when fusionning photogrammetric data and lidar data for feature extraction. More generally, this method can be applied to any other sorts of 3D data and provides an efficient algorithm for matching 3D datasets [C5087]

"Effects of forest spatial structure on large footprint lidar waveform"

Large footprint lidar has demonstrated its great potential for accurate estimation of many forest parameters, e.g.,

forest height, forest biomass and vertical structure of forest canopy. In addition to the canopy vegetation, many factors such as atmosphere, underlying surface, the shape of crown, et al., influence the lidar waveform. The illuminating intensity of the laser beam across the lidar footprint is a Gaussian distribution and reduces from 1.0 to e^{-2} from the center to the edge of the footprint. Hence the forest stand structure plays an important role in the lidar waveform. The contribution of each tree to the lidar waveform varies with its location in a forest stand. This paper simulated the random, uniform and clumped tree distribution patterns in a stand. Then waveforms were simulated using a three dimensional lidar waveform model developed by Sun and Ranson. The results show that the tree distribution patterns affect the lidar waveform profiles. The area (or energy) under the waveform from vegetation (AWAV) and the height of median energy (HOME) were used to estimate the effects. Following trends have been revealed from the simulation: for AWAV and HOME, uniform > random > cluster. There is no obvious difference between regular and random. The waveform area (AWAV) varies much more than HOME. For the clumped case, the number of clusters does not have much effect on the lidar waveform [C5088]

"Web-based visualization and animation of geospatial data using X3D"

In this case study, we utilize X3D (eXtensible 3D) for the geoscientific visualization of an interferometric (InSAR) data set of Kilauea volcano, Hawaii. We describe the modeling and animation of the geospatial data using X3D features and tools and demonstrate the Web-based interaction of the user with the displayed 3D content [C5089]

"SAR based products for the implementation of humanitarian aid and development assistance projects within the UNOSAT project"

The UNOSAT service is an ESA Earth Observation Market Development initiative whose objective is to encourage, facilitate, accelerate and expand the use of accurate geo-information derived from EO satellite imagery by professionals involved in the implementation of humanitarian aid and development assistance projects. In this paper, we focus on the role of SAR within this context. Space-borne SAR has a particularly good potential to support disaster management and humanitarian relief projects thanks to its all-weather capability, its capabilities for change detection, the large existing data archives, and, of course, the geometric and thematic information content of the images. Basic processing techniques, including precision image co-registration, multi-temporal analysis, terrain corrected geocoding, interferometry, and radargrammetry are well developed and operational. Advanced techniques like differential interferometry and interferometric point target analysis (IPTA) became more and more operational during the last years and provide unique information about terrain stability and deformation [C5090]

"A simulator of synthetic aperture radar images; land, ocean surface, and man-made targets"

Synthetic aperture radar (SAR) images are very useful for many applications. However, SAR images require a great deal of experience for the interpretation, since the appearances are very different from optical images. Additionally, the appearances change significantly by the observational condition, such as frequency and incident angle. We propose a SAR image simulating algorithm developed for the aid of the SAR image analysis and training. The simulator is also intended to support the SAR system configuration design by providing the expected images. The main features of the algorithm are the capability of wide area simulation and the low computational costs. The simulated image of 10 km square area is shown and compared with the real image [C5091]

"Optimal siting of hydrological monitoring stations with respect to remote sensing-based geo-environmental patterns"

The management of sustainable and dependable water resources in a semi-arid coastal watershed in South Texas, such as the Choke Canyon Reservoir Watershed (CCRW), is deemed critical because of complex relationships among ecosystems, social development, human health, and economic progress. To retrieve key hydrological information constrained by a limited budget, a set of hydrological monitoring stations in support of investigation of drought and flood impacts in the CCRW were identified by a grey integer programming (GIP) approach under uncertainty. The area of interest is divided into eight hundred cells in GIS for the 15,000-square-kilometer watershed area. Each cell size is 4-by-4 kilometer. The cells are assigned weights that could quantify monitoring values in terms of soil permeability, precipitation rate, evaporation rate, predicted soil moisture, evapotranspiration rate, and the normalized difference vegetation index (NDVI). RADARSAT and LANDSAT satellite images are acquired in support of determination for part of the weighted values, such as soil moisture and vegetation index, in the hydrological cycle. The weights are aggregated as coefficient matrices in a GIP model that help identify the most suitable locations. Fifteen cells are chosen out of eight hundred candidates and are ranked consecutively. Eventually, only five sites were selected after a site investigation based on site accessibility and practical uses of the selected sites. It may help collect a vital database at strategic locations,

including wind speed, wind direction, soil moisture, ambient temperature, soil temperature, and relative humidity periodically for drought and flood management in the future [C5092]

"Near real time vessel detection using spaceborne SAR imagery in support of fisheries monitoring and control operations"

The system components for the operation supply of maritime target positions detected in SAR imagery are described, together with their implementation details and practical performance parameters. Integration of detected target information within European fisheries monitoring systems based on VMS is demonstrated [C5093]

"Remote sensing study based on IRSA Remote Sensing Image Processing System"

The IRSA Remote Sensing Image Processing System is multi-functional software used for satellite image processing. It consists of over ten parts of the routine and typical used modules in Remote Sensing Image Processing project, such as viewer & file import/export, basic processing, image restoration. As an indigenous developed software, IRSA combines the advantages and kernels of many import famous systems, such as ERDAS imagine, PCI, ENVI and ER-mapper, and avoids some infrequently used functions or details. Hence, it appears concisely, refinedly and practically, acceptable and understandable. Based on this characteristic, we develop an additional set of interrelated data together with the system to face the college students and people who are not familiar with the Remote Sensing Image Processing work. Our experiences prove that we are successful. With the detailed help documents and instruction as well as our elaborately chose, arranged data, the students can study the system step by step. From these data, they get very intuitionistic and sensible cognition to the remote sensing study [C5094]

"Lateral and subsidence movement estimation using InSAR"

Ground movement poses a hazard to buried infrastructure (e.g., pipelines) as either massive instantaneous movement leading to serious failures or as small incremental movement over a period of time resulting in catastrophe, are common. Conventional ground motion detection and measurement techniques require regular costly surveys and operational cost increase in geographically dispersed areas. The measurement of ground movement (e.g., subsidence) using DInSAR (Differential Interferometric Synthetic Aperture Radar) is a well established technique and many studies have been completed to validate its performance. In these studies, ground movement is generally derived from a single look direction (e.g., subsidence only). Strictly speaking, if one look direction is used to obtain ground movement estimates, then only one dimension of movement can be derived. This can produce significant errors in measuring subsidence, especially in the case of localized movement producing significant lateral movement. This paper discusses a technique for extracting lateral ground displacement using interferometry and a data fusion, least squares estimation technique from multiple SAR look directions. It is shown that meaningful three dimensional movement estimates can be derived within expected sensor error, with a dramatic reduction in errors of subsidence measurements over a single look direction measurement. The validation was accomplished using a time series of satellite data collected over a pipeline right of way in 2001, along with a series of traditional surveys for comparison [C5095]

"Short wave spectrum modulation by a surface current field and long waves for SAR imaging process simulation"

In the framework of the SAR imaging process simulator we are developing, the modification of the short wave spectrum by ocean surface is of great importance. Short waves at the sea surface produce the backscattering of the radar wave. So the modulation of the short wave distribution by ocean surface induces the modulation of the SAR image. In this paper we present a two-step algorithm designed to simulate the modulation of the short waves by both current and long waves. First of all the modulation of the long waves by current is taken into account. Then the modification of the short wave spectrum by long-wave orbital velocity and current is considered. To achieve the calculation we use the action balance equation (ABE) based on a weak interaction theory. ABE theory and the two-step algorithm are described here [C5096]

"Wind parameter analysis of two offshore windpark sites"

Due to the shortage of suitable sites on land offshore wind farming has grown rapidly in Europe over the last decade. For the optimal siting, building and operation of these wind parks, remote sensing techniques can help in many different ways. In this study a special application of the well known wind field measurement technique based on synthetic aperture radar (SAR) data is presented. SAR scenes as acquired by the European satellites ERS-2 or ENVISAT permit the estimation of 2D wind fields with a resolution of less than 1 km and a coverage

of up to 500 km. With this capability SAR is an efficient instrument to obtain wind information on spatial scales relevant for offshore wind farming. In the analysis the two wind parks sites "Horns Rev" and "Butendiek" in the North Sea are compared. While "Horns Rev" is already in operation "Butendiek" is still in the planning stage. The objective is to assess the expected power yield in the new wind park in comparison to the existing wind farm. For the investigation ERS-2 image mode scenes of 100 by 100 km size were used, which are ideally suited for this application, because both wind farm sites are covered by a single scene. Scatterplots of SAR derived wind speed and wind direction obtained for both wind farms are presented and discussed [C5097]

"Multilayer perceptron classification for ENVISAT-ASAR imagery"

This paper describes the application of neural networks to targets classification from multi-polarization ENVISAT-ASAR imagery. The used neural network is multilayer perception (MLP) with fast learning (FL), which is fully interconnected network. Accordingly, the training data sets may be taken from a known truth data in the ground. And finally, the results of proposed method are compared with that of the other classification ones, the in situ test data are from Zhaoqing in Guangdong Province of China [C5098]

"Analysis of polarimetric marine scattering at different range resolutions"

In this work we deal with the problem of analyzing and modeling marine (lake) surface scattering as seen by high resolution radars, with the aim of highlighting, where possible, the differences due to changes in the range resolution and polarization [C5099]

"Enhancement of Doppler centroid for ocean surface current retrieval from ERS-1/2 raw SAR"

Ocean surface current information is one of the important factors which are employed for a variety of scientific pursuits especially on ocean environment. Although remote sensing techniques have been developed up to now, the investigation of ocean surface current using synthetic aperture radar (SAR) is not easy of access. This paper presents the results of ocean current observation using ERS-1 raw SAR data which were obtained off the coast of Jeju Island. We extract the ocean current based on the concept in which Doppler frequency shift and the ocean current are closely related. Moving targets cause Doppler frequency shift of the backscattered radar radiation of SAR, thus the line-of-sight velocity of the scatterers can be evaluated. The Doppler frequency shift can be measured by estimating the difference between Doppler centroid obtained and reference Doppler centroid calculated. Theoretically, the Doppler centroid is zero, however, squinted antenna which is affected by several physical factors causes Doppler centroid to be nonzero. The Doppler centroid can be estimated from measurements of sensor trajectory, attitude and Earth model. By compensating ERS attitude errors, we could enhance Doppler centroid accuracy and verify that the extracted ocean surface current is more coincident with the in-situ data. We present here the results of estimated ocean surface current and observed in-situ data, which are in agreement within the limit of error bounds [C5100]

"Comparison between simulations and interferometric polarimetric SAR P-band data on a pine-trees forest"

The interpretation of SAR data remains particularly difficult in case of forests, which makes the use of modelling very helpful. On the other hand, the potential of combined use of interferometric and polarimetric data has been already demonstrated to provide key forest parameters. In this paper, we present comparisons between interferometric polarimetric images of a forest simulated by a coherent scattering model derived from L. Thirion (2003) and L. Thirion (2004), and real airborne and full polarimetric interferometric P-band data measured over maritime pine trees. Results are presented that demonstrate the efficiency of the model to retrieve polarimetric and interferometric parameters on this forest. Finally, a first step of simplification and inversion of the model, relying on the analysis of the scatterers contributions, is proposed [C5101]

"Influence of antenna aperture length on observations of the Kuroshio surface current by the NICT HF ocean radar"

A HF long-range (over 200 km) ocean radar system, developed by Japan's National Institute of Information and Communications Technology, was used to observe the Kuroshio surface current in the southern part of the East China Sea. The observations began in July 2001. In this paper, we show the relationship between the antenna aperture length (beam-width) and the accuracy of Kuroshio surface current speeds measured using post-processed signals received by the radar [C5102]

"Mesoscale and submesoscale zoo observed with HF radar in Monterey Bay"

Shore-based high-frequency Doppler radar observations collected in Monterey Bay between 1999 and 2001 are

utilized for the reconstruction of high-resolution surface currents: mesoscale and submesoscale ageostrophic spiral eddies, eddy dipoles, eddy tripoles and multi-eddy systems with lifetimes about 4-12 hours (sub-inertial periods). Our analysis demonstrates topography nature of all these eddies because of rectification of tides in the submarine canyon system. Spiral mesoscale eddies generated in the head of Monterey and Soquel Canyons have induced strong alongshore water transport qualified as Stokes drift [C5103]

"Inversion of vegetation height using SIR-C dual frequency polarimetric SAR interferometry data"

From the frequency characteristic of L and C band, in this paper, a new phase based method of vegetation height estimation using dual frequency SIR-C polarimetric SAR interferometry data is presented. Compared the preliminary result with field measurement data, it indicates that the inversion algorithm can obtain the height of vegetation with an acceptable accuracy [C5104]

"A novel Radon transform-based method for ship wake detection"

Based on the gliding-box algorithm and the Radon transform algorithm, a novel method for detecting ship wakes in synthetic aperture radar (SAR) images is proposed. The method is applied to both simulation images and real SAR image, and the result shows that the detection accuracy is satisfactory in strong noise environment. One significant feature of the new algorithm is that it can even detect ship wakes which are significantly shorter than the image dimensions [C5105]

"Remote sensing of frozen lakes on the North Slope of Alaska"

We used synthetic aperture radar (SAR) images from the ERS-2 remote sensing satellite to map the freeze condition of lakes on Alaska's North Slope, the geographic region to the north of the Brooks Range. An image from March 1997, to coincide with the period of maximum freeze depth, was used for the frozen lake mapping. Emphasis was placed on distinguishing between lakes frozen to the lakebed and lakes with some portion unfrozen to the bed (a binary classification). The result of the analysis is a map identifying lakes as frozen to the lakebed and lakes not frozen to the lakebed. This analysis of one SAR image has shown the feasibility of a simple technique for mapping frozen lake condition for supporting decision making and understanding impacts of climate change on the North Slope. [C5106]

"Validation of a glacier surface mass balance model using remote sensing"

A method to validate spatialized mass balance model over glaciers using optical remote sensing data, for the time series period 1984-2002 is presented. To model the mass balance, we use the snow model CROCUS, adapted for glaciers. Results are discussed for St. Sorlin Glacier, French Alps. The snow line calculated in the model is compared with satellite images. Comparison of altitude gives a correlation $R^2 = 0.94$, and a RMSE of 30 m. [C5107]

"To measure the cumulate crustal deformation of important faults system on the Western China by PS InSAR technique"

This work puts forwards a plan to measure the cumulate long period slow slip of some active fault zone by applied PS InSAR technique and introduces some prophase work. At first, some scenes ERS-1/2 SAR data from strong earthquakes in West China are processed by D-InSAR technique. Next, corner reflector experiment field is established in where fault slibs in intensity and earthquake happen in high frequency, and the cumulate long period crustal deformation and coseismic deformation of important structural region will be measured at high precision. [C5108]

"Angular and frequency correlation for sea-ice thickness retrieval"

A combined spatial and frequency domain interferometer or angular and frequency correlation (ACF/FCF) between two radar beams in the VHF-band is applied for the direct measurement of sea-ice thickness. This measurement is critical because the thickness of sea ice within the polar region indicates the state of ocean circulation and the associated air-sea heat exchange, which profoundly affects the global heat balance and ocean thermohaline circulation. This new instrument technology-cryospheric advanced sensor (CAS)-can measure sea-ice thickness, tilling a critical gap in measuring the polar region. In this paper, we present the algorithm development and demonstration by simulations of estimating the height of the sea-ice that led to the robust design of CAS interferometric system. Sea-ice thickness is derived from the interferometric phase of the ACF/FCF function of two VHF-band-scattered returns of two radar waves that have different frequencies, incident angles, and observation angles. The inversion calculation to estimate the ice thickness is based on several methods, gradient-descent (GD). least-square (LSQ) method, and genetic algorithm (GA). Compared with a GD

method, and LSQ method, GA does not require the knowledge of the derivative of the ACF/FCF function. Good agreement is shown with GD and LSQ results, when a single unknown variable-sea-ice thickness-is to be determined. To support the inversion calculations and analysis, we developed an analytical model. The analytical model used to formulate the ACF/FCF function depends on the age of the ice being measured. The analytical model for first-year ice is based on the small perturbation method (presented here) and, for multiyear ice, the Kirchhoff approximation (presented in accompanying paper by the authors). [C5109]

"Ice sheet motion in inland Antarctica from JERS-1 SAR interferometry"

From a series of three JERS-1 SAR interferograms over the Yamato mountains area in the Antarctica, ice surface movement is detected. In spite of less accurate orbit information, baselines are estimated using 1 km global DEM and referring phases over bare rock areas. The Detected movement fields from three interferograms resemble, but different subtly [C5110]

"Feature extraction of SAR data based on eigenvector of texture samples"

Feature extraction of SAR data based on eigenvector of texture samples tries to find the principle components of the distribution of training sets. These eigenvectors can be considered as a set of features, which together characterize the variations between training samples for each class. Defining covariance matrix is also an important issue to achieve significant classification accuracy. In this study, classification is performed based on eigenvector of textures and gray level cooccurrence matrix. Both statistical based decision rules and neural networks are applied as a classifier to test the performance of the feature extraction method based on eigenvector of texture samples and cooccurrence matrix. [C5111]

"Scattering mechanism identification based on the rotation and eccentric angles of polarimetric SAR data"

In this paper we introduce two novel parameters for polarimetric SAR (POLSAR) images. For this purpose, a 2times2 matrix is defined to take into account the independent elements of the covariance matrix. To understand the geometry of this new matrix, an equation of ellipse is defined. As a result, the geometry of the ellipse is completely tied up with the eigenvalues and eigenvectors. Two novel parameters, the rotation and eccentric angles of the ellipse which can directly be derived from the eigenvalues and eigenvectors, are presented. The results indicate that different scattering mechanisms can be represented with the rotation and eccentric angles. Results obtained from the proposed parameters, when compared with the results derived from existing features, were in agreement in terms of the scattering mechanisms, as well as terrain cover types present in the test site [C5112]

"Analyses of C-band microwave backscatter to wind roughened first-year sea ice melt ponds"

Variations in wind forcing over summer first-year sea ice (FYI) melt ponds occur at hourly to weekly scales and are a significant contributor to backscatter (σ°) variability observed from space borne synthetic aperture radar (SAR) platforms (e.g., ENVISAT-ASAR and RADARSAT-1). This variability impairs our ability to use SAR to derive information on summer sea ice thermodynamic state and energy balance parameters such as albedo and melt pond fraction. The surface roughness contribution to like-polarized, C-band σ° estimates from FYI melt ponds in the Canadian Arctic is addressed through a spectral and statistical analysis of surface wave height profiles for varying wind speeds, upwind fetch lengths, and melt pond depths. Our hypothesis is that the perturbation of wind-roughened melt pond surfaces to wavelengths that are resonant to C-band SARs is driven by upwind fetch and wind speed. Significant scale surface roughness was observed even at wind speeds of 3 m s⁻¹ resulting in σ° (HH) ranging from -6 dB at 20° incidence to -24 dB at 50° incidence. Results from a multivariate linear regression analysis show that 53.4% of observed variance in σ° (HH or VV) can be explained by wind speed (0.9 m height), upwind fetch from melt pond edges, and depth of melt ponds, with no appreciable difference in the relative contribution of those explanatory variables. [C5113]

"Comparison of SAR data and operational sea ice products to EM ice thickness measurements in the Baltic Sea"

In February 2003, sea ice thickness measurements using an electromagnetic induction (EM) instrument were made in the Gulf of Bothnia and Gulf of Finland. We have made comparisons between the EM measurements and Radarsat-1 ScanSAR Wide mode SAR data, and also between our operational sea ice products (digitized ice thickness charts, and ice thickness charts refined by the latest Radarsat-1 image). The SAR images are in 100 m resolution, and the other products are in 500 m resolution [C5114]

"SSALTO/DUACS and operational altimetry"

The SSALTO/DUACS multiple altimeter processing system provides MERCATOR, GODAE, and climate forecasting centers with directly usable, high quality near real time altimeter data. Commercial applications for the fishery and offshore industries are also developed. An overview of the SSALTO/DUACS system is given and its main applications and users are described. [C5115]

"ENVISAT RA-2/MWR cross-calibration and validation final results"

ESA launched its environmental research satellite, ENVISAT, on 1 March 2002. It carries a suite of 10 instruments offering opportunities for a broad range of scientific research and applications. In particular, ENVISAT carries a radar altimeter (RA-2), a microwave radiometer (MWR), and a precise tracking system (DORIS). The evaluation of the quality of the ENVISAT altimetry geophysical data products and the cross-calibration on ERS-2 and other flying altimeters has been performed during the commissioning phase within a team of scientists drawn up from the pre-launch announcement of opportunity. The results obtained from this teamwork are presented here. [C5116]

"Approaches to automate image geocoding and registration"

Coregistration and geocoding are standard methods to generate registered stacks of multiple remote sensing image data. It is shown that pixel-based image matching is a useful tool to automate these procedures. Demonstration examples are provided for a multi-temporal set of ERS SAR images. [C5117]

"Sampling the mesoscale ocean surface currents with various satellite altimeter configurations"

Ten-day composites of maximum cross correlation (MCC) ocean surface current vectors from 1 km spatial resolution advanced very high resolution radiometer (AVHRR) thermal infrared images are used to simulate the ocean surface current retrieval capabilities of three satellite altimeter configurations over a large California coastal region. Ground track positions of the nadir sampling TOPEX/Poseidon (TP; now the Jason-1) satellite altimeters are used to compute the cross track components of the corresponding MCC vectors for a ten-day composite period. Next, the TP and Jason-1 "tandem mission" sampling is simulated for the same region and temporal sample. Finally, a similar approach is used to simulate the current retrievals from the proposed wide swath ocean altimeter (WSOA), which will have the capability to retrieve both along and cross track components of the surface velocity over a spatial swath rather than just nadir sampling. Visual comparisons of raw vector fields and through differences and wavenumber spectra from optimally interpolated (OI) currents from the "simulated altimetry" with the corresponding MCC fields demonstrates that the combined coverage from Jason and TOPEX results in a better representation of the currents than that of Jason alone and that the retrieved currents from the WSOA altimeter provide an even greater improvement over the tandem mapping of the TP and Jason-1 altimeters. [C5118]

"Calibrating the Jason-1 measurement system"

We present calibration results from Jason-1 (2002-) and TOPEX/Poseidon (1992-) overflights of dedicated verification sites on the Mediterranean island of Corsica and on a California offshore oil platform (Harvest). Harvest served for a decade (1992-2002) as a calibration site for the TOPEX/Poseidon (T/P) mission, and is serving in a similar capacity for Jason-1. Initiated in 1996, the Corsica experiment features a fiducial reference station near Aspretto, and a primary sub-satellite tide-gauge deployment site 40 km south at Cape Senetosa. Both Corsica and Harvest feature carefully designed collocations of space-geodetic and tide-gauge systems to support the absolute calibration of the altimetric sea-surface height (SSH). By incorporating improved estimates of the Jason-1 sea-state bias and columnar atmospheric wet path delay, we observe a bias of about 12 cm. [C5119]

"On estimation of snow water equivalence using L-band and Ku-band radar"

The study of snow has become an important area of research in the natural sciences, particularly in hydrology and climatology. This study shows a concept of estimating snow water equivalence under the consideration of a dual frequency L- and Ku-band polarization system. [C5120]

"Radiometric and geometric correction of RADARSAT-1 images acquired in alpine regions for mapping the snow water equivalent (SWE)"

In this paper, introduced is an application of two radiometric slope correction methods on standard RADARSAT images in a mountainous environment like the Alps. Because of the highly varying topography, such corrections

are needed to reduce the distortions on the backscattering coefficients when trying to monitor the snow characteristics from SAR data in alpine regions. This paper discusses the results obtained by the two different methods over dry and wet snow cover; both algorithms significantly reduced the effect of local slope facing the radar, but may not compensate enough for the steep slope over 30°. [C5121]

"Polarimetric study of scattering from dry snow cover in alpine areas"

This paper introduces a qualitative characterization of dry snow scattering behaviour in Alpine areas. An electromagnetic scattering model is developed, based on the vector radiative transfer equation, to simulate the fully polarimetric response of a snow cover. Multi-temporal and multi-frequency polarimetric SAR data acquired over Alpine test sites are analyzed by comparing polarimetric indicators to simulated ones with various sets of snow cover characteristics. [C5122]

"Impact of using several altimeters for improving numerical wave analyses and forecasts"

Meteo-France Marine and Oceanography Division is using data from the European Space Agency (ESA) satellite ERS2 to improve analyses and forecasts of the sea-state. As it travels along its orbit above the earth's surface, the measuring platform's onboard altimeter measures significant wave heights and wind speeds. These parameters are assimilated into Meteo-France's sea-state forecasting model. Envisat (ESA satellite) and Jason (satellite of CNES, the French space agency and NASA, the US space agency), successors of ERS2 and Topex respectively will provide similar and validated data in 2003, in "real time". In addition, data from the US Navy satellite GFO are also available on a NOAA ftp server, the United State Oceanographic and Atmospheric Administration. Preliminary results related to the benefit of using these new data in addition to ERS2 ones for numerical wave analyses are presented. The usefulness of using several altimeters for wave forecasting systems is shown by experiments for assessing their input which are conducted within Meteo-France's Marine and Oceanography Division, with the support of the CNES. [C5123]

"Combined active and passive microwave remote sensing of snow in Finland"

We examined the use of data from active (QuikScat on SeaWinds) and passive (SSM/I on DMSP) space-borne microwave sensors for monitoring key snow parameters in Finland. The feasibility of these data for the task was determined both separately and using a combined data set. The results are based on satellite and ground truth data for 21 test sites in Finland covering the winters of 1999-2000, 2000-2001, and 2001-2002. We show that a Ku-band scatterometer with a fixed incidence angle provides reasonable accuracy for retrieval of dry snow water equivalent (SWE). Using the combined active/passive data set retrieval accuracy is better than with SSM/I data. QuikScat data can also be used for determining onset of snow melting and snow-covered area (SCA) in spring. [C5124]

"A constrained spectral unmixing approach to snow-cover mapping in forests using MODIS data"

A snow-cover mapping method accounting for forests (SnowFrac) is presented. SnowFrac uses spectral unmixing and endmember constraints to estimate the snow-cover fraction of a pixel. The unmixing is based on a linear spectral mixture model, which includes endmembers for snow, coniferous trees, branches of leafless deciduous trees and snow-free ground. Model input consists of a land-cover fraction map is applied in the unmixing procedure to identify the number and types of endmembers for every pixel, but also to set constraints on the area fractions of the forest endmembers. Results are presented for non-forested areas, deciduous forests, coniferous forests and mixed deciduous/coniferous forests. Results are also compared to the MODIS L2 500 snow product. [C5125]

"Analysis of system concepts for bi- and multi-static SAR missions"

The performance and capabilities of a bistatic spaceborne synthetic aperture radar (SAR) are analyzed, where the transmitter and receiver are in different orbits. Such a configuration may be optimized for a broad range of applications like frequent monitoring, wide swath imaging, single-pass cross-track interferometry, along-track interferometry, resolution enhancement or radar tomography. [C5126]

"GLORIA: Geostationary/Low-Earth Orbiting Radar Image Acquisition System: a multi-static GEO/LEO synthetic aperture radar satellite constellation for Earth observation"

In this paper, we present a novel approach to continuous remote sensing of Earth. The proposed concept "GLORIA" drastically enhances the ability of scientists to study the Earth in a manner not possible before. The proposed system is based on a constellation of few geostationary, radar transmitter satellites and several low Earth orbiting synthetic aperture radar receiver satellites. Just as the sun is the radiation source for optical

remote sensing, transmitters of microwave energy in a geostationary orbit provide the energy for radar remote sensing. Advantages of such a constellation lie in (1) a much larger number of observables, due to multi-static measurements, which significantly enhances the accuracy of retrieval algorithms, 2) the distribution of failure risk is by eliminating total system failure if a single satellite stops operating, 3) simple modular system design of small satellites through separation of transmitters and receivers (reducing weight, cost and power consumption by each satellite), and 4) flexibility in operation, that is, the receivers can be configured for different modes.

[C5127]

"A further insight into the potential of bistatic SAR in monitoring the Earth surface"

This contribution discusses some relevant features of bistatic scattering from vegetation, based on a simulation analysis using a theoretical model developed at Tor Vergata. This paper is focused on land cover monitoring by a combination of monostatic and bistatic radar. The main mechanisms contributing to bistatic scattering are highlighted and its exploitation in monitoring vegetation covered surfaces is discussed. [C5128]

"Landmine detection by a broadband GPR system"

Most of the landmine detection techniques by GPR use a monostatic type radar system, which is suitable for detecting landmines buried in shallow soil, which is normally less than 10 cm. The shallow target is difficult to detect by conventional GPR due to its low range resolution. We developed a broadband Vivaldi type antenna, which operates at 1GHz-10GHz. Using this antenna, we made a prototype of a GPR system, which operates at 2GHz-5GHz. By scanning the antenna on a 2D plane, we could obtain clear 3-D images of mine-like targets buried in dry sand. We proposed an array signal processing technique using CMP method, and found it is effective for rejection of the ground surface clutter, even if the ground surface has roughness. [C5129]

"Buried land mine detection using complex natural resonances on GPR data"

In this paper, we discuss a modified Prony's algorithm for use in buried land mine detection from ground penetrating radar (GPR) data. The algorithm finds the dominant complex natural resonances (CNRs) for vectors of time-domain GPR data. We consider the identification of objects present in two-dimensional images. The CNR features of an unknown image are processed through distance-based detectors with the CNR features of known objects from an object library. We analyze our algorithm performance versus SNR and also analyze performance for different distance detectors. [C5130]

"Effective clutter removal for detecting non-metallic mines in various soil fields"

In this paper, an effective method for removing the clutter effects from the data collected using a stand-off impulse GPR with a small electromagnetic probe is presented. The method requires no a priori knowledge about the target and/or ground characteristics. Essentially, it combines successive processing and spatial variable moving averaging (SVMA) to eliminate the clutter and to enhance the detection of small land mines shallowly buried in different soils. In addition, this method can use measured GPR data to infer the effective soil permittivity. [C5131]

"Analysis of space-surface interferometric bistatic radar"

The concept and preliminary analysis of the Interferometric SS-BSAR system is discussed in this paper. [C5132]

"Millimeter-wave polarimetric bistatic radar scattering from rough soil surfaces"

Polarimetric measurements of the bistatic scattered fields from a rough, dry, soil surfaces, were performed recently at 35 GHz over the entire upper hemisphere, at both low and high incidence and scattering angles, and at near forward and backward directions. These measurements are discussed in this paper and the angular dependence of the bistatic scattering coefficients, σ_0 , and the correlation between various polarization combinations are presented as well. [C5133]

"Automated image matching between geocoded Landsat-TM scenes and MOMS-2P stereo imager for DEM and orthoimage production"

The German along-track stereo scanner MOMS-2P delivered 3-line stereo imagery of many parts in the world from 1996 till 1999. Its satellite platform was the Russian space station Mir. The relative accuracy of the exterior orientation of the MOMS camera based upon GPS and gyro measurements (1 m and 1-2 arcseconds, respectively) was sufficient with respect to MOMS ground pixel size of 17 m. In order to get the absolute orientation, bias and drift parameters and some values of the interior orientation of the camera have to be

estimated via bundle adjustment. For this task, ground control points (GCP) have to be provided. For large areas in Afghanistan, Jordan, and Libya, geocoded thematic mapper imagery was available. Automated image matching is used to extract thousands of GCP even though the time gap between Landsat and MOMS imaging ranges from 8 to 11 years. The geoid height of the GCP is taken from available digital elevation models (DEM) of lower accuracy. The GCP enter a bundle adjustment which results in improved values of exterior and interior orientation. These are then used in DEM derivation and orthoimage production for the three MOMS viewing directions. DLR's MOMS stereo workstation software is used for all these tasks. The fit between TM and MOMS orthoimages and between the orthoimages of the off-nadir looking MOMS channels is checked via automated image matching. Mean and standard deviations of the shifts are found to be in sub-pixel range. [C5134]

"Fusion of airborne laser altimeter and RADARSAT data for DEM generation"

This paper describes a geostatistical method for the generation of an improved accuracy digital elevation model (DEM) through the fusion of airborne laser altimeter data and a stereo-radargrammetric DEM. The results show that the accuracy of the DEM (canopy-top and ground-level) after data fusion is significantly better than that of the initial radargrammetric DEM. For the canopy-top DEM, the standard deviation of elevation errors falls from 21 m to 14 m or from 25 m to 11 m, depending on the validation source adopted. [C5135]

"Seasonal polarimetric measurements of soil moisture using tower-based GPS bistatic radar"

The results of GPS L-band ($L1$, $\lambda = 19$ cm) surface reflection measurements observed using multiple polarizations and receiving antenna gains are described. The measurements were performed using the 300 m tall ETL Boulder Atmospheric Observatory (BAO) tower during summer through fall of 2002. In this experiment, the first seasonal measurements of bare soil moisture from a stationary location using bistatic reflection of signal of opportunity were performed. Several receiving antennas offering various gain and polarization sensitivities were used. Theoretical modeling of bistatic surface scattering shows that the magnitude and width of the reflected waveform depend on the dielectric permittivity of the soil, vegetation cover, and soil roughness. By observing from a fixed tower over low grass, the roughness of the reflecting area remains constant, hence variations in the signal are uniquely related to changes in the dielectric permittivity, and therefore, to soil moisture. To investigate polarization sensitivity of the reflected signal to soil moisture, four endfire (-12 dB) antennas with complete circular and orthogonal polarization sensitivities were used. The high-gain antennas increased the received dynamic range and reduced surface multipath radio wave interference. Seasonal retrievals of soil-moisture content from multi-polarization GPS reflection data is presented and compared with in-situ soil moisture measurements. [C5136]

"Galileo signal-based bistatic system for avalanche prediction"

The tool for avalanche prediction based on the Space Surface Interferometric Bistatic Synthetic Aperture Radar (SS-InBSAR) is discussed in this paper. The forthcoming Galileo navigation satellites signals are considered as the electromagnetic source of the novel bistatic SAR. [C5137]

"Topics in passive bistatic remote sensing"

This paper presents a succinct overview of a research effort involving passive bistatic remote sensing. Included were antenna analysis, direction of arrival estimation analysis, waveform analysis, direction of arrival error analysis, and receiver location analysis. [C5138]

"New approach for snow water equivalent (SWE) estimation using repeat pass interferometric SAR"

Retrieval of Snow Water Equivalent (SWE) using conventional InSAR processing is difficult due to InSAR phase wrap. The problem appears when the snow layer variation exceeds some tens of cm because of the high InSAR phase sensitivity to snow depth. This paper describes the concept of applying delta-K technique on InSAR data for deriving SWE of dry snow. The technique solves the conventional problem of InSAR phase wrap from pixel to pixel even for the most extreme cases. Experimental results show that the delta-K InSAR phase can be estimated to a few degrees accuracy for an area of 10^4 10 km² corresponding to roughly SWE of 100 mm. [C5139]

"Variograms: practical method to process polarimetric SAR data"

Most application of polarimetric SAR imagery require more efficient processing technique which achieves two fundamental goals. The first one is to detect and classify the constituent remotely sensed scenes from pixels to pixels in the imagery. The second one is to reduce the data dimensions without loss of critical information

because the fully polarimetric SAR data can be processed just as multi-dimensional images, which could like multi-bands spectrometer images. It is the increased use of spatial data in remotely sensed images that we can get the valuable extraction. But there is composing complexity among the polarimetric imagery texture comparing some hyperspectral images. Some strong backscatters may exist under arid surfaces and contaminate some adjacent pixels. The contamination of imagery decreases the precision of classification. To determine the pixel distance in spatial coordinate is a key to debar some difficulty in front of polarimetric SAR data. The approach to link the nature and cause of spatial variation in image is to use the variograms and subsequent Kringing theory. The data results from the fully polarimetric images prove that the variograms are the tool used to link models of radar backscattering scenes. Some directional variograms aim to indicate the backscattering anisotropy, the height of the sills of the variograms are related to the kinds of the remotely sensed objects and the range of the influence is related to the acting distance on pixels of scenes. [C5140]

"Enhanced resolution in 3-D interferometric ISAR imaging using an iterative SVA procedure"

Multi-dimensional high resolution is one of the most important factors in automatic target recognition (ATR) using the synthetic aperture radar (SAR) or inverse SAR (ISAR) images. In this work, we propose a resolution enhancement technique in three-dimensional (3-D) interferometric SAR/ISAR (IF SAR/ISAR) imaging using an iterative sidelobe apodization procedure. [C5141]

"A change detection technique for repeat pass interferometric SAR"

In the coherent change detection application of repeat pass SAR interferometry (InSAR) the scene coherence is used to detect areas of man-made scene disturbance. The sensitivity of this technique however is dependent on the extent of decorrelation across the scene that arises due to processing aberrations, system noise and environmental effects. Formulating the detection problem as a hypothesis testing leads to a new log likelihood change statistic with significantly improved detection performance according to Priess et al. (2003). The statistic however, requires accurate estimates of the unknown hypothesis parameters to be obtained from the interferometric image pair. The pair extends work by Priess et al. (2003) by examining the loss in detection performance that arises due to errors in the estimates of the scene partial coherence and interferometric phase required in the formulation of the log likelihood change statistic. The technique is applied to a repeat pass InSAR image pair collected using the DSTO Ingara X-band SAR where these parameters must be estimated adaptively over the scene. [C5142]

"Examination of forest polarimetric backscattering with coherent cylinder model"

In this work a coherent backscattering model for cylinders has been employed to simulate L-band and C-band polarimetric backscattering from a pine forest. Scattering covariance matrix, entropy, alpha angle, polarimetric coherence and temporal coherence are calculated and compared with SAR measurements. The results show that direct backscattering from tree crowns is an important scattering mechanism. Realistic ground reflection modelling was shown to be very important. By simulating the tree growth, general agreement between the known biomass and backscattering parameters was achieved. [C5143]

"Visualisation of cross-polarised response patterns over short vegetation"

The analysis of polarimetric response patterns for earth science applications has been hindered by difficulties in attributing phenomenological response patterns to interactions between polarized waves and multi-layered landscapes, such as forested and agricultural areas. Traditional analysis of response patterns relies on the use of areal responses to characterize landscapes. It is shown in this paper, however, that the variability of response patterns within apparently homogenous areas may provide extra information on the nature of polarimetric interactions. A new technique is described, which allows the synoptic analysis of response patterns over these sub-scenes. Using this technique, it is found that response patterns over forested areas are too variable to provide a basis for classification. However, an area of reed beds within the forest image produces a response pattern that is consistent over large areas. This distinctive pattern is more widespread in the agricultural scene, suggesting that it may be the result of coherent interactions between stalks and the underlying surface. The results of this approach are made more significant by the fact that the characteristic response pattern cannot be achieved by additively combining idealized response patterns, and suggests that the response is caused by coherent effects. As the use of additive modelling is common within polarimetric radar research, it is proposed that further research into the nature of the observed response patterns may provide useful additional information which can be incorporated into future models. [C5144]

"Application of Gaussian Markov random field model to unsupervised classification in polarimetric SAR image"

The aim of this paper is to demonstrate that the Gaussian Markov random field (GMRF) model can be successfully applied to the classification of multi-frequency polarimetric SAR data. As a special case of MRF, the GMRF has been shown to be an accurate compact representation from a single-band textured images or multi-band textured images. To apply the method to the classification of inter-channel correlated polarimetric SAR data, we first transformed the data into combination of uncorrelated principal component images. Both intensities (hh, hv, and vv) and phase difference (ϕ_{hh-vv}) images of L- and P-band data are considered for classification in the study area in Jeju Island, South Korea. The properties of the transformed data reveal that the images tend to be Gaussian and they are mutually uncorrelated. The GMRF model therefore can be applied to the classification of the transformed polarimetric SAR data. As the GMRF model is a type of classifier based on segment merging, the classification process begins from the initial guess consisting of large amounts of segments. Spatially and statistically similar regions are combined to update the segmented map for each iteration. The final classification map based on polarimetric characteristics shows improvements in the accuracy and efficiency of the classification frame for the tested polarimetric SAR data. [C5145]

"Current maps and bathymetry from P-band SAR images: preliminary results"

Microwave remote sensing at very long wavelength is already used and validated for coastal zone regions and regions covered by ice (Antarctica) using airborne systems. For many other applications, a high potential exists and the PYLA 2001 experiment allowed the acquisition of data for fields still under preliminary tests. The experiment was carried on a Transall aircraft (French army/DGA) and used the SAR sensor RAMSES (multifrequency/multipolarization) from ONERA by P. Paillou et al. (2001). For the experiment, the acquisition was performed in P band (435 MHz). The aim was to explore potentials of the low frequency domain for sub-surface moisture detection (Pyla sand dune), biomass evaluation (Nezer forest), mapping of the ocean bathymetry and salinity (Arcachon inlet, estuary of the river Gironde), and archaeology (St Germain d'Esteuil, Dignac, Moulin du Fa). A dedicated P-band calibration site was set up in order to fully exploit the polarimetric information. This part of the study consists of analyzing SAR images from RAMSES (P band) in order to be able to take into account the effect of longer surface waves, winds and currents on the surface roughness in the Arcachon inlet. Tidal currents associated with long oceanic waves recorded at the mouth of the inlet, including the northern channel and sand banks of the ebb tidal delta. The analysis provides tools allowing the production of current maps, which are in turn compared to in-situ measurements by GPS on surface drifting buoys and to current velocity fields provided by a 2DH numerical model, MARS-2D. The evaluation of the ability of a 1D hydrodynamical model applied to SAR images in order to reproduce currents in the area presented. Multipolarization images can be used in order to separate the information associated with the ocean surface (tilt) modulation, which is different for each polarimetric image, from the hydrodynamic modulation, similar for each image. The tilt modulation is representative of a Real Aperture Radar-like (RAR) image. The data being available quite late, we just performed correlations between each set of data by using polarimetric coefficient. We obtain good answers on the information associated with the motion of the scatterers. [C5146]

"Sea-surface current measurements with an X band radar"

A measurement system is under development, which uses a coherent X band radar operating from land based stations. By measuring the radar backscattering over several tidal cycles, tidal current patterns are observed in a test area which is 500 X 700 m in size. The radar is operated from two stations to obtain radial Doppler-velocity components which are corrected for Bragg-wave velocities and wind-drift and combined to current vectors. While the operation of radar from space and current gauges from ships is elaborate, the herein presented measuring system offers a low cost facility with high mobility. It has the potential for current monitoring as well as for case studies of changes in current dynamics which have an impact on erosion and sand transport, coastline changes and safety of navigation. [C5147]

"SAR observations of typical phenomena in the Black Sea shore area"

Summer/autumn experiments conducted for the past four years by Space Research Institute RAS near Ghelendzhik, Black Sea shore, allowed to closely monitor sea and atmosphere dynamics in the region. Over 35 ERS-2 SAR images obtained exhibit large variety of important phenomena: atmospheric and oceanic fronts pollution and other slicks, atmospheric convection, vortices, lee patterns, etc. Available extensive data covering all-year sea state, NOAA data and hydrometeorological condition help to adequately interpret SAR signatures. The focus is on three phenomena: lee structures in the atmosphere downwind from the coastal ridge and their dependencies of their growth rate and spatial characteristics on wind speed and direction and medium stratification; vortices which are a frequent occasion in the 100-km coastal zone where north-western current predominates; considerable oil pollution of the coast registered in the end of July 2002. [C5148]

"Velocity field retrieval from long term coherent points in radar interferometric stacks"

This paper addresses the question of how to robustly estimate linear deformation at a large number of points from differential phase in an interferometric stack. The so-called "Permanent Scatterers technique" (Ferretti et al. 2001), uses a relatively large number of differential interferograms of the same area, co-registered at the same master SLC image. Linear deformation rates and DEM errors are estimated for pixels that have limited temporal decorrelation. This straightforward and generic setup has been used in a network approach that uses connections between nearby points to compute a velocity field for large areas. [C5149]

"Polarised AIRSAR along track interferometry for shoreline change modeling"

This study is introducing a new approach of ATInSAR hologram for modeling shoreline change. AIRSAR data with L and C bands utilized to model the shoreline change. Based on the phase information in along track interferometry, and ATInSAR hologram the quantitative information such as current velocity and swell wave height have been modeled. The phase information in ATInSAR hologram images can be transferred to wave refraction pattern. These information have been used to model the shoreline change rate. [C5150]

"Phase difference based multiple acquisition phase unwrapping"

This work addresses the derivation of a phase-difference (gradient) based maximum likelihood (ML) phase unwrapping algorithm. In particular, we determine and study the structure of the ML phase unwrapping on a 2D grid in the multi-channel case and compare it with existing phase unwrapping algorithms. This allows us first to frame single-channel, phase based phase unwrapping algorithm in a general formulation. Second, among the known single-channel, phase-difference based phase unwrapping algorithms we identify those achieving a ML solution. Although achieving results similar to existing phase-based ML phase unwrapping algorithm in the multi-channel case, our approach allows to easily incorporate possible a priori knowledge about the absolute phase variation dynamics. [C5151]

"SMOS: analysis of perturbing effects over land surfaces"

Surface soil moisture is a key variable of water and energy exchanges at the land surface/atmosphere interface. But currently there are no means to assess it on a global and timely fashion. The ESA Earth Explorer Opportunity mission Soil Moisture and Ocean Salinity (SMOS) is the first attempt to fill such a gap. SMOS is based upon an L-band 2-D interferometer, an innovative concept of bi-dimensional aperture synthesis method to obtain surface measurement with an appropriate resolution from a tractable (in terms of dimensions) space-borne instrument. Moreover, the sensor has new and very significant capabilities especially in terms of multi-angular view configuration. However as for most of space borne instrument, retrieval of surface parameters/variables will be hampered by several factors. This fact is enhanced for sensors having a coarse spatial resolution. In the specific case of SMOS the ground resolution of 40 km means that the influence of different contributors to the signal has to be accurately assessed and eventually corrected. Finally many pixels will be affected by topography effects. It is thus important to assess exactly which level of topography distorts significantly the brightness temperatures and to which extend so as to be able to either correct soil moisture retrieval for topography effects or flag the data. The goal of this paper is to present the topography effects. The latter has been analyzed in depth by modeling the signal issued from mountainous terrain including moisture and vegetation gradient. The adjacency and shadowing effects were in particular addressed. The second step was to develop a simplified characterization of the topography through a statistical description which is then used to assess exactly the level of topography which has an influence of the signal and from which one has to take it into account in the retrieval process. The potential of SMOS, depending on the view angle configuration and the use of the sole 1.4 GHz is thus investigated over complex targets. These questions are key issues to define the exact range of configurations where SMOS meets the scientific requirements of the mission. [C5152]

"A study on cloud-top height retrieval by using MISR and MODIS data"

Information about cloud heights can be retrieved by satellite images. Cloud heights can affect total liquid and water content. Cloud heights are needed to determine the reflecting layer reference altitude (RLRA). Multiangle imaging spectroradiometer (MISR) and moderate resolution imaging spectroradiometer (MODIS) can retrieve information about clouds. MISR determined cloud-top height geometrically by a stereophotogrammetric technique. MODIS estimates cloud top pressure by a CO2slicing method. To ensure the retrieval of cloud heights, it is important to look for good algorithms that process this kind of information. But the way the instruments process cloud information is different. The objective of this research is to study, analyze and implement the existing algorithms used for the retrieval of cloud-top heights, from both MODIS and MISR instruments. In this paper, the algorithm to retrieve cloud-top heights will be presented. An analysis on cloud information from both techniques will lead to a better understanding of the earth's climate system. [C5153]

"Optimal precipitation estimation using multisensor microwave datasets"

The quantification and variability of water cycle and its mechanisms are key scientific issues. Systematic errors and biases in precipitation measurements can be eliminated using merging techniques from multisatellite data and data assimilation techniques. Microwave measurement data sources are used in this investigation to merge precipitation estimates from several satellites to produce optimal precipitation datasets. The emphasis of the research is on several case studies with different synoptic conditions and backgrounds to enhance the global precipitation measurement. Analysis and detection of severe snowfall in high latitudes and light rain over desert using AMSU-B and AMSR-E data are discussed. Space-based precipitation estimation is validated using ground-based radar (WSR88D) and rain gauge data for different cases representing different synoptic conditions and surface types. Three hourly global precipitation assimilation schemes for a land-atmosphere couple model system using merged, satellite-based precipitation is explained and the sensitivity of the couple system to the precipitation assimilation is explored. The high frequency passive microwave, such as 150 GHz, is useful particularly for ice and mixed precipitation. Results of the comparative study of precipitation totals based on multisensor estimate, Doppler radar estimate and gauge data are presented. [C5154]

"Measuring vertical rainfall velocity through spaceborne Doppler radar: performance analysis and system requirements"

In this paper we will present the results of the trade studies on the performance of a spaceborne Doppler radar in measuring vertical rainfall velocity. Particular emphases will be placed on: 1) the choice of the PRF vs. antenna size ratio, 2) the choice of the observational strategy, 3) the choice of the operating frequency; and the 4) processing strategy. The results show that accuracies of 1 m/s or better can be achieved with the currently available technology and with careful selection the system parameters. [C5155]

"An overview of MODIS on-orbit calibration and instrument performance"

The MODIS ProtoFlight Model on-board the EOS Terra spacecraft was launched on December 18, 1999 and the Flight Model 1 on-board the EOS Aqua spacecraft was launched on May 04, 2002. Together they have produced over 5 years of calibrated data sets from which many land, oceans, and atmosphere products have been developed and provided to the science community and public users for better understanding of both long- and short-term changes in the global environment. Overall, both Terra and Aqua MODIS have been performing well with constant on-orbit calibration and characterization efforts. The Level 1B algorithms and the corresponding production code used to generate the calibrated data sets are mature and stable. [C5156]

"Multiyear MODIS observation of global aerosols from EOS Terra/Aqua satellites: validation, variability, and application"

The multiyear MODIS (Moderate Resolution Imaging Spectroradiometer) measurements are full of exciting aerosol events, such as the well-known Asian/Saharan dust outbreaks, biomass burning in South Africa, Southeast Asia, Central America, and Southern Africa, and air pollution all over the world. The MODIS aerosol optical depths (τ_a) are validated against AERONET (aerosol robotic network) and other radiometer/sunphotometer (e.g., airborne sunphotometer, shadowband radiometer, microtops, etc.) measurements within the expected retrieval errors of $\Delta\tau_a = \pm 0.05 \pm 0.2 \tau_a$ (e.g., 25% for $\tau_a = 1$) over land and $\Delta\tau_a = \pm 0.03 \pm 0.05 \tau_a$ (e.g., 8% for $\tau_a = 1$) over ocean. The comparisons of monthly MODIS V4 (version 4) and GACP (global aerosol climatology project) AVHRR (advanced very high resolution radiometer) aerosol optical depths with AVHRR show that the difference of aerosol loading are generally larger in the northern hemisphere than in the southern hemisphere from March to August 2000 and February 2001 in both hemispheres. Similar conclusions can also be drawn from regional analysis, except in pristine oceans in the northern hemisphere where MODIS and AVHRR aerosol retrievals are in agreement throughout the year. The preliminary results of correlating MODIS aerosol optical depths with PM_{2.5} (particulate matter with diameter [C5157]

"Development of a classification algorithm for operational polarimetric NEXRAD radar"

Classification of meteorological and nonmeteorological radar echoes will be one of the key functions of the operational polarimetric NEXRAD radar. In this paper, basic principles of the classification for several cases are presented. The data were obtained from the polarimetric prototype of the NEXRAD radar. [C5158]

"Soil moisture retrieval over the southern Great Plains: comparisons between experimental remote sensing data and operational products"

The southern Great Plains region of the US has been a focus area for experimental remote sensing of surface

soil moisture since the 1970's. Intercomparison of soil moisture retrieval using both experimental data and operational data is carried out during the SGP99 remote sensing campaign in July 1999. Passive microwave measurements obtained from the airborne ESTAR instruments at L-band and TRMM microwave imager (TMI) measurements at X-band were processed to retrieve surface soil moisture during SGP99 and compared to field measurements. TMI retrieved soil moisture for June-September 1999 were compared with operational soil moisture sensors in the Oklahoma (OK) Mesonet system. To mimic operational products, the correction for vegetation and surface roughness in the TMI retrievals are based on average literature values, and surface temperatures estimated from a land surface hydrologic model forced with operational products. [C5159]

"Airborne GPS bistatic radar soil moisture measurements during SMEX02"

To further investigate the potential for remotely sensing soil moisture using the L-band GPS bistatic radar concept, a GPS bistatic radar participated for the first time in airborne measurements during the Soil Moisture Experiment 2002 (SMEX02) in Ames, Iowa. A 12 channel GPS navigation receiver was modified to perform bistatic radar measurements and mounted on the JPL PALS instrument. The reflected GPS signal-to-noise ratio measurements generated a ground track which was sensitive to the surface characteristics. Assuming surface roughness and vegetation cover to be constants over the duration of the study period, the temporal changes in the measured signals were suspected to be proportional to varying soil moisture content. The bistatic signal measurements were interpolated to a UTM grid to produce daily maps of relative change of surface soil moisture over the study region. The maps of the study region showed a transition from very dry surface soil moisture conditions to very wet conditions following precipitation events occurring in the middle of the study period. Additionally, the maps showed sensitivity to localized rainfall in areas without precipitation. The scattered signal measurements were also compared with in situ soil moisture measurements at 32 field sites and found to follow the general soil moisture trend as a function of time. These positive initial results from the first controlled experiment of GPS bistatic radar for measuring soil moisture were encouraging. Additional analyses with the present data set and comparison with other remote sensing instruments (PALS) are planned as well as participation in future campaigns. [C5160]

"Validation of aircraft and satellite remote sensing of brightness temperature and derived soil moisture using a hydrologic/radiobrightness model"

This investigation is aimed at using a coupled hydrologic/radiobrightness model to validate remotely sensed brightness temperatures measured from aircraft and the satellite and derived moisture. The advantage of this approach is that the model can bridge the discontinuities in space and time among many observations at disparate scales and provide estimates of measurement uncertainty. This effort was focused on data generated during the Soil Moisture Experiments in 2002. Results are preliminary at this time and have served to raise numerous questions that are directing current and future research. [C5161]

"Numerical simulation of multiple effects due to convective clouds on satellite radar reflectivity at 14 and 35 GHz"

Spaceborne precipitation radars are usually designed to operate at attenuating wavelengths, mostly at X, Ku and Ka band. At these frequencies and above, convective rainfall clouds can cause severe attenuation. Moreover, raindrops and precipitating ice can give rise to appreciable multiple scattered radiations which apparently tends to enhance the nominal attenuated reflectivity. In order to properly describe radar observations in such conditions, apparent reflectivity has to be modeled taking into account both path attenuation and incoherent effects. To this aim, a general definition of volume radar reflectivity is introduced and a Monte Carlo model of backscattered specific intensity is implemented. Spaceborne apparent reflectivity due to multiple scattering is shown to be significantly different from the attenuated one for the near-surface layers of mature convection at Ku band and even for growing convection at Ka band. A discussion about this discrepancy is carried out at Ku band showing its possible impact for estimated rainrate profiles. If precipitation incoherent effects are formally treated as perturbation factors of the specific attenuation model, constrained single-frequency inversion techniques are shown to be suitable to minimize rainrate retrieval errors due to multiple scattering. [C5162]

"Active rain gauge concept for moderate to heavy precipitation using W-band and S-band Doppler radars"

Previous research studies have used multifrequency radar Doppler spectra to study different aspects of precipitation, and have demonstrated its utility as an accurate profiling rain gauge method (Firda, 1999). Recently this concept have been used to retrieve the drop size distribution (DSD) and vertical air motion in rain using a dual-frequency cloud profiling radar system, operating at 33GHz (Ka-band) and 95GHz (W-band), will provide measurements over a wider dynamic range of rain conditions, extending the active rain-gauge concept to

heavier rain rates. The use of the W-band signal will provide accurate measurement of the vertical air motion in rain. Considering the conditions of heavy rain in which case large nonspherical raindrops exist, the actual drop's shapes will be corrected. Data will be processed as suggested by Firda et al., 1999. This research's goal is to develop software to retrieve several cloud characterization parameters, such as drop size distribution and vertical air motion from collected data during November 2001 at the Cloud and Radiation Testbed (CART) site in Lamont, Oklahoma. Rain rate estimates, drop size distribution and the vertical air motion retrieval used to study the inner processes of rain will be presented. [C5163]

"Neural networks and tree classifiers: an application to rainfall estimation"

The cloud discrimination methods, used to retrieve rainfall fields, are based on statistical relations. Two nonlinear regression methods, artificial neural network and tree classifier are compared in combining TRMM with GOES data. [C5164]

"NASA Advanced Component Technology Program, investments in remote sensing technologies"

Investments in remote sensing technologies have become increasingly important as Earth scientists strive to better understand changes of the Earth System on a global scale. This paper discusses investments in active and passive remote sensing technologies that will provide new measurement capabilities for advanced observing satellites systems. Such measurements will enable more reliable predictions of weather, climate and other globally important elements of the Earth's system. The Earth Science Technology Office, Advances Component Technology program manages this portfolio of technology developments for the Earth Science Enterprise. [C5165]

"Compact dual-frequency microstrip antenna feed for future soil moisture and sea surface salinity missions"

The development of a compact, lightweight, dual-frequency antenna feed for future soil moisture and sea surface salinity (SSS) missions is described. The design is based on the microstrip stacked-patch array (MSPA) to be used to feed large lightweight deployable rotating mesh antenna for spaceborne L-band (~ 1 GHz) passive and active sensing systems. This paper describes the design of a single-element stacked patch element and the 7-element array configuration. [C5166]

"Microwave Observatory of Subcanopy and Subsurface (MOSS): a low-frequency radar for global deep soil moisture measurements"

Measurements of deep and subcanopy soil moisture are critical in understanding the global water and energy cycle, as well as the interaction of the carbon and water cycles, but are presently not available on a synoptic basis. In this paper, a low-frequency UHF/VHF radar mission concept is presented and technology challenges to implement it are discussed. This mission concept is currently being studied under a NASA/ESTO instrument incubator program (IIP) project. The progresses of several aspects of the project are discussed. [C5167]

"The use of polarimetric and interferometric SAR data in floodplain mapping"

Recent advances in polarimetric SAR show promise for augmenting the capability of traditional interferometric SAR. In particular, a polarimetric topography technique provides useful slope information, and polarimetric interferometry may be used to decompose the response into vegetation and ground surface contributions. Here we discuss an integrated approach that utilizes the combined capability of regular (single channel) interferometry, polarimetric interferometry and polarimetric topographic mapping for topographic mapping of flood-prone areas. [C5168]

"Segmentation of textured scenes using polarimetric SARs"

The methods currently used for classification or segmentation of polarimetric SAR images are based on the multivariate complex Gaussian model. This should limit the application of these methods to "homogeneous" Gaussian areas, since their performances are significantly degraded in the presence of spatial texture. We show that image segmentation can be viewed as a likelihood approximation problem. The optimum criterion is derived for segmentation of K-distributed textured polarimetric SAR images. The product model is assessed and applied only within areas in which the model is valid. The new method is validated for ice type segmentation using Convair-580 SAR data collected in 1993 over Cornwallis Island in Canada. [C5169]

"Consolidation of a pixel-based classification using neighborhood information"

A two-step consolidation process is presented that reduces the effect of speckle in the classification result. The degree of consolidation or smoothing can be adjusted using a classification confidence measure and a threshold for the amount of neighborhood agreement needed. Results from AIRSAR ice data shown are compared to a classification result from pre-filtered data. [C5170]

"2-micron coherent Doppler lidar for space-based global wind field mapping"

A space-based 2-micron coherent Doppler lidar can have a significant impact on climate research and numerical weather forecasting. This paper describes the key challenges of deploying such an instrument in space, and provides a status of the technology development activities. [C5171]

"First observations with the UMass dual-beam InSAR"

A dual-beam along-track interferometric synthetic aperture radar which is self contained within an aircraft pod has been developed to study coastal regions. System hardware is described. Initial test flights aboard the NOAA WP-3D research aircraft were performed to evaluate system performance over land and water surfaces. Notable look-angle dependencies are observed in the sea surface NRCS under very low wind conditions. [C5172]

"Very wideband radar imaging with the airborne SAR sensor PAMIR"

At FGAN, a new very wideband radar is under development. The system will serve as an experimental airborne platform operating in the X-band and is called PAMIR (Phased Array Multifunctional Imaging Radar). In this paper high resolution SAR and ISAR images acquired within the first flight campaign are presented. A spatial resolution in the sub-decimetres regime could be achieved. [C5173]

"Conceptual spaceborne Ka-band spotlight synthetic aperture radar with reconfigurable aperture"

Two principal objectives of this investigation are: a) to produce using a reconfigurable aperture circular beam footprints for grazing angles from 15° to 70°, and b) to maintain high efficiency high-power 35 GHz solid-state devices in a feed array. An elliptical reflector 8.51 m high and 2.9 m wide is proposed with a near-zone programmable, transmit-receive phased array feed in a beam waveguide to deliver 25.5 W/m² at the radiating aperture. By redirecting the beam to track a particular area, called the "spotlight-mode", fine azimuth resolution and multi-look images can be produced. A 700 km altitude orbit is assumed and the resolution goal is 1.0 m. [C5174]

"Investigations on a new high resolution wide swath SAR concept"

This paper investigates a specific application of digital beamforming in order to provide new class of SAR instruments offering high resolution, wide swath and continuous coverage. [C5175]

"On the concept of an all digital sensor design"

The digital communications revolution that began in the last decade has produced technology advances that have yet to be included in the design of remote sensing sensors especially high resolution optical and RF sensors. Current wireless telephony operates with software radios as an integral design construct with improved performance over analog equivalents. The commercial technology sector driven by aggressive business plans and deployment strategies allowed the development of RF components, processors and embedded software implementation, to enable all digital system architectures. Traditional design approaches used in the telecommunications industry have not typically been transferred to the sensor design community. This paper addresses a new sensor design approach that incorporates the technology and philosophy of the telecommunications industry. [C5176]

"Potential of digital beamforming in bi- and multistatic SAR"

Digital beamforming on receive is an innovative concept to gather additional information about the direction of scattered radar echoes during the acquisition of synthetic aperture radar (SAR) images. This additional information can be used to suppress range and azimuth ambiguities, to improve geometric and/or radiometric resolution, and to increase the unambiguous swath width. It is shown that this technique is especially promising in combination with bistatic SAR constellations, where digital beamforming on the receive will allow for more compact antenna structures. Furthermore, an extension of digital beamforming to multistatic SAR formations will enable a reduced antenna aperture for each receiver, thereby allowing cost-effective and powerful SAR missions with wide swath coverage in the future. [C5177]

"Soil moisture retrieval and AMSR-E validation using an airborne microwave radiometer in SMEX02"

Field experiments were conducted to evaluate the effects of dense agricultural crop conditions on soil moisture retrieval using passive microwave remote sensing. Aircraft observations were collected using a new version of the Polarimetric Scanning Radiometer (PSR) that provided C band and X band channels. Observations were also available from the Aqua satellite Advanced Microwave Scanning Radiometer (AMSR-E) at the same frequencies. Soil Moisture Experiments 2002 (SMEX02) was conducted over a three-week period during the summer near Ames, Iowa, an area which is dominated by corn and soybeans. Aircraft data were processed and channels selected to minimize radiofrequency interference. A preliminary comparison of the aircraft (PSR) and satellite (AMSR-E) 10.7 GHz data showed comparable brightness temperature values. Sensitivity of brightness temperature to soil moisture was observed for nearly all the ground validation sites, even under dense corn canopies. Similar sensitivities were observed for C and X band channels. These results illustrate the potential to develop soil moisture retrieval techniques for wide range of agricultural conditions using AMSR-E frequencies.

[C5178]

"Quantitative analysis of SMEX'02 AIRSAR data for soil moisture inversion"

In July 2002, the AIRSAR system flew several data acquisition flights during the SMEX'02 field experiment in Iowa. The test site was chosen specifically because of the varying vegetation cover to allow more quantitative testing of the radar inversion algorithms under these conditions. Field conditions were generally favorable for this experiment, and data were acquired during an initial dry period, followed by a wet period after significant rain, and again followed by a drier period. This paper discusses in detail the characteristics of the AIRSAR data acquired, and provides an initial quantitative assessment of the accuracy of the radar algorithm under these vegetated conditions. [C5179]

"Soil moisture retrieval through changing corn using active/passive microwave remote sensing"

Soil moisture is a critical state variable in land surface hydrology. Large-scale soil moisture mapping based on microwave remote sensing would be valuable in many different practical and theoretical applications, and a real potential exists for new space missions in the near future which will utilize simultaneous active/passive microwave measurements for global soil moisture retrieval. This paper discusses the experiment for the retrieval of soil moisture using radar and radiometric measurements. It was shown that combinations of simultaneous radar and radiometer data can enhance soil moisture retrievals, especially in the presence of dynamic vegetation. [C5180]

"VIIRS sensor performance"

This paper summarizes the anticipated performance of the National Polar-orbiting Operational Environmental Satellite System (NPOESS) Visible Infrared Imaging Radiometer Suite (VIIRS) sensor. Predictions are generated from models and demonstration hardware based on the design described in a companion paper. VIIRS risk-reduction will continue as the Engineering Development Unit (EDU) is assembled and tested over the next year facilitating performance verification and lowering flight unit development risk. [C5181]

"Introduction, overview, and status of the NPOESS aerosol polarimetry sensor (APS)"

The National Polar-orbiting Operational Environmental Satellite System (NPOESS) added several new aerosol and cloud Environmental Data Records (EDRs) to the NPOESS Integrated Operational Requirements Document (IORD) in 2001 that require procurement of an Aerosol Polarimetry Sensor (APS). The APS provides a unique along-track scan to produce EDRs directly underneath the satellite to estimate climate trends. APS will measure orthogonal polarizations in nine spectral bands between 0.4 and 2.4 μm and will be launched on the first NPOESS operational satellite planned for 2009 in a 2130 local ascending node time orbit. The APS contractor was selected in early 2003 for a fall 2003 contract start. This paper describes the APS requirements and provides an overview of the design approach. [C5182]

"Integrating SAR and optical products for crop management (Isocrop) biophysical parameter retrieval using X and L band SAR data"

The Isocrop project has obtained near simultaneous L and X band SAR data, superspectral data and in situ ground truth data at two winter wheat test sites over several growing seasons using airborne DLR E-SAR and Specim AISA sensors. This paper describes the development of retrieval algorithms and information products based on the SAR data which are capable of providing useful information for the management of winter wheat

crops. These algorithms are based on exploiting the correlation between biophysical parameters including mean backscatter, ratios of backscatter and components derived from a range of polarimetric scattering models. These algorithms and products are intended to support the application of X and L band data from the proposed satellite borne TerraSAR system. [C5183]

"Need for developing multi-band single and multiple pass POLinSAR monitoring platforms in air and space"

In this overview, reasons are provided on why we do need to place multi-modal, multi-band single and multiple pass POLinSAR monitoring platforms into air and space. The questions "on what POLinSAR monitoring can provide that POL-SAR and IN-SAR by themselves cannot accomplish" is assessed; whereupon facts and justifications on placing POL-IN-BISAR satellite clusters into space are presented. Reasons for this technology becoming a basic requirement for current, near-future and much more so for future all day & night year-round monitoring of the terrestrial covers are analyzed in view of the un-abating and uncontrollable terrestrial population explosion, which has, does and for ever will result in unavoidable conflicts deteriorating unfortunately at times into terrorism. The pertinent questions on how to reduce the exorbitant cost for initiating this "home-globe security protection" technology are therefore also broached, and the expected benefits are laid out. The pertinent National and International airborne and space borne multi-modal, multi-band SAR remote sensing and security conflict surveillance support agencies are herewith invited for co-sponsoring our proposal, which is timely and fleets of orbiting multi-band POLinSAR platforms are urgently required to be placed into space. [C5184]

"Analysis of anisotropic behavior using sub-aperture polarimetric SAR data"

In this paper, a fully polarimetric analysis method is introduced to decompose synthesized polarimetric images into sub-aperture data sets, which corresponds to the scene responses under different azimuthal look-angles. A statistical analysis of polarimetric parameters permits to clearly discriminate media showing a non-stationary behavior during the SAR integration. A method is proposed, which eliminates the influence of azimuthal backscattering variations in conventional polarimetric SAR data analysis. [C5185]

"Full polarimetry versus partial polarimetry for quantitative surface parameter estimation"

The performance difference between full polarimetry (fp) and partial polarimetry (pp) systems is still an important open question according to Imbo and Souyris (2000) and Lee et al. (1995), especially in the frame of future low-cost spaceborne SAR studies. The aim of this paper is to briefly present a fully polarimetric model, the recent F-Bragg model (Breuer et al., (2002, 2003)), and compare it to its restriction to partial polarimetry. In a second step the inversion possibilities of fp and pp F-Bragg are investigated. [C5186]

"Influence of resolution cell size for surface parameters retrieval from polarimetric SAR data"

This paper introduces a study of the influence of the size of SAR resolution cell on polarimetric scattering characteristics over rough surfaces. Surface scattering is shown to be dependent on the cell size to correlation length ratio. SAR resolution is taken into account by dividing a surface spectrum in two parts: a low-frequency spectrum corresponding to local slopes and a high-frequency component, defining the roughness inside a resolution cell. Backscattering coefficients are calculated for each resolution cell with the IEM model using local incidence angles. Surface scattering is characterized with three polarimetric indicators $H/A/\alpha_{\perp}$, highly related to the soil characteristics. These models are validated on indoor polarimetric SAR measurements acquired at the JRC laboratory. [C5187]

"Pi-SAR image analysis using polarimetric scattering parameters and total power"

This paper tries to classify POL-SAR image data using polarimetric entropy, averaged alpha angle, and total power. Using unsupervised classification scheme with iterative Maximum Likelihood (ML) classifier, it is possible to classify residential areas with trees and vegetation areas. The results are shown using Pi-SAR image data comparing with other representative methods. [C5188]

"Polarization orientation estimation and applications: a review"

We review estimation algorithms and applications of polarization orientation angle shifts induced by terrain slopes. We develop a unified analysis of estimation algorithms based on circular polarization covariance matrix. The effect of radar frequency, scattering media, and polarimetric calibration will also be discussed. Applications to DEM generation, polarimetric SAR data compensation and ocean surface feature characterization will be mentioned. SIR-C, and JPL AIRSAR L-band and P-band polarimetric SAR images are used for demonstration.

[C5189]

"Classification of tree types by polarimetric Pi-SAR"

In order to classify tree types, we introduce a new technique, which detects the change of Polarimetric Entropy parameters. We define the difference of the two-dimensional polarimetric entropy parameters, and applied the proposed technique to Pi-SAR airborne polarimetric SAR data. The result in an urban area shows that the seasonal change is very random and we could not find significant changes between two scenes. Then, we applied the technique in a forested region. The change in coniferous trees and broadleaf trees is statistically different. Using the change in polarimetric entropy properties, we find this technique can be used for tree type classification. [C5190]

"The SAR train concept: required antenna area distributed over N smaller satellites, increase of performance by N"

The concept implements the coherent combination of the N SAR flying along a same arc as seen from the ground. A particular case is with N SAR in visibility and a single transmit. A "Signal Cleaning" SAR Train keeps unchanged the maximum antenna area of each individual SAR and brings a factor N advantage on both the SNR and the ambiguity protection. The main formation constraint is the width of the tube containing the satellite trajectories on an earth frame. An "Antenna distributing" SAR Train enables the distribution of an unchanged total minimum antenna area into N smaller elementary antennas, together with the multiplication by N of the merit factor (swath over azimuth resolution ratio). Application for $N > 2$ requires very tight along track SAR spacing accuracy. Use of appropriate spread spectrum waveforms instead of conventional pulse waveforms removes the major part of the extra orbit constraints induced by "Antenna distributing" and enables it for any value of N. A Train of N SAR in visibility eases the metrology of the formation (DGPS) and the global energy efficiency is increased by N since with only single transmit SAR the same performance is achieved. Moreover, the orbit constraints are relaxed by 2. As part of its application, the concept can circumvent the matter of huge antenna size for SAR mission in P band or at very high altitude, all the more as in these cases the tube width constraints are reduced (function of λ and altitude). [C5191]

"A study of the X-band entropy of breaking ocean waves"

In this paper we develop a simple model for the polarimetric radar backscatter from breaking ocean waves. We show that the dynamics of the breaking process lead to characteristic variations in the wave depolarization processes. We compare the model prediction with X-band grazing incidence radar data collected for breaking ocean waves in the surf zone. [C5192]

"WindSat SDR and EDR on orbit calibration and validation"

The Coriolus spacecraft was successfully launched on 6 January 2003. Its primary payload is the WindSat fully polarimetric radiometer. WindSat is a first-of-its-kind instrument that will remotely sense the speed and direction of near surface winds over the ocean by measuring the partial correlation between orthogonally polarized components of natural thermal emission radiated by the ocean surface at microwave frequencies. The ability of WindSat to successfully retrieve wind vector depends critically on two issues, hardware calibration of the four Stokes brightness temperatures and the relationship between those TBs and the ocean surface wind vector. An approach is described to detecting and estimating possible errors in both the hardware calibration and forward model based on a new type of statistical analysis of the on-orbit radiometer measurements. [C5193]

"A study of sea emission models for WindSat"

Three physical models for the microwave polarimetric brightness temperature of the sea surface are reviewed and compared. Two of these models are based on the composite surface theory, but use slightly different forms for the sea surface spectrum. The third model is based on a small slope approximation. All models are shown to predict similar zeroth, first, and second harmonic azimuthal variations of sea brightness and to show reasonable agreement with empirical results. However some discrepancies exist that is examined. [C5194]

"Scene characterization using sub-aperture polarimetric interferometric SAR data"

In this paper, a fully polarimetric analysis method is introduced to decompose synthesized interferometric SAR images into sub-aperture data sets, which correspond to the scene responses under different azimuthal look-angles. A statistical analysis of polarimetric parameters permits to clearly discriminate media showing a nonstationary polarimetric behavior during the SAR integration. A method is proposed to observe the polarimetric interferometric properties of anisotropic targets. [C5195]

"Coherence estimation and speckle filtering based on scattering properties"

In this paper, we propose a new speckle filter for polarimetric SAR that preserves pixels' scattering properties. The basic principle is to select pixels of the same scattering characteristics to be included in the average. To achieve this, the algorithm first applies the Freeman and Durden decomposition to separate pixels into three scattering categories: surface, double bounce and volume, and then unsupervised classification is applied. Speckle filtering is performed using the classification map masks. Pixels centered in a 9x9 window are filtered by including only pixels in the same and two neighboring classes from the same scattering category. This algorithm is extended to the coherence estimation of polarimetric interferometry SAR data. The effectiveness of this new algorithm is demonstrated with JPL AIRSAR and E-SAR data. [C5196]

"Measurement of ocean wave spectra using polarimetric SAR data"

New methods have been investigated which use fully-polarimetric synthetic aperture radar (SAR) image data to measure ocean wave slope spectra. Independent techniques have been developed to measure wave slopes in the orthogonal SAR (azimuth/range) directions. These measurements must still contend with motion-induced nonlinearities in the SAR processing. The methods are, however, physically based, robust, and utilize a parametrically simpler modulation transfer function. NASA/JPL/AIRSAR L-band data from California coastal waters has been used. Wave spectra measured using the new methods are compared with spectra developed using both conventional SAR intensity-based methods and NDBC buoys. [C5197]

"Radiometric normalization of optical remote sensing imagery"

Sensor viewing angle effects, which are caused mainly by an atmosphere and a sun-sensor-target geometry, are observed quite often in images acquired by optical remote sensing sensors, especially airborne sensors with a wide field of view. We propose an image-based empirical radiometric normalization method, which is based on a linear regression applied over linear models between the observed radiance and the target radiance for each surface class separately. The experiments for data acquired by airborne multispectral scanner DAEDALUS AADS 1268 ATM show the effectiveness and potential of the proposed method especially for the mosaicking and classification applications. [C5198]

"Multi-waveform full-polarimetric GPR for landmine detection"

A full-polarimetric ultra wideband GPR front-end has been developed in IRCTR especially for landmine detection application. A number of new ideas have been implemented in the design. A principally new antenna system design and an ability to perform quasi-simultaneous measurements with two transmit polarization and in two different frequency bands are main novelty aspects of the radar. Additionally in comparison with commercially available video impulse GPR systems the front-end has considerably larger bandwidth, ability to measure polarimetric structure of the scattered field and very high precision of scattered field measurements. [C5199]

"Ultra wideband endfire synthetic aperture radar for landmine detection"

The detection of landmines is an important and challenging application for remote sensing technologies. The use of ground penetrating radar is an established technique but requires close coupling between the antennae and the ground and generally suffers from a poor area coverage rate. In order to clear mines rapidly along a route using a vehicle mounted system, a forward looking sensor is required that can operate effectively in a stand off configuration and detect surface laid, flush and buried mines. Reliable detection is required against a background of vegetation and other, surface and buried mines. Reliable detection is required against a background of vegetation and other, surface and buried, clutter. The Remote Minefield Detection System (REMIDS) is a technology demonstration programme funded by the UK Ministry of Defence designed to use an Ultra Wideband Synthetic Aperture Radar (UWBSAR) and a polarimetric infrared camera. The UWBSAR is a 3GHz bandwidth impulse radar with onboard data collection and offline image processing. The UWBSAR has been successfully trialled against landmines. Previous trials have mounted the radar on an airship and employed a conventional side-looking imaging geometry. In contrast, for the trials reported in this paper, the radar was mounted on a trolley to simulate a ground vehicle and operated in a forward-looking mode. The resulting use of an endfire synthetic aperture radar rather than the more conventional broadside aperture is the principal development reported in this paper. This coarsens the resolution and introduces a left-right ambiguity into the data. Previous trials have also highlighted the lack of a comprehensive data set containing controlled targets and a range of clutter conditions. The current trials were therefore conducted on a purpose built 80m test track which contained five different soil types, a range of surface conditions and over 200 targets of varying types and burial depth. The trials campaign collected over 500 data sets by varying the conditions of data collection in terms of polarisation, antenna height, antenna separation, incidence angle, power levels and pulse repetition frequency. The

experimental configuration allowed the track of the platform to be repeated to sufficient accuracy to allow the synthesis of multiple baselines in the vertical and horizontal. The principal conclusions from the trials analysis are 1) that the data set collected is of good quality and comprehensive in terms of targets and background; 2) the endfire synthetic aperture configuration worked as anticipated; and 3) the left-right ambiguity can be resolved if a suitable antenna configuration is used. [C5200]

"Impact of ground clutter on buried object detection by ground penetrating radar [Ground penetrating radar penetrating]"

We performed careful analysis of the measure data to determine the clutter level and responses of different targets in different types of soils under different environmental conditions. We found that even in a dry sand ground clutter level is higher than responses of many types of antipersonnel mines. As a result, the signal-to-clutter ratio for GPR targets becomes nonsufficient for reliable detection by widely used detection procedures. A new detection algorithm, which should partly overcome this problem, has been developed. The performance of the algorithm on real GPR data is encouraging. [C5201]

"Relative radiometric correction on remotely sensed data for land cover change detection: an unsupervised clustering approach"

This paper proposes and automated radiometric normalization process that uses an unsupervised clustering to adjust a cluster-by-cluster mapping to minimize the effects of the influences of radiometric difference on image interpretation and classification. [C5202]

"A methodology for true orthorectification of large-scale urban aerial images and automatic detection of building occlusions using digital surface model"

In urban area with high buildings, conventional orthorectification using digital terrain model (DTM) cannot meet the requirements of true orthoimage generation. Using digital surface model (DSM) integrating from DTM and digital building model (DBM), we propose a methodology in the study to automatically orthorectify large-scale urban aerial image and detect building occlusions for true orthoimage generation. Principle behind the methodology is the optical characteristic of buildings in photogrammetry, in which roof and root sharing the same coordinate are featured with different distances to imagery center. Therefore, in practical operation, we first compute the distances of input image pixels to imagery center and their coordinates is output orthoimage. A data matrix is used to remember the distances and coordinated. Then we compare the coordinates in the matrix. When pixels have the same coordinate, the one with the longest distance represents building root. For true orthoimage generation, only gray value of the roof need to convert into the output image and others are treated as occluded area. By creating an index image, the occluded area can be recorded for next step processing, such as refilling from neighboring orthoimages. Therefore, using a data, matrix and an index image, we are able to automatically orthorectify large-scale urban aerial images and detect building occlusions for true orthoimage generation, provided that the digital surface model is available and the overlap of neighboring image is large enough to ensure 100% visibility of the occluded area. [C5203]

"Automatic shadow detection and radiometric restoration on digital aerial images"

This paper develops automatic procedures for shadow detection and radiometric restoration of features under cast shadows in aerial images. Techniques including recursive quad-tree image partition, adaptive thresholding, region growing segmentation, mathematical morphology, and local histogram matching are applied to automatically extract the regions of building-cast shadows and to restore the brightness of those pixels within the shadow regions. Empirical results show that the detail information of features within the shadow regions is enhanced by applying the techniques developed in this paper. [C5204]

"Detection of chlorophyll fluorescence in vegetation from airborne hyperspectral CASI imagery in the red edge spectral region"

This work provides a description of the investigations conducted to assess the detection of chlorophyll fluorescence from hyperspectral CASI data. The viability of retrieval of solar-induced fluorescence through airborne imaging spectrometer measurements of radiance of targets under natural illumination is studied. A method based on in-filling of fluorescence signals in atmospheric oxygen absorption lines is applied to study sites of corn crop grown under different stress conditions due to variation in nitrogen treatment. Results of the relationships found between measurements of laser-induced fluorescence and chlorophyll concentration at the ground level with the in-filling of the 762 nm oxygen band and optical indices calculated from CASI imagery R685/R655, derivative D730/D706, and the double-peak derivative f/reflectance index Dpi (D688-D710)/

D6972 are presented. [C5205]

"Observational architectures for enabling earthquake forecasting"

Observational architectures for allowing the eventual forecasting of earthquake are discussed. Current science requirements suggest that L-band InSAR systems with short repeat periods would be best suited to such measurements. Constellations of such sensors in orbits around 2000-5000 km altitude might provide optimal Earth coverage for interferometry, while higher orbits around 10,000-40,000 km might approach the goal of around-the-clock for disaster-response applications. [C5206]

"Rainfall over land from the AMSR-E"

Significant improvements in the retrieval of instantaneous rain rates over land have occurred through the continued evolution of the Goddard Profiling Algorithm (GPROF), which has been used in the TRMM mission and most recently, the Aqua Advanced Microwave Scanning Radiometer (AMSR-E). At present, GPROF V6 incorporates a probability of convective rain, in conjunction with a convective and stratiform set of rain radiance vectors, which are then used to compute a final surface rain rate. Preliminary results with TMI and AMSR-E over the United States in the instantaneous scale suggest low bias errors and high correlations when compared with rain gauge adjusted radar rainfall estimates. Discussion on the use of specialized ground validation sites at Eureka, California and Iowa City, Iowa are also presented. [C5207]

"Geometrical performance of the VEGETATION products"

VEGETATION data are mainly used for multitemporal applications, which induces high level geometrical specifications, especially for multitemporal registration. To comply with them, the VEGETATION 1 image location is improved by a systematic use of ground control points. These are provided by a ground control points data base generated through VEGETATION 1 chips using space triangulation method. Consequently, since its launch onboard SPOT 4 in March 1998, VEGETATION 1 has showed a very good and stable geometrical performance. VEGETATION 2, launched onboard SPOT 5 in May 2002, completes now VEGETATION 1 for operational production. It is so essential to ensure geometrical continuity between both sensors. On SPOT 5, a stellar sensor provides a very good estimation of satellite altitude, implying a very good absolute image location: it is not necessary to improve VEGETATION 2 images using ground control points. However, it was necessary to perform a fine geometrical calibration of VEGETATION 2 cameras that was realized during the commissioning phase using ground control points of the VEGETATION 1 data base. Today we can say that VEGETATION 2 geometrical performance is at least as good as VEGETATION 1's and geometrical continuity is guaranteed. The object of this paper is to present VEGETATION 1 geometrical performance and the methods and results of VEGETATION 2 geometrical commissioning phase. [C5208]

"Possible approaches to remote sensing of photosynthetic activity"

Remote sensing of photosynthesis by fluorosensing and related techniques is a complementary approach to gas exchange and circulation models that helps to monitor accurately the spatial and temporal changes in biosphere primary production. Although important advances have been made in the fields of fluorosensing during the past ten years, a comprehensive review of the different techniques available and their scope is lacking. The aim of the present review is to examine the emerging techniques in order to evaluate their potential for application at different integration levels, from leaf canopy, and from ground measurements to satellite detection. It is also intended to highlight the actual limitations and the necessary preparatory steps towards a space mission. Finally, the information that could be obtained from satellite measurements will be reviewed. [C5209]

"A high spectral resolution sensor for active and passive remote sensing of vegetation fluorescence"

The present paper describes main technical features and experimental results of a high spectral resolution sensor that can operate both as a passive and active sensor. The sensor features a high spectral resolution detection system (521 channels, up to 0.04-nm spectral resolution) and allows the remote detection of both laser-induced fluorescence of vegetation and reflectance plus solar-induced fluorescence spectra. [C5210]

"A semi-empirical algorithm for estimating soil moisture from dual-frequency microwave AMSR data"

In this paper the development of a semi-empirical algorithm for estimating soil moisture content from dual-frequency (C- and X-bands) microwave AMSR data is demonstrated. The algorithm is based on a simplified form of the radiative transfer theory and computes the optical depth through the polarization index at X-band.

Validation of the algorithm was attempted first with SMMR data collected in Russia in 1979-1981. [C5211]

"A hybrid scattering model for surface parameter estimation using polarimetric SAR interferometry"

In this work the potential of using the interferometric coherence at different polarization over surface scatterers to extract information about surface parameters is investigated. The sensitivity of the individual coherence contributions to surface roughness and moisture conditions is discussed and simulated using a novel hybrid polarimetric surface scattering model. The model itself consists of a coherent part obtained from the extended Bragg model and incoherent part obtained from the integral equation model. Finally, the experimental airborne SAR data are used to validate the proposed model at different polarizations. [C5212]

"Optimal image classification employing "optimal" polarimetric variables"

Analysis of polarimetric SAR data often proceeds after first identifying important degrees of freedom in the data, thereby reducing the dimensionality of the problem. Various derived parameters (e.g. entropy, polarization fraction) and/or descriptions of polarimetric data (e.g. scattering matrix, covariance matrix, Stokes Parameters) are employed to effectively reduce the dimensionality of the data while at the same time preserving the relevant polarimetric information. The classification presented in this work involves two steps: first determine the reduced set of variables, from the data, that "optimally" represents the polarimetric information. Second, employ these newfound variables to segment (and classify) the polarimetric SAR image. Finally, the classification results are compared with standard statistical maximum likelihood techniques. [C5213]

"Evaluation of the Wishart test statistics for polarimetric SAR data"

A test statistic for equality of two covariance matrices following the complex Wishart distribution has previously been used in new algorithms for change detection, edge detection and segmentation in polarimetric SAR images. Previously, the results for change detection and edge detection have been quantitatively evaluated. This paper deals with the evaluation of segmentation. A segmentation performance measure originally developed for single-channel SAR images has been extended to polarimetric SAR images, and used to evaluate segmentation for a merge-using-moment algorithm for polarimetric SAR data. [C5214]

"Global SWE monitoring using AMSR-E data"

We demonstrate the "baseline" global snow water equivalent retrieval (SWE) algorithm using Advanced Microwave Scanning Radiometer EOS (AMSR-E). Daily, pentad and monthly records for March 2003 of AMSR-E SWE estimates are generated and gridded to the 25 km EASE-grid projection. The estimates are tested using ground measurements from the World Meteorological Organization Global Telecommunications Network. Preliminary bias characteristics are evaluated. A fraction of the error is related to uncertainties about the grain size changes throughout the winter season that directly affect the parameterization of the snow depth estimation in algorithm. The algorithm includes the need for a correction of forest cover and this effect is clearly observed in the retrieval. AMSR-E has twice the spatial resolution of the Special Sensor Microwave Imager and is able to characterize snow variability at the local scale. Development of the algorithm is focused on a dynamic parameterization of the snow grain size and density via a dense media radiative transfer model plus the inclusion of a high quality forest correction data set. [C5215]

"Polarimetric optimisation applied to permanent scatterers identification"

In this work, the potential of full-polarimetric SAR data to enhance the performance of permanent scatterers candidates (PSC) detection is investigated. In particular, the problem of finding the polarisation states that maximise the signal amplitude inverse coefficient of variation (ICV) is analyzed. Under the hypotheses of Rice statistics and high signal to clutter ratio (SCR), the problem can be cast into a form equivalent to the optimisation of the ratio between PS (target) and clutter backscatter. Then, solution can be derived for the optimal transmit and receive polarisation states. In the paper, selected typologies of PS and clutter are investigated. The approach is validated through Monte Carlo simulation of the multitemporal polarimetric response of PS-like SAR pixels. Results indicate that optimal ICV values of polarimetrically complex PSC pixels are higher than in the ERS case of the single VV channel, thus leading to increased stability of the subsequent parameter retrieval. Moreover, simulation of ICV vs. SCR suggest that a higher number of PSC may be detected by using optimal polarisation states than in the conventional VV channel alone. [C5216]

"On the sensitivity of polarimetric coherence to small and large scale surface roughness"

The objective of this paper is to investigate the effect of a two-scale surface roughness description on the polarization coherence in circular polarization (i.e. PRRL). Under the assumption of sufficiently smooth surfaces,

the small-slope approximation (SSA) model is employed to derive a first order expression for PRRL. In the paper the sensitivity of PRRL to azimuth slopes is presented. [C5217]

"Phenomenology of millimeter-wave signal propagation and scattering for detection of targets camouflaged under foliage"

In this paper, we report on a series of foliage penetration experiments aimed at demonstrating the potential application of nadir looking, millimeter-wave radars in detecting targets under foliage cover. An algorithm is developed that classifies the radar return and isolates the radar return from hard targets. [C5218]

"Investigating relationship between correlation lengths and physical properties of wet snow"

Relationship between correlation lengths and snow wetness is investigated by fitting to experimental data. The strong fluctuation theory is applied to calculate the backscattering from a half space of wet snow. The effective permittivity of wet snow is calculated using the two-phase model with non-symmetrical inclusions. In the two-phase model, wet snow is assumed to consist of dry snow (host) and liquid water (inclusions). The shape and size of water inclusion are considered using an anisotropic and azimuth symmetric correlation function. Numerical results for the backscattering coefficients of wet snow versus snow wetness are illustrated at 17 Ghz. [C5219]

"Modeling the SAR response of pine forest in Southern Finland"

Ground data, biologically accurate model trees, an optical mosaic, a ground digital elevation model, and a top surface model for a forested site at Tuusula, Southern Finland have been used to construct a natural model forest. Model calculations include the SAR imaging process and predict SAR image structure. CARABAS low frequency SAR images of the forested site are compared with SAR image calculations, and fractional Brownian motion based texture images. Simulated intensities and textures agree well with observation. [C5220]

"The CALIPSO mission"

The Cloud-Aerosol Lidar and Infrared Pathfinder Satellite Observations (CALIPSO) satellite flies in a polar orbit as part of the Aqua constellation to vertically profile aerosols and clouds using the first satellite lidar dedicated to atmospheric sensing. The payload also includes passive visible and infrared sensors, which use data from the lidar to improve their retrieval accuracies. These measurements are used to improve our knowledge of the role of aerosols and clouds in the climate system. [C5221]

"Extending climate data records from the EOS era into the NPOESS era"

In preparation for the future National Polar Orbiting Operational Satellite System (NPOESS) NASA and the Integrated Program Office are conducting the NPOESS Preparatory project (NPP), a mission to provide risk reduction for the NPOESS and data continuity for global change researchers. We summarize the sensor capabilities, orbital characteristics, and the data that produces the Climate Data Records (CDRs). We describe NASA plans to work with the IPO and its systems contractor, Northrop Grumman Space Technologies, on sensor characterization and calibration, algorithm evolution and the production of CDRs. [C5222]

"A model study of leaf curvature effect on microwave vegetation scattering"

This article describes a model based on radiative transfer theory, where the leaves geometry is represented by a curved rectangular dielectric sheet. [C5223]

"Radar remote sensing of forests at low frequencies: a 3D electromagnetic scattering model"

A 3D electromagnetic scattering model is developed to study the interactions between a forest and a low frequency radar wave. [C5224]

"GOMOS validation"

GOMOS (Global Ozone Monitoring by Occultation of Stars) on Envisat measures ozone, NO₂, NO₃, H₂O, aerosols, neutral air density, and temperature in the stratosphere and mesosphere by detecting the absorption of starlight in UV, visible and infrared wavelengths. During bright limb conditions, GOMOS also observes scattered solar radiation. GOMOS delivers ozone concentration profiles at altitudes 15-100 km with a vertical resolution of about 1.5 km and with a global coverage. As a self-calibrating method, stellar occultation measurements provide a basis for a long-term monitoring of ozone profiles. We present results achieved during the first year of the

GOMOS validation program. The validation is based on comparisons with lidars, ozone sondes, balloon borne instruments, other satellites as well as with climatological and meteorological data. [C5225]

"First scientific results on GOMOS/ENVISAT"

GOMOS on board ENVISAT is the first stellar occultation spectrometer providing vertical profile of ozone and minor species from the upper troposphere to the mesosphere on a regular basis. First results indicate that GOMOS reach its expected accuracy after improvements of data processing. [C5226]

"Automatic co-registration of space-based sensors for precision change detection and analysis"

A variety of techniques were developed at JPL to assure sub-pixel co-registration of scenes and orthorectification of satellite imagery to other georeferenced information to permit precise change detection and analysis of low (e.g. 1-4km weather satellite) and moderate (e.g. 30m Landsat) resolution space sensors. The methodology employs the additive composition of all pertinent dependent and independent parameters contributing to image-to-image tiepoint misregistration within a satellite scene. Mapping and orthorectification (correction for elevation effects) of satellite imagery defies exact projective solutions because the data are not obtained from a single point (like a camera) but as a continuous process from the orbital path. Standard image processing techniques can apply approximate solutions with sufficient accuracy, but some advances in the state-of-the-art had to be made for precision change-detection and time-series applications. The basic technique first involves correlation and warping of raw satellite data to an orthorectified Landsat data base to give an approximate mapping. Then digital elevation models are used to correct perspective shifts due to height and view-angle. The image processing approach requires from three (e.g. geosynchronous weather satellite imagery) to six (e.g. polar weather satellite imagery) sequential processing steps that warp the dataset by resampling pixel values. To avoid degradation of the data by multiple resampling, each warp is represented by an ultra-fine grid of tiepoints. For successive warps, the grids can be composed mathematically into a single grid such that only one re-sampling occurs. Ultra-fine grids can currently be up to 1000 Ч 1000, or more million points. [C5227]

"Host medium transformation of the early-time radar response of a buried dielectric target"

This paper addresses the problem of predicting the early-time radar response of a low-metal content landmine buried in a lossy soil given its response in a lossless soil. To make the problem tractable, we consider plane wave scattering from a homogeneous dielectric target embedded in a layered host medium with a global loss model. Using similarity analysis and the Born approximation, a transformation law for the scattered field is derived which relates the early-time target response in the lossy host medium to that in a corresponding lossless host medium. We also present a transformation law for the target impulse response, which follows directly from the transformation for the scattered field. The derived transformation law is tested using early-time responses of a mine-like target obtained from 3D finite-difference time-domain (FDTD) simulations. Based on these tests, the ability of the transformation law to predict changes in the early-time response of a non-metallic landmine as a result of changes in the electromagnetic properties of the host medium is discussed. [C5228]

"Characterization of shallow underground targets using wideband microwave reflectometry"

In this paper, the use of a combined signal processing technique of target discrimination for the step-frequency ground penetrating radar is investigated. To construct the radar range profile from the backscattered signal, a real part of the inverse discrete Fourier transform is multiplied by the pseudospectrum obtained from the same data via eigenvector method. The signatures of small underground objects can be subdivided in four categories designated conditionally as front wall; back wall; inclusion of high density; inclusion of low density. Experimental studies have shown that the technique is valid for both strong and weak scatterers. The approach can be extended to the discrimination of complex targets such as landmines by creating a set of templates. [C5229]

"Imaging of high-frequency full-vectorial GPR data using measured footprints"

For proper imaging and inversion, four parameters need to be known accurately. These are position of the transmitter and receiver antennas, the wave velocity distribution in the medium, the polarization and the amplitude characteristics of the antennas used. The position information problem is solved by introducing an automated acquisition frame with high accuracy in horizontal and vertical positioning of the antennas over a fixed area. For object detection and characterization purposes, we use elevated antennas, which imply that at least a two-medium background medium must be used for accurate velocity information. The velocity in air is known, while that of the Earth must be obtained from independent measurements. The polarization and amplitude characteristics can be obtained for elevated antennas by modeling the transmitter and receiver and validate the model with measurements in air. A second way of obtaining information on the wave field, both polarization and amplitude, that is emitted into the ground is to record it in a certain plane in the air. In a

configuration with constant velocity horizontal layers, only the down-going wave field, in the upper half space below the antennas, contributes to the down-going wave field in the layered earth. Accurate knowledge of this down-going wave-field allows wave-field extrapolation into the layered earth, which technique can then be used in multi-component imaging algorithms accounting for polarization and amplitude. Here, the effects of knowing the four parameters are shown. It demonstrated that the multi-components or full polarimetric, imaging technique is a tool of full operational value only when all four parameters are accurately known. [C5230]

"Ultra high resolution wind retrieval for SeaWinds"

The SeaWinds series of scatterometer instruments were designed to measure vector winds over the ocean at a nominal resolution of 25 km. However, the radar backscatter measurements from which the wind is inferred are made at finer resolution than this. Further, the spatial sampling of the backscatter measurements can support reconstruction of finer scale backscatter values which can then be used to estimate the near-surface wind vector field at high resolution (pixel spacing of 2.5 km). At this resolution, the data can be used to study coastal and mesoscale wind features such as tropical cyclones and convective storms. In this paper we use simulation and actual data to validate the accuracy of the retrieved winds and analyze the effective resolution of the wind estimates. An empirical technique to compensate for the estimate bias is developed and applied and an improved method for ambiguity selection is developed. Comparison of the derived vector winds with a variety of other wind sensors is very encouraging. [C5231]

"Radar methods for atmospheric stratification condition unambiguous determination by synergy data of sea surface altimetric and scatterometric observations"

The results of theoretical researches and numerical estimations of sea surface radar backscattering coefficient temperature-wind dependencies are presented. A radar method for atmospheric stratification condition evaluation, based on a joint application of data of sea surface altimeter and scatterometer observations, is suggested. [C5232]

"Operational estimation of coastal wind vectors from RADARSAT SAR imagery"

In this paper we are concerned with automated approaches for generating wind vectors, an in particular with comparing approaches that differ in the spatial scales of the features used to estimate wind direction from the SAR imagery. One group (Veridian Systems Division) has focused on using larger scales (3 to 16 km) and estimating directions from either a spectrum of the image or from a projection of the imagery in different directions. The other group (GKSS Research Center) has focused on much smaller spatial scales (0.4 to 1.6 km), which extract directions either in the spectrum of the image or from local gradients derived from the image. [C5233]

"Combined active/passive hurricane wind retrieval algorithm for the Seawinds scatterometer"

Because of their high wind gradient structures, tropical cyclones (TCs) present a major challenge to space-borne scatterometer measurements of ocean surface wind vectors. Frequently spiral bands of strong rains accompany the high winds, and this precipitation attenuates the ocean backscatter measured by the scatterometer. Furthermore, traditional geophysical model functions (GMF), which relate wind speed and direction with radar backscatter (σ_0), have not been tuned for the high wind conditions of TC's. The SeaWinds scatterometer has the ability to measure simultaneously the ocean backscatter and brightness temperature. By using this combined active/passive approach, simultaneous wind and rain estimates are made in TC's. Rain rate, determined passively, is used to model both the attenuative and scattering effects of rain. These parameters are used to correct the measured ocean σ_0 at 12.5 km resolution. Wind speed retrievals are performed using a special TC-GMF developed using airborne scatterometer measurements in hurricanes. SeaWinds wind speed results for several hurricanes occurring between 1999 and 2002 compare well with high-resolution surface wind fields available from NOAA's Hurricane Research Division aircraft flights. [C5234]

"Combined active and passive microwave sensing of ocean surface wind vector from TRMM"

This paper presents a new ocean wind vector measurement technique that uses the combined passive and active microwave measurements respectively from the Tropical Rainfall Measuring Mission (TRMM) Microwave Imager (TMI) and the Precipitation Radar (PR). The wind speed is inferred by TMI over a wide swath that includes the narrower PR swath. The PR scans cross-track $\pm 18^\circ$; and near the swath edges, where the radar backscatter responds to both the magnitude and direction of the surface wind, we use the microwave radiometer estimate of wind speed and the measured σ_0 at incidence angles greater than 15 degrees to derive wind direction. Because the PR provides only a single azimuth look, multiple possible wind direction solutions exist. The ability to select the proper (single) direction is beyond the scope of this paper; but comparisons are

presented between the "closest" retrieved TRMM wind vectors and near-simultaneous wind vectors measured by the QuikSCAT satellite scatterometer to demonstrate the potential for measuring ocean surface vector winds. [C5235]

"Ocean winds retrieved from X-band radar-image sequences"

A new method for retrieving wind speeds and directions using nautical radar-image sequences is presented. The method consists of two parts, one for wind direction and another for wind speed retrieval. Wind directions are locally extracted from wind induced streaks, which are approximately in line with the mean wind direction. The algorithm assumes wind direction as normal to the local gradients of the amplitude image. Wind speeds are derived from the radar cross section, by parameterization of its dependency on the wind vector, which is performed by training of a neural network. For verification of the method the wind direction and speed from nearly 1400 radar-image sequences are compared to in situ data from a wind sensor. The accuracy and limitations of the method are discussed. A second new method is introduced, which enables to retrieve spatial and temporal wind fields from radar-image sequences. Thereby the wind streaks are available in space and time. The local velocity and direction of the wind pattern of each point in the investigated area is determined using tensor-based techniques. This method has the advantage that no calibration of the radar images or training of a neural network is necessary. [C5236]

"Systematic tropospheric aerosol lidar measurements over Potenza in the frame of EARLINET"

27 months of systematic lidar measurements of aerosol backscatter and extinction have been performed since May 2000 in Tito Scalo (Potenza) (Southern Italy, 40°36'N, 820 m a.s.l.) in the frame of the EARLINET project. A statistical analysis on the backscatter properties in the UV of tropospheric aerosols has been performed and presented. [C5237]

"On the suitability of TerraSAR-X split antenna mode for current measurements by along-track interferometry"

Latest concepts for the TerraSAR-X hardware design include the availability of a split antenna mode, in which the fore and aft halves of the SAR antenna array with a total length of 4.8 m can act as separate receiving antennas for along-track interferometry (ATI). The effective ATI time lag is 0.17 ms. We discuss in this paper whether the split antenna mode is suitable for ocean current measurements. Typical (tidal) currents in coastal areas are on the order of 1 to 2 m/s. To measure them, the ATI time lag should ideally be 20 times longer than the time lag of TerraSAR-X. Furthermore, the backscattered power from the ocean at low wind speeds can be below the noise floor of the instrument. However, the high resolution of TerraSAR-X permits averaging over many pixels to reduce noise. Simulated data products suggest that TerraSAR-X is capable of measuring currents with satisfactory accuracy at a spatial resolution of about 1 km, which is sufficient for many applications. [C5238]

"Evaluation of TerraSAR-X Spotlight processing accuracy based on a new Spotlight raw data simulator"

This paper evaluates the Spotlight processing accuracy for TerraSAR-X. It describes the developed Spotlight raw data simulator. Approximations in the Sliding Spotlight processing are calculated and verified by using this simulator. Based on a worst case scenario, raw data were simulated and processed with an Extended Chirp Scaling algorithm for Sliding Spotlight. The simulation results demonstrate the applicability of the processing algorithm for TerraSAR-X. [C5239]

"The CloudSat Mission"

The CloudSat Mission deploys the first spaceborne 94 GHz cloud profiling radar in space. The mission was selected under the NASA Earth System Science Pathfinder Program (ESSP <http://essp.gsfc.nasa.gov>) with a scheduled launch for the alter part of 2004. The unique feature of the CloudSat radar lies in its ability to observe jointly most of the clouds and precipitation within its nadir field of view. The CloudSat satellite also flies as part of a constellation of satellites that includes EOS Aqua and EOS Aura at each end of the constellation. CloudSat, as second ESSP mission that flies an aerosol lidar (CALIPSO) and another small satellite, PARASOL, carrying the POLDER polarimeter inserted in the formation between the larger EOS spacecraft. This constellation is referred to as the A-train. An overview of the CloudSat mission, its science goals, science products and validation are summarized. CloudSat seeks to solve a number of outstanding cloud-climate problems and thereby spur improvements in both weather forecasting and climate prediction. It aims to evaluate quantitatively the representation of clouds and cloud processes in global atmospheric circulation models, and the relationship between the vertical profiles of cloud liquid water and ice content and cloud radiative properties, including the

radiative heating by clouds. [C5240]

"Operational sea ice monitoring with RADARSAT-2-a glimpse into the future"

In order to assess the potential of RADARSAT-2, a field-validated airborne and satellite SAR sea ice dataset was collected over young and first year sea ice at multiple polarizations. Some preliminary observations are presented. [C5241]

"Synthetic Aperture Radar for Search and Rescue: studies at natural resources Canada-update"

The use of Synthetic Aperture Radar to assist Search and Rescue in the location of downed airplanes is being explored in studies at Natural Resources Canada (Canada Centre for Remote Sensing). Test imagery in polarimetric mode is being acquired by the C-SAR on board the Environment Canada Convair-580. This paper discusses algorithm studies and recent results. [C5242]

"Clutter effects on ground moving target velocity estimation with SAR along-track interferometry"

The SAR interferogram, defined as the product of the first channel and the complex conjugate of the second, is one way of comparing two SAR channels. When the two sub-apertures are aligned along the flight path, targets with non-zero radial velocities can be detected by exploiting the phase information of the interferogram. This paper examines the effect of clutter interference on the interferometric phase and provides a simple method for mitigating the clutter contamination by using time-frequency (TF) analysis techniques and a velocity-offset matched filter (VOMF). Both simulated and airborne results are presented. [C5243]

"Using Pol-InSAR at X-band: preliminary observations"

First Page of the Article [C5244]

"Signal theoretical aspects of bistatic SAR"

First Page of the Article [C5245]

"Non-cooperative bistatic SAR imaging system: spatial resolution analysis"

First Page of the Article [C5246]

"Forest height feature extraction in polarimetric SAR interferometry by using rotational invariance property"

First Page of the Article [C5247]

"The effect of temporal decorrelation on the inversion of forest parameters from Pol-InSAR data"

First Page of the Article [C5248]

"Polarimetric SAR interferometry applied to land ice: first results"

First Page of the Article [C5249]

"Oceanographic applications of spaceborne bistatic SAR"

First Page of the Article [C5250]

"Remote sensing to support Australia's commitment to international agreements: a role for synthetic aperture radar"

First Page of the Article [C5251]

"Operational wetlands monitoring for the Ramsar convention: TESEO powers a breakthrough"

First Page of the Article [C5252]

"Desertification-a land degradation support service"

First Page of the Article [C5253]

"Interpretations of the omega-K algorithm and comparisons with other algorithms"

First Page of the Article [C5254]

"Radar processing and geometric specificity of bistatic data"

First Page of the Article [C5255]

"Wavenumber domain SAR focusing with integrated motion compensation"

First Page of the Article [C5256]

"Mesoscale soil moisture estimation from SAR data using subscale landuse information"

The variation of soil moisture and its spatial pattern within a watershed is highly dynamic. Hydrological processes, such as runoff production or evapotranspiration, largely depend on the spatial distribution of soil water content, which is impossible to measure on ground over larger areas. ENVISAT ASAR image products have high potential for the generation of soil moisture maps. Especially wide swath images, covering large areas with adequate spatial and temporal resolution, are very interesting from the user point of view. The quality of the soil moisture products, derived from SAR data mainly depends on the information about the land cover. Especially for mesoscale images, an adequate parameterisation of the land cover is difficult. We therefore investigate the effect of different landuse parameterisations on the accuracy of mesoscale soil moisture inversion. An algorithm for the derivation of mesoscale soil moisture maps is proposed. [C5257]

"Surface soil moisture estimation using active microwave ERS wind scatterometer and SAR data"

This paper presents an original methodology to retrieve surface (2greater than 0.8) are observed for three studied watersheds in France with an rms error smaller than 4% between real and retrieved moistures. [C5258]

"A soil moisture algorithm using tilted Bragg approximation"

A successful soil moisture algorithm using radar data must identify the soil moisture effect and the surface roughness dependence explicitly since rough surface scattering depends on both the roughness and the dielectric constant of an imaged surface. For bare surfaces, several algorithms have been developed to estimate soil moisture using polarimetric radar data. These algorithms were empirically derived from either experimental data or numerical data instead of starting from rough surface scattering theories. In this paper, we present a soil moisture algorithm theoretically derived using the tilted Bragg approximation. With appropriate approximations using the tilted Bragg theory, we have derived both co- and cross-polarization ratios. Then, a soil moisture algorithm is developed based on these two ratios. This new algorithm is compared with the existing empirical methods using input data from the IEM (Integral Equation Method) an experimental radar data. We also briefly discuss the effect of vegetation on this soil moisture algorithm. [C5259]

"Multisource image fusion by using the redundant wavelet decomposition"

We propose in this paper a method for combining simultaneously multispectral (XS), panchromatic (P) and radar (SAR) images by suing conjointly the Intensity Hue Saturation (HIS) transform and the Redundant Wavelet Decomposition (RDW). The fusion is accomplished through two steps. Firstly, XS images are represented in the HIS system in order to isolate the spectral components (H,S) from the spatial information (I) component. Secondly, features coming from P and SAR images are incorporated into the (I) component by using the RWD. The obtained fused images show the contribution of the P image for discriminating lines and edges. While the SAR image provides an information on the surface roughness and the detection of point targets as houses, boats, and water-land transitions. [C5260]

"Application of log-cumulants to change detection on multi-temporal SAR images"

Satellite SAR images acquired on repeated orbits became a useful source of information to monitor changes in many areas where optical data are rarely available. In this paper, two different approaches which take the specificity of speckle distributions into account are proposed to detect changing areas. The first one consist in detecting changes of the mean radiometry by applying in a temporal direction a conventional "edge detector". The second one consists in detecting temporally heterogeneous areas by measuring 3-dimensional texture parameters using second kind statistics. The results obtained with these two approaches and their

complementarity are illustrated on a 7 image time series acquired by satellites ERS. [C5261]

"Entropy among a sequence of SAR images for change detection"

The coherence map between two images is frequently used to detect changes in a sequence of temporal SAR images and to evaluate the interferometric image quality. Recently, an alternative method for change detection was proposed: the entropy image. This paper performs the entropy calculation among several temporal SAR images. With this method, it is possible to calculate the entropy between two images considering intermediary, previously, or later acquired images, which contain information about the change process. It is shown that this method can improve the change detection performance in low coherence areas (using intermediary images) or in high coherence areas (using former or further images). Simulated images were used to show the performance of the method and to compare this method with coherence and entropy only between two images. [C5262]

"Analysis of multi-frequency polarimetric data for assessment of bare soil roughness"

The aim of this study is to assess the bare soil surface roughness parameter, i.e. the root mean square height (hrms) when the moisture is constant, using anechoic chamber measurements based on fully polarimetric scatterometer data. An incidence angle based algorithm has been proposed to assess the bare soil height hrms. For this purpose, sets of experimental backscattering data have been evaluated on different types of rough surfaces (Rough Gaussian, hrms= 2.5 cm, Smooth Gaussian, hrms= 0.4 cm and Medium Mixed surface, hrms= 0.9 cm) with known geometrical and dielectric properties. The scattering matrix of those three surfaces under test was measured in monostatic mode vs. frequency (1-19 GHz) and incidence angles ($\theta = 10^\circ$ to 50° in steps of 10° for hrms= 2.5 cm and 0.9 cm and 5° for hrms= 0.4 cm) data. An empirical relationship has been developed between backscattering, hrms and incidence angle independently for L-, C-, X- and Ka-band for all polarizations (i.e. HH, VV and HV). This relationship provides the calculated backscattering values, which is helpful in the inversion process. A good agreement has been obtained between the observed and calculated hrms. The analyses show the strong dependence of hrms on incidence angle, polarization and frequency. This type of work is also helpful in the near future to predict the optimum sensor parameters (i.e. incidence angle, polarization and frequency) for measuring the bare soil roughness. [C5263]

"Surface parameter retrieval from polarimetric and multi-frequency SAR data"

The aim of this paper is to present a surface model inversion using the integral equation formulation of backscattering coefficients. A quantification of the influence of surface parameters such as roughness and soil moisture on polarimetric indicators for various frequency bands is led. Finally, a technique is introduced to retrieve a surface RMS height and dielectric constant from multi-frequency data. The inversion technique is applied to polarimetric and multi-frequency measurements acquired at EMSL, JRC laboratory. [C5264]

"Temporal and spatial soil moisture change pattern detection using multi-temporal Radarsat SCANSAR images"

The research has been done to derive the soil moisture information at local scale by using single polarization, single frequency sensors such as ERS-1/2, Radarsat, and JERS-1. There is a need to develop a technique to estimate soil moisture information from these currently available data sources at both regional and local scales. In this study, a soil moisture change detection algorithm was developed for using the multi-temporal 50m resolution Radarsat SCANSAR image data. It was based on the theory model analysis results, with the correction of vegetation and incident angle effects. The relative soil moisture change value can be derived. The results were compared with in-situ measured soil moisture data from 3 different sampling sites at study area. The validation indicated our algorithm with RMSE error of 0.44 in estimating soil moisture change ratio. [C5265]

"A coherent EM scattering model for dual baseline POLInSAR"

First Page of the Article [C5266]

"Surface roughness characterization for SAR applications"

In this paper is proposed an alternative description of the roughness state of bare soil surfaces at the scale of the "homogenous" agricultural field. As a first step, the roughness power spectra of experimental profiles acquired over various test-sites in Europe are thoroughly investigated to characterize the main features of the different tillage states. Then, a novel roughness parameter is obtained by integrating the filtered power spectral density of the surface over a frequency band centered on the resonant Bragg frequency. This parameter can describe the roughness effectively seen by the SAR sensor at the scale of the field. Finally, the roughness parameter stability and its impact on the backscattered σ° are assessed with a view on investigating issues of

parameters retrieval. [C5267]

"Model-based methods for soil moisture estimations from SAR data"

In this paper, two model-based methods for the soil moisture retrieval from SAR data are investigated. These methods implicitly consider the physical theory relating the direct relationships between geophysical parameters and SAR measurements and, moreover, can incorporate a priori information to make the parameter estimation more accurate. Given that the inverse problem of recovering soil moisture from SAR observations doesn't have a unique solution, the proposed methods perform a probabilistic estimation of such parameter, finding solutions representative of an unknown probabilistic distribution such as the mean or the most probable solutions. The methods are a Neural Network based-methods and a Mixture Model method. The difference of the solution found by these methods are discussed. Moreover, simulations about soil moisture estimations from ERS and ENVISAT ASAR data are presented. [C5268]

"Influence of surface roughness frequency components of radar backscattering: consequences on roughness sampling"

Natural soil surfaces present multiple, random roughness scales (or frequency components). Proper estimation of the correlation length, L , of a low frequency (LF) roughness component (typically $L > 20$ cm) requires excessively long profiles (> 10 m). Consequently, usually applied sampling protocols were not suitable for an accurate determination of L . The objective of the study was to establish to which extent the low frequency component has a significant impact on the soil microwave backscattering. We implemented a model based on the Method of Moments (MM) to generate profiles presenting arbitrarily chosen multiple random roughness scales. It is shown that for angle of incidence lower than 40° , adding a low frequency component with a component greater than 4 times the wave length does not affect the MM results. If profiles of 2 meters are used, we obtained much better results when the low frequency is removed. [C5269]

"Abyss-Lite: improved bathymetry from a dedicated small satellite delay-Doppler radar altimeter"

We describe the rationale, scientific basis, and implementation of a mission to map the ocean's bottom topography with a spatial resolution of 6 km based on a high-precision radar altimeter on a dedicated free-flying spacecraft. [C5270]

"Future radar altimeter concepts for ocean applications"

Alcatel Space is currently leading a study for ESA for reviewing the user needs in ocean and ice altimetry and for proposing and studying new altimeter concepts. The paper presents the results of this study focusing on ocean mesoscale sea surface topography (sea state applications not addressed) applications and swath interferometric radar altimeter concepts. [C5271]

"Phase B and breadboard results of the Ka-band altimeter for future microsatellite altimetry missions"

CNES is studying in partnership with scientific laboratories and industry the feasibility of a high-resolution ocean topography mission based upon a new class of wide-band, Ka-band altimeter. This paper presents the altimeter/radiometer design and performance as well as results from the breadboard activities. The accommodation on a microsatellite is also shown. [C5272]

"JASON-1 calibration campaign at the Ibiza island area"

A Spanish/French JASON-1 calibration campaign is being prepared for June 2003 in the area of Ibiza island in the NW Mediterranean Sea. The main objective, with a direct absolute altimeter calibration, is to map with a new designed, building and calibrated GPS catamaran, the mean sea surface MSS/local geoid gradient in the north area of Ibiza island at one crossing point of an ascending and descending satellite track. One part of a descending orbit in the SE of the island is also included. It is expected to have a new tide gauge at Ibiza harbor at that time. This campaign with its associated strategies is expected to have French support (CNES, LEGOS, CERGA and Noveltis) and is based in the experience obtained by three previous campaigns made in March 1999, July 2000 and August 2002 in the Cape of Begur/Llafranc/Palamos area. Direct absolute altimeter calibration was made from direct overflights using GPS buoys with a toroidal design performed at the ICC based in the original design of the University of Colorado at Boulder. The TOPEX Alt-B bias was estimated processing altimeter and GPS data. Other main objective of the campaign was to map GPS buoys the mean sea surface, MSS, along an ascending T/P groundtrack about 15-20 km from the coast, using coastal tide gauge measurements. In this case indirect absolute altimeter calibration is possible for any other altimetric satellite

crossing the MSS, with the only requirement that tide gauges are operational during the overflight. Two tide gauges were placed temporarily in Llafranc harbor and was used the data from the permanent L'Estartit tide gauge. The MSS provides with a reference for the altimetric measurement. The tide gauge provides with the temporal variable part of the sea level. The purpose of this presentation is to present and first results of the expected new JASON-1 calibration campaign in June 2003 at the Ibiza island area. [C5273]

"Comparison of microwave radiometer brightness temperature over a hot reference area"

Nadir-looking microwave radiometers are flown on different altimeter missions to correct the altimeter range for water vapor and cloud liquid water path delay in troposphere. Actually four sensors, TOPEX, JASON-1, ERS-2, and ENVISAT microwave radiometers (MWR) provide continuous measurement and the aim of this paper is to compare their measured brightness temperatures over the same hot reference continental area. [C5274]

"Innovative radar altimeter concepts"

In the frame of the study "Innovative radar altimeter concepts", founded by the European Space Agency (ESA), the authors analyzed potential advanced measurement concepts for radar altimeters of future generation, studied the feasibility of the identified techniques and proposed a design for an instrument based on the most promising system concept. This paper summarizes the major results of the study. [C5275]

"Application of GPS in airborne SAR image based disaster evaluation"

In the process of airborne SAR image based disaster evaluation, the first step is to complete image rectification, so the image rectification time is the bottleneck of the whole disaster evaluation process. Dynamic GPS data recording instrument positioned on the airborne SAR airplane can record the precise parameters of the SAR such as the velocity, the latitude, the longitude, the elevation and so on. The parameters are the key parameters to determine the relationship between the pixels of the SAR image and the points on the ground in the F. Leberl formula that is the SAR imaging equation. Thus dynamic GPS data can directly transform coordinates of image pixels to geographical coordinates. With the geographical coordinates, we can rectify the airborne SAR image quickly to make preparation for other processing of disaster evaluation. [C5276]

"ASAR AP mode performance and applications potential"

This paper reviews results from the post launch and commissioning period of ENVISAT in the alternating polarization mode of the ASAR instrument. Particular emphasis is placed on intercomparison of data from point targets deployed in Canada, and the Netherlands and differences in their information are explored. [C5277]

"The ASAR wide swath mode products"

This paper focuses on the characterization of the medium resolution generated by the ASAR ground processing facility installed on the ENVISAT ground segment from the ASAR wide swath mode of acquisition. It introduces the description of their main processing algorithmic features and includes details of the instrument settings used during this acquisition mode and their optimization throughout the ENVISAT commissioning phase period. [C5278]

"Geometric performance of ENVISAT ASAR products"

We describe validation measurements of the geometric accuracy of ASAR images, measured redundantly via independent methods. Our tests include image (IM), alternating polarization (AP), and wide swath (WS) mode acquisitions over a variety of test sites. ASAR's slant range products (IMS/APS) require a slightly different validation methodology than ground range precision (IMP, APP) and medium resolution products (IMM, APM, WSM). A third approach is required for ellipsoid-geocoded products (IMG, APG). The most highly accurate validation is possible with single look complex (SLC) data (IMS and APS products), as all other product types lose resolution during multilooking. For a library of ground control points (GCPs) including map features such as bridges or road intersections, as well as (where available) transponders and corner reflectors, we use surveyed or map-measured position information (together with the delay value in the case of transponders) to solve the zero-Doppler iteration and predict the position of the GCP as an azimuth and slant range coordinate in the radar image. In the case of ground range products (e.g. IMP, APP, IMM, APM, WSM) the predicted slant range value is additionally transformed by a slant to ground range transformation to determine the predicted image coordinate. The GCP feature is then either measured by inspection of a detected image, or localized automatically within the neighborhood of the prediction. GCPs are measured within the radar geometry image products, derivative geocoded products, and topographic maps, providing their measured map, radar geometry, and nominally geocoded GTC locations. Radar image locations are compared to map reference values and

statistics of differences are tabulated. We compare the accuracies of the estimates achievable using transponders and map GCPs. Based on the suite of products (and accompanying orbit information) available to us, we establish a methodology for estimating a preliminary sampling window start time bias. The multiple validation and estimation techniques used ensure robust determination of ASAR geolocation accuracy. [C5279]

"Soil dielectric spectroscopic parameters dependence on humus content"

The purpose of this paper is to apply generalized refractive mixing dielectric model (GRMDM) based on the Debye relaxation formula to soils with various humus contents. With this approach, the soil types containing 6.6% and 0.6% of natural humus. Complex dielectric constant or complex refractive index were measured as a function of moisture at the frequencies of 0.55; 1.1; 1.8, 3.0, 11.5, 13.5 and 16.3 GHz with the temperature being of 20-24 °C. Using measured data only at 1.8, 3.0, 4.3 GHz, the GRMDM parameters-relaxation time, static dielectric constant, and conductivity for both types of water in soil were attained for both types of soil. Though variation in the relaxation parameters with humus content is moderate, this factor has to be taken into account when soil moisture remote sensing algorithms are being designed for agricultural areas. For this purpose, the GRMDM can be applied, with a soil humus content being one of its physical parameters. [C5280]

"ASAR instrument performance and product quality status"

This paper presents the main characteristics of the advanced synthetic aperture radar (ASAR) instrument on board ENVISAT, ASAR products, the challenges in the ASAR calibration and product validation, the methodology used to perform the sensor performance monitoring and product calibration based on the special ASAR features and dedicated calibration sites and finally a summary on the product quality status will also be provided. [C5281]

"ASAR image mode product quality"

This paper gives details of the Envisat ASAR image mode products quality analysis. Initially, a description of the analysis methodology and performance assessment tools and the image properties are given followed by the image quality analysis. This analysis includes format verification, impulse response function measurements, equivalent number of looks and radiometric resolution determination, analysis of azimuth ambiguities, localization accuracy, preliminary radiometric calibration and the derivation of noise equivalent radar crosssection. [C5282]

"Current navy applications of satellite remotely sensed data"

The satellite programs office of the commander, naval meteorology and oceanography command provides guidance for acquisition, assimilation, and application of satellite remotely sensed data for navy meteorology and oceanography (METOC). Access to required satellite data through direct receipt or shared acquisitions is a primary mission. If data are not available from other military, civilian, or foreign sources, the satellite programs office supports future satellite programs such as Coriolus/WindSat. Algorithm development, data assimilation and fusion techniques, and display tools are also supported. Recent efforts include modification of navy training to provide up-to-date remote sensing techniques to enlisted sailors and officers in school and in the field. The naval meteorology and oceanography command provides METOC support to the navy in the form of global and regional analyses and forecasts of atmospheric and oceanic conditions and their impact on platforms, weapons, and sensors. Navy METOC also supports the analysis of hyperspectral data to determine the utility for coastal applications such as bathymetry, submerged hazards, and visibility. Altimetry is used daily to provide an all weather look "into" the water column that is essential to determine the distribution of water masses and currents in the ocean. Visible imagery for R&D sensors is being used to determine the presence of dust, fire and volcanic ash in various regions of the world. Real-time organic acquisition of the data allows rapid processing of the data in tactical situations. [C5283]

"Terrain categorization using a background spectral library"

We describe development of a background spectral library for northeastern Virginia, USA, based on hyperspectral images and an extensive land cover database. The library consists of mean spectra and standard deviations measured in 14 areas of uniform land cover. Terrain categorization products include classification maps and fractional abundance maps determined by linear mixture analysis. There is excellent qualitative agreement between the linear unmixing results and the known land covers. [C5284]

"Raw data based two-aperture SAR ground moving target indication"

This paper investigates the capability of classical two-channel SAR ground moving target indication (GMTI) techniques, such as displaced phase center antenna (DPCA) or along-track interferometry (ATI) when

implemented on azimuth-uncompressed SAR data, rather than the processed SAR image. By transforming the data into the Doppler frequency domain complete target detection and parameter estimation scheme is proposed. In contrast to the conventional image based algorithms, the proposed techniques are able to detect even fast movers. The GMTI feasibility is demonstrated with measured airborne data. [C5285]

"Multi-sensor approach for assessing the taiga-tundra boundary"

Monitoring the dynamics of the tundra-taiga boundary is critical for our understanding of the causes and consequences of the changes in this area. Because of its inaccessibility, remote sensing data plays an important role. In this study, we examined the use of several remote sensing techniques for identifying the existing tundra-taiga ecotone. These include Landsat, MISR and RADARSAT data. High-resolution IKONOS images were used for local ground truth. It was found that on Landsat ETM+ summer images, reflectance from tundra and taiga at band 4 (NIR) is similar, but different at other bands such as red, and MIR bands. When the incidence angle is small, C-band HH-pol backscattering coefficients from both tundra and taiga are relatively high. The backscattering from tundra targets decreases faster than taiga targets when the incidence angle increases, because the tundra targets look smoother than taiga. Because of the shading effect of the vegetation, the MISR data, both multi-spectral data at nadir looking and multi-angle data at red and NIR bands, clearly show the transition zone. [C5286]

"Preliminary design of a SAR-GMTI processing system for RADARSAT-2 MODEX data"

The RADARSAT-2 satellite includes an experimental mode, called the moving object detection experiment (MODEX), which is to be used to perform ground moving target indication (GMTI) using a C-band synthetic aperture radar (SAR). During MODEX operation, the SAR antenna is partitioned into two subapertures along the satellite track to sequentially observe the same scene from the same spatial point. By appropriate processing of the returned signals from each channel, detection of temporal changes in the scene (i.e. moving targets) can be accomplished. The MODEX configuration will be used by the Canadian Department of National Defense RADARSAT-2 GMTI demonstration project, which aims to develop a SAR-GMTI processing system to investigate the military and commercial utility of space-based moving target measurements. This paper discusses a conceptual SAR-GMTI processor design in terms of selected algorithms and their performance, such as along track interferometry (ATI), displaced phase center antenna (DPCA) and iterative moving target (terrain) matched filtering (MTMF). Processing issues arising in space based radar (SBR) GMTI are also discussed. It is anticipated that the ultimate processor design will incorporate these algorithms as independent processing configurations, along with selection rules that will optimize their use to the contents of the image scene. [C5287]

"3D global ozone proxy fields and the NPOESS OMPS assimilation experiment, for improved numerical weather predictions for military operations"

Important classes of military operations would benefit from improved long term weather forecasts. Because the radiative effects of ozone influence jet streams, the use of daily measurements of stratospheric ozone should improve long term forecasting. Ozone data will be provided operationally by the National Polar-Orbiting Operational Environmental Satellite System (NPOESS) Mapping and Profiler Suite (OMPS) instrument. An assimilation experiment (OMPS-AE) will use data from an OMPS on the NPOESS Preparatory Project (NPP) spacecraft for testing ozone assimilation and forecasting algorithms. The development of those algorithms is being aided by using proxy 3D global fields which are calculated by combining sparse measurements of ozone with operational meteorological analyzed fields. We describe this data fusion method, and the validation and properties of the resulting ozone proxy. [C5288]

"Automatic structures detection and spatial registration using multisensor satellite imagery"

Mesoscale processes such as upwellings, eddies, or thermal fronts are very energetic and their knowledge is very important not only to study oceanic circulation but also areas of applications that include acoustic propagation anomalies, fisheries management and exploitation, coastal monitoring and offshore or ocean oil detection and exploitation. A variety of techniques and algorithms have been developed to detect such structures. The foremost difficulties encountered in the preceding approaches are the presence of noise, mainly due to clouds and other atmospheric phenomena. In this context, the proposed methodology, due to its region-based nature, overcomes the edge detection inconveniences and obtains the proper structure identification. Moreover and in order to perform an exhaustive analysis of the structure dynamics, it is necessary to compare image sequences. In this context, the use of spatial registration techniques is necessary to achieve that pixels in different images correspond to the same geographic region. An automatic contour based approach for high accuracy registration of multisensor and multitemporal remote sensing images is presented. It avoids the use of ground control points, while exploiting the maximum reliable information in both images. These automatic tools,

that combine structures detection techniques and multitemporal and multisensoral registration, have been applied to AVHRR, SeaWiFS and MODIS images of the Canary Island and Alboran Sea areas and have demonstrated that it can be a fundamental tool to validate marine and coastal dynamic studies using remote sensing data.

[C5289]

"The analysis and application of spline interpolation for multisensor and multiresolution image registration"

We briefly introduce B-splines of continuous expression, discrete expression, and their interesting properties as well as describing the fundamental processing steps of image registration. In virtue of error analysis and image registration, we approve spline interpolation and approximation in resampling and transformation reliable and efficient. [C5290]

"A fusion strategy for extraction of urban road nets form multiple images"

We give an overview of our work on automatic road extraction in urban areas. Special emphasis is on the aspect of fusing information from high resolution multiview aerial images. [C5291]

"Synergistic use of DAIS bands to retrieve land surface emissivity and temperature"

Land surface temperature is an important key for environmental studies like energy balances and climate models. As is well-known, to retrieve land surface temperature from remotely sensed data, land surface emissivities are needed due to the nondeterministic nature of the temperature/emissivity separation from thermal infrared measurements: if thermal radiation is measured in N spectral bands, there will be $N+1$ unknowns (N emissivities and a single surface temperature). In this paper, two methods to estimate land surface emissivity from the Digital Airborne Imaging Spectrometer (DAIS) sensor are considered: the temperature/emissivity separation method (TES) developed by Gillespie et al. (1998), in which thermal infrared data are needed, and the NDVI thresholds method (NDVITHM) developed by Sobrino et al. (2001), in which visible and near-infrared data are also needed. Once the LSE has been estimated, LST can be retrieved using a single-channel or two-channel method using only one thermal channel or a combination of two thermal channels respectively. These methods usually use the atmospheric water vapor content as input data, so a method based on the ratios between absorbent and transparent bands in the red and near-infrared region to estimate atmospheric water vapor is also presented. The final results obtained for the validation carried out over the Barrax test site (Albacete, Spain) in the framework of the DAISEX (DAIS experiment) campaigns supported by ESA show deviations of around 0.01 for LSE and deviations between 1 K and 1.5 K for LST. [C5292]

"Multi sensor block adjustment"

Spatio-triangulation process, based on a multisensor block adjustment, is applied to 40 different VIR and SAR images: Landsat-7 ETM, panchromatic SPOT-4 HRV, multiband ASTER, RADARSAT (fine, standard, wide modes) and ERS-1. The images were acquired over Rocky Mountains, Canada from different view/look angles (nadir, across- and in-track) creating various intersection geometries in the overlap areas. Only 1:50,000 paper maps were available for this area. A physical multisensor geometric correction model and algorithms developed at the Canada center for remote sensing were used for the processing. Preliminary results of block formed with all images gave positional errors of around 20-26 m. These errors result from medium-resolution sensors (ERS-1, RADARSAT standard/wide modes, Landsat-7 ETM), from weak intersection geometry between some images, but these errors also include the 1:50,000 map errors (25-30 m). [C5293]

"Multisource urban classification: joint processing of optical and SAR data for land cover mapping"

In this paper we present and compare different techniques for the fusion of multitemporal SAR and multiband optical images. We consider both neuro-fuzzy and statistical approaches for the exploitation of the contextual information and the classification, and different schemes for the multisensor fusion. The proposed techniques are applied to a set of two multitemporal SAR and a Landsat multiband image of an urban area. Results show that it is possible to fully exploit the potentialities of the two sensors, by appropriately fusing their information. In particular, the proposed schemes are useful to retain at the same time the change detection capability and the best possible classification accuracy, thus they are of practical interest for civil protection applications. [C5294]

"Parameter estimation and classification of multiscale remote sensing data"

In this article we describe a Bayesian model for integration of multiscale image data. The approach is based on the concept of a reference resolution. Data at this and lower resolutions are connected to the reference resolution through a fully specified statistical model. Algorithms for parameter estimation and classification based

on the multiscale model are proposed, and results and comparisons with singlescale classification are presented. [C5295]

"Analysis of interferometric signals based on coherence and power spectral density"

In the paper of Holzner and Bamler (2002) it was proven that two interferometric burst-processing options are equivalent. In order to address this question interferogram sample coherence and power spectral density were applied. This paper proposes to use these two expectation values as a general instrument to explore various SAR modes and their interferometric signal properties. Moreover, this method is a way to represent and investigate the behavior of the interferometric signals in a unified and concise way. In turn, this approach will help to design new algorithms for SAR interferometry. Burst-mode interferometry serves as an example. All the known properties of interferometric burst-mode signals—for the cases of non-zero fringe frequency, burst pattern misalignment, and misregistration—can be inferred very easily. In order to amplify the spectral behavior of interferometric burst-mode signals the results are contrasted/referenced to the ones obtained for strip-map interferometry. On this basis, the expectations for spotlight interferometry can be predicted and discussed. [C5296]

"Monitoring areal deformation via multipass SAR differential interferometry"

We propose a new approach for monitoring the evolution of Earth surface deformations via differential SAR interferometry. It allows us to overcome the limitations of standard techniques by incorporating the knowledge of the deformations associated to tie points and available spatial deformation models. [C5297]

"Resolving the acquisition ambiguity for atmospheric monitoring in multi-pass radar interferometry"

Atmospheric signal in spaceborne radar interferograms can be used for both meteorological interpretation in atmospheric studies, as well as for subtracting it from interferograms intended for surface deformation or topography studies. We show that atmospheric signal can be conveniently described stochastically by a power-law behavior, where the absolute amount of energy in the signal, related to the weather situation, can be described using a χ^2 probability density function, based on EUREF GPS data. We present a single master stacking as well as cascaded interferogram stacking as methods to derive the atmospheric phase screen from the data. [C5298]

"Traffic monitoring using SRTM along-track interferometry"

In February 2000, the shuttle radar topography mission SRTM was flown as the first single-pass SAR interferometer in space. The goal was to obtain a global digital elevation model. Therefore, a secondary receive-only antenna on the top of a 60 m long deployable mast supplemented the primary transmit and receive antenna mounted in the shuttle cargo bay. Due to mechanical constraints, the interferometric baseline did not only consist of the terrain height sensitive across track component but also contained an along track component of 7 m. The resulting time lag between the data acquisitions by the two antennas causes phase differences, which are proportional to the line-of-sight velocity of moving targets. Since this system ability has been expected prior to the SRTM launch, a traffic monitoring experiment has been carried out during the mission, which showed a surprisingly good agreement between the GPS velocity measurements on ground and the measurement from space. A strategy to exploit the along track interferometric (ATI) phase and the coherence together with the azimuth displacement of moving vehicles in focused SAR images has been developed and applied on sample test sites for traffic monitoring on highways. [C5299]

"A three-step phase correction approach for airborne repeat-pass interferometric SAR data"

The operational use of airborne interferometric SAR data acquired in repeat-pass mode for DEM generation, polarimetric SAR interferometry, SAR tomography, and differential SAR interferometry is restricted due to imperfections of the available GPS-based motion compensation data, as well as due to the adopted strategies for efficient SAR raw data processing and motion compensation. A three-step correction approach is proposed, partly based on the availability of a (high resolution) digital elevation model of the area of interest, which might be obtained e.g. through the use of single-pass SAR interferometry. Attention is given to the implementation of these methods for squinted geometries. The performance is demonstrated using data of the DLR-owned E-SAR system in repeat-pass imaging mode. [C5300]

"Permanent Scatterers: precision assessment and multi-platform analysis"

The Permanent Scatterers (PS) technique is an advanced tool for processing series of interferometric SAR data aiming at millimetric precision ground deformation mapping. The approach is based on a joint time-space-

acquisition geometry analysis that is carried out at individual point-wise radar targets. The aim of this paper is twofold: (1) describe the main issues related to the precision of PS products; (2) show preliminary PS results obtained using, instead of ESA-ERS scenes, data acquired by other spaceborne SAR platforms characterized different acquisition parameters (namely RADARSAT and JERS). [C5301]

"Differential tomography: a new framework for SAR interferometry"

In this paper, a new interferometric mode crossing the differential SAR interferometry and multibaseline SAR tomography concepts, can be termed differential SAR tomography, is proposed. Its potentials, coming from the joint elevation-velocity resolution capability, are discussed both in terms of possible novel imaging products, and improved operation of conventional differential interferometry and SAR tomography. Processing is cast in a bidimensional baseline-time spectral analysis framework, with sparse sampling. The use of a modern data-dependent bidimensional spectral estimator is proposed for joint baseline-time processing. Promising simulated results are reported. [C5302]

"Development of a high stability L-band radiometer for ocean salinity measurements"

An NEDT analysis of a Dicke radiometer with noise diode injection is presented. The analysis is formulated for a calibration that would form separate running averages of receiver noise temperature and of gain in order to minimize the NEDT and maximize the antenna observation duty cycle relative to the reference and noise diode duty cycles. Results are applied to the Aquarius ocean salinity radiometer problem to show that near ideal total-power radiometer performance is possible. [C5303]

"Hurricane wind and rain measurements using a dual polarized C/Ku-band airborne radar profiler"

Airborne ocean backscatter dual polarization measurements at C and Ku-band obtained in high wind speed conditions (20 to 60 m/s) are presented. The VV and HH NRCS measurements are compared. The preliminary comparisons show that the HH NRCS measurements are slightly more sensitive to the surface wind speeds for high wind speed and precipitation conditions. [C5304]

"QuikSCAT wind retrievals for tropical cyclones"

The use of QuikSCAT data for wind retrievals of tropical cyclones is described. The evidence of QuikSCAT σ_0 dependence on wind direction for >30 m/s wind speeds is presented. The QuikSCAT σ_0 s show a peak-to-peak wind direction modulation of 1 dB at 35 m/s wind speed, and the amplitude of modulation decreases with increasing wind speed. A correction of the QSCAT1 model function for above 23 m/s wind speed is proposed. We explored two microwave radiative transfer models to correct the effects of rain for wind retrievals. Both radiative transfer models have been used to retrieve the ocean wind vectors from the collocated QuikSCAT and SSM/I rain rate data for several tropical cyclones. The resulting wind speed estimates of these tropical cyclones show improved agreement with the wind fields derived from the best track analysis for up to about 15 mm/h SSM/I rain rate. A comparative analysis of maximum wind speed estimates suggests that other rain parameters likely have to be considered for further improvements. [C5305]

"Aspects of the SMOS pre-launch calibration"

A synthetic aperture radiometer system, SMOS, is under development for launch in 2007. The synthetic aperture concept requires calibration activities of novel nature in addition to traditional radiometer calibration exercises. Especially very accurate antenna pattern measurements are an issue. [C5306]

"Development of airborne aperture synthetic radiometer (HUT-2D)"

An L-band airborne radiometer using two-dimensional aperture synthesis (HUT-2D) is under development in Helsinki University of Technology (HUT) for remote sensing. The low measurement frequency is suitable for soil moisture and sea surface salinity measurements. The instrument's technical characteristics are similar to those of the European Space Agency's (ESA) SMOS (Soil Moisture and Ocean Salinity) satellite instrument in order to support ESA in satellite mission instrument development work. The HUT-2D instrument overview and recent test results are presented in this paper. [C5307]

"Performance of STAR-Light receivers during CLPX"

STAR-Light is a 10 element, 1.4 GHz aperture synthesis radiometer being developed at the University of Michigan. It features 3 new technologies: 1) 2-dimensional aperture synthesis using 3-bit correlation, 2) Direct Sampling Digital Receiver (DSDR) architecture, and 3) band definition in the digital definition in the digital

domain. The instrument successfully completed Critical Design Review in the spring of 2002 and is being fabricated as funds become available. As a test of robustness of the receiver design, we are using four STAR-Light receivers in a dual-polarized 1.4 GHz radiometer, and two are used as IF amplifiers in a dual-polarized 6.7 GHz radiometer. Both radiometers will eventually be fully polarimetric. The system is currently deployed near Fraser, Colorado, as part of the NASA Cold Lands Processes Experiment (CLPX) to occur in February and April, 2003. We will report on the performance of these receivers in this relatively harsh environment. [C5308]

"ASAR ERS interferometric phase continuity"

For ten years, a long history of data was acquired by the SAR sensors on the satellite ERS-1 and ERS-2 offering a wide range of interferometric applications. In 2002, the more advanced satellite ENVISAT was launched. The SAR on board on ENVISAT (ASAR) can continue the success of the remote sensing mission of the ERS satellites and preserve or even increase the value of the archived ERS data. The subject of this study is to demonstrate the continuity of the interferometric measurements by the combination of the SAR scene of the different sensors to interferograms (cross interferometry). [C5309]

"ENVISAT multipolarised ASAR data for flood mapping"

During the August 2002 Elbe river flood, different satellite data were acquired, and especially ASAR data from ENVISAT. The advanced synthetic aperture radar instrument was activated in different image modes. Thus, the comparison with quasi-simultaneous ERS-2 data enables to evaluate the contribution of polarisation configurations on flood surface detection. This study highlights the increased capabilities of ASAR for flood mapping, especially benefit of a common use of like- and cross-polarisations. [C5310]

"Cloud liquid water retrievals from aqua AMSU/HSB"

The aqua satellite of NASA's Earth observing system carries, among other instruments, the atmospheric infrared sounder, the advanced microwave sounding unit-A, and the humidity sounder for Brazil, which are used cooperatively to retrieve numerous geophysical parameters, including profiles of atmospheric temperature, ozone, water vapour, and cloud liquid water. This paper discusses the method of obtaining nonprecipitating cloud liquid water and some results from the first year of operation; for example, images of retrieved cloud liquid water show the positions of weather fronts. The retrieval process consists of several stages; cloud liquid water is estimated in the first stage, using the microwave channels. This algorithm seeks to minimize, by iteration, a cost function composed of quadratic functions of the differences between observed and computed brightness temperatures and the differences between the retrieved and a priori atmosphere/surface parameters. The algorithm uses internally a condensation model that relates water vapour and cloud liquid water to a single profile of a humidity variable, through which the a priori statistics of water vapour are introduced. The transition between vapour and liquid (saturation point) is a parameter found by the algorithm, thus allowing for possible error in the retrieved temperature profile. In simulations, the integrated cloud liquid water has rms errors of 50g/m² over water surfaces, and 150g/m² over land surfaces. [C5311]

"ENVISAT ASAR scanSAR interferometry"

We summarize a technique capable to combine SAR acquisitions in different modes, like scanSAR/scanSAR or scanSAR/SAR, and we presents preliminary results achieved by processing early ENVISAT acquisitions in AP and WSM mode. [C5312]

"Validation of ASAR wave mode level 2 product"

One month (March 2003) of ASAR wave mode level 2 data are validated using collocated with ECMWF WAM spectra and wind speed data. The geophysical validation of wind and wave parameters shows good agreement in terms of mean wave periods, T_p , T_{p12} , but the ASAR tends to measure a longer mean swell period ($\approx 0.7s$). for the ASAR level 2 significant waveheight, H_s , saturation effects at high sea-states are observed. Less saturation effects observed when considering only waves with periods above 12s, H_{p12} . Good correlation is also observed for the mean spectral wave direction, π_{12} , for the long wave part of the spectrum. The saturation in H_{sis} mostly due to the well-known effect of azimuth roll-off, which increases with increasing wind sea states. Statistics and global maps comparison are also presented, showing the capabilities of ASAR wave mode to provide global coverage of wave spectral parameters. [C5313]

"ERS-ENVISAT permanent scatterers interferometry"

The permanent scatterers (PS) technique (Ferretti et al, 2001, 2000, Colesanti et al., 2003), is a powerful and fully operational tool for monitoring ground deformations on a high spatial density grid of point-wise targets,

exploiting long series of SAR data. The most attractive aspects of this approach is the capability of providing measurements relative to individual radar targets with unprecedented precision. Up to now, PS analyses have been carried out on ERS, RADARSAT, and JERS data sets. The purpose of this presentation is to discuss the feasibility of updating results obtained by means of a PS analysis on ERS interferometric data using ENVISAT ASAR images. In particular, the main goal is to stitch coherently the new ENVISAT ASAR measurements to the already available ERS displacement time series relative to individual PS. To this end, we will model the interferometric phase of point-wise targets taking account the different ERS and ENVISAT carrier frequencies. Then, we identify the main constraints to be met at individual permanent scatterers in order to guarantee the feasibility of coherent stitching. [C5314]

"Calibrating the quickSCAT/SeaWinds radar for measuring rainrate over the oceans and improving wind vector estimates"

The sensitivity of the SeaWinds scatterometer to rainrates as small as 0.5 mm/hr (for winds less than 6m/s) is a result of backscattering and attenuation by the rain column. This creates both a need to correct the measured radar cross sections, to improve the accuracy of wind vector estimates, and an opportunity to estimate the ocean rain rate to supplement ocean precipitation studies. Both the sea surface and atmospheric rain contribute to the total radar cross section. A comprehensive method is being developed to identify, separate and estimate these two different targets. The goal is to utilize this new method to correct the measured NCRS so that the sea surface reflection can be estimated in a manner that will lead to more accurate wind vector estimates. Also an opportunity exists to estimate the ocean rain rate to supplement ocean precipitation studies. [C5315]

"Campaign mode observation of tropical convection using ground-based radar systems"

Tropical convection plays an important role in enhancing rainfall and also creates uncertainty in the model-based predictions of weather in tropics due to the latent heat released into the troposphere. Ground-based radar systems are important tools available for the effective characterization of convective events. Availability of different radar systems ideally suited to study tropical convection in an area popularly known as the Golden triangle for weather observations in southern part of India, led to the organization of an interagency program for a campaign mode of observations using the different radar systems and associated rain gauges etc. to observe tropical convection during the period Oct-Dec, on a few days when the north east monsoon was prevalent over the east coast of peninsular India. The Golden triangle consists of Sriharikota Island where the Space Launch Complex of ISRO is located at the Satish Dhavan Space Center, the Cyclone Detection Radar site of IMD at Chennai and the National MST Radar Facility (NMRF) at Gadanki in close proximity to the temple city of Tirupati. An indigenously developed S band Doppler weather radar is commissioned at Sriharikota Island on the east coast of India in December 2002, as an interagency program between India Meteorological Department and Indian Space Research Organization. A siphoning type fast response rain gauge and a tipping bucket rain gauge are located within 10 km from the radar. Another S band DWR is located in Chennai, India by IMD. These radars have the capability to measure precipitation and Doppler velocity and provide in real time the 3 base products viz., reflectivity, velocity, and spectral width of the hydrometeors within radar sample volume with good accuracy up to 250 km. From these base products, other meteorological products like rainfall rate, rainfall accumulation, Cappi, echotop etc. are derived. Indian MST radar, a VHF profiler (at 53 MHz) normally used for estimating the winds and turbulence and an L band lower atmospheric wind profiler operating at 1357.5 MHz for estimating the winds, turbulence, and precipitating weather systems in tropical latitudes are operating at NMRF since 1990. Apart from these radar systems, a disdrometer and an optical rain gauge are also located at this facility as collocated instrumentations for the measurement of rainfall rate and rainfall accumulation. All these three locations are geographically located within 80-100 km from each other and form a triangle. These instrumentation systems provide an excellent ground-based network for the characterization of tropical convection. The paper describes the campaign details including the detailed characteristics of the radar systems used and provide intercomparison of the data obtained as the convective systems transited over the terrain which is essentially coastal for Chennai and SHAR and mountainous for Gadanki. [C5316]

"Sensitivity analysis of self-consistent polarimetric rain retrieval to C-Band radar observables"

Numerical simulations are used to investigate the sensitivity of C-Band rain retrieval to polarimetric radar observables. The simulator is based on a T-matrix solution technique, while the hydrometeor distribution have been characterized with respect to dielectric composition (water, ice, and mixed phase), raindrop size distribution (normalized gamma distribution), shape (ellipsoid with parameterized aspect ratio), and angle orientation. The self-consistent ZPHI approach is here adopted and the sensitivity analysis is performed in order to evaluate the expected errors of this method to radar observables. Since differential phase shift KDP is affected by the spatial variation of the backscattering differential phase shift δ , a new neural-network estimation technique is applied to remove δ effects on KDP estimate. The performance of these correction procedures and the effects of an error

bias on radar measurements is evaluated by using mono-dimensional Gaussian raincell models. [C5317]

"A two-scale differential SAR interferometry approach for investigating earth surface deformations"

This paper presents a DIFSAR approach that allows us to detect and follow the temporal evolution of surface deformations at different spatial scales. In particular, our solution extends the capability of the algorithm referred to as small baseline subsets (SBAS) technique (Berardino et al., 2002), and allows us to investigate large scale deformation phenomena as well as displacements of single buildings or structures. The proposed technique relies on small baseline DIFSAR interferograms only, in order to mitigate the decorrelation phenomena, and requires two different sets of data generated at low (multi-look) and high (single-look) spatial resolution, respectively. The algorithm has been tested with the data acquired by the European Remote Sensing (ERS) satellites which are relative to the city of Napoli (Italy) and surroundings; the results have been validated by using geodetic data. [C5318]

"An overview of the Keys area precipitation project (KAPP)"

As part of the NASA tropical rainfall measuring mission ground validation (TRMM-GV) program, a field campaign was conducted in Florida Keys during August-September 2002. The purpose of the field campaign was to study the characteristics of rainfall over the Florida Keys, utilizing Key West WSR-88D, NASA's s-band polarimetric radar (NPOL), and a network of rain gauges and disdrometers. This study focuses on the performance of the rain gauges and disdrometers and its impact on the radar rainfall algorithms. [C5319]

"Multivariate probability matching of satellite infrared and microwave radiometric measurements for rainfall retrieval at the geostationary scale"

The objective of this paper is to investigate how the synergy between low-earth-orbit (LEO) microwave (MW) and geostationary earth orbit (GEO) infrared (IR) radiometric measurements can be exploited for satellite rainfall detection and estimation. Rainfall retrieval is pursued at the space-time scale of typical geostationary observations, that is, at a spatial resolution of few kilometers and a repetition period of few tens of minutes. The basic idea behind the investigated statistical integration methods follows an established approach consisting in using the satellite MW-based rain-rate estimates, assumed to be sufficiently accurate, to calibrate spaceborne IR measurements on limited sub-regions and time windows. The proposed methodology is focused on a new statistical approach, namely the multivariate probability matching (MPM). The MPM method is rigorously formulated and systematically analyzed in terms of relative detection and estimation accuracy. [C5320]

"Radar estimate of attenuation at K band in stratiform rain using a physical model of the melting layer"

A technique for the identification of the microphysical characteristics of stratiform precipitation is presented. It allows to estimate the attenuation at microwave frequencies from radar measurements of reflectivity. [C5321]

"NPOESS Field Terminal Segment"

The National Polar-orbiting Operational Environmental Satellite System (NPOESS) Field Terminal Segment (FTS) consists of three components: the signal processing subsystem, the data processor element, and the mission application subsystem (MAS). The NPOESS program scope of work for field terminals includes development of procurement specifications for High Rate Data (HRD) field terminal and Low Rate Data (LRD) field terminal configurations, development and delivery of the data processor element software, and generation of interface control documents for the field terminal interfaces. [C5322]

"Improving the detection capability of spatial failure modes using downward-looking sensors in terrain database integrity monitors"

This paper discusses various methods of improving the detection capability of horizontal and vertical failure modes for a terrain database integrity monitor that is purely based on the inputs from downward looking sensors. Terrain database integrity monitors which use radar altimeter and GPS inputs have previously been proposed for Synthetic Vision Systems (SVS). An SVS provides pilots with either a Heads Down Display (HDD) or a Heads Up Display (HUD) containing aircraft state, guidance and navigation information, and a virtual depiction of the terrain as viewed "from the cockpit". The source used to generate the terrain depicted on these displays is a Digital Elevation Model (DEM). Due to the compelling nature of the displays, it is quite possible for the pilots to use the display for functions other than its original intended function. It may be hard to avoid such a scenario, especially if the system is certified as an advisory system. When using SVS display technology for functions other than advisory it may be necessary to include a DEM integrity monitor whose performance is specified by

probabilities of Missed Detection, Fault-Free Detection and Time-to-Alarm. Ideally, the DEM represents the height or elevation of the terrain at corresponding coordinates (e.g. latitude and longitude) expressed in a predefined vertical datum. However, the given elevations deviate from the true elevations due to systematic and blunder errors that are present in the DEM primarily due to the way in which they are generated from different sensor technologies such as photogrammetry, remote sensing, etc. and the manual post-processing process. Another source of error of lesser significance is the flat earth approximation over relatively larger areas, while collecting the data. The described integrity monitor method is based on the comparison of the DEM terrain profile with an independent terrain profile synthesized from a downward looking sensor (Radar Altimeter) and GPS-Wide Area Augmentation System (WAAS) measurements. Due to the inherent presence of sensor measurement noise and random errors in the DEM, it is not possible to detect vertical biases and horizontal translations in the DEMs in an absolute sense, but only in a statistical manner. When considering the probability-of missed detection, a region of uncertainty can be defined as the geo-spatial region that contains the set of all possible aircraft positions surrounding the true position which do not result in an integrity alarm, given the presence of a DEM failure. The integrity monitor's capability to detect horizontal failure modes is directly related to the extent of the uncertainty or missed detection region; the smaller the region, the better the integrity monitor is capable of detecting a horizontal failure. A method is proposed to detect horizontal failures, which monitors the Kalman filter's covariance matrix over the region of uncertainty. A similar concept as that used for integrity monitoring has been explored for its potential applications in terrain navigation. Flight test data from NASA's flight trials at Eagle/Vail (EGE), Colorado and Ohio University's flight trials in Juneau (JNU), Alaska is used to evaluate the performance of the proposed methods. [C5323]

"Wireless IC Doppler radars for sensing of heart and respiration activity"

Remote monitoring of respiration and heart activity can be implemented using wireless communications technology and Doppler radar techniques. Such monitoring has been demonstrated by leveraging existing wireless technology. RFIC's developed for wireless base stations have been reused to produce hybrid and fully integrated Doppler radars for vital signs sensing. Heart and respiration activity were observed using these radars at a distance of up to one meter. This technology can potentially enable low-cost, noninvasive long term monitoring of chronic and recovering patients. [C5324]

"Recursive transform-based phase unwrapping"

We present an improved transform-based phase unwrapping (PU) system that employs a recursive structure. Each stage, which is identical with others, performs PU by FFT method and gives a solution as well as a residual (phase) error. The residual error is then reprocessed by the following stages. Experimental results for simulated and real InSAR phase images show significant improvement over conventional results of a single stage system. [C5325]

"Modeling and simulation of the fused Bayesian-regularization method for remote sensing imagery with synthetic aperture arrays"

A new fused Bayesian regularization (FBR) method for enhanced remote sensing imaging based on a new concept of aggregated statistical-deterministic regularization was developed recently. In this study, we represent the results of modeling and extensive simulation of the FBR algorithms for enhanced reconstruction of the spatial spectrum patterns (SSP) of the point-type and spatially distributed wavefield sources as it is required for the remote sensing imagery with synthetic aperture arrays. The simulations were performed in the MATLAB computational environment for the family of the SAR imaging algorithms that employed different modifications of the FBR method. The presented results enable one to evaluate the operational performance of the FBR method that was not previously reported in the literature. [C5326]

"Synthetic aperture antenna for near field applications"

Preliminary results of implementation of a new approach to design of scanning antennas are presented. Combining mechanical movement of a simple radiator along a real aperture of a stationary antenna with the concept of the antenna aperture synthesizing is the main idea of that approach. Helical-slot synthetic aperture antenna has been suggested, designed and tested in Ka-band. The tests shown a good agreement with theoretical evaluations, as well as a high efficiency of the suggested antenna in transmit/receive operating mode. The antenna in the near-field zone for relatively small real antenna apertures provides a high azimuth resolution. [C5327]

"Performance evaluation of a memory-based TCP-friendly rate adaptation algorithm for a real-time radar application"

Implementing a TCP-friendly congestion control mechanism is imperative for emerging UDP-based real-time, high-bandwidth applications such as multimedia. VCHILL project for digitized radar data transfer over the Internet is one such application for which a source based TCP-friendly rate adaptation based on loss (TRABOL) algorithm is deployed and shown to be TCP-friendly over applicable timescales. Comparison of the TRABOL-based radar application with other non-congestion controlled UDP flows shows that the application performs better with TRABOL and is fair towards neighboring TCP flows. Implementation of a simple memory-based mechanism as an add-on to the TRABOL algorithm enhances the performance of the application. [C5328]

"Air- and space borne remote sensing systems for traffic data collection -European contributions"

The increasing volume of traffic and transport rates in Europe and in other continents require new methods of traffic data recording as well as an intelligent traffic management, which fits the intermodal and cross-boarder traffic. Simultaneously it has to take in account that the EU enlargement in particular into Eastern European economic areas corresponds with an expandability of trans-national traffic management in Europe. The air and space borne remote sensing technologies have the highest potential to solve the sustainable traffic problems. With this it is merely possible to open up potentials of traffic route infrastructure identified by scientific research and to transfer the results of present rural approaches to European scale. It will result in a standardization of traffic data in terms of quality and quantity which is the key point for an integrated and sustainable traffic management in Europe for the future. A special session for the European contributions on this new ITS-topic gives the possibility for a better cooperation in international research. [C5329]

"Role of nonlinear optics in NASA remote sensing program"

Nonlinear optics is essential to the development of lidar and DIAL wavelengths. Harmonic generation is used to generate widely spaced wavelengths needed for atmospheric component measurement. Seeding is accomplished by using the idler from a LiNbO₃parametric oscillator pumped by Nd:YAG laser. [C5330]

"Modelling of remote sensing characteristics of salt wet soils in decimeter wavelength range"

This paper describes the modelling of microwave remote sensing characteristics, which could prove to be valuable in monitoring processes on desertization, as sample salinisation of soils. This paper presents the results of numerical experiments on modeling the influence of salinity of wet soils on their radar sensing characteristics in P- (70 cm) wavelength range with the influence of a vertical profile of the soil humidity distribution. [C5331]

"Co-histogram and its application in remote sensing image compression evaluation"

Peak signal-to-noise ratio (PSNR) has found its application as an evaluation metric for image coding, but in many instances it provides an inaccurate representation of the image quality. The new tool proposed in this paper is called co-histogram, which is a statistic graph generated by counting the corresponding pixel pairs of two images. For image coding evaluation, the two images are the original image and a compressed and recovered image. The graph is a two-dimensional joint probability distribution of the two images. A co-histogram shows how the pixels are distributed among combinations of two image pixel values. By means of co-histogram, we can have a visual interpretation of PSNR, and the symmetry of a co-histogram is also significant for objective evaluation of remote sensing image compression. Our experiments with two SAR images and a TM image using DCT-based JPEG and wavelet-based SPIHT coding methods perform the importance of the co-histogram symmetry. [C5332]

"Road network extraction in remote sensing by a Markov object process"

In this paper, we rely on the theory of marked point processes to perform an unsupervised road network extraction from optical and radar images. A road network is modeled by a Markov object process, where the objects correspond to interacting line segments. The prior model, called "quality candy" model, is constructed so as to exploit as far as possible the geometric constraints of this type of line network. Data properties are taken into account in the density of the process through a data term based on statistical tests. Optimization is realized by simulated annealing using a RJM-CMC algorithm. Some experimental results are provided on aerial and satellite images (optical and radar data). [C5333]

"Removal of impulse bursts in satellite images"

Characteristics of impulse bursts in satellite images are analyzed and methods for burst removal are considered. Artificial compact burst model is proposed and test images are created. An advanced multipass algorithm for the detection and removal of compact bursts in the presence of both additive and multiplicative noise is proposed. The efficiency of the algorithm is evaluated quantitatively using the artificial test images and visually using the

artificial test images and real radar and optical satellite images. It is shown through experiments that the proposed method removes impulse bursts efficiently while preserving information [C5334]

"Remote sensing of troposphere for aviation safety: antenna aspect"

Techniques of microwave remote sensing of the atmosphere with the emphasis to the aviation applications are considered. Some results recently obtained are presented including joint research projects of NAU and IRCTR. Specificity of antennas is discussed. The paper mainly reflects the works, which were done with author participation, and does not aspire to saturation coverage. [C5335]

"Global three-dimensional FDTD modeling of impulsive ELF propagation about the Earth"

This paper has reported the initial application and validation of the FDTD method to model impulsive ELF propagation within the entire Earth-ionosphere cavity. This technique permits direct, 3-D, time-domain calculation of impulsive, round-the-world ELF propagation accounting for arbitrary horizontal as well as vertical geometrical and electrical inhomogeneities and anisotropies of the excitation, ionosphere, lithosphere, and oceans. We expect that this model will be useful in studies of ELF propagation phenomena which form the physics basis of important remote-sensing investigations of lightning and sprites, global temperature change, and subsurface structures. [C5336]

"Neural network for LIDAR detection of fish"

In this paper we present a neural network for detection of fish, from light detection and ranging (LIDAR) data and have described a classification method for distinguishing between water-layer, bottom and fish. Four multi-layer perceptrons (MLP) were developed for the classification purpose, where classes include fish, bottom and water-layer. The LIDAR data gives a sequence of intensity of laser backscatters obtained from laser shots at various heights above the Earth surface. The data is preprocessed to remove the high frequency noise and then a window of the sample is selected for further processing to extract features for classification purposes. We have used linear predictive coding (LPC) analysis for the feature detection purpose. The results show that the detection technique is effective and can do the required classification with a high degree of accuracy. We have tried our approach with four different MLPs and are presenting the data obtained from each of them. [C5337]

"Multiscale SAR image segmentation using a double Markov random field model"

In this paper, we propose a multiscale Bayesian segmentation algorithm for SAR image. This approach uses a hierarchical two-level Markov random field (MRF) to represent both texture and region label over the wavelet lattice. The high level uses an isotropic multilevel logistic (MLL) random field to characterize the blob-like region formation process at each scale and the interscale dependencies over the corresponding multiresolution region. At lower level a novel causal Gaussian autoregressive (CGAR) process is proposed to describe the fill-in of multiresolution region. Once the multiscale double MRFs model is established, in term of sequential maximum a posteriori (SMAP), model parameter estimate and region segmentation are performed alternately from coarse to fine scale. Our segmentation method is tested on both synthetic and ERS-1 SAR images. [C5338]

"Comparing RADARSAT-1 and IKONOS satellite images for urban features detection"

In this paper, a comparison of the visual appearance and detection of different man-made objects in an urban area in Norway is presented using IKONOS and RADARSAT-1 images. Results show that RADARSAT-1 fine mode images add very limited information to the IKONOS panchromatic image for many mapping applications. One explanation for the seemingly lack of information from the synthetic aperture radar (SAR) data, is that the IKONOS sensor image the Earth ground with a resolution of 1 m, while the RADARSAT-1 fine mode only has 9 m resolution. Despite these matters, it is shown that RADARSAT-1 may uniquely detect certain objects or structures and thereby give additional knowledge to the interpretation of an IKONOS image. Multi-temporal RADARSAT-1 acquisitions can also be used to detect man-made changes at times when weather conditions hamper optical image acquisitions. It is expected that new SAR satellites with resolutions down towards 1 m, work much better as a complementary, all-weather information source to the optical ones. [C5339]

"Ground penetrating radar (GPR) studies at the ElectroScience Laboratory (ESL)"

There are a number of factors to be considered in making many GPR measurements. These include (a) electronic hardware (b) antenna systems (c) electromagnetic properties of the ground (d) target identification and remote sensing concepts and (e) use of numerical simulations. The purpose of this paper is to review the contributions made at the ESL for these factors and to discuss future potential advances in the state of the art. [C5340]

"Microwave remote sensing research at the ElectroScience laboratory"

The ElectroScience Laboratory (ESL) at The Ohio State University has made many important contributions to the development of microwave remote sensing, both in theory and practice. The term "remote sensing" is very broad, and could be interpreted to include ESL efforts in areas such as ground penetrating radar technologies, studies of microwave propagation through the atmosphere, contributions to the development of polarimetric concepts for radar, studies of the ionosphere, and experiments and modeling of optical propagation in the atmosphere. More general ESL contributions that play a role in the remote sensing area also include the development of new antennas, radar technologies, and general electromagnetic modeling methods. However, this paper focuses specifically on the "microwave remote sensing" area, where applications involve active or passive microwave sensors used to observe geophysical environments in order to retrieve information about those environments. [C5341]

"Research on the quickly evaluation of flooding disaster based on the parallel geographic image processing system"

Using parallel geographic image processing system, the flooding disaster will be monitoring and evaluating in time. Using ParGIP to establish background database and process RS images, we can get the losses of the disaster by overlaying operation in 24 hours. According to the experiment in the Poyang Lake region, this method can promote the speed and the efficiency of the monitoring and evaluating of flooding disaster to several times. [C5342]

"Antenna-based processing of the radar data for zone detection in remote sensing imagery"

A new approach is addressed to perform antenna-based processing of radar imagery data aimed at reconstruction/enhancement of the images degraded by a spatially-shift-invariant radar spread function and contaminated with additive Gaussian noise. The fused maximum entropy-variational method is developed and computationally implemented using the modified Hopfield neural network. Enhanced zone detection and image denoising are achieved using the proposed approach. [C5343]

"Remote monitoring of sea surface HFSWR"

The paper considers an excellent electrodynamics model of an excited sea surface when it is interpreted by spectral components of the backscattered HF signal for remotely monitored targets. A peculiarity of the application of the electrodynamics model is supposing that the excited sea surface section is a quasi-periodic random antenna array with elementary resonators. [C5344]

"Estimation of ocean surface currents beyond the region of overlap of dual-site HF radar"

High-frequency ground wave radar (HFGWR) has emerged as a valid tool for the sensing of ocean parameters. If there are at least two radars covering the same patch of ocean then geometric considerations can be used to construct a complete vector current. Unfortunately, the region of overlap for two radar sites is smaller than the total single site coverage and other techniques are needed to estimate vector currents outside the common coverage area. The continuity of flow equation uses knowledge of vector currents within the overlap and radial current information outside the overlap to extrapolate tangential current data outside the overlap thereby increasing the region where vector current information is known. This approach has not been previously applied to a narrow-beam, long-range radar. Tests of the radar facilities conducted in the summer and fall of 2002 show that this technique achieved good comparisons between the radar-derived vector currents and continuity-derived vector currents for ranges up to 350 km for one azimuthally adjacent range cell. [C5345]

"An optimal wavelet for raw SAR data compression"

Synthetic aperture radar (SAR) is a sophisticated remote sensing tool that is capable of providing high resolution images from a moving platform. Due to the very poor correlation and high entropy of SAR raw data, redundancy reduction techniques have not proven successful and a lossy compression is necessary. In a previous work, we have presented a compression of the raw SAR signal using five kinds of wavelets. The quality reconstruction was very good, however, due to noise like characteristics of the raw SAR signal, none of the standard wavelets was very efficient in compacting energy in the transform domain. In this paper, we propose to determine an optimal 2-D wavelet which is learned directly from the raw SAR data. The optimality criterion in the learning processes is redundancy minimization in the transform domain. Experiments show that this optimal wavelet performs better than the standard wavelets. [C5346]

"Agent communication based SAR image parallel processing"

Airborne SAR remote sensing image has the characteristic of large data volume and computation burden, so the processing needs very large computer memory and stronger computation ability. Based on the introduction of the SAR image processing procedure, we study the SAR image processing using computer parallel computation technology. The parallel processing mechanism is based on the parallel computer cluster operation and the large virtual shared memory technology. In the client/server architecture based SAR image parallel system, agent based network communication plays an important role in the computer performance monitor and burden distribution. In the end, the application of the SAR image parallel processing system in the disaster monitor and assessment system is introduced. The application result illustrates the high efficiency of the system and the feasibility of our research. [C5347]

"Vegetation and forestry study by radar remote sensing"

Remote sensing data obtained by airborne side-look radars over wide frequency ranges is analyzed. Relationships between backscattered signal and parameters of the investigated underlying surface have been derived. The classification of vegetation growth and forestry on test sites has been performed. [C5348]

"Progress in high-spectral resolution lidars for remote sensing of the environment"

Recent progress in the high-spectral resolution lidar technique is reviewed. The new system is used for precise remote sensing of atmospheric aerosol parameters, temperature and wind velocity for practical applications in meteorological and industrial monitoring. [C5349]

"Automatic correction of optical alignment deterioration of a continuously operated Mie lidar"

Alignment of the laser beam and telescope axes is crucial to the acquisition of high quality lidar data. For a continuously operated Mie lidar, a routine alignment correction is needed to ensure that its data are not influenced by the misalignment and thus truly represent the aerosol and cloud behavior. This paper describes the operation of such a lidar system with automatic correction of optical alignment. [C5350]

"ACA lidar system for continuous monitoring of aerosols, dust and cloud in troposphere at Suwon, Korea"

Using by Automatic Control Aerosol (ACA) Mie lidar system, continuous time-height indication plots of range corrected backscattered intensity, depolarization ratio, and IR/visible ratio of Asian dust, aerosols, and cirrus clouds in the altitude range of 0.5-15 km have been measured and analyzed. [C5351]

"An algorithm of bridge detection in remote sensing images based on fractal"

This paper presents a new method to detect the bridge in synthetic aperture radar (SAR) images based on fractal. In this method, the gray surface of SAR image is model as a DFBR (discrete fractional Brownian random) field. In the homogenous region of SAR image, the H (Hurst) exponent of DHFR is almost the same but in the sharply change region such as the boundaries of bridge, the H occurs as singularity. According to this characteristic, the bridge can be detected and extracted. In order to alleviate the influence of the speckle of SAR image, an idea of mean was introduced into this algorithm. Experiment results show this algorithm is very effective and superior to other classical edge detection operators. [C5352]

"An algorithm for remote sensing imaging of moving target with conventional narrow-band radar"

This paper studied the problem of imaging the moving target in cross range direction by using conventional narrow-band radar and indicates that the key technique to obtain the cross range profile of target is motion compensation. In this paper, after the analysis in theory, a motion compensation algorithm based on third order polynomial coefficients estimation was proposed. In order to optimize these estimating coefficients, an optimal criterion was also presented. Moreover, this paper also proposed an algorithm to estimate the cross-range resolution. Simulation results show the presented method of cross range imaging is effective and the algorithm of estimating the resolution is reasonable. [C5353]

"Compact long-path absorption laser radar system for measuring greenhouse molecular concentration"

A compact long-path absorption laser radar system has been developed incorporating a single-mode optical parametric oscillator with the PPMgLN crystal for methane concentration measurements. Spatial distribution can

be derived using topographic targets as the reflectors at several directions. [C5354]

"Ocean imaging using multichannel along track interferometry"

An airborne multichannel along track interferometer (MATI) is described and discussed. This MATI system is based on an X-band SAR installed in a BAE/BAC 1-11 aircraft which can be set up with 2, 3 or 4 beams. It is demonstrated that a MATI can be used to Doppler filter radar signals acquired from a moving platform which are scattered by moving and partially coherent scatterers. Processing techniques are described for the removal of phase errors. These phase errors are caused primarily by the separation of the antennas in range due to the aircraft installation, and by aircraft roll, pitch and yaw motions. The basis of the processing technique is a two stage phase screen which is capable of compensating the differential phase errors between each image in a multichannel set to the precision required for Doppler filtering. It is shown that optimal filtering may be applied to the scattered radar signals by adaptively varying complex weights applied to each channel until an extremum of a selected image measure is obtained. Hence, if a certain type of scatterer is associated with energy located in a particular part of the Doppler spectrum, and an image feature results from the modulation of this type of scatterer, then the visibility of the feature can be maximised using an adaptive MATI. An example is presented showing the technique applied to a sandbank image. [C5355]

"Atmospheric radar for the 0.5-110 km region"

Radar can be used to make measurements of the dynamics and structure of the atmosphere by detecting irregularities in refractive index due to variations in humidity and temperature in the lower atmosphere (0-20 km), and due to variations due to fluctuations in electron density in the mesosphere lower thermosphere (MELT) region of the upper atmosphere (50-110 km). MF and HF radars have been used to routinely investigate the MLT for over 50 years. Wind profiling radars operating in the VHF band have been used for about 25 years to investigate the stratosphere troposphere (ST) region, but only routinely in the last 15 years. Considerable development has occurred within the past decade. In particular, great attention has been paid to interferometric and imaging techniques, to a re-examination and extension of MF radar techniques, to the application of VHF radars developed for atmospheric research to meteor studies, and finally, a rebirth of dedicated meteor radars has occurred. Here we briefly describe some of these recent improvements. [C5356]

"Low-cost realisation of space-borne synthetic aperture radar-MICROSAR (September 2003)"

This paper presents an overview of the MicroSAR satellite, showing the approach adopted to realise a truly low cost space-borne SAR system. The rationale leading to the proposed design, an outline of the overall structure of the associated imaging system, a review of the performance estimated for the resulting MicroSAR imaging system and a view of the airborne demonstrator, are provided. [C5357]

"Advanced synthetic aperture radar imaging and feature analysis"

We review and discuss advanced algorithms for synthetic aperture radar image formation, the effect of motion perturbation on radar imaging, synthetic aperture radar imaging of ground moving targets, and micro-Doppler feature analysis. [C5358]

"Multi-image satellite SAR interferometry: state of the art and future trends"

In this paper, we wish to review briefly the principles underlying a recently developed approach, known as the permanent scatterers (PS) technique and aimed at the joint exploitation of a series of spaceborne interferometric SAR images for the retrieval of high precision elevation and ground deformation data on a sparse grid of privileged point-wise radar targets. [C5359]

"Description and applications of the multipolarized dual band OrbiSAR-1 InSAR sensor"

In the last decade, interferometric SAR (InSAR) has reached a wide acceptance as being a suitable tool to generate high-precision digital elevation models. Especially in tropical areas, with nearly permanent cloud coverage, InSAR provides a cost-efficient means for mapping large areas in short time periods. However, the interaction of microwaves with vegetation is strongly dependant on their frequency, demanding a careful interpretation of the extracted information. Short waves like X-band are mainly scattered back from the top of the canopy, whereas P-band penetrates the foliage and gets reflected from trunk and soil, thus carrying the phase information (and therefore the height information as well) from bald earth. For the generation of topographic maps, generally the ground elevation rather than the surface elevation is required, whereas the surface and ground elevation together enable the estimation of additional physical parameters like vegetation height, density, or biomass. [C5360]

"An algorithm of road detection in remote sensing images based on B-spline wavelet"

This paper presents a new method to detect the road in synthetic aperture radar (SAR) images based on B-spline wavelet. In this method, B-spline wavelet is constructed firstly. The roads can be detected by searching the maximal amplitude of the SAR images' wavelet transform. In order to alleviate the influence of the speckle of SAR image, an idea of mean was introduced into this algorithm. Experiment results shows that the algorithm is very effective and superior to other classical edge detection operators. [C5361]

"Microwave remote sensing: needs and requirements concerning technology"

Spaceborne microwave remote sensing instruments, like the imaging radiometer and the synthetic aperture radar, are over time faced with two partly conflicting requirements: performance expectations (resolutions, sensitivity, coverage) steadily increase with resource allocations (weight, power, bulk, cost) decrease. This results in needs and requirements to the development of advanced technology thus enabling the future advanced systems to be viable and realistic. [C5362]

"Advance MMICs for remote sensing and radar applications"

Modern remote sensing systems and radars are more and more based on electronically steered antennas. Instead of using one high power tube, each radiating element must contain a full T/R module allowing an individual modulation of amplitude and phase of both transmit and receive signal. The key elements in such systems are monolithic microwave integrated circuits. In this paper some general information about these components are given as well as the latest achievements in terms of power amplifiers are described. The CHA7010 is a 10W power amplifier (in pulse mode) featuring high PAE and small size. [C5363]

"Ultra-wideband MMICs for remote sensing applications"

This paper presents an overview of the current activity at the Technical University of Denmark in the field of ultra-wideband monolithic microwave integrated circuits (MMICs) for next generation high resolution synthetic aperture radar (SAR) systems. The transfer function requirements for MMIC components in a wideband SAR system are described. The design and performance of a DC-to-X-band SiGe HBT quadrature mixer and a C-band GaAs pHEMT downconverter are described. Experimental results demonstrate the usefulness of the designs for quadrature modulations/demodulation and downconversion of ultra-wideband linear FM-modulated signals. [C5364]

"Optimisation transmitter-receiver location in bistatic SAR"

This paper presents the results of space ambiguity functions of bistatic and multistatic synthetic aperture radar. We have obtained equations, which make it possible to optimize the attitude of transmitter and receiver in order to provide maximum distance resolution. Presented are results of simulation of aerospace SAR with pseudo noise signals. [C5365]

"Research institute "Orion" has more that 40 years experience in the field of microwave and millimeter-wave technology"

"Orion" facilities currently include a modern CAD system for computer aided design; microelectronics assembly area; semiconductor integral circuit processing facility. The space of semiconductor and microwave tube facility is subdivided into several areas for specific technological processes that include final fabrication and testing. Microwave tube facility enables "Orion" to develop and fabricate microwave and millimeter wave medium power TWT and klystrons. The variety of C.W. and pulsed, narrow band and wide band TWT are developed for the frequency bands up to 40 GHz. Semiconductor facility enables "Orion" to fabricate PIN diodes, Schottky, Gunn and IMPATT diodes for production of microwave and millimeter wave components. Microwave systems on the basis of such components perform critical functions ranging from communication, radiometry, and spectroscopy to radar, remote sensing and physical measurements. This "Orion" capability is the key to success of several strategic commercial and military products. [C5366]

"Spaceborne synthetic aperture radar (SAR) systems: state of the art and future developments"

This paper first summarizes the state of the art in spaceborne SAR systems and applications. The second part of this paper gives an overview of new concepts, techniques and technologies for future SAR systems, allowing an increase of flexibility the SAR operation mode as well as a reduction in the overall system costs. Several innovative concepts and technologies as bi and multistatic configurations, parasitic SAR, sparse aperture

systems and digital beamforming will play an important role for future spaceborne SAR constellations. [C5367]

"Optimal design of broadband loaded receiving antenna for HFSWR using simulated annealing"

One of the major challenges in using coast-based high frequency surface wave radar (HFSWR) is, for the purpose of the long-range detection of ships and aircraft as well as icebergs, or the remote sensing of the ocean environment using the coast-based HFSWR, how the size of transmitting and receiving antennas are reduced at lower end of the HF band. In this paper, according to the operating frequency bandwidth for a HFSWR, where both the gain and the voltage standing wave ratio (VSWR) of a receiving monopole can satisfy the requirement of engineering design, it mainly describes the process in which the loading circuit parameters, locations of the loads along the antenna, as well as matching network parameters are optimized by the simulated annealing algorithm (SAA) to achieve a VSWR less than 3 in the operating frequency bandwidth. Several examples antennas illustrate that the SAA is an effective method for designing HF broadband loaded antennas. [C5368]

"Low-grazing backscattering efficiency from clustering vegetation"

A low-grazing scattering model for vegetation where leaves occur in clusters is developed in this paper. Taken into account of the coherent effects from different clustering scatters. Monte-Carlo method is applied to simulate the low-grazing backscattering from the clustering vegetation that which is distributed randomly or regularly respectively. The results are good used to explain the backscattering enhancement and the grazing incidence characteristic of the clustering vegetation. [C5369]

"Wave scattering in random media and its application to remote sensing"

This paper deals with wave scattering by a body in a continuous random medium and multiple scattering by a discrete random medium with many dielectric particles; in particular, addresses methods for analyzing the above two types of scattering and shows the scattering characteristics computed by the methods. The application is also discussed to remote sensing of water contents in soil. The results presented here have been derived from my laboratory. [C5370]

"Determination of vertical distributions of aerosol optical parameters by use of multiwavelength lidar data"

We propose a lookup table method to derive vertical distributions of aerosol optical parameters in the troposphere from multiwavelength observations using a Mie-scattering lidar. The method is characterized by the capability of treating generalized aerosol size distributions, as well as by rapid convergence of the iteration procedure. The methodology and numerical simulation are described. [C5371]

"Progress in high-spectral resolution lidars for remote sensing of the environment"

Recent progress in the high-spectral resolution lidar technique is reviewed. The new system is used for precise remote sensing of atmospheric aerosol parameters, temperature and wind velocity for practical applications in meteorological and industrial monitoring. [C5372]

"ISAPE'03. 2003 6th International Symposium on Antennas, Propagation and EM Theory (IEEE. Cat. No.03EX681)"

First Page of the Article [C5373]

"Urban land-cover classification: an object based perspective"

Up to date and accurate urban land cover information is needed in a variety of applications, e.g. urban planning and management. However, depending on traditional surveying tools, especially in large metropolitan cities, to produce such data is a time consuming and expensive task. This has initiated the need to classify remotely sensed data to extract urban land cover information. A new classification approach (object based) has been recently proposed and is currently being investigated. In this research the classification accuracy of object-based classification is tested against statistical classifiers using two images (Landsat and IRS). Results have shown that object based classification yields better classification results. [C5374]

"Gigabit networking: digitized radar data transfer and beyond"

Gigabit networking makes possible the remote access to expensive and specialized facilities that were inaccessible in the past due to limited bandwidths. VCHILL project for digitized radar data transfer is one such

real-time application that will tap the next generation Internet technology to provide interactive access to real-time and stored data generated by weather radars, thus revolutionizing the way experiments are carried out. The design and implementation of the deployment of an efficient congestion control algorithm for this application are presented. The TCP-friendly rate adaptation based on loss (TRABOL) algorithm is a source-based rate control mechanism that controls the transmission rate based on the feedback about losses experienced by the client station. The performance results show that the deployment of this algorithm makes the application TCP-friendly. [C5375]

"Landmine detection technology research programme at TNO"

This presentation gives an overview of most of the activities on research and development in the technology area for landmine detection at TNO in the Netherlands. The projects cover the range from military applications to humanitarian demining. In the "conventional" detection systems area the activities on an instrumented prodder, metal detection, ground penetrating radar thermal infrared are covered. Signal processing and sensor fusion are key activities in this area. The focus for these techniques is on vehicle mounted and airborne multi-sensor systems. The activities are supported by more fundamental modelling of the interaction of sensors with the landmines. Especially the effects of the environment of the mines (background clutter, scenario) on this interaction are taken into account. [C5376]

"Output characterization of ground-based and integrated optical sensor for retrieved aerosol error minimization"

Lidar (Light Detection and Ranging) Raman outputs signals cannot be acquired in digital way because of technical restrictions in its present configuration. On the contrary, DIAL (Differential Absorption Lidar) Lidar has this opportunity due to the instrumentation operating mode. Remote-monitoring laser instrumentation has the capability of detecting energy backscattered from the atmosphere, namely coming particularly from aerosol particles. In spite of the presence of filtering devices in the system, output signal is affected by different noises. One of the main optical sensing instrumentation, based on laser technique, is lidar (light detection and ranging). In this paper we describe an alternative way of characterizing information content of an experimental lidar in order to minimize the error of retrieving aerosol. In this way, by using digital filtering, we can optimize the output signal with respect to noise. We also do a comparison between traditional window technique and adjustable one using Kaiser procedure. [C5377]

"Non-uniform sampling issues arising in shallow angle wave profiling LIDAR"

Non-uniform sampling has been identified as a fundamental property in the shallow angle remote sensing required to collect the data required to build DSWP prediction models for moving vessels. The dependence of typical DSWP models on traditional discrete spectral techniques introduces the requirement to re-map sets of N non-uniform sea profile data onto uniformly sampled equivalents. The high computational cost of the general change of basis involved in this process and its detrimental effects upon prediction time motivated an examination of approximation methods. A metric IF is discussed which measures the degree of departure from uniformity in terms of the Primary Band Limitation property which is associated with a generalisation of Nyquist's theorem. Various levels of approximation are examined based upon the extent of the departure of Γ from unity. The major conclusion is that for each set of N remotely sensed data values which constitute a sea profile scan it is possible to assess the level of computational sophistication required to render the data set suitable for use in DSWP. This ability is central to the design of an the intelligent system architecture which is required to operate a viable DSWP unit. [C5378]

"On the estimation of interferometric phases for multibaseline SAR interferometry using a relaxation-based technique"

In this paper, we examine how one can exploit baseline diversity of a multichannel interferometric SAR system to overcome the layover problem. The problem arises when different height contributions collapse in the same range-azimuth resolution cell, due to the presence of strong terrain slopes or discontinuities in the sensed scene. We propose a multilook approach to counteract the presence of the time-and-space varying amplitude distortion which is due to the extended nature of natural targets; to this purpose we extend a recent relaxation based approach by estimating the interferometric phases using a nonlinear least squares estimation technique that is based on a deterministic modelling of the amplitude distortion. [C5379]

"High frequency radar astronomy with HAARP"

At high frequency, radio waves will interact with space plasmas and surfaces of local astronomical objects,

producing an echo that can provide new diagnostic data. The availability at high power radars operating at high frequencies opens a window for the remote investigation of our surrounding space environment. We discuss and illustrate this technique with some specific examples. [C5380]

"Terahertz-frequency remote-sensing of biological warfare agents"

This paper presents a detailed assessment of terahertz-frequency spectroscopy as a technique for the remote detection of biological warfare agents. Design studies are presented for a differential-absorption-radar (DAR) approach that utilizes the spectral signatures of *Bacillus* (B.) *subtilis* spores within the terahertz (THz) regime as the detection mechanism. The signature data used in these studies is taken from laboratory measurements performed on uniform thin films of B. *Subtilis* spores and the system performance is assessed for both incoherent and coherent detector modalities. These studies consider DAR remote sensing of biological (bio) clouds at significant ranges (i.e., 1 km) and include the effects of realistic atmospheric conditions. A high-level remote-sensor design is used to estimate the probabilities of detection (pd) and false-alarm (pfa) associated with this general technique. These studies suggest useful remote-detection performance can be achieved (i.e., $pd > 0.9$ & pra_{10-4} for bio-cloud densities 3cm^{-3}) at 1 km ranges if the THz signature information remains predictably stable under varying atmospheric conditions (e.g., changes in humidity, spore activity state, etc). Furthermore, a realistic bio-agent airframe attack scenario is utilized to demonstrate standoff detection of bio-clouds with 100% confidence while outside the threat-level concentrations. All together, these results demonstrate that standoff detection of bio-agents is feasible for threat-level concentrations in practical battlefield environments at sufficient ranges to provide for early warning. [C5381]

"Generalized optimization of polarimetric contrast enhancement"

The optimization of polarimetric contrast enhancement (OPCE) is one of important problems in radar polarimetry. The traditional OPCE is to choose optimal polarization states for enhancing a desired target versus an undesired target/clutter. The contrast enhancement enables us to discriminate or distinguish the desired target from background or from the undesired target. We propose a generalized OPCE (GOPCE). For the GOPCE problem, we need to find not only three coefficients such that the ratio of two factors associated with the desired target and clutter is maximal, but also optimal polarization states such that the received power ratio of the target and clutter is maximal. Both the factors consist of three parameters, i.e., the Cloude entropy (Cloude, S.R. and Pottier, E., IEEE Trans. Geosci. Remote Sensing, vol.35, p.68-78, 1997) and two special similarity parameters (Yang, J. et al., Electron. Lett., vol.37, p.193-4, 2001). The optimal coefficients of the GOPCE are obtained by solving an eigenvalue problem. Using an example, we demonstrate that the GOPCE can be employed for detecting roads in a forest area by using polarimetric SAR data. [C5382]

"Ground-based polarimetric SAR systems for environment studies"

Polarimetric SAR interferometry is a compound technique that has shown an ability to extract geophysical parameters from SAR images and is useful in terrain classification and surface change detection. SAR is a well-known technique for airborne or spaceborne remote sensing. It can usefully be exploited in a ground-based radar imaging system as well. By using radar polarimetry, a ground-based SAR system can be used for monitoring seasonal vegetation changes. We have developed a ground-based polarimetric SAR system for environmental studies. It is based on a vector network analyzer, polarized antennas and a scanning control unit. We describe the ground-based polarimetric SAR system and present some experimental results of monitoring trees with seasonal variation. [C5383]

"A new method of high-accuracy level-measure based on combining radar frequency-modulation and phase-discrimination"

The basic principle of frequency-modulation radar level gauge is analyzed briefly. A new method to improve the precision of radar level gauge is proposed based on combining radar frequency-modulation and phase discrimination. The method adopts frequency-modulation technique to get rough data of an unknown level, uses phase-discrimination technique to get subtle data, and then joins them together to get high accuracy composition data of the level. Effective conditions for data composition of rough data and subtle data are also discussed especially. [C5384]

"Range correlation effect on ISM band I/Q CMOS radar for non-contact vital signs sensing"

A quadrature direct conversion microwave Doppler radar has been fully integrated in $0.25\ \mu\text{m}$ CMOS. This ISM band radar chip has been used to detect heart and respiration movement 50 cm from the subject. While oscillator phase noise is a performance-limiting factor in CW radar systems, the range correlation effect enables measurement of small phase modulations in spite of the notoriously high phase noise of the on-chip CMOS

oscillator. This is the first reported quantitative experimental verification of the range correlation effect. [C5385]

"Advanced Gaussian MRF rotation-invariant texture features for classification of remote sensing imagery"

The features based on Markov random field (MRF) models are usually sensitive to the rotation of image textures. The paper develops an anisotropic circular Gaussian MRF (ACGMRF) model for modeling rotated image textures and retrieving rotation-invariant texture features. To overcome the singularity problem of the least squares estimate (LSE) method, an approximate least squares estimate (ALSE) method is proposed to estimate the parameters of ACGMRF model. The rotation-invariant features can be obtained from the parameters of the ACGMRF model by the one-dimensional (1D) discrete Fourier transform (DFT). Significantly improved accuracy can be achieved by applying the rotation-invariant features to classify SAR (synthetic aperture radar) sea ice and Brodatz imagery. [C5386]

"Refraction and shoaling of surface waves by currents and topography as observed by HF radars"

Phased-array Doppler radars were deployed immediately south of the mouth of the Chesapeake Bay during the COPE-3 experiment in the fall of 1997. The radars collected the Doppler spectra and extracted surface current vectors for a period of 45 days. Significant wave height and peak period estimates were obtained from the Doppler spectra using the method originally developed by Barrick (1977). The study region was strongly impacted by the outflow from the Chesapeake Bay. The buoyant plume that emanated from the bay during ebb tides was observed in the surface current maps produced by the HF radars. Significant surface current shear existed at the boundary where the buoyant plume overrode denser shelf water, resulting in a convergence frontal zone. The refraction and shoaling of the surface waves was observed as they propagated over these regions. The current-induced shoaling of incident waves was isolated from the effects of local topography. The location of significant wave height growth and dissipation was found to be dependent upon the tidal stage and the wind and wave direction. Regional remote sensing of both waves and currents was necessary to identify these high energy regions which are of considerable interest for studies of mixing at the estuarine front as well as for the safe maritime operations. [C5387]

"A comparison of near-surface current measurements by ADCP and HF-Radar on the west Florida shelf"

Surface currents (0.5 m) were measured during an eleven-day deployment of a pair of CODAR Ocean Sensors 25 MHz SeaSonde™ HF-Radars. The radar footprint overlooked of an array of acoustic Doppler current profilers on the West Florida Shelf (WSF) located between the 10 m to 30 m isobaths. An earlier study compared the hourly-averaged HF-Radar current vectors at grid points near the ADCP moorings, and found correlation coefficients (R) of 0.8 to 0.9 for the alongshelf components but 0.6 or less for the cross-shelf components, which are small in magnitude. The study noted that the alongshelf surface currents measured by the radar are about 30% larger than those of the ADCPs measured 2 to 3 m below the surface according to standard deviations and linear regression slopes. In this study we focus on the mooring located near the center of the radar coverage and explore the near surface shear and wind forcing. A fit of the M2tide, which is barotropic on the WSF, to the ADCP and radar vector time series yielded current tidal ellipse parameters that are in close agreement, suggesting that the low-frequency, upper-layer shear may be real. Alongshelf wind and radar current speed (at 0.5 m) were more strongly correlated than the alongshelf wind and ADCP current at 2.5 m depth. Both the principal axis analyses and the complex vector correlations indicate directional differences of 6° to 12° counterclockwise rotation (looking down) for currents with respect to wind, i.e., to the left of the wind, which is attributed primarily to the location of the coastal wind station. [C5388]

"Intercomparison of an ADCP, ADP, standard and long-range HF radar: influence of horizontal and vertical shear"

A nested HF radar network has been deployed along the New Jersey coast as part of the New Jersey Shelf Observing System (NJSOS). A standard range (about 50 km) system setup for continuous operation since 1999 includes two sites in Brant Beach and Brigantine, New Jersey. A second longer range system (about 170 km) includes four New Jersey sites set up in Wildwood, Tuckerton, Loveladies, and Sandy Hook. The first of the long-range sites was deployed in Spring 2000. Both the long-range and standard-range systems provide real-time maps of surface currents, with resolutions of 1.5 km (standard) and 6 km (long-range). During the summer of 2001, three Workhorse ADCPs and two SonTek ADPs were deployed along a line perpendicular to the coast. All of these in situ current meters were deployed for six weeks within the footprints of the two CODAR networks. Comparisons were made between the ADCP/ADP time series and radial CODAR time series provided by the long-range and standard-range sites closest to the line of current meters. Additional comparisons were drawn

between the total current fields of the standard and long-range CODAR systems with the in situ current meters. Several forcings were examined to explain the differences in the observations including vertical and horizontal shears. [C5389]

"Constructing surface current maps from HF radars with different operating frequencies"

HF radars operating at decameter wavelengths (3 to 30 MHz) in ground wave mode are capable of mapping near-surface currents. Several different HF radar systems are often in operation to observe an area, using different radar operating frequencies. Users of the data products of HF radars need to know the likely uncertainties or 'errors' caused by the use of data from radars with different operating frequencies and how to merge the data from these different systems into a single current map. During the year 2000 two MCR's operating at 4.8, 6.8, 13.4 and 21.8 MHz were sited at Moss Landing and Santa Cruz, California, collecting current maps at hourly intervals. We show that the current maps over Monterey Bay constructed from 4.8 MHz and from 21.8 MHz data have difference vectors that are between 1 and 7 cm/s when averaged over a ten day period. We also present a physical model that predicts the difference between current vectors observed at different frequencies in the 3 to 25 MHz range. The predicted difference in current speed between currents observed at 4.8 and 21.8 MHz is ≈ 5 cm/s for a 10 m/s wind speed and ≈ 9 cm/s for a 15 m/s wind speed. Typical maximum wind speeds on Monterey Bay are 10 to 15 m/s. We discuss briefly how HF radar observations at different frequencies can be used to produce a current map corresponding to a single reference frequency of 13.5 MHz. [C5390]

"Compression of RADARSAT data with block adaptive wavelets"

Summary form only given. A new algorithm, referred to as the wavelet packet-based embedded blocking code (WPEB), was developed for synthetic aperture radar (SAR) data compression. This algorithm combines the different properties of wavelet packet decomposition, block coding, and speckle reduction. Better results were obtained by using the wavelet packet transform that decomposes the higher frequencies. The higher coding efficiency can be obtained by dynamically allocating bits according to block variances. The examples using RADARSAT data have shown that compression performance is better than conventional wavelet methods. Visual image interpretation was found acceptable at 1 bpp. [C5391]

"Initial river test of a monostatic RiverSonde streamflow measurement system"

A field experiment was conducted on May 7-8, 2002 using a CODAR RiverSonde UHF radar system at Vernalis, California on the San Joaquin River. The monostatic radar configuration on one bank of the river, with the antennas looking both upriver and downriver, provided very high-quality data. Estimates of both along-river and cross-river surface current were generated using several models, including one based on normal-mode analysis. Along-river surface velocities ranged from about 0.6 m/s at the river banks to about 1.0 m/s near the middle of the river. Average cross-river surface velocities were 0.02 m/s or less. [C5392]

"Profiling river surface velocities and volume flow estimation with bistatic UHF RiverSonde radar"

During the summer of 2000, a bistatic UHF radar-the RiverSonde-was designed, built, and tested on rivers and canals in the Central Valley of California. The transmitter and receiver were on opposite banks. They simultaneously transmit to and receive from elliptical time-delay cells that span the river, with the transmit and receive antennas as their focal points. With 30 MHz bandwidth, the cell span up/down-river is 10 m. A three-element receive array employs the direction finding MUSIC algorithm to determine echo bearing. Velocity along the river channel is measured vs position across the river from the first-order Bragg-echo Doppler shifts. Radiating less than 1 W power, received surface-echo signal-to-noise ratios of 40 dB were received, both across narrow canals and across the American River that was 80 meters wide. Our tests and analyses were sponsored by and conducted along with the U.S. Geological Survey in Menlo Park, CA. "Surface truth" velocity profiles were established by current meters suspended from a boat, from a bridge, and from timing the drifts of tennis balls between two transverse cuts. RMS velocity differences between 6%-13% of the typical average flow velocity were observed. The rms differences between the three "surface truth" measurements themselves also fell within the same span. From the velocity profiles across the river, estimates of total volume flow for the four methods were calculated based on a knowledge of the bottom depth vs position across the river. The flow comparisons for the American River were much closer, within 2% of each other among all of the methods. Sources of positional biases and anomalies in the RiverSonde measurement patterns along the river are identified and discussed. [C5393]

"Fitting normal modes to HF radial and total surface current vector data over enclosed bays and estuaries"

A technique referred to as Normal Mode Analysis (NMA) has recently been developed for representing total vector CODAR HF radar data in Monterey Bay. These modes satisfy the coastal boundary constraint of no flow normal to the shore, and inherently represent both divergent and rotational flow as two sets of ortho-normal basis functions. In prior investigations by others, the domain had a large open boundary at which additional information from a numerical model was needed to completely represent the surface flows in the Bay. The modes were fitted to data only in the two-site overlap region where total vectors were calculated. We apply NMA for completely enclosed bays, using two-dimensional finite element methods to derive these modes where the shoreline is the mathematical boundary for the problem. This is an improvement over prior studies with open boundaries where additional information was needed to represent the flow within. We also extended this methodology by fitting to radial velocities from each radar by itself-as well as simultaneous radial data from multiple coastal radars viewing the same bay. It was applied to Corpus Christi Bay where two SeaSondes have been operated by Texas A&M University for two years. First, we employed simulations, where we resolved arbitrary current flow patterns into two sets of radial data. Noise was added to the vectors, and the extraction accuracy was studied. Ability to derive meaningful total velocity patterns depends on the noise level; the percent coverage of the bay by the radial measurements, and the availability of simultaneous radial data from different sites/angles. Surprisingly good extraction is often obtained with only single radar coverage. Finally, this method is now tested here with actual, hourly SeaSonde HF radar data over this Bay, both at the single-site radial level and by employing both sites. Comparisons are made with the real-time total-vector maps produced by the radar software over the common coverage area. Our bay-conforming natural mode-pattern resonances will be used in ongoing studies that relate their strengths to wind stress across the bay surface. [C5394]

"Marrying quantitative and graphic tidal analysis tools with HF radar current map outputs"

Separating off the tidal portion of flow from measured data and resolving into its individual constituents is an important part of coastal oceanographic analyses. HF radar surface-current maps taken hourly over many weeks or months offer a wealth of tidal information. Recent findings by several groups-based on HF current maps-show striking relations for the M2 tidal constituent strengths and ellipse axes with near-shore bathymetry. We have married the classic and popular Foreman tidal analysis MATLAB package directly to CODAR SeaSonde current map outputs via convenient graphical user interfaces. These algorithms allow one to resolve time series of total surface-velocity vectors at each map grid point into tidal constituents. Alternatively, the user can click to select specific points where such analyses are to be done, for example at an offshore structure or ADCP mooring. Based on measurements accumulated into a folder over any period of time, the algorithms will display the energy and signal-to-noise ratio of the extracted constituents, allowing the user to select which to retain for further analysis, display, or prediction. Ellipses for any of the constituents can be plotted over the Cartesian grid or at the specific points of interest. Movies of individual or summed tidal components can be made over any period from the past into the future. Finally, these tidal flows can be subtracted from the HF mapped current maps to give the de-tided residual circulation. [C5395]

"Simplified calculation of constituent tidal currents and height from HF radar profiles across the mouth of bays and sounds"

A dominant part of the circulation in nearly enclosed bays, estuaries, or sounds is dictated by tidal inflow at its mouth, called co-oscillatory forcing. The remaining flow component is usually due to winds. HF radar measurements over an area at the entrance can be used to determine the sinusoidal tidal velocity constituents along a line across the mouth. We use this complex spatial profile at different phases of the tidal cycle as the boundary excitation condition to solve a scalar second-order partial differential equation (PDE) for tide height. For the remaining boundary condition, the flow normal to the shore is taken to be zero. The bathymetry of the bay is included in the PDE. This is then solved by a powerful finite-element code, PDE2D. From the tide height distribution, the velocity circulation is simply calculated as its gradient. We present results applying this method to simple, canonical bay shapes and bathymetries. The effect of the bottom shape is studied, as well as the different excitation profiles at the mouth. Both tide height and vector current field are calculated and compared for the different geometries and excitations. Our future studies are applying this to Long Island Sound, for example, where three SeaSondes straddle the mouth at the Eastern end, owned and operated by University of Rhode Island and University of Connecticut. Our studies reported here of canonical bay and bottom shapes serves as a guide and check in applications to these real-world situations. To our present lowest order of approximation, friction and dissipative effects that cause tidal-phase time lags at different points are neglected. Higher-order nonlinearities are also neglected. Both of these effects are being included in subsequent studies. The main advantage of our method for co-oscillatory tidal analysis is simplicity: it avoids the complexities and computational requirements of full-up numerical primitive equation methods. The goal is to provide this as an algorithmic tool to run on the standard PCs that control and process data for the many HF radars being operated in bays. From a radar-measured profile of the tidal constituents across the mouth, we hope to estimate tidal circulation and tide heights throughout the bay, in areas well away from the entrance-where HF radars make

their measurements. [C5396]

"High frequency radar measurements of friction velocity in the marine boundary layer"

This work uses the hydrodynamic theory of the turbulent boundary layer to interpret High Frequency (HF) radar data and to address the potential of HF radar for determination of the friction velocity in the water over a broad spatial region. Recent advances in HF radar instrumentation have resulted in the development of a radar capable of detecting small changes in surface wave phase velocities as a result of an underlying current. The development of a multi-frequency radar system extends this capability to the determination of the vertical distribution of the flow in the water column, or current shear. In this work, the Levenberg-Marquardt method of nonlinear least squares is used to determine the near surface current profile based on a theoretical model of the effect of the current on the phase velocity of a surface gravity wave. The results of this analysis are compared to in situ measurements of wind velocity and measurement-based calculations of friction velocity. The results show that estimates of the friction velocity compare well with in situ measurements under moderate wind conditions. [C5397]

"Vector wind field measurements using multifrequency HF radar"

It is well known that HF radars are capable of measuring wind direction by using the relative strength of the echoes from the approaching and receding ocean waves at the Bragg resonant wavelengths. Here we examine the ability of multifrequency HF radar to measure wind speed as well as direction. In this study we use data collected over Monterey Bay, California in December of 2000. At that time the M1 buoy (deployed by the Monterey Bay Aquarium Research Institute, MBARI) measured wind speed and direction. Two multifrequency coastal radars (MCR's) operated near Santa Cruz and Moss Landing, California. Using the method of partial least squares we developed an algorithm for estimating the surface wind vector from multifrequency HF radar data. Comparison with surface truth from the M1 buoy indicates that the method produces excellent results. The wind speed was estimated with a standard error of prediction of a little over 1 m/s, bias of ≈ 0.5 m/s and R^2 of 0.71. We think that this method will find useful application in measuring the detailed structure of the wind field in coastal regions on a few kilometer size scale. [C5398]

"Uncertainties in SeaSonde current velocities"

This paper describes the methods used to derive uncertainties in SeaSonde radial and total velocity vectors. Studies of baseline deviations are used to illustrate/validate the results. Recommendations are made for further work leading to reduction of the uncertainties. [C5399]

"An efficient compensation approach for nonuniform sampling of rotating angle in ISAR imaging"

In this paper under the assumption that radar also transmits narrow-band tracking signal accompanying transmission of wide-band signal and PRF (pulse repeating frequency) value is much higher than that of signal required by non-overlap imaging, the target moving trace may be estimated by using narrow-band signal. Furthermore, PRF is modified by referring the estimated moving trace. With these efforts, nonuniform sampling of rotating angle is well-compensated for imaging. Actually, most imaging radars can provide such narrow-band tracking signal and also operate with PRF high enough. [C5400]

"Information extraction from high resolution SAR data for urban scene understanding"

The high complexity and the increased importance of geometry in growing resolution synthetic aperture radar (SAR) data in urban environments poses a limit on the usability of lattice-based scene models. Geometrical models based on marked point processes can be employed to provide better descriptions of the scene. A Gibbs potential based on a hierarchical Bayesian description of the direct model of the acquisition is defined on the process: an a-priori measure of plausibility for the scene takes into account interactions between scene objects, while a Bayesian likelihood term is based on the decomposition of scene objects into basic elements and on their mapping in the data space. Multiple reflections of the radar signals are considered and exploited. The resulting detectability measure is compared to a hypothesis in a likelihood ratio. The resulting posterior potential is optimized by Monte Carlo methods. The resulting algorithm is applied on a diverse set of single submeter resolution SAR intensity images on urban scenes, providing descriptions of the 3-d structure of the imaged urban areas in terms of separate objects. [C5401]

"Visibility analysis of man-made objects in SAR images"

The increasing resolution of SAR data offers the possibility to utilize this data for a detailed scene interpretation in urban areas. Different SAR specific phenomena like foreshortening, layover, shadow and multipath-

propagation burden the interpretation. A high resolution LIDAR DEM of an urban scene is incorporated to investigate the impact of the phenomena on the visibility of man-made objects by a SAR measurement from a given sensor trajectory and orientation. LIDAR data as ground truth is well suited for this task, because it contains elevation information of man-made and natural objects. Incoherent sampling of the DEM simulates shadow and layover areas. By a variation of viewing and aspect angles a large number of such simulations are carried out. From this set of segmentations the n best are determined with respect to the visibility of roads and buildings. Furthermore, the locations of total reflection or double-bounce scattering in the vicinity of buildings are determined. [C5402]

"Simulation and analysis of fine resolution SAR images in urban areas"

This paper provides a preliminary discussion on the simulation and the analysis of fine resolution SAR data in urban areas. It presents a very interesting data set obtained by means of a precise SAR simulator and some road extraction results on the same data set. Despite some possible improvements, the research shows the huge potentiality of SAR data for urban area mapping and monitoring. [C5403]

"Fusion of LIDAR data and aerial imagery for automatic reconstruction of building surfaces"

An approach for building reconstruction based on fused information extracted from different data sources, namely LIDAR data (light detection and ranging) and aerial imagery, is proposed. The building reconstruction is performed within the scope of a general surface estimation process. This surface estimation aims at generating a DTM including buildings and vegetation removed. The buildings are reconstructed by applying polyhedral models. Thus a large variety of building types can be described with the only limitation, that the roof surface consists of planes. [C5404]

"SPOT5 THX: a 2.5m fused product"

SPOT5 was launched on the 4th of May 2002 by an Ariane 4 rocket from Kourou, French Guyana. Like previous SPOTs, SPOT5 is able to acquire both high resolution panchromatic data and low resolution multispectral images (green-red-infrared images), with a 2.2 s time delay between the two acquisitions. The swath remains equal to 60 km but panchromatic resolution has been increased from 10 m to 2.5 m using an optimal quincunx sampling scheme named THR mode, while multispectral sampling was improved from 20 m to 10 m. Like other high resolution remote sensing systems, SPOT5 makes it possible to produce high resolution multispectral images by merging panchromatic and multispectral data. The main difficulty consists in panchromatic/multispectral geometric registration since the misregistration depends on attitude perturbations and local relief, which leads to use automatic correlation. To merge registered multispectral and panchromatic images, CNES selected a simple but efficient method, based on intensity/hue/saturation transform. This method was successfully compared to a set of other merging techniques through an experiment including quantitative and qualitative assessment by experts. The final false colored product, named THX, is a three band multispectral image covering a 60 km \times 60 km area per scene with a 2.5 m sampling interval, which may be converted into a pseudo colored using a matrix transformation. Panchromatic/multispectral fusion finally proves to be of utmost importance for global system optimization, since it allows to generate on ground a product that could not be produced on board, mainly for transmission and data storage limitations. [C5405]

"Classification of X-band high resolution SAR images over urban areas: Markovian segmentation using Mellin transform"

This paper presents a classification method devoted to high-resolution SAR amplitude images over dense urban areas. The classification method is based on a statistical approach involving a Markovian segmentation process. Our contribution is the introduction of Fisher distributions to fit urban area statistics at best. This implies the use of second kind statistics at best. This implies the use of second kind statistics built upon Mellin transform. The estimation process and the Markovian process are described here. Our goal is both to explain how these distributions can be used in a classification process and to discuss some results. The theory is explained and its validity regarding our data is presented. Then the discussion focuses on the application of this theory to real data. [C5406]

"Information extraction from high resolution SAR data for urban scene understanding"

The high complexity and the increased importance of geometry in growing resolution synthetic aperture radar (SAR) data in urban environments poses a limit on the usability of lattice-based scene models. Geometrical models based on marked point processes can be employed to provide better descriptions of the scene. A Gibbs potential based on a hierarchical Bayesian description of the direct model of the acquisition is defined on the process: an a-priori measure of plausibility for the scene takes into account interactions between scene objects,

while a Bayesian likelihood term is based on the decomposition of scene objects into basic elements and on their mapping in the data space. Multiple reflections of the radar signals are considered and exploited. The resulting detectability measure is compared to a hypothesis in a likelihood ratio. The resulting posterior potential is optimized by Monte Carlo methods. The resulting algorithm is applied on a diverse set of single submeter resolution SAR intensity images on urban scenes, providing descriptions of the 3-d structure of the imaged urban areas in terms of separate objects. [C5407]

"Texture analysis and classification of SAR images of urban areas"

In SAR image classification texture holds useful information. In a study after the ability of texture to discriminate urban land-cover, a set of measures was investigated. Among them were histogram measures, wavelet energy, fractal dimension, lacunarity and semivariograms. The latter were chosen as an alternative for the well known gray-level cooccurrence family of features. The study was done on the basis of non-parametric separability measures and classification techniques applied to ERS-1 SAR data. The conclusion is that texture improves the classification accuracy. The measures that performed best were mean intensity (actually no texture), variance, weighted-rank fill ratio and semivariogram, but the accuracies vary for different classes. Despite the improvement, the overall classification accuracy indicated that the land-cover information content of ERS-1 leaves to be desired. [C5408]

"Urban change detection in the Helsinki metropolitan region using Radarsat-1 fine beam SAR images"

This paper describes the potential of Radarsat-1 fine beam intensity SAR images in urban mapping and change detection. The main objective was to determine the possibility of building detection e.g. as a function of height, orientation, roof material and roof type in the Helsinki metropolitan region. Altogether, 22235 buildings were used to estimate the effect of height, and then 14270 buildings were used to estimate the effect of orientation. Additionally, a smaller and more detained set of buildings was selected from various environments e.g. from forested and dense urban areas. It was shown that height and orientation were the main factors affecting on the detectability of the buildings. The results indicate that approximately 39% of the buildings can be detected using the Radarsat-1 SAR; densely build up areas are clearly visible in Radarsat fine beam images, but in small-house areas buildings that are surrounded by forest are visible only in very rare cases. [C5409]

"Flood monitoring in urban areas: statistical vs. neurofuzzy approach"

The paper aims at investigating different classification and segmentation tools for flood monitoring using satellite SAR images. To this aim, two different approaches, namely statistical segmentation and neurofuzzy classification are compared and discussed. The methods show, in general, the possibility to provide to a good extent accurate maps of the flooded areas using simple processing schemes. This stresses the effectiveness of satellite SAR images for real-time flood monitoring. [C5410]

"Infrastructure analysis from high resolution SAR and InSAR imagery"

In this paper, we present a methodology for the extraction of building dimensions from high resolution SAR and 3-d (InSAR) imagery. For flat and sloping roof buildings we show how differing imaging geometries produce fundamental limitations on the structural information that may be obtained. The procedure is applied real imagery and initial results are discussed. [C5411]

"Integrating high resolution air-borne linear CCD (TLS) imagery and LIDAR data"

3D building modeling can be more easily generated with several methods. LIDAR data have high potential of automation; though they have such disadvantages as low resolution and no texture. On the other hand, generally, a resolution of the aerial images is higher than that of LIDAR data. The extraction of buildings from aerial images in dense urban environment is easier from aerial images than from LIDAR data. However, the fully automated 3D modeling of buildings from aerial images in dense urban environment is not successful. The objective of this research is to develop a methodology to automatically generate 3D modeling of buildings. The generation of 3D buildings data is done by integrating high resolution air-borne linear CCD, low resolution DSMs (created from LIDAR) and existing 2D digital maps. The detail representation of roof shapes such as gables is created by using the knowledge of buildings. [C5412]

"Urban area analysis based on ESPRIT/MUSIC methods using polarimetric interferometric SAR"

This paper describes the analysis of man-made area using fully polarimetric interferometric SAR data at L-band. This approach uses a polarimetric interferometric classification procedure to determinate the nature of the

different media of the scene under study. An interferometric phase estimation based on ESPRIT methods is applied to the retrieval of the height of different media and specifically for the characterisation of the buildings. [C5413]

"TerraSAR-X: a new perspective for scientific use of high resolution spaceborne SAR data"

TerraSAR-X is a new German radar satellite that shall be launched in mid 2005 with a lifetime of 5 years. It carries a high frequency X-band SAR sensor that can be launched in three different modes and polarizations. The spotlight-, stripmap- and scanSAR-modes provide high resolution images for detailed analysis as well as wide swath data whenever a larger coverage is required. Imaging will be possible in single, dual and quad-polarization. TerraSAR-X will be an operational SAR system for scientific and commercial applications. The various capabilities of the SAR system are presented as well as the corresponding product types. Based on these characteristics the scientific potential of TerraSAR-X with respect to urban areas is highlighted. Finally, the TerraSAR system is described consisting of the space, the ground segment and the user infrastructure. DLR is responsible for the scientific users while the commercial sector will be handled by the Infoterra GmbH. [C5414]

"Spectral interpretation based on multisensor fusion for urban mapping"

This paper is concerned with fusing aerial imagery, LIDAR point clouds, and hyperspectral imagery for the purpose of automated urban mapping. Instead of performing traditional supervised and unsupervised classification of hyperspectral data we propose a region growing approach from seed pixels that originate from fusing LIDAR and aerial imagery. This requires a thorough alignment of all sensors involved—a problem that is solved with sensor invariant features. The common system is the geodetic reference frame in which the LIDAR points are computed. The alignment results in transformations from sensor space to object space and back, avoiding resampling the sensor data. After describing the major aspects, an example demonstrates the feasibility of the proposed fusion approach. [C5415]

"Information content in SAR images of urban areas"

In this paper we present a SAR raw signal simulator based on a model of the electromagnetic field scattered by an urban structure and on a radar model. The simulation scheme also accounts for the time-domain problems related to the optical path length of the scattering contributions. Examples of simulated images are provided, along with a discussion devoted to identify the information content in SAR images of urban areas and to point out results useful for the image interpretation. [C5416]

"Estimation of ocean wave spectra from microwave backscatter and emissivity measurements"

The microwave reflectivity of the ocean surface is determined mainly by the surface roughness or wave spectrum. Since direct measurement of the wave spectrum at centimeter wavelengths is very difficult, microwave measurements are currently the largest source of information for this region of the spectrum. This paper discusses a procedure to determine a form for the equilibrium spectrum that is consistent with backscatter measurements over a range of incidence angles and look directions, and presents results using the backscatter data summarized by the CMOD4 model function. [C5417]

"Analytical formulation of the scattering by a slightly rough dielectric boundary, covered with a homogenous dielectric layer"

Characterization of the radar response of a multi-layer dielectric media with slightly rough interface has a number of applications, including remote sensing of snow non-destructive evaluation and quality control of multi-layered MMIC, etc. For the case of snow-pack remote sensing, the premise is to compare the scattered fields of the rough surface with snow with that on bare rough surface and then attribute the variation in the scattered power and coherence to the snow parameters. In this approach, first, the snow cover is modeled by a homogenous dielectric layer having a smooth top surface above a ground plane with a rough surface. In situations where the scattering from the rough surface become comparable to with the snow volumetric scattering, the volume scattering is added incoherently to the surface scattering, and then, the coherence is computed. In this paper, a small perturbation solution is developed to predict the bistatic scattering coefficients and the coherence of a slightly rough surface covered with homogenous dielectric layer. [C5418]

"2nd GRSS/ISPRS Joint Workshop on Remote Sensing and Data Fusion over Urban Areas. URBAN 2003 (Cat. No.03EX646)"

First Page of the Article [C5419]

"Land cover classification of urban and sub-urban areas via fuzzy nearest-mean reclustering of SAR features"

This paper describes a nonparametric algorithm based on fuzzy-reasoning concepts and suitable for land use classification, either supervised or unsupervised, starting from pixel features derived from SAR observations. Pixel vectors constituted by features calculated from the backscattering coefficients in one or more bands and/or polarizations are clustered. At each iteration step, pixels in the scene are classified based on the minimum attained by a weighted Euclidean distance from the centroid representative of each cluster. Upgrade of centroids is iteratively obtained both from the previously obtained classification map and by thresholding a membership function of pixel vectors to each cluster. Such a function has been derived based on entropy maximization of the resulting clusters. To yield the weighted distances from a pixel vector, its features are weighted by means of progressively refined coefficients, whose calculation still relies on the membership function through a least squares algorithm. Refinements of the feature-dependent weights are introduced to optimize individual classes. Possible "a priori" knowledge coming from ground truth data may be used to initialize the procedure, but is not required. Experimental results carried out on SIR-C SAR data of the city of Pavia and its surroundings demonstrate the usefulness of a nonparametric classification to discriminate land use in general, and urban and built-up areas in particular, from SAR observations analogous to those which are routinely available from Envisat. A training set, even of very small size, may be utilized. However, its knowledge affects initialization only and is unnecessary for the iterative refinement procedure. Pixel-based classification attains almost 70% accuracy without any postprocessing. [C5420]

"Automatic structure detection in a point-cloud of an urban landscape"

A method for detecting urban structures in an irregularly spaced point-cloud of an urban landscape is proposed. The method is especially designed for detecting structures that are extensions to the bare-earth (e.g., bridges, ramps, etc.). The method involves a segmentation of a point-cloud followed by a classification. Both the segmentation and classification of the data are based on the analysis of a data structure in which the point-cloud is represented as an orthogonal set of profiles. Also proposed is a conceptual and logical model of the landscape for the structure detection problem. [C5421]

"Extraction of 3D information using overlay detection on SAR images"

This paper presents a study of height recovery using overlay detection in semi-urban areas. The input data are a lonely SAR image and a map of the buildings. The first part of the paper presents the different steps of the proposed algorithm (primitive selection, overlay extraction and height recovery), and the second part is dedicated to the method evaluation on two SAR images of the same area but acquired with different incidence angles. [C5422]

"Model-based processing of multifrequency polarimetric SAR images of urban areas"

In this paper, we describe a two-step classification scheme for fully polarimetric SAR images. The classification scheme is composed of the cascade of an optimum segmentation stage, and an ML supervised classifier. Different segmentation schemes are described, specifically designed for mono- or multifrequency images. The classification scheme is applied to a set of fully polarimetric, multifrequency SIR-C images of the town of Pavia, in Northern Italy, considering all the possible pairs of polarimetric channels and the two bands individually and jointly, aiming at identifying the best combination for practical applications. Results show that for urban areas, the best performance is achieved by jointly processing the three polarimetric channels, and the minimum performance degradation is achieved considering the HH and the HV channels. [C5423]

"Multi-platform permanent scatterers analysis: first results"

The PS technique is an advanced tool for the joint exploitation of series of interferometric SAR data for measuring millimetric ground deformation effects on privileged radar targets. In this paper we briefly discuss some preliminary results obtained in the first attempt to apply the permanent scatterers (PS) technique on a RADARSAT data set. [C5424]

"A differential SAR interferometry approach for monitoring urban deformation phenomena"

This paper presents a new DIFSAR approach that allows us to detect and follow the temporal evolution of localized deformations. This approach, which is suitable for monitoring single buildings or structures, extends the capability of the algorithm referred to as SBAS technique, originally developed for investigating large scale deformation phenomena. The proposed technique relies on small baseline interferograms only, in order to preserve the DIFSAR capability to provide spatially dense deformation maps; moreover, it requires two different

sets of DIFSAR interferograms generated at low (multi-look data) and high (single-look data) spatial resolution, respectively. The algorithm has been tested with data acquired by the European remote sensing (ERS) satellite relative to the area of the city of Napoli (Italy) and the results have been validated by using geodetic data.

[C5425]

"Backscatter ionogram inversion"

A backscatter ionogram, BSI, is a plot showing the group path or time delay against operating frequency when using ground-based swept frequency radar. In the case of ground backscatter, the received signals are reflected from distant locations on the Earth's surface. The ionosphere is the medium through which both the transmitted and received signals traverse. A backscatter ionogram contains useful information regarding the state of the ionosphere at the time and over the range of the returned signal, which could be a few thousand kilometers from the transmitter/receiver location. Backscatter ionograms differ from the more conventional vertical incidence ionograms, where the received signals are reflected from a region of the ionosphere vertically above the sounder location. Methods of inverting backscatter ionograms to obtain ionospheric profiles offer an important means of remote sensing the distant ionosphere and regions in which land and sea scatter occur. Thus, backscatter ionograms can play an important role in the frequency management systems of over-the-horizon radar. [C5426]

"Analysis of X-SAR SRTM elevation data to estimate surface cover heights over land areas"

We present the first results of the SRTM AO-038 project in Norway. The SRTM X-SAR elevation data are evaluated with respect to digital reference maps and surface cover types like agricultural fields, forest, lakes and infrastructure. Optical satellite images, aerial photos and field observations are used to aid in the analysis of the SRTM elevation data. The X-SAR SRTM DEM gave better elevation accuracies over many open agricultural areas as compared to the 1:50000 topographic DEM commonly used in Norway. The SRTM DEM gave surface cover elevations rather than ground elevations in areas of dense forest. These SRTM elevation offsets in forested areas may be used further to categorize the forest cover type. [C5427]

"Monte Carlo simulations of surface clutter in GPR scenarios"

The clutter caused by scattering from a rough air-ground interface is analyzed numerically. The simulations have been done using Monte Carlo approach. Statistical properties of the scattered field have been analyzed. It has been found that the phase of the reflected electromagnetic field nearby a rough air-ground interface follows the profile of the interface and this phase modulation of the reflected field is responsible for the forming of the clutter. Furthermore it is demonstrated that the correlation function of the phase of the reflected field coincides with the correlation function of the rough surface, while for the correlation of the reflected field it is valid only if the magnitude of the surface clutter is considerably less than the mean value of the ground reflection. [C5428]

"Scattering by rough surfaces: comparison between simulations and experimental radar data"

The Curvilinear Coordinate Method is an efficient and versatile tool for analyzing random rough surfaces. In this paper, we present the model and some comparisons between simulations and experimental radar measurements over bare soils. The comparisons are convincing. [C5429]

"RADARSAT-1 image quality maintained in extended mission"

RADARSAT-1, the first Canadian SAR remote sensing satellite has successfully completed its design lifetime of five and a quarter years. It is in extended mission operation meeting customer demand. The Image Quality Control program is kept fully operational. Measured results indicate image quality performance is better than system specification and maintained. This paper briefly describes image quality results and recalibration work.

[C5430]

"Terrain interpretation from SAR techniques"

Our results have shown that selective processing of RADARSAT-1 images has assisted in regional terrain mapping of large areas the northern boreal forest region in Canada. Terrain roughness information derived from RADARSAT-1 when fused with high resolution DEM data provided image maps that are useful for landform interpretation. [C5431]

"Validation of the X-SAR SRTM DEM for ERS and JERS SAR geocoding and 2-pass differential interferometry in alpine regions"

The X-SAR SRTM DEM of the alpine region in Switzerland was validated for SAR geocoding and 2-pass

differential interferometry using ERS and JERS data. The absolute horizontal and vertical accuracies of the X-SAR SRTM DEM are in general in line with the nominal indications, but in very rugged areas we found horizontal offsets of up to 50 m in both northing and easting directions and some extreme absolute height errors up to even 1000 m. Also visible in the X-SAR SRTM DEM is an important noise for the slopes of SAR illumination. The ERS and JERS SAR images geocoded with the X-SAR SRTM DEM do not contain significant geometric artifacts, but, in parallel to what was discussed before, show in comparison to the map offsets in both easting and northing directions. The matching of geocoded products of descending and ascending modes is very good, i.e. on the order of 1 to 2 pixels. Considering that in our geocoding approach the geocoded SAR images are accurately co-registered to the DEM, the horizontal offsets have no influence for 2-pass differential interferometry. We found that the X-SAR SRTM DEM is well suited for ERS and JERS interferograms of the descending mode of baselines up to 100 m. For the differential interferometric analysis of ERS SAR data in ascending mode, however, attention has to be paid to the noise of the slopes facing away from the X-SAR. [C5432]

"Radargrammetry and space triangulation for DEM generation and image ortho-rectification"

In 2002 ENVISAT with the advanced SAR (ASAR) as one important instrument was launched. As compared to the preceding SAR sensors on ERS-1 and ERS-2 the ASAR has beam-steering capability permitting the acquisition of data over the same area under the different incidence angles as required by radargrammetry. In this paper a concept of combined use of radargrammetry and space triangulation to derive digital elevation models (DEMs) is presented. Space triangulation with opposite side acquisitions is used to determine a number of control points. Radargrammetry is then used to derive a DEM using these control points as reference. Preliminary test on the different steps of the combined method are presented. [C5433]

"Radargrammetry of opposite-side stereo Magellan synthetic aperture radar on Venus"

Radargrammetry of opposite-side stereo SAR is demonstrated using Magellan SAR images of Venus. Large areas of gentle slope can be successfully matched to generate DEM using conventional stereo-match algorithm while high to moderate relief regions need further treatment using shape-from-shading. The initial stereo-match points are classified into three categories; GOOD, BAD, and TOPO, and different methods are applied to different regions to iteratively improve DEM. [C5434]

"Airborne X-band SAR imaging with 10 cm resolution-technical challenge and preliminary results"

RAMSES airborne SAR system bandwidth was recently increased to 1.2 GHz in X and Ku bands, yielding (unweighted) 3 dB range resolution of 11 cm. Synthesis of SAR images with matching cross-range resolution, requires long integration time thus disqualifies temporal-domain back-injection synthesis algorithm as impractically slow. The wider relative bandwidth also disqualifies simplified range/Doppler types of algorithms because the hypothesis of proportionality between Doppler and squint is no more valid. Therefore, we implemented a fast frequency-domain synthesis algorithm (Ω -k or range-migration algorithm) and designed a new deterministic motion and antenna pattern compensation method for it. Since the required accuracy on carrier trajectory exceeded the performance of our differential GPS-hybridized inertial navigation unit, we implemented an autofocus based on the phase tracking of several isotropic point-like echoes. Since the resolution cell is only a few wavelength wide, clutter appearance and statistics is unusual. We present here some typical examples for high resolution clutters and compare with texture simulations from optical 2 1/2 D surface modelling. [C5435]

"Examination of crop characteristics using microwave data"

The numeric inversion of water-cloud model of synchronized microwave bands of ERS-2 and JERS satellites gave the possibility of obtaining crop characteristics. Model performance was validated by comparison between backscattering coefficients simulated and measured by satellites. The contribution of various crop characteristics was presented and compared to measured soil-vegetation parameters at the ground level during satellite overpasses. [C5436]

"A new image registration method for multi-frequency airborne high-resolution SAR images"

High resolution airborne synthetic aperture radar (SAR) is useful for surveillance and remote sensing applications. The higher resolution leads to more speckle as well as a need for more accurate pixel-level registration. Also, the curvature of the Earth needs not to be taken into account while registering two images because the swath of terrain being imaged in an airborne SAR is small. This article describes a new technique for registering multi-frequency airborne high-resolution SAR images. The image registration is set forth based on the fundamental principle of relaxation method, which uses image segment comprising of the relaxation registration results of point feature as global control. In order to guarantee the accuracy and reliability of image

registration, line moment of edge feature is first used as match units to develop the traditional relaxation method. Airborne SAR images in Ku-band and X-band are used to test the new image registration method. Experimental results show that the proposed method outperforms standard image registration techniques in terms of reliability and rapidity in most cases. It also achieves better performance than wavelet pyramid method. [C5437]

"Using graph matching to compare VHR satellite images with GIS data"

We propose a graph matching methodology based on relaxation labeling to compare road junction in VHR satellite images with GIS road data. Use is made of the spatial layout between points based on the relative angle. The technique finds correspondences between set of points taking into account error on the spatial location and spurious or missing points. An analysis is given to determine the weights of the algorithm based on the expected graph error. [C5438]

"A comparative analysis of data on multiyear sea ice distribution in the Arctic as retrieved from satellite passive microwave radiometer and radar images"

This study deals with a comparison of estimates on multiyear sea ice distribution in the Arctic, derived from SSM/I data using NORSEX algorithm and from satellite radar. Conducted analysis revealed qualitative correspondence of these estimates, as well as underestimation of SSM/S-derived values. The difference between these estimates can be explained by some inaccuracy in the input parameters, such as sea ice emissivities, air and ice temperatures, as well as by their spatial and temporal variations. [C5439]

"The origin, evolution and legacy of SEASAT"

On the morning of June 26, 1978 a satellite was launched into Earth orbit from Vandenberg Air Force Base near Lompoc, California. The satellite, "SEASAT" opened a new age of space remote sensing using active radar to image and probe planetary processes. SEASAT began as a rough theme to use an array of active and passive microwave technologies, largely untried in space, to remotely sense synoptic ocean properties. This challenging prospect was the dream of scientists, aligned as the NASA sanctioned SEASAT Users Working Group", that had worked for more than five years to develop the appropriate sensor technologies and experiments for SEASAT. This group had staunchly championed the program throughout the approval and development process. This paper describes the epic SEASAT mission from its origin as an idea in 1972 until it became a reality collecting global ocean data in 1978. The path of the program is traced step-by-step through: definition studies performed by NASA Centers and the Navy Applied Physics Laboratory; establishment of the NASA SEASAT program Office in 1974 to develop the plan to secure mission level status and funding; identity as an approved new program in 1975; the selection of an industry team to implement SEASAT under the guidance of the Jet propulsion Laboratory; international expansion of the program with scientific participation and mission contributions (data collection stations, tracking sites, experiments) from Canada, Europe and Australia; the successful launch of SEASAT in June 1978, initiating a host of scientific demonstration and validation experiments; and the unexpected demise of SEASAT after 110 days in space. The paper concludes with a view of SEASAT's heritage expressed in terms of the derivative missions that have followed. [C5440]

"Ocean surface wave imaging from Seasat to Envisat"

The questions about the correct SAR imaging theory of ocean surface waves and the best inversion algorithm for retrieving two-dimensional ocean wave spectra from SAR image spectra has haunted remote sensing scientists for the last 25 years. Here a short historical review is presented. [C5441]

"SEASAT sees the winds with SAR"

The original justification for the inclusion of an L-band synthetic aperture radar on Seasat was for the measurement of ocean surface wave spectra. Indeed, the initial research on ocean wave measurement from Seasat evolved to the point where SAR imagery from the subsequent ERS-1, ERS-2, and ENVISAT satellite SARs are routinely combined with wave model estimates to produce ocean surface wave spectra. The scatterometer on Seasat was the primary means of measuring ocean surface wind speed direction. Nonetheless, patterns of SAR-measured normalized radar cross section clearly showed spatial structures associated with variations in wind speed and direction. In the last five years, it has become more apparent that SAR imagery can be used to make high spatial resolution estimates of wind speed. In this paper, we trace the evolution of SAR wind speed measurement capabilities from Seasat to the present. [C5442]

"Present status of GCOM mission"

Global Change Observation Mission (GCOM) is a follow on mission of ADEOS, ADEOS2 and TRMM. It is under

phase A study in NASDA (National Space Development Agency of Japan). GCOM is not a series of satellites but a mission and its concept is to continuously monitor geophysical parameters which are critical to understand global change phenomena, especially phenomena related to climate change. Those parameters include, but not limited to, optical thickness of aerosols and clouds, water and energy fluxes, carbon fluxes, sink and source of greenhouse gases, atmospheric constituents, etc. The measurement of geophysical parameters will continue more than 15 years after the launch of ADEOS2. The first generation satellites of GCOM after ADEOS2 is now composed of 3 satellites, i.e. GOSAT (joint program of NASDA and MOE), CCOM (tentative name), and GPM core satellite (joint program of NASDA and NASA). The main target of GOSAT is to clarify the sinks and sources of greenhouse gases, especially carbon dioxide, in the continental scales by monitoring atmospheric greenhouse gases distribution. The target of CCOM is to measure geophysical parameters which are uncertain in the today's climate models. GPM core satellite is a follow on of TRMM and the target of GPM core satellite is to measure precipitation. GOSAT will carry at least 2 instruments, i.e. an instrument which can measure tropospheric carbon dioxide, and SWIFT (Stratospheric Wind Interferometer: stratospheric wind sensor). CCOM will carry three core instruments, i.e. SGLI (GLI follow on, which covers from UV to IR), AMSR2 (AMSR follow on), alpha-Scat (SeaWinds follow on). Other instruments may be added based on an AO process. GPM core satellite will carry 2 instruments, i.e. DPR (Dual Precipitation Radar: PR follow on) and a microwave radiometer. The orbit of CCOM will be a sun synchronous orbit, which is almost the same as ADEOS2. The orbits of GOSAT and GPM core satellite will be around 700 km and 400 km, respectively. These 3 satellites are planned to be launched in 2007 and 2008. [C5443]

"POLDER on ADEOS-2"

POLDER on ADEOS-1 in 1996 was ahead of the series of multithematic radiometers now observing the Earth continuously: SeaWiFS (1997), MODIS (1999 on Terra, 2002 on Aqua), MERIS (2002 on Envisat). A second POLDER instrument was launched by ADEOS-2 on 14 December 2002. POLDER-2 will follow on the unique measurements of directional and polarization signatures of the atmosphere and Earth surfaces initiated by POLDER-1. From these observations a comprehensive set of geophysical parameters on aerosols, clouds, ocean color and land surfaces will be produced and distributed to the scientific community for Earth monitoring and climate research. A second generation of scientific algorithms has been developed based on the experience of POLDER-1 data analysis. An overview of POLDER-2 demonstration products will be given with first in-flight results. The POLDER website (<http://smc.cnes.fr/POLDER/>) has been renewed and provides already enhanced information on POLDER products. [C5444]

"ADEOS-II calibration and validation plan"

ADEOS-II is the second global observation satellite of Japan following ADEOS to improve satellite-based global change observation system, and to obtain Earth observation data set for elucidation of the global water and energy cycle, carbon cycle, stratospheric ozone depletion and so on. For these mission objectives, five remote sensing instruments are onboard ADEOS-II that was launched on December 14, 2002. NASDA is responsible to check out ADEOS-II, and to calibrate and validate AMSR and GLI sensor characteristics and their data products. After launch for four months, the first check out phase is planned for satellite function and performance and during the phase the first-light images of AMSR and GLI is obtained. Before data distribution for general uses, NASDA is planning the calibration and validation phase for eight months after the first check out phase. This paper describes overview of NASDA's Calibration and Validation Plan. [C5445]

"Geophysical interpretation of ScanSAR data in relation to SSM/I data and numerical models of Arctic sea ice"

Characterizing the variability of sea ice in the Polar Regions is fundamental for the understanding of global climate and the geophysical processes governing climate changes. Arctic sea ice distribution and circulation are analyzed with the help of ScanSAR images, numerical models and passive microwave data from the late summer period of 1996. The results from an automatic SAR ice concentration algorithm are compared statistically to an 18 km spatially gridded Arctic ice-ocean numerical model and an SSM/I NASA Team 2 ice concentration algorithm. Furthermore, the SAR and the Arctic ice-ocean numerical model datasets are also compared quantitatively in terms of geophysical properties (ice concentration and ice motion) to a 55.5 km gridded barotropic Arctic numerical model. [C5446]

"Polar sea ice mapping using SeaWinds data"

Microwave remote sensing provides an excellent means for mapping polar ice extent. In this study, a new algorithm for polar sea ice mapping is developed for use with the SeaWinds instrument. The approach utilizes a priori information within the framework of Bayes detection to produce sea ice extent maps. Statistical models for

sea ice and ocean are represented in histograms which are filtered using a principal component (PC) based filtering technique. Spatial a priori information is incorporated through the loss terms associated with Bayes risk. Sea ice extent maps produced by the algorithm correlate well with the Remund-Long algorithm. [C5447]

"Ice thickness estimation using SAR data and ice thickness history"

We introduce an algorithm for sea ice thickness estimation by augmenting the sea ice thickness history derived from the daily digitized ice charts for the Baltic Sea ice. This algorithm is designed for operational use and utilizes the C-band Radarsat-1 data. [C5448]

"Spatial decision support system for sediment related disaster prevention planning"

In this paper, we present the basic issues related to the enforcement of The Law Related to Promotion of Measures for Sediment-related Disaster Prevention in a restricted area etc. due to Sediment-related disaster (simplified as Law for Prevention of Sediment-related Disasters), put into effect by Japanese Ministry of Land, Infrastructure and Transport since April 2002. We also present the technical problems, our implementation of spatial decision support system and finally the examples of analysis results. [C5449]

"A new approach for tracking the trajectory of oceanic warm pool"

During the past two decades, the western Pacific warm pool (WP) is of growing concern following the recognition of its significant role in global climate change and its strong association with El Nino-Southern Oscillation phenomena. A fundamental issue in WP related studies is to locate its centroid and track its trajectory. The method used by some previous researchers for estimating the WP position seems to oversimplify the problem to a purely geometric one. This, however, is found to be systematically biased in both zonal and meridional directions. A new scheme for determining the WP centroid, which takes into account the thermal structure of the surface water, is proposed, resulting in a significant improvement in precise tracking of the WP trajectory compared to previous results. The proposed scheme may also be applicable to the determination of centers or axes of other oceanic features such as eddies, fronts and currents. [C5450]

"Evaluation of ice concentration algorithms using data fusion of SSM/I and Radarsat"

The sea ice concentration from the enhanced NASA Team (NT2) algorithm was evaluated against coincident Radarsat images. The evaluation uses a new data fusion technique accounting for the sensor's antenna pattern. Evaluation can be performed visually or statistically. This study involves cases from the Gulf of St. Lawrence, Canada during the winter of 2000. Results show good agreement between the data sets. [C5451]

"Classification of urban SAR imagery using object oriented techniques"

This paper describes the development of techniques for the production of urban mapping data from interferometric polarimetric synthetic apertures radar (SAR) data. The information contained in the radar originates from four types of data properties: radiometric, i.e. the channel intensities; polarimetric, e.g. decomposition properties entropy and alpha; interferometric, e.g. coherence and interferometric height; and geometric, e.g. shape and area. A multi-scale analysis, using the infrastructure provided by eCognition image analysis software, enables these different sources of information to be brought together. Ambiguities that result from the use of radiometric and polarimetric information alone are eliminated. A map product with broad classification information is produced. Validated results for urban scenes are presented, that were produced using data from the Deutsche Luft und Raumfahrt system E-SAR. [C5452]

"Comparison of wind vectors and air-sea temperature differences measured during SHOWEX"

During ONR's Shoaling Waves Experiment (SHOWEX) off the coast of North Carolina in November and December 1999, measurements of wind speed and direction as well as air and water temperatures were made using a variety of techniques. This paper shows a comparison of the measurements taken on December 3, 1999. [C5453]

"Air-sea interaction with multiple sensors-Seasat legacy"

By flying a number of ocean observing sensors together, Seasat demonstrated potential of not only sensor synergism, but also science synergism, which has illuminated the path of spacebased air-sea interaction studies in more than two decades since its demise. Two topics-El Nino and tropical cyclone, are discussed as examples of the science synergism inspire by Seasat. [C5454]

"Mapping wetlands of the North American boreal zone from satellite radar imagery"

The accurate assessment of spatial and temporal distributions of wetlands can have a large impact in improving the estimates of the global net carbon exchange. This paper presents the methodology and sample results for the first large-scale wetlands map of the North American boreal zone, derived from JERS-1 and ERS-2 SAR imagery. The finished product will be a consistent baseline map, which can be subsequently used for time-series analyses when continuous satellite radar observations become available. The wetlands class maps are generated using a combination of optimization-based class rule definitions and a supervised classification algorithm. The wetlands class types are those defined by the Canadian Wetlands Classification System. Results are validated at a number of study sites and compared to existing local-scale wetlands maps. [C5455]

"Combining SAR and scatterometer data to improve high resolution wind speed retrievals"

With the December 14, 2002 launch of the SeaWinds scatterometer on ADEOS-2 complementing a similar instrument aboard QuickSCAT, we now enjoy global wind speed measurements at 25 km resolution from two active microwave scatterometers. WindSat launched on January 6, 2003 with the mission to test the possibility of making wind vector measurements of comparable precision and resolution as conventional scatterometry by using polarimetric radiometry. However, the relatively coarse resolution of these instruments makes it difficult to measure winds in coastal areas. Here we show that by combining scatterometer wind direction measurements with high, sub-kilometer resolution radar cross section measurements from the RADARSAT-1 synthetic aperture radar (SAR) we can make significantly improved wind speed retrievals in coastal areas. Recently ASAR data from ENVIASAT have become available. We have just begun using this data source for SAR wind speed retrievals and have found that these data avoid some of the problems encountered with RADARSAT-1 imagery. [C5456]

"RADARSAT mapping of BORA/SIROCCO winds in the Adriatic Sea"

We examine the spatial variability of the wind/roughness fields over the Adriatic Sea during BORA/SIROCCO wind events using RADARSAT synthetic aperture radar (SAR) imagery, QUICKSCAT scatterometer wind measurements, and simulations derived from high-resolution atmospheric Limited Area Model Italy (LAMI) and Coupled Ocean/Atmospheric Mesoscale Prediction System (COAMPS). BORA winds are manifested in SAR imagery as jet-like structures exhibiting intense roughness modulations along the eastern coast. SIROCCO winds produce more uniform roughness signatures and extend over the southern Adriatic. On the basis of comparisons with the SAR imagery, the atmospheric models are able to replicate the gross morphological structures of the wind field. However, higher resolution models are required for simulating more local orographic effects. [C5457]

"The development and application of a sea surface stress model function for the QuickSCAT and ADEOS-II sea winds scatterometers"

A prototype of new geophysical model function is developed: it derives sea surface stress from the backscatter of an active microwave sensor (SeaWinds). The results are compared to values derived with a common drag coefficient, and to values derived from a state of the art surface flux model, which has been validated over a wide range of wind and wave conditions. The new model function determines friction velocity, which is the square root of the kinematic stress. The friction velocities appear to be underestimated for typical open ocean values, but appear to be excellent for stronger winds. [C5458]

"Improving on the monostatic radar cross section of targets by employing sea clutter to emulate a bistatic radar"

Aircraft that employs radar cross-section reduction techniques typically have a significantly larger bistatic radar cross-section. This paper discusses the possibility of utilising an airborne monostatic radar configuration over an oceanic region to emulate a bistatic radar. This is achieved by employing the reflective nature of the ever-present sea clutter to effectively create a "pseudo-transmitter" on the sea's surface. In addition to improving the radar cross-section of targets, this emulated bistatic radar system reduces the target's capability to locate the airborne receiver. The reflection and scattering characteristics of the sea's surface are also discussed and rudimentary models reflecting these characteristics with regard to the forward scatter region are developed. [C5459]

"Estimation of soil moisture using Radarsat repeat-passes"

The method for developing a soil moisture inversion algorithm can be approached in two ways: the multiple-incident angle approach and the change detection method. The paper discusses how these two methods can be

used to predict surface soil moisture. In the multiple incident angle approach surface roughness can be mapped, if multiple incident angle viewing is possible, and if the surface roughness is assumed constant during data acquisitions. A backpropagation neural network is trained with the data set generated by the IEM (Integral Equation Method) model. The training data set includes possible combinations of backscatter as a result of variation in soil moisture within the period of data acquisitions, and the inputs to the network are backscatter acquired at different incident angles. The outputs are correlation length and r.m.s. height. Once the roughness is mapped, soil moisture can be determined. The next approach is the application of the change detection concept. In this approach, the change in soil moisture over two different periods is determined from Radarsat data using a simplified algorithm. The methods would be applied to Radarsat data acquired over Ames, Iowa during the period June-July 2002. [C5460]

"The National Polar-orbiting Operational Environmental Satellite System future US operational Earth observation system"

Over the last nine years the Integrated Program Office has been developing the National Polar-orbiting Operational Environmental Satellite System (NPOESS). NPOESS spacecraft will be launched into three orbital planes beginning later this decade to provide significantly improved operational capabilities and benefits to satisfy the critical civil and national security requirements for space-based, remotely sensed environmental data. [C5461]

"New-ice detection using microwave sensors"

Twice-daily backscatter maps constructed from SeaWinds scatterometer data are used to monitor the rapid growth of the 2001 Odden. Scatterometer-only derived parameters are used to discriminate new-ice from open water areas. Validation is performed using RADARSAT and ERS-2 SAR scenes. It is shown that SSM/I derived information not only lag those of the scatterometer by twelve to twenty four hours, but would have told a totally different time evolution of the Odden. [C5462]

"SPOT5 geometric image quality"

SPOT5 geometric image quality's point is different from other SPOT satellites: with improved location accuracy, resolution and stereoscopic acuity, the challenge is not only to fulfill specifications but also to get a geometrically optimized system. That's why a phase of fine geometrical calibration was carried on during SPOT5's first year in orbit, in the continuity of first two months commissioning phase. This paper deals with improvements realized during optimization phase: first, each detection line's absolute calibration of viewing angles has been processed; second, continuous calibration sites observations have been carried on allowing location performances' improvement. [C5463]

"Pushing the limits of SPOT HRV resolution with steered viewing modes"

SPOT 1 to 4 satellites have been designed to provide pictures with a swath of 60 km for nadir viewing and operate in two modes: a panchromatic mode with a sampling interval of 10 meters, and a multispectral mode with a sampling interval of 20 meters. Since the modulation transfer function (MFT) is significant at Nyquist 2D-frequencies, C.N.E.S. has been undertaking new studies to find a way to increase the sampling density and therefore improve the resolution. Without any change in the spacecraft electronics or optics, a method which consists in accurately steering the satellite attitude around its 3 axis was proposed and validated on SPOT1 during in-flight campaigns in December 1998 and June 1999. The acquired pictures actually demonstrated the resolution improvement. After a presentation of the SPOT1 image chain, this paper describes the different steered modes, focuses on ground processing methods and compares the results on the pictures in order to evaluate their actual resolution. [C5464]

"SAR measurements of ocean wind and wave fields in hurricanes"

Spaceborne synthetic aperture radar (SAR) is still the only instrument providing directional information on surface wind and ocean waves on a global and continuous basis. From RADARSAT-1, many SAR images have been collected over the past years, which cover several hurricanes and allow investigation of the wind and wave fields under these extreme situations. A time-frame of 27 days of ERS-2 SAR wave mode data was processed, which covers several tropical cyclones in the Atlantic Ocean, of which Hurricane Edouard has been investigated in detail together with additional data available from scatterometers, buoys and weather centers. The wind fields and wave parameters are extracted from SAR imagery and compared to results of the numerical model output provided by the European Centre for Medium-Range Weather Forecast (ECMWF) and co-located ERS-2 scatterometer measurements. For each wave system, spectral parameters such as wavelength, wave propagation direction and wave age are calculated and compared to the numerical model output provided by ECMWF. [C5465]

"Coherence estimation from multilook detected SAR images"

This work presents an unsupervised method capable to provide estimates of temporal coherence starting from a couple of multilook detected SAR images of the same scene. The method relies on a robust measurement of the temporal correlation of speckle patterns occurring between the two pass dates. Thanks to the accurate speckle assessment, the temporal correlation coefficient (TCC) of speckle between two overlapped images taken different times is estimated. A nonlinear transformation aimed at decorrelating the data across time while retaining the multiplicative noise model is defined starting from the pixel the pixel geometric mean and ratio of the two overlapped observations. Such a reversible transformation is applied to the couple of images to expedite assessment of temporal speckle patterns correlation. The TCC of speckles is estimated from the noise variances of a transformed couple of images by inverting the relationship yielding the noise variances of the transformed data. Experiments are carried out on two SAR observations from the ERS-1/2 Tandem mission. Starting from the SLC pair, coherence is first estimated to be used as reference. Then, detected 5-looks images are produced and TCC is measured on square blocks, to yield the desired coherence estimate. A linear regression fit shows a good degree of matching with the true coherence values, which holds also on textured areas. Experiments show a good degree of accuracy, when the TCC of speckles is estimated on 32×32 blocks of geometric mean and ratio of detected 5-looks amplitude images. The method yields acceptable results also in the presence of strong reflectors and textures (urban area) where intensity-based coherence estimators generally fail. [C5466]

"Unsupervised classification of polarimetric SAR images using neural networks"

We study two unsupervised algorithms for polarimetric SAR image classification. The first one is Cloude's decomposition algorithm. The main advantage of this unsupervised algorithm is to provide terrain identification information where the most important kinds of scattering medium can be discriminated. However, his main advantage is the arbitrary location of decision boundaries. To surmount this insufficiency, we present the second algorithm based on neural networks. We propose a new scheme of unsupervised classification that combine the most important kind of trained nets. [C5467]

"Novel registration technique of InISAR and InSAR"

In InISAR system, the pixels between two ISAR images derived from corresponding antennas usually do not register properly without prior compensation. A three-dimension motion compensation method, or 3D focusing, is put forward in this paper. While the multi-antenna-pair configuration in radar system, the angular motion parameters both in the azimuth and pitching are estimated accurately and the phase unwrapping processing can be avoided in the procedure of obtaining phase unambiguous. Simulation data is used to illustrate the accuracy of the proposed method. The method has also been extended to stripmap SAR for the interferometric 3D imaging of moving and/or man-made objects. [C5468]

"The estimation of ship velocity from SAR imagery"

The estimation of ship heading and speed from a high resolution Synthetic Aperture Radar (SAR) image of a ship and its wake is important for monitoring and tracking ships from satellites. Though the ship can often be imaged clearly, its orientation may be difficult to estimate from its image because of the effect of ship motion. The wake can provide direct information about the ship heading; the cross-range separation between the location of the ship in the image and the wake provides an estimate of the speed. The performance of algorithms on ship and wake extractions from Radarsat and other satellite imagery is discussed. [C5469]

"The SSCM for ship characterization using polarimetric SAR"

Ship characterization is investigated using the symmetric scattering characterization method (SSCM), which was introduced by Touzi and Charbonneau (2002). The SSCM method appears to be very promising for ship identification. Identification of ship targets with significant symmetric scattering is shown to lead to accurate pitch measurement, under certain conditions. [C5470]

"Multiscale classification and filtering of SAR images using Dempster-Shafer theory"

Classification of high resolution SAR images is difficult due to the presence of speckle noise. We propose to use a multiscale decomposition that allows different trade-off between spatial precision (resolution) and radiometric uncertainty (noise reduction). Classification decisions at large scale are certain but spatially imprecise whereas decisions at high resolution are uncertain but spatially precise. We first decompose the SAR image in low and high frequency images at different scales using a stationary wavelet transformation. Then low pass images are classified by maximum likelihood based on a Gaussian mixture estimation. Wavelet coefficients in high frequency

images enable us to identify stationary homogeneous regions within the image where classification decisions are expected to be stable across scales. Decisions at different scales are merged using Dempster-Shafer theory which gives us an adequate framework to manipulate both uncertainty and imprecision. Finally, resulting multiscale decisions are injected in a stochastic classification algorithm (MPM) as a hidden "evidential" Markov random field. The proposed algorithm is evaluated on artificial SAR images. We also propose to filter wavelet coefficients based on the resulting multiscale confidence map. [C5471]

"A ground-based interferometer for the safety monitoring of landslides and structural deformations"

This paper concerns the use of Ground-Based Synthetic Aperture Radar (GB-SAR) interferometer for the measurement of terrain movements and structural deformations in man-made structures. This instrument can measure displacements with a precision up to a fraction of millimetre. The spatial extension of the monitored area can be of a few squared kilometres. With respect to other traditional geotechnical instruments, the presented GB-SAR interferometer can remotely monitor the target scene, providing deformation maps and not only point-like measurements. [C5472]

"Contributions of InSAR to study active tectonics of Taiwan"

Presents four case examples of contribution on InSAR to active tectonics issues in Taiwan Island that is one of the most seismically active regions in the world. For these studies, differential InSAR technique is used in a 2-pass approach, the resulting interferograms combine images of the ERS-1/2 satellites from 1993 to 2001. The results illustrate the different tectonic processes that InSAR can investigate in Taiwan: (1) regarding the 1999 Chi-Chi earthquake event, InSAR allows to capture coseismic displacements, and to detect displacements at nearby faults triggered by the earthquake, (2) in the Tainan area (SW Taiwan), InSAR can measure the interseismic crustal deformation field (uplift of an anticline) over eight years, (3) for the Fengshan fault and Longitudinal Valley fault, InSAR is able to monitor fault creep. This study makes it possible to consider InSAR as a tool (in complement to the GPS network) for monitoring several active faults in Taiwan that have the potential to produce earthquakes. [C5473]

"Curvature effects in ocean surface scattering"

EM scattering from ocean surface are described using a generalized curvature expansion of the fields at an elevated non-perfect conducting surface. The new theory describes in general the scattering of EM waves from an undulated ocean surface, and reconstructs perfectly the case of Bragg scattering (Wright, 1966), and the case of perfect conducting surface (Elfouhaily et al., 1999). The formalism is applied to the case of backscattering, and expression from normalized radar cross section for different polarization combinations is given. [C5474]

"Remote sensing observation of mining induced subsidence by means of differential SAR-interferometry"

We applied the differential SAR-interferometry to detect subsidence in the brown coal mining area of the Lower Rhine Embayment, Germany. The displacement is caused by groundwater withdrawal. For this approach, 40 ERS-1/2 scenes covering a time interval of about 4 years were processed. In a first evaluation, a mean displacement rate of about 50 mm/yr was observed. This estimation agrees very well to the leveling measurements. In addition, we applied the Permanent Scatterer techniques in order to get a detailed understanding by pointwise information beside the spatial data. [C5475]

"Land subsidence monitoring service in the Lagoon of Venice"

In order to provide the best knowledge of the subsidence process around the Lagoon of Venice to the authorities that manage the area, SAR-based monitoring techniques (differential SAR interferometry and the interferometric point target analysis) will be integrated with levelling and GPS surveys into an overall database and information system. In this contribution the different monitoring techniques are briefly introduced, the results presented and compared, and the integration concept explained. [C5476]

"Monitoring slow mass movements with the Permanent Scatterers technique"

In this paper we wish to show a few exemplificative results obtained in the framework of a wide area Permanent Scatterers analysis financed by Regione Lombardia. The core purpose was the identification and description of slope instability/failure phenomena in a relevant part of the Lombardy alpine territory (Northern Italy). [C5477]

"Measurement of the dielectric constant of seawater at L-band"

Accurate relationships between salinity and dielectric constant (which determines emissivity) are needed for sensor systems such as SMOS and Aquarius that will monitor salinity from space in the future. This paper describes a resonant cavity technique for the measurement of the dielectric constant of seawater as a function of its salinity. The purpose of the new measurements is to establish the dependence of the dielectric constant of seawater on salinity in contemporary units (e.g. psu) and to take advantage of modern instrumentation to increase the accuracy of these measurements. [C5478]

"Satellite measurements of backscatter from rain-induced roughness on the sea surface using QuickSCAT and TRMM"

The presence of rain affects the ability of the SeaWinds scatterometer to estimate surface wind speed and direction. There are several aspects of this problem. Studies are in progress to evaluate the effect of rain-induced sea surface roughness on the normalized radar cross section (NRCS) measured by the SeaWinds satellite radar on the QuikSCAT (QSCAT) satellite. In order to accomplish the wind measurement, the effect of attenuation and scattering by the atmospheric rain must be removed. The QSCAT NRCS data is collocated in space and time with the TRMM satellite, in the neighborhood of an NDBC buoy, to permit the calculation and removal of the contribution from the atmospheric precipitation. The buoy wind speed and direction provides critical information on the impact of this effect on the operational performance of this instrument, and to assist with other comparisons. Vertical profiles of the atmospheric water content and reflectivity are available from the TRMM sensors. The buoy winds are essential to estimate the nominal surface NRCS that is augmented by the rain-splash contribution. [C5479]

"Oceans 2003. Celebrating the Past ... Teaming Toward the Future (IEEE Cat. No.03CH37492)"

First Page of the Article [C5480]

"Operational oceanographic applications for the Wide Swath Ocean Altimeter"

The Wide Swath Ocean Altimeter (WSOA) is an interferometric radar instrument presently being developed by the Jet Propulsion Laboratory for integration to the Ocean Surface Topography Mission. The Naval Research Laboratory has a long history of working with satellite remote sensing instruments and applying the information to ocean environment prediction. Traditional nadir altimeter satellites measure sea level at the satellite nadir point with a footprint of about 7 km at intervals of about 6.5 km along the ground track. While the information is very useful for ocean monitoring and prediction, the limited spatial extent creates a large possibility that ocean mesoscale features such as eddies or current meanders may not be sampled. The wide swath instrument provides a much greater spatial density of measurements. The intrinsic instrument resolution is about 1 km in the across-track direction and 11 km in the along-track direction. The instrument provides measurements within these cells across a 200 km wide swath. Errors levels are high, and averaging to 15 km bins greatly reduces error levels. [C5481]

"A relationship between atmospheric rain reflectivity and elevation variance due to drop impact on the sea surface"

The additional surface roughness created by drops impacting the sea surface can bias wind speed estimates obtained from satellite scatterometric measurements. The additional roughness essentially depends on the rain content in very large drops. The estimate of this contribution will be highly dependent on the model chosen for the drop size distribution. However, it has been observed that the reflectivity of the drops falling in the atmosphere has a drop-size dependence that is very similar to that of the surface roughness induced by rain. This paper shows how reflectivity data can be used to improve the estimate of the elevation variance resulting from drop impact. [C5482]

"Rain effects on SeaWinds data"

The effects of rain on SeaWinds data are investigated using one year of SeaWinds σ^0 data, SSM/I and TMI rain rates collocated within 5 minutes of the SeaWinds observation, and tri-linearly interpolated ECMWF 10-m wind analyses. Attenuation and volumetric backscattering are parameterized in terms of rain rate, and the modification of the surface radar cross-section by rain roughening is found. The effects of different rain drop size distributions and non-uniform beamfilling are investigated. [C5483]

"Rain, wind, and backscatter: modeling rain effects on Ku-band ocean wind scatterometers"

Spaceborne Ku-band ocean wind scatterometers (SeaWinds, NSCAT) enable frequent global coverage of meso-scale ocean surface winds. These instruments measure the normalized backscatter cross-section (σ^0) of the ocean's surface from multiple look directions and use this information to estimate ocean surface wind vectors. Although σ^0 is strongly related to surface winds, at Ku-band it is also impacted to varying degrees by rain. Arguably, the most important error source for Ku-band wind scatterometers is rain contamination. In order to calibrate out the effects of rain as much as possible, we must understand the impact of rain on the backscatter measurements which are used to retrieve wind vectors. [C5484]

"Radar method for atmospheric stratification condition unambiguous determination by synergy data of sea surface altimetric and scatterometric observations"

The results of some theoretical and experimental investigations show that the difference of near sea surface air and water temperatures influences on microwave reflective characteristics of ruffled sea surface. The cause of this influence is temperature dependence of the sea surface wind wave spectrum. Besides, temperature-wind variations of radar backscattering coefficient are commensurable. Therefore, for a solution of the sea surface remote sensing inverse problem applied to near surface wind field parameters (wind speed and wind direction) retrieval it is necessary to have exact information about the condition of atmospheric stratification. However, at present, it is unknown effective and correct methods for atmospheric stratification condition precise and remote evaluation. [C5485]

"Towards an operational spaceborne system for high-resolution current measurements in coastal areas"

Along-track interferometric synthetic aperture radar (along-track InSAR) is a new technology for imaging surface current fields from airborne or spaceborne platforms with accuracies of 0.1 m/s or better, spatial resolutions on the order of 10 to 1000 m, and swath widths of up to more than 100 km, depending on platform and instrument parameters. This is particularly attractive for the mapping and monitoring of current fields in coastal areas. The SRTM experiment on a Space Shuttle in early 2000 offered a first chance to demonstrate current measurements by InSAR from space. Although the SRTM configuration was not well suited for current measurements and the coverage of the ocean was very limited, some images of coastal scenes exhibit clear signatures of typical surface current patterns, which have been found to be in good agreement with theoretical predictions and to resolve current variations on spatial scales of about 1 km. The German satellite TerraSAR-X, which will be launched in 2005, will offer similar current measuring capabilities. Concepts for more specific, further optimized InSAR missions for oceanic applications are currently under investigation. We give an overview of these developments. [C5486]

"Impact of seawinds scatterometer data on ocean surface analysis and weather prediction"

Scatterometer observations of the ocean surface wind speed and direction improve the depiction and prediction of storms at sea. These data are especially valuable where observations are otherwise sparse—mostly in the Southern Hemisphere and tropics, but also on occasion in the North Atlantic and North Pacific. The Sea Winds scatterometer on the QuikScat satellite was launched in June 1999 and it represents a dramatic departure in design from the other scatterometer instruments launched during the past decade (ERS-1,2 and NSCAT). This paper will be limited to results from the SeaWinds scatterometer on Quikscat. This presentation shows the influence of QuikScat data in data assimilation systems both from the NASA Data Assimilation Office (GEOS-3) and from NCEP (GDAS). The strategy for assessing the impact of SeaWinds in NWP was largely described and parallels the approach used for the geophysical validation of NSCAT data. [C5487]

"The delay-Doppler radar altimeter: robust and improved measurement capabilities"

A delay-Doppler radar altimeter exploits coherent signal processing in addition to incoherent waveform averaging to achieve significantly better measurement precision and instrument efficiency than are possible from a conventional incoherent instrument such as TOPEX or Jason-1. The required processing can be built into the on-board system, whose output waveforms yield geophysical parameters with the analysis algorithms already developed for conventional altimetric data. The approach enables new architectures, ranging from a single-frequency geodetic instrument (Abyss-Lite), to a three-satellite constellation of TOPEX-class altimeters (WITTEX) small enough to fit into one launch vehicle. [C5488]

"Ocean observations with a space-based delay-Doppler altimeter constellation"

A constellation of (nominally) three DDA satellites can all be placed in the same orbit plane by a single launch vehicle. Earth rotation spreads their respective nadir tracks by a spacing that is proportional to their along-orbit

separation. This constellation which we have called WITTEX (Water Inclination Topography and Technology Experiment) is a candidate approach that would meet nearly all of the requirements identified by the user community for oceanographic altimetry. The WITTEX constellation can be tuned to favor dense spatial coverage, relatively tight temporal coverage, or other priorities. In addition the constellation can be used in a dual-use mode as was Geosat, in that geoid observations over a dense ground track can be made, after which the constellation can be maneuvered into an oceanographic exact repeat mission. [C5489]

"GEOSAT follow-on GFO radar altimeter satellite performance"

Under a Navy Contract with Ball Aerospace and Technologies Corporation, the first GFO satellite was completed in 1997 and launched on 10 February 1998 on an Orbital Taurus launch vehicle. The satellite was operationally accepted on 29 November 2000. With an anticipated 8-year or more life, GFO (<http://gfo.bmpcoe.org/Gfo>) is a DoD satellite mission managed by the PEO C4I and Space, Meteorological and Oceanographic (METOC) Systems Program Office (PMW 155) located in San Diego, California. The satellite is in the same Exact Repeat Orbit (ERO) as the original GEOSAT (800 km by 108 degrees inclination). All GFO's data products are available to the scientific community and are distributed by NOAA's Laboratory for Satellite Altimetry. The primary program objective was to develop an operational series of radar altimeter satellites to maintain continuous ocean observation for accurate global measurements of both mesoscale and basin-scale oceanography. Since its acceptance, Computer Sciences Corporation (CSC), under contract with the Navy, has provided a team known as the GFO Calibration and Validation (Cal/Val). This team, assisted by NASA and NOAA personnel, has undertaken extensive and continuing calibration and validation activities on an exact repeat cycle basis. This paper will discuss the results of those Cal/Val efforts and present charts showing the performance history of the satellite, its sensors (both the Radar Altimeter and the Water Vapor Radiometer), and other relevant performance measures such as orbit accuracy. [C5490]

"Modeling rain effects on microwave backscatter from the ocean"

During the Kwajalein Experiment (KWAJEX) in 1999 the effect of rain on Ku band normalized radar cross sections of the sea, σ_0 , was measured for a wide range rainfall rates and incidence angles. The primary result was that rain significantly increases the cross section at moderate to high incidence angles, obscuring, if not eliminating backscatter from wind-generated waves. To verify our understanding of the effect of rain on sea surface roughness and to extend it to smaller incidence angles and other microwave frequencies we modeled microwave backscatter from a rain-disturbed ocean surface. To do this, we developed a realistic representation of the ocean surface perturbed by wind and rain which accounts for the damping of surface waves by rain-induced subsurface turbulence and for the enhancement of gravity-capillary and short gravity waves by rain-generated ring-waves. The spectral representation of the ocean surface is used as input to a scattering model. The multiscale scattering model used here separates surface waves into three distinct scales (short, intermediate, and long) and evaluates σ_0 for each scale. Since rain significantly alters short gravity waves (i.e. the intermediate scale), the explicit calculation in the model of backscatter from these waves makes it ideal for diagnosing the effects of rain. We will show that values of σ_0 computed by the model are in quantitative agreement with KWAJEX data. We will also show modeled rain effects on the cross section at low incidence angles for a variety of microwave frequencies. [C5491]

"Probing of the artificial hole in the ionosphere with the HF skywave radar"

This paper explains the experiment in which HF skywave radar probed the artificial ionospheric hole, which is caused by the flames of the rocket vertically launched and penetrated the ionosphere. After the rocket had passed through the ionosphere, the minimum time-delay P_{min-f} on the backscatter ionograms obviously appeared with wave and focusing stripes resulting from the irregular structure etc. The results indicated that there was a low electron density zone, the artificially created hole in the ionosphere along the propagation path. Under the asymmetry quasi-cosine ionospheric hole model, the experimental P_{min-f} was simulated with the technique of ray tracing. It was deduced that the range size of the hole in the ionosphere along the radar beams was some 573 km and the critical frequency of the center was 2.6 MHz lower than the background critical frequency (12 MHz). The ionospheric environment 350 km away from the launching site was disturbed and the propagation velocity of the ionospheric disturbance was about 50 m/s. [C5492]

"L-band VV clutter analysis for natural land"

Land clutter is statistical by nature, and its values vary in many dimensions. This paper analyzes L-band VV polarized land clutter characteristics acquired by the NASA JPL AirSAR system. In particular, this paper mainly concentrates on the distribution of clutter values with respect to grazing angle for typical vegetation communities in the Northern Territory region in Australia. [C5493]

"HF surface wave radar for oceanography-a review of activities in Germany"

The remote sensing group of the University of Hamburg is working in the field of HF radar since 1980. For the start three CODAR systems have been purchased from NOAA/ERL (developed by D. Barrick's NOAA group). Based on 16 years of experience a new system called WEllen RADar (WEERA) has been designed at the University of Hamburg in 1996. The new design aims to be as flexible as possible in order to allow easy adjustment to different requirements, i.e. working frequency, spatial resolution, and antenna configurations. The first part of this paper describes the technical solutions available to achieve resolution in range and azimuth. Modulation techniques for range resolution like Pulses and Frequency Modulation (FMCW) are compared, as well as Direction Finding and Beam Forming for azimuthal resolution. A short introduction to the algorithms is given. The second part discusses the hardware and software components which form a WEERA and are now commercially available. The third part shows an example of a monitoring system bringing together HF radar remote sensed data and numerical models. [C5494]

"Subsurface sounding of Mars: multi-pulse detection of water-related interfaces"

We introduce optimized multi-pulse algorithms for the analysis of Mars surface and subsurface radar data, referring in particular to the data which should be acquired by the MARSIS instrument in the near future. The proposed processing schemes aim at detecting the presence and estimating the depth of water-related subsurface interfaces. A statistical model is introduced to cope with the expected scenario, and maximum likelihood based detection and estimation techniques are derived. The performance of the new techniques is deeply investigated, proving the effectiveness of the proposed approaches. [C5495]

"Limits to the extraction of information from multi-hop skywave radar signals"

The performance of HF skywave radar systems is customarily referred to in terms of single-hop propagation, a mechanism which provides illumination of the Earth's surface out to ranges of around 4000 kilometres. In practice, the process of ionospheric reflection often supports multiple hops, though the signals are inevitably subjected to much greater distortion and contamination. In this paper, we address the issue of adequacy of conventional models of multi-hop propagation. We formulate a detailed model which accounts for intermediate surface scattering, and obtain a representation in terms of integrals in x - k space. We proceed to evaluate the resulting expressions for several cases of interest. The results demonstrate that it is vital to understand the complexities of multi-hop propagation if this method of observation is to be exploited for remote sensing of the ocean at extreme ranges. [C5496]

"Mars Advanced Radar for Subsurface and Ionosphere Sounding (MARSIS): subsurface performances evaluation"

According to the Mars Express mission, the MARSIS primary scientific objectives are to map the distribution of water, both liquid and solid, in the upper portions of the crust of Mars. Three secondary objectives are also defined: subsurface geologic probing, surface characterization, and ionosphere sounding. In order to obtain the primary objectives the Radar Sounder design was based on the Ice/water interface and Dry/ice interface scenario: defining the material composition of the first layers and porosity and the pore filling materials. Concerning the surface, we have characterized the geometric structure in terms of a large-scale morphology, on which a small-scale geometric structure, due to rocks, is superimposed, taking into account also that recently the structure of the planet's surface was described by means of fractals and in particular the new MARS surface models obtained by processing of the MOLA data. According to these models, this paper provides a description of the operational planning approach and expected performances of MARSIS. [C5497]

"The National Polar-orbiting Operational Environment Satellite System capabilities for operational ocean remote sensing"

Over the last decade, the tri-agency Integrated Program Office (IPO), comprised of the National Oceanic and Atmospheric Administration (NOAA), the Department of Defense (DoD), and the National Aeronautics and Space Administration (NASA), has been managing the development of the National Polar-orbiting Operational Environmental Satellite System (NPOESS). Once operational, NPOESS will replace NOAA's Polar-orbiting Operational Environmental Satellite (POES) and DoD's Defense Meteorological Satellite Program (DMSP) systems. Ocean measurements comprise one-fourth of the 55 user-validated requirements for geophysical measurements that will be made by NPOESS sensors. Ocean requirements have directly and substantially "driven" the design and acquisition strategy for three NPOESS sensors: the Visible/Infrared Imager Radiometer Suite (VIIRS); the Conical-scanning Microwave Imager/Sounder (CMIS); and the Altimeter. With these instruments, NPOESS will deliver higher resolution (spatial and temporal) and more accurate measurements of

sea surface temperature (SST), ocean surface wind vectors/stress, ocean color and derived parameters, sea ice (edge motion, age, surface temperature, thickness), oceanic heat flux, significant wave height, and sea surface topography. NPOESS spacecraft will be launched into three orbital planes beginning later this decade to provide significantly improved operational capabilities and benefits to satisfy the critical civil and national security requirements for space-based, remotely sensed environmental data. NPOESS will transform today's relatively short-term, space-based ocean research missions into a sustained, operational ocean remote sensing observation program. [C5498]

"Statistical analysis of real sea clutter data measured by a high resolution radar at low grazing angles"

Summary form only given. The exact knowledge of the sea clutter properties is of great importance for a modern maritime surveillance radar because they are directly involved in the optimization of the detection process, mainly through the CFAR processor design. Although sea clutter has been investigated by many authors for many years, a generally accepted model still does not exist. [C5499]

"Ring-wave measurements form natural rain"

We present preliminary results of our efforts to measure ring-waves generated by natural rain. Winds at sea are monitored by remote sensing of radars observing sea surface roughness. Yet rain also roughens the sea surface. Improved understanding of sea-surface roughness during rain contributes to better measurements of winds and rain at sea. [C5500]

"Investigations with SECAR-a bistatic HF surface wave radar"

This paper describes a bistatic HF surface wave radar, designated SECAR, which was deployed near Darwin, Australia, and used to conduct a variety of scientific investigations related to radar design, siting and target detection, as well as providing a test-bed for evaluating the operational utility of HFSWR as an element of a national surveillance network. The scientific results are significant because of their implications for improved radar design and effective deployment. [C5501]

"Scattering of ultrashort electromagnetic pulses by nonlinearly reflecting targets"

Nonlinear radiolocation is very promising for future remote sensing systems and it has been proposed for sensible determination and recognition of objects, including elements with different nonlinear electromagnetic characteristics. It is based on the fact that generation of higher harmonics occurs under scattering of electromagnetic waves by nonlinearly loaded conducting targets. Investigating re-reflected harmonics, one can determine a nonlinear object, and also obtain additional information. The paper investigates numerically the scattering of ultrashort electromagnetic pulses by the following models of nonlinear scatterers: nonlinearly loaded vibrator; two-dimensional plate. The calculations give the possibility of determining optimal values of electromagnetic probing pulse duration needed to obtain the maximal useful reflected signal. [C5502]

"Oil slick detection by SAR imagery: potential and limitation"

Ocean pollution by oil slicks is a major environmental hazard highlighted by the spectacular accidents of Exxon Valdez, Erika and Prestige. But, these oil tanker accidents only account for 5% of total oil pollution worldwide, 95% coming from wild discharges. In order to monitor and therefore to detect surface pollution, an effective tool has to be found. Satellite detection is well adapted to this problem, and especially synthetic aperture radar (SAR) can fill the lack of pollution survey which affects seas and coasts. Indeed SARs image oil slicks allowing estimation of the pollution risk in coastal areas. On satellite or aircraft, SAR is an interesting tool because, on the one hand, SAR images can be acquired through clouds unlike infrared or optical images. On the other hand, it is well suited to the detection of slicks because slicks modify seawater viscosity, producing a strong impact on short waves measured by SAR. The backscatter is attenuated and oil spills appear as a dark patch on the SAR image. Studies had shown that it is not easy to always detect oil slicks as backscatter depends strongly on wind and sea surface conditions among other restrictive factors. A comprehensive synthesis of previous studies shows the suitable SAR acquisition modes to detect slicks, function of the influence of SAR parameters such as polarization (VV), wavelength (C-band), incidence angle (20 to 45°), satellite or aircraft flight direction, waves and wind directions. We present here cases of easy and ambiguous detection to show the possibilities offered by SAR to automatically detect slicks, in order to improve the pollution detection and the drift forecasting in case of accidents for example. For this, ERS SAR and ENVISAT ASAR ocean images examples are shown, applying segmentation algorithms and a new approach with an original method based on ocean surface characterization. [C5503]

"A modified velocity projection method for estimating the subsurface velocity structure of the Chesapeake Bay outflow plume"

We describe a methodology for estimating subsurface velocity structure in a buoyant outflow plume from a set of available observations. The observational data include HF Doppler radar, SST and sea surface color. In addition, plume-specific temperature and salinity information from in situ observations are used minimally, if available. Detailed application of the methodology is shown via a case study for the Chesapeake Bay during November 1997. The proposed methodology depends on developing a zero-order dynamical feature model for a typical plume. Theoretical models and past synoptic observational data sets are used to design the 'plume feature model'. The feature model's primary parameters include the location and extent of the frontal boundary, a simplified gravity current structure in the vertical with prescribed (or inferred) density stratification, and spatial gradient of salinity across the plume. These parameters are inferred from remote sensing or minimal strategic in situ observations. For the Chesapeake Bay case study, a previously developed velocity projection method by Shen and Evans (2002), which obtains subsurface current structure within the Ekman layer depth from surface currents (HF Doppler radar) and wind observations, is employed in a modified configuration. The 'feature model' density stratification in shallow water is incorporated now in the dynamical projection equations. The resulting subsurface projected currents are compared with available ADCP profiles. The difference between the density-stratified estimate and ADCP is further used to calibrate and improve the zero-order dynamical feature model parameters. This synergistic approach can now be applied to other shallow water features such as salt lenses and other anomalous entities. [C5504]

"A new temporal interpolation method for high-frequency vector wind fields"

A new technique for the time interpolation of the forcing fields that recovers the movement of propagating features is introduced and applied to vector wind fields. The method involves the decomposition of the fields into their complex empirical orthogonal functions, and the interpolation of the temporal functions for the significant modes. The technique is tested using atmospheric model vector wind fields sampled at coarse temporal resolution to demonstrate the recovery of the wind fields at the intermediate times. The technique is also applied to a gridded vector wind product from satellite scatterometer data. [C5505]

"A new method for calibration of SAR image"

With the rapid development of remote sensing technology in these years, people can get a lot of synthetic aperture radar (SAR) images of the earth's surface easily. The problem is that, people need to know the exact properties of the ground surface from the SAR images which is derived from the different kinds of remote sensing system. So the calibration of SAR image is needed. In this paper, a new methodology for calibration of SAR images and its realization for existing airborne strip map SAR system are put forward. After analysis of the range-Doppler imaging algorithm, a system model is given, and a calibration method is proposed in this paper. Computer simulation is used to verify the validity of this calibration method. [C5506]

"Feature-based multi-resolution SAR and TM images auto-registration"

This paper introduces a method for automatic registration and fusion of multi-resolution SAR and TM images. We use a new model to extract and match features from multi-resources images, and register the images by affine transformation using accurate RCPs derived by feature-based algorithms. After registration, we fuse SAR and TM images by ratio method. The result shows that the algorithm is efficient. [C5507]

"Improved global marine gravity by retracking altimeter waveforms"

We present a new global marine gravity anomaly model with errors nearly a factor of two lower than our previous global models. This improvement is achieved by re-tracking the raw echoes of the ERS-1 radar altimeter. Ocean surface waves are a fundamental limitation to the recovery of gravity anomalies from satellite altimeter profiles. For example, to recover the gravity field at an accuracy of 1 mGal at 20-km full wavelength requires measuring the ocean surface height change over a 10-km horizontal distance to a precision of 1 cm. Standard processing of altimeter data provides a height precision of only about 5 cm at this length scale. These standard products are optimized for recovery of ocean surface height, significant wave height and wind speed and are based on tracking algorithms having at least three unknown parameters. The most precise retracking algorithms are heavily weighted to match the onset time of the leading edge but we show this onset time is nearly perfectly correlated with the wave height parameter. If one assumes the wave height changes only slowly with distance, re-tracking can be performed with a more precise, two-parameter model. Repeat cycles across the South Pacific (area of high sea state) show improvement in along-track slope error from 6.39 microradian to 3.34 microradian and there is a corresponding improvement in resolution from 40 km to 31 km. In addition there

are improvements in ocean coverage, especially near coastlines and on the shallow continental margins. The quality of the retracked ERS-1 data are superior to non-retracked Geosat geodetic mission data suggesting the Geosat data can be improved as well. [C5508]

"Integrating bathymetry, topography, and shoreline, and the importance of vertical datums"

NOS/NOAA has developed a vertical datum transformation tool, VDatum, which allows transformation of bathymetric and topographic elevation among 28 different orthometric, ellipsoid/3-D, and tidal datums. This tool is based on the latest geoid, ellipsoid, and tidal hydrodynamic models. A national vertical datum transformation database ("National VDatum") is being developed and populated by NOS, and a major effort remaining is the tidal modeling of every bay and estuary in the US, plus some refinements of the geoid model in Alaska. The use of VDatum will be a cornerstone of the new way that NOS will acquire, handle and process bathymetric and shoreline data and efficiently use these data to produce NOAA nautical chart and electronic vector products and to support coastal resource managers. Some applications for which National VDatum is critical include: (1) the sharing of geospatial data among NOAA, USGS, FEMA, NIMA, and other federal and state agencies, which datum incompatibilities have limited in the past; (2) the implementation of a full National Bathy/Topo Program with the U.S. Geological Survey, VDatum being required for the blending of NOAA's bathymetric data with USGS's topographic data; (3) the measurement of consistently defined MHW shoreline from RTK-GPS-referenced Lidar elevation data from the intertidal zone, transformed with VDatum to the MHW datum, with the zero line then being the shoreline; (4) meeting local coastal user needs for being able to blend their bathymetric and topographic data with that obtained by other groups; local users are requesting a National VDatum for this reason; (5) the implementation of a seamless National Bathymetric Database, using VDatum to transform all historical data sets to a common datum (MLLW); (6) improving the efficiency and accuracy of RTK-GPS-referenced hydrographic surveys by eliminating the need for simultaneous tide installations, settlement/squat corrections, and time-consuming post processing; (7) the ability to use high-quality 3rd-party bathymetric data in NOAA nautical chart products, with VDatum solving the datum incompatibility problems that have prevented this; (8) marine boundary applications; and (9) the ability to link with creation of GIS layers and digital elevation models required for habitat restoration projects. [C5509]

"Fine resolution satellite-based winds for episodic events"

Improvements are made to regularly gridded wind fields, based on seawinds scatterometer observations, with the goal of better representing episodic wind forcing for meteorological studies and for forcing ocean models. [C5510]

"The determination of surface salinity with SMOS-recent results and main issues"

The European Space Agency SMOS (Soil Moisture and Ocean Salinity) mission aims at obtaining global maps of both variables from space for large scale climatic studies. It uses an L-band microwave interferometric radiometer with aperture synthesis (MIRAS) to measure brightness temperature (TB) emitted by the Earth surface and then compute from it the two geophysical parameters. The retrieval of salinity is a complex process that requires the knowledge of other environmental information and an accurate processing of the radiometer measurements. Here we present the recent results obtained from different studies and campaigns as part of the SMOS mission and highlight the different issues still to be solved. [C5511]

"Uncertainties on salinity retrieved from SMOS measurements over global ocean"

In order to prepare the Soil Moisture and Ocean Salinity (SMOS) mission, we present 1) the sea surface salinity precision that could be achieved with the SMOS radiometer measurements and 2) the time and space scales over which averaged SMOS Tb should remain relatively constant in order to prepare after-launch monitoring of radiometer drifts. Leaving aside errors due to the instrument and the image reconstruction process, the SSS averaged over 200 x 200 km² areas and over 10 days retrieved from SMOS measurements should meet the GODAE requirements with a precision better than 0.1 psu in most oceanic regions, assuming random noise on W and SST of 2 m s⁻¹ and 1 °C, respectively. On another hand, this requirement will not be met if no a priori information on the wind speed is available. However, it is likely that SMOS Tb will suffer from temporal drifts and/or from regional biases linked to sun disturbances for instance. In these biases are going to be monitored using Tb averages, it will be necessary to take into account wind speed variability. [C5512]

"A cardioid model for multi-angular radiometric observations"

L-band passive microwave remote sensing sensors are able to provide estimates of surface soil moisture, on both spatial and temporal scales compatible with applications in the fields of meteorology and hydrology. A radiometric system using a 2-D interferometric design with multi-angular viewing capabilities will be borne by the

Soil Moisture and Ocean Salinity (SMOS) space mission. The basic rationale for retrieving soil moisture from radiometric measurements is the assumption that the surface layer can be modeled as a dielectric medium. Its dielectric constant then depends on several physical parameters, including soil moisture; emissivities for various incidence angles are computed using Fresnel's formulas. Many controlled field experiments have demonstrated the validity of this approach. Scenes exist however (e.g. ice covered or frozen surfaces, complete desert areas) where surface soil moisture is not a relevant concept. For such scenes, information should however be available on the complex dielectric constant itself. This communication describes a methodology which aims at retrieving in an optimized way the dielectric constant information available from multiangular radiometric data. [C5513]

"Triple-frequency radar for cloud and precipitation microphysics research"

The University of Massachusetts (UMass), Colorado State University (CSU) and the National Center for Atmospheric Research (NCAR) are collaborating to develop an advanced multifrequency radar (MFR) system for studying clouds and precipitation, which should become operational in 2004. This highly portable radar consists of three polarimetric Doppler subsystems operating at Ku-band (13.4 GHz), Ka-band (35.6 GHz) and W-band (95 GHz), a programmable scanning pedestal, and a unique single aperture antenna that generates colocated matched beams at each frequency. This combination of frequencies allows measurement of a wide range of atmospheric targets including weakly reflecting clouds and precipitation. [C5514]

"IGARSS 2003. 2003 IEEE International Geoscience and Remote Sensing Symposium. Proceedings (IEEE Cat. No.03CH37477)"

First Page of the Article [C5515]

"The Soil Moisture and Ocean Salinity mission"

Surface soil moisture is a key variable of water and energy exchanges at the land surface/atmosphere interface. But currently there are no means to assess it on a global and timely fashion. Similarly, our current knowledge of sea surface salinity is very reduced. One way to overcome this issue would be to use an adequate space-borne instrument. The most promising instrument would then be an L-band microwave remote sensing sensors as they are able to provide estimates of surface soil moisture and sea surface salinity, on spatial and temporal scales compatible with applications in the fields of climatology, meteorology and large scale hydrology. The ESA Earth Explorer Opportunity mission SMOS is the first to attempt to fulfill such a gap. SMOS is based upon an L-band 2-D interferometer. It is thus an innovative concept of bi-dimensional aperture synthesis method to obtain surface measurement with an appropriate resolution from a tractable (in terms of dimensions) space-borne instrument. Moreover, the sensor has new and very significant capabilities especially in terms of multi-angular view configuration. This paper will describe the SMOS concept in terms of instrument (characteristics) and will investigate the main aspects of the retrieval capabilities of the 2-D microwave interferometer for monitoring soil moisture, vegetation biomass and sea surface salinity. The analysis is based on model inversion taking into account the instrument characteristics. The standard error of estimate of the surface variables is computed as a function of the sensor configuration system and of the uncertainties associated with the spatial measurements. The inversion process is based on a standard minimisation routine that computes both retrieved variables and standard error associated with the retrievals. Nevertheless, retrieving surface variables from such as instrument is not necessarily straightforward. Over the oceans, a very high sensitivity and accuracy are acquired. Over the land the main issues are linked to mixed pixels and topography. Using other sensors/mission (such as Aquarius over the oceans) and assimilation techniques will be used to address these issues. The potential of SMOS, depending on the view angle configuration and the use of the sole 1.4 GHz is thus investigated. These questions are key issues to define the observation configuration of SMOS that meets the scientific requirements and the technical constraints of the spatial missions. [C5516]

"NEOS: the North East Ocean Observing System by: Scott Glenn & NEOS partners"

Ocean.US is coordinating the development of a National Federation of Regional Associations of Coastal Ocean Observing Systems. It is anticipated that on the order of ten regional associations will evolve. These associations will coordinate regional enhancements of the existing and expanding national backbone of coastal ocean observations. [C5517]

"Performance of a VHF ocean surface radar in the surf zone"

In the high VHF band (152.2 MHz) the Bragg scattering waves on the sea surface have wavelengths of about 1 m. The radar Doppler spectrum of echoes can be heavily modulated by swell in open water, and in the surf zone the effect is enhanced. Under these conditions the Bragg first-order lines are broadened. This paper reports on a study to evaluate the integrity of the surface current maps produced by the VHF coastal ocean surface radar

within the surf zone. Comparisons are made with radar data under calm conditions, and with currents measured with an acoustic current profiler mounted on the bottom. The radar current measurements are slightly more noisy under rough conditions, but it is clear that this technology has potential to monitor rip currents and coastal vortices in the surf zone when conventional techniques become strained. [C5518]

"Surface transport and mixing in Monterey Bay. I: Objective surface current maps"

"Summary form only given". HF radars measure synoptic surface currents near the coast at time intervals like one hour with spatial resolution of a few kilometers. Although increasing numbers of HF radars make synoptic surface current maps routinely available, these maps are not useful for environmental or ecological studies, which require quantitative descriptions of near surface transport to study the impacts of upwelling, the ecology of nearshore habitats, or the effects of harmful algal blooms or oil spills. Particle studies provide a natural way to reveal synoptic surface transport properties embedded in a synoptic Eulerian velocity archive. Particle trajectories cannot easily be computed directly from an HF radar surface current archive, since the measurements contain space and time gaps and do not extend to the shoreline. Here we apply a technique called normal mode analysis (NMA) to objectively map HF radar surface current archives in Monterey Bay so that particle trajectories can be reliably computed. The NMA technique uses two sets of basis functions (vorticity modes and divergence modes) and exactly enforces no normal flow at the coastline and a specified normal flow (obtained from the radar measurements themselves) along the open boundaries. Spatial filtering is applied to reduce white noise, and an eight hour low-pass filter (with a sharp cutoff) is used to limit large accelerations while preserving semidiurnal fluctuations. The resulting objective maps typically recover about 70% of the mean kinetic energy in the radar measurements. This is the first of three talks describing the computation of synoptic maps of particle properties from HF radar measurements in Monterey Bay. [C5519]

"A complex of polarimetric, combined active-passive sensors of L-, C-, and X-band of frequencies for vessel and airborne application"

Summary form only given. A complex of polarimetric (dual polarization), combined active-passive devices of L-, C-, and X-band of frequencies for land and sea surface microwave reflective and emissive characteristics simultaneous and coincident measurements is presented. The complex is dedicated to solve the problem applied to near sea surface wind and surface wave fields' parameters precise and unambiguous retrieval, as well as for sea surface signatures detection and identification. The methodology of experiments' performance and field calibration will be discussed. The results of preliminary measurements of sea surface radar backscattering coefficients and brightness temperatures under various conditions of observation (angle of incident, location and polarization), air-water temperatures, wind and wave parameters will be presented. Relationships between sea surface radar backscattering coefficients, brightness temperatures, statistical characteristics of radar signal frequency's distributions and the parameters of observed media will be built. As well as correlative properties between fluctuations of sea radar backscattering coefficients, radar signal frequency distribution characteristics and brightness temperatures due to the change of sea surface principal parameters air-water temperatures, wind speed and direction, sea wave force and swell condition will be presented. Vessel and airborne application properties of such a complex application for sea surface mapping will be discussed. [C5520]

"Bound waves and radar backscattering from the sea surface"

New effects recently revealed in field experiments conducted in IAP RAS on radar probing of the sea surface and associated with strong nonlinearity of short gravity-capillary waves and generation of high-order harmonics and "parasitic" capillary ripples (bound waves) are discussed. Wave tank experiments on radar probing of short wind waves in the presence/ absence of films are also described and relative intensities of linear and bound waves are estimated. Field and wave tank experiments has confirmed the expected intensification of modulation of Bragg ripples due to long surface waves, the modulation coefficient has been shown to be several times the modulation on a clean water surface. [C5521]

"Ocean environment sensing using polarimetric and interferometric SAR"

New methods have been investigated which use fully polarimetric synthetic aperture radar (POLSAR) image data to measure ocean wave slopes. Independent techniques have been developed to measure wave slope spectra in both the radar azimuth and range directions. Wave spectra measured using the new methods are compared with spectra developed using conventional SAR intensity-based methods, and with spectra from in situ buoys. Wave-current interactions may also be measured using the same measurement techniques. NASA/JPL/AIRSAR L-band image data from California coastal waters and from the New York Bight are used in the studies. NRL has also recently lead two collaborative field experiments that feature Along-Track Interferometric SAR (AT-INSAR) systems. In April, 2003, NRL, NASA JPL and UCLA collaborated in a study of sub-mesoscale coastal eddies

that featured the NASA/JPL/AIRSAR. NRL has also recently collaborated with the University of Massachusetts in a deployment of their Dual Beam Interferometer on the west coast of Florida. This paper presents preliminary data from both of these experiments. [C5522]

"Posteriori estimation of low altitude propagation loss from radar sea clutter data"

This paper describes the estimation of propagation loss and its statistical properties based on observations of radar sea clutter data. This problem is solved by first finding an ensemble (about 105 models) of relevant refractivity model parameters and then using all these models to map into the propagation loss domain. In this mapping each refractivity model is weighted according to its data likelihood function. [C5523]

"Detection of small targets in ocean wave clutter using panchromatic time series imagery"

Visual detection of small objects on or near the ocean surface from an aircraft is important for search and rescue, and detection of stealthy boats and other militarily important targets. This is made difficult by a combination of the rapidly moving sensor platform and the typically high level of modulations in scattered light at the surface. To achieve reasonable search rates, the observer must scan through modest grazing angles (i.e., look towards the horizon) where the ocean clutter that limits detection performance is varying light from wave facets and white caps. This paper describes a technique for significantly improving the signal-to-clutter ratio. A time series of images is mapped to a common reference frame at the level of the mean ocean surface, separating time and space variations, and the temporal dwell is utilized. For moored targets, the signal may be simply integrated up in time, while for drifting and powered targets, it must be integrated along the appropriate target velocity vector. Specific examples are provided for navigation buoys, small surface floats and slowly moving boats, most of which are difficult if not impossible to find in any single image frame. Achieved gain using panchromatic images is shown to approach 20 dB in cases where the velocity vector is known or can be calculated from the data. [C5524]

"Bistatic mapping radar BISAR"

Synthetic aperture radar (SAR) is a system of active prints that are loaded in a sensor able, to carry out the cartography of natural scenes with a better resolution. SAR supplies images based on the waves reflected by the Earth's surface that do not appear on classical optical images. Indeed, radar waves may describe drifted ice in aquatic surfaces; they can penetrate under vegetation and even slightly into the basement. However, the main problem with this approach is the interpretation of the radar image that is different from usual graphics. When the radar is composed of a simple antenna, we speak about a monochromatic configuration. The antenna works in alternative it will function as a transmitter and then switch to a receiver. The radar can be designed to operate with two separate antenna to perform the transmit and the receive functions, and this may be called bistatic radar. The bistatic system has particular features coming from the separation between the transmitter and the receiver. In this configuration, the transmitter illuminates the scene with beam pointed to its centre. The diffused signal is then picked up by the receiver. Technological progressions enabled to place the receiver and the transmitter aboard satellites, ships, planes or other carrier. The delocalisation of both the transmitter and receiver makes it possible to improve the capacity of detection and identification of the radar, and thus to increase the detection capacity of a furtive target. This paper presents the potential scientific objective of the bistatic synthetic aperture radar (BISAR). First, it begins by an extension of modelling, proposed by literature such as monostatic scalar radar model and vertical model (that take in account the polarisation wave in the transmitter and the receiver) are presented. Then, the next part will be devoted to the development of two bistatic methods that are an extension of monostatic approaches. Namely, method of coherent summation and method of adapted filtering. [C5525]

"A new ocean SAR imaging process simulator"

In this paper, we develop the concept of a new ocean SAR imaging process simulator. We intend to come up with a simulator more complete than those which have been developed until now. Indeed, in addition to the large number of oceanic and atmospheric phenomena considered, the simulator should lead to cope with various radar configurations (spaceborne, airborne, grazing-angle). The simulator is based on several interconnected units allowing to model the sea surface features and their interactions with the radar electromagnetic waves. We develop the hydrodynamic modulation of the short waves by the long waves which are at the core of the process. The peculiarities of different type of radars and radar carriers are also included. [C5526]

"Multi-frequency HF radar for mapping current shear and vector winds"

A new radar is in final stages of development and testing by Imaging Science Research (ISR), Inc., under sponsorship by the Office of Naval Research. The system is based on digital receiver technology incorporated

into a PC operating environment. The capability of broad band operation across the whole HF band and beyond allows for new applications in both ocean sciences and ship traffic control. Use of bistatic geometry simplifies logistics and allows all data acquisition and processing to be done at a single site. The use of multiple frequencies for ocean science application allows one to measure current shear in the vertical dimension over depths of the order of a few meters. Recent results by other co-workers has shown that under some conditions, such vertical shear can be used to infer wind speed over the radar cell by matching the stress across the surface boundary layer. [C5527]

"Recent results from a nested multi-static HF radar network for the NorthEast Observing System (NEOS)"

Summary form only given. A nested HF radar network has been deployed along the New Jersey coast as part of the New Jersey Shelf Observing System (NJSOS) and the larger regional NorthEast Observing System (NEOS). A 25 MHz standard system (range about 50 km) setup for continuous operation since 1999 includes two sites in Brant Beach and Brigantine, New Jersey. A second 5 MHz long-range system (range about 170 km) includes four New Jersey sites set up in Wildwood, Tuckerton, Loveladies, and Sandy Hook, and one Massachusetts site in Nantucket. Both the long-range and standard-range systems provide real-time maps of surface currents, with resolutions of 1.5 km (standard) and 6 km (long-range). Recent additions to the network included GPS synchronization, which allows all long-range sites to operate on a single frequency without interfering with each other. In addition to single frequency operation, the GPS synchronization allows the existing coastal stations to be bistatically linked to each other. Without adding additional hardware, four coastal sites provide four monostatic radial current maps and 12 bistatic hyperbolic current maps simultaneously. This both increases data coverage and reduces measurement error. Two bistatic transmitting buoys (one 25 MHz and one 5 MHz) complement the coastal sites. This operational, nested, and multistatic network provides real-time current maps for scientific and operational users. [C5528]

"An alternate analysis for the second-order high frequency bistatic radar cross section of the ocean surface-patch scatter and its inversion"

In this paper, the verification of the second-order high frequency (HF) ocean surface cross section for a surface patch remote from the transmitter and receiver is presented. The bistatic result is shown to reduce to the proper monostatic models when the appropriate geometry for backscatter is introduced. In particular, the electromagnetic coupling coefficient for the bistatic case is seen to incorporate its monostatic counterpart. It is well-known that the second order portion of the HF radar spectrum of the ocean echo contains substantial information on the surface gravity wave spectrum. Thus, the initial analysis forms the basis for the extraction of ocean surface parameters from bistatic HF radar data. An inversion technique for extraction of ocean surface wave parameters from bistatic HF radar data is briefly developed here. The inversion results from simulated spectra are seen to be very reasonable. [C5529]

"The SAHARASAR project: potential support to water prospecting in arid Africa by SAR"

First Page of the Article [C5530]

"A modified apodization method in SAR/ISAR processing"

SAR/ISAR image processing involves a 2D Fourier transform that produces high intensity sidelobes which obscure low intensity scatters in the image. Although the sidelobe can be reduced using parametric windows, the image resolution becomes worse. The apodization technique can reduce sidelobe level while maintaining the image resolution. In this paper, based on the analysis of the apodization algorithm, a modified apodization method was present via stronger constraint. The modified method has higher resolution and lower sidelobe level than the original method. This method was proved correct with a real ISAR image. [C5531]

"Generation of geometrically and radiometrically terrain corrected ScanSAR images"

Inclined surface topography diminishes the geometric and radiometric quality of synthetic aperture imagery. The correction of these effects becomes indispensable when quantitative image analysis is performed with respect to the derivation of geo- and biophysical parameters. Due to their spatial extent and frequent availability, ScanSAR image products extend the operative range of microwave imagery and have a high potential for numerous operational applications over larger areas. The study presents a procedure for a pre-operational terrain correction of ScanSAR imagery as acquired by RADARSAT and ENVISAT ASAR. [C5532]

"Speckle filtering of SAR images using Hülder regularity analysis of the sparse code"

This paper introduces a novel approach for filtering speckle in SAR images using the Hülder regularity analysis of the sparse code. Recently, sparse code shrinkage was proposed for filtering images corrupted with additive white Gaussian noise. Sparse coding is a method for finding a representation of the data in which only a small portion of the basis is simultaneously active. In the proposed approach, first the sparse code representation for the SAR image is obtained. Then, the pointwise Hülder exponent is computed for each of these basis functions and used as a cost function for basis enhancement. This enhancement is the key for reducing speckle in SAR images. As the results show, the reconstructed images have a better visual perception as compared to those obtained by adaptive filtering techniques and coefficient shrinkage based algorithms. [C5533]

"Extraction of vegetation parameters based on simulated annealing algorithm using polarimetric SAR interferometry data"

An inversion scheme of vegetation parameters based on a simulated annealing algorithm using polarimetric SAR interferometry (Pol-InSAR) data is presented. Comparing the result of inversion with field measurement, it indicates that the inversion algorithm can obtain the height of vegetation with good accuracy. [C5534]

"Impact of ScanSAR images' radiometric calibration on vessels and identification"

Image quality and radiometric calibration of several RADARSAT ScanSAR processors has been compared to assess impact of different processors on the vessel cross section and on the background, respect to the automatic detection as well. Several ocean scenes processed by four different ScanSAR processors have been analysed and some variability in image quality and radiometric calibration have been found. In this study cross sections of the same targets, present in the selected images and identified thanks to the Vessel Monitoring System (VMS) data, have been analysed to find out the differences among them and where it is possible to link these differences to some specific parameters. [C5535]

"Simulation study of stochastic dark line features in in correlated K-distributed images"

Intensity fluctuation of synthetic aperture radar (SAR) images, due to speckle and texture, statistically brings series connections of dark pixels. Resolution enhancement of SAR systems can provide texture with correlation properties. In this paper, simulation studies are carried out to investigate the relation between occurrence of the stochastic dark line features and texture correlation. [C5536]

"Enhanced zone detection in radar images via fusing the maximum entropy and variational analysis methods"

A new approach is addressed for denoising and reconstruction of the radar images degraded by spatially-shift-invariant linear system and contaminated with additive Gaussian noise. The fused Maximum Entropy-Variational Analysis method is developed and computationally implemented using the modified Hopfield neural network. The enhanced zone detection and image denoising are achieved using the proposed approach. [C5537]

"An estimation method of target location and scattered waveforms for UWB pulse radar systems"

This paper presents a method of estimating target location and scattered waveforms, whose accuracies are interdependent. The technique relies on iterative improvements of estimated dominant-frequency waveforms. Description of the algorithm is followed by statistical simulation examples. The performance of the technique is contrasted with conventional methods and statistical bounds in terms of target locating accuracy. Results indicate that our proposed method has a remarkable performance, which is close to the theoretical limit. [C5538]

"Using radarsat to detect and monitor stationary fishing gear and aquaculture gear on the eastern Gulf of Thailand"

Five Radarsat-1 images from the fine beam mode (F2, F4, F5) taken between April and July 2002 were processed and statistically analyzed to determine their fishing and aquaculture gear detection abilities. Combinations of these multi-temporal and multi-angle images were used to attempt detection and separation of the gear types. Image processing techniques such as speckle filtering, region-based segmentation and supervised classification were applied to test the ability to separate the backscatter signals of four different gear types common to the study area. [C5539]

"All direction auto-adaptive dynamic window filter for noise suppression in SLC SAR image"

To smooth coherent speckle noise and preserve edge information in SLC SAR images as precise as possible, a new algorithm called all direction auto-adaptive dynamic window filtering method based on coherent speckle

statistic characteristic and analysis of spatial filtering algorithms for SAR image, is developed in this paper. For every processing pixel the filtering window is divided into mutually exclusive all direction sub-windows according to the complexity of image texture and edge existence. Local relative standard deviation is used to determine whether the local filtering window area is homogeneous. Then a Kuan filter and a 3x3 directive operator are incorporated to process the SAR image. The proposed method can auto-adaptively modulate its filtering window size and selection of filtering pixels. The developed method is applied to a single-look ERS SAR image. Experimental results show that the performance of the method is satisfactory in both speckle suppression and preservation of image details. [C5540]

"Edge detection and extraction for SAR images"

Edge information is useful for various remote sensing applications: classification, relief reconstruction, image analysis. A lot of methods have been proposed to process edge extraction, with respect to the hypothesis of additive noise. All these methods are usually based on differential operators followed by a non local-maxima suppression or a zero-crossing search. In SAR imagery, presence of speckle noise makes derivative methods not applicable because of non-constant false alarm results. Usually, ratio operators are used for SAR image processing. In this paper, we propose a new edge detector based on a ratio. This operator has the particularity to deliver signed results. Then we apply two edge extraction methods: the first one based on a non local-maxima suppression, and the second on a non zero-crossing suppression. [C5541]

"Airport detection and runway recognition in SAR images"

This paper presents a novel approach to the detection of airport runway in SAR imagery, which combines a region-based method and a Hough transform analysis stage using contextual information to identify suitable signatures. For the recognition of runway, the points are grouped using a Hough transform to find potential runway; finally, The result of this procedure is the fast and accurate identification of airfield runways. Recognition results on high resolution SAR images are given. [C5542]

"Texture estimation in SAR images of forests"

Texture information plays an important role in interpreting remote sensing images, especially high spatial resolution images. Image texture measures the relationships between pixels and their neighbors. For SAR images, it is apparent that there are fluctuations in addition to speckle. Physically, these appear to be caused by variations in the scene structure. Texture reveals the intrinsic spatial variability of natural scenes and is a valuable feature to discriminate different land types. Many methods and models to describe and estimate texture have been developed. A major problem with texture models is the efficiency and computational complexity. We are faced with a compromise between choosing some simple parameters that fail to reproduce the observed image characteristics accurately and more sophisticated models (with many degrees of freedom) that better fit the observation but are slow to compute. In this paper, we investigate two texture models based on the two types of measurements: correlation length and Gaussian Markov random field(GMRF). The particular application of this study is to use the texture from JERS and RADARSAT data from the Amazon to better distinguish different classes within the forest. The texture information can be used by the classification and segmentation processes to improve the accuracy of the results. The estimated texture helps improve the estimation accuracy of forest parameters such as biomass and tree height. [C5543]

"A new parameter for IFPOL coherence optimization methods"

The interferometric coherence optimization methods are based on the definition of projection vectors, which is the way to combine the information occurring from the polarimetric channels of both interferometric images. Optimization algorithms have already been proposed. In order to know in which cases these algorithms really improve the scalar interferometric result, a new entropy parameter H' calculated with the eigenvalues found by the second optimization method and called IFPOL entropy is introduced. The physical significance of this entropy parameter is first explained. Particular cases where this parameter is equal to 1 are studied. Finally, we explain how this parameter H' can be used in order to obtain more information on the scene and, for example, to improve terrain classification methods. [C5544]

"A philosophical discussion of the physical limits of radar"

Any radar setup is limited by the physical properties of the electromagnetic radiation used to gather information about a target. Some of the limits on accuracy are due to the quantum nature of the photons, others due to the limitations of the electronic equipment used to perform the modulations. The techniques used to record the characteristics of the radiation are as important as the method by which that information is analyzed and interpreted. In each stage of the travels of the radiation, from creation and propagation to recording and analysis,

the physical properties of the photons involved play a key role in the behavior of the radiation. The techniques by which these properties are modulated, monitored and recorded are also important. In this paper, these topics are discussed and weighed in detail. From this understanding of the flow of information a theoretical apparatus will be constructed that will be capable of recovering a maximum of that information for later use. [C5545]

"Leaf area index inversion using multiangular and multispectral data sets"

Leaf area index (LAI) is an important parameter for describing vegetation canopy structure in the terrestrial ecosystem. LAI is closely related to plant transpiration, sunlight intercept, photosynthesis and Net Primary Productivity. Multiangular remote sensing is capable of providing more three-dimension information of vegetation, and it is powerful in solving the problem of the same object with different spectrum or vice versa. As a result, multiangular remote sensing and Bidirectional Reflectance Distribution Function (BRDF) model based inversion may be more suitable for Leaf Area index (LAI) retrieval over row crop canopies. However, it's still difficult to get LAI without enough a priori knowledge due to the underdetermined problems in inversion. We use the multispectral information to get the a priori estimation of LAI, and then perform BRDF model inversion. Different from the general one channel based BRDF model inversion methods, our new methods use the multiangular and multispectral data sets together to increase the available information in inversion, i.e., it is a synthetic method. From the inversion results we found that the new synthetic method is more effective in LAI inversion. [C5546]

"Spectral and radiometric distortion evaluation of pan-sharpened XS imagery obtained from compressed XS and pan data"

This work reports about an original application concerning lossy compression of multispectral (XS) and panchromatic (Pan) images collected by spaceborne platforms. Generally, the former is a set of three or four narrow-band spectral images, while the latter is a single broadband observation imaged in the visible and near-infrared wavelengths. Since high resolution spectral observations having high SNR are difficult to obtain, and especially to transmit, the Pan image, having resolution typically four times that of XS, but slightly lower SNR, is added to the XS data and used with the main purpose of expediting both visual and automatic identification tasks, possibly through an integration (merge) with the lower resolution XS data. Whenever XS data at the same resolution of the Pan data and with adequate SNR were hypothetically available on board, the bottleneck of downlink to receiving stations would impose severe limitations in the bit rate, so that a lossy compression would be mandatory. The consequence of the loss of information is a distortion, both radiometric and especially spectral, which may be easily quantified. [C5547]

"Unsupervised Bayesian reconstruction of microwave images from real data"

We address the problem of non-linear microwave imaging for the reconstruction of dielectric profiles. We propose a statistical based inversion algorithm, adopting the Bayesian (MAP) framework and a complex Gaussian MRF model for the image. The use of statistical algorithms for the estimation of the complex MRF parameter leads to a robust and effective non-linear inversion method. Some experiments on real data are able to show the good performance of the method. [C5548]

"Linear distribution-based retrieval of underground voids"

This paper deals with the problem of determining the shape of unknown scattering voids embedded in a homogeneous half-space from the measurements of the magnetic scattered field over a measurement domain parallel to the air-soil interface. The formulation accommodates the distributional nature of the induced surface equivalent current densities. Thus, as unknown, a single layer distribution whose support accounts for the boundary of the scatterers is chosen and is reconstructed by a singular value decomposition based algorithm. Numerical examples resulting from the application of such algorithm are presented. [C5549]

"TSVD spatial resolution enhancement of microwave radiometer data: a sensitivity study"

In this paper a sensitivity study of the truncated singular value decomposition (TSVD) for spatial resolution enhancement of radiometric data is detailed. A large set of meaningful experiments is presented and discussed. [C5550]

"Fusion of airborne synthetic aperture radiometer and Landsat ETM+ images"

Unlike optical images, the microwave radiometer image contains information of ground brightness temperature. To integrate some features of microwave radiometer images and optical images, some transform schemes, such as intensity-hue-saturation (IHS), principal component analysis (PCA) and wavelet transform (WT), were applied

to merge the airborne synthetic aperture radiometer images and Landsat ETM+ images. The experiments show that the wavelet based transform method shows the best potential among the three methods. [C5551]

"Water body extraction from multi-source satellite images"

This paper introduces an original entropy-based method for water body extraction from multi-source satellite images. The proposed method is remarkably simple and relies only on the assumption that water body in the image is a smooth area. This assumption is most of the time verified in optical and radar images, which makes the approach insensitive to image sensors. Experimental results illustrate the robustness of the proposed approach. [C5552]

"Improvement research on texture-detection in full-polarization SAR image filter"

The Polarimetric Whitening Filter (PWF) method for speckle reduction in polarimetric synthetic aperture radar (SAR) is stated with some traditional covariance matrix parameter estimate methods. Aimed at their defects in parameter estimation, an enhanced auto-adaptive edge-detection method for parameter estimating is presented. Because of the lack of point target and line detection in the above-mentioned methods, a new parameter estimation method is then introduced. Finally, results of the above-mentioned methods applied in PWF are submitted. Detail analyses and comparisons are also given. It is proved that the new parameter estimation method is the most robust. [C5553]

"Polarimetric SAR image processing: Wishart vs. "H/A/alpha" segmentation and classification schemes"

In this paper we analyze the potentialities of two different representations commonly used for polarimetric SAR images, for segmentation and classification purposes. The first representation is based on the covariance matrix of the considered polarimetric channels, while the second is based on the "H-A-alpha" decomposition. For both representations, we devise a segmentation + classification scheme, and we evaluate their performance on a set of C- and L- band polarimetric AirSAR images. On the basis of the achieved results, we devise a hybrid scheme, that uses a segmentation algorithm based on the full covariance matrix, then jointly classifies the pixels of the identified homogeneous regions considering the "H-A-alpha" representation. Results show that the hybrid scheme provides a significant performance improvement with respect to the approaches based on a single representation. [C5554]

"Performance assessment of multitemporal SAR images' visual interpretation"

Trying to compute or find items on SAR images, is often hard to achieve for photo-interpreters due to the speckle. Hence, the choice of a filtering approach often appears to be a tough choice. With the large number of images acquired on an area it is now possible to use multitemporal filters. When using those kind of filters the difficulty lies in finding a trade-off between temporal and/or spatial loss. Most of the time photo-interpreters set their choice on a subjective criterion. In this paper visual interpretation performance is tested to achieve an objectivity on the choice of different filtering approaches. [C5555]

"SAR DEM filtering by mean of Bayesian and multi-scale, nonstationary methods"

Several signal processing techniques are presented and evaluated to filter/enhance SAR digital elevation models (DEMs). The results are compared to a topographic digital terrain model (DTM) in the context of 3D visualization and real-time rendering. Through the DLR X-SRTM DEM, the interest of InSAR data for such applications is illustrated. [C5556]

"Extraction of momentum flux of monochromatic gravity waves using spectroscopic imaging"

Atmospheric gravity waves play a significant role in the dynamics and thermal balance of the upper atmosphere. The vertical fluxes of horizontal momentum characterizing the cross-correlation between the wave-induced vertical wind perturbations and the associated horizontal wind have proved to be difficult to measure. In this paper, we develop a novel technique for calculating momentum fluxes of monochromatic wave components from spectroscopic imaging and meteor radar wind measurement. Our approach uses the two-dimensional (2-D) cross-periodogram of two consecutive Doppler-shifted time differenced (TD) images to identify a dominant wave component and extract the wave parameters. Besides estimating the average perturbation of the dominant wave in the whole field of view (FOV), 2-D short-time Fourier transform is applied to the TD images to obtain the strongest perturbation of this wave in a portion of the FOV. With the wave parameters acquired, we calculate the momentum flux of the dominant wave component. The alternation of the direction and strength of dominant waves can be tracked for each clear night. Nightly averages provide information for investigating seasonal and

geographical variation in momentum flux of gravity waves. [C5557]

"Wavelet footprints for speckle reduction of SAR images"

Wavelet footprints, proposed by Dragotti (2002), are used for speckle reduction of synthetic aperture radar (SAR) images. Wavelet footprints contain all wavelet coefficients associated with a singular structure of a signal. Consequently, the dependency across scales that is inherent in wavelet transformation is eliminated. In the present paper, coefficients of wavelet footprints are thresholded with hard thresholding. The denoising method shows great promise for speckle removal and hence provides good detection performance for SAR based recognition. [C5558]

"A novel multi-channel SAR moving targets detection and image method"

Provides a novel multi-channel SAR moving targets detection and image (MTDI) method. After clutter is cancelled by using three apertures, two ways of signals through which moving targets can be detected are gained. Then Doppler centroid and Doppler frequency rate can be estimated, so both the real positions and velocities of moving targets will be acquired. Finally some typical computer simulation results are presented which illustrate the method's validity. [C5559]

"Operation and processing for scan mode patch-mapping SAR"

The operation and processing for an airborne scan mode patch-mapping synthetic aperture radar (SAR) system are discussed, which serves for moderate fine-resolution mapping of medium-sized terrain patches. The scanning angular scope and velocity are determined by the desired imagery patch size and cross-range resolution respectively. The linear range-Doppler algorithm is employed in image formation. Finally, the experimental result of the test campaign of the described system is also presented in the paper. [C5560]

"Speckle reduction of SAR images using adaptive curvelet domain"

Synthetic aperture radar (SAR) images are corrupted by speckle noise due to random interference of electromagnetic waves. The speckle degrades the quality of the images and makes interpretation, analysis and classification of SAR images harder. In this paper we will consider the use of the curvelet transform (CT), for speckle reduction of SAR images. The CT is a new approach for image representation approach that codes image edges more efficiently than the wavelet transform. Edges are very important in image perception and with fewer coefficients to represent edges, a better denoising scheme can be achieved. We will use three denoising methods: Wavelet-domain hidden Markov tree models, hard thresholding of the curvelet coefficients, and an adaptive combined method (ACM) proposed here, which uses the desired aspects of both aforementioned methods. [C5561]

"Platform and mode independent SAR data processor based on the extended chirp scaling algorithm"

This paper describes a SAR processor implementation being able to process data acquired in StripMap, ScanSAR or SpotLight, from airborne and space borne platforms. Together with the radar imaging techniques, the processing software has been developed to be able to dynamically adapt its performance to the memory and CPU resources of the computer running it and automatically calculates the optimum number of blocks used to process big images. Maximum portability has also been one of the major tasks and user interface has enhanced capabilities. Extended Markup Language (XML) standard has been adopted for parameter, setup and report files to simplify the software toolkit manual and, at the same time, to improve the user experience. The aim of this flexible core is to help design processors for future systems where, for example, transmitter and receiver are not in the same platform and thus, can follow different paths. The processing kernel and the specific modules for each operating mode and platform have been validated using raw data from ERS-1, RADARSAT and E-SAR, while in order to validate SpotLight mode, simulated data have been used for both air- and space borne platforms. [C5562]

"An approach to SAR imaging by means of non-uniform FFTs"

In this study, the potential use of the non-uniform FFT (NUFFT) in SAR imaging is analyzed. The main objective has been the improvement of the computational efficiency and image accuracy of seismic migration SAR processing. Different NUFFT methods have been implemented and tested in order to choose an adequate technique for the imaging problem. Our approach consists in substituting both the Stolt interpolation and the final range inverse FFT, in the ω -k algorithm, by a single NUFFT. Numerical simulations illustrate the performance of the new method and the influence of the selection of NUFFT parameters in the precision and computation time

of the SAR imaging algorithm. [C5563]

"Change detection on SAR images by using a parametric estimation of the Kullback-Leibler divergence"

Presents a method for performing change detection using a pair of SAR images acquired at different dates. The main difficulty with SAR images is the presence of speckle noise which may produce noisy change images if they are acquired with slightly different angles. The technique proposed in the present paper uses a parametric estimation of the probability distributions locally in each image as a characterization of the surfaces. The change is measured as a distance between these probability laws. The dissimilarity measure between the statistical distributions used here is a symmetric version of the Kullback-Leibler divergence. [C5564]

"A source estimation method to locate anomalous electromagnetic source in ELF band with global noise separation by ICA"

The Japanese Islands are located in an active position of seismic activity and have therefore often been afflicted by the damage of an earthquake. There is a report that disorder of an electromagnetic (EM) wave occurs in nature as a precursor of crustal activity. In order to detect the sign, we have measured EM waves of 223 Hz at about 40 sites in Japan. Our final goal is to sense seismic activity and to predict earthquakes. To locate local sources radiating anomalous EM waves, we need to separate global noise components due to tropical thunder in the equatorial region from observed data. Therefore, in this paper, in order to separate global noise components, we perform independent component analysis. Our goal in this paper is to estimate a local anomalous EM wave source. [C5565]

"Study on analysis of EM radiation source based on eigenvector"

Occurrence of anomalous Electro-Magnetic (EM) radiation is known as a precursor of earthquakes. Our goal is to locate anomalous EM source caused by seismic activity for earthquake prediction. For the purpose, we have been measuring EM wave of 223 Hz at about 40 sites in Japan. Measured signal contains much noise caused by far thunder lightning around equators, human activities, near field lightning and so on. This paper shows that the principal component analysis methods for covariance matrices of measured signals are effective for removing a component caused by thunder lightning around equator and for separating each EM source. Moreover, it is shown that a result of elimination of noise caused by far lightning around equators, estimation of thunder lightning location in near field agrees with real thundercloud observed by radar system, and estimation of sources of anomalous EM radiation occurred before earthquake. [C5566]

"Study on locating simulation of EM radiation source and transfer characteristic in ELF electromagnetic field"

The Japanese Islands are located in an active position of seismic activity and therefore often have been afflicted by the damage of an earthquake. There is a report that disorder of an electro-magnetic (EM) wave occurs in nature as a precursor of crustal activity. In order to detect the sign, we have been measuring EM waves of 223 Hz at about 40 sites in Japan. Our final goal is to determine the EM source more correctly. To locate the radiation source by multi point observations of EM power, EM wave propagation characteristic needs to be clear. In the presumed method of a generation source, we assume the attenuation model that EM wave intensity declines by the α power of the distance from the EM source. α is an unknown value, however, this paper analyzes α by locating the thundercloud position which generates the EM wave. [C5567]

"A SAR time series analysis toolbox for extracting fire affected areas in wetlands"

During the period 1999-2000 frequent fires occurred in the delta of Paranar' River, Buenos Aires, Argentina. A set of 13 ERS 2 images were collected within the frame of the ESA AO3 232 project. One of the basic concerns when trying to make use of these data for time series analysis is the need of tools for calibration of the SAR data, image coregistration, reduction of the radiometric uncertainty, and creation of the specific change detection algorithm. This paper presents the efforts made toward setting a processing procedure for these tasks. It combines ESA SARtoolbox with software developed within the ENVI-IDL environment that includes image coregistration, a temporal filter for increasing the number of looks but avoiding a loss in spatial resolution, and a change detection algorithm that maps the observed increase-decrease in the SAR response due to fires in this area. [C5568]

"The development of a processing environment for time-series analysis of SeaWinds scatterometer data"

The analysis of Earth observation data is normally undertaken within the spatial, or image, domain. With sensors obtaining highly frequent observations it is sometimes difficult to understand the temporal evolution and specific characteristics of the data if the analysis of the data is performed solely in the spatial domain. This paper provides an overview of the processing chain that has been developed to extract time series data sets consisting of backscattering coefficient σ^0 measurements from the SeaWinds sensor on NASA's QuikSCAT platform. The current global, operational, solution for land surfaces is outlined along with some typical processing times. Due to the volume of the orbital data sets from the SeaWinds sensor, emphasis is drawn upon the fact that within the operational processing chain robustness and stability of the processing environment is critical. The time series data sets are used to analyse the dynamics of freeze-thaw events across the Siberian biome. This work has been undertaken within the framework of the SIBERIA II project. [C5569]

"Eolian deformation detection and modeling using airborne laser altimetry"

Monitoring of landscapes or sea bottoms by means of laser altimetry or multibeam results in huge amount of data covering the same area in different epochs. Often stable benchmarks are not available in the area covered. We propose a geodetic/geostatistical method to analyze possible deformations in such area out of time series of data. The method is used for a deformation analysis of six consecutive years of laser data covering a dune section on the south-west coast of the island of Texel, the Netherlands. [C5570]

"Stochastic modelling for structure reconstruction from high-resolution SAR data"

The exploitation of metric resolution SAR data for the reconstruction of the structure of the observed scenes poses specific problems related both to the complexity of acquired scene details and to the peculiarities of the SAR acquisition system. On the one hand, much more complexity is transferred through the system from the scene into the data: new kinds of complex man-made scene objects are acquired. Layover and shadowing and responses from single scatterers tend to dominate the data. On the other hand, multiple signal reflections, sidelobe effects, radiometric pollution and many other effects related to the increased resolution of the system have to be taken into account. We show how, by properly modelling in stochastic terms the peculiarities of both the acquisition system and of the scene and by composing them in a Bayesian framework, new methods are developed that allow the reconstruction of the imaged structures from SAR data. Particular interest is devoted to the application of the developed algorithms in urban environments on data resolutions ranging from a few metres to fifty centimetres. [C5571]

"Linear structures' detection on SAR multi-temporal sets using the Polar Transform"

The Polar Transform (PT) is an efficient tool for detecting and linking the nearly aligned pixels. The method proposed in this paper uses this ability of the PT in order to extract the linear structures in the multi-temporal SAR images with strong speckle. Our algorithm consists in three steps: homomorphic channel summation, edge detection and linear structure extraction by PT. The homomorphic summation reduces data dimension and, meantime, filters the speckle. Since, in the sum image, the residual noise is additive, the edge detection, in the second step, is done by using Sobel's detector, which is a low computation algorithm. The resulting binary image is transformed by using the PT. The linear structure is detected by looking for the maximum in the transformed image and, then, it is extracted by an inverse polar transformation. The reconstructed linear structure has the same position as in the multi-temporal images and its pixels are perfectly linked. [C5572]

"Extended range migration algorithm for squinted spotlight SAR"

Several algorithms are available for SAR data processing and it has been shown that they lead to acceptable results in standard situations. However, processing of SAR data is a very difficult task if high resolution is to be achieved in spotlight mode with a large squint angle. In this case the echoes of a scene span a wide range area and the storage in a rectangular data field is inefficient. This paper presents an extended range migration algorithm which solves the problem by an adaptation of the receiver range gate. Then, the signal can be described in modified range and wave number components leading to a reduction of the memory requirement. Because of the limitation of the processed data to the scene echoes the processing efficiency increases. Beside the theoretical presentation of the new method the applicability is shown using simulated data. [C5573]

"A solution for linking the sparse aligned pixels in multi-temporal SAR sets"

In the edge detection of noisy images, low rates of false alarms may be obtained only for high detection thresholds. Unfortunately, a high threshold reduces not only the false alarms, but also the rate of true detections. Consequently, in the detected image, the edges are constituted by sparse pixels whose linking is a rather difficult task. This is, also, the case of SAR images, where speckle behaves like a strong multiplicative noise.

The paper proposes a method for linking the sparse aligned pixels resulting from the linear structure detection in multi-temporal SAR sets. Our method rests on the Polar Transform (PT). Applied to the data volume represented by the multi-temporal sets and not a single image as in regular applications, the PT has a double effect: it links the sparsely detected pixels and, meantime, performs a data fusion. This latter action enhances the ability of the PT. [C5574]

"Quality evaluation for efficient ScanSAR data processing algorithms"

Next generation Synthetic Aperture Radar (SAR) spaceborne sensors are being deployed with different acquisition modes including Scanning SAR (ScanSAR). That is due to the wider swath that ScanSAR provides. In this frame, this paper takes some known SAR processing techniques and studies their application to ScanSAR raw data processing. The methods based on Spectral Analysis (SPECAN) are convenient to treat ScanSAR data due to their burst processing capability in comparison with other methods designed for Standard high precision products. In this work, a careful study about special features of ScanSAR data is carried out. Then, a technique is selected and evaluated using a simulation environment. [C5575]

"The role of context for road extraction from SAR imagery"

This paper deals with automatic road extraction from airborne SAR imagery. Automatic extracted road networks are often incomplete. Even sophisticated road extraction approaches that are developed for optical imagery often fail to extract a complete road network. In SAR imagery in contrary to optical imagery, roads are more affected by high backscattering context objects. These local context objects like trees, bridges, or vehicles can disturb road extraction, but they can also support it. We show that an explicit modeling of context objects, leads to improved extraction results. [C5576]

"Mutual information based registration of SAR images"

Interpolation artifacts caused by the discrete nature of digital images and interpolation kernels have been previously reported in the literature for mutual information based image registration. Unfortunately they become pronounced in the case of SAR (synthetic aperture radar) image registration, exacerbated by speckle noise. We analyzed the two widely used interpolation algorithms in image registration, namely bilinear interpolation and partial volume interpolation. According to simulation results, we found that the former algorithm produces an extremely non-smooth metric function, whereas the latter method introduces a spurious global optimum at some position of misalignment, instead of the position of perfect registration, under certain circumstances. To make the mutual information criterion useful for the application of SAR image registration, we proposed two pre-processing steps including speckle reduction and an appropriate selection of the number of bins for histogram construction. Simulation results indicate that, by this effort, interpolation artifacts in the mutual information function can be significantly suppressed, and as a consequence, accurate registration is allowed. In conjunction with the two proposed pre-processing steps, we implemented a multiscale elastic registration algorithm. An example of registering a pair of JERS-1 (L-band, HH-polarization) and RADARSAT (C-band, HH-polarization) images verified the potential of this algorithm. [C5577]

"Real time phase preserving SAR processor based on COTS architecture"

Pushed by the continuous improvement of digital processing capability, nowadays a relatively low cost real time strip map synthetic aperture radar (SAR) processor is feasible. This paper first selects an adequate SAR processing algorithm and second looks for a suitable COTS platform based on digital signal processors for achieving real time processing without any accuracy loss. [C5578]

"Applying fractional Fourier transform to radar imaging of moving targets"

A fractional Fourier transform based method for radar imaging of moving targets is presented in this paper. Compared with the traditional joint time-frequency approaches, it can achieve a better result of clutter cancellation by using optimal filtering in the fractional Fourier domain due to linear and rotational properties of this transform. By using this method, we can carry out moving targets detection, LFM signal parameters estimation as well as clutter cancellation at the same time under the time-frequency analysis. The effectiveness of this method has been tested through simulation. [C5579]

"High resolution airborne FM-CW SAR: digital signal processing aspects"

There is a growing interest in miniaturized cost-effective, high resolution imaging radar. Existing imaging systems are generally too heavy or too expensive. Frequency modulated continuous wave (FM-CW) radars are usually more compact and less expensive and combining this technology with synthetic aperture radar (SAR) methods

leads to an interesting sensor for small-scale applications. The radar delivers signal in frequency domain rather than in the time one so special processing algorithm, which takes the typical characteristics of FM-CW radar signal into account, has to be used. Frequency shift information of the FM-CW signal is being used to obtain both range and azimuth resolution. Although these shift occur at different scales, there may be a mix up: this has been investigated. [C5580]

"Analysis of range ambiguity suppression in SAR by up and down chirp modulation for point and distributed targets"

This Paper provides a demonstrative derivation of the effect of up and down chirp modulation on point and extended target signals. Analysis has been performed with respect to signal amplitude, signal extension, modulation rate and phase behavior. The suppression of "point target" range ambiguities is investigated for the a possible TerraSAR-X parameter setting. Extended targets have been simulated and filtered. A Range-Ambiguity Simulator is under development which is based on airborne X-band data from the Experimental SAR (E-SAR) of DLR. The simulator concept is presented. [C5581]

"Robust Doppler Centroid estimate for ERS and ENVISAT"

The algorithm presented is capable of retrieving the correct DC ambiguity and to fit a fine polynomial estimate both on uniform and contrasted scenes. The core of the algorithm exploits a block wise processing: in each block a coarse unambiguous estimate is provided by exploiting both a second order statistic estimator (WDAR) and a higher order technique (MLBF). The final, fine estimate of the unambiguous Doppler is achieved by jointly exploiting the coarse unambiguous estimate with a fine, ambiguous one. The proposed algorithm accounts carefully for large variation of DC with range, like for recent Emergency Backup Mode of ERS and RADARSAT. The final estimate and its confidence is provided by a weighted average of the block measures. Tuning of the weights and additional check ensure robustness. The estimate of the offset frequency constant is then approached and a solution for calibrating its value is provided. [C5582]

"SAR raw data aspects and focusing via high precision algorithms"

In this study synthetic aperture radar (SAR) raw data are analyzed and processed via various processing algorithms. Characterization of the surface reflectivity pattern is performed. Surface reflectivity pattern is obtained by using SAR raw data and transfer function of the system. Two algorithms, namely narrow focusing and wide focusing, are examined for boresight geometry. With the approach used in the study, operation on a certain amount of data set is possible without having to process the whole data. This is quite advantageous since it provides time efficiency and ability to focus on desired geographical regions. Advantages of this procedure are given and applications to ERS-2 raw data for Istanbul, Turkey, are presented. Statistical analysis of the raw data is clearly shown. [C5583]

"Phase accuracy of motion compensated airborne SAR images"

We study the effects of residual uncompensated trajectory deviations on the phase accuracy of motion compensated SAR images. We show that linear and quadratic deviations interact with the SAR processing and generate additional phase artifacts with respect to what is expected by simple geometric considerations. [C5584]

"A multi-layer feed-forward perceptron for microwave signals processing"

This paper investigates the processing of radar signals using artificial neural networks. Today, the use of FMCW radar is considered to control the agricultural implements working depth, in order to overcome the limitations of sensors based on optical or ultrasound devices towards agricultural environment (dust, rain, etc.). The objective is to determine the radar-target distance R with a direct identification of the discrete-time radar signal $S_b[n]$. The neural network structure is a multi-layer feed-forward perceptron. Using simulation studies, we illustrate the capability of this neural network in determining the relation between R and S_b . The first training strategy uses non-disturbed input data, but this solution leads to an important overfitting when noise is added to the input signals. The second strategy reduces this sensitivity by carrying out the training phase with noisy input data. A comparison of accuracy and computing times is achieved between neural network and spectral analysis (FFT). [C5585]

"Perceptual grouping of regular structures for automatic detection of man-made objects"

Human observers perceive man-made objects in images from the visual spectrum domain as well as in IR or SAR imagery. Mechanisms like perceptual grouping are crucial to this capability. In this paper two examples for grouping in different image sources are discussed. The first example is activity estimation in urban areas from

thermal IR images. The grouping of vehicles into rows is performed along the margins of the roads. The other example is related to the detection of industrial buildings from InSAR data. Such buildings often show salient regular patterns of strong scatterers on their roofs. A previous segmentation which uses the intensity, height and coherence information extracts building cues. Strong scatterers are filtered by a spot detector and localized by a cluster formation. These scatterers are grouped in rows by a process that uses the contours of the building cues as context. [C5586]

"Modelling the radiometric response of a dynamic, 3D structural model of Scots pine in the optical and microwave domains"

A dynamic 3D structural model is used to simulate the structural growth stages of a Scots pine canopy from age 5 to 50 years. The 3D structural output of the model agrees with observed measures of Scots pine canopy structure. Needles are added to the structural model according to measured density and phyllotaxy (distribution). The 3D structural models are used to drive both optical and microwave models of canopy radiometric response. Simulated canopy radiometric response is compared with airborne hyperspectral reflectance data (HyMAP) and airborne synthetic aperture radar (ASAR) backscatter data, recorded during the SAR and Hyperspectral Airborne Campaign (SHAC) conducted over the UK during 2000. Simulations are shown to agree well in general with observations. This method is shown to be suitable for exploring the impact of canopy structure on the measured remotely sensed signal. [C5587]

"Hierarchical decision tree classification of SAR data with feature extraction method based on spatial variations"

The binary decision tree classification and feature extraction method based on texture features is applied to SAR data. In order to achieve more complex analysis it is advantageous to use binary decision trees, in which the decision between only two classes must be assigned at each node. Pixel based feature extraction methods reduce classification performance because of the speckle and also conventional texture analysis is not applicable to every part of an image. Therefore, a decision-making process, which can be applied to every pixel of an image, is required. The results show that computation time and accuracy of classification process are improved. [C5588]

"Forest biomass inversion from SAR using object oriented image analysis techniques"

Recent advancements in object oriented image classification provide possibilities to investigate new approaches for inversion techniques for synthetic aperture radar (SAR) images to derive bio-/geophysical parameters, like forest biomass. A study was performed on ERS and JERS SAR data in the Raco test site in Michigan. Both data sets were acquired within 10 days during summer 1992. Ground reference data were available from 80 forest stands with biomass ranges from early regrowth to mature stands for various pine species. Ecognition software was used to perform image segmentation. It was found that the software generated excellent image objects which correlate spatially well with existing stand boundaries and ecological units. However, the SAR data needed to be pre-filtered to reduce the influence of speckle to achieve better segmentation results. Also, improved segmentation was found when ERS and JERS data were used jointly in the segmentation process. Mean backscatter values of the 4 hectare test stands were compared with the mean backscatter of the larger image objects which contain the test stands. A comparison of the 4 ha test stands with the image objects containing these stands showed a signal correlation with an r^2 of 0.89. The derivation of biomass was then compared using the stand data only or the image objects only. While the r^2 values were about 0.1 higher for the stand derived regression equations, virtually the same model coefficients (slope, intercept) were achieved with the biomass regression with stand data and image object data. This shows, that models which are developed on carefully selected stand data can be transferred to image objects which resulted from prior segmentation of the SAR data. [C5589]

"Multiscale oil slick segmentation with Markov chain model"

A Markov chain model is applied for the segmentation of oil slicks acquired by SAR sensors. Actually, oil slicks have specific impact on ocean wave spectra. Initial wave spectra may be characterized by three kinds of waves, big, medium and small, which correspond physically to gravity and gravity-capillary waves. The increase of viscosity due to the presence of oil damps gravity-capillary waves. This induces a damping of the backscattering to the sensor, but also a dampening of the energy of the wave spectra. Thus, local segmentation of wave spectra may be achieved by the segmentation of a multiscale decomposition of the original SAR image. In this work, the unsupervised segmentation is achieved by using a vectorial extension of the Hidden Markov Chain (HMC) model. Parameters estimation is performed using the general Iterative Conditional Estimation (ICE) method. The problem of estimating multi-dimensional and non-Gaussian densities is solved by using a Principal

Component Analysis (PCA). The algorithm has been applied on an ERS-PR1 image. It yields interesting segmentation results with a very limited number of false alarms. Also, the multiscale segmentation proved to be an interesting alternative to classify marginal or degraded slicks. [C5590]

"Two-dimensional sea surface current fields derived from multi-sensor satellite data"

We used multi-sensor satellite images to compute small-scale surface currents in the Northern Baltic Sea. The images were acquired by the Thematic Mapper (TM) aboard Landsat, by the Synthetic Aperture Radar (SAR) aboard ERS-2, and by the Wide-Field Scanner (WiFS) aboard IRS-1C within two hours on 15 July, 1997, over the Northern Baltic Proper. Most of them show manifestations of an ongoing algae bloom, which are driven by the local currents. Pairs of images acquired at either different electromagnetic frequencies (TM and SAR) or at the same electromagnetic bands (TM and WiFS) are used for applying cross-correlation or partial differentiation techniques, respectively. Our results are insofar promising as the computed two-dimensional surface current fields complement existing data from numerical models. However, limitations of the proposed method are due to the strong dependence of the visibility of algae bloom manifestations on local weather conditions and to the low availability of satellite data. [C5591]

"Range-velocity mitigation via SZ phase coding for NEXRAD WSR-88D radars"

A fundamental limitation of pulsed weather radar is range-velocity ambiguity. Increasing (decreasing) the PRT (pulse repetition time) increases (decreases) the unambiguous range while decreasing (increasing) the unambiguous velocity. It has recently been shown that SZ phase coding of the transmit pulses allows for increased unambiguous range while maintaining a constant unambiguous velocity. To date statistical SZ phase coding performance has been investigated using numerically simulated Gaussian shaped weather spectra. However, experimental weather spectra are frequently non-Gaussian in shape, and thus SZ performance evaluation with experimental data would be more realistic. In this paper SZ phase coding is applied to experimental data offline and the results are compared to numerical simulations. [C5592]

"Orbit estimation of the interferometric cartwheel using an extended linearized Kalman filter"

We derive models and relations which might be useful for the calibration and orbit determination of cartwheel configurations such as proposed by Massonnet (2001). The aim is to develop a method to obtain precise position and velocity estimates for each individual cartwheel satellite from noisy and erroneous measurements (e.g. GPS). For later interferometric SAR processing precise estimates of the baseline vectors between the satellites are essential, because every error in the position of the antenna leads to a multiple error in height of the digital elevation model. The whole approach is based on state space arguments giving rise to Kalman filtering methods. [C5593]

"Multiple classifier system based on attractor dynamics"

A new method is proposed for combining outputs of several classifiers. The method is based on the theory of dynamical systems. In our formulation each classifier output represents a forcelet in a phase space of the dynamical system. Depending on interactions (superposition) of forcelets the system can perform in two different regimes: non linear averaging among several classifiers outputs and selection among them. We show that the attractor dynamics method outperforms both the winner takes all algorithm and the single best classifier. [C5594]

"Modelling the radiometric response of a dynamic, 3D structural model of wheat in the optical and microwave domains"

A dynamic 3D structural model of wheat is used to simulate growth stages of a wheat canopy. The 3D information regarding canopy structure output by this model is used to drive two models of canopy radiometric response, one in the optical and one in the microwave domain. The radiometric response of the canopy in the optical and microwave domains is simulated and the sensitivity of the canopy response to variation in the canopy structural and radiometric parameters is examined. The modelled canopy response is compared to field-measured hyperspectral reflectance in the optical, and airborne synthetic aperture radar (E-SAR) backscatter measurements in the microwave. The modelled signal is shown to agree in general with observations. It is demonstrated that the major growth development stages of the wheat canopy which impact the remote sensing signal in the optical and microwave domains can be modelled in this way. This method is shown to be suitable for exploring the impact of canopy structure on remotely sensed measurements. [C5595]

"Biophysical parameter retrieval from forest and crop canopies in the optical and microwave domains using 3D models of canopy structure"

3D structural models of a (dynamic) wheat canopy and a Scots pine canopy are used to drive models of canopy scattering behaviour in the optical and microwave domains. These models have been shown to be capable of simulating canopy reflectance and backscatter using scattering models in the optical and microwave domains. By varying the structural and radiometric parameters governing the simulated canopy response, look-up tables (LUTs) of reflectance (optical) and backscatter (microwave) are constructed. These LUTs are used to 'invert' the scattering models against reflectance and backscatter observations made from airborne reflectance and SAR backscatter data. The practicability of this approach is demonstrated. It is shown that combined optical and microwave retrievals are possible without the need for simplified mathematical models of scattering behaviour and time-consuming numerical inversion techniques. Once LUTs have been generated, inversion against observations is very rapid and flexible. [C5596]

"Classification of surface covers by combining optical and microwave data for Baikal Lake region"

Integration of optical and microwave remote sensing data is an effective way to conduct more detailed classification of the surface covers. For this work we analyzed MSU-E optical data and SIR-C quad-pol data (both C- and L-bands) that cover southeastern part of Baikal Lake region. Using two sources of data, we compared the results of several classification methods and verified them during field trip. We focused our attention mostly on forest classification. Besides we got classification results for water surfaces and marshlands. [C5597]

"Feature detection from preprocessed sea ice SAR data based on higher-order statistics"

We apply higher-order statistics to filtered Radarsat-1 SAR image data over the Baltic Sea to detect edges and spotlike features. [C5598]

"Assessment of environmental sensitivity index of flooding areas in western Amazonia using fuzzy logic in the dual season GRFM JERS-1 SAR image mosaics"

This study focuses on improving information about oil spill environmental sensitivity in Western Amazonia, Brazil, using a pair of multiseasonal (1995 low flood to 1996-high flood) GRFM JERS-1 SAR mosaics. Fuzzy analysis is carried out to extract information about landscape modifications within half hydrological cycle. The oil spill hazard information derived from JERS-1 SAR data is straightforward to interpret and constitutes a representation of the original Environmental Sensitivity Index (ESI) product conceived by PETROBRAS. [C5599]

"Environmental monitoring of tropical wetlands in semi-arid Sub-Saharan Africa-what about remote sensing?"

Heterogeneous socio-ecological and socio-economic interrelations of local, regional and continental phenomena determine the ecological balance of semi-arid regions in Sub-Saharan Africa. Multitemporal monitoring for change detection and analysis of regional patterns of degradation is one of the main steps to understand processes of degradation and desertification. Operationalized earth observation by medium-to-high-resolution spaceborne remote sensing is the tool for monitoring dynamics of land cover change in order to support regional planning for sustainable development. Neither existing satellite platforms and sensor systems nor the management of data acquisition and distribution for the users in Sub-Saharan countries meet the requirements determined by the key-words low-cost, non-profit, decentralized, appropriate. There is urgent need for establishing a sustainable programme of earth observation of Sub-Saharan regions based on free of charge data with medium-to-high spatial and spectral resolutions. [C5600]

"Spectral mixture analysis of ASTER image in Brazilian Savanna"

The present work aims to evaluate the advantages of the ASTER sensor for the distinction of Brazilian Savanna vegetation types from spectral mixture analysis. The study area is the Military Instruction Field which has an extensive area with approximately 115.014 ha of native Brazilian Savanna. The methodology used can be divided in three stages: a) preprocessing, b) endmembers identification and c) Spectral Mixture Analysis (SMA). The images were acquired with atmosphere correction. The union of the spatial dimensions between VNIR and SWIR images was done by duplicating the pixels size from the SWIR image. Since the study area is located in two adjacent ASTER images a mosaic was done in order to combine both. Endmembers were detected in three steps: a) spectral reduction by the Minimum Noise Fraction (MNF) transformation, b) spatial reduction by the Pixel Purity Index (PPI) and c) manual identification of the endmembers using the N-dimensional visualizer. The spectral classification was done using the Spectral Mixture Analysis (SMA). The classification was done relative to the different vegetation types and bodies of water with vegetation occurrence. The amount of nonphotosynthetic vegetation (NPV) and photosynthetic vegetation (PV) is preponderant in the distinction

between the vegetation types. These procedures allowed identifying the main scenarios in the study area.

[C5601]

"Mesoscale modeling investigation using PENNSTATE/NCAR MM5 model and remote sensing technology for weather simulation and prediction"

The objective of present study is to adapt the MM5 climate and weather prediction model for possible use in areas where solar cookers and solar Stirling engines will be used under the NASA/HBCU Renewable Energy and Technology Utilization project. Equipments that use solar energy for cooking and heating are valuable in areas that predominantly include third world countries where other resources are limited. In such conditions solar energy cannot be wasted; hence to make use of it at the right time effectively, accurate prediction of sunshine is absolutely necessary. The MM5 modeling system is used as a research tool for diagnostics and prediction of mesoscale weather patterns and circulations. Two regions were chosen as case study-Washington D.C. and Louisiana. NCEP/NCAR global analysis data is used to construct the initial and boundary conditions. Later the simulation uses the remote sensing data including satellite and radar for model initialization and run. The model is run for a 48 hour time period on 14-15 June, 2002 over Washington D.C. and 2-3 October, 2002 over the Louisiana costal region. Cloud cover, precipitation and sunshine are the major parameters of model simulation and forecast. Better prediction of sunshine help solar energy equipments be better utilized. [C5602]

"Correction of local and global tropospheric effects on differential SAR interferograms for the study of earthquake phenomena"

The presence of atmospheric contributions in SAR interferograms represents the main limit for the detection of ground deformation movements. This paper presents a methodological approach to reduce at both global and local scales the tropospheric contributions in the interferograms. It first requires the refined knowledge of the permanent scatterers that can only be obtained from the analysis of a large population of interferograms. The correction of global scale atmospheric contribution exploits the correlation between phase and topography and the correction of local artefacts is based on correlation between interferograms containing one common acquisition. [C5603]

"The extraction of canopy-understory vegetation-topography structure using helicopter-borne LIDAR measurement between a plantation and a broad-leaved forest"

The relationship between stratification of canopy layers, understory vegetation and topography was investigated using helicopter-borne laser scanner data. The study plot was established ranging from an evergreen broad-leaved forest to a plantation of hinoki cypress (*Chamaecyparis obtuse*). LIDAR measurement was conducted with high density of footprints (23.4 points/m²) and both first pulse data and last pulse data were recorded. A local minimum filter was used to generate a digital elevation model (DEM). Adjoining spaces with 1 m wide along a certain direction in the stand were assumed and whole measurement data within every space were projected to a corresponding vertical plane to comprehend a canopy structure. It was found that through this processing that a series of vertical projective planes described stratification of canopy layers, gap structure, distribution of understory vegetation as well as topography. [C5604]

"A three-dimensional radar backscatter model for larch forest using L-system"

A three-dimensional backscatter model for larch forest stands is described, with an emphasis on the construction of the tree model using Lindenmayer system (L-system). This model calculates the incoherent backscatter from larch forest composed of realistic tree structures. Using L-system, tree architectures were generated faithful to the real stand tree structure. The tree models simulated by L-system give exact position information of tree architecture and are used for calculating the probability density functions of tree components and improve the precision of radar backscatter model. Here, we define five major components of the radar backscatter model: direct crown backscatter, direct ground backscatter, direct trunk backscatter, multi-path interactions between crown and ground, and double-bounce from trunk-ground interactions. Total backscatter from a simulated larch forest is computed by incoherent summation of the components. In this paper, the 3D radar model is introduced based on a description of L-system model of larch tree. Next, the polarization radar returns of larch stands are simulated and analyzed at L-, C-, X- and P-band with different incident angles. This 3D larch radar model gives reasonable results of backscattering coefficients averaged over the entire larch stands. [C5605]

"Determination of the displacements along the Maergaichaka fault, using remote sensing data, Tibet, China"

ERS-I/ERS-2 synthetic aperture radar interferometry and Landsat TM was used to study the Maergaichaka fault

where Manyi earthquake occurred on Nov. 8, 1997 in Tibet, China. We derived an accurate digital elevation model (DEM) and the deformation interferogram of the Manyi earthquake using a tandem ERS-1/ERS-2 image pair and modeled the left-lateral slip of the fault in three dimensions using a half-infinite elastic model. Detailed geological and geomorphological offsets revalued using river valleys and structural markers on the Landsat ETM images at different scales are used to constrain the localization, total displacement at the Maergaichaka fault, Tibet, China. The river network morphology associated with small rivers is offset by several meters to several kilometers along the Maergaichaka fault. Our results indicate that the left-lateral slip of the fault has accommodated the shortening of the India-Eurasian lithospheric plates. [C5606]

"Examples of data collected from "PRIRODA-MIR" Space Station by microwave radiometers, optical and infrared sensors over the territory of Africa"

This paper discusses examples of data collected from the "PRIRODA-MIR Space Station" over the territories of some African countries. Among these countries are Egypt, Ethiopia, Somali, Botswana, and some others. The measurements have been conducted with the aid of microwave radiometers, thermal infrared, near-infrared sensors, and optical instruments. [C5607]

"SAR-image classification with a directional-oriented discrete Hermite transform and Markov random fields"

A novel classification scheme for SAR images based on the perceptual classification of image patterns in the discrete Hermite transform (DHT) domain over a roughly hexagonal sampling lattice has been developed. In order to obtain the DHT referred to a rotated coordinate system the set of coefficients of a given order are mapped through a unitary transformation based on the generalized binomial function. This representation allows a perceptual classification, including constant patterns (0-D), oriented structures (1-D), and non-oriented structures (2-D). Classification is based on light adaptation and contrast masking properties of the human vision. Finally, classification is improved by means of a probabilistic approach based on Markov random fields. [C5608]

"Towards a quantitative understanding of the effects of wind motion on airborne and satellite SAR imagery of vegetation"

The monitoring of environmental land resources with airborne and satellite Synthetic Aperture Radar (SAR) is time-critical and relies on the availability of good quality images often acquired within specific time windows when there are marked differences in backscatter between and among vegetation. Wind disturbance can differentially alter the backscatter and image statistics of different vegetation types in a scene, and cause rapid temporal decorrelation between images. Recently, this temporal behavior has been utilized as a discriminant between vegetation types. However, to date, almost all this work has been based on empirical inspection and supposition, with little or no validation by field observation or modeling. In this paper we present results from a model developed to provide realistic wind-induced motions based on extensive field observations. The results allow us to make a quantitative assessment of the behavior and quality of SAR imagery according to wind conditions, vegetation response, and imaging scheme. We also look at ways of alleviating wind effects by use of appropriate data collection and processing schemes. It is found that the effect of the motion on the imagery is a complex interaction between the motion that describes the characteristic period of oscillation of the target and the way the imaging process samples that motion. There are also critical dependencies on radar frequency, range and resolution. With consideration of the latter dependency we look to likely future SAR platforms which promise markedly increased spatial resolution, but for which motion effects will become more acute. [C5609]

"Combination of SAR, SPOT, and geophysical data for geological mapping: the Nyanga Basin (SW Gabon) example"

Using spaceborne Radarsat and SPOT data, and airborne geophysical data (magnetometry and radiometry) as well, the mapping of the lithostructural units of the Nyanga syncline is enhanced. These data, analyzed with the help of a GIS, contribute to the improvement of the geological knowledge. [C5610]

"The contribution of spaceborne SAR interferometry to geomorphological analyses"

Interferometric SAR data are used to derive morphometric terrain attributes required by geomorphological and hydrogeological applications. Instead of generating an interferometric Digital Terrain Model (DTM) and subsequently derive the terrain attributes, we compute these quantities directly from the interferogram. Experiments demonstrate that, when compared with traditional DTM-based measures, SAR-based attributes seem more stable and offer best performances. Results shown in this paper have been obtained by processing ERS-1/2 SAR data referring to a typical Alpine mountain basin. [C5611]

"Landslide tracking with a curve evolution model driven by interferometric data"

We are interested in the problem of modeling the propagation of landslides. We use an image processing approach based on the computation of a geodesic distance map. We determine the evolution of an initial curve along a given surface. The model can incorporate various properties coming from the geometry of the surface or independent measures. In an application, we focus on landslides study in the context of natural risk management. The model is driven by geometrical constraints and SAR interferometric measures. [C5612]

"Sensitivity of DEMs generated from interferometric cartwheel configurations"

Former analysis revealed that the vertical height accuracy of digital elevation models (DEMs) generated by synthetic aperture radar interferometry (InSAR) mainly depends on the precise knowledge of baseline length, baseline tilt angle and interferometric phase offset. Recently slightly different formations of passive microsatellites which simultaneously receive signals transmitted from an active spaceborne radar system and have near circular orbits were proposed. This paper presents the sensitivity of DEMs generated from such constellations to important interferometric parameters. PALSAR (ALOS), ASAR (Envisat) and TerraSAR-X are considered as illuminating SAR systems and a three dimensional SAR geometry that includes an ellipsoidal Earth geometry (WGS84) is applied. [C5613]

"Estimating orbital trajectories from fringe gradients in SAR interferograms for measuring crustal strain"

We develop and assess a new orbital tuning approach by applying differential synthetic aperture radar (SAR) interferometry. We use interferograms of the same site for estimating across-track and radial orbit adjustments from fringe gradients caused by orbit uncertainties. Our approach eliminates these fringes by using the improved short-arc orbit estimates. Taking six estimates from the Delft Institute for Earth-Orientated Space Research (DEOS), the approach yields mean standard deviations of 2.4 cm for the across-track and 4.5 cm for the radial components. The interferograms calculated with our post-fit orbital estimates compare favorably with those corrected with a conventional orbital tuning approach. We can now distinguish between orbital and deformation contributions to interferometric SAR phase gradients and are able to measure surface deformation changes over an interseismic time interval longer than one year. Our new approach is limited, however, to well-correlated interferograms where it is possible to measure the fringe gradient. We have also applied Permanent Scatterers (PS) technique to 42 SAR images acquired by ERS between August 1992 and June 1998. This approach estimates the average range change rate of more than 3 million PS with a formal standard deviation of 0.3 mm/yr along the line of sight. We obtain a phase coherence factor greater than 0.8 and a standard deviation of 3 mm for a single line of sight measurement. This velocity field is much easier to interpret than the separate interferometric pairs. Interpreting these interesting features in terms of geophysical models of inter-seismic and post-seismic deformation, however, will require further research effort. [C5614]

"Evaluation of the potential of radar ENVISAT data for the updating of numerical thematic maps on the coastal fringe of French Guyana"

The objective of this study is to value the potential of radar satellites data, in particular ENVISAT, for the updating and the revision of existing thematic maps on the coastal plain of French Guyana. The scale of work retained is the 1: 50000. The cartographic updating consists in removing on the old map the geographical elements that disappeared and adding evolutions undergone by the landscape between two dates given. Our methodology of updating takes support on the topographic (IGN, National Geographic Institute, France), and Vegetation (LET, Terrestrial Ecology Laboratory) numerical existing maps. In humid tropical context, the images radar is the only one to be efficient to provide information on deposits of surface, and the occupation of soil. It has been carried out in this study a follow-up of the evolution of the coastline between 1992 (ERS) and 2002 (ENVISAT), and a comparison of the potential of ERS, JERS, and ENVISAT for the cartography of the coastal plain. Results from previously studies have been used as control data. Data extracted after Remote Sensing treatments have been integrated in a Geographical Information System. [C5615]

"US National Large-scale City orthoimage standard initiative"

The early procedures and algorithms for national digital orthophoto generation in the National Digital Orthophoto Program (NDOP) were based on earlier USGS mapping operations, such as field control, aerotriangulation (derived in the early 1920s), the quarter-quadrangle-centered (3.75 minutes of longitude and latitude in geographic extent), 1:40,000 aerial photographs, and 2.5 D digital elevation models. However, large-scale city orthophotos using early procedures have disclosed many shortcomings, e.g., ghost image, occlusion, shadow. Thus, to provide the technical base (algorithms, procedure) and experience needed for city large-scale digital

orthophoto creation is essential for the near future national large-scale digital orthophoto deployment and the revision of the Standards for National Large-scale City Digital Orthophoto in National Digital Orthophoto Program (NDOP). This paper will report our initial research results as follows: (1) high-precision 3D city DSM generation through LIDAR data processing, (2) spatial objects/features extraction through surface material information and high-accuracy 3D DSM data, (3) 3D city model development, (4) algorithm development for generation of DTM-based orthophoto, and DBM-based orthophoto, (5) true orthophoto generation by merging DBM-based orthophoto and DTM-based orthophoto, and (6) automatic mosaic by optimizing and combining imagery from many perspectives. [C5616]

"InSAR coherence optimisation using second kind statistics"

We present an optimization of the estimated interferometric synthetic aperture radar (InSAR) coherence, that we had presented in IGARSS'01, which is based on a binary mixture modelisation of the coherence images. The proposed approach is based on a second kind statistics defined as the Mellin-transform of its probability density function (pdf). The Mellin transform of coherence pdf is then computed analytically. It will serve for interferogram parameters estimation by zone growing. Results are validated on a test zone of highly energetic relief (Mustang). [C5617]

"Influence of hydrometeors on InSAR observations"

Repeat-pass synthetic aperture radar interferometry is an important tool for measuring Earth surface topography and/or surface deformations. These observations, however, are highly affected by the atmosphere. Therefore, an accurate description of atmospheric distortions is very important to improve an accuracy of interferometric measurements. In this paper we discuss influence of hydrometeors on the microwave propagation. On examples of two interferograms we show that there is a strong increase in a propagation delay associated with rain. To validate this observation we have used weather radar measurements to estimate contribution of rain droplets on the propagation path. It is shown that in some cases, a rain induced propagation delay can be of several centimetres. [C5618]

"Simulation of interferogram image for spaceborne SAR system"

In interferometric synthetic aperture radar (InSAR) processing, simulation of interferogram is a common practice. It is used as synthetic data to test and validate the whole chain of InSAR processing from the interferogram creation to the DEM reconstruction. Simulators for interferometry, those have been reported in the literature, are developed in very simplified imagery geometry model. In this paper, a interferogram simulator which deal with real radar sensor parameters and orbit data is presented. [C5619]

"The research of difference interferometric SAR technique"

This paper discusses several processing algorithms of D-InSAR based on experience accumulated by our predecessors, and puts forward a new method, "new" 4 pass D-InSAR, with its formula. [C5620]

"Retrieval of multi-scale roughness parameters and soil moisture by numerical inversion"

The aim of this present work is to find an inverse model to retrieve roughness geometric and dielectric parameters of natural rough surfaces from radar backscattering data. The bi-dimensional surfaces are described by means of the fractional Brownian motion random process, using the bi-dimensional wavelet transform. Multi-scale roughness is characterized by two parameters, the first one proportional to the standard deviation and the other one related to the fractal dimension. Soil moisture is related to the complex dielectric constant. To simulate radar backscattering we used the small perturbation model in which the radar backscattering coefficient can be expressed as the product of two factors, the first dependent on polarisation but independent of surface roughness and vice versa the second dependent on roughness but independent of polarisation. Thus, this model simplifies the procedure of inversion and the co-polarised ratio between hh and vv polarisation is independent of roughness and a minimisation over only two parameters is performed to retrieve the complex dielectric constant independently of the employed geometric surface description. Once the dielectric constant is known, the retrieval of multi-scale surface roughness parameters is performed in a successive step by using multi-frequency and multi-incident angle data. [C5621]

"Performance assessment of multi-frequency SAR interferometry based on statistical estimation"

We show the information theoretic performance of two maximum likelihood techniques to solve the problem of phase unwrapping in SAR interferometry. Bias and minimum variance of the estimators, in terms of the Cramer Rao lower bounds, are computed. [C5622]

"Comparative study of InSAR topography reconstruction algorithms based on look vector's orthogonal decomposition"

For topography reconstruction by InSAR, different orthogonal bases have been introduced and corresponding reconstruction algorithms have been derived in the previous research. In this paper, analytical analyses on these algorithms show that these algorithms are equivalent to each other if only no simplified models are introduced in the orthogonal decomposition, regardless of different orthogonal bases having been defined. [C5623]

"Comparison of satellite baseline estimation methods for interferometry applications"

Baseline is a very important parameter in SAR interferometry (InSAR) processing and applications. It impact generation and quality of DEM from interferogram. Although a variety of baseline estimation methods are reported in the literature, to our knowledge, a systematical comparison on such methods is still unavailable. In this paper, some representative methods of baseline estimation are compared and their advantages and disadvantages are assessed and outlined. The comparison is carried out with ERS-1/2 tandem data over the Jingjiang area of China. [C5624]

"Decision level fusion of multi-frequency polarimetric SAR and optical data with Dempster-Shafer evidence theory"

This paper investigated and tested the multi-source data fusion of multi-frequency SAR data with optical sensor, utilizing the mathematical theory of evidence. In this type of data fusion, the correct definition of uncertainty and mass function is very important. Firstly each mono-source data is independently classified using the Bayesian maximum likelihood classification method and the fusion is processed during the decision making stage. For the representation of support and plausibility, mass of evidence is assigned to the candidate labels associated with the frequencies of neighborhood pixels' decision. Then the mass is weighted again by both the distance effect and the global source-specific reliability. In the combination and fusion stage, unions of classes get same mass values to emboss its uncertainty of decision making. Finally Dempster's orthogonal sum method was used to combine the evidence information and the associated level of ignorance, and then the maximum support rule decides the final land-cover types. Classification accuracies before and after each step of fusion processing are compared with reference training data set. We applied this method to the NASA/JPL polarimetric AIRSAR data and KOMPSAT-1 (Korea Multi-Purpose SATellite-1) EOC (Electro Optical Camera) panchromatic data and obtained noticeably better land-cover classification results. [C5625]

"Information and understanding: analysis of remotely sensed data"

A review is given of the development of the field of image understanding in remote sensing, with an emphasis on the contributions of David Landgrebe and his group at the Laboratory for Applications of Remote Sensing, Purdue University. The differences in approach required for multispectral, hyperspectral and radar image data are emphasised, in which the seminal contributions to the field by Landgrebe as well as others are summarised. The treatment concludes by examining the current problem of thematic mapping from mixed spatial data types, such as would be found in a geographical information system. Rather than seeking techniques that "fuse" available data types as a means for deriving joint inferences, it is proposed instead that the most practical means is to have each individual data source analysed separately by the most appropriate techniques and the fuse at the label level using the facilities of an expert consultant. [C5626]

"Combining MISR, ETM+ and SAR data to improve land cover and land use classification for carbon cycle research"

Accurate and reliable information about land cover and land use is essential to carbon cycle and climate change modeling. While historical regional-to-global scale land cover and land use data products had been produced by AVHRR and MSS/TM, this task has been advanced by sensors such as MODIS and ETM since the latter 1990s. While the accuracies and reliabilities of these data products have been improved, there have been reports from the modeling community that additional work is needed to reduce errors so that the uncertainties associated with the global carbon cycle and climate change modeling can be addressed. Remotely sensed data collected in different wavelength regions, at different viewing geometries, usually provide complementary information. Their combination has the potential to enhance remote sensing capabilities in discriminating important land cover components. In this paper, we studied multi-angle data fusion, and optical-SAR data fusion for land cover classification at regional spatial scale in the temperate forests of the eastern United States. Data from EOS-MISR, Landsat-ETM+ and RadarSat-SAR were used. The results showed significantly improved land cover classification accuracy when using the data fusion approach. These results may benefit future land cover products for global change research. [C5627]

"Multisensor image fusion and mining: from neural systems to COTS software with application to remote sensing AFE"

We summarize our methods for the fusion of multisensor/spectral imagery based on concepts derived from neural models of visual processing (adaptive contrast enhancement, opponent-color contrast, multi-scale contour completion, and multi-scale texture enhancement) and semi-supervised pattern learning and recognition. These methods have been applied to the problem of aided feature extraction (AFE) from remote sensing airborne multispectral and hyperspectral imaging systems, and space-based multi-platform multi-modality imaging sensors. The methods enable color fused 3D visualization, as well as interactive exploitation and data mining in the form of human-guided machine learning and search for objects, landcover, and cultural features. This technology has been evaluated on space-based imagery for the National Imagery and Mapping Agency, and real-time implementation has also been demonstrated for terrestrial fused-color night imaging. We have recently incorporated these methods into a commercial software platform (ERDAS Imagine) for imagery exploitation. We describe the approach and user interfaces, and show results for a variety of sensor systems with application to remote sensing feature extraction including EO/IR/MSI/SAR imagery from Landsat and Radarsat, multispectral Ikonos imagery, and Hyperion and HyMap hyperspectral imagery. [C5628]

"Multispectral satellite image analysis based on the method of blind separation and fusion of sources"

The number of satellite images is in full evolution allowing us to improve the extraction of useful information related to the physical reality of natural scenes. In this paper, we propose a new hybrid approach of multi-spectral analysis of satellite images. This approach consists in a method of blind separation of sources. This method allows us to decompose a pixel into information coming from independent sources. Algorithms adapted in the context of our work, operating in the two dimensional space, have been used for the separation. These algorithms produces many sources, in order to choose among them the most significant having a maximum value of entropy representing a maximum information about one class of land use. In order to have a classified image with good classification, we proceed with the fusion of these sources using a technique of maximum likelihood classification. We validated our approach on optical images of the satellite SPOT 4 and radar images of the satellite ERS 2 representing a central Tunisian region. The results obtained consists in the production of five classes of land use. [C5629]

"Change detection in urban context with multitemporal ERS-SAR images by using data fusion approach"

We propose in this paper, a new method for change detection in urban context with multitemporal SAR images. The method operates in two steps: change measures computation between the two SAR images, and the fusion of previous change measures with an interpretation measure, used as prior information, with the help of fuzzy subsets theory. This interpretation attribute comes from an optical image, across NDVI (Normalized Difference Vegetation Index). The proposed method is applied on two ERS-SAR images and one multispectral optical SPOT (2001) image of the urban area of Douala city, in order to appreciate changes between (1994) and (1999). The method allows the global change analysis in urban context at a pixel scale and at an area larger than a pixel. [C5630]

"RADARSAT-1 and LANDSAT7 ETM+ integration for kimberlite exploration in the Buffalo Head Hills area, northern central Alberta"

The objective of this study was to develop a method of data integration involving intensity, hue, and saturation (IHS) enhancement using RADARSAT-1 Principal Component and Landsat7 ETM+ band 6 imagery. RADARSAT-1-PC2 image provides optimal topographic enhancement of the surface expression characterizing known kimberlite pipes in the Buffalo Head Hills, and complement associated thermal anomalies observed in the Landsat7 ETM+ band6. The IHS data fusion of RADARSAT-1-PC2 with Landsat7 ETM+ band 6L images resulted in a virtual image with 12.5 m resolution. Locations of some of the known kimberlite pipes were defined by the brighter absolute radiance response in band 6L compared to the host sedimentary rocks (Lower-Upper Cretaceous shales). Cross verification of the outlined thermal anomalies has been achieved using high-resolution aeromagnetic (HRAM) data. [C5631]

"Classification of polarimetric synthetic aperture radar images using fuzzy clustering"

Clustering is a well known technique for classification in polarimetric synthetic aperture radar (POLSAR) images. Pixels are represented as complex covariance matrices, which demand dissimilarity measures that can capture

the phase relationships between the polar components of the returns. Four dissimilarity measures are compared to judge their efficacy to separate complex covariances within the fuzzy clustering process. When these four measures are used to classify, a POLSAR image, the measures that are based upon the Wishart distribution outperform the standard metrics because they better represent the total information contained in the polarimetric data. The Expectation Maximization (EM) algorithm is applied to a mixture of complex Wishart distributions to classify the image. Its performance matches the FCM clustering results yielding a tentative conclusion that the Wishart distribution model is more important than the clustering mechanism itself. [C5632]

"Analysis of high resolution polarimetric SAR in urban areas"

Parallel to the conventional (statistical, spectral) description of mixed urban classes for image segmentation, the description on the basis of cues and related spatial properties is used within the classification process. Recently we concentrate very much on strong model-based classification, which may lead to a classification not covering the whole area due to the implementation of insufficient models (class descriptions). Major interest is related to urban features like urban fabric, continuous urban fabric (dense, medium dense), discontinuous urban fabric (dense residential, sparse residential, residential blocks) as well as industrial areas. [C5633]

"Study on the spectral quality preservation derived from multisensor image fusion techniques between JERS-1 SAR and Landsat TM data"

The advantage of multisensor data fusion stems from the fact that the use of multiple types of sensors increases the accuracy with which a quantity can be observed or characterized. The response of radar is more a function of geometry and structure than surface reflection as occurs in the optical wavelengths. A suitable fusion method has to be chosen with respect to the used spectral characteristic of the multispectral bands and the intended application. This paper describes a comparative study of multisensor image fusion techniques in preserving spectral quality of the fused images. Image fusion techniques applied in this study are: wavelet, intensity-hue-saturation (IHS), principal component analysis (PCA), and high pass filtering (HPF). With these image fusion techniques, a higher spatial resolution JERS-1 SAR is fused with Landsat TM data. The merging process is carried out at the pixel level and the comparison of the resulting images is explained based on the measurement in preserving spectral quality of the fused images. Assessment of the spectral quality is performed by graphical and statistical methods between the original TM image and the fused images. The factors computed to qualify the fused images are: mean, standard deviation, coefficient correlation, and entropy. With a visual inspection, wavelet and PCA techniques seem to be better than the other techniques. PCA provided the greatest improvement with an average entropy of about 5.119 bits/pixel. [C5634]

"Determination of optimal SAR illumination aspects in build-up areas"

The increasing resolution of SAR data opens the possibility to utilize such data for scene interpretation in urban areas. SAR specific illumination phenomena like foreshortening, layover, shadow, and multipath-propagation burden the interpretation. In this paper a high resolution LIDAR DEM is incorporated to determine the visibility of objects by a SAR measurement from a given sensor trajectory and orientation in an urban environment. Shadow and layover areas are detected by incoherent sampling of the DEM. By a variation of viewing angle and aspect a large number of such simulations are carried out. From this set a subset of a number of best simulations is determined for two example tasks, namely the analysis of objects on roads and the detection and reconstruction of buildings. Dominant scattering can interfere large parts of the scene. Such strong backscatter can be caused by specular reflection on gabled roofs or double-bounce on corner structures at building walls and roofs. The approach is extended to the detection of such structures. [C5635]

"Automatic registration of electro-optical and SAR images"

Presents a new and robust method to perform multisensor image registration from dissimilar sources. It is a proof of concept demonstration. It is based on multiple transformations of two quite dissimilar images into new domains, where local or global similarities are extracted. [C5636]

"Hydrometeor classification system using dual-polarization radar measurements"

Hydrometeor classification system using fuzzy logic technique based on dual-polarization radar measurements is presented. In this study, five radar measurements (horizontal reflectivity, differential reflectivity, specific differential phase, correlation coefficient, and linear depolarization ratio), and height relating to environmental melting level are used as input variables of the system. The hydrometeor classification system chooses one of nine different hydrometeor categories as output. The system presented in this paper is a further development of an existing hydrometeor classification system model developed at Colorado State University. The hydrometeor classification system is evaluated by comparison against the in situ sample data collected by instrumentation on T-28 aircraft

during Severe Thunderstorm Electrification and Precipitation Study (STEPS). [C5637]

"Discriminating urban environments using multi-scale texture and multiple SAR images"

In this work we improve a methodology for discriminating urban environments by means of textural features in SAR images. In particular, we introduce multi-scale co-occurrence features and show how the feature set may be chosen as a function of the training set and the mapping classes. Moreover, we provide and compare results obtained by different satellite SAR sensors on the same urban test site, as well as a combination of these sets. Finally, a short analysis of the polarization effects and their importance in this framework of analysis is considered. The results are extremely encouraging, and show the potential of this technique, even if more research is needed to exploit the capabilities of the new generation of low-Earth orbit SAR satellites. [C5638]

"Anisotropy in reflected GPS measurements of ocean winds"

The probability density function (PDF) of the ocean surface slope can be estimated from the code-correlation waveform of reflected GPS signals. Anisotropy in this PDF is found to correspond to the local near surface wind direction, suggesting the ability to resolve this direction using scattered signals from two or more GPS satellites. A two-stage estimation process was applied to sets of waveform data collected from an airborne delay-mapping GPS receiver. First, an isotropic normal distribution was assumed for the PDF. The mean square slope (MSS) was fit to the measured waveform data for each satellite independently. Differences between the MSS estimates from two satellites at different azimuths were observed. In the second step, a bidirectional normal PDF was used with MSS constrained to that obtained in the first step, and an assumed value was given for the ratio of upwind to crosswind slopes. The direction of the principal axes was then varied to minimize the total residuals for both satellites. The results were compared with buoy recordings of the local wind direction. [C5639]

"Experimental study of a polarization-rotating Van Atta array with reduced co-polarized radar cross-section"

Fundamental experiment was conducted on a Van Atta array as a candidate of calibration target for airborne SAR. The problem of direct scattering from the elements was solved by giving a quarter-wavelength displacement between two sub-arrays. The result showed a good retrodirectivity with smooth reflection pattern as a function of the rotation angle and polarization rotating characteristic, while the directly backscattered waves were suppressed well. [C5640]

"Reflection characteristics of a retrodirective PARC"

Reflection characteristics of a retrodirective PARC (polarimetric active radar calibrator) were measured in a radio anechoic chamber. The reflection beamwidth was twice as wide as that of a conventional array reflector of the same size, and the measured RCS was 40.8 dBm² that almost agreed with the predicted value of 41.5 dBm². [C5641]

"An unsupervised classification method for polarimetric SAR images with a projection approach"

Two unsupervised training algorithms are presented based on a projection method for polarimetric SAR images. For this, polarimetric features, including the entropy H , angle α , anisotropy A , the largest eigenvalue of the coherence matrix λ_1 and coherence γ , are computed. Based on these features three noncorrelated and independent variates, which are the first three principle components are extracted using the principle component analysis. Then, a three-dimensional Cartesian coordinate is constructed using those three resultant variates. In order to reasonably define the initial cluster centers for the unsupervised classification, a projection method is proposed. As a result, a sophisticated two-dimensional feature space is obtained. Two initial cluster center determination algorithms, the histogram and histogram-quadrant methods, based on the above two-dimensional feature space are presented. Unsupervised classifications (with a minimum distance decision rule) are conducted based on the defined initial cluster centers. The classification results show that these approaches have high performance in convergence, speed, data volume and accuracy of training and classifying. [C5642]

"The DSTO Ingara airborne X-Band SAR polarimetric upgrade: first results"

The Ingara airborne multi-mode X-Band imaging radar system developed by DSTO has been upgraded to a fully polarimetric collection capability with a 600 MHz bandwidth. The initial trial of the upgraded system in December 2002 included the collection of synthetic aperture radar data sets of a calibration scene including interferometric repeat passes. The application of calibration techniques to the data yields a measured channel cross talk less than -30 dB. [C5643]

"The analysis of interferometric SAR imaging precision in the distributed micro-satellite system"

The INSAR imaging is one of the principal working patterns of the distributed satellite SAR system. This paper research mainly the influence of the Earth-movement and the distributed satellite circling to the INSAR imaging precision, analyze and derive the corrected imaging formula and the error curvature, and analyze in detail the height error shift in the variant latitudes and rotating angles. The results of simulation verify that when the latitude is lower and the rotating value is larger, the height error is higher. And the height error is the highest near the equator. [C5644]

"Calibration concept for the TerraSAR-X instrument"

The paper describes the calibration measures planned for the TerraSAR-X SAR instrument, due for launch in 2005. TerraSAR-X is a high-resolution X-Band SAR satellite that operates in Strip-map, Spotlight and ScanSAR modes and has selectable or dual polarization. It can image on the left or right side of the sub-satellite track, which is achieved by rolling the satellite. There are also experimental modes for wide bandwidth, providing even higher resolution, as well as for full polarization and along track interferometry (ATI), the latter two being achieved by splitting the receive antenna into two halves. Due to the high degree of flexibility of the instrument, e.g. the large number of modes and possible antenna beams, and the tight performance requirements, the calibration of the sensor is a major challenge and new concepts are needed to keep the costs affordable. [C5645]

"CALIPSO and CloudSat missions offer student opportunities in atmospheric research, remote sensing, and data comparisons globally"

CALIPSO and CloudSat will provide a unique data set on aerosol-cloud interactions that will substantially increase our understanding of the climate system and potential for climate change. [C5646]

"Earth observation instrument frequencies: a valuable resource to protect"

At the World Radiocommunication Conference 2003 (WRC-03) of the International Telecommunication Union (ITU) several issues related to Earth observation will be on the agenda and decisions will be taken with respect to these so-called agenda items. In this paper the current status of some of the WRC-03 agenda items will be given where Earth observation is directly involved through its active instruments, the so-called Earth Exploration Satellite Service (active), or its passive instruments, the so-called Earth Exploration-Satellite Service (passive). The paper discusses and presents the status up-to-date for the following agenda items for WRC-03: (1) Agenda Item 1.5: introduction of Radio Local Area Networks (RLANs) in the bands 5150-5350 MHz and the band 5470-5725 MHz. The 5250-5350 MHz band is an extensively used band for remote sensing by SARs, scatterometers and altimeters. This agenda item also asks for an extension of the EESS (active) band from 5460-5570 MHz to facilitate wideband (up to 320 MHz) active sensors. (2) Agenda Item 1.38: the possible allocation of 6 MHz for EESS (active) in the frequency range 420-470 MHz (P-band). A new frequency allocation in P-band would enable a future satellite project to carry a P-band radar for e.g. penetrating forest canopies for biomass estimation and ice-sheet sounding on Antarctica for retrieval of the bedrock topography. (3) Agenda Item 1.8.2: the protection of EESS (passive) sensors from unwanted emissions in adjacent and nearby bands. The issue of unwanted emissions is difficult to tackle both from a technical and regulatory point of view especially when linked to the protection of exclusive passive band. At the time of the IGARSS conference itself, the outcome of these WRC-03 agenda items including the upcoming agenda items for the next World Radiocommunication Conference (planned in 2007) will be known and will be presented. Consequentially, the Earth observation community will be informed at a very early stage which issues are selected for the next World Radiocommunication Conference where EESS (both active and passive) is directly involved as well as the implications of the outcome of the issues leading to WRC-03. [C5647]

"Outreach activities of the Polar Radar for Ice Sheet Measurement (PRISM) project"

The PRISM project at the University of Kansas has developed a multifaceted outreach program designed to interest students and the general public in research conducted in harsh polar environments. This outreach program involves K-12 students and teachers, undergraduate students from a minority institution, undergraduate journalism students with an interest in science and technology reporting, and the general public. [C5648]

"Locating calibrators in airborne InSAR calibration"

The condition number of sensitivity matrix is a key factor that influences the performance of InSAR calibration. On the basis of InSAR calibration theory, basic principles of locating calibrators are proposed, and constraints of locating calibrators are also derived. Under the theory of condition number minimization, an algorithm of locating

calibrators is presented to minimize the sensitivity matrix condition number. Theoretic analyses and computing results show that the algorithm is efficient. [C5649]

"On the stability of large antennas as calibration targets"

Large radar cross section (RCS) and high temporal stability are the typical requirements expressed nowadays to external calibration targets to be used for spaceborne SAR calibration. The use of ground-based large parabolic reflector antennas may be a good alternative to active radar calibrators or corner reflectors. Outstanding stability of the antennas RCS was demonstrated in a calibration series under AO3-343 in 1999-2000. Under the extension of the project in 2002 with a goal of preparation to ENVISAT mission we were able to demonstrate the repeatability of the series of observations made before as well as our ability to control polarisation of backscattered signal and to show phase stability of the backscatter, what is important for repeated orbits interferometry. [C5650]

"Impact of different correlation receiving techniques on the imaging performance of UWB random noise radar"

Cross correlation receiver is one of the most important parts in a random noise radar system. In this paper, the impact of different correlation receiving techniques on the imaging performance of ultra wideband (UWB) random noise radar is studied. Three types of correlation receivers, namely, the ideal analog correlation receiver, the digital-analog correlation receiver, and the fully digital correlation receiver, are discussed. [C5651]

"Improved polarimetric SAR classification by application of terrain azimuth slope corrections"

In polarimetric SAR imagery, along-track or azimuth slopes cause a shift in the polarization orientation angles. By estimating the orientation angle shift, Schuler et al. have been able to generate topographic models in good agreement with DEMs produced by other means. An improved method for estimating the orientation angle was developed by Lee et al. along with a unified analysis of available techniques. Another way to view this work is as a means of correcting the polarimetric SAR imagery for the terrain-induced slope effects in order to improve the accuracy of geophysical parameters derived from the SAR imagery. In this paper the techniques of Lee et al. are used to correct C and L-band polarimetric AIRSAR imagery taken in 1996 over the flanks of Mt Tongariro, New Zealand. We then use the corrected and uncorrected data in classification schemes and compare the results to demonstrate the effects of the azimuth slope corrections. The volcanic Mt Tongariro provides a rich variety of surface slopes, and a variety of vegetation is present including exotic forest, native forest, scrub, grasses and bare ground. Class statistics extracted from fore- and back-slopes (in the azimuth direction) are observed to cluster more tightly than for uncorrected data. This effect is more pronounced for L-band than for C-band. The largest effects were seen in targets of low polarisation entropy such as exotic forest. These corrections result in a modest improvement in the overall classification accuracies. [C5652]

"Comparison of multipolarization SAR systems depending on the way of the full scattering matrix measurements"

A number techniques, providing simultaneous or quasi-simultaneous measurements of the co-polarized and cross-polarized components in each orthogonal polarization are discussed in the report. Among the techniques of the measurements separation are time separation (SIR-C case), spatial/temporal separation from the same orbit of a squint SAR, repeated orbits interferometry mode, carrier separation and orthogonal codes separation. Each of the techniques under discussion is characteristic by the required PRF or swath width, data rate, level of polarization coupling and ambiguities. The comparison of the distortions is being made as well as a comparison of the SAR parameters. [C5653]

"Validation of bidirectional reflectance models using the first scene acquired by the CHRIS sensor over the Jornada Experimental Range"

Multi-angular reflectance data over desert grasslands and shrublands in the USDA, ARS Jornada Experimental Range near Las Cruces, New Mexico, were obtained by the Compact High Resolution Imaging Spectrometer flown on the PROBA satellite on August 5, 2002. An experimental satellite-borne sensor, the CHRIS, is one of the few sources of consistent multi-angular reflectance data on kilometer scales, providing up to five looks at a given target within the space of a few minutes. Two images acquired at different sun-target-sensor geometries were used to examine the validity of a simplified geometric-optical model (SGM) of bidirectional reflectance which incorporates a priori, empirical knowledge of the scattering properties of the underlying soil. The model is based on principles of geometric-optics while providing a mechanism for encapsulating volume scattering effects. It has been subjected to sensitivity studies and tested using a radiosity-based method, with simulations driven by

detailed plant maps and measurements of the optical properties of plants and soils. However, up to this point it has only been tested against multi-angular data acquired from the air by tilting a digital multispectral camera; work here using data from the CHRIS sensor extends and corroborates the results presented in the previous studies. [C5654]

"Combined field and laboratory goniometer system-FIGOS and LAGOS"

Ground level measurements of surface directional reflectance properties can be performed either in the field or within a laboratory setup. The latter has the advantage of independence on weather conditions, constant illumination and neglectable atmospheric disturbances. On the other hand, the artificial laboratory light sources usually are less parallel and less homogeneous than the clear sky solar illumination. In order to compare these two types of measurements (or replace one by the other) a careful correction of the data (BRDF retrieval) with respect to the mentioned sources of error is necessary. For the field case, this can be done following the well known procedures proposed by Martonchick and others. The purpose of this paper is to present our laboratory goniometer system and a corresponding BRDF retrieval solution. The RSL laboratory goniometer system (LAGOS) is based on the field goniometer (FIGOS) with the addition of a 1000 W brightness-stabilized quartz tungsten halogen lamp and lens system, placed in a dark room for minimization of stray light. The inhomogeneity of the illuminated area has been directly measured and found to be within 10% mean deviation for the zenith position. A simulation of the complete geometry of LAGOS, including the angular distributions and inhomogeneity of the light source as well as the changing position of the radiometer footprint allows us to estimate the measurement error for any target with known BRDF. The same algorithm can be used as core for the BRDF retrieval. [C5655]

"Wavelet-based system for classification of airborne laser scanner data"

A new semi-automatic processing system for classification of airborne laser scanner cloud points is developed. To mitigate the difficulty caused by the complex distribution of objects on Earth's surface, wavelet was adopted in size-based clustering of laser points. A hybrid method of processing laser scanner data in both grid and raw formats was also adopted to speed up the processing time and adjust the smoothing effect of interpolation. The processing focused on processing the data acquired over urban area. This paper presents and explains the components of the system using the test data acquired over Shinjuku area, Tokyo, Japan. [C5656]

"Cabannes versus Rayleigh scattering and terrestrial backscatter ratio revisited in LITE in support of CALIPSO"

In order to make optimal quantitative use of multi-wavelength spaceborne lidar data in the upcoming satellite lidar mission CALIPSO (Cloud-Aerosol Lidar and Infrared Pathfinder Satellite Observations), it is essential that the lidar be well calibrated. In view of the use of a narrow bandwidth receiver filter in CALIPSO, it is necessary to quantitatively distinguish Cabannes scattering from the full bandwidth Rayleigh scattering for correct calibration of the 532 nm channel based on Rayleigh normalization. This also affects the 1064 nm calibration when it is implemented by the 532/1064 calibration ratio approach. Secondly, the calibration obtained by normalizing to a nearly Rayleigh background signal depends on the backscatter ratio R , defined as the ratio of the total backscattering coefficient [aerosol backscattering coefficient, $\beta_a(z)$, plus molecular backscattering coefficient, $\beta_m(z)$] to the molecular backscattering coefficient, $\beta_m(z)$. How well this backscatter ratio, R , can be estimated in clean air regions will play an important role in lidar measurements of aerosol and cloud by CALIPSO. The LITE (Lidar In-space Technology Experiment) mission, the first lidar designed for atmospheric studies to fly in Earth orbit, provided an important database for doing the analysis and simulations for future lidar systems on free-flying satellite platforms. This paper presents calculations of Rayleigh/Cabannes scattering cross sections that should apply for CALIPSO by incorporating different depolarization factors appropriate for different spectral bandwidths. LITE data are analyzed to recover estimates of R characteristic of clean air regions. Errors in recovering R resulting from uncertainties in the calibration constant and two-way transmission from the calibration reference height are simulated and assessed. [C5657]

"Polarization characteristics of a mixed seeding pasture and its application for predicting the ratio of legumes"

Reflectance (R), polarized reflectance (Q) and degree of polarization (P) were measured for a mixed seeding pasture consisting of white clover and tall fescue in 8 spectral bands in the visible, near- and short-wave infrared wavelength ranges. Horizontal leaves in the white clover canopies generated more polarized light than vertical leaves of the tall fescue. Polarization (Q and P) increased as the ratio of legumes (ROL, leaf area ratio of white clover to the total) increased in the mixed sown canopies. A multiple regression model that used a Q and R_s of 3-bands that were all acquired at view zenith angle 60° explained 90% of the variation of ROL with RMSE 11%.

The regression model was validated by a data set provided in the next growing season. The model including polarization information was comparatively more stable inter-annually than the model of reflectance only. It is effective to utilize the polarization information of reflected light as a method of estimating ROL of mixed seeding pastures where planophyll and erectophyll plant species coexist. Polarization is appropriate for ROL monitoring in pastures. [C5658]

"An approach to multistatic spaceborne SAR/MTI processing and performance analysis"

Multistatic spaceborne SAR offers in addition to powerful Earth imaging and remote sensing the possibility to detect the presence of slowly moving objects due to the large baselines. In contrary to monostatic multi-subaperture systems with classical STAP processing the multi-satellite system overcomes the problem of blindness against certain directions of target motion. Moreover velocity and direction of target motion can be estimated with considerably higher accuracy when taking advantage of the geometry of the multistatic configuration. For this purpose non-classical algorithms have to be developed. Furthermore, the application of optimum detection schemes and the exact analysis of MTI performance are challenging tasks. Indeed the high system complexity and the huge amount of data to be analysed make the MTI processing exceedingly difficult. Therefore only sub-optimum methods can be implemented. In this paper we propose a sub-optimum approach for multistatic spaceborne moving target detection. First of all we define a signal model for both moving targets and clutter proceeding from an arbitrary multistatic configuration. Secondly, we present the sub-optimum statistical processing based on the exploitation of the covariance matrix describing the common statistical properties of the random vector composed of a selected number of resolution cells in the range-Doppler-space for all sensor channels. Then we analyse the MTI performance of representative multistatic configurations. Finally this method is applied to simulated data of multistatic satellite systems. [C5659]

"Orbital SAR simulator of fishing vessel polarimetric signatures based on high frequency electromagnetic calculations"

This paper continues the work developed in related to a numerical tool able to simulate the full-polarimetric raw data for a given orbital SAR system from a realistic vessel model. This simulator makes possible the construction of a precise database of vessel radar signatures that will be used to develop classification algorithms. The simulator will be also useful to determine the system parameters of a future orbital SAR sensor dedicated to sea activity monitoring. This paper is focused on the validation tests and the new improvements developed. [C5660]

"Development of a new C-band polarimetric Doppler weather radar in Japan"

Communications Research Laboratory (CRL) has developed a new C-band (5340-MHz) multi-parameter Doppler radar system with a bistatic Doppler radar network. The purpose is to establish the next-generation technology of precipitation observation for meteorological and hydrological applications, such as weather forecasting and run-off analysis for predicting floods. This new radar is named COBRA (CRL Okinawa Bistatic polarimetric RADar). The weather targets of the system are typhoons, Baiu-frontal rainfall, meso-scale precipitation in subtropical zones, and clear-air turbulence. Two transmitter (klystron) units are used for to observe the polarization characteristics of precipitation particles. The transmission polarization for each pulse is selected from six possible polarizations. The return signal is measured simultaneously by two receivers, one for the horizontal polarization and the other for the vertical polarization. [C5661]

"Fully polarimetric classification accuracy"

Assuming that polarimetric data is entirely described by the underlying complex covariance matrix, this paper gives expressions for the maximum likelihood classification accuracy, and applies these to real data. This assumes negligible interclass environmental variation and a homogeneous image structure which is overly simplistic. By including a model of environmental variation, more realistic results may be possible. [C5662]

"Newest technology of mapping by using airborne interferometric synthetic aperture radar systems"

Various remote sensing technologies are presently used to derive land surface and sub surface information. Each individual system (sensor) has its own advantages and disadvantages. The new airborne interferometric RADAR system OrbiSAR-1, developed, manufactured and operated by Orbisat da Amazonia's Remote Sensing Division, created a new way of automated mapping. Due to the use of microwaves as sending and receiving impulses of the sensor, the system is independent of day light and can therefore even map at night. As the microwaves are not influenced by the presence of clouds, the system can even map in bad weather situations, like rain or closed cloud coverage. [C5663]

"Targets classification of semi-arid region using polarimetric SAR data \$an example in Xinjiang, China"

This paper develops a classification way using polarimetric synthetic aperture radar (SAR) data. Polarization of radar electromagnetic wave is a very important factor of backscattering theory and geosciences applications. However, polarimetric SAR images are still difficult to interpret and therefore there is a need to improve the classifier that can make use of the polarimetric information. Under the certain circumstance the present paper attempts to classify remotely sensed scenes by all the complete polarization response parameters, which are presented as data dimensions for classification arithmetic. The test site is located in Hetian of Xinjiang, China. SIR-C data were acquired in the test site in 1994. Fully polarimetric SAR data can be processed as multi-dimensions images. But the polarimetric information is related greatly with variable targets. Firstly, we decompose the backscattering matrix and get polarimetric ratios, polarimetric degree, and polarimetric entropy. These polarimetric parameters are considered as data dimensions in which elements change in terms of probability functions with variable targets. Training samples were then generated from the outputs of the unsupervised classification of K-means, to be used in subsequent supervised classifications of two frequencies (C- and L-band for SIR-C data) and various polarization combinations. The estimation of the classifier tallies with the local municipal statistics. The result shows that classification precision can be improved finely with the polarimetric technique. [C5664]

"Utilization of the radar polarimetric covariance matrix for polarization error and precipitation canting angle estimation"

The 343 radar polarimetric covariance matrix provides a complete set of measurements from distributed particles. Via optimum polarization theory, radar system polarization errors and particle orientation distribution parameters can be estimated. While the theory of covariance matrices and associated optimum polarizations for random media have been known for some time, the application to retrieval of microphysical information of precipitation is much more recent. Well calibrated covariance matrices and in particular the calibration of the phases of the two co-to-cross covariance terms hhS_{vh}^* and vvS_{hv}^* is necessary before optimum polarization analysis. [C5665]

"A RF model of an active array antenna for a spaceborne SAR"

LSAR is to be a space-based synthetic aperture radar (SAR) capable of high resolution imaging of the surface of the Earth. Applications for LSAR include the observation of oil slicks, ice packs, shipping lanes, industrial pollution, forests and agricultural usage. LSAR will travel in a low Earth orbit focusing a narrow radiation pattern upon the Earth in the plane of travel and a series of wide beams in a plane transverse to this. Whereas the narrow along track or azimuth beam formed from the long antenna dimension is fixed normal to the spacecraft, the wide elevation beams formed from the short antenna dimension have the ability to scan over the surface of the Earth. [C5666]

"Humidity gradients derived from wind profiler radar and RASS in presence of elevated ducts"

Wind profiler radars, developed over a decade ago, provide a wealth of information about wind and turbulence in the troposphere. Refractive index gradients retrieved from these radars combined with temperature gradients obtained from a radio acoustic sounding system (RASS) can provide continuous humidity gradient profiles in the lower troposphere. This technique has a distinct advantage over humidity gradient retrievals from radiosondes, which are launched periodically (with a period of 6 hours or 12 hours). The 482 MHz wind profiler and RASS data from the Meteorological Observatory at Lindenberg, Germany, have been analysed in the presence of ducting conditions to obtain height profiles of humidity gradient. These profiles compare well with those retrieved from radiosonde data analysis. [C5667]

"A topological feature extraction system from lidar data with the application of radiowave propagation modelling"

Various implemented software programs and GIS software applications were employed to investigate an effective method of extracting features (primarily buildings) from a LIDAR dataset (Vosselmann, 1999). Boundaries or outlines define the features, with the result being an external output file containing vector data of these features. The method involved the use of various GIS and image processing functions. These functions include in sequence, classification and smoothing using majority and median filters. The goal of classification and smoothing is to condition the tile for edge detection. The fundamental problem with the LIDAR dataset is the classification of pixel heights, in order to provide clear-cut boundaries between topographical features, such as ground level and roof level of buildings. To overcome this, various sized filters were investigated (30, 545, and

70) as well the number of iterations of the filter to find the optimal classified and smoothed dataset. An edge detection function was performed by determining slope values for the tile. Thresholding was applied next to aid in the sequential processes, thinning and expanding, by removing spurious pixels. The resulting feature outlines were vectorised. Subsequent functions were applied to improve accuracy of feature outlines. Visibility analysis has been implemented, showing visible and obstructed pixels. Basic radiowave propagation techniques have also been implemented for use on the LIDAR data. These include LOS and single-knife edge diffraction. The vectorised features can now be utilised in developing further propagation techniques, such as reflection and scattering. [C5668]

"A novel approach for synthetic aperture radar image processing based on Genetic Algorithm"

In this study, an evolutionary computing algorithm is utilized for data preparation and analysis of synthetic aperture radar (SAR) imagery for planetary geology. Since its invention by J.H. Holland in the 1990s, the Genetic Algorithm (GA) has already gained popularity in a wide range of engineering applications. The genetic approach is used for processing of SAR imagery to find a region of a pre-defined criterion. It was seen that the algorithm is superior to deterministic methods in terms of processing times and finding the global minimum points. The proposed method is suitable to SAR image processing where huge amounts of data have to be processed in very short time intervals. [C5669]

"A comparison of non-parametric spectral estimators for SAR imaging"

Nonparametric spectral estimators have many applications including target range signature estimation and synthetic aperture radar (SAR) imaging. In this paper we explain how to apply nonparametric approaches to SAR imaging. We present an important nonparametric spectral estimation method which is the Capon algorithm. We compare the Capon method with other nonparametric methods such as APES, Periodogram, and FFT for their resolution, sidelobe levels, and spectral peaks. And we also show by means of experimental examples that the forward-backward Capon gives much better estimation than the forward only Capon. [C5670]

"EMI and atmospheric noise measurements for determining HF bandwidth occupancy profile of East-Mediterranean Sea"

Surveillance potential of Over-The-Horizon Radar (OTHR) systems increases the interests on the high-frequency (HF) band of the EM spectrum. The frequency management systems in these radars tackle with the problem of channel occupancy and atmospheric noises both of which may change very rapidly even in a short portion of a day. In this work EMI and atmospheric noise measurements have been realized over a certain period in autumn, winter, spring and summer at distinct regions of the East Mediterranean Sea. Dynamic characteristics of channel availability and noise floor have been determined based on time-slots in a day, days in a season and compared with International Telecommunication Union (ITU-R) predictions by analyzing measurement data. [C5671]

"Melting layer model evaluation in Singapore"

Propagation characteristics in the melting layer are not only relevant to slant path attenuation predictions for satellite links but also for spaceborne radar remote sensing of rainfall. In the latter case, the radar retrieval algorithms rely heavily on accurate estimates of the melting layer attenuation, since the radar signal traverses this region twice, both in the forward direction and in the return direction. Several models have been proposed for predicting the attenuation in the melting layer. One such method is the non-coalescence-non-break up (N-N) model based on spherical melting particles made of dielectric composites, Nishitsuji and Hirayama (1971). The model assumes the melting particles to be composed of a homogenous mixture of water, ice and air, and calculates the complex permittivity from Wiener's theory. The calculation includes the parameter "form factor", U , as well as the volume content of water, ice and air. The height variation of these parameters has been inferred fairly accurately in the past from satellite propagation data, Awaka et al. (1985). This paper compares the N-N model predictions with Doppler radar measurements taken in Singapore. Comparisons are presented in terms of the radar reflectivity (dBZ) as well as the mean fall speed (V_{view}) and the Doppler width (w). [C5672]

"Method for remote sensing of the atmosphere by using laser generated flashes"

In this paper, a new atmospheric monitoring method by using pulsed flashes is described. The formula for calculating the volumes of local regions in the case when scattering angles are not equal to 90° and for the extinction coefficient K between flashes is introduced. [C5673]

"Remote analysis of gas mixtures using an optical parametric oscillator based lidar system"

A scheme for lidar measurements of multicomponent gas mixtures in the mid-IR region using a newly developed

fast-switching, frequency-agile optical parametric oscillator (OPO) system combined with multivariate statistical methods has been implemented and tested. The scheme adopted was able to predict the composition of the remote hydrocarbon gas mixture within the uncertainty of the pre-determined gas composition. [C5674]

"Laser technology maturation and risk reduction for space-based remote sensing"

This paper presents a multiCenter efforts leading to formulation of an integrated NASA strategy to provide the technology and maturity of systems necessary to make Lidar/Laser systems viable for space-based study and monitoring of the earth's atmosphere. The goal of such a strategy is to assure the availability of the suite of technologies required to enable the successful development of the broad range of lidar missions envisioned by NASA. The Strategy Team also recommended development of eye-safe space-based solid-state laser transmitters for multiple lidar applications. The concern of eye-safety is promoting the development of solid-state eye-safe laser transmitters in the UV and mid-IR. Using the non-linear optical devices, such as optical parametric oscillator (OPO), optical parametric amplifier (OPA), and wave mixing technologies; the tunable wavelength range can be extended to target the different atmospheric constituents, such as ozone, carbon monoxide, ammonia, methane, etc. [C5675]

"Studying of the modeling optimum methods of random processes and fields"

In the paper the modeling of random processes and fields has been carried out. The way of increase of modeling accuracy has been described. [C5676]

"Z-R relationship for individual snowfall and its evaluation"

Relationship between radar reflectivity factor (Z) and precipitation rate (R) is important in estimating precipitation rate. This is called "Z-R relationship" and generally derived in the power-law form. A new snowfall observation system and techniques were proposed to determine the detailed Z-R relationship corresponding to each snowfall event. The best-fit Z-R relation for each snowfall event was calculated. It was possible to classify Z-R relationship of snowfall into 3 types. Effects of size distribution and fall velocity of snow particles on the Z-R relationship were examined. [C5677]

"Wireless LAN PC card sensing of vital signs"

Heart and respiration activity can be monitored remotely without any sensors attached to the subject, using the microwave Doppler radar principle. Implementation of this function using wireless LAN PC cards is described. Heart rate was successfully obtained with two minimally modified LAN cards each driven by a laptop computer, at a distance of 40 cm from the subject. This is the first demonstration of the use of a modified wireless terminal for remote sensing of vital signs. [C5678]

"Hidden Gauss Markov model for multiscale remotely sensed image segmentation"

Hidden Markov models are useful tool for tackling numerous problems especially in statistical signal and image processing. This paper presents a wavelet domain approach to remotely sensed image segmentation based on Hidden Markov Tree (HMT) models. The essence of this work is based on capturing the statistical properties of the wavelet coefficients by a tree-structured model. One important drawback to the HMT model is the need for iterative training of the HMT model parameters for a given data set. Following the fast training we perform likelihood computation algorithm for texture classification at different scales and directly segment wavelet-compressed images. We demonstrate the performance of the algorithm with SPOT and RADARSAT images. The findings are found to be encouraging. [C5679]

"Monitoring freeze-thaw events in Siberia using the seawinds Ku-band scatterometer: first results"

In this paper we will report the first results of our work carried out within the framework of the SIBERIA II project. This project has the aim to demonstrate the viability of full greenhouse gas (GHG) accounting using a set of multi-sensor Earth Observation instruments, detailed existing databases of field information and some of the worlds most advanced climate models. Freeze-thaw information is intended to be used for validation and input into the GHG models. Utilising the high temporal sampling of the SeaWinds sensor on QuikSCAT, along with a unique gridding and extraction method, from observational to analysis space, we present a new approach for freeze-thaw detection by time series analysis and evaluation of the temporal characteristics of the backscattered signal. [C5680]

"Geoscience laser altimeter system (GLAS) for the ICESat mission-pre-launch performance"

GLAS is a space lidar on NASA's ICESat Mission. GLAS was qualified and delivered and ICESat is scheduled for launch in December 2002. This talk summarizes the as-built characteristics of GLAS and its predicted measurement performance. [C5681]

"3-dimensional mid-infrared remote sensing of gas concentrations in combustions"

First Page of the Article [C5682]

"Advanced MMICs for Remote Sensing and Radar Applications"

Modern remote sensing systems and radars are more and more based on electronically steered antennas. Instead of using one high power tube, each radiating element must contain a full T/R module allowing an individual modulation of amplitude and phase of both transmit and receive signal. The key elements in such systems are monolithic microwave integrated circuits. In this paper some general information about these components are given as well as the latest achievements in terms of power amplifiers are described. The CHA7010 is a 10W power amplifier (in pulsed mode) featuring high PAE and small size. [C5683]

"Microwave Remote Sensing: Needs and Requirements Concerning Technology"

Spaceborne microwave remote sensing instruments, like the imaging radiometer and the synthetic aperture radar, are over time faced with two partly conflicting requirements: performance expectations (resolution, sensitivity, coverage, a.o.) steadily increase while resource allocations (weight, power, bulk, cost) decrease. This results in needs and requirements to the development of advanced technology thus enabling future advanced systems to be viable and realistic. [C5684]

"Development and application of a SAR training processor"

In order to make the concepts of SAR more accessible to a general audience, a SAR Training Processor (STP) was developed. The SAR Training Processor was used in lecture and laboratory exercises for graduate-level Remote Sensing classes and for public seminars. The software allows the user to interactively visualize data and explore the effects of processing options. Users can view any intermediate processing results, modify the processing steps, and change processing parameters. The processor can be run either from the command line or from a graphical user interface. Examples of exercises that demonstrate SAR principles and strategies for using the STP are given. [C5685]

"Proceedings of International Conference on Recent Advances in Space Technologies (IEEE Cat. No.03EX743)"

First Page of the Article [C5686]

"Potentials for high-resolution imaging with small satellites"

In the field of space-borne topographic mapping instruments the trend to smaller ground sample distances (GSD) can be observed, making use of the best technology available at the given time. From the 80 m GSD of ERTS (later renamed Landsat-1), the first satellite dedicated to civil space-borne Earth surface imaging launched in 1972, the GSD now approaches 1 m. Mass and power consumption of spacecraft and instruments follow similar trends. Alternatives to passive optical systems such as SAR and laser altimeters also benefit from the immense improvement in very diverse fields of technology. Nevertheless, the most promising prospects for topographic mapping with small satellites are connected with passive optical systems, especially push-broom systems. The paper tries to contribute to the answer of the question, how far can we go with decreasing instrument size, mass and power consumption, and decreasing the GSD at the same time. After explaining the basic topographic mapping concepts, the paper deals with important parameters for mapping with small satellites: spatial resolution, radiometry, mass, volume, power consumption, microelectronics, pointing accuracy and stability, data volume and transmission. From the technology point of view, small satellite missions for topographic mapping are feasible. One system is already in Earth orbit, others are in the planning stage. There is a good chance to install mapping systems with a low cost space segment. It is a question of market requirement and behavior whether or not these small satellite based mapping systems can successfully compete with existing space-borne or airborne based mapping systems. [C5687]

"Synthetic aperture radar image processing using cellular neural networks"

In this paper, Cellular Neural Networks (CNNs) have been applied to noisy Synthetic Aperture Radar (SAR) image to improve its performance and appearance. The image has been obtained from Erzurum, Turkey.

Because of the importance of imaging quality and appearance for remote sensing applications, CNN has been applied to data for image processing applications that for noise filtering and edge detection. In training, Recurrent Perceptron Learning Algorithm (RPLA) is used as a learning algorithm. According to templates SAR-image has been tested and obtained satisfactory results. [C5688]

"Automatic detection of flooded areas on ENVISAT/ASAR images using an object-oriented classification technique and an active contour algorithm"

Two techniques for extracting flooded areas out of radar-imagery in a time-efficient way are presented in this paper. The results of the object-oriented classification technique, based on the commercial eCognition software, and the active contour technique, are both obtained on 2 ENVISAT ASAR images; one recorded during a flood period in Flanders on 2 January 2003 and one during a non-flooded region on 26 June of the same year. In both techniques the net flooded result is based on the subtraction of the existing water bodies (i.e. lakes, rivers, canals, ...) obtained from the non-flooded reference image, from the image recorded during the flooded period. [C5689]

"Applying space technologies for human benefit; the Canadian experience and global trends"

In the era since Canada followed the Soviet Union and the United States into space, space technology has evolved enormously. No longer the exclusive purview of fully developed countries, space is being harnessed for the benefit of humanity by even small countries and individual establishments. The exploitation of space applications is limited only by the imagination and resolve of the interested parties. Canada's initiation into space took the form of Alouette 1, launched in 1962 to learn more about the physics of electromagnetic phenomena interfering with its radio communications with its northern areas. International collaboration has played an important role and continues to be emphasized as its exploitation of space progressed from science and communications to remote sensing to space robotics. Even today, Canada has declined to develop an independent launch capability, preferring to collaborate with the nations endowed with such a capability. Recent developments in Canada have seen collaboration extend inward, with federal/provincial and private/public sector cooperation on selected space missions. Such collaboration has proven very beneficial to Canada and is recommended globally. Canadian harnessing of space technology began in the domain of communications, moving from R&D into phenomena affecting communications to the world's first domestic geostationary satellite communications system. Today, Canadians have access to not only our own domestic comsats but also international service providers which include Canadian elements. Canadian involvement in space robotics received a big boost with the contribution of the CANADARM to NASA for use on their space shuttles. It grew further with the CANADARM-2 for the International Space Station (ISS), a sophisticated robot which is still evolving, the third main element not yet launched. This arm is available for use by the international partners on the ISS, a major international scientific collaboration. [C5690]

"TerraSAR-X, German X-band remote sensing system"

TerraSAR-X is the latest development at EADS Astrium GmbH of Synthetic Aperture Radar using an active phased array for spaceborne remote sensing. Its technical implementation is based on core technologies which have been developed and qualified in a demonstrator programme (DESA). New capabilities have been added like full polarimetry and along track interferometry via a Dual Receive Antenna. The programmatic implementation follows a Public Private Partnership (PPP) between the German Aerospace Center, DLR and EADS Astrium GmbH. EADS Astrium is investing into TerraSAR-X to build-up a data service for world wide customers through the founded Infoterra GmbH. [C5691]

"DCT and wavelet based image compression in satellite images"

Synthetic aperture radar (SAR) and SPOT images are becoming increasingly important and abundant in a variety of remote sensing and tactical applications. Thus, there is a strong interest in developing data encoding and decoding algorithms that can obtain higher compression ratios while keeping image quality to an acceptable level. This study aims to compare most of the well-known compression techniques namely discrete cosine transform and discrete wavelet transform. It investigates RADARSAT and SPOT images of different regions of different characteristics. RADARSAT-1 fine and standard beam mode images of the different regions in Istanbul are used to test the performance of the compression algorithms. The regions, which have been investigated, were sea areas, forest areas, built environment-residential and industrial areas which define different patterns of urban land use. The studies showed that homogeneous areas like forest and sea gave better compression results compared to heterogeneous areas like industrial and environmental. The second purpose of this study is to compare the two compression algorithms. The discrete wavelet based algorithm gave much better results compared to the discrete cosine transform based algorithm. The results changed according to the quantization

process and the transform-coding algorithm. [C5692]

"The Imaging Wind and Rain Airborne Profiler-a dual frequency dual polarized conically scanning airborne profiling radar"

The University of Massachusetts (UMass), with support from ONR, NOAA and NASA, has developed a novel radar system called the Imaging Wind and Rain Airborne Profiler (IWRAP). IWRAP is a dual frequency (C/Ku band) dual polarized airborne radar that profiles the volume and surface backscatter and Doppler simultaneously at 30, 35, 40 and 50 degrees incidence, while conically scanning at 30 to 90 rpm. Its range resolution can be set at 15, 30, 60 or 120 m. From these measurements the ocean surface wind field, 3-D boundary layer winds within rain bands can be mapped. IWRAP was flown during the 2002 NOAA/NESDIS/ORA Hurricane Ocean Winds Experiment, which was conducted in conjunction with the 2002 NOAA/AOML/HRD Hurricane Field Program. This paper presents the system design, radar processing algorithms and initial results from the 2002 hurricane flights. [C5693]

"Design and development of a dual-frequency (Ku/Ka), dual-polarization, wide-angle scanning airborne rain radar antenna system"

A compact, dual-frequency (Ku/Ka-band), dual-polarization, wide-angle scanning antenna system has been developed as part of an airborne instrument for measuring rainfall. This system is an upgrade version of a prior single frequency airborne rain radar instrument, and was designed to generate spatially coincident horizontally and vertically polarized beams at both frequencies with 3-dB beamwidths that match within 25 percent, and have low-sidelobe levels over a wide scan angle at each polarization-and-frequency combination. The calculated results, as well as the measured electrical performance over wide-angle scanning, are presented. [C5694]

"Regularization of Laplace transform inversion for subsurface conductivity and permittivity profile estimation using GPR signals"

This paper deals with the regularization problem raised by the inversion of GPR radargram. The determination of subsurface conductivity and permittivity profiles leads to Laplace transform inversions for real data. A very recent method to solve this severely ill-posed problem is presented and evaluated using a standard 2D FDTD numerical GPR model for multilayered media. [C5695]

"Noise radar using random phase and frequency modulation"

Pulse compression radar is used in a great number of radar applications. Excellent range resolution and high ECCM performance can be achieved by wide-band modulated long pulses, which spread out the transmitted energy in frequency and time. By using random noise as waveform, the range ambiguity can be suppressed as well. The same limit in Doppler resolution is achieved as for a coherent Doppler radar when the time compression of the reference is tuned to that of the target. Mostly, the random signal is transmitted directly from a noise generating HF-source. A sine wave, which is phase or frequency modulated by random noise, is an alternative giving similar performance but higher transmitted mean power when peak-limited transmitters are applied. A narrower modulation noise bandwidth can also be applied to generate the same output bandwidth. For phase modulation, the bandwidth amplifying factor is simply the rms value of the phase modulation, and for a frequency modulating waveform, the output rms bandwidth equals the rms-value of the frequency modulation. The results also show that the range sidelobes can be highly suppressed compared with the sidelobes of the modulating signal. The mean and variance of the correlation integral are derived in terms of the autocorrelation function of the modulation. The combined effects of low range sidelobes and enhanced range resolution make frequency and phase modulation attractive. [C5696]

"An adaptive clutter rejection scheme for atmospheric radars"

Clutter rejection is among the most important issues in radar signal processing, for which adaptive antenna technique is a powerful means. Compared to other applications of the adaptive antenna, however, atmospheric radars require strict conditions; The main antenna beam pattern should not be altered since the target region is defined by its shape. Especially, the loss of the antenna gain should be kept to no more than about 0.5 dB in order to maintain the high sensitivity of the system. Also, clutter from surrounding mountains is often stronger than the desired weak scattering from atmospheric turbulence. We propose a new algorithm which satisfies the above conditions, and confirm its capability by applying to actual radar data. Despite the fact that no information is given on the spectral features of the desired and undesired signals, only the clutter echoes from surrounding mountains were effectively cancelled without affecting the desired echoes from atmospheric turbulence. [C5697]

"SAR/MTI from helicopters"

MTI/SAR is a well established technique for airborne surveillance. In a helicopter these two modes of operation can be combined as well. The helicopter can also easily move in the vertical direction, making SAR mapping of the height profile of the ground surface possible. In this paper, MTI/SAR from a helicopter is studied in more detail. Relationships are developed between the involved parameters, and the performance is displayed in some examples. Phase error compensation is needed by IMU or autofocus due to the non-linear movement of the antenna along the SAR path. Highly improved mapping performance can be achieved by using an ESA with multiple beam generation, or high speed scanning. For high resolution mapping in three dimensions interferometric SAR is needed. [C5698]

"Assessment of a digital quadrature demodulator for a stepped frequency radar"

A direct digital demodulator for a stepped frequency radar was modeled and its performance estimated by computer simulation. The performance of a prototype was evaluated. Timing jitter was found to be the most significant cause of error in both cases. [C5699]

"Calibration of HF radar systems with ships of opportunity"

This paper addresses the application of ships of opportunity to determine the proper phase corrections for HF ground-wave phased array radar systems. Such HF radar systems are being used more and more extensively for measurements of coastal ocean surface currents. In order to correctly determine the spatial bearing of the currents that such systems measure, antennas must be appropriately calibrated for amplitude and phase variations within the array. Phase and amplitude corrections are often accomplished through ship-based transponder runs. Such calibration runs, however, require the use of a ship and thus are expensive and may not be done as frequently as is needed, such as if there are changes in the elements of the array or the local terrain. A technique is described below that can potentially make use of ships of opportunity with unknown bearings to determine the required phase corrections for the array elements and to determine the bearing of the unknown ship. Examples run thus far from transponder data collected with an 8-element loop receiving antenna array indicate that with this technique, for cases where the SNR exceeds 20 dB, the antenna phase corrections are generally within 0.2-0.3 radians of the values obtained from a direct transponder run where the ship's bearing is known. When the ship's bearing is assumed unknown and is uniquely determined from different radar frequencies, for cases where the SNR exceeds 20 dB, the results for the ship bearing are consistent to within 2-3°. [C5700]

"Radar sea echo in UHF in coastal zone: experimental observations and theory"

We present the results of a preliminary experiment of remote sensing of near-shore environment by an UHF radar initially devoted to atmospheric wind profiling. VV and HH Doppler signatures of the sea surface during a one-day experiment are analyzed in terms of signal decay with distance and Doppler spectra morphology. Marked differences between VV ("slow" scatterers) and HH spectra ("fast" scatterers) were observed. VV spectra could be partly reproduced considering a first-order Bragg theory. [C5701]

"Merging surface current data from HF radars operating at different frequencies"

HF radars operating at decameter wavelengths (3 to 30 MHz) in ground wave mode are capable of mapping near-surface, coastal ocean currents. Several different HF radar systems are often in operation to observe a given area, using different radar operating frequencies. Users of the data products of HF radars need to know the likely uncertainties and biases caused by the use of data from radars with different operating frequencies and how to merge the data from these different systems into a single current map. During the year 2000 two MCR's operating at 4.8, 6.8, 13.4 and 21.8 MHz were sited at Moss Landing and Santa Cruz, California, collecting current maps at hourly intervals. We show that the current maps over Monterey Bay constructed from 4.8 MHz and from 21.8 MHz data have rms current speed differences of about 10 cm/s. We also present a physical model that predicts the difference between current speeds observed at different frequencies in the 3 to 25 MHz range as a result of wind stress induced, vertical current shear. We demonstrate theoretical and empirical methods for mitigating what we think is wind-stress-related bias between current observations at different HF radar operating frequencies. [C5702]

"P band data collection and investigations utilizing the RAMSES SAR facility"

ONERA, the French aerospace research agency, has developed a multi-frequency, full polarimetric and high resolution airborne SAR facility named RAMSES, which has been expanded with a P-band (435 MHz) capability at the end of year 2000. The Gironde area was chosen as a suitable test-site for fieldwork validation of P-band

capabilities in coordination with the "low frequency radar working group" set up by CNES (French Space Agency), the DGA (DOD Procurement Agency) and the CEV (French Flight Test Center). This experiment has explored the capabilities of this low frequency band for sub-surface moisture detection (on the "Pyla" sand dune), biomass assessment (on the Nezer forest), mapping of the ocean bathymetry/salinity (on the "bassin d'Arcachon", estuary of the Gironde), and archaeology (imaging of buried Roman-era artifacts). After a short description of the radar P and of the experience feedback of campaign "PYLA 2001" on the P-band radar, we present a preliminary synthesis of the results on the different sites. The "PYLA 2001" campaign results are encouraging. We therefore plan further experiments at the beginning of 2004 over Egypt (with simultaneous band P+L). In conclusion, we present the future research trend at ONERA in the domain of lower frequency (VHF/UHF) SAR. [C5703]

"Wideband radar phenomenology of forest stands"

In this paper, experimental ultra wideband radar backscatter response of a forest stand for remote sensing using applications are presented. The radar signal is a zero-mean pulse with a duration of 1.5 ns, and rise time of 0.1 ns occupying a bandwidth 3 GHz from 0.5 GHz-3.5 GHz. The transmitter pulse amplitude exceeds 240 V in a 50 ohm transmission line giving rise to a peak power of about 1.15 kW. The transmit and receive antennas are broadband and with voltage standing-wave ratio of better than 1.2 up to 12.0 GHz. The radar is capable of transmitting both horizontal and vertical polarizations. Radar ranging of up to 180 m was achieved with a pulse repetition rate of 5 kHz. This radar was deployed to measure polarimetric backscatter from a 40-year old larch plantation stand with viewing angle varying from 50° to 75°. For calibration, a corner reflector with 1 m side length was applied. Attenuation of the radar signal propagating through the canopy was extracted from the backscatter response of the forest. Two specific features are observed from the attenuation data one having an exponential and the other having a power law dependence with distance. For the pulse scattered by the trihedral reflector imbedded in the forest, a phase diagram representing the parametric relation between the quadrature components of the receive signal is analyzed. The results obtained in this study show new possibilities for radar remote sensing of forest parameters with ultra wideband radars. [C5704]

"Development of the ultra-wideband LORA SAR operating in the VHF/UHF-band"

LORA (low-frequency radar) is a new airborne VHF/UHF-band radar which has both synthetic-aperture radar (SAR) and ground moving target indication (GMTI) modes. The main motivation for the system is to facilitate detection of man-made objects in a variety of conditions, i.e. stationary or moving, located in open terrain or in concealment under foliage. The LORA system will operate in several configurations extending from 20 MHz to 800 MHz. Initial flight trials during 2002 were successfully conducted using the 200-400 MHz band. SAR image examples are shown including both forested areas and man-made objects. A second band, 400-800 MHz, has also been completed but not yet flight tested. A third band, 20-90 MHz, is being added and will be completed during 2003. [C5705]

"Weathering the storm: developments in the acoustic sensing of wind and rain"

An Acoustic Rain Gauge (ARG) analyses the underwater sound levels across a wide frequency range, classifies the observed spectrum according to likely source and then determines the local wind speed or rain rate as appropriate. This paper covers a trial on the Scotian Shelf off Canada, comparing the geophysical information derived from the acoustic signals with those obtained from other sources. [C5706]

"A new diffraction tomography algorithm for ground penetrating radar"

A new diffraction tomography algorithm for the detection of near-surface buried objects with ground penetrating radar is derived. By allowing the transmitter and receiver to move independently improved image quality is achieved. [C5707]

"GPR-based shape reconstruction of metallic objects"

The problem of determining the shape of buried objects for multifrequency plane wave incidence in a 2D geometry is dealt with. The problem is tackled by searching for the support of the currents induced on the contour of the objects, is formulated as the inversion of the linear operator arising from the application of the Kirchhoff approximation and is solved by means of the Singular Value Decomposition approach. The presented numerical results show the effectiveness of the proposed inversion algorithm. [C5708]

"Combining GPR and EMI data for discrimination of multiple subsurface metallic objects"

Cleanup of subsurface metallic objects such as unexploded ordnance (UXO) constitutes an urgent problem

worldwide. The heart of the problem is discrimination, as opposed to detection. Ultra-wideband electromagnetic induction sensors (UWB EMI), operating from a few Hz up to 100s of kHz, have shown considerable promise in subsurface discrimination of metallic objects. Unfortunately, a great many objects, including widespread clutter items, produce very broad, smooth EMI signal patterns, over a number of decades of frequency. Shape identification is complicated by the sensitivity of EMI fields to metal type. UWB ground penetrating radar (GPR) has also shown definite discrimination capability for characterizing subsurface metallic targets. Uninfluenced by metal type, GPR is capable of registering complex natural resonances from which target length can be estimated. Further, examination of the spatial patterns of GPR signals can indicate the (X,Y,Z) locations of targets, even of multiple targets present simultaneously in the incident beam. In this paper we consider potential collaborative roles of UWB GPR and UWB EMI for discrimination of multiple subsurface metallic objects. Rigorous 3-D FDTD models demonstrate GPR's ability to estimate target positions, orientations, and length even when reflections overlap. These data can then be used to constrain inversion of UWB EMI patterns. Processing of EMI measurements based on prior estimates of object location and orientation successfully extracts distinct frequency response signatures for two very closely spaced objects. [C5709]

"Estimation of target position and velocity using data from multiple radar stations"

By using high resolution range information from multiple radar stations in monostatic or bistatic modes, the position estimates can be highly improved compared with conventional measurements from a single radar. In this paper, fundamental geometry relationships and the possible accuracy of target position and velocity estimates are analyzed when data from several radars are combined. The velocity error is proportional to the wavelength and the Doppler resolution, which is limited by the available time of measurement. The estimation error increases when the radars are close, or when the target is close to the radar level surface. For ground stations, the accuracy in estimated target altitude is usually significantly lower than the position data in the horizontal plane. Examples and simulation results are presented, displaying the performance of three radars working in bistatic and monostatic modes. The analysis is generalized to an arbitrary number of radar stations. [C5710]

"On the use of the specular direction copolarised ratio for the retrieval of soil dielectric constant"

In this paper we propose a soil dielectric constant retrieval scheme based on the use of the ratio of power densities scattered at hh and vv polarisations along the specular direction for different incidence angles and/or frequencies. The method relies on the minimum squares technique, and is based on the observation that, at variance with the backscattering case, in the specular case the small perturbation method (SPM) and the Kirchhoff approach (KA), both under the scalar approximation (SA) and under the stationary phase approximation (SPA), lead to the same expression of the copolarised ratio, that should hold under a wide range of surface roughness. We present method of moments (MoM) simulations that confirm this expectation, and we test the validity of the overall retrieval scheme. [C5711]

"A two-scale model for the ocean surface bistatic scattering"

An improvement of the two-scale model for the solution of the electromagnetic bistatic scattering from sea surface is presented. The simplest two-scale model combines the small perturbation theory with geometrical Optics. A cut-off frequency separating the two domains has to be chosen. This is a difficult task, since, except for low winds, the domains of validity of the two approximations do not overlap. We suggest to replace the small perturbation theory by the Small Slope Approximation of Voronovich. It allows the cut-off spatial frequency to be shifted so that the use of geometrical Optics is restricted to larger scales. [C5712]

"Analysis of GPR scattering by multiple subsurface metallic objects to improve UXO discrimination"

Detection and identification of buried unexploded ordnance (UXO) is an emerging problem worldwide. Recent ultra wideband (UWB) field tests between 10s of MHz and 100s of MHz have demonstrated that certain of the target's dimensions can be estimated from analysis of complex natural resonances in the scattered signal. However, the problem becomes much more complicated at highly contaminated UXO sites where clutter items, from which subsurface UXO must be distinguished, appear simultaneously within the field of view of the sensor. This often occurs in realistic field conditions, where GPR discrimination capabilities are typically limited by ground clutter, coupling between antenna and ground, and limited view of the target due to innocuous items. Under extreme shielding by clutter, the incident field cannot excite strong currents on the target and in turn the scattered field from the object cannot easily be separated from the responses of the clutter. To investigate this, we pursue simulations here designed to test subsurface side-looking EM field scattering from multiple buried objects placed in a uniform ground. The numerical calculation is performed using the finite difference time domain (FDTD) method in conjunction with generalized perfectly matched layer GPML. The results are analyzed for a cylinder and plate placed in a uniform ground. [C5713]

"Analysis and simulation of sea clutter at high range resolution and low grazing angles"

Sea clutter data provided by Thales Naval France are analyzed in order to determine their statistical and correlation properties. The K-compound distribution is found to match the best the amplitude pdf of the data. A new method is proposed for estimating the associated scale and shape parameters. Two innovative approaches are also described for simulating the sea clutter. The first one is based on the K-compound pdf model, while the second one is a 2D MA kernel based generating procedure. [C5714]

"Surface and volume scattering from natural and manmade rough surfaces in the process of setting up data base coefficients"

We propose and set out analytical formulations based on electromagnetic asymptotical methods to evaluate the power scattered by natural and man-made rough surfaces. Then we are interested in studying the evolution, according to the surface roughness and dielectric parameters, of scattering coefficients in the process to set up coefficients data base. [C5715]

"Study of the backscattering coefficient and the interferometric coherence of mangrove forests"

We propose to use a coherent model in order to compute the backscattering coefficient σ and the interferometric coherence γ of several stands of mangrove forests at P band. At this frequency, we may expect strong coherent effects reflecting the interactions between the ground and the forest scatterers. Simulation results are discussed: the different contributions are analyzed in order to quantify their impact on σ and γ . [C5716]

"Frozen soil dielectric model using unfrozen water spectroscopic parameters"

In this paper, the generalized refractive mixing dielectric model (GRMDM) introduced in was extended over freezing temperatures. Two types of unfrozen soil water, bound either by hydrophilic soil particle or ice crystal surfaces, have been identified. With this approach, the soil unfrozen water spectroscopic parameters in the microwave band were retrieved using the bentonite soil dielectric data measured at 0.6, 1.11, and 1.43 GHz, and 25°C down to -30°C. Based on these results, a dielectric model for frozen soil was proposed which allows for predicting complex dielectric constant as a function of frequency and temperature. [C5717]

"Research on parallel computation based remote sensing image processing for natural disaster monitoring and assessment"

The serious natural disasters such as flood and earthquake break out in a short time. Remote sensing such as airborne SAR can acquire the image of the disaster area quickly. But the airborne SAR remote sensing image has the property of large volume data, so the processing needs very large computer memory and strong computation ability. In this paper, based on the analysis of the SAR image processing procedure, we study the SAR image processing method using computer parallel computation technology, which is based on the parallel computer cluster operation and the large virtual computer memory sharing technology. We also introduce the application of the SAR image parallel processing system in the disaster monitor and assessment to validate the high efficiency of the system and the feasibility of our research. [C5718]

"Modeling radar backscatter from breaking waves on the surface"

A model for describing radar sea clutter is proposed. It consists of two parts, an oceanographic and an electromagnetic one. The former contains swell, small capillary and gravity waves as well as breaking wave events. The latter combines ray tracing, Bragg scattering and the Method of Moments. It is shown that the combination of the two models is capable of well reproducing several key aspects of radar sea clutter. [C5719]

"Interferometric Point Target Analysis with JERS-1 L-band SAR data"

Interferometric Point Target Analysis (IPTA) is a method that exploits the temporal and spatial characteristics of interferometric signatures collected from point targets that exhibit long-term coherence to map surface deformation. This paper demonstrates the viability of this technique for L-band data collected by the JERS-1 sensor during the time period 1992-1998. A data set covering Koga, Japan is used for demonstration and indicates regions of substantial subsidence. [C5720]

"Interferometric point target analysis for deformation mapping"

Interferometric Point Target Analysis (IPTA) is a method to exploit the temporal and spatial characteristics of interferometric signatures collected from point targets to accurately map surface deformation histories, terrain

heights, and relative atmospheric path delays. In this contribution the IPTA concept is introduced, including the point selection criteria, the phase model and the iterative improvement of the model parameters. Intermediate and final results of an IPTA example using a stack of ERS-1 and ERS-2 data, confirm the validity of the concept and indicate a high accuracy of the resulting products. [C5721]

"Perturbation caused by cloud in ERS SAR interferogram"

In repeat-pass SAR interferometry, errors by the tropospheric radar phase delay has been pointed out. We analyze ERS SAR data pairs covering the Kanto Plains, which is a region including Tokyo, Japan. Fringe features that are independent from actual deformations are found from generated interferograms. The fringe patterns are depends on the data; same feature appears on the interferograms generated from the same data. One of the significant patterns is detected in the interferograms from data obtained in August 1999, all of the interferograms by this data contain same fringe feature. A SPOT HRV image acquired 18 minutes after the SAR data reveals patterns of cloud distribution that are similar to the fringe features in the interferograms. It shows a possibility for cloud-induced perturbations in radar signals. Optical sensor imagery with a spatial resolution equivalent to that of the SAR imagery is useful for the evaluation of interferometric fringes. [C5722]

"Multi-temporal repeat-pass interferometry for an improved analysis of Arctic glaciers"

This paper describes a new technique to separate topography- and displacement-related phase components in SAR interferograms of Arctic glaciers. Compared to standard 4-pass-interferometry, a combination of several interferograms in a least-squares adjustment on the basis of a extended glacier flow model is proposed. The method enables to detect areas with significant changes of glacier flow velocity, supports a detailed accuracy analysis, and allows the estimation of the influence of systematic errors. The paper includes a description of the model, accuracy analysis and an error budget. [C5723]

"Calibration of interferometric airborne SAR images using a multisquint processing approach"

This paper presents a technique to calibrate interferometric airborne SAR images based on a multisquint processing approach, i.e., by processing the same image pairs with different squint angles we can combine the interferograms to obtain the desired phase correction. Airborne single-pass interferometric data from the DLR's E-SAR is used to validate the method. [C5724]

"Options for high-precision motion compensation for airborne differential SAR interferometry"

Differential interferometry using space-borne SAR sensors has become an established technique for detecting and monitoring centimetre-scale deformations of the Earth's surface, as well as glacier flows and land slides. Although often very efficient, the use of space-borne SAR data has several drawbacks, namely phase artifacts caused by atmospheric effects and very low coherence due to long data acquisition intervals. Airborne sensors on the other hand may overcome most of the problems mentioned above and provide a much higher flexibility in sense of spatial resolution, used wavelength and data acquisition. However, the use of airborne sensors has been prevented by insufficiently accurate motion compensation of the sensor platform. In this paper, the performance and deficiencies of the different approaches for estimation of residual motion errors are compared and evaluated, in the face of their application in airborne differential SAR interferometry. Some preliminary results of airborne differential SAR interferometry, obtained using an optimised motion compensation scheme, will also be shown. The analysis carried out in this paper is based on repeat-pass interferometric data acquired by DLR's experimental SAR system (E-SAR) in L-band. [C5725]

"Experiences with SRTM/X-SAR phase unwrapping using the minimum cost flow method"

With the Shuttle Radar Topography Mission (SRTM) flown in February 2000, the most comprehensive interferometric SAR data of the Earth's land mass so far were acquired. At the German Aerospace Center the X-SAR data are processed to a precise and homogeneous Digital Elevation Model (DEM). One of the most critical processing steps is phase unwrapping (PU). We are using an implementation of the Minimum Cost Flow (MCF) algorithm. Now that a total of 16,000 interferograms between $\pm 60^\circ$ latitude have been processed, this offers the unique opportunity to study the behavior of the MCF algorithm using a very large data pool. In this paper we report on the practical experiences with MCF gained during operational SRTM/X-SAR data processing. We present the results of a throughput analysis. Further, the problems experienced with MCF PU of the X-SAR data are discussed. It is shown how specific adoptions of the MCF cost functions can help to overcome them. The paper also presents the methods of PU quality assessment used in our operational processing. [C5726]

"LaRA-2002: results of the airborne laser and radar altimeter campaign over Greenland, Svalbard, and Arctic sea ice"

The primary objectives of LaRA-2002 were to assemble measurements of land and sea ice with simultaneous observations from a low-altitude aircraft by laser and radar altimeters. Data from the mission was expected to illustrate similarities and differences between these two very different means of measuring surface height. These objectives were met. This paper provides an overview of the project, and includes highlights of the results.

[C5727]

"Investigation of overlap correction techniques for the Micro-Pulse Lidar NETWORK (MPLNET)"

The Micro-Pulse Lidar NETWORK (MPLNET) uses elastic-scattering lidars stationed at sites around the globe to produce aerosol and cloud vertical profiles on a continuous year-round basis. Processing of MPLNET data requires a correction for the lidar overlap function in the 0-6 km range, to take into account the loss in near-field receiver efficiency. This correction is normally determined from recording horizontal profiles that require a 10 km clear line-of-sight and homogeneous atmospheric conditions, limiting the practicality in which successful corrections can be obtained. An alternative overlap correction method using a secondary receiver is considered that eliminates the need for horizontal measurements. A review of both methods is presented, including a discussion of signal uncertainties. [C5728]

"Estimation of aerosol concentration from elastic scattering LIDAR data"

West Desert Test Center (WDTC) at Dugway Proving Ground uses measurement, modeling and simulation capabilities to characterize and referee customer standoff biological and, to a lesser extent, chemical detection systems. The WDTC LIDAR model of aerosol clouds uses a Mie scattering model and associated joint aerosol cloud distribution function $N(a,r)$, where a is the particle radius and r is the position vector of the particle. We make the key simplifying assumption that the two parameters a and r are statistically independent. Justification for this well-mixed assumption is that aerosol particles with dimensions of less than a few microns remain in the atmosphere for a long time, typically days. Large particles are removed by gravity segregation. For the associated inverse problem, the LIDAR elastic scattering equation is formally inverted to yield an estimate of the aerosol particle concentration $\rho(r)$. Inversion requires knowledge of boundary conditions along an arc of constant range $R=R_f$. Given a seed value on the arc from a point detector, a two-frequency algorithm is shown to correctly populate all values on the arc $R=R_f$, leading to near-real-time accurate inversions over the entire LIDAR sweep. Numerical results in a noise background and a representative choice of numerical parameters are given. [C5729]

"The vector digital TV filtering and phase unwrapping"

In this paper, we analyzed the relation between "noises" and interferometric synthetic aperture radar (SAR) phase unwrapping, and applied novel digital TV filtering methods to the interferograms. The filtering algorithm has less computation load than iteration anisotropic diffusion filtering and provides reliable accuracy for our phase unwrapping. The numerical results proved phase fringes protected and residues largely reduced, which lay the foundation for efficient branch-cut phase unwrapping. [C5730]

"Phase unwrapping based on active contour model"

A new phase unwrapping method based on active contour model is presented in this paper. Active contour model offers a general frame for the edge feature extraction. It defines an initial contour by some high level information, and then deforms it towards the desired feature. Then contour map is obtained, on which the fringe lines are continuous and closed. Actually the interferogram is divided into some blocks by the fringe lines and the border of the image. Finally, we do phase unwrapping for the whole image block by block. The advantages of our method are its robust to image noise and easy contour initialization. Experiment on the real data and the comparison with one traditional method demonstrate the efficiency and robust of our method. [C5731]

"Derivation of soil surface properties from airborne laser altimetry"

A technique is presented and tested which enables land surface roughness on the vertical scale of a few centimetres to be estimated from an aircraft-mounted scanning laser altimeter, or LiDAR (Light Direction And Ranging) system. While the systematic uncertainty in measuring land elevation using a LiDAR system is around 20 cm, we demonstrate that sequential laser pulse returns are highly correlated in height, and after detrending to remove the effects of topographic slope, show variation that can enable different physical soil treatments to be distinguished. Test sites were created on Sonning Farm in Reading, UK, with treatments including rolling flat, ploughing and potato-ridging. The standard deviation of detrended returns from 26 LiDAR acquisitions show a

clear variation between the different treatments which would enable surface roughness to be estimated without fieldwork. This provides a useful variable to models of overland water flow which will strongly influence sediment erosion, transport and deposition and flood extent. [C5732]

"Phase statistics and quality evaluation of deformation maps with multiple-image differential interferometry"

This paper presents a closed formulation to evaluate the quality of terrain deformation maps obtained with multi-image differential interferometry. The analytical formulation, based on the application of the asymptotic covariance matrix, that propagates the interferogram coherences to the linear deformation and DEM error accuracies when using a stack of interferograms, is developed and validated with real data from the ERS satellites. [C5733]

"The MANTISSA project: first results from the Italian field experiments"

An innovative method of estimating rainfall via the attenuation it causes to a ground-based microwave link is described. First results from field experiments carried out in Italy are also presented. [C5734]

"High resolution FM-CW SAR performance analysis"

The combination of compact FM-CW technology and high resolution SAR techniques seems of special interest for the implementation of a low cost, airborne imaging radar. A project has been started to investigate the feasibility of FM-CW SAR. A system simulation is in development to estimate the performance of FM-CW SAR. The performance is probably limited by phase noise. Therefore, a study has been made of the effects of phase noise and a time domain description of phase noise has been developed. [C5735]

"Data-linking for integration of remote sensing and in-situ measurements for airborne atmospheric experiments"

This paper describes recent work using data communications links to integrate ground-based remote sensing and in-situ aircraft measurements during a number of atmospheric research experiments conducted by the Meteorological Service of Canada (MSC) in collaboration with the National Research Council (NRC) using its Convair 580 aircraft. These systems have been deployed to provide real-time or near real-time information between aircraft and ground-based sensors and information sources to help coordinate and integrate measurements as well as to provide decision-making information to optimize aircraft and ground-based sensor deployment. These include the use of a wide-area satellite telephone and line-of-sight VHP/UHF data-links for both general-purpose and specialized applications. Both technologies provide a data communications capability with various pros and cons, which can be exploited as required for different applications. This approach can be used in real-time to coordinate and position remote sensing instruments, which is invaluable for inter-comparisons between aircraft in-situ and ground-based remote sensing measurements particularly for radar observations. [C5736]

"HF ocean radar observation of surface currents induced by a typhoon in the East China Sea"

A long-range (200 km) high-frequency (HF) ocean radar system was developed by Japan's Communications Research Laboratory (CRL) to monitor the Kuroshio upstream region of the East China Sea. Sea surface observation began in July 2001. In this paper, we present the validation results of surface currents obtained by the radar in comparison with currents measured using a moored current meter. We also present the results of observing temporal variations in the Kuroshio over a year and the surface currents induced by a strong typhoon. [C5737]

"Short-time observation of coastal currents with DBF radar"

We have developed a DBF (Digital Beam Forming) radar which can complete one round observation of surface current every 15 minutes by a digital beam forming system. The predominant frequency is 41.9 MHz, range-directional resolution 500 m, maximum reach 25 km, azimuthal resolution 13-17° and velocity resolution 2.13 cm/s. We applied the DBF radar for current observation in the northern area of Ise Bay and compared the data with those collected synchronously by current meters set at 1 m and 2 m depth at two stationary points for eight days. The correlation coefficient between the DBF radar and the current meter at 1 m depth was 0.7-0.8 and the standard error 5-10 cm/s. In view of the fact that the measurement depth for the DBF radar was about 30 cm they seem to be coincided well. Next, we assimilated the continuous observation data of the DBF radar into a quasi three dimensional model of coastal currents by the nudging method in order to infer spatial and temporal changes of the currents. When the inferences of three-dimensional current were compared with the data gained

by concurrently implemented ADCP spot observation at 4 measurement points, the current distribution for the surface-to-3 m depth layer was improved well as to speed and direction. [C5738]

"Geometries for streamflow measurement using a UHF RiverSonde"

Three geometries for a UHF streamflow radar system are examined: bistatic across the channel, monostatic on a bank, and monostatic in the center of the channel. The radar operates by analyzing the frequency spectrum of the received energy and determining the angles of arrival of energy at each frequency, so it is important to understand how the various geometries affect the width of the frequency spectrum and its angular distribution. We argue that placing the radar and antenna on one bank, with the antennas looking broadly across the river, generally produces the best results. The broad frequency spectrum allows many points to be analyzed, most of which have single-angle direction solutions (which generally are more robust than dual-angle solutions), and all the equipment can be placed at a single location. [C5739]

"A Doppler knife-beam radar altimeter concept for novel sea state parameters"

This paper extends our theoretical and experimental researches on microwave backscattering at small incidence angles as applied to remote sensing of the ocean. A new concept of a Doppler radar with a knife-beam antenna pattern is proposed. With a nadir-pointing rotating antenna the radar will be able to measure a number of key sea state parameters previously unavailable, such as the long wave slope, the direction of wave propagation. Preliminary theoretical analysis and numerical simulations predict that in a space-borne scenario, signals may be isolated for scattering cells of the order 14x14 km over a swath approximately 250 km wide. [C5740]

"EBiRa: Experimental Bistatic Radar for air surveillance"

This paper describes the concept and reports the status of the FGAN Experimental Bistatic Radar (EBiRa). The main field of this bistatic radar investigation is air surveillance operation with host off ground-based cooperative illuminators. Also possible is the use of noncooperative illuminators like FM radio stations, TV stations, or monostatic radars which are located in the observation area. The receiver and transmitter are build up with commercial-off-the-shelf components to reduce cost and shorten the development time. New digital signal generation and processing technologies came into operation for both units. [C5741]

"Assessment of local topographic maps obtained by ground-based SAR interferometry"

A procedure to derive a digital elevation model (DEM) over a region spanning a few square kilometres by means of a ground-based interferometric synthetic aperture radar (GB-InSAR) is described. The results obtained at a test-site near the village of Sauze d'Oulx, Italy, are presented. The comparison with an existing DEM shows the good accuracy of the proposed DEM retrieval technique. [C5742]

"The study of the parameters to interferometric SAR height-measurement and velocity-measurement precision in the Cluster Micro-Satellite system"

The Cluster Micro-Satellite synthetic aperture radar system is an innovative SAR system brought forward recently. CT-InSAR and AT-InSAR is the principal working models in this system. This paper researches chiefly the influence of the difference of all kinds of parameters in the system to the height precision of CT-InSAR and analyzes the measurement precision requirement of all sorts of data in the swath. And we analyze the requirement of the velocity measurement precision to the baseline precision. The simulation result enunciates that the requirement of baseline precision of CT-InSAR is much more precise than that of AT-InSAR. [C5743]

"Ultra-wideband MMICs for remote sensing applications"

This paper presents an overview of the current activity at the Technical University of Denmark in the field of ultra-wideband monolithic microwave integrated circuits (MMICs) for next-generation high-resolution synthetic aperture radar (SAR) systems. The transfer function requirements for MMIC components in a wideband SAR systems are described. The design and performance of a DC-to-X-band SiGe HBT quadrature mixer and a C-band GaAs pHEMT downconverter are described. Experimental results demonstrates the usefulness of the designs for quadrature modulation/ demodulation and downconversion of ultra-wideband linear FM-modulated signals. [C5744]

"A ground based remote sensing radar technique for dynamic testing of large structures"

In this paper, the authors describe an innovative survey radar technique, based on microwave holographic images, for dynamic testing of large structures providing both vibration amplitude pattern and frequency.

Theoretical background is provided and experimental results obtained during a dynamic test on a concrete and masonry building are reported. [C5745]

"A bandwidth extrapolation technique of polarimetric radar data and a recursive method of polarimetric linear prediction coefficient estimation"

Resolution of a radar is limited in range by its bandwidth. One of the various super-resolution techniques for improving its resolution is bandwidth extrapolation (BWE). In the technique, a linear prediction model is fitted to the data, and the model is used to extrapolate the bandwidth. In this paper, the concept of BWE is extended, and a new algorithm called polarimetric bandwidth extrapolation (PBWE) applicable to polarimetric radar data is proposed. It is shown through numerical simulations that utilization of full polarization information allows PBWE to improve the resolution beyond the conventional BWE method. Some results of physical simulation experiment using a W-band polarimetric FMCW radar and corner reflectors are shown to confirm the advantage of PBWE. [C5746]

"Joint distributions for correlated radar images"

First Page of the Article [C5747]

"Adaptive spectral estimation for multibaseline SAR tomography with airborne L-band data"

First Page of the Article [C5748]

"Texture classification approach using conditional local variance model"

First Page of the Article [C5749]

"High resolution multi-spectral analysis of urban areas with quickbird imagery and synergy with ERS data"

First Page of the Article [C5750]

"Target detection and analysis based on spectral analysis of a SAR image: a simulation approach"

First Page of the Article [C5751]

"Aggregating the statistical estimation and variational analysis methods in radar imagery"

First Page of the Article [C5752]

"Measurement of sea level by L-band SAR"

First Page of the Article [C5753]

"Estimate of net primary production of aquatic vegetation of the amazon floodplain using SAR satellite data"

First Page of the Article [C5754]

"Impact of new technologies on future space-borne radar design"

First Page of the Article [C5755]

"Conceptual studies for exploiting the TerraSAR-X dual receive antenna"

First Page of the Article [C5756]

"Microstrip permanent scatterers for SAR interferometry applications"

First Page of the Article [C5757]

"Physical analysis of atmospheric delay signal observed in stacked radar interferometric data"

First Page of the Article [C5758]

"Tidal flat DEM generation by satellite remote sensing"

First Page of the Article [\[C5759\]](#)

"Challenges and proposed solutions for validation of spaceborne rain rate estimates"

First Page of the Article [\[C5760\]](#)

"Observations and modelling of the response of along-track SAR interferometry to mesoscale ocean features"

First Page of the Article [\[C5761\]](#)

"Regrowth biomass estimation in the amazon using JERS-1/RADARSAT SAR composites"

First Page of the Article [\[C5762\]](#)

"Combined land-cover classification and stem volume estimation using multitemporal ERS tandem INSAR data"

First Page of the Article [\[C5763\]](#)

"Investigation of ocean wave groups using radar-image sequences"

First Page of the Article [\[C5764\]](#)

"A new wind sea /swell classification method for complex ENVISAT ASAR wave mode data"

First Page of the Article [\[C5765\]](#)

"Mediterranean sea wind and wave characteristics from satellite, buoy and numerical model data"

First Page of the Article [\[C5766\]](#)

"The potential of ALOS single polarization INSAR for estimation of growing stock volume in Boreal forest"

First Page of the Article [\[C5767\]](#)

"Dual-frequency rain profiling method without the use of surface reference technique"

First Page of the Article [\[C5768\]](#)

"Utilization of range profile data of surface echo from TRMM/PR"

First Page of the Article [\[C5769\]](#)

"Evaluation of TRMM PR attenuation by radar mirror image"

First Page of the Article [\[C5770\]](#)

"Height-biomass allometry in temperate forests performance accuracy of height-biomass allometry"

First Page of the Article [\[C5771\]](#)

"Potential of polarimetric SAR interferometry for forest carbon accounting"

First Page of the Article [\[C5772\]](#)

"Ground validation during EGPM: possible concepts for an Italian distributed site"

First Page of the Article [\[C5773\]](#)

"Puerto Rico deployable radar network design; site survey"

The Microwave Remote Sensing Laboratory (MIRSL) at the University of Massachusetts and the Cloud Microwave Measurements of Atmospheric Events (CLiMMATE) Laboratory at the University of Puerto Rico at Mayaguez are collaborating to modify a MK2 marine radar donated by Raytheon for use as meteorological radar nodes in a proposed weather radar network. This will be the first network to measure lower atmospheric phenomena in Puerto Rico. The radar consists of an antenna, a rotator, and a transceiver that will be placed at top of a tower or building, along with a data processing system. This paper derives two important equations describing the curved earth effect on beam propagation for radar range calculation. It also describes the method used to survey the MIRSL Tilton Farm field site, and the eleven campuses of the University of Puerto Rico backbone and justifies their fixed offset antennas' elevation angle and location. [C5774]

"Polarimetric properties of chaff"

The paper presents the scattering models of chaff that capture the essential polarimetric properties as well as some data to support the properties. Two simple scattering models are used to compute polarimetric variables. The models are Herizian dipole and thin wire antenna. The result shows that two models produce very similar results if the chaff length is half the radar wavelength or less. [C5775]

"Research on information system for natural disaster monitoring and assessment"

The serious natural disasters such as flood and earthquake result in great loss to human every year. It is of great significance to monitor and assess the situation of a disaster with information system based on GPS, RS, GIS and so on. In this article the construction of information system for serious natural disaster monitoring and assessment is studied, which uses the dynamic GPS, Airborne SAR, GIS, parallel computation remote sensing image processing technology and so on. The whole system can be divided into two parts, i.e. the air part and the ground part. The prominent advantage of the system is its approximate real time processing of the disaster situation information. We introduce the elements of the two parts and their function in the system in detail. And the key technology to implement the quick image processing is also introduced in detail. At last the application efficiency is introduced. [C5776]

"NEXRAD data quality by spectral processing. Spectral processing on NCAR's S-Pol radar"

The WSR-88D radar system (NEXRAD) is developing a phase coded pulsing scheme using spectral processing that will improve data quality by removing overlaid echo contamination. A prototype spectral processor has been implemented on NCAR's S-Pol research radar for validation testing. Spectral processing will simultaneously enhance the anomalous propagation clutter mitigation technique, which uses a fuzzy logic based radar echo classifier, and allow future data quality enhancements. [C5777]

"Investigations in radar rainfall estimation using neural networks"

Rainfall on the ground is dependent on the four dimensional distribution of precipitation aloft. In principle one can obtain a functional relation between the rain rate on the ground and the four-dimensional radar observations aloft. However it is difficult to express this in a useful form. Neural networks provide a mechanism to solve this complex problem. Using ground measurements of rain rate as the target output neural networks have been developed in the past that use the radar measurements as input and produce rainfall rates on the ground. Several topics related to neural network based radar rainfall estimates are addressed in this paper. This paper investigates the input vector types and sizes that are useful in a radar rainfall estimation context. Similarly, the neural network is trained with an initial data set, but updated adaptively. Various updating mechanisms are investigated with respect to accuracy of rainfall estimation. Two years of data from the Weather Surveillance Radar-1988 Doppler (WSR-88D) radar and a network of gages from Melbourne, Florida are used to evaluate the topics listed here. [C5778]

"Effective shape of raindrops. Polarimetric radar perspective"

In this study, polarimetric radar measurements are used for estimating mean shape of raindrops for several rain events. A linear dependence of the axis ratio on equivolume raindrop diameter is assumed, and the slope β of such dependence is obtained from the measurements of reflectivity factor Z , differential reflectivity ZDR , and specific differential phase KDP . Within-the-storm and between-the-storm variations of the parameter β are the primary focus of this investigation. [C5779]

"A degree estimation model of earthquake damage using temporal coherence ratio"

A degree of earthquake damage can be estimated using temporal decorrelation by employing a coherence ratio which is defined by dividing a post-event coherence image by a pre-event image. In the case of applying both C

and L bands SAR data for evaluating the damage of the 1995 Hyogoken-Nanbu Earthquake in Japan, the probability of the degree of damage could be approximated by a linear function of the coherence ratio. In this paper, we examine whether the post-earthquake damage estimation model is applicable for the 1999 Kocaeli earthquake in Turkey as another case. As a result, significant correlation between the probability of the degree of damage and the grade of damage surveyed by disaster researchers is also clarified by employing the coherence ratio computed from three ERS- 1/2 SAR data set including the event. [C5780]

"MINERVA: an INSAR monitoring system for volcanic hazard"

MINERVA (Monitoring by Interferometric SAR of Environmental Risk in Volcanic Areas) is a small scale service demonstration project financed by ESA in the Data User Programme framework. The objective of the project is the design, development and assessment of a demonstrative information service based on the interferometric processing of images from the ASAR instruments on board ERS1/2 and ENVISAT-I. The system is based on a new approach for the processing of INSAR data, which allows to optimize the quality of interferograms spanning from 35 days up to several years, and to merge them to generate a single solution describing the temporal evolution of the ground deformations in the examined risk area. The system allows to update this solution each time a new SAR image is available, and constitutes therefore an innovative tool for monitoring of the ground displacements in risk areas. [C5781]

"Monitoring of the forests state in the Chernobyl area using remote sensing data"

The study of the area of Chernobyl nuclear power plant (NPP) using spaceborne SAR and optical data is devoted to the monitoring of the forests state in the surrounding area. The use of a SIR-C/X datatake from SRL-2 flight and series of ERS SAR data for the year interval 1992-1997, obtained at different meteorological conditions and in different seasons of the year, JERS-1 along with optical data were discovered to be very helpful for the classification of vegetation types, study of the forests state after the nuclear accident in the area. Various products derived from remote sensing data allowed to detect forest fire areas and to make conclusion about domination of damage from fires occurred significantly later the accident. [C5782]

"On the use of ERS INSAR data in the ecological monitoring of the Baikal region"

The goal of our paper is a study of the potential of ERS SAR for the ecological monitoring of the Baikal lake region, the area of global importance as economical area and natural environmental reserve. The Ust-Barguzin test site is characterized by a very complicated topography average slopes of 15°-25° and appears to be severe examination for modern phase unwrapping techniques, as the area rich with layovers/foreshortenings on the SAR images. In our research we used a set of ERS SAR data obtained during tandem mission in 1997-1998. The coherence maps and DEM of the area of study were generated. A use of especially developed phase unwrapping technique allowed to generate DEM of the area from a pair of tandem scenes. An intensity images were combined into multitemporal images. Study of the multitemporal images, coherence and DEM maps allowed us to make classification of the forested/deforested areas, the areas with various soils type and moisture. The results of DINSAR processing of the ERS data for the study area with high seismic activity are discussed also. The data collected during field trip in the beginning of September 2000 are compared with results of ERS data analysis. [C5783]

"Analysis of two dimensional sea surface elevation fields using spaceborne SAR"

Space borne synthetic aperture radar are able to provide high resolution measurements of ocean waves on a global scale. The present study uses a reprocessed data set of complex SAR images acquired by the European Remote Sensing satellite ERS-2 to estimate different wave parameters relevant for ship security. In addition, a new method is presented to derive two dimensional sea surface elevation fields from complex SAR data. The method permits to analyze wave fields in more detail than conventional SAR wave measurement techniques, which only estimate the wave spectrum. The technique provides parameters like maximum to significant wave height ratios, wave steepness, or the probability of wave breaking. Global maps and statistics of the new parameters are presented. [C5784]

"SLAM, the development of an EO service to support the legal obligations of Swiss and Italian Geological Risk Services in landslide risk forecasting and prevention"

The necessity to identify and monitor slope movement is of paramount importance to reduce the socio-economic toll that every year is paid in developing as well as in developed countries. From the late 80's Italian and Swiss legislations regarding hydro-geological risks, have identified landslide hazard maps as essential tools to mitigate the risk associated to landslides. Several projects funded by the European Space Agency within the framework of its Data User Program (DUP), have investigated the feasibility and the operational applicability of spaceborne

imagery to respond to the needs of governmental institutions that have a mandate in landslide analysis and prevention. Techniques based on SAR interferometry and on the combination of state of the art Remote Sensing observations with CIS modeling have been analysed in order to assess the contribution of Satellite Remote Sensing information in support to the practices of the Geological Risk Services Agencies. [C5785]

"Landslide identification by SAR interferometry: the Sarno case"

This paper reports on the results of the application of SAR interferometry to the study of a landslide disaster which happened in the Sarno area (Italy) in 1998. A DEM generated by means of an ERS-1/2 tandem pair has been compared with a topographic one allowing the identification of the areas mostly affected by the landslide. [C5786]

"Estimating multiyear sea-ice concentration using passive microwave data and MLP neural networks"

Three ice-type classification methods utilizing SSM/I passive microwave data were compared. Each applied a multilayer perceptron (MLP) neural network (NN) with OKEAN (radar and passive microwave) sea-ice learning data, a different learning algorithm based on, respectively, error back propagation and simulated annealing (M1), dynamic learning and polynomial basis functions (M2), and dynamic learning with two-step optimization (M3). M2 and M3 methods used the Kalman filtering technique. Our studies demonstrated, that for sea-ice inversions the modified MLP NN with M1 algorithm was more efficient because M2 and M3 algorithms caused overfitting. Multiyear (MY) sea-ice concentration maps were generated from SSM/I Tbs (19 GHz V, 19 GHz H and 37 GHz V channels) using modified MLP NN with M1 algorithm, OKEAN and ERS learning data. These maps were compared with respective MY sea-ice concentration maps developed using NASA Team algorithm (NTA). Our studies demonstrated the superiority of the NN method compared to the NTA. [C5787]

"On the potential of multi-polarization and multi-temporal C-band SAR data in classifying crops"

We report on an investigation aimed at evaluating the performance of a neural-network based crop classification technique, which makes use of multi-polarization and/or multi-temporal back-scattering coefficients measured at C-band. [C5788]

"Impact of interception on the thematic analyses of SAR data in agricultural areas"

The objective of this study is to analyse and interpret the impact of intercepted rainfall on the thematic analyses of SAR data acquired in agricultural areas. The investigations were carried out using airborne E-SAR data at X-, C- and L-band. Furthermore, TerraSAR simulated data were analysed with respect to future spaceborne missions. The strongest effect of plant surface wetness on crop recognition was found at C-band. Single classes showed changes in user's or producer's accuracy up to 30%. For classifications based on X-and L-band data- the future TerraSAR configuration-better classification results were achieved when free vegetation water was present. Thus, the matutinal overflight time of TerraSAR over Germany can be considered as an advantage for crop mapping issues. [C5789]

"Field studies on the action of rain on the radar backscattering from wind-roughened water surfaces"

In order to gain further insight into the radar backscattering from rain-and wind-roughened water surfaces, we performed field experiments at the mouth of the river Elbe in the German Bight. The backscattered radar power from the water surface was measured at different wind speeds, wind directions, and rain rates, as well as at different radar frequencies, polarizations, and incidence angles. Our results show that the dominant scattering mechanism at VV-polarization is Bragg scattering which shows a strong dependence on the Bragg wavelength. The enhancement and reduction of the surface roughness by splash products and sub-surface phenomena, respectively, result in a transition wavenumber between enhancement of the radar backscattering (due to additional surface roughness) and its reduction (due to wave damping) of about 100 rad/m. We hypothesize that this transition wavenumber depends on the drop-size distribution of the rain. Taking into consideration the different dependencies on rain rate of the radar backscatter at different frequencies and polarizations, we suggest a method to estimate rain rates by calculating the ratio of the radar cross-sections at L band, VV-polarization and at C band, HV-polarization. Provided an availability of synthetic aperture radar (SAR) data at the respective frequency/polarization combinations, this method will allow for investigating the nature of small-scale (convective) rain events over the ocean by analyzing multi-frequency/multi-polarization SAR images. [C5790]

"Techniques for reducing SAR antenna size"

First Page of the Article [C5791]

"Instrument concept of NEXRAD in space (NIS)-a geostationary radar for hurricane studies"

First Page of the Article [C5792]

"Aerosol Arctic Campaign at ALOMAR (69N, 16E, Norway) in June-July 2002"

The GOA Aerosol Arctic Campaign 2002 was carried out during the months of June and July at ALOMAR (Arctic Lidar Observatory for Middle Atmosphere Research). Aerosol measurements at this latitude are scarce, so the aim of this campaign is the characterization of the Arctic aerosols. Two instruments, the Cimel photometer at the AERONET network and the EPP-3000 spectrometer, are used for the measurements. This work is focuses on the Cimel data. These data show a low aerosol optical thickness (AOT), with an average value of 0.135 at 440 nm. The AOT decreases strongly with wavelength, so the Engström parameter $\alpha(440,670,870)$ presents high values, with an average of 1.61 for a log-log fit at these three wavelengths. [C5793]

"Propagation within boundary layers over sea at millimeterwaves and infrared wavelengths"

Air-sea interaction processes in the marine boundary layer have a severe impact on the performance of infrared and radar sensors. Multispectral mm-wave/IR-sensors may exhibit complementary performance thus leading to a combined optimum performance. Propagation models have to be tested in order to cope with the varying environment and allow a performance prediction for sensors in different bands of the electromagnetic spectrum. To validate existing propagation models like TERPEM for radar and IRBLEM for IR performance and to compare IR and mm-wave propagation over the sea under various atmospheric conditions, joint experiments were conducted over transmission ranges well beyond the horizon, assisted by a careful environmental characterization. The paper describes the experimental approach and gives representative results for measurement and simulation. [C5794]

"Use of ERS/SAR measurements for soil geometric and aerodynamic roughness estimation in semi-arid and arid areas"

This paper discusses the potential of radar signal to characterise the bare surface roughness in arid or semi-arid regions. The used microwave sensor is the SAR of ERS. Ground truth measurements were acquired over different arid sites in the South of Tunisia. An empirical approach is proposed to derive the surface roughness from SAR measurements. The relationships with two different kinds of roughness have been studied: the geometric roughness, which is characterised by a rather new parameter called Zs, and the classical aerodynamic roughness Z0. [C5795]

"Lidar measurements of tropospheric ozone over Reunion Island: influence of the synoptic situations"

A tropospheric ozone lidar located at Reunion Island has provided an opportunity to investigate the daily vertical ozone distribution in the latter part of biomass burning season, during November-December 1999. The comparison with austral winter 1998 daily ozone profiles show that each daily ozone profile is very stratified with ozone enhancements ([C5796]

"Development of a multiple adjustment processor for generation of DEMs over large areas using SAR data"

During the last years orbital SAR data have been acquired for almost every place in the world. This fact can be used for generating large digital elevation models (DEM) of remote areas using SAR interferometry (InSAR). Nevertheless, the generation of large quality DEMs using this technique presents several problems, such as temporal decorrelation (even with a one-day temporal gap between acquisitions), baseline errors or SAR parameters calibration. These factors can dramatically degrade the quality of the final DEM and, therefore, advanced InSAR techniques are needed to minimize or compensate for these errors. In this paper the Institut Cartogràfic de Catalunya (ICC) presents a robust method for generating very large, high quality DEMs using a set of SAR interferograms. The method is based on a simultaneous multiple adjustment of critical parameters for the SAR images using three types of phase-registered points: control points, known-height and corresponding points. Results for the area of Tierra del Fuego (Argentina) are also presented. [C5797]

"Two polarization radar imagery of sea surface: the dependence on atmospheric stability"

It is shown that the two polarizations of microwave radar signal at low grazing angles sense different scatterers:

horizontally polarized signal scatters predominantly from steep waves, while vertically polarized one scatters primarily from free Bragg waves. Ocean radar images being sensitive to surface wind fluctuations may be treated as an indicator of atmospheric boundary layer conditions. Radar images of surface imprints of atmospheric patterns near a coastal mountain ridge are considered. In this case the stratification of atmospheric boundary layer near sea surface plays the major role in the formation of lee structures downwind the ridge. [C5798]

"Interferometric coherence for change detection in the Nasca region of Peru"

The Nasca Lines in Southern Peru are important for their archaeological and cultural significance as well their impact on local economies as a famous tourist landmark. Recent anecdotal evidence implies that a combination of enhanced El Nino conditions and increased anthropogenic degradation are leading to the gradual erosion of the surface upon which the lines and geoglyphs are etched. A combination of barren desert, wide expanse and centimetre scale impacts makes effective mapping of such a large area very difficult. In this study it is shown that interferometric coherence using ERS data between 1997 and 1999 is sensitive to the small scale degradation across the Nasca pampa. As such it provides a potential tool for long term mapping and quantification of the degradation. [C5799]

"GPR for archaeological investigations: real performance assessment for different surface and subsurface conditions"

This paper assesses GPR (Ground Penetrating Radar) performance for archaeological investigations. We exploit extensive data acquisition campaigns to characterize the instrument behavior in different operative conditions and we select ad hoc processing techniques to optimally extract target signatures from the collected data. The extensive analysis demonstrates the real effectiveness of GPR surveys in archaeological investigations. [C5800]

"Polar radar for ice sheet measurements"

First Page of the Article [C5801]

"Relating micro ave backscatter azimuth modulation to surface properties of the greenland ice sheet"

First Page of the Article [C5802]

"Quantifying the biomass of australian subtropical woodlands using SAR inversion models"

First Page of the Article [C5803]

"Comparison between SAR and wind scatterometers data for surface parameters monitoring over a sahelian agropastoral area"

First Page of the Article [C5804]

"Greenland ice sheet elevation change from 1992 to 1999 derived from ERS-1 and ERS-2 satellite altimeter measurements"

First Page of the Article [C5805]

"Increasing temporal resolution in greenland ablation estimation using passive and active microwave data"

First Page of the Article [C5806]

"The GBFM radar mosaic of the Eurasian Taiga: a groundwork for the bio-physical characterization of an ecosystem with relevance to global change studies"

First Page of the Article [C5807]

"Model based PolSAR and PolInSAR speckle noise reduction"

First Page of the Article [C5808]

"Estimating vegetation bias in polarimetric SAR interferometry"

First Page of the Article [C5809]

"The dependence of polarimetric coherence on surface roughness for very rough surfaces"

First Page of the Article [C5810]

"On the retrieval of forest biomass from SAR data by neural networks"

First Page of the Article [C5811]

"Individual tree detection using CARABAS-II"

First Page of the Article [C5812]

"Characteristics of radar reflectivity of rain forests measured by space-borne Ku-band radar"

First Page of the Article [C5813]

"Preliminary ASTER and INSAR imagery combination for mud volcano dynamics, Azerbaijan"

First Page of the Article [C5814]

"Adaptive algorithms for the fully-automated retrieval of cloud and aerosol extinction profiles from CALIPSO lidar data"

First Page of the Article [C5815]

"Retrieval of cloud emissivity and particle size frame of the CALIPSO mission"

First Page of the Article [C5816]

"Synergies of CALIOP with aqua-train instruments"

First Page of the Article [C5817]

"SIBERIA-II: sensor systems and data products for greenhouse gas accounting"

First Page of the Article [C5818]

"Combining microwave radiometer and wind profiler radar measurements to improve accuracy and resolution of atmospheric humidity profiling"

First Page of the Article [C5819]

"Cloud-Aerosol Lidar with Orthogonal Polarization (CALIOPe)"

First Page of the Article [C5820]

"Selection algorithm for the CALIPSO lidar aerosol extinction-to-backscatter ratio"

First Page of the Article [C5821]

"The two emergencies of "El Salvador" in the frame of the international charter "space and major disasters""

First Page of the Article [C5822]

"Subsidence monitoring over oil fields with L-band SAR interferometry"

First Page of the Article [C5823]

"Surface statistics of the saharan ergs observed in the $\gamma\theta$ azimuth modulation"

First Page of the Article [C5824]

"LITE aerosol retrievals at 1064 nm with improved aerosol retrieval approaches in support of CALIPSO"

First Page of the Article [\[C5825\]](#)

"Geoscience laser altimeter system (GLAS) on the ICESat mission: pre-launch and on-orbit measurement performance"

First Page of the Article [\[C5826\]](#)

"Atmospheric measurements by the geoscience laser altimeter system: initial results"

First Page of the Article [\[C5827\]](#)

"Precision geolocation determination and pointing management for the advanced land observing satellite (ALOS)"

First Page of the Article [\[C5828\]](#)

"Calibration and validation of palsar (II) use of polarimetric active radar calibrator and the Amazon rainforest data"

First Page of the Article [\[C5829\]](#)

"Detection and monitoring of unstable high-mountain slopes with L-band SAR interferometry"

First Page of the Article [\[C5830\]](#)

"Wavelet packet remote-sensing images coding algorithm based on quadtree classification and UTCQ"

First Page of the Article [\[C5831\]](#)

"Adapted vector-lifting schemes for multiband textured image coding"

First Page of the Article [\[C5832\]](#)

"Level 1 data processing algorithm for ALOS PRISM and AVNIR-2"

First Page of the Article [\[C5833\]](#)

"Retrieval of land surface parameters in the zone of Chotts, Tunisia, from SIR-C/X-SAR data"

First Page of the Article [\[C5834\]](#)

"Wavenumber spectra of the Mediterranean Sea winds derived from the NASA QuikSCAT data"

First Page of the Article [\[C5835\]](#)

"Ocean wave spectrum and radar cross-section analysis from coincident ENVISAT ASAR observations and airborne polarimetric radar measurements performed during the VALPARESO experiment"

First Page of the Article [\[C5836\]](#)

"Use of SAR cross spectra for wind retrieval from envisat ASAR wave mode data"

First Page of the Article [\[C5837\]](#)

"A JERS-1 radar mosaic for subsurface geology mapping in East Sahara"

First Page of the Article [\[C5838\]](#)

"Development status of the cloud profiling radar for the cloudsat mission"

First Page of the Article [\[C5839\]](#)

"Comparison of spatial and spectral sea state parameters measured by space borne SAR, nautical radar and in situ sensors"

First Page of the Article [\[C5840\]](#)

"Investigation of wavelets for raw SAR data compression"

First Page of the Article [\[C5841\]](#)

"The dual-frequency precipitation radar for the GPM core satellite"

First Page of the Article [\[C5842\]](#)

"Precipitation processing system for the global precipitation measurement mission"

First Page of the Article [\[C5843\]](#)

"On the use of the log-normal particle size distribution to characterize global rain"

First Page of the Article [\[C5844\]](#)

"A compact and flexible multi-DSP system for real-time SAR applications"

First Page of the Article [\[C5845\]](#)

"Issues and challenges for standardizing level zero format for SAR data"

First Page of the Article [\[C5846\]](#)

"Japan's progress for the global precipitation measurement (GPM)"

First Page of the Article [\[C5847\]](#)

"Estimation of raindrop size distribution from TRMM precipitation radar observations"

First Page of the Article [\[C5848\]](#)

"NEXLASER-an unattended tropospheric aerosol and ozone lidar-first results"

First Page of the Article [\[C5849\]](#)

"Use of Raman lidar for validation of aqua retrievals and the study of airs radiances"

First Page of the Article [\[C5850\]](#)

"Lidar observations of etna volcanic aerosol"

First Page of the Article [\[C5851\]](#)

"Analysis of built-up areas from polarimetric interferometric SAR images"

First Page of the Article [\[C5852\]](#)

"Estimation of coupling between mobile vehicular radars and satellite radiometers"

First Page of the Article [\[C5853\]](#)

"Design of an L-band microwave radiometer with active mitigation of interference"

First Page of the Article [\[C5854\]](#)



"DInSAR measurements of reclaimed coastal land"

The subsidence rate in a reclaimed coastal land has been estimated using JERS-1 L-band SAR two-pass differential interferometry (DInSAR). Owing to the severe temporal decorrelation induced by frequent soil loading and to the intense deformation gradient, the L-band was effective for observation of subsidence in the reclaimed land. Permanent scatterers were also used to remove residual phase. We evaluated the accuracy of the estimated subsidence rate using field measurements obtained by magnetic probe extensometer with an accuracy of ± 1 mm from 42 ground stations. Two-dimensional subsidence map was achieved from 5 qualified interferograms. The correlation coefficient between the two-dimensional radar measurements and the in situ data was 0.87 with an r.m.s. error of 1.44 cm. The results demonstrate that L-band DInSAR is useful for geological engineering applications. [C5855]

"Frozen ground deformation monitoring using SAR interferometry"

The interferometric SAR technique has demonstrated its capability to measure ground deformation in wide range of application. The seasonal freeze/thaw transition will cause the deformation of ground surface, which is the main factor for engineering construction in permafrost region. China begins construction of Qinghai-Tibet railway in 2002. About 550 km of the railway will pass through permafrost areas. Thawing and temperature rising has a great influence on railway stability. In this study, five scenes SAR SLC images, including Tandem data, are used to produce multiple interferograms. Two typical methods for deformation detection are discussed. One is the InSAR measure with the high accurate DEM used to reduce the terrain effect, the other is differential InSAR. The data of deformation in experiment site are compared quantitatively with precise and accurate geodetic data derived from field measurement respectively. The analysis of precision and reliability of two methods showed that the InSAR measure with the high accurate DEM is the suitable technique for deformation monitoring using ERS-1/2 SAR data in Qinghai-Tibet Plateau. Additionally, an InSAR monitoring system of frozen ground deformation is proposed for the Qinghai-Tibet railway building. [C5856]

"Simulation of abandoned mining induced surface movements for estimating DInSAR detection limits"

Underground mining activities very often cause changes to the surface. Beside the strong influences of active mining, former mining activities with still existing cavities in the underground do influence the surface as well, causing a risk for people and infrastructure. The main risk is induced by sudden falls of the surface. In contrast to surface deformations induced by active mining these deformations are difficult to predict. The risk justifies the monitoring of ground movements in historical mining areas. One technique evaluated is Differential Interferometric Synthetic Aperture Radar (DInSAR). The main difference to other applications of DInSAR is, that location, subsidence rate and spatial extent can just roughly be estimated using related historic information about former mining activities. In addition, the expected character of the subsidence complicates the separation between deformation signal and atmospherical artifacts. In order to get a first idea about the limits of the technique, circular shaped deformation models with different extents and maximum vertical displacements have been modeled and integrated into the DInSAR processing chain. The final results have been evaluated qualitatively and quantitatively in order to get an idea about the detection limits of DInSAR using ERS-1/2 data. The qualitative assessment shows that subsidence cones of circular shape with radii below 400 m cannot be reliably identified in a single interferogram in the investigated case. In the quantitative assessment the highest relative RMS errors between model and result were found for subsidence cones with small radii and small maximum vertical displacements. Furthermore it could be shown that the use of multiple interferograms by applying stacking techniques leads to a better detection limit of the DInSAR method. [C5857]

"High resolution image reconstruction by GPR using MUSIC and SAR processing method for landmine detection"

Landmine detection is a difficult and very sensitive task as it may cost a human life even with a slight mistake or misdetection. In addition, the invention of non-metallic landmines made the scenario much more complicated and difficult. Various landmine detection techniques have been proposed, such as a metal detector, an electromagnetic induction (EMI), and so on. However, the probability of false alarm is very high in such techniques, which is considered as a severe problem. In this paper, ground penetrating radar, which has the capability to detect the non metal and the plastic mines, has been proposed to detect landmines. In addition, super resolution technique MUSIC algorithm and SAR (Synthetic Aperture Radar) has been implemented for the signal processing and image reconstruction of a GPR signal. [C5858]

"Ground-based SAR interferometry as a tool for landslide monitoring during emergencies"

This work concerns the application of ground-based synthetic aperture radar (GB-SAR) interferometry as a tool

for the landslide monitoring during emergencies. An example of application of this technique to the Cortenova landslide, Italian Alps, is described. The deformation maps provided by GB-SAR interferometry allows for the study of the landslide temporal evolution and the volume estimation of the material involved in the mass movement. This information is important for the assessment of future risk scenarios needed to draw up the emergency plans for civil protection purposes. [C5859]

"Land subsidence in the Firenze-Prato-Pistoia basin measured by means of spaceborne SAR interferometry"

This work concerns the application of space-borne SAR interferometry (InSAR) to the study of the land subsidence problem affecting the urban areas of the Firenze-Prato-Pistoia basin (Central Italy). Such a phenomenon is mainly related to the large amount of ground-water pumped for the industrial activities of this area. The interferometric analysis has been carried out by means of both traditional Differential Interferometry (DInSAR) and Permanent Scatterers technique (PS) by using SAR data acquired by the ESA ERS1/2 satellites. Different patterns of terrain subsidence have been detected in the industrial areas of the monitored basin. [C5860]

"Comparison between InSAR and leveling"

The Differential SAR Interferometry (DInSAR) technique has been applied to a test site located near Vauvert (France). A subsidence phenomenon has been previously observed by leveling. Precise monitoring of the phenomenon is needed in relation with deep (more than 1 km) exploitation of underground salt by solution mining, in order to constrain further geomechanical modeling studies for a better knowledge of its evolution. The InSAR measurements has been compared to the available leveling data. [C5861]

"Siral the radar altimeter for the cryosat mission, pre-launch performances"

First Page of the Article [C5862]

"Towards an atmosphere free interferogram; first comparison between ENVISAT's ASAR and MERIS water vapor observations"

During ERS-1 and ERS-2 missions, the application of synthetic aperture radar interferometry (InSAR) become known as a very important method for topographic mapping and high accuracy surface displacement measurements. Further investigations, however, showed that expected accuracy couldn't be achieved. It appeared that radiowave propagation through the atmosphere causes significant distortion to the observed signal and obscures effects of topography and/or deformations. Therefore, it became clear that in order to achieve very accurate measurements of surface displacements additional knowledge of state of atmosphere during InSAR measurements is necessary. In this paper the possibility of using Medium Resolution Imaging Spectrometer (MERIS) in combination with Advanced SAR (ASAR), both are on board of ENVISAT, for obtaining atmosphere free interferograms is discussed. [C5863]

"Rain-flagging of the Envisat altimeter"

As the goals for altimetric measurements become ever more precise, there is concern about the reliable detection and discarding of rain contaminated data. A dual-frequency rain detection technique developed for the Ku- and C-band TOPEX altimeter, is adapted for the Ku- and S-band RA-2 altimeter on Envisat. Of particular concern is the selection of a suitable threshold to minimise the quantity of good data inadvertently discarded. [C5864]

"Remotely sensed determination of flood surface gradients for hydrological modelling of semi-arid floodplains"

The wetland and riparian communities associated with most inland Australian rivers rely on periodic flooding and drying cycles for their healthy maintenance and ecological functioning. Community composition, structure and location are determined primarily by elevation and hence access to flood waters. As most inland rivers are heavily regulated, determination of the timing and size of environmental flow releases from water storages is essential for the proper management of these areas. Modelling of flood surface gradients across large floodplains is one means used to determine which areas of the floodplain and consequently which vegetation communities will be flooded for a given environmental flow release. Traditionally, these gradients have been determined by cell-based analysis using aerial photography and contour maps. Various Landsat TM derived water detection algorithms and L-band SAR backscatter thresholding techniques were explored to detect floodwater boundaries during flooding of a large wetland area on the Macquarie River in central western New

South Wales, Australia. These were used in conjunction with a Digital Elevation Model of the area in a GIS environment to model the flood surface gradient and determine the relationships between elevation, flooding and distance from flood entry point. Results showed that automated determination of the flood surface gradient from the satellite imagery achieved better results than manual cell-based analysis and facilitated more accurate modelling of the effects of flow releases. The development of such techniques will permit better use of water resources for sustainable management of important wetland and riparian communities in the future. [C5865]

"Preliminary assessment of SRTM X band DEMs of Southern Africa for hydrogeological studies"

The Table Mountain Group (TMG) Aquifer Feasibility Study and Pilot Project is a major hydrogeological project in the mountains fringing the eastern side of the Cape Town metropolitan area. An earlier study using a 30 m×30 m DEM demonstrated that the TMG topography is spatially and structurally well correlated with the patterns of fracture deformation, partly inherited from the break-up of the Gondwanaland supercontinent, in part produced by uplift and erosion under the present-day plate-tectonic stress regime. The advent of the SRTM datasets seems thus to be potentially a good source of high resolution DEM data for such applications, but the differences between radar derived and stereo optical data must be assessed. For example, and as is shown, X Band radar data is sensitive to the height of vegetation. Although, not as important for this application, the absolute height accuracy of the X Band DEMs is also assessed via a corner reflector deployed during the mission, as well as other spot heights. [C5866]

"Rain effects on SeaWinds data"

One year of SeaWinds σ₀ data are used with SSM/I and TMI rain rates collocated within 5 minutes and tri-linearly interpolated ECMWF analyses to investigate the effects of rain on SeaWinds data. By parameterizing attenuation and volumetric backscattering in terms of rain rate, the modification of the surface radar cross-section by rain can be found. Uncertainty exists in the rain modification of the surface radar cross-section for different rain rate-wind speed regimes, but its magnitude and azimuthal behavior are sufficiently important to require attention for accurate rain contamination correction. [C5867]

"Joint-Time Frequency Analysis for investigating layered structures by surface penetrating radar"

A Continuous Wave Step Frequency Radar system, working at high frequencies, is suggested as a tool for intra-wall inspection. A processing technique based on Joint Time Frequency Analysis (JTFA) is applied to simulated and experimental data. [C5868]

"Experimental validation of an electromagnetic model for rice crops using a wide-band polarimetric radar"

A physics-based electromagnetic model specially tailored for the computation of the radar backscatter from rice crops is being developed. The model produces estimates of the coherent polarimetric backscatter response as a function of the sensor parameters and the physical description of the scene. This model is currently under validation against experimental data gathered in the European Microwave Signature Laboratory (EMSL). First results, obtained by a direct comparison of simulated and measured backscattering coefficients (with HH, HV and VV polarizations), show a reasonable agreement. The dependence on incidence angle, frequency and morphological characteristics of the rice plants is currently being assessed. [C5869]

"Multi-resolution imaging spectroscopy resolving the structure of heterogeneous canopies for forest fire fuel properties mapping"

Coniferous forests represent canopies with a high heterogeneity in the horizontal and as well in the vertical dimension. Consequently the interaction of incident radiation is dominated by the complex 3-D canopy structure and architecture. Radiative transfer approaches based on coupled leaf and canopy radiative transfer models still allow the simulation of the canopy reflectance as a function of leaf optical properties, canopy structure and viewing geometry as well as the retrieval of biophysical and biochemical canopy variables. High resolution imaging spectrometry supported by LIDAR data and radiative transfer models of different levels of complexities (SAIL, GeoSAIL) are employed to assess the influence of canopy heterogeneity and structure at different spatial scales. We discuss the relevance of single scene components and canopy structure to the recorded canopy reflectance and present a strategy to support radiative transfer models for biophysical and biochemical parameter retrieval relevant for forest fires. [C5870]

"Relating SAR image texture and backscatter to tropical forest biomass"

Twenty six texture measures (derived from local statistics, grey-level co-occurrence matrix (GLCM), sum and

difference histogram (SADH) and variograms) were calculated for simulated images and their ability to discriminate image texture independently of image contrast was determined. The seven texture measures able to discriminate texture independently of contrast (and therefore able to estimate biomass independently of backscatter) were entropy (derived from local statistics), contrast, entropy, correlation and chi-square (derived from the GLCM), mean of sum vector (derived from the SADH) and range (derived from the variogram). These measures were calculated for Japanese Earth Resources Satellite (JERS-1) Synthetic Aperture Radar (SAR) images and related to the biomass of regenerating forest and mature forest plots from two study areas in Brazilian Amazonia. It was hypothesised that texture (a measure of both biomass and canopy unevenness) could be related to tropical forest biomass up to and beyond the saturation of the backscatter/biomass relationship. The results showed that only GLCM derived contrast increased the correlation between backscatter and biomass. The combination of GLCM contrast with backscatter has the potential to increase the accuracy of biomass estimation over the use of backscatter alone. [C5871]

"The effect of sub-pixel areal distribution of snow on the estimation of snow depth from spaceborne passive microwave instruments"

The mapping of estimated snow depth (SD) or snow water equivalent (SWE) from spaceborne passive microwave imagery is usually achieved by detecting a snow scattering signal from the land surface and then by calibrating the magnitude of the scattering with snow depth or snow water equivalent. Scattering is estimated from the brightness temperature difference between 19 GHz and 37 GHz vertical polarization channels of a microwave radiometer (or frequencies not too dissimilar to these). If a snow scattering signal is present, it is generally assumed that snow covers the entire area of a coarse spatial resolution passive microwave pixel (or footprint). For seasonal snowpacks, this is a reasonable assumption because at high latitudes in general, snow cover is often spatially continuous over wide areas during the winter season. However, for spatially discontinuous snowpacks (such as early winter snow, ephemeral snow covers or perhaps regions marginal to mid-winter continental snow covers), snow might be detected in a microwave pixel but it may be inaccurate to assume that snow covers the entire pixel; snow might be spatially localized but dominant enough radiometrically to trigger a snow scattering signal. In this paper we investigate the effect of sub-pixel scale fractional snow extent on the microwave detection of snow. Under cloud-free conditions determined by the Moderate Resolution Imaging Spectroradiometer (MODIS) MOD10_L2 product, we compare the snow scattering signal for various DMSP Special Sensor Microwave Imager pixels with the MODIS MOD10_L2 snow product (500 m² 500 m spatial resolution). Using the 25 km² 25 km EASE grid projection for the passive microwave imagery, comparisons are made between the microwave scattering signal and the percentage of MODIS pixels classed as 100% snow within the 25 km² 25 km. We also compare microwave snow scattering signals with the degree of MODIS snow pixel clustering/dispersion within 25 km² 25 km pixels. This research has important implications for the errors of passive microwave mapping of SD or SWE in discontinuous snow covered regions. [C5872]

"Estimation of red pine tree height using Shuttle Radar Topography Mission and ancillary data"

In this paper accurate tree height retrieval for red pine and Austrian pine is demonstrated using C-band Shuttle Radar Topography Mission (SRTM) height and ancillary data. The tree height retrieval algorithm is based on modeling uniform tree stands with a single layer of randomly-oriented vegetation particles. For such scattering media, the scattering phase center (SPC) height, as measured by SRTM, is a function of tree height, incidence angle, and the extinction coefficient of the medium. The extinction coefficient for uniform tree stands is calculated as a function of tree height and density using allometric equations and a fractal tree model. The algorithm outputs tree height estimates that are significantly closer to the true tree height than the raw SRTM SPC height values obtained from the height difference between the SRTM data and the National Elevation Dataset (NED). The accuracy of the proposed algorithm is demonstrated using SRTM and TOPSAR data for 15 red pine and Austrian pine stands. [C5873]

"Investigating the performance of radar configurations in crop monitoring"

This paper describes an algorithm aimed at monitoring the soil moisture and the growth cycle of wheat fields using radar data. The algorithm is based on neural networks trained by an electromagnetic model and multitemporal ground data measured on fields taken as a reference. The retrieval procedure is tested using multitemporal signatures collected at a test site. [C5874]

"Estimating vegetation biophysical properties from high resolution images: a comparison between radar and optical data"

This paper is devoted to the comparison of high resolution (≈ 1 squared-meter pixels) images acquired in the solar (visible and near infrared) and radar domains over crops. [C5875]

"Experimental validation of a GPR dedicated to the Martian subsurface exploration (Pyla sand dune)"

In the frame of the NETLANDER project, we have developed a ground penetrating radar (GPR) aimed at initial observations of the geological features in the deep Martian subsurface and the detection of potential liquid water reservoirs. Initial ground tests at 2, 3 and 4 MHz were recently performed on the Pyla Dune, which is a sand dune nearly 100 meter high along the south-west Atlantic coast in France. The horizontal reflecting layer located at the base of the dune together with the known permittivity value of the sand offer the opportunity to test the performance of the device in a rather well-documented and simple environment. These first experimental results are reported in the paper. We will focus on the precise measurement of the electric antenna characteristics and the analysis of the backscattered signals using both electric and magnetic components of the received field. Comparisons with numerical simulations taking into account the actual environment of the GPR are also presented for comparisons. [C5876]

"Complex impedance mapping using GPR survey methods"

GPR surveys are normally processed to provide reflection images free of static offsets and long period drift. However in many surveys the raw data is observed to contain systematic decays consistent with Cole-Cole models of complex impedance. The resulting time-constants can be used to provide additional constraints for geotechnical investigations of moisture content and plasticity in soils. [C5877]

"Some estimations of water lenses position based on experimental data obtained by SAR operating at P and VHF bands"

The materials presented below concern the questions of utilization of airborne SAR operating at four frequencies (4, 23, 68 and 254 cm). Results of algorithms for inverse problem solution (which is incorrect) development are presented. These problems are the moisture profile determination, detection of subsurface cracks, splits, cavities and so on using the results of radar mapping at different wavelength ranges. The outputs were approbated to explain the results of radar sensing in the regions of desert with water lenses. [C5878]

"Surface soil moisture estimation from SAR data over wheat fields during the ADAM project"

Surface soil moisture estimation from SAR (ERS-2 and Radarsat) images was investigated using the "water-cloud" model. It was verified that the "water-cloud" model can adequately represent the backscattering coefficients over winter wheat fields, during the entire growing season, as a function of canopy water content and surface soil moisture. [C5879]

"Influence of the soil tillage and degradation due to rain upon the radar scattered signal"

The study presented here is deals with the effect of bare soils roughness (including soil tillage and state of degradation due to rain fall) upon microwave scattering. Many theoretical as well as experimental studies have already been completed to point out the influence of soil roughness on backscattering. Nevertheless, the interpretation of radar measurements in terms of soil roughness still remains a difficult task given the geometrical complexity of real soils and the influence of soil moisture. Electromagnetic simulations of the radar signal are an essential step to understand the influence of such parameters on the back-scattered signal. For the purpose of this paper, a data base of real bare soil geometrical descriptions retrieved by using a stereovision method is used and the back-scattered signal is obtained for each kind of soil by a rigorous differential electromagnetic method. [C5880]

"A phase signature for detecting subsurface moisture using polarimetric L-band SAR: example of the Pyla dune-France"

We investigate the penetration capabilities of L-band microwaves for the mapping of subsurface moisture. Our experimental site is the Pyla dune, a bare sandy area allowing high signal penetration and presenting large subsurface wet structures (paleosoils) at varying depths. We established that a phase signal is correlated to the buried and wet paleosoils: a phase difference between HH and VV channels reaching 25° was clearly observed on L-band airborne SAR data. This phase signature was confirmed by fieldwork measurements and fits the semi-empirical model proposed by Oh et al. [C5881]

"Precipitation measurements using the QuikSCAT Radiometer"

Microwave brightness temperatures are obtained from the SeaWinds scatterometer on the QuikSCAT satellite.

These QuikSCAT Radiometer (QRad) measurements are used to infer instantaneous oceanic rain rates using a statistical retrieval algorithm that is based upon collocated TMI measurements. QRad instantaneous rain rate measurements have been binned in 0.5 hour local time windows onto a $0.5^{\circ} \times 0.5^{\circ}$ ocean grid. Also, an average rain rate product is produced, where QRad instantaneous rain rates have been averaged for five-day intervals (pentads) in the 0.5 hour local time windows. The scientific utility of QRad rain measurements is that they provide increased temporal and spatial sampling, which complements that provided by the TRMM Microwave Imager (TMI) and the Special Sensor Microwave Imagers (SSMIs) on the three DMSP satellites. Examples for the year 2000 are presented with corresponding rain rate measurements derived from TMI and SSMI. The results demonstrate that QRad rain measurements agree well with these independent rain observations. [C5882]

"Validation and error characterization for the Global Precipitation Measurement"

In this paper, we have dealt with the validation and error characterization for the Global Precipitation Measurement (GPM) research initiative. The GPM is a three-year on-orbit duration program with a five-year duration goal. The Core satellite launch is scheduled tentatively for Fall 2008. Presently, GPM is in formulation stage in which the team is developing concepts and requirements prior to design work. As a part of formulation, ground validation is developing its requirements with a top level schedule requirement of commencing GV operations two years prior to the Core satellite launch. The rationale is that GV will benefit from a two-year head start in preparation for the Core observations. The requirements for GV are being developed in collaboration with, and vetted by, the precipitation science community. [C5883]

"The Bayesian Algorithm for Microwave Precipitation Retrieval (BAMPR): potential and application to TRMM data"

The Bayesian Algorithm for Microwave Precipitation Retrieval (BAMPR) is a cloud resolving model (CRM)-based retrieval technique for estimating surface rainfall and precipitating cloud profiles by means of microwave radiometric measurements from space. In this paper is illustrated the version of BAMPR tailored for the multi-frequency microwave radiometer aboard of the Tropical Rainfall Measuring Mission (TRMM), called TRMM Microwave Imager (TMI). Since the inversion procedure is based on a cloud-radiation database (CRD) pre-generated by performing radiative transfer calculations on the CRM numerical outputs, the important aspect of CRD representativeness is described. Results of applying BAMPR to a selected event observed by TRMM are finally discussed. [C5884]

"Global ocean wave measurements from ENVISAT ASAR data using a parametric inversion scheme"

Two-dimensional ocean wave spectra are measured from ENVISAT ASAR wave mode cross spectra on a global scale. The measurement is performed using a parametric retrieval scheme, which makes use of prior information taken from numerical wave models. The Partition Rescale and Shift algorithm (PARSA) is based on a partitioning technique, which splits an a prior wave spectrum into its wave system components. Integral parameters of these systems, such as mean direction, mean wavelength, waveheight, and directional spreading are then adjusted iteratively to improve the consistency with the SAR observation. The method takes into account the full nonlinear SAR imaging process and uses a maximum a posteriori approach, which is based on statistical model quantifying the errors of the SAR imaging model, the SAR measurement, and the prior wave spectra. The method is applied to a global data set of ENVISAT ASAR data acquired during the CAL/VAL phase. The benefit of cross spectra compared to conventional symmetric image spectra is demonstrated. [C5885]

"ASAR multi-swath techniques"

In 2002 ENVISAT with the advanced SAR (ASAR) as one important instrument was launched. As compared to the preceding SARs on ERS-1 and ERS-2 the ASAR has additional functionality with many different modes. Important aspects of the ASAR include the alternating polarization modes for quasi simultaneous acquisition of data at two different polarizations, and beam-steering capability, which permits to acquire data at different incidence angles. To optimize the use of the new functionality adequate processing techniques are required. This is particularly important for data acquired in different swaths, i.e. with different image geometries. In this paper ASAR multi-swath techniques are discussed, including image co-registration, multi-channel filtering, and multi-swath multi-temporal techniques. [C5886]

"Validation of GOMOS O3 vertical profiles"

In this paper, we present the results of validation studies of O3 profiles measured by the instruments GOMOS (global ozone monitoring by occultations of stars), one of three instruments dedicated to atmospheric chemistry

measurement along with MIPAS and SIAMACHY, on board the ESA satellite ENVISAT launched on 1 march 2002. [C5887]

"Sampling simulation of five sun synchronous orbit satellites' group and TRMM rainfall estimation using radar-AmeDAS composites"

Sampling error of rainfall rate was estimated by using radar-AMeDAS composites in $5^{\circ}45'$ and $1^{\circ}41'$ grid box for five sun synchronous orbit satellites and TRMM. It was influenced by satellite altitude, swath width, local time. Sampling error caused by altitude occupied half of sampling error. It was discovered that sampling error depend on sampling period as period- 12 /. [C5888]

"Calculations of surface clutter interference with precipitation measurement from space by 35.5 GHz radar for Global Precipitation Measurement Mission"

Surface clutter interference with precipitation measurement from space using 35.5 GHz radar was evaluated for the Global Precipitation Measurement (GPM) Mission. The GPM Mission is unique in that it consists of a core satellite with dual-frequency precipitation radar (13.6 GHz and 35.5 GHz) and eight small companion satellites that are equipped with microwave radiometers. The 35.5 GHz precipitation radar has very high sensitivity; its designed minimum detectable rain rate at the rain top is 0.3 mm/h. In this study, a Taylor distribution with random errors in the excitation current is considered in calculating the radiation pattern of a 35.5 GHz slotted waveguide planar phased array antenna. The signal-to-clutter power ratio (S/C) was evaluated for the antenna pattern given by the Taylor distribution (peak side lobe level=-35dB, $n=6$; the same values as for the TRMM PR), where S is the received power from the rain scattering volume and C is the backscattered power from sea surface. Uniform rain rates of 0.3 and 1.0 mm/h were assumed in the calculation of S. We show that the interference of surface clutter with precipitation measurement can be suppressed more at 35.5 GHz than at 13.6 GHz because of the short wavelength. The calculated S/C ratio distribution showed that the effect of the side lobe clutter is not negligible, especially for low rain rates (less than 1.0 mm/h), but it is negligible for heavier rain (over 1.0 mm/h). The calculations also show that the effect of the main lobe clutter is severe and not negligible for either light or heavy rain. The conclusion is that 35.5 GHz precipitation radar can accurately observe rain with a planar phased array antenna fed with a Taylor distribution ($n=6$, peak side lobe level=-35 dB). [C5889]

"Evaluation of precipitation type determination from TRMM observations"

The TRMM mission is dedicated to observing and understanding the impact of tropical rainfall. Two of the important products of the TRMM mission are classification of precipitation into convective and stratiform type as well determination of the height of the bright band. Currently TRMM uses an algorithm to arrive at these products based on a characterization of horizontal and vertical variability of reflectivity. This paper presents result of a new algorithm developed using wavelets transform. The algorithms for wavelet analysis based products of both convective/stratiform classification as well as bright band detection are described. The results obtained from wavelet algorithms are compared against both the current products as well as ground radar inferences. The results show that the wavelet-based analysis provides fairly accurate results for both convective/stratiform classification as well as bright band determination. [C5890]

"Impact of ASAR ENVISAT directional wave spectra on wave forecast"

In order to improve the wave forecast, the assimilation of directional wave spectra in wave model has been developed at Meteo France. The assimilation scheme is tested for real ENVISAT ASAR wave spectra provided by the European Space Agency. The scheme takes into account the limitation in frequency related to the ASAR instrument. The preliminary results show that the assimilation of wave spectra is efficient and works correctly. The impact of the assimilation on wave parameters is significant and stays effective in the forecast period. In addition, statistical analysis has shown good skill in term of root mean square and assimilation index for the analyzed wave parameters (wave height, direction and frequency). [C5891]

"Deep convection observed from split window of GOES and PR/TRMM, LIS/TRMM"

Deep convection over South America is investigated in terms of cloud type classified by the split window (11 and 12 μm) using the hourly data of GOES, and rainfall by the PR (Precipitation Radar), and lightning activity by the LIS (Lightning Imaging Sensor) on board TRMM (Tropical Rainfall Measuring Mission) as case studies. [C5892]

"Spaceborne passive microwave measurement of snowfall over land"

A physically based retrieval algorithm was developed to estimate snowfall over land. The retrieval algorithm relies on the MM5 model that generates the vertical structure of a snow cloud, including snow mass, snow

particle effective diameter, and water vapor. The MM5 cloud simulation was used to provide statistics for generating the cloud characteristics. The snow cloud profile and surface emissivity were then used in radiative transfer calculations that were optimized against AMSU-B observations at 89, 150 and 183.3 ± 7 , ± 3 , and ± 1 GHz. The multi-parameter cloud model that produced brightness temperatures that best fit the AMSU-B observations was selected as the retrieved profile. The retrieved snowfall distribution was validated with radar reflectivity measurements obtained from the operational NWS radar network. [C5893]

"Precipitation retrievals using radiometric and spatial information of passive microwave radiometers"

The effect of rainfall inhomogeneity within the sensor field-of-view (FOV), the so-called beam-filling error, affects significantly the accuracy of rainfall retrievals. Observational analyses of Tropical Rainfall Measuring Mission (TRMM) Microwave Imager (TMI) and Precipitation Radar (PR) data show that the beam-filling error can be examined in terms of the coefficient of variation (CV, standard deviation divided by mean rain rate) that provides a measure of the spatial variability. Furthermore, the CV of surface rainfall from PR is related to its vertical structure and has some correlation with the TMI 85 GHz brightness temperature (T_b), especially at the high rain rates. Based on these findings, we exploit the 85 GHz spatial variability in the context of a Bayesian-type inversion method for rainfall retrieval. The spatial variability at various domain sizes (thus CV in a vector form) is blended with the sets of multi-channel brightness temperatures (T_b vector) for the Bayesian inversion. The a-priori databases for the inversion are constructed from the collocated TMI and PR observations at the PR resolution. Through synthetic retrievals we demonstrated that the inclusion of CV information of the T_b remarkably improved the rainfall retrieval accuracy by reducing the effect of the rainfall inhomogeneity. [C5894]

"The ship detection capability of ENVISAT's ASAR"

Norway has used spaceborne SAR systems for operational fisheries monitoring since 1998. RADARSAT-1 has been the main source of data. With ENVISAT, there are plans to increase usage of satellite data. First, however, it is important to verify which modes and products are most useful for operational purposes. At FFI, we are in the process of analysing ENVISAT data for evaluating the ship detection capabilities of the ASAR instrument. The Alternating Polarisation (AP) mode is of particular interest, as this represents a new spaceborne capability for routine observations. The first results are promising for VV/VH AP data for ship detection. [C5895]

"Tunable solid-etalon filter for the ICESat/GLAS 532 nm channel lidar receiver"

We report on the tunable solid-etalon filter used in ICESat/GLAS 532 nm channel lidar receiver. [C5896]

"Using multitemporal RADARSAT-1 data to extract paddy rice structure in southern China"

RADARSAT-1 data has been widely used to monitor paddy rice in the world since RADARSAT-1 satellite was launched in 1995. In China, Crop structure adjustment policy has brought great change of rice area. Government managers of agricultural industry need timely crop structure information to monitor the performance of implementing the crop structure adjustment policy. But crop structure information based on statistical data from reporting system cannot meet the urgent and timely needs of governors for rice structure information. RADARSAT-1 brought a new data source for extracting rice information with high accuracy. Using multitemporal RADARSAT data can obtain all rice area with different season in a farming year in certain area. This paper presents the methods of remote sensing for study on rice structure using multitemporal RADARSAT data. Then, this paper instructs and analyses the rice structure in the Wuhan city area in 2002. [C5897]

"Design and analysis of multi-mode cluster SAR"

This paper presents the basic configuration of the Distributed Satellite Synthetic Aperture Radar System, discusses the working mode of the system, and indicates the specific performance of the system compare with the conventional SAR system. [C5898]

"ENVISAT ASAR for land cover information"

In 2002 ENVISAT with the advanced SAR (ASAR) as one important instrument was launched. As compared to the preceding SARs on ERS-1 and ERS-2 the ASAR has additional functionality with many different modes. Important aspects of the ASAR include the alternating polarization modes for quasi simultaneous acquisition of data at two different polarizations, and beam-steering capability, which permits to acquire data at different incidence angles. In this paper the use of the ENVISAT ASAR for land cover information retrieval is discussed. For multi-incidence angle data a coefficient to characterize the incidence angle dependence is proposed. [C5899]

"Microwave instruments development in ESA's Earth Observation Future Programmes"

This paper presents an overview of the microwave instruments currently in development under the Future Programmes of the ESA's Earth Observation Envelop Programme. The description of the instruments will be structured according to two broad categories of future missions, i.e. the Earth Explorer and Earth Watch candidates. [C5900]

"Centimetric sea surface height accuracy using the Wide-Swath Ocean altimeter"

In this paper, we present error sources and predicted performance of the Wide-Swath Ocean altimeter, an instrument which has been proposed as an experiment for the NASA/CNES Ocean Surface Topography Mission. The data obtained by this instrument will allow the detailed study of ocean mesoscale phenomena, with a space-time resolution which cannot be achieved by a single conventional nadir altimeter. [C5901]

"Self characterization of modelling parameters for synthetic aperture imaging radiometers"

It is now well established that Synthetic Aperture Imaging Radiometers (SAIR) promise to be powerful sensors for high-resolution observations of the Earth at low microwave frequencies. Within this context, the European Space Agency (ESA) is currently developing the SMOS mission. This propagation of modelling errors within a reconstruction process that attempts to retrieve the brightness temperature of a scene under observation from interferometric measurements depends on the knowledge of the values of the parameters involved in the modelling of the instrument. This contribution describes an approach to characterize these modelling parameters, once the instrument has been launched into space, with an accuracy such that the propagation of errors through the reconstruction process is still under control. [C5902]

"A numerical study of the nonlinear ocean-SAR spectral transform"

Direct numerical simulations of the ocean-to-SAR mapping and the corresponding spectral transform have been carried out using both the linear Gaussian wave model and random Gerstner waves. It is demonstrated that specular reflection can play a significant part in the SAR imaging process for steep range travelling waves. Some consequences for the SAR image spectra are illustrated for both wave models. [C5903]

"Ocean wind field retrieval using ENVISAT ASAR data"

In the last years several algorithms for high-resolution ocean surface wind field retrieval from space borne synthetic aperture radar (SAR) have been developed. These algorithms were specially designed for the C-band SARs aboard the European satellites ERS-1 and ERS-2 operating at vertical (VV) polarization in transmit and receive and the Canadian satellite RADARSAT-1 operating at horizontal (HH) polarization. This paper shows the application of the algorithms to data of the advanced SAR (ASAR) from the European satellite ENVISAT. The wind retrieval algorithm consist of two parts. In the first wind directions are extracted from wind-induced streaks visible in most SAR images at scales between 200 and 1600 m using two different methods. In the second part wind speeds are derived from the normalized radar cross section (NRCS) and image geometry of the calibrated SAR images, together with the local wind direction resulting from the first step. For the wind speed retrieval the semi empirical C-band scatterometer model CMOD5 is used. CMOD5 was originally developed for the scatterometer aboard ERS-1 and 2 operating at VV polarization and consequently requires modification if applied to HH-polarized SAR data. In case of HH-polarization the CMOD5 model is extended by considering the polarization ratio. It is shown that the quality of ENVISAT ASAR data is very well suited for measuring high-resolution ocean wind fields, which are especially important in coastal zones. [C5904]

"Wide-angle azimuth antenna pattern estimation in SAR images"

We propose a novel technique to estimate the Azimuth Antenna Pattern (AAP) from SAR images. The technique first perform azimuth focusing at enhanced resolution, then selects those scatterers that are less affected by ambiguous returns and finally derive the AAP by spectral analysis. Results achieved by processing ENVISAT-ASAR data are presented. [C5905]

"Qualification of SRTM DEM. A first approach toward an application dependant qualification framework"

The now well-known SRTM (Shuttle Radar Topography Mission) mission, launched in February, 2000 for 11 days, used C-band and X-band interferometric SAR to acquire data all over the Earth surface. These data allowed to generate the world's largest DEM. The aim of our study is to assess the quality of the SRTM DEM derived from the X-SAR system, compared with the quality of a reference DEM and of DEM from other sources.

An important aspect of the study is to be able to conclude on the real relevancy of the SRTM product compared to the already existing products, for instance is it to be considered as a new global topographic reference or should it be only limited to some applications. The chosen test site is the Grand Morin, watershed of the Seine river nearby Paris, France, that exhibits a wide thematic diversity. Beyond the qualification of SRTM products, we tried to develop a systematic framework for the analysis of quality, which constitutes a challenging issue nowadays. [C5906]

"Validation of SRTM-derived surface currents off the Dutch coast by numerical circulation model results"

The feasibility of exploiting the along-track separation of 7 m between the two X band antennas of SRTM for ocean current measurements was already demonstrated by us at IGARSS 2002. We presented an SRTM image of the Dutch Waddenzee with clear phase variations in water-covered areas, which could be converted into line-of-sight current variations by about 1.3 m/s. A comparison with a current map from a tidal atlas showed good qualitative agreement, but digital reference data for a quantitative validation of the SRTM results were not available. In this work we present a detailed comparison of the SRTM data with simulated current fields from the numerical circulation model KUSTWAD. We obtain an overall correlation of 0.558, a regression coefficient of 1.011, and an rms difference between SRTM and KUSTWAD currents of 0.24 m/s. Furthermore, we analyze the correlation of spatial variations in the measured and simulated current fields on different length scales. We find that SRTM can resolve the current variations which are relevant to KUSTWAD down to scales on the order of 1 km. [C5907]

"The terraSAR-X satellite project"

The objective of TerraSAR-X is the setup of an operational space borne X-Band SAR system in order to produce remote sensing products for commercial and scientific use. The TerraSAR-X project is conducted under the aegis of the DLR Space Flight Management and comprises a space and a ground segment. The space segment is designed and built by ASTRIUM GmbH, the ground segment is set up by several institutions of DLR, namely the German Remote Sensing Data Center, the Remote Sensing Technology Institute, the German Space Operations Center and the Microwaves and Radar Institute. [C5908]

"Rapid Environmental Assessment at high latitudes"

Rapid Environmental Assessment (REA) includes the use of satellite, airborne, and in situ observations together with geophysical models to provide the best possible estimate of the prevailing conditions during a military operation. Increasingly, the focus is on analysis (nowcasting) and short term forecasting. Requirements vary widely however, depending on the types of vessels involved and the nature of the operation. We have worked closely with the Royal Norwegian Navy (RNoN) to develop a REA capability for high latitudes to meet the requirements of the RNoN. [C5909]

"An Automatic Ship Detection system using ERS SAR images"

An ASD (Automatic Ship Detection) system is introduced in this paper. ASD system is mainly composed of a ship detector and a wake detector. The post-processing procedures improve the detection accuracy. Ship parameters, which include ship length, ship beam, ship position, ship orientation and ship speed, are also estimated. [C5910]

"Multi-sensor synergetic analysis of mesoscale oceanic features: Campos Basin, southeastern Brazil"

This study presents a combined use of multi-sensor remote sensing and in situ data for the analysis and interpretation of oceanic features observed at the continental shelf and slope of the Campos Basin, southeastern Brazilian coast. Ocean color (SeaWiFS), thermal infrared (AVHRR), scatterometer (QuikSCAT) and SAR (Radarsat-1) data were integrated in order to associate the different SAR backscatter patterns to physical and biological forcing processes. The interpreted SAR feature included processes such as oceanic fronts, meandering and eddies, upwelling plumes, wind variability and algae bloom. The correct interpretation of these features was only possible through the use of the multi-sensor synergetic approach complemented by timely field verification. [C5911]

"P-band radar data classification by neural network for Amazonian land cover assessment"

This work presents the evaluation of the P-band data discrimination properties using Fuzzy-ART artificial neural network (AMN) unsupervised methodology for land cover mapping in the Amazon tropical forest. [C5912]

"The effect of seasonal and weather conditions to land cover class separability in ERS radar data"

The effect of seasonal and weather conditions to the separability of land cover classes were studied using ERS SAR intensity and coherence images. Generally, the classes are more separable in individual coherence images than in individual intensity images. The exception is springtime during snowmelt, when intensity images are better. Temporal averaging and some texture measures increase class separability. [C5913]

"Dim target detection in IR maritime surveillance systems"

In this paper we present an automatic procedure for the detection of long-range airborne targets in maritime naval surveillance systems. The algorithm performance is investigated via simulation and compared to the one of the classical moving window detection algorithm. [C5914]

"Fractal mapping for sea surface anomalies recognition"

The aim of this paper is to investigate whether fractal maps extracted from sea SAR images are useful for discriminating the sea from other entities or anomalies. Fractal mapping consists of locally estimating the fractal dimension of the image. To this purpose four different methods based on covering and spectral analysis are proposed and compared when applied to real ERS1-2 GEC images. Wind falls, sea and line coast are well distinguishable in the fractal maps. This result clearly shows that the use of image fractal processing is a promising and powerful technique for identifying sea surface anomalies. [C5915]

"HF radar detects submesoscale spiral eddies in Monterey Bay"

Shore based high-frequency Doppler radar observations are utilized for the reconstruction of high-resolution surface currents in Monterey Bay and off Monterey: meso-scale ageostrophic spiral eddies with scales equal to 10-20 km and lifetimes up to 6-12 hours. We have found that cyclonic spiral eddies are generated by the shear instability in the transition zone of the California coast. However, observed anticyclonic spiral eddies with smaller sizes and life times have explicit topographic nature. The spiraling order (So), Rossby (Ro) and Reynolds (Re) numbers for eddies were estimated to identify different stages of eddy evolution. [C5916]

"Utilization of Hopfield neural network and quasi-linear model for longshore current pattern simulation from RADARSAT"

This study introduced a new approach for modeling longshore current pattern from sequential RADARSAT SAR images. Doppler frequency gradient shift from the two sequential RADARSAT images has been estimated. This model utilized to simulate the longshore current pattern. The quasi-linear model used to map the longshore pattern detected by Doppler frequency shift into the real longshore current simulated from significant wave height at breaking zone. A Hopfield neural network was applied to compare between longshore current estimated from Doppler frequency gradient shift and ones modeled from quasi-linear. [C5917]

"Use of synoptic real data for relating the sea surface roughness to the backscattering signal fractal dimension"

In this paper the authors analyze the correlations between sea surface roughness, wind intensity and radar backscattering time series, by using the fractal geometry. The aim is to provide evidence, by using real data, of correlation between the sea surface roughness and the backscattering fractal dimension. The results have highlighted good correlations and shown the usefulness of the fractal dimension as a parameter for sea surface roughness characterization. [C5918]

"Microwave radiation and backscatter of the sea surface perturbed by underwater gas bubble flow"

Field experiments conducted over the past few years have demonstrated the efficiency of microwave remote sensing methods in localizing underwater gas spurts on the sea surface. This problem is closely related to the tasks of monitoring the state of underwater gas pipes and localizing natural underwater gas jets. This paper discusses the experimental data obtained and suggests, based on this analysis, an approach to the important problem of developing a model that would give an adequate description of electromagnetic properties of the sea surface perturbed by a flow of gas bubbles. [C5919]

"Retrieval of surface-current fields and bathymetries using radar-image sequences"

An algorithm for retrieving high-resolution surface-current fields and bathymetries using nautical radar-image

sequences is presented. The image sequences are acquired by a common marine X-Band radar. The algorithm retrieves 3d wave-number frequency spectra for each pixel in the analyzed area. With the local 3d spectra maps of hydrographic parameters, wave spectra with its integral spectral parameters, e.g. the local significant wave height, are determined. Thereby areas of about 2 km in radius are covered by the radar. The spatial distribution of these parameters gives a better understanding of the processes near the shoreline for better application of coastal or river training measures. Especially in harbor areas and regions with coastal structures, where the wave fields are highly inhomogeneous due to shallow-water effects like refraction and shoaling as well as building effects like diffraction, is the potential of the developed method. The method is also applicable on moving vessels to get permanently information about local currents, changing water depths in near-shore regions around the ship, especially when the ship is approaching or leaving a harbor. [C5920]

"The internal wave extraction from composing sea surface using SAR image"

The major goals of the variable SARs were applications in ocean wave research and wave forecasting. Two-dimensional ocean wave spectra can be derived from SIR-C/X-SAR images by inversion of the SAR imaging mechanism. But for a composite sea surface, i.e., there exist local wind-generated waves, long wave (or swell) from far fetch, internal waves and/or wave breakers, to separate very certain wave information or wave spectrum is difficult in practice. Inversion of a 2D spectrum of internal wave surface of South-China Sea is computed from SIR-C/X-SAR image data. A new inversion method is presented which estimates two dimensional wave spectra. The scheme uses prior information from ocean wave models to add missing information and to account for the fact that the SAR ocean wave imaging mechanism model is not a one to one imaging process. The scheme takes the shape of different ocean wave components as information and uses the SAR information to adjust the mean wavelengths, propagation directions and waveheights of the prior spectrum. The scheme is based on stochastic models for both the measurement error and the prior distribution. The method can separate internal wave from wind-generated waves efficiently. [C5921]

"Glacier mass balance determination by remote sensing in the French Alps: progress and limitation for time series monitoring"

This paper presents an approach founded on an indirect methodology to determine the distribution of mass balance at high spatial resolution using remote sensing and ground stakes measurements. A recent time series of images from optical and SAR data are selected on 3 outlet glaciers well suited in the French Alps to evaluate the accuracy of the computed mass balance. The method is based on the snowline determination as a proxy of the equilibrium line altitude (ELA). The key of the transfer is the activity coefficient (db/dz) for the annual mass balance calculation. Comparison between measured and computed mass balance provide a good correspondence ($R^2=0.90$) and allows extending the method on large-scale areas. The limitations are cloudiness for optical data and high slope distortion on SAR images. [C5922]

"Relation between ground features and mathematical morphology using JERS-1/SAR data during flooding time in paddy areas"

The conventional method of detecting flood extent using satellite SAR data is derived from signal intensity changes for each pixel between before and during the flood time. SAR signal intensity should include the information of interaction between ground features and microwave radar. Using mathematical morphology, particular ground feature can be investigated, such as regularly straight lined levees of consolidated paddy fields. [C5923]

"Assessing L-band SAR modes for commercial forest management"

The use of remote sensing in UK forestry has previously been limited to Interpretation of aerial photographs. One new technique which is near commercial realisation is Synthetic Aperture Radar (SAR). Various approaches to using SAR data exist. This paper demonstrates the use of dual-baseline coherence to classify a forested landscape to improve upon a basic backscatter intensity approach, and to give an indication of vegetation density. It is shown that enhancements to the classification are possible, although a few inconsistencies are highlighted. SAR has the capabilities to aid commercial forest management, through complimenting and enhancing current practices, although further research is required to fully quantify the value. [C5924]

"A production line for forest stem volume measurements from VHF SAR data"

Retrieval of forest stem volume has been the main civilian application investigated for VHF SAR data during recent years. Based on promising results obtained from previous studies, a project was defined with the objective to develop a fully integrated system for retrieval of stem volume at high spatial resolution from

CARABAS-II VHF SAR images. Using the developed production line, stem volume can easily be retrieved within predefined forest stands or within homogeneous areas defined by segmentation of optical satellite images. In order to evaluate the accuracy and efficiency of the production line, CARABAS-II images have been collected and analyzed over a test area covering 25425 km². The major part of the area is owned by the Swedish forest company Holmen Skog AB. For coniferous forest stands, exhibiting normal forest production conditions, the accuracy in terms of root mean square error (RMSE) for estimation of forest stem volume is about 44 m³ha⁻¹ (22% of the average stem volume) in the range of 70-400 m³ha⁻¹, using the developed production line. In comparison to earlier research tools, the developed production line speeds up the analyses approximately 10 times. [C5925]

"Fire scar detection in Central Portugal using RADARSAT-1 and ERS-2 SAR data"

A comparative study on backscatter returns from multi-temporal RADARSAT-1 and ERS-2 SAR data has been conducted on a fire-disturbed region of Central Portugal. Six images were examined to detect changes between forest and burnt forest areas. A local incidence angle normalization to 23° was applied to allow a comparison between scenes from different beam modes and SAR instruments. A number of widely distributed sample plots were chosen to characterize different vegetation classes. Both sensors were able to discriminate burnt and unburnt classes. However, no discrimination was possible between the three cover type classes considered, neither before nor after the fire. The similar response from both instruments was associated to the volumetric scattering produced on C-band by vegetation. Small differences in backscatter values can only be explained by the soil moisture changes between the dates in which the images were acquired. [C5926]

"Mapping surface-water with Radarsat at arbitrary incidence angles"

Generally, the contrast between water and land in SAR images decreases with decreasing incidence angle. Thus, surface water detection by intensity thresholding requires high incidence angle data. In this work we demonstrate a texture based surface water detector that produces accurate results, independently of the incidence angle. [C5927]

"Simulations of "The historic Southeast Louisiana and Southern Mississippi flood activity during May 8-10th, 1995" to build a prototype GIS/RS based ERAISA (Environmental Risk Assessment Integrative Systems Approach) for Gulf Coastal states of the United States"

The Gulf Coastal states region of United States is prone to the highest national frequency of both severe weather and climate problems accompanied by economic losses (e.g., severe convection, flooding, tropical cyclones, ice storms etc.). A GIS/remote sensing (RS) framework is necessary to properly understand physical processes, investigate cause and affect relationships and develop conceptual models of the behavior of environmental systems. Our goals included focusing on the environmental effects and impacts of heavy rains and flash flooding and finally to produce a prototype GIS/RS Environmental Risk Assessment System (ERAISA) for the region of interest. We selected "The historic Southeast Louisiana and Southern Mississippi flood activity during May 8-10th, 1995" as our study case. The NCAR/Penn State Mesoscale Model (MM5) is used to study the effects of warm sea surface temperature anomalies, sea surface pressure and winds on the precipitation characteristics of this event. Mesoscale model simulations are used to forecast and better understand the physics associated with the flood event. Each component is modified to accommodate the detailed study. For the preliminary model run, a doubly nested domain centered over the Central Gulf of Mexico with grid spacing of 90 km and 30 km is employed. MM5 is run for each 6 hr period, from the initial storm development-May 8th and through May 10th. NCEP/NCAR reanalysis data and synoptic data are used for constructing the initial and boundary conditions. The model simulations are compared with radar data for further comparisons and validations. The phenomenon of interest-flooding here is narrowly defined in order to depict, analyze and predict (or manage) environmental dynamics through the use and application of GIS and RS data and technologies. A major goal is to unify our understanding and knowledge of similar historic events into a more comprehensive integrative framework from different disciplines-meteorology, marine and fisheries sciences, environmental sciences etc., and develop a system of Integrated Environmental Risk Assessment for the Gulf Coast, which would be ultimately used for operational use. [C5928]

"Polarimetric analysis of P-BAND SAR data acquired over a forested area: "the PYLA 2001 experiment""

P-band airborne SAR (the French RAMSES facility) data were acquired in the framework of the PYLA 2001 project. Images from the Nezer forest are investigated by means of a Van Zyl classification scheme. A new relation between the classification in terms of backscattering mechanisms and the mean height of the trees is proposed. [C5929]

"Biomass estimation of Thetford forest from L-band SAR data: potential and limitations"

This paper summarises the results of two pieces of work (i) a comparison of the relative ability of the AirSAR and E-SAR sensors, to estimate stand volume, age and height, (ii) an analysis of the sensitivity of observed backscatter change to changes in stand height and volume between 1991 (AirSAR data) and 2000 (E-SAR data). In both cases the method employs neural network and linear multivariate models to generate relationships between backscatter and stand volume/age/height. Experiment 1 shows the estimates of tree height, age and timber volume, from the AirSAR and E-SAR sensors have similar levels of accuracy, with the use of the E-SAR coherence data appearing to compensate for the lack of P-band data. The results of experiment 2 show change in height and percentage volume are estimated with a percentage RMSE of less than 10%. [C5930]

"Comparison of tree height estimations from C and L-band InSAR data"

Average height of forest stand is an important parameter related to forest ecological function and carbon cycling. Estimation of stand height using remote sensing data becomes possible due to the new technologies. Interferometry synthetic aperture radar (InSAR) technology uses the phase information of radar returns to get three-dimensional information of the earth surface. The existence of trees in a radar pixel modifies the phase information, so InSAR data has been studied for its potential of tree height estimation. In this study, the C and L-band InSAR data acquired during STR-C/X SAR Mission (1994) were used to estimate average tree height of forest stands in the Daxinganling forest region in Northeast China. The DGPS is used to locate each forest sample plot and the tree heights were measured in 1999. Tree heights in 1994 were deduced from the 1999 field measurements and the tree growth table. The results from C and L bands were compared. Following conclusions were drawn from the study: (i) Stand height information can be acquired from the digital surface model (DSM) generated from InSAR data, (ii) If the forest stand is very uniform in terms of tree height and density, the C-band InSAR data gives better result than L band. Otherwise, the results from L-band InSAR data are more stable, (iii) Multi-temporal InSAR technology may be used to monitor stand height increment. [C5931]

"Blue-ice domain discrimination using interferometric coherence in Antarctic Grove Mountains"

Discrimination of blue-ice domain is very important for meteorolite searching and Antarctic inland ice sheet evolution research. Application of SAR interferometric coherence to blue-ice domain target discrimination is studied over polar inland ice. For the region of Grove Mountains in East Antarctica, interferometric coherence analysis is carried out for a pair of tandem ERS- 1/2 SLC full scenes acquired in February 1996. The investigation indicates significant differences in coherence between blue-ice and other ice sheet features, providing possibilities for target discrimination. The generated blue-ice domain map is compared to a reference blue-ice domain map extracted from TM image acquired in 1990. The final results indicates good consistency. [C5932]

"Stem volume retrieval at stand level using multiple low-frequency SAR images"

In this paper the ground slope effect on stem volume retrieval from VHF-band SAR images has been studied using multiple co-registered images acquired from different flight headings. Accurate measurements of the topography were used as additional input data to a model of the backscatter amplitude variation with ground slope and aspect angle. Modeling this topographical effect on the radar backscatter provides a base for improvement of the stem volume retrieval. [C5933]

"Radarsat data for Siberian plain ecosystems classification"

Radarsat data validity in classification of Siberian plain taiga ecosystems along the Yenisei River (IGBP transect, 90°E) was analyzed. Six test areas were selected. Those areas represent a variety of the main ecosystem and physical-geographical conditions from the tundra to the southern taiga (forest) zones. The analysis of Radarsat signal amplitude, textural characteristics and digital elevation fused data allowed the detection of 18 on-ground classes. For the purpose of classification the importance of parameters are arranged as follows: relief, signal amplitude, skewness, variance, mean Euclidean distance and kurtosis. The main advantage of the Radarsat data is its ability to detect hydromorphic elements (7 bog types were determined). [C5934]

"Tropical forest biomass measurement by backscatter and DEM information as derived from airborne SAR"

A new approach to tropical forest biomass monitoring with airborne interferometric X- and P-band SAR data is presented. For the first time radar backscatter is used along with remotely sensed vegetation height to measure tropical forest biomass. The statistical models yield excellent fit statistics, and the well-known 'backscatter

saturation effect' is overcome. This research is discussed in more detail. [C5935]

"Effect of dielectric properties of moist salinized soils on backscattering coefficients extracted from RADARSAT image"

This paper presents the experimental results regarding changes in the dielectric properties of artificially moistened and salinized soils and on soil samples taken from a salt lake. The complex dielectric constants of soil samples were measured using a microwave network analyzer. We evaluated the real and imaginary parts of dielectric constants of artificially moistened and salinized soil samples prepared in the laboratory as a function of microwave frequency, salinity, and water content. The frequency and the salinity of soils have little influence on the real part of dielectric constant ϵ' . The results show that, in the frequency range of 1-6 GHz, the imaginary part ϵ'' has greater sensitivity to soil salinity. The dielectric constant measurements for soil samples collected in Jilantai Salt Lake are in agreement with the results of the artificially moistened and salinized laboratory soil samples. These dielectric measurements were subsequently compared with the backscattering coefficients extracted from a RADARSAT image (C-HH) that was acquired at same time with the soil sampling at the Jilantai Salt Lake area. We discovered that the correlation coefficient between σ_0 extracted from the RADARSAT image and ϵ'' measured in the soil sample is 0.70. The correlation coefficient between σ_0 and the soil sample salinity is 0.69. This suggests that soil salinity has a significant contribution to the backscattering coefficient, σ_0 recorded in a SAR image. Consequently, a SAR image can be a useful tool for monitoring soil salinity. [C5936]

"Precision ocean salinity measurements using the Passive Active L/S-band aircraft instrument"

Ocean salinity measurements using the Passive Active L/S-band instrument flying on the NCAR C-130 aircraft were made in July 2002 near Monterey, CA. When the radiometer data were corrected for the SST using the Klein and Swift salinity model and surface roughness effects using the L-band scatterometer, the retrieved salinity measurements had an RMS difference of 0.2-0.3 psu when compared with the R/V Point Sur ship measured salinity data. [C5937]

"Aquarius instrument design for sea surface salinity measurements"

Sea surface salinity is a key parameter for the study of ocean circulation, global water cycle and hence climate changes. In response to these measurement needs, Aquarius was selected recently for the third NASA Earth System Science Pathfinder (ESSP) Announcement of Opportunity for a planned launch date in September 2008. The characteristics of the Aquarius instrument are provided in this paper. [C5938]

"Calibration of the CONSERT/ROSETTA radar"

The ROSETTA/ESA probe will probably rendezvous Comet 67P/Churyumov-Gerasimenko in 2014 and launch a Lander at the nucleus surface. The CONSERT instrument will perform the sounding of the comet nucleus by measuring a 90 MHz electromagnetic wave propagation from the Lander to the orbiter throughout the nucleus. The goal of this sounding is to determine the internal structures of the comet nucleus at different scales and to deduce information on its composition (density, type and abundance of the refractor). CONSERT is an original concept of spaceborne transmission radar based on the propagation throughout the nucleus while the classical radars are based on the reflection. This instrument fulfills three functions: a chronometer to measure the propagation delay, an imager based on the multipath propagation and a radiometer to estimate the wave attenuation. The calibration of the instrument should characterize these three functions but due to the novelty of the instrument concept we have no classical set of parameters to quantify the instrument performances from a data-inversion point of view. The instrument design and the absence of calibration channel due to mass and power constraints require specific signal processing and calibration protocol. In this paper, we review the instrument, its objectives and its time transponder structure. Then we present the philosophy of the calibration. In particular we present the results of the instrument ground calibration and the planned in-fly calibration. [C5939]

"Marsis radar signal simulation"

We are going to present here a radar sounding simulation which could be used to validate the radar echoes processing and to support the interpretation of the future Marsis data. In order to follow the Marsis radar sounding process scheme, the first step in the building of our simulation was to model the Martian surface. Many surface modelisation methods have been developed and can be found in the literature, but considering the fact Martian surface is mostly smooth, the modelisation algorithm we developed uses the Facet Method scheme. We will show that this method is a valuable process to model a smooth surface. This method is a very fast one, the computation time it takes is short comparatively to other methods. We will discuss the implementation of the algorithm and show results. Then this surface model allowed us to simulate the global radar echoes. We will present results of simulations using the model of Martian surface and adding some subsurface structures. The

instrument simulation we defined makes strict reference of the Marsis radar settings, anyway it may model any SAR radar with a nadir looking configuration. [C5940]

"Potentiality of RADARSAT-1 images in the detection of salt affected soils in the arid zone: Wadi El-Natrun, Egypt"

This paper presents a simulation comparative study of the effect of salt on the imaginary part (ϵ'') of the dielectric constant (ϵ) and therefore on the backscattering coefficient (σ_0). Mixing model is adapted to estimate this effect on Soil of Wadi El-Natrun area, west desert of Egypt, as a representative area of salt affected soils in the arid zone. Small perturbation backscattering coefficient model (SPM) is also used to estimate the best mode of RADARSAT-1. S1 and S3 were found to be the best choice to detect such type of soil for this area and similar one. [C5941]

"Iceberg identification in the Eurasian Arctic using SAR images"

SAR studies on iceberg identification were conducted in Franz-Joseph Land, Novaya Zemlya, and Severnaya Zemlya. Field observations were used for SAR image interpretation. [C5942]

"A low frequency wideband depth sounder for sea ice"

Sea ice plays an important role in the Earth climate system. Techniques used in the past to determine sea ice thickness had fundamental limitations in terms of spatial and temporal coverage. We performed extensive simulations using published ice-core data from both polar regions, and our results suggested the use of a UHF radar system (300-1300 MHz) for sounding thin Antarctic sea ice and thin ice in the Arctic and a VHP radar system (50-250 MHz) for sounding thick Arctic sea ice. Based on the simulation results, we designed a prototype radar system that operates on both the frequency ranges. We have successfully used the system to collect data over sea ice at Barrow, Alaska. The experiments show that with our system, we can measure sea ice thickness with less than 20 cm uncertainty in thickness. [C5943]

"Sensitivity of satellite observations to snow characteristics"

The sensitivities of a large range of satellite observations to snow characteristics are evaluated and compared, for a winter season, for the Northern hemisphere. Satellite measurements include passive (SSM/I emissivities) and active (ERS scatterometer) microwaves, along with visible reflectances (AVHRR). The satellite responses are systematically compared with in situ snow measurements at 493 stations, in North America and Eurasia. Passive microwaves at high frequency (85 GHz) are very sensitive to the presence snow on the ground, even for very low snow depth. None of the tested satellite measurements is well correlated with the snow depth, at a global scale, making snow depth retrieval from these observations difficult. Active microwave observations show a high sensitivity to the onset of snow melting. [C5944]

"Development of a cross-platform (SMMR and SSM/I) passive microwave derived snow water equivalent dataset for climatological applications"

When Special Sensor Microwave/Imager (SSM/I; in operation 1987 to present) and Scanning Multichannel Microwave Radiometer (SMMR; 1978-1987) data are combined, the time series of dual polarized, multichannel, spaceborne passive microwave brightness temperatures extends from 1978 to the present. The Meteorological Service of Canada (MSC) has developed operational snow water equivalent (SWE) retrieval algorithms for western North America that can be applied to both SMMR and SSM/I data. Evaluation of this cross-platform time series shows that SWE estimates derived during SMMR winter seasons are systematically and significantly lower than retrievals during SSM/I seasons if no brightness temperature adjustments are employed. An examination of co-located brightness temperatures over terrestrial surfaces of central North America during the SMMR and SSM/I overlap period of August 1987 show that SSM/I brightness temperatures systematically exceed SMMR measurements, with the magnitude of this difference dependant on overpass time and brightness temperature magnitude. Regression relationships were determined using data from the overlap period, and utilized to adjust midlatitude terrestrial SMMR data to an SSM/I F-8 baseline. A SWE time series was subsequently reprocessed using these adjusted SMMR brightness temperatures. The resulting SWE dataset produces a time series of acceptable cross-platform homogeneity when assessed with in situ SWE measurements and remotely sensed snow extent data. Climatological research questions that demand a time series of significant length can now be confidently addressed with this passive microwave derived dataset. [C5945]

"An ultra-wideband radar for measurements of snow thickness over sea ice"

Snow cover of variable thickness exists on sea ice with thickness fluctuations in the range from less than a few

centimeters to several meters depending on snow drifts and ice type. Snow largely controls the thermal and electrical properties of a sea ice cover. Because of its low thermal conductivity, it effectively insulates the sea ice surface from cold polar air and modifies the heat flux between the atmosphere and ocean. It also changes the sea ice albedo. Additionally, thick snow cover acts as a mechanical load and can depress the ice surface below sea level, causing the ice floe to be flooded with sea water. Thus accurate knowledge of snow thickness on sea ice is essential for determining the overall heat budget in the polar regions, which in turn can impact global ocean circulation and climate. We developed an ultra-wideband radar for measuring snow thickness. It operates over the frequency range from 2-8 GHz in FM-CW mode. We used a phase-locked YIG oscillator to generate a very linear 2-8 GHz chirp by using a low-frequency (5-20 MHz) digital chirp generator as a reference signal for the phase detector. We also constructed a receiver with a large dynamic range and fast settling time. The received signal was digitized using a 12-bit A/D converter and stored for further processing. We also developed simple models to simulate radar performance. We modeled snow as a multi-layered media and sea ice as dielectric half-space, and performed extensive simulations using snow geophysical data collected during Antarctic cruises to optimize radar performance. We evaluated the radar's performance by measuring its response to point targets such as a delay line and corner reflectors. With the Hanning window function, the measured radar range resolution is about 3.75 cm. We collected data on snow-covered ground in conjunction with measurements of snow parameters such as density, particle size, and roughness. The results from these measurements show that we can clearly delineate returns of the snow-air and snow-ground interfaces for 6-cm-thick dry snow. [C5946]

"Optical flow and scale-space theory applied to sea-ice motion estimation in Antarctica"

Sea-ice motion in Antarctica is studied applying methods from computer vision and scale-space theory to a sequence of images obtained from scatterometer data. The proposed method can obtain a dense motion vector field for any specific observation scale. Spatial and temporal scales are used to focus on relevant geophysical features and events. A preprocessing stage involving spatial and temporal filtering at selected scales reduces noise and artifacts produced in the image generation phases, allowing reliable feature extraction and tracking at relevant scales. Optical flow (OF) methods provide a dense estimation of the motion field. The limitations and advantages of this approach are discussed. Optical flow sea-ice motion data are in agreement with sea winds data obtained independently and with very different methodologies. OF results are compared to data from wavelet methods. [C5947]

"Variations of sea ice extent in the Caspian and Aral seas derived from combination of active and passive satellite microwave data"

The paper discusses time and space variations of ice cover in the Caspian and Aral seas. We use the synergy of data from active (radar altimeter) and passive (radiometer) microwave instruments onboard the TOPEX/Poseidon satellite, as well as passive microwave data from SSMR and SSM/I sensors. The results indicate significant spatial and temporal variability of ice conditions, with a marked decrease of both duration of ice season and ice extent during winters 1998/99-2001/02. The satellite-derived time series of sea ice parameters are very valuable in view of the heterogeneous and mostly unpublished data on ice conditions over the Caspian and Aral seas since the mid-1980s. [C5948]

"Detection of oil slick signatures in SAR images by fusion of hysteresis thresholding responses"

A new method is proposed in this paper to detect oil slick signatures in oceanographic SAR images. This method is based on directional behavioural oil slick in the sea surface. Therefore, directional hysteresis thresholding responses are first computed in order to bring to the fore dark spots, and increase pixels connexity in each Freeman direction. Those responses are then merged with the help of a Context Independent Constant Behaviour (CICB) operator. The proposed method is tested on ERS SAR amplitude images of Mediterranean and Atlantic seas. The obtained results are promising and show a good qualitative detection. [C5949]

"Evaluation of ENVISAT ASAR data for measurement of surface wind field over the Korean east coast"

The detailed knowledge of ocean surface wind field is useful for understanding of ocean circulation and variability in a specific spatial and temporal window. An efficient way to obtain such information in sufficient density is through satellite remote sensing. The most recent environmental observation satellite, ENVISAT, has an Advanced Synthetic Aperture Radar (ASAR), which operates at C-band frequency. The ASAR has the potential of retrieving sea surface wind field more accurately than the ERS-1/2 AMI because the ASAR can collect high resolution images with a various viewing geometry and simultaneously in two polarization mode. Several ASAR images including alternating polarization mode and wide swath mode were obtained off the eastern coast of

Korean peninsula during the winter season. Simultaneously, we installed two corner reflectors on the near beach to calibrate ENVISAR ASAR data. In this paper we combined polarization ratio models and modified C-band VV-polarization wind speed retrieval models (CMOD_4 and CMOD_IFR2) to apply them to ASAR alternating polarization mode data. We compared the resulting wind fields estimated from ENVISAT ASAR data with wind speed and direction measured by the several coastal automatic weather systems and two ocean buoys which are deployed at 10 km and 100 km off the east coast of Korean peninsula respectively. [C5950]

"Estimation of directional wave spectra from SAR image"

A new inverse estimation method based on a Bayesian theorem is proposed for estimating directional wave spectra from SAR image. Numerical simulation was used to examine the validity and accuracy of the proposed method. The benchmark directional wave spectra and the estimated directional wave spectra were compared, and they show good agreement. [C5951]

"Correcting scatterometer ocean measurements for rain effects using radiometer data: application to SeaWinds on ADEOS-2"

Measurements of ocean scattering by the SeaWinds on ADEOS-II can be corrupted by presence of rain. To correct for this, we must first estimate the rain rate and storm height, and use these to estimate the attenuation through and backscatter from the rain. ADEOS-II carries the AMSR radiometer, with rain rate as one product. Either this or an algorithm using the brightness temperature can provide attenuation. Finding storm height requires correlation with some measured parameter; after studying several approaches, we found that the storm height relates well enough with rain rate to use the AMSR rain rate as the input to get height. We show here the results of simulations of performance of the correction algorithm using the imperfect actual correlation between storm height and rain rate. We find that corrections are possible up to a rain-rate threshold that depends on the surface wind speed and direction. Above the threshold, one must discard the data by setting a rain flag. We show threshold curves for allowable errors (due to rain height errors) of 5%, 10%, and 15%. Unacceptable errors are largely due to rain echo that greatly exceeds the surface echo. [C5952]

"Offshore wind maps from ERS-2 SAR and wind resource modelling"

ERS-2 SAR satellite scenes in PRI format are calibrated and processed into offshore wind maps for a site in the North Sea. The wind direction is retrieved by the two-dimensional Fast Fourier transform method, and the wind direction is used as input to the CMOD-IFR and CMOD-4 scatterometer algorithms for the calculation of wind speed maps. The wind speed maps are regridded to 400 m by 400 m in order to reduce noise. Each of the wind maps are compared to high-quality meteorological in-situ observations collected from a 62 m tall mast located 14 km offshore. The development of offshore wind farms is in rapid growth. In the planning phase of such wind farms, it is important to assess the wind resources. A new wind resource mapping method based on satellite SAR images may prove useful. A pc-software has been developed for applied use and is presented here. [C5953]

"RADARSAT-1 SAR scenes for wind power mapping in coastal area: Gulf of St-Lawrence case"

Mapping of offshore wind fields is expected to receive increasing attention within the wind power community in the near future to estimate the wind power potential on coastal areas. RADARSAT-1 satellite can be used for wind resource mapping in coastal regions at a high spatial resolution if wind direction data are available. This paper presents an approach to obtain accurate wind maps from RADARSAT-1 scenes on the Gulf of St. Lawrence using collocated data (in situ and QuickSCAT measurements) and hybrid model (CMOD-IFR2 with polarization ratio). We indicate the theoretical best configuration of RADARSAT-1 products for wind retrieval using a hybrid model. Based on a set of six SAR scenes chosen to match the most typical wind conditions, first results are discussed. Those results already indicate accurate wind estimation close to the coast. Also wind patterns over large area are available and can help to plan more accurate wind power measurements. Specific considerations of wind power mapping are reviewed and finally, future developments of the project are presented. [C5954]

"Evaluating the offshore wind potential. A combined approach using remote sensing and statistical methods"

In the framework of the current development of offshore wind energy exploitation, an accurate evaluation of the wind potential is crucial for siting windmills. There is a strong need for accurate statistical data from non-intrusive means, such as spaceborne radar data. This paper deals with the methodology developed to provide accurate offshore wind potential statistics. The method developed to obtain accurate wind maps from ERS SAR (synthetic aperture radar) images is presented. Then, considering the need of dense statistical information for evaluating

the wind potential, a data fusion methodology is exposed. [C5955]

"An empirical model to retrieving ocean wave period from nadir altimeter data"

Accurate measurement of the ocean wave period is of much scientific interest both operationally and for research. Shipping and offshore industries are keen to obtain real-time and climatological information on wave period in the open ocean to assist the design of sea-going structures and maximise safety at sea. Similarly, wave period is relevant for short-to-medium term ocean and weather forecasting, and more broadly, to ocean circulation and climate research, given the reported dependence of atmosphere-ocean momentum transfer on some measure of sea state development. In principle, full ocean wave spectra can be obtained from satellite synthetic aperture radars (SAR), yet the systematic extraction of wave period information from SAR has so far not been pursued. Hence, global wave period information is presently available only through numerical wave models, and there remain concerns about the lack of large scale validation of the geographical distribution and temporal variability of the modelled ocean waves. Here, we propose that ocean wave period information can be retrieved with adequate accuracy using satellite altimeters. There is evidence that satellite altimeter data contain wave period information, in addition to that on wave height. The existence of sea state development effects on the retrieval of altimeter wind speed is well documented and a few earlier studies have already considered the development of altimeter wave period models. However, the sea state dependence in these semi-empirical models is complex, and in both cases, the datasets of collocated altimeter/buoy measurements used to develop the models spanned only a small range of environmental conditions. In this paper, we present preliminary results of a new, purely empirical, wave period algorithm developed on the basis of the largest to-date dataset of collocated altimeter/buoy spectra measurements. The empirical wave period model is validated using independent collocated altimeter/buoy data, and by computing global monthly wave climatology. These are compared with existing wave period climatologies derived from numerical wave models. [C5956]

"An airborne campaign measuring wind signatures from the sea surface using an L-band polarimetric radiometer"

A series of circle flights have been carried out over the sea surface, using the EMIRAD L-band polarimetric radiometer. Motion compensation is applied, and polarimetric azimuth signatures are generated. Single tracks show geophysical noise, typically about 2 K, but averaging decreases the noise, producing signatures with variations below 500 mK. A harmonic analysis of the results provides no clear signature, and for the 2nd, 3rd, and 4th Stokes parameters it is shown, that a significant part of the signal must be due to Gaussian noise. The 1st Stokes parameter is shown to have a 500 mK 2nd harmonic, but a comparison of the signature to the downwelling galactic background radiation indicates, that the signature may not origin from the wind driven sea surface pattern. [C5957]

"Operational applications of RADARSAT-1 for the monitoring of natural oil seeps in the South Gulf of Mexico"

The origin of the oil activity in Campeche Sound is closely related to the activity of the natural oil seeps. At the moment, the operational areas with greater production in the Cantarell field from PEMEX Exploration and Production (PEP), coincide with the activity of the most important seep in the south of the Gulf of Mexico. With the intention of establishing the origin and magnitude of the hydrocarbon contributions of the natural seeps in this area, the Northeast Marine Region (RMNE) of PEP, with the support of the Subdivision of Technology and Development (STDP) of PEP and the Corporative Unit of Geographic Information Systems (SICORI) developed during the 2000-2001 with RADARSAT International and RADARSAT Resource Center in Brazil a progressive application of the RADARSAT-1 satellite to evaluate oil seep potentiality in detection and measurement, being allowed to establish a proven method for the monitoring of oil seep behavior. The methodology is applied in a continuous way from 2002 and includes a regional criterion for the selection of images, basic and advanced digital analysis utilizing the Unsupervised Semivariogram Textural Classifier (USTC), and meteo-oceanographic calibration. The methodology also correlates geologic and environmental information. The results shown activity of the Cantarell seep in 79.5% of the 83 images analyzed during 2000-2002. Area coverage of Cantarell seep from 66 images ranks between 0.04 to 207.4 km², with an average area of 32 km². RADARSAT-1 analysis identified that the main hydrocarbon contribution, in area as well as frequency for South Gulf of Mexico, comes from the natural oil seeps, particularly from the Cantarell field. This project also demonstrates the viability of the integration of disciplinary groups within PEMEX for the development of new technologies with multiple applications that allow the optimization of resources and enhance the availability of environmental tools. [C5958]

"Automatic detection of oil spills in ENVISAT, Radarsat and ERS SAR images"

We present a framework for automatic detection of oil spills in SAR images. Multi incident angle and multi

polarization SAR data are ingested into the framework in order to optimize revisit times and thereby the temporal and spatial coverage. Dark spots in the images are primarily detected by adaptive thresholding. For each of them a number of features are computed in order to classify the slick as either an oil slick or a 'look-alike' (other oceanographic phenomena which resemble oil slicks). A classification scheme is utilized based on statistical modeling. A data set of about 100 images from each of the sensors ERS, Radarsat and ENVISAT is or will soon be available to train and test the algorithm. In this paper, only results from ERS and Radarsat are reported because the access of ENVISAT images has been delayed. [C5959]

"Passive polarimetric remote sensing of the ocean surface during the Rough Evaporation Duct experiment (RED 2001)"

This paper describes the deployment of a fully polarimetric K-band radiometer in the Rough Evaporation Duct (RED) experiment, which was conducted during August and September of 2001. The calibration of the four Stokes parameters is described, along with a comparison of the measurements with results of both the Klein-Swift and Ellison et al. sea surface dielectric models. The purpose of the experiment was to improve physical forward models of the ocean surface emission in order to improve wind vector retrieval algorithms. [C5960]

"Spatial domain techniques to derive sea state parameters from ERS and ENVISAT SAR imageries"

So far mainly one dimensional wave measurements (e.g. buoy time series) have been collected and analyzed. Using new measurement techniques, like Synthetic Aperture Radar (SAR) based ones (e.g. using ERS-1/2 and ENVISAT SAR Imagettes), it is now possible to retrieve two dimensional sea surface elevations. New analysis techniques have been found to examine these data. As in time series wave crests and troughs follow each other simply as alternating maximum and minimum points, in two dimensions the situation is more complicated. A so-called 'Spider' algorithm has been developed creating an assignment of corresponding crest and trough points on a two dimensional sea surface. This allows examination of individual wave parameters like individual wave height or steepness to be compared with global and statistical ones on the surface itself, like significant wave height and sea surface gradient. In addition, grouping parameters can be generalized in the spatial domain. Image analysis also allows parameters not available in one dimension like the crest/trough lengths. For statistical examinations, these parameters have been calculated on some 34,000 SAR imageries, globally distributed in a 3 week period in the southern winter. [C5961]

"A scatterometer inversion procedure for the Mediterranean Sea"

In this paper we present a scatterometer inversion procedure capable to deal with data frames in which we have triplets and doublets. This is actually the case of the Wind SCatterometer (WSC) on board of the ERS-2 satellite over the Mediterranean Sea. A set of meaningful experiments is presented. [C5962]

СПИСОК ЛИТЕРАТУРЫ

C4491. Johnson J.T. A study of rough surface thermal emission and reflection using Voronovich's small slope approximation. 2004. IGARSS '04. Proceedings. 2004 IEEE International Geoscience and Remote Sensing Symposium. - Anchorage, AK, 20-24 Sept. 2004. - Vol. 1. - P. 398-401. ↑

C4492. Sletten M.A. Experimental investigation of radar backscatter from plunging breakers using an ultrawideband radar and visible/infrared cameras. / Sletten M.A., Smith G.B., Liu X., Duncan J.H. // 2004. IGARSS '04. Proceedings. 2004 IEEE International Geoscience and Remote Sensing Symposium. - Anchorage, AK, 20-24 Sept. 2004. - Vol. 1. - P. 394-397. ↑

C4493. Smith J.R. Forward scattering phenomena at low grazing. / Smith J.R., Mirotznik M.S. // 2004. IGARSS '04. Proceedings. 2004 IEEE International Geoscience and Remote Sensing Symposium. - Anchorage, AK, 20-24 Sept. 2004. - Vol. 1. - P. 402-405. ↑

C4494. You H. Correlation time analysis of delay-Doppler waveforms generated from ocean-scattered GPS signals. / You H., Garrison J.L., Heckler G., Smajlovic D. // 2004. IGARSS '04. Proceedings. 2004 IEEE International Geoscience and Remote Sensing Symposium. - Anchorage, AK, 20-24 Sept. 2004. - Vol. 1. - P. 428-431. ↑

- C4495.** Rappaport C. A simple approximation of transmitted wavefront shape from point sources above lossy half spaces. 2004. IGARSS '04. Proceedings. 2004 IEEE International Geoscience and Remote Sensing Symposium. - Anchorage, AK, 20-24 Sept. 2004. - Vol. 1. - P. 421-424. ↑
- C4496.** Li Y. Microwave scattering from 3-D breaking water wave crests. / Li Y., West J.C. // 2004. IGARSS '04. Proceedings. 2004 IEEE International Geoscience and Remote Sensing Symposium. - Anchorage, AK, 20-24 Sept. 2004. - Vol. 1. - P. 406-409. ↑
- C4497.** Mette T. Applying a common allometric equation to convert forest height from Pol-InSAR data to forest biomass. / Mette T., Papathanassiou K., Hajnsek I., Pretzsch H., Biber P. // 2004. IGARSS '04. Proceedings. 2004 IEEE International Geoscience and Remote Sensing Symposium. 20-24 Sept. 2004. - Vol. 1. - {no data available}. ↑
- C4498.** Lakshmi V. Microwave remote sensing: a perspective from the last few field experiments. / Lakshmi V., Bolten J., Narayan U. // 2004. IGARSS '04. Proceedings. 2004 IEEE International Geoscience and Remote Sensing Symposium. 20-24 Sept. 2004. - Vol. 1. - {no data available}. ↑
- C4499.** O'Neill P. Comparison of soil moisture retrieval algorithms using simulated HYDROS brightness temperatures. / O'Neill P., Njoku E., Chan T., Crow W., Hsu A., Shi J.C. // 2004. IGARSS '04. Proceedings. 2004 IEEE International Geoscience and Remote Sensing Symposium. 20-24 Sept. 2004. - Vol. 1. - {no data available}. ↑
- C4500.** Dong Qing. Optimum polarimetric analysis of backscattering from rough sea surface. / Dong Qing, Guo Huadong. // 2004. IGARSS '04. Proceedings. 2004 IEEE International Geoscience and Remote Sensing Symposium. 20-24 Sept. 2004. - Vol. 1. - {no data available}. ↑
- C4501.** Valade C. Homomorphic wavelet transform and new subband statistics models for SAR image compression. / Valade C., Nicolas J.-M. // 2004. IGARSS '04. Proceedings. 2004 IEEE International Geoscience and Remote Sensing Symposium. 20-24 Sept. 2004. - Vol. 1. - {no data available}. ↑
- C4502.** Yueh S.H. Windsat validation using seawinds, windrad and polscat measurements. / Yueh S.H., Wilson W.J., Dinardo S., Hsiao S.V. // 2004. IGARSS '04. Proceedings. 2004 IEEE International Geoscience and Remote Sensing Symposium. - Anchorage, AK, 20-24 Sept. 2004. - Vol. 1. - P. 390-393. ↑
- C4503.** Sanchez F.I. Design and implementation of a miniaturized water vapor profiling radiometer. / Sanchez F.I., Reising S.C., Jackson R.W. // 2004. IGARSS '04. Proceedings. 2004 IEEE International Geoscience and Remote Sensing Symposium. 20-24 Sept. 2004. - Vol. 1. - {no data available}. ↑
- C4504.** Tsutsui K. Data fusion techniques of heterogeneous sensor images for debris hazard assessments. / Tsutsui K., Miyazaki S., Nakagawa H., Shiraishi T., Rokugawa S. // 2004. IGARSS '04. Proceedings. 2004 IEEE International Geoscience and Remote Sensing Symposium. 20-24 Sept. 2004. - Vol. 1. - {no data available}. ↑
- C4505.** Aggarwal V. Multiple-model multiscale data fusion regulated by a mixture-of-experts network. / Aggarwal V., Nagarajan K., Slatton K.C. // 2004. IGARSS '04. Proceedings. 2004 IEEE International Geoscience and Remote Sensing Symposium. 20-24 Sept. 2004. - Vol. 1. - {no data available}. ↑
- C4506.** Rincon R.F. Forward and backscattering measurements of rainfall using the NASA Microwave Link. / Rincon R.F., Lang R., Meneghini R., Kurum M., Stich J. // 2004. IGARSS '04. Proceedings. 2004 IEEE International Geoscience and Remote Sensing Symposium. - Anchorage, AK, 20-24 Sept. 2004. - Vol. 1. - P. 432-435. ↑
- C4507.** Hallberg B. Performance simulation of spaceborne P-band SAR for global biomass retrieval. / Hallberg B., Smith G., Olofsson A., Ulander L.M.H. // 2004. IGARSS '04. Proceedings. 2004 IEEE International Geoscience and Remote Sensing Symposium. - Anchorage, AK, 20-24 Sept. 2004. - Vol. 1. - P. 503-506. ↑
- C4508.** De Grandi G. The GBFM radar mosaic of the Eurasian Taiga: selected topics on geo-location and preliminary thematic products. / De Grandi G., Spirolazzi V., Rauste Y.A., Curto L., Rosenqvist A., Shimada M. // 2004. IGARSS '04. Proceedings. 2004 IEEE International Geoscience and Remote Sensing Symposium. - Anchorage, AK, 20-24 Sept. 2004. - Vol. 1. - P. 507-510. ↑
- C4509.** Gong Min. Analysis of the virtual baseline of cluster SAR satellites. / Gong Min, Zhang Chuanwu,

Zhang Xiaoling, Huang Shunji. // 2004. IGARSS '04. Proceedings. 2004 IEEE International Geoscience and Remote Sensing Symposium. - Anchorage, AK, 20-24 Sept. 2004. - Vol. 1. - P. 500-502. ↑

C4510. Costantini M. SAR interferometric baseline calibration without need of phase unwrapping. / Costantini M., Minati F., Quagliarini A., Schiavon G. // 2004. IGARSS '04. Proceedings. 2004 IEEE International Geoscience and Remote Sensing Symposium. - Anchorage, AK, 20-24 Sept. 2004. - Vol. 1. - P. 493-495. ↑

C4511. Addesso P. On the influence of the surface fractal dimension on the IFSAR baseline decorrelation. / Addesso P., Longo M., Restaino R., Tesaro M. // 2004. IGARSS '04. Proceedings. 2004 IEEE International Geoscience and Remote Sensing Symposium. - Anchorage, AK, 20-24 Sept. 2004. - Vol. 1. - P. 496-499. ↑

C4512. Peng Xu. Texture classification using optimized support vector machines. / Peng Xu, Min Dai, Chan A.K. // 2004. IGARSS '04. Proceedings. 2004 IEEE International Geoscience and Remote Sensing Symposium. 20-24 Sept. 2004. - Vol. 1. - {no data available}. ↑

C4513. Ersahin K. Incorporating texture information into polarimetric radar classification using neural networks. / Ersahin K., Scheuchl B., Cumming I. // 2004. IGARSS '04. Proceedings. 2004 IEEE International Geoscience and Remote Sensing Symposium. 20-24 Sept. 2004. - Vol. 1. - {no data available}. ↑

C4514. Folkesson K. Automatic segmentation of multiple VHF-band SAR images to improve stem volume retrieval. / Folkesson K., Smith G., Ulander L.M.H. // 2004. IGARSS '04. Proceedings. 2004 IEEE International Geoscience and Remote Sensing Symposium. - Anchorage, AK, 20-24 Sept. 2004. - Vol. 1. - P. 519-522. ↑

C4515. Mette T. Biomass estimation from polarimetric SAR interferometry over heterogeneous forest terrain. / Mette T., Papathanassiou K., Hajnsek I. // 2004. IGARSS '04. Proceedings. 2004 IEEE International Geoscience and Remote Sensing Symposium. - Anchorage, AK, 20-24 Sept. 2004. - Vol. 1. - P. 511-514. ↑

C4516. Santoro M. Evaluation of JERS-1 L-band SAR backscatter for stem volume retrieval in boreal forest. / Santoro M., Schmullius C., Askne J., Eriksson L. // 2004. IGARSS '04. Proceedings. 2004 IEEE International Geoscience and Remote Sensing Symposium. - Anchorage, AK, 20-24 Sept. 2004. - Vol. 1. - P. 515-518. ↑

C4517. Zrnic D.S. Use of backscatter differential phase in weather surveillance radars. / Zrnic D.S., Melnikov V.M., Ryzhkov A.V. // 2004. IGARSS '04. Proceedings. 2004 IEEE International Geoscience and Remote Sensing Symposium. - Anchorage, AK, 20-24 Sept. 2004. - Vol. 1. - P. 456-458. ↑

C4518. Ferraiuolo G. A Bayesian technique for terrain mapping using multi-frequency ground based interferometric SAR systems. / Ferraiuolo G., Leva D., Nico G., Pascasio V., Schirizzi G., Tarchi D. // 2004. IGARSS '04. Proceedings. 2004 IEEE International Geoscience and Remote Sensing Symposium. - Anchorage, AK, 20-24 Sept. 2004. - Vol. 1. - P. 469-472. ↑

C4519. Reinking R.F. Radar radial velocity variance measurements to decipher mountain-influenced Kelvin-Helmholtz waves, slope flows, and rotors. 2004. IGARSS '04. Proceedings. 2004 IEEE International Geoscience and Remote Sensing Symposium. - Anchorage, AK, 20-24 Sept. 2004. - Vol. 1. - P. 444-447. ↑

C4520. Lim S. Retrieval of reflectivity in a networked radar environment. / Lim S., Chandrasekar V., McLaughlin D. // 2004. IGARSS '04. Proceedings. 2004 IEEE International Geoscience and Remote Sensing Symposium. - Anchorage, AK, 20-24 Sept. 2004. - Vol. 1. - P. 436-439. ↑

C4521. Cuccoli F. Spatial rainfall rate estimation through combined use of radar reflectivity and raingauge data. / Cuccoli F., Facheris L., Giuli D., Meoni L. // 2004. IGARSS '04. Proceedings. 2004 IEEE International Geoscience and Remote Sensing Symposium. - Anchorage, AK, 20-24 Sept. 2004. - Vol. 1. - P. 440-443. ↑

C4522. Chen C.W. Mitigation of tropospheric InSAR phase artifacts through differential multisquint processing. 2004. IGARSS '04. Proceedings. 2004 IEEE International Geoscience and Remote Sensing Symposium. - Anchorage, AK, 20-24 Sept. 2004. - Vol. 1. - P. 485-488. ↑

C4523. Marinkovic P. Advanced InSAR coregistration using point clusters. / Marinkovic P., Hanssen R. // 2004. IGARSS '04. Proceedings. 2004 IEEE International Geoscience and Remote Sensing Symposium. - Anchorage, AK, 20-24 Sept. 2004. - Vol. 1. - P. 489-492. ↑

C4524. Veneziani N. Height retrieval by using a pseudo-differential approach in SAR interferometry preliminary results with actual SAR data. / Veneziani N., Giacobazzi V.M., Bovenga F. // 2004. IGARSS '04. Proceedings.

2004 IEEE International Geoscience and Remote Sensing Symposium. - Anchorage, AK, 20-24 Sept. 2004. - Vol. 1. - P. 481-484. ↑

C4525. Shimada M. Repeat pass SAR interferometry of the Pi-SAR (L) for DEM generation. / Shimada M., Furuta R., Watanabe M., Tadono T., Rosenqvist A. // 2004. IGARSS '04. Proceedings. 2004 IEEE International Geoscience and Remote Sensing Symposium. - Anchorage, AK, 20-24 Sept. 2004. - Vol. 1. - P. 473-476. ↑

C4526. Eineder M. Avoiding phase unwrapping in DEM generation by fusing multi frequency ascending and descending interferograms. / Eineder M., Adam N. // 2004. IGARSS '04. Proceedings. 2004 IEEE International Geoscience and Remote Sensing Symposium. - Anchorage, AK, 20-24 Sept. 2004. - Vol. 1. - P. 477-480. ↑

C4527. Bignami C. Comparing and combining the capability of detecting earthquake damages in urban areas using SAR and optical data. / Bignami C., Chini M., Pierdicca N., Stramondo S. // 2004. IGARSS '04. Proceedings. 2004 IEEE International Geoscience and Remote Sensing Symposium. 20-24 Sept. 2004. - Vol. 1. - {no data available}. ↑

C4528. Zhanqiang Chang. Study on land subsidence evolvement tendency by means of "integrated DInSAR". / Zhanqiang Chang, Jingfa Zhang, Qingshi Guo, Lixia Gong. // 2004. IGARSS '04. Proceedings. 2004 IEEE International Geoscience and Remote Sensing Symposium. 20-24 Sept. 2004. - Vol. 1. - {no data available}. ↑

C4529. Zou Q. Wind vector inversion from RADARSAT SAR images: a new algorithm. / Zou Q., He Y., Perrie W., Vachon P. // 2004. IGARSS '04. Proceedings. 2004 IEEE International Geoscience and Remote Sensing Symposium. 20-24 Sept. 2004. - Vol. 1. - {no data available}. ↑

C4530. Horstmann J. Evaluation of an operational SAR wind field retrieval algorithm for ENVISAT ASAR. / Horstmann J., Koch W. // 2004. IGARSS '04. Proceedings. 2004 IEEE International Geoscience and Remote Sensing Symposium. 20-24 Sept. 2004. - Vol. 1. - {no data available}. ↑

C4531. Soisuvarn S. Validation of ocean surface wind vector sensing using combined active and passive microwave measurements. / Soisuvarn S., Jones W.L., Kasparis T. // 2004. IGARSS '04. Proceedings. 2004 IEEE International Geoscience and Remote Sensing Symposium. 20-24 Sept. 2004. - Vol. 1. - {no data available}. ↑

C4532. Berizzi F. Sea SAR image analysis by fractal data fusion. / Berizzi F., Martorella M., Bertini G., Garzelli A., Nencini F., Dell'Acqua F., Gamba P. // 2004. IGARSS '04. Proceedings. 2004 IEEE International Geoscience and Remote Sensing Symposium. 20-24 Sept. 2004. - Vol. 1. - {no data available}. ↑

C4533. Chambenoit Y. Different fusion strategies to detect geographical objects by active contours in multitemporal SAR images. / Chambenoit Y., Trouve E., Classeau N., Rudant J.-P., Bolon P. // 2004. IGARSS '04. Proceedings. 2004 IEEE International Geoscience and Remote Sensing Symposium. 20-24 Sept. 2004. - Vol. 1. - {no data available}. ↑

C4534. Tupin F. Merging of SAR and optical features for 3D reconstruction in a radargrammetric framework. 2004. IGARSS '04. Proceedings. 2004 IEEE International Geoscience and Remote Sensing Symposium. 20-24 Sept. 2004. - Vol. 1. - {no data available}. ↑

C4535. Farina P. Landslide risk analysis by means of remote sensing techniques: results from the ESA/SLAM project. / Farina P., Moretti S., Colombo D., Fumagalli A., Manunta P. // 2004. IGARSS '04. Proceedings. 2004 IEEE International Geoscience and Remote Sensing Symposium. 20-24 Sept. 2004. - Vol. 1. - {no data available}. ↑

C4536. Lukowski T.I. Pipeline encroachment monitoring using polarimetric SAR imagery. / Lukowski T.I., Power D., Yue B., Randall C.J., Youden J., Howell C. // 2004. IGARSS '04. Proceedings. 2004 IEEE International Geoscience and Remote Sensing Symposium. 20-24 Sept. 2004. - Vol. 1. - {no data available}. ↑

C4537. {no data available}. IGARSS 2004. 2004 IEEE International Geoscience and Remote Sensing (IEEE Cat. No.04CH37612). 2004. IGARSS '04. Proceedings. 2004 IEEE International Geoscience and Remote Sensing Symposium. 20-24 Sept. 2004. - Vol. 1. - {no data available}. ↑

C4538. Guo Huadong. Environmental monitoring with remote sensing data from Chinese spacecraft. / Guo Huadong, Wang Weimin, Wang Changlin, Zhong Ruofei, Zhu Boqin, Chen Jinsong. // 2004. IGARSS '04. Proceedings. 2004 IEEE International Geoscience and Remote Sensing Symposium. 20-24 Sept. 2004. - Vol. 1. - {no data available}. ↑

- {no data available}. ↑

C4539. Wei Song. An improved method of Doppler centroid estimation in SAR. / Wei Song, Fang Zhihong, Wang Hongyuan. // 2004. IGARSS '04. Proceedings. 2004 IEEE International Geoscience and Remote Sensing Symposium. 20-24 Sept. 2004. - Vol. 2. - P. 1530-1533. ↑

C4540. Boncori J.P.M. Implementation of a co/decoding method in SAR processing based on time domain correlation. 2004. IGARSS '04. Proceedings. 2004 IEEE International Geoscience and Remote Sensing Symposium. 20-24 Sept. 2004. - Vol. 2. - P. 1522-1525. ↑

C4541. Boerner E. A new method for Total Zero Doppler Steering. / Boerner E., Fiedler H., Krieger G., Mittermayer J. // 2004. IGARSS '04. Proceedings. 2004 IEEE International Geoscience and Remote Sensing Symposium. 20-24 Sept. 2004. - Vol. 2. - P. 1526-1529. ↑

C4542. Yinghai Ke. 3-D hurricane boundary layer wind retrieval algorithm for airborne Doppler radar measurements. / Yinghai Ke, Xuehu Zhang, Xiuwan Chen, Jilong Yang, Esteban D., Carswell J., Frasier S., McLaughlin D.J., Chang P., Black P., Marks F. // 2004. IGARSS '04. Proceedings. 2004 IEEE International Geoscience and Remote Sensing Symposium. 20-24 Sept. 2004. - Vol. 1. - {no data available}. ↑

C4543. Thompson D.R. Comparison of high-resolution wind maps from SAR imagery with in situ measurements from the ONR CBLAST experiments. / Thompson D.R., Monaldo F.M., Farrar J.T., Weller R.A., Elfouhaily T.M., Grimmer T.K. // 2004. IGARSS '04. Proceedings. 2004 IEEE International Geoscience and Remote Sensing Symposium. 20-24 Sept. 2004. - Vol. 1. - {no data available}. ↑

C4544. Fernandez D.E. C- and Ku-band ocean backscatter measurements under extreme wind conditions. / Fernandez D.E., Kerr E., Frasier S., Carswell J., Chang P., Jelenak Z., Connor L., Black P., Marks F., Alex Zhang. // 2004. IGARSS '04. Proceedings. 2004 IEEE International Geoscience and Remote Sensing Symposium. 20-24 Sept. 2004. - Vol. 1. - {no data available}. ↑

C4545. Moore R.K. Correcting SeaWinds measurements for rain effects. / Moore R.K., Braaten D., Natarajakumar B., Kurisunkal V.J. // 2004. IGARSS '04. Proceedings. 2004 IEEE International Geoscience and Remote Sensing Symposium. 20-24 Sept. 2004. - Vol. 1. - {no data available}. ↑

C4546. Adams I.S. High quality wind retrievals for hurricanes Isabel and Fabian using the SeaWinds scatterometer. / Adams I.S., Jones W.L. // 2004. IGARSS '04. Proceedings. 2004 IEEE International Geoscience and Remote Sensing Symposium. 20-24 Sept. 2004. - Vol. 1. - {no data available}. ↑

C4547. Ainsworth T.L. Polarimetric SAR image classification-exploiting optimal variables derived from multiple-image datasets. / Ainsworth T.L., Lee J.-S. // 2004. IGARSS '04. Proceedings. 2004 IEEE International Geoscience and Remote Sensing Symposium. 20-24 Sept. 2004. - Vol. 1. - {no data available}. ↑

C4548. Lopez-Martinez C. Statistical assessment of eigenvector-based target decomposition theorems in radar polarimetry. / Lopez-Martinez C., Pottier E. // 2004. IGARSS '04. Proceedings. 2004 IEEE International Geoscience and Remote Sensing Symposium. - Anchorage, AK, 20-24 Sept. 2004. - Vol. 1. - P. 192-195. ↑

C4549. Kimura H. Improvement of polarimetric SAR calibration based on the Quegan algorithm. / Kimura H., Mizuno T., Papathanassiou K.P., Hajnsek I. // 2004. IGARSS '04. Proceedings. 2004 IEEE International Geoscience and Remote Sensing Symposium. 20-24 Sept. 2004. - Vol. 1. - {no data available}. ↑

C4550. Monaldo F.M. Application and extension of a quasioperational approach to wind speed measurement from spaceborne synthetic aperture radar. / Monaldo F.M., Thompson D.R., Pichel W.G., Clemente-Colon P. // 2004. IGARSS '04. Proceedings. 2004 IEEE International Geoscience and Remote Sensing Symposium. 20-24 Sept. 2004. - Vol. 1. - {no data available}. ↑















C4551. Pichel W.G. SAR-derived winds in coastal Alaska waters. / Pichel W.G., Xiaofeng Li, Friedman K.S., Clemente-Colon P., Beal R., Monaldo F., Wackerman C. // 2004. IGARSS '04. Proceedings. 2004 IEEE International Geoscience and Remote Sensing Symposium. 20-24 Sept. 2004. - Vol. 1. - {no data available}. ↑

C4552. Lee J.S. Polarimetric analysis of scatterometer data for ocean surface wind measurement. / Lee J.S., Yueh S.H., Schuler D.L. // 2004. IGARSS '04. Proceedings. 2004 IEEE International Geoscience and Remote Sensing Symposium. 20-24 Sept. 2004. - Vol. 1. - {no data available}. ↑

- C4553.** Schuler D.L. Spiral eddy detection using surfactant slick patterns and polarimetric SAR image decomposition techniques. / Schuler D.L., Lee J.S., De Grandi G. // 2004. IGARSS '04. Proceedings. 2004 IEEE International Geoscience and Remote Sensing Symposium. 20-24 Sept. 2004. - Vol. 1. - {no data available}. ↑
- C4554.** Skriver H. Knowledge-based sea ice classification by polarimetric SAR. / Skriver H., Dierking W. // 2004. IGARSS '04. Proceedings. 2004 IEEE International Geoscience and Remote Sensing Symposium. - Anchorage, AK, 20-24 Sept. 2004. - Vol. 1. - P. 204-207. ↑
- C4555.** Leducq P. Matching-pursuit based analysis of fluctuating scatterers in polarimetric SAR images. / Leducq P., Ferro-Famil L., Pottier E. // 2004. IGARSS '04. Proceedings. 2004 IEEE International Geoscience and Remote Sensing Symposium. 20-24 Sept. 2004. - Vol. 1. - {no data available}. ↑
- C4556.** Lopez-Sanchez J.-M. Characterization of the electromagnetic response of maize crops with polarimetric backscatter profiles. / Lopez-Sanchez J.-M., Ballester-Berman J.D., Fortuny-Guasch J. // 2004. IGARSS '04. Proceedings. 2004 IEEE International Geoscience and Remote Sensing Symposium. 20-24 Sept. 2004. - Vol. 1. - {no data available}. ↑
- C4557.** Howell C. Iceberg and ship discrimination with ENVISAT multipolarization ASAR. / Howell C., Youden J., Lane K., Power D., Randell C., Flett D. // 2004. IGARSS '04. Proceedings. 2004 IEEE International Geoscience and Remote Sensing Symposium. 20-24 Sept. 2004. - Vol. 1. - {no data available}. ↑
- C4558.** Kunz L.B. Melt detection in Antarctic ice-sheets using spaceborne scatterometers and radiometers. / Kunz L.B., Long D.G. // 2004. IGARSS '04. Proceedings. 2004 IEEE International Geoscience and Remote Sensing Symposium. 20-24 Sept. 2004. - Vol. 1. - {no data available}. ↑
- C4559.** Akers E.L. Design, fabrication, and evaluation of a mobile robot for polar environments. / Akers E.L., Harmon H.P., Stansbury R.S., Agah A. // 2004. IGARSS '04. Proceedings. 2004 IEEE International Geoscience and Remote Sensing Symposium. 20-24 Sept. 2004. - Vol. 1. - {no data available}. ↑
- C4560.** Sivashanmugam S. A Bayesian network for autonomous sensor control during polar ice sheet measurements. / Sivashanmugam S., Tsatsoulis C. // 2004. IGARSS '04. Proceedings. 2004 IEEE International Geoscience and Remote Sensing Symposium. 20-24 Sept. 2004. - Vol. 1. - {no data available}. ↑
- C4561.** Kuchikulla A. A wideband radar depth sounder for measuring the thickness of glacial ice. / Kuchikulla A., Gogineni S.P., Kanagaratnam P., Akins T.L. // 2004. IGARSS '04. Proceedings. 2004 IEEE International Geoscience and Remote Sensing Symposium. 20-24 Sept. 2004. - Vol. 1. - {no data available}. ↑
- C4562.** Paden J. Multiband multistatic synthetic aperture radar for measuring ice sheet basal conditions. / Paden J., Mozaffar S., Dunson D., Allen C., Gogineni S., Akins T. // 2004. IGARSS '04. Proceedings. 2004 IEEE International Geoscience and Remote Sensing Symposium. 20-24 Sept. 2004. - Vol. 1. - {no data available}. ↑
- C4563.** Winstead N.S. Synthetic aperture radar and high-resolution MM5 simulations of barrier jets in coastal Alaska. / Winstead N.S., Colle B.A., Bond N. // 2004. IGARSS '04. Proceedings. 2004 IEEE International Geoscience and Remote Sensing Symposium. 20-24 Sept. 2004. - Vol. 1. - {no data available}. ↑
- C4564.** Parthasarathy R. A compact high-resolution radar for determining snow accumulation rates. / Parthasarathy R., Kanagaratnam P., Akins T., Gogineni S., Jezek K. // 2004. IGARSS '04. Proceedings. 2004 IEEE International Geoscience and Remote Sensing Symposium. 20-24 Sept. 2004. - Vol. 1. - {no data available}. ↑
- C4565.** Lane K. Validation of synthetic aperture radar for iceberg detection in sea ice. / Lane K., Power D., Youden J., Randell C., Flett D. // 2004. IGARSS '04. Proceedings. 2004 IEEE International Geoscience and Remote Sensing Symposium. 20-24 Sept. 2004. - Vol. 1. - {no data available}. ↑
- C4566.** Braaten D. Virtual PRISM-on the ice via the web with the polar radar for ice sheet measurements project. / Braaten D., Holvoet J., Gogineni S. // 2004. IGARSS '04. Proceedings. 2004 IEEE International Geoscience and Remote Sensing Symposium. 20-24 Sept. 2004. - Vol. 1. - {no data available}. ↑
- C4567.** Churchill S. Data fusion: remote sensing for target detection and tracking. / Churchill S., Randell C., Power D., Gill E. // 2004. IGARSS '04. Proceedings. 2004 IEEE International Geoscience and Remote Sensing Symposium. 20-24 Sept. 2004. - Vol. 1. - {no data available}. ↑

- C4568.** Torma M. Fusion of low resolution optical and high resolution SAR data for land cover classification. / Torma M., Lumme J., Patrikainen N., Luojus K. // 2004. IGARSS '04. Proceedings. 2004 IEEE International Geoscience and Remote Sensing Symposium. 20-24 Sept. 2004. - Vol. 4. - P. 2680-2683. ↑
- C4569.** Torma M. Effect of texture measures to separability of land cover classes using ERS SAR images. / Torma M., Luojus K. // 2004. IGARSS '04. Proceedings. 2004 IEEE International Geoscience and Remote Sensing Symposium. 20-24 Sept. 2004. - Vol. 4. - P. 2684-2687. ↑
- C4570.** Qiming Zeng. A novel hybrid method to unwrapping interferometric phase. / Qiming Zeng, Jian Jiao, Hua Zhang. // 2004. IGARSS '04. Proceedings. 2004 IEEE International Geoscience and Remote Sensing Symposium. 20-24 Sept. 2004. - Vol. 4. - P. 2632-2635. ↑
- C4571.** Zheng Zhao. InSAR technology processing and result analysis. / Zheng Zhao, Jixian Zhang, Zhiyong Wang, Haitao Li, Wujun Gao, Bin Pan, Rongbin Wang. // 2004. IGARSS '04. Proceedings. 2004 IEEE International Geoscience and Remote Sensing Symposium. 20-24 Sept. 2004. - Vol. 4. - P. 2636-2638. ↑
- C4572.** Stoll B. A simple class-set based vegetation classification of a South Pacific volcanic island (Moorea Island, French Polynesia) using both AirSAR and MASTER data. / Stoll B., Capolsini P. // 2004. IGARSS '04. Proceedings. 2004 IEEE International Geoscience and Remote Sensing Symposium. 20-24 Sept. 2004. - Vol. 4. - P. 2688-2691. ↑
- C4573.** Donato T.F. Temporal analysis of RADARS AT-1 imagery from Delaware Bay. / Donato T.F., Eguiluz A., Garvine R.W., Xiao-Hai Yan. // 2004. IGARSS '04. Proceedings. 2004 IEEE International Geoscience and Remote Sensing Symposium. 20-24 Sept. 2004. - Vol. 4. - P. 2734-2737. ↑
- C4574.** Feng H. Use of a global wave model to correct altimeter sea level estimates. / Feng H., Vandemark D., Chapron B., Beckley B. // 2004. IGARSS '04. Proceedings. 2004 IEEE International Geoscience and Remote Sensing Symposium. 20-24 Sept. 2004. - Vol. 4. - P. 2738-2741. ↑
- C4575.** San Martin M.T. FCM and HCA performance analysis for crop type classification of SAR imagery. / San Martin M.T., Sadki M. // 2004. IGARSS '04. Proceedings. 2004 IEEE International Geoscience and Remote Sensing Symposium. 20-24 Sept. 2004. - Vol. 4. - P. 2692-2694. ↑
- C4576.** Chan S.H. Cross-validation of Jason-1 and QuikSCAT wind speeds. / Chan S.H., Halterman R.R., Long D.G. // 2004. IGARSS '04. Proceedings. 2004 IEEE International Geoscience and Remote Sensing Symposium. 20-24 Sept. 2004. - Vol. 4. - P. 2730-2733. ↑
- C4577.** Wu Tao. Spectral filtering for radar interferometry: position analysis of filtering. / Wu Tao, Zhang Hong, Wang Chao. // 2004. IGARSS '04. Proceedings. 2004 IEEE International Geoscience and Remote Sensing Symposium. 20-24 Sept. 2004. - Vol. 4. - P. 2629-2631. ↑
- C4578.** Gens R. Development of a Radarsat-1 interferometric baseline catalog. 2004. IGARSS '04. Proceedings. 2004 IEEE International Geoscience and Remote Sensing Symposium. 20-24 Sept. 2004. - Vol. 4. - P. 2604-2606. ↑
- C4579.** Hanssen R.F. Stochastic modeling of time series radar interferometry. 2004. IGARSS '04. Proceedings. 2004 IEEE International Geoscience and Remote Sensing Symposium. 20-24 Sept. 2004. - Vol. 4. - P. 2607-2610. ↑
- C4580.** Zhang Bo. Rapid object recognition from high resolution SAR image supported by geo-database. / Zhang Bo, Wang Chao, Zhang Hong. // 2004. IGARSS '04. Proceedings. 2004 IEEE International Geoscience and Remote Sensing Symposium. 20-24 Sept. 2004. - Vol. 4. - P. 2582-2584. ↑
- C4581.** Budillon A. Multi-channel along track interferometry. / Budillon A., Pascasio V., Schirizzi G. // 2004. IGARSS '04. Proceedings. 2004 IEEE International Geoscience and Remote Sensing Symposium. 20-24 Sept. 2004. - Vol. 4. - P. 2601-2603. ↑
- C4582.** Rabus B. Interferometric point target analysis of RADARSAT-1 data for deformation monitoring at the Belridge/Lost Hills oil fields. / Rabus B., Werner C., Wegmueller U., McCardle A. // 2004. IGARSS '04. Proceedings. 2004 IEEE International Geoscience and Remote Sensing Symposium. 20-24 Sept. 2004. - Vol. 4. - P. 2611-2613. ↑

- C4583.** Zhiyong Wang. New methods of the filtering the phase noise in the interferometric SAR. / Zhiyong Wang, Jixian Zhang, Zheng Zhao. // 2004. IGARSS '04. Proceedings. 2004 IEEE International Geoscience and Remote Sensing Symposium. 20-24 Sept. 2004. - Vol. 4. - P. 2622-2625. ↑
- C4584.** Wei Song. The improvement of the conventional GMTI method with single-channel SAR. / Wei Song, Wang Hongyuan. // 2004. IGARSS '04. Proceedings. 2004 IEEE International Geoscience and Remote Sensing Symposium. 20-24 Sept. 2004. - Vol. 4. - P. 2626-2628. ↑
- C4585.** Kun Ren. Preprocessing to improve the quality of SAR interferogram. / Kun Ren, Xiangquan Shi, Lei Bian, Feng Wang, Guang Wu. // 2004. IGARSS '04. Proceedings. 2004 IEEE International Geoscience and Remote Sensing Symposium. 20-24 Sept. 2004. - Vol. 4. - P. 2614-2617. ↑
- C4586.** Tang Zhi. Motion error analysis and compensation for airborne formation flying InSAR. / Tang Zhi, Li Jingwen, Zhou Yinqing. // 2004. IGARSS '04. Proceedings. 2004 IEEE International Geoscience and Remote Sensing Symposium. 20-24 Sept. 2004. - Vol. 4. - P. 2618-2621. ↑
- C4587.** Martini A. Multi-frequency polarimetric snow discrimination in Alpine areas. / Martini A., Ferro-Famil L., Pottier E. // 2004. IGARSS '04. Proceedings. 2004 IEEE International Geoscience and Remote Sensing Symposium. - Anchorage, AK, 20-24 Sept. 2004. - Vol. 6. - P. 3684-3687. ↑
- C4588.** Qin Yu. Modeling of snow wetness inversion using multi-polarization SAR at C-Band. / Qin Yu, Jiancheng Shi, Yun Shao, Wei Liu. // 2004. IGARSS '04. Proceedings. 2004 IEEE International Geoscience and Remote Sensing Symposium. - Anchorage, AK, 20-24 Sept. 2004. - Vol. 6. - P. 3696-3699. ↑
- C4589.** Sanz-Marcos J. Bistatic parasitic SAR processor evaluation. / Sanz-Marcos J., Mallorqui J.J., Broquetas A. // 2004. IGARSS '04. Proceedings. 2004 IEEE International Geoscience and Remote Sensing Symposium. - Anchorage, AK, 20-24 Sept. 2004. - Vol. 6. - P. 3666-3669. ↑
- C4590.** Pulliainen J. Estimation of snow pack characteristics and snow covered area in boreal forests from ERS-2 SAR and Envisat ASAR data. / Pulliainen J., Luojus K., Hallikainen M., Metsamaki S., Koskinen J., Kama J.-P., Huttunen M., Rasmus S. // 2004. IGARSS '04. Proceedings. 2004 IEEE International Geoscience and Remote Sensing Symposium. - Anchorage, AK, 20-24 Sept. 2004. - Vol. 6. - P. 3680-3683. ↑
- C4591.** Jaruwatanadilok S. Snow thickness estimation using correlation functions at C-band. / Jaruwatanadilok S., Kuga Y., Ishimaru A., Hussein Z.A., McDonald K.C. // 2004. IGARSS '04. Proceedings. 2004 IEEE International Geoscience and Remote Sensing Symposium. - Anchorage, AK, 20-24 Sept. 2004. - Vol. 6. - P. 3705-3708. ↑
- C4592.** Cao Laming. SAR image segmentation by 2-D fuzzy entropy. / Cao Laming, Zhang Kunhui, Xia Liangzheng. // 2004. IGARSS '04. Proceedings. 2004 IEEE International Geoscience and Remote Sensing Symposium. - Anchorage, AK, 20-24 Sept. 2004. - Vol. 6. - P. 3798-3801. ↑
- C4593.** Chen Weirong. Road network extraction in high resolution SAR images. / Chen Weirong, Wang Chao, Zhang Hong. // 2004. IGARSS '04. Proceedings. 2004 IEEE International Geoscience and Remote Sensing Symposium. - Anchorage, AK, 20-24 Sept. 2004. - Vol. 6. - P. 3806-3809. ↑
- C4594.** Nies H. A data fusion approach for distributed orbit estimation. / Nies H., Loffeld O., Knedlik S., Gebhardt U., Wiechert W. // 2004. IGARSS '04. Proceedings. 2004 IEEE International Geoscience and Remote Sensing Symposium. - Anchorage, AK, 20-24 Sept. 2004. - Vol. 6. - P. 3736-3739. ↑
- C4595.** Hayes D.S. Creating a geographic footprint from LIDAR data in ArcGIS. / Hayes D.S., Vu N., Zhang W. // 2004. IGARSS '04. Proceedings. 2004 IEEE International Geoscience and Remote Sensing Symposium. - Anchorage, AK, 20-24 Sept. 2004. - Vol. 6. - P. 3770-3773. ↑
- C4596.** Tulu Z. Design considerations for bistatic radar probing of winds in clear air conditions. / Tulu Z., Frasier S.J. // 2004. IGARSS '04. Proceedings. 2004 IEEE International Geoscience and Remote Sensing Symposium. 20-24 Sept. 2004. - Vol. 6. - P. 3662-3665. ↑
- C4597.** Pierdicca N. A joint analysis of microwave radiometer and scatterometer data to characterize meso-scale structures in the Mediterranean Sea. / Pierdicca N., Pulvirenti L., De Biasio F., Zecchetto S. // 2004. IGARSS '04. Proceedings. 2004 IEEE International Geoscience and Remote Sensing Symposium. 20-24 Sept. 2004. - Vol. 4. - P. 2760-2763. ↑

- C4598.** Xie Tao. The scattering fields of 2-D sea fractal surface with finite conductivity illuminated by ellipse polarization wave. Part One. Scattering fields in Cartesian coordinates. / Xie Tao, BinHong Li, WenJun Chen, YiJun He. // 2004. IGARSS '04. Proceedings. 2004 IEEE International Geoscience and Remote Sensing Symposium. 20-24 Sept. 2004. - Vol. 4. - P. 2772-2775. 
- C4599.** Iris S. RADARSAT-1: Canadian Space Agency Hurricane Watch program. / Iris S., Burger G. // 2004. IGARSS '04. Proceedings. 2004 IEEE International Geoscience and Remote Sensing Symposium. 20-24 Sept. 2004. - Vol. 4. - P. 2742-2745. 
- C4600.** Chandrasekar V. Simulation of X-band radar observation of precipitation from S-band measurements. / Chandrasekar V., Gorgucci E., Lim S., Baldini L. // 2004. IGARSS '04. Proceedings. 2004 IEEE International Geoscience and Remote Sensing Symposium. 20-24 Sept. 2004. - Vol. 4. - P. 2752-2755. 
- C4601.** Xie Tao. The scattering fields of 2-D sea fractal surface with finite conductivity illuminated by ellipse polarization wave. Part two. Scattering matrix and numerical results. / Xie Tao, YiJun He, BinHong Li, WenJun Chen. // 2004. IGARSS '04. Proceedings. 2004 IEEE International Geoscience and Remote Sensing Symposium. 20-24 Sept. 2004. - Vol. 4. - P. 2776-2779. 
- C4602.** Joong-Sun Won. Characteristics of permanent scatterer in coastal area. / Joong-Sun Won, Seung-Kuk Lee, Sang-Wan Kim, Sang-Hoon Hong, Kyoung-Ok Kim. // 2004. IGARSS '04. Proceedings. 2004 IEEE International Geoscience and Remote Sensing Symposium. - Anchorage, AK, 20-24 Sept. 2004. - Vol. 6. - P. 3633-3635. 
- C4603.** Donato T.F. Synthetic aperture radar simulations from an idealized tidal channel. / Donato T.F., Romeiser R., Lyzenga D.R., Xiao-Hai Yan. // 2004. IGARSS '04. Proceedings. 2004 IEEE International Geoscience and Remote Sensing Symposium. 20-24 Sept. 2004. - Vol. 6. - P. 3646-3649. 
- C4604.** Ghedira H. Combination of passive and active microwave data for soil moisture estimates. / Ghedira H., Lakhankar T., Jahan N., Khanbilvardi R. // 2004. IGARSS '04. Proceedings. 2004 IEEE International Geoscience and Remote Sensing Symposium. 20-24 Sept. 2004. - Vol. 4. - P. 2783-2786. 
- C4605.** Arakelyan A.K. Polarimetric, L-band, combined radiometer and short pulse scatterometer system. / Arakelyan A.K., Goulyan A.G., Karapetyan V.R., Martirosyan R.M., Pirumyan H.A., Saakyan Yu.A., Hambaryan A.K., Smolin A.I., Karyan V.V., Hambaryan V.K., Arakelyan A.A. // 2004. IGARSS '04. Proceedings. 2004 IEEE International Geoscience and Remote Sensing Symposium. 20-24 Sept. 2004. - Vol. 4. - P. 2787-2790. 
- C4606.** Spencer M.W. The HYDROS radiometer/radar instrument. / Spencer M.W., Njoku E., Entekhabi D., Doiron T., Piepmeier J., Girard R. // 2004. IGARSS '04. Proceedings. 2004 IEEE International Geoscience and Remote Sensing Symposium. 20-24 Sept. 2004. - Vol. 1. - {no data available}. 
- C4607.** Shimada M. Determination of polarimetric calibration parameters of L band SAR using uniform forest data. / Shimada M., Tadono T., Watanabe M. // 2004. IGARSS '04. Proceedings. 2004 IEEE International Geoscience and Remote Sensing Symposium. 20-24 Sept. 2004. - Vol. 1. - {no data available}. 
- C4608.** Rincon R.F. NASA's L-Band Imaging Scatterometer. / Rincon R.F., Hildebrand P., Hilliard L., Mead J. // 2004. IGARSS '04. Proceedings. 2004 IEEE International Geoscience and Remote Sensing Symposium. 20-24 Sept. 2004. - Vol. 1. - {no data available}. 
- C4609.** Fischman M.A. Digital beamforming developments for the joint NASA/Air Force Space Based Radar. / Fischman M.A., Le C. // 2004. IGARSS '04. Proceedings. 2004 IEEE International Geoscience and Remote Sensing Symposium. 20-24 Sept. 2004. - Vol. 1. - {no data available}. 
- C4610.** Moriyama T. A study on extraction of urban areas from polarimetric Synthetic Aperture Radar image. / Moriyama T., Uratsuka S., Umehara T., Satake M., Nadai A., Maeno H., Nakamura K., Yamaguchi Y. // 2004. IGARSS '04. Proceedings. 2004 IEEE International Geoscience and Remote Sensing Symposium. 20-24 Sept. 2004. - Vol. 1. - {no data available}. 
- C4611.** Tran T.N. Initialization of Markov Random Field clustering of large polarimetric SAR images. / Tran T.N., Wehrens R., Buydens L.M.C., Hoekman D.H. // 2004. IGARSS '04. Proceedings. 2004 IEEE International Geoscience and Remote Sensing Symposium. 20-24 Sept. 2004. - Vol. 1. - {no data available}. 
- C4612.** Jingjuan Liao. Monitoring for 2003 Huai River flood in China using multisource SAR data. / Jingjuan

Liao, Yun Shao, Shixin Wang. // 2004. IGARSS '04. Proceedings. 2004 IEEE International Geoscience and Remote Sensing Symposium. 20-24 Sept. 2004. - Vol. 4. - P. 2260-2263. ↑

C4613. Sang-Eun Park. Physical interpretation on eigen-analysis of the polarimetric coherency matrix for microwave scattering from vegetation. / Sang-Eun Park, Wooil M Moon. // 2004. IGARSS '04. Proceedings. 2004 IEEE International Geoscience and Remote Sensing Symposium. 20-24 Sept. 2004. - Vol. 1. - {no data available}. ↑

C4614. De Grandi G. A wavelet multiresolution technique for polarimetric texture analysis and segmentation of SAR images. / De Grandi G., Hoekman D., Lee J.-S., Schuler D., Ainsworth T. // 2004. IGARSS '04. Proceedings. 2004 IEEE International Geoscience and Remote Sensing Symposium. 20-24 Sept. 2004. - Vol. 1. - {no data available}. ↑

C4615. Novo-Gradac A.-M. An overview of NASA's Laser Risk Reduction Program. / Novo-Gradac A.-M., Heaps W., Upendra Singh. // 2004. IGARSS '04. Proceedings. 2004 IEEE International Geoscience and Remote Sensing Symposium. 20-24 Sept. 2004. - Vol. 1. - {no data available}. ↑

C4616. Antonello G. SAR interferometry from satellite and ground-based system for monitoring deformations on the Stromboli volcano. / Antonello G., Tarchi D., Casagli N., Farina P., Guerri L., Leva D. // 2004. IGARSS '04. Proceedings. 2004 IEEE International Geoscience and Remote Sensing Symposium. 20-24 Sept. 2004. - Vol. 1. - {no data available}. ↑

C4617. Kwoun O.-I. Deformation of the Aniakchak caldera, Alaska, mapped by InSAR. / Kwoun O.-I., Zhong Lu. // 2004. IGARSS '04. Proceedings. 2004 IEEE International Geoscience and Remote Sensing Symposium. 20-24 Sept. 2004. - Vol. 1. - {no data available}. ↑

C4618. Pugh M.L. Neural image fusion of remotely sensed electro-optical and synthetic aperture radar data for forest classification. / Pugh M.L., Waxman A.M., Duggin M.J., Hassett J.M. // 2004. IGARSS '04. Proceedings. 2004 IEEE International Geoscience and Remote Sensing Symposium. 20-24 Sept. 2004. - Vol. 1. - {no data available}. ↑

C4619. Singhroy V. Identifying SAR permeability zones on groundwater recharge areas. / Singhroy V., Bajc A., Molch K. // 2004. IGARSS '04. Proceedings. 2004 IEEE International Geoscience and Remote Sensing Symposium. 20-24 Sept. 2004. - Vol. 1. - {no data available}. ↑

C4620. Tapley I. The geology, landforms and topography of sub-Antarctic Macquarie Island, Australia, as revealed by AIRSAR. / Tapley I., Dijkstra A.H., Brolsma H. // 2004. IGARSS '04. Proceedings. 2004 IEEE International Geoscience and Remote Sensing Symposium. 20-24 Sept. 2004. - Vol. 1. - {no data available}. ↑

C4621. Hlavka D.L. Initial validation and results of Geoscience Laser Altimeter System optical properties retrievals. / Hlavka D.L., Hart W.D., Palm S.P., McGill M.J., Spinhirne J.D. // 2004. IGARSS '04. Proceedings. 2004 IEEE International Geoscience and Remote Sensing Symposium. 20-24 Sept. 2004. - Vol. 1. - {no data available}. ↑

C4622. Raney R.K. Simultaneous laser and radar altimeter measurements over land and sea ice. / Raney R.K., Leuschen C.J. // 2004. IGARSS '04. Proceedings. 2004 IEEE International Geoscience and Remote Sensing Symposium. 20-24 Sept. 2004. - Vol. 1. - {no data available}. ↑

C4623. Rostan F. CryoSat payload calibration and characterization. / Rostan F., Mallow U., Riegger S. // 2004. IGARSS '04. Proceedings. 2004 IEEE International Geoscience and Remote Sensing Symposium. 20-24 Sept. 2004. - Vol. 1. - {no data available}. ↑

C4624. Rey L. SIRAL the radar altimeter for the CryoSat mission, pre-launch performances. / Rey L., de Chateau-Thierry P., Phalippou L., Calvary P., Mavrocordatos C. // 2004. IGARSS '04. Proceedings. 2004 IEEE International Geoscience and Remote Sensing Symposium. 20-24 Sept. 2004. - Vol. 1. - {no data available}. ↑

C4625. Lukowski T.I. Synthetic aperture radar for search and rescue: polarimetry and interferometry. / Lukowski T.I., Bing Yue, Mattar K. // 2004. IGARSS '04. Proceedings. 2004 IEEE International Geoscience and Remote Sensing Symposium. 20-24 Sept. 2004. - Vol. 4. - P. 2479-2482. ↑

C4626. Margarit G. Analysis of the limitations of coherent polarimetric decompositions on vessel classification using simulated images. / Margarit G., Fabregas X., Mallorqui J.J., Broquetas A. // 2004. IGARSS '04.

Proceedings. 2004 IEEE International Geoscience and Remote Sensing Symposium. 20-24 Sept. 2004. - Vol. 4. - P. 2483-2486. ↑

C4627. Carriero F. CryoSat Ground Segment: PDS-IPF infrastructure design overview. / Carriero F., Grimont P., Nasuti C., Mantovani P., Petiteville I., Pastori M., Spaventa V., Viau P., Vollono A., Zelli C. // 2004. IGARSS '04. Proceedings. 2004 IEEE International Geoscience and Remote Sensing Symposium. 20-24 Sept. 2004. - Vol. 4. - P. 2472-2474. ↑

C4628. Fukuda S. Relating polarimetric SAR image texture to the scattering entropy. 2004. IGARSS '04. Proceedings. 2004 IEEE International Geoscience and Remote Sensing Symposium. 20-24 Sept. 2004. - Vol. 4. - P. 2475-2478. ↑

C4629. Touzi R. Target scattering decomposition of one-look and multi-look SAR data using a new coherent scattering model: the TSVM. 2004. IGARSS '04. Proceedings. 2004 IEEE International Geoscience and Remote Sensing Symposium. 20-24 Sept. 2004. - Vol. 4. - P. 2491-2494. ↑

C4630. Venkataraman G. Fusion of optical and microwave remote sensing data for snow cover mapping. / Venkataraman G., Mahato B.C., Ravi S., Rao Y.S., Mathur P., Snehmani. // 2004. IGARSS '04. Proceedings. 2004 IEEE International Geoscience and Remote Sensing Symposium. 20-24 Sept. 2004. - Vol. 4. - P. 2554-2557. ↑

C4631. Wu Fan. Residential area information extraction by combining China airborne SAR and optical images. / Wu Fan, Wang Chao, Zhang Hong. // 2004. IGARSS '04. Proceedings. 2004 IEEE International Geoscience and Remote Sensing Symposium. 20-24 Sept. 2004. - Vol. 4. - P. 2568-2570. ↑

C4632. Qong M. A new polarization state conformation and its application to coherence optimization in PolInSAR. 2004. IGARSS '04. Proceedings. 2004 IEEE International Geoscience and Remote Sensing Symposium. 20-24 Sept. 2004. - Vol. 4. - P. 2495-2498. ↑

C4633. Shishkova O. A multi-frequency polarimetric scattering model for subsurface structure detection. / Shishkova O., Hajnsek I. // 2004. IGARSS '04. Proceedings. 2004 IEEE International Geoscience and Remote Sensing Symposium. 20-24 Sept. 2004. - Vol. 4. - P. 2499-2502. ↑

C4634. Mavrocordatos C. Development of ASIRAS (Airborne SAR/Interferometric Altimeter System). / Mavrocordatos C., Attema E., Davidson M., Lentz H., Nixdorf U. // 2004. IGARSS '04. Proceedings. 2004 IEEE International Geoscience and Remote Sensing Symposium. 20-24 Sept. 2004. - Vol. 4. - P. 2465-2467. ↑

C4635. Franssoru J.E.S. Estimation of forest stem volume using optical SPOT-5 satellite and laser data in combination. / Franssoru J.E.S., Magnusson M., Holmgren J. // 2004. IGARSS '04. Proceedings. 2004 IEEE International Geoscience and Remote Sensing Symposium. 20-24 Sept. 2004. - Vol. 4. - P. 2318-2322. ↑

C4636. Magnusson M. Combining CARABAS-II VHF SAR and Landsat TM satellite data for estimation of forest stem volume. / Magnusson M., Fransson J.E.S. // 2004. IGARSS '04. Proceedings. 2004 IEEE International Geoscience and Remote Sensing Symposium. 20-24 Sept. 2004. - Vol. 4. - P. 2327-2331. ↑

C4637. Puestow T.M. Near real-time monitoring of river ice in support of flood forecasting in eastern Canada: towards the integration of Earth observation technology in flood hazard mitigation. / Puestow T.M., Randell C.J., Rollings K.W., Khan A.A., Picco R. // 2004. IGARSS '04. Proceedings. 2004 IEEE International Geoscience and Remote Sensing Symposium. 20-24 Sept. 2004. - Vol. 4. - P. 2268-2271. ↑

C4638. Shixin Wang. Assessing the efforts of the flood diversion and storage in the drainage area of Huaihe River using remote sensing. / Shixin Wang, Shirong Chen, Yi Zhou, Qing Zhao. // 2004. IGARSS '04. Proceedings. 2004 IEEE International Geoscience and Remote Sensing Symposium. 20-24 Sept. 2004. - Vol. 4. - P. 2276-2279. ↑

C4639. Nakamura K. Study on the forest observation in Kushiro wetland by using dual-frequency and fully polarimetric airborne SAR (Pi-SAR) data. / Nakamura K., Wakabayashi H., Shinsho H., Maeno H., Uratsuka S., Nadai A., Umehara T., Moriyama T. // 2004. IGARSS '04. Proceedings. 2004 IEEE International Geoscience and Remote Sensing Symposium. 20-24 Sept. 2004. - Vol. 4. - P. 2332-2335. ↑

C4640. Miranda F.P. Generation of multi-temporal JERS-1 SAR mosaics over the Manaus-Coari-Urucu Region, Western Amazonia, Brazil. / Miranda F.P., Beisl C.H., Forsberg B., Arruda W.C., Pedroso E.C. // 2004.

IGARSS '04. Proceedings. 2004 IEEE International Geoscience and Remote Sensing Symposium. 20-24 Sept. 2004. - Vol. 4. - P. 2384 vol.4. ↑

C4641. Wallington E.D. Forest height estimation from X-band SAR. / Wallington E.D., Izzawati, Woodhouse I.H. // 2004. IGARSS '04. Proceedings. 2004 IEEE International Geoscience and Remote Sensing Symposium. 20-24 Sept. 2004. - Vol. 4. - P. 2393-2396. ↑

C4642. Walker W.S. A comparison of forest canopy height estimates derived from SRTM and TOPSAR in the Sierra Nevada of California. / Walker W.S., Pierce L.E., Kelndorfer J.M., Dobson M.C., Hunsaker C.T., Fites J.A. // 2004. IGARSS '04. Proceedings. 2004 IEEE International Geoscience and Remote Sensing Symposium. 20-24 Sept. 2004. - Vol. 4. - P. 2336-2339. ↑

C4643. Watanabe M. Tight correlations between forest parameters and backscattering coefficient derived by the L-band airborne SAR (PiSAR). / Watanabe M., Shimada M., Rosenqvist A., Romshoo S.A., Ohta K., Tadono T., Matsuoka M., Furuta R. // 2004. IGARSS '04. Proceedings. 2004 IEEE International Geoscience and Remote Sensing Symposium. 20-24 Sept. 2004. - Vol. 4. - P. 2340-2343. ↑

C4644. Fornaro G. Motion compensation of squinted airborne SAR raw data: role of processing geometry. / Fornaro G., Franceschetti G., Perna S. // 2004. IGARSS '04. Proceedings. 2004 IEEE International Geoscience and Remote Sensing Symposium. 20-24 Sept. 2004. - Vol. 2. - P. 1518-1521. ↑

C4645. Dengxin Hua. UV Rayleigh lidar for measuring atmospheric temperature profiles of the troposphere. / Dengxin Hua, Uchida M., Kobayashi T. // 2004. (CLEO). Conference on Lasers and Electro-Optics. 16-21 May 2004. - Vol. 1. - P. 2 P. vol.1. ↑

C4646. Hirano Y. High-performance 1.5 μm coherent Doppler LIDAR for wind-field measurement. 2004. (CLEO). Conference on Lasers and Electro-Optics. 16-21 May 2004. - Vol. 1. - P. 2 P. vol.1. ↑

C4647. Goldman A. Anomaly subspace detection based on a multi-scale Markov random field model. / Goldman A., Cohen I. // 2004. Proceedings. 2004 23rd IEEE Convention of Electrical and Electronics Engineers in Israel. 6-7 Sept. 2004. - P. 444-447. ↑

C4648. Wolf J.P. Probing the atmosphere using a femtosecond terawatt lidar. / Wolf J.P., Kasparian J., Mejean G., Salmon E., Yu J., Boutou V., Courvoisier F., Rodriguez M., Woste L., Bourayou R., Sauerbrey R. // 2004. (CLEO). Conference on Lasers and Electro-Optics. 16-21 May 2004. - Vol. 1. - P. 2 P. vol.1. ↑

C4649. von der Lippe C.M. Photonics technology development for optical fuzing. / von der Lippe C.M., Liu J.J., Keeler G.A., Serkland D.K., Geib K.M., Peake G.M., Mar A. // 2004. LEOS 2004. The 17th Annual Meeting of the IEEE Lasers and Electro-Optics Society. 7-11 Nov. 2004. - Vol. 1. - P. 264-265. ↑

C4650. Schirone L. EMI in orbiting sounding radar from ripple in solar arrays. / Schirone L., Seu R. // 2004. Proceedings. 2004 IEEE Aerospace Conference. 6-13 March 2004. - Vol. 1. - {no data available}. ↑

C4651. Hampson G.A. Design and demonstration of an interference suppressing microwave radiometer. / Hampson G.A., Ellingson S.W., Johnson J.T. // 2004. Proceedings. 2004 IEEE Aerospace Conference. 6-13 March 2004. - Vol. 2. - P. 993-999. ↑

C4652. Woeste L. Femtosecond white-light filaments: A new tool in atmospheric research. 2004. LEOS 2004. The 17th Annual Meeting of the IEEE Lasers and Electro-Optics Society. 7-11 Nov. 2004. - Vol. 2. - P. 623-624. ↑

C4653. Lukin V. Iterative DCT algorithm for digital elevation model reconstruction from isogram maps. / Lukin V., Ponomarenko N., Sharonov V., Zelensky A. // 2004. Proceedings of the International Conference Modern Problems of Radio Engineering, Telecommunications and Computer Science. 24-28 Feb. 2004. - P. 165-168. ↑

C4654. Ostermeyer M. 0.5 J frequency stabilized diode pumped solid state laser for a next generation lidar system. / Ostermeyer M., Kappe P., Wulfmeyer V., Menzel R. // 2004. (CLEO). Conference on Lasers and Electro-Optics. 16-21 May 2004. - Vol. 2. - P. 2 P. vol.2. ↑

C4655. Hrabar S. Introduction to special session on electromagnetics in communications. 2004. MELECON 2004. Proceedings of the 12th IEEE Mediterranean Electrotechnical Conference. 12-15 May 2004. - Vol. 2. - P. 489-490. ↑

- C4656.** Sankaran K. Radar remote sensing for oil spill classification (optimization for enhanced classification). / Sankaran K., Guasch J.F. // 2004. MELECON 2004. Proceedings of the 12th IEEE Mediterranean Electrotechnical Conference. 12-15 May 2004. - Vol. 2. - P. 511-514. ↑
- C4657.** Abramov S.K. Influence of multiplicative noise variance evaluation accuracy of mm-band SLAR image filtering efficiency. / Abramov S.K., Lukin W., Ponomarenko N.N., Egiazarian K.O., Pogrebnyak O.B. // 2004. MSMW 04. The Fifth International Kharkov Symposium on Physics and Engineering of Microwaves, Millimeter, and Submillimeter Waves. 21-26 June 2004. - Vol. 1. - P. 250-252. ↑
- C4658.** Natarov M.P. Orthomode transducer for mm-wave range. / Natarov M.P., Rud L.A., Tkachenko V.I. // 2004. MSMW 04. The Fifth International Kharkov Symposium on Physics and Engineering of Microwaves, Millimeter, and Submillimeter Waves. 21-26 June 2004. - Vol. 2. - P. 641-643. ↑
- C4659.** Czarnecki W. Analysis of 2-D correlation properties of sea surface backscattered signal. / Czarnecki W., Darlak J. // 2004. MIKON-2004. 15th International Conference on Microwaves, Radar and Wireless Communications. 17-19 May 2004. - Vol. 2. - P. 555-558. ↑
- C4660.** Xiaoli Sun. Cloud and aerosol lidar channel design and performance of the Geoscience Laser Altimeter System on the ICESat mission. / Xiaoli Sun, Abshire J.B., Krainak M.A., Spinhirne J.D., Palm S.P., Lancaster R.S., Allan G.R. // 2004. (CLEO). Conference on Lasers and Electro-Optics. 16-21 May 2004. - Vol. 2. - P. 2 P. vol.2. ↑
- C4661.** Hasegawa N. Surface-structure identification using THz radar techniques with spatial beam filtering and out-of-focus detection. / Hasegawa N., Ronnburg K., Lissauskas A., Thomson M., Löffler T., Roskos H.G. // 2004. (CLEO). Conference on Lasers and Electro-Optics. 16-21 May 2004. - Vol. 2. - P. 2 P. vol.2. ↑
- C4662.** Boerner W.-M. From airborne via drones to space-borne polarimetric-interferometric SAR environmental stress-change monitoring-comparative assessment of applications. / Boerner W.-M., Morisaki J.J. // 2004. MIKON-2004. 15th International Conference on Microwaves, Radar and Wireless Communications. 17-19 May 2004. - Vol. 3. - P. 901-904. ↑
- C4663.** Boerner W.-M. Recent advances in the development of polarimetric interferometric SAR imaging in microwave remote sensing of the terrestrial covers: need for developing multi-band single and multiple pass POLinSAR monitoring platforms in air and space. / Boerner W.-M., Morisaki J.J. // 2004. MIKON-2004. 15th International Conference on Microwaves, Radar and Wireless Communications. 17-19 May 2004. - Vol. 3. - P. 1079-1082. ↑
- C4664.** Weissman D.E. Corrections to the seawinds scatterometer wind vectors by removing the effects of rain from the NRCS. / Weissman D.E., Bourassa M.A., Durden S.L. // 2004. IGARSS '04. Proceedings. 2004 IEEE International Geoscience and Remote Sensing Symposium. - Anchorage, AK, 20-24 Sept. 2004. - Vol. 2. - P. 791-794. ↑
- C4665.** Ebuchi N. Evaluation of ocean surface vector winds observed by QuikSCAT/seawinds and ADEOS-II/seawind. / Ebuchi N., Graber H.C., Caruso M.J. // 2004. IGARSS '04. Proceedings. 2004 IEEE International Geoscience and Remote Sensing Symposium. - Anchorage, AK, 20-24 Sept. 2004. - Vol. 2. - P. 795-798. ↑
- C4666.** Phalippou L. End to end performances of a short baseline interferometric radar altimeter for ocean mesoscale topography. / Phalippou L., Guijarro J. // 2004. IGARSS '04. Proceedings. 2004 IEEE International Geoscience and Remote Sensing Symposium. - Anchorage, AK, 20-24 Sept. 2004. - Vol. 2. - P. 765-768. ↑
- C4667.** Vogel P. The L-band SAR pre-development. / Vogel P., Ludwig M., Klooster K., Head A. // 2004. IGARSS '04. Proceedings. 2004 IEEE International Geoscience and Remote Sensing Symposium. - Anchorage, AK, 20-24 Sept. 2004. - Vol. 2. - P. 769-773. ↑
- C4668.** Kelly K.A. Impact of ocean currents on scatterometer winds in the tropical Pacific Ocean. / Kelly K.A., Dickinson S., Jiang C.L., Johnson G.C., Thompson L.A. // 2004. IGARSS '04. Proceedings. 2004 IEEE International Geoscience and Remote Sensing Symposium. - Anchorage, AK, 20-24 Sept. 2004. - Vol. 2. - P. 799. ↑
- C4669.** Yisok Oh. Comparison of two inversion methods for retrieval of soil moisture and surface roughness from polarimetric radar observation of soil surfaces. 2004. IGARSS '04. Proceedings. 2004 IEEE International Geoscience and Remote Sensing Symposium. - Anchorage, AK, 20-24 Sept. 2004. - Vol. 2. - P. 807-810. ↑

- C4670.** Low A. A two parameter backscattering model for bare soil surfaces: from theory to application. / Low A., Mauser W. // 2004. IGARSS '04. Proceedings. 2004 IEEE International Geoscience and Remote Sensing Symposium. - Anchorage, AK, 20-24 Sept. 2004. - Vol. 2. - P. 811-814. ↑
- C4671.** Kim Y. Vegetation effects on soil moisture estimation. / Kim Y., van Zyl J. // 2004. IGARSS '04. Proceedings. 2004 IEEE International Geoscience and Remote Sensing Symposium. - Anchorage, AK, 20-24 Sept. 2004. - Vol. 2. - P. 800-802. ↑
- C4672.** Sikdar M. A modified empirical model for soil moisture estimation in vegetated areas using SAR data. / Sikdar M., Cumming I. // 2004. IGARSS '04. Proceedings. 2004 IEEE International Geoscience and Remote Sensing Symposium. - Anchorage, AK, 20-24 Sept. 2004. - Vol. 2. - P. 803-806. ↑
- C4673.** Wang F. Forward model and sensitivity study of uplink large array calibration using in-orbit targets. / Wang F., Sarabandi K. // 2004. IGARSS '04. Proceedings. 2004 IEEE International Geoscience and Remote Sensing Symposium. - Anchorage, AK, 20-24 Sept. 2004. - Vol. 2. - P. 761-764. ↑
- C4674.** Winter E.M. Endmember-based in-scene atmospheric retrieval (EMISAR). 2004. Proceedings. 2004 IEEE Aerospace Conference. 6-13 March 2004. - Vol. 3. - {no data available}. ↑
- C4675.** Silbert M. Measuring the performance of track-to-track fusion systems. / Silbert M., Burroughs A. // 2004. Proceedings. 2004 IEEE Aerospace Conference. 6-13 March 2004. - Vol. 3. - {no data available}. ↑
- C4676.** Njoku E. The HYDROS mission: requirements and system design. / Njoku E., Spencer M., McDonald K., Smith J., Houser P., Doiron T., O'Neill P., Girard R., Entekhabi D. // 2004. Proceedings. 2004 IEEE Aerospace Conference. 6-13 March 2004. - Vol. 2. - P. 1000-1007. ↑
- C4677.** Aina L. Multi-use, low SWaP, ultra-sensitive photoreceiver arrays for ladar & remote sensing. / Aina L., Fathimulla A., Hier H., Jiang W., Foshee J., Arnold J. // 2004. Proceedings. 2004 IEEE Aerospace Conference. 6-13 March 2004. - Vol. 3. - {no data available}. ↑
- C4678.** Beale D.A.R. An assessment of multi-static radar remote sensor networks. / Beale D.A.R., Hume A.L., Cage J., Williams P. // 2004. Proceedings. 2004 IEEE Aerospace Conference. 6-13 March 2004. - Vol. 3. - {no data available}. ↑
- C4679.** Ranson K.J. Landcover attributes from ICESat GLAS data in Central Siberia. / Ranson K.J., Sun G., Kovacs K., Kharuk V.I. // 2004. IGARSS '04. Proceedings. 2004 IEEE International Geoscience and Remote Sensing Symposium. - Anchorage, AK, 20-24 Sept. 2004. - Vol. 2. - P. 753-756. ↑
- C4680.** Aguasca A. A solid state L to X-band flexible ground-based SAR system for continuous monitoring applications. / Aguasca A., Broquetas A., Mallorqui J.J., Fabregas X. // 2004. IGARSS '04. Proceedings. 2004 IEEE International Geoscience and Remote Sensing Symposium. - Anchorage, AK, 20-24 Sept. 2004. - Vol. 2. - P. 757-760. ↑
- C4681.** Powell W. Reconfigurable computing as an enabling technology for single-photon-counting laser altimetry. / Powell W., Hicks E., Pinchinat M., Dabney P., McGarry J., Murray P. // 2004. Proceedings. 2004 IEEE Aerospace Conference. 6-13 March 2004. - Vol. 4. - P. 2327-2339. ↑
- C4682.** Trianni G. ENVISAT-1 data for urban area detection and characterization. / Trianni G., Dell'Acqua F., Gamba P., Lisini G. // 2004. IGARSS '04. Proceedings. 2004 IEEE International Geoscience and Remote Sensing Symposium. - Anchorage, AK, 20-24 Sept. 2004. - Vol. 2. - P. 735-738. ↑
- C4683.** Lihua Jin. Spaceborne spotlight SAR processing using the frequency-scaling algorithm. / Lihua Jin, Xingzhao Liu, Zhixin Zhou. // 2004. Proceedings of the IEEE Radar Conference. 26-29 April 2004. - P. 563-567. ↑
- C4684.** Fuks I.M. Travel time and intensity statistics of the pulsed signals backscattered by a rough surface [geophysical remote-sensing applications]. / Fuks I.M., Godin O.A. // 2004. IEEE Antennas and Propagation Society International Symposium. 20-25 June 2004. - Vol. 1. - P. 910-913. ↑
- C4685.** Wheeler K. An L-band SAR for repeat pass deformation measurements on a UAV platform. / Wheeler K., Hensley S., Lou Y., Miller T., Hoffman J. // 2004. Proceedings of the IEEE Radar Conference. 26-29 April 2004. - P. 317-322. ↑

- C4686.** Uppuluri A.V. MATLAB-based ERS SAR data acquisition and processing software for classroom use. / Uppuluri A.V., Jost R.J. // 2004. Proceedings of the IEEE Radar Conference. 26-29 April 2004. - P. 524-528. ↑
- C4687.** El-Ocla H. On indirect method of RCS calculation of conducting targets in random media. / El-Ocla H., Tateiba M. // 2004. IEEE Antennas and Propagation Society International Symposium. 20-25 June 2004. - Vol. 1. - P. 958-961. ↑
- C4688.** Hacıhaliloglu I. DCT and DWT based image compression in remote sensing images. / Hacıhaliloglu I., Karta M. // 2004. IEEE Antennas and Propagation Society International Symposium. 20-25 June 2004. - Vol. 4. - P. 3856-3858. ↑
- C4689.** Oughstun K.E. Optimal pulse penetration in Rocard-Powles-Debye model dielectrics using the Brillouin precursor. 2004. IEEE Antennas and Propagation Society International Symposium. 20-25 June 2004. - Vol. 4. - P. 4228-4231. ↑
- C4690.** {no data available}. IEEE Antennas and Propagation Society Symposium (IEEE Cat. No.04CH37529). 2004. IEEE Antennas and Propagation Society International Symposium. 20-25 June 2004. - Vol. 4. - {no data available}. ↑
- C4691.** Dehmollaian M. Simulation of radar scattering from electrically large objects under tree canopies. / Dehmollaian M., Il-Suek Koh, Sarabandi K. // 2004. IEEE Antennas and Propagation Society International Symposium. 20-25 June 2004. - Vol. 4. - P. 3852-3855. ↑
- C4692.** Im E. Advanced geostationary radar for hurricane monitoring and studies. / Im E., Durden S.L., Rahrnat-Sarnii Y., Fang H., Cable V., Lou M., Huang J. // 2004. Proceedings of the IEEE Radar Conference. 26-29 April 2004. - P. 307-311. ↑
- C4693.** Shkvarko Y.V. Neural network-based signal processing for enhancing the multi-sensor remote sensing imagery. / Shkvarko Y.V., Montiel J.L.L., Rizo L., Salas J.A. // 2004. CONIELECOMP 2004. 14th International Conference on Electronics, Communications and Computers. 16-18 Feb. 2004. - P. 168-172. ↑
- C4694.** Araujo R.T.S. Spots segmentation in SAR images for remote sensing of environment. / Araujo R.T.S., Medeiros F.N.S., Costa R.C.S., Marques R.C.P., Moreira R.B., Silva J.L. // 2004. 6th IEEE Southwest Symposium on Image Analysis and Interpretation. 28-30 March 2004. - P. 95-99. ↑
- C4695.** Aloisio G. A problem solving environment for remote sensing data processing. / Aloisio G., Cafaro M., Epicoco I., Quarta G. // 2004. Proceedings. ITCC 2004. International Conference on Information Technology: Coding and Computing. 5-7 April 2004. - Vol. 2. - P. 56-61. ↑
- C4696.** Vazquez-Bautista R.F. The fused Bayesian maximum entropy-variational analysis method for computer reconstruction of remote sensing imagery. / Vazquez-Bautista R.F., Shkvarko Y.V., Morales-Mendoza L.J., Rizo-Dominguez L. // 2004. CONIELECOMP 2004. 14th International Conference on Electronics, Communications and Computers. 16-18 Feb. 2004. - P. 272-276. ↑
- C4697.** Belhadj Z. Unsupervised classification of polarimetric SAR images using neural nets. / Belhadj Z., Yahia M. // 2004. Proceedings. 2004 International Conference on Information and Communication Technologies: From Theory to Applications. 19-23 April 2004. - P. 335. ↑
- C4698.** Lou Y. On-board processor for direct distribution of change detection data products [radar imaging]. / Lou Y., Hensley S., Le C., Moller D. // 2004. Proceedings of the IEEE Radar Conference. 26-29 April 2004. - P. 33-37. ↑
- C4699.** Rosen P.A. Developments in repeat pass interferometric radar for Earth and planetary sciences. 2004. Proceedings of the IEEE Radar Conference. 26-29 April 2004. - P. 207-211. ↑
- C4700.** Farah I.R. Analyzing satellite image with blind separation of sources, knowledge based system and fusion of multisource images. / Farah I.R., Ahmed M.B. // 2004. Proceedings. 2004 International Conference on Information and Communication Technologies: From Theory to Applications. 19-23 April 2004. - P. 337. ↑
- C4701.** Farah L.B. A sensitivity analysis of radar backscattering coefficient to multiscale roughness description and radar parameters using the small perturbation model. / Farah L.B., Bennaceur R., Belhadj Z., Boussema R. // 2004. Proceedings. 2004 International Conference on Information and Communication Technologies: From

Theory to Applications. 19-23 April 2004. - P. 341-342. ↑

C4702. Ksendzuk A.V. Optimisation of the spatial attitude of the bistatic and multistatic synthetic aperture radar. / Ksendzuk A.V., Volosyuk V.K., Sologub N.S. // 2004. MSMW 04. The Fifth International Kharkov Symposium on Physics and Engineering of Microwaves, Millimeter, and Submillimeter Waves. 21-26 June 2004. - Vol. 1. - P. 178-180. ↑

C4703. Meshkov E.M. Characteristics of a signal backscattered from a rough water surface at small incidence angles. / Meshkov E.M., Karaev V.Yu., Kanevsky M.B., Balandina G.N., Zuikova E.M., Gol'dblat V.Yu., Titov V.I. // 2004. MSMW 04. The Fifth International Kharkov Symposium on Physics and Engineering of Microwaves, Millimeter, and Submillimeter Waves. 21-26 June 2004. - Vol. 1. - P. 187-189. ↑

C4704. Gogineni S. High-resolution mapping of near-surface internal snow layers with a wideband radar. / Gogineni S., Kanagaratnam P., Braaten D., Akins T., Parthasarathy B. // 2004. GPR 2004. Proceedings of the Tenth International Conference on Ground Penetrating Radar. 2004. - P. 769-771. ↑

C4705. Yanovsky F. Doppler-polarimetric method of turbulence intensity retrieving in rain using remote sensing with microwave radar. / Yanovsky F., Averyanova Y. // 2004. MSMW 04. The Fifth International Kharkov Symposium on Physics and Engineering of Microwaves, Millimeter, and Submillimeter Waves. 21-26 June 2004. - Vol. 1. - P. 97-102. ↑

C4706. Gorishniak V.P. Passive multichannels millimeter-waves imaging system. / Gorishniak V.P., Denisov A.G., Kuzmin S.E., Radzikhovsky V.N., Shevchuk B.M. // 2004. MSMW 04. The Fifth International Kharkov Symposium on Physics and Engineering of Microwaves, Millimeter, and Submillimeter Waves. 21-26 June 2004. - Vol. 1. - P. 202-204. ↑

C4707. Gutnik V.G. Wind influence on sea radar backscattering intensity. / Gutnik V.G., Kulemin G.P., Sharapov L.I. // 2004. MSMW 04. The Fifth International Kharkov Symposium on Physics and Engineering of Microwaves, Millimeter, and Submillimeter Waves. 21-26 June 2004. - Vol. 1. - P. 220-222. ↑

C4708. Sologub N.S. Optimal and quasioptimal processing algorithms in the multisatellite SAR in terms of the stochastic vector fields. / Sologub N.S., Volosyuk V.K. // 2004. MSMW 04. The Fifth International Kharkov Symposium on Physics and Engineering of Microwaves, Millimeter, and Submillimeter Waves. 21-26 June 2004. - Vol. 1. - P. 244-246. ↑

C4709. Lutsenko V.I. The arrival angle performances for signals scattered by the targets and sea surface and their usage for detection efficiency improvement. 2004. MSMW 04. The Fifth International Kharkov Symposium on Physics and Engineering of Microwaves, Millimeter, and Submillimeter Waves. 21-26 June 2004. - Vol. 1. - P. 214-216. ↑

C4710. Kulemin G.P. Dual-polarization determination of soil parameters: theory and experimental data comparison. 2004. MSMW 04. The Fifth International Kharkov Symposium on Physics and Engineering of Microwaves, Millimeter, and Submillimeter Waves. 21-26 June 2004. - Vol. 1. - P. 217-219. ↑

C4711. Serbin G. GPR measurement of crop canopies and soil water dynamics- implications for radar remote sensing. / Serbin G., Or D. // 2004. GPR 2004. Proceedings of the Tenth International Conference on Ground Penetrating Radar. 2004. - P. 497-500. ↑

C4712. Yingjian Liu. Automatic detecting system for ship wakes in SAR images. 2004. WCICA 2004. Fifth World Congress on Intelligent Control and Automation. 15-19 June 2004. - Vol. 4. - P. 3032-3036. ↑

C4713. {no data available}. GPR 2004 Conference is organized. 2004. GPR 2004. Proceedings of the Tenth International Conference on Ground Penetrating Radar. 2004. - Vol. 1. - P. iii. ↑

C4714. Kona K.S. A novel feed system for soil moisture spaceborne radar: dual-frequency dual-polarized stacked patch microstrip array. / Kona K.S., Manteghi M., Rahmat-Samii Y. // 2004. IEEE Antennas and Propagation Society International Symposium. 20-25 June 2004. - Vol. 4. - P. 4368-4371. ↑

C4715. Papila I. Multiscale segmentation of remotely sensed images using pairwise Markov chains. / Papila I., Ersoy O. // 2004. IEEE Antennas and Propagation Society International Symposium. 20-25 June 2004. - Vol. 2. - P. 2123-2126. ↑

- C4716.** Tripoli L. Modelling and migration of two dimensional GPR images. / Tripoli L., Elkhetai S.I. // 2004. GPR 2004. Proceedings of the Tenth International Conference on Ground Penetrating Radar. 2004. - Vol. 1. - P. 99-102. ↑
- C4717.** {no data available}. GPR 2004 conference is organised in cooperation with. 2004. GPR 2004. Proceedings of the Tenth International Conference on Ground Penetrating Radar. 2004. - P. iii. ↑
- C4718.** Whiting B.M. GPR investigations of a prehistoric native american village site, lower snake river Floodplain, Idaho, USA. / Whiting B.M., Orvald T.O. // 2004. GPR 2004. Proceedings of the Tenth International Conference on Ground Penetrating Radar. 2004. - P. 451-454. ↑
- C4719.** Brown R. System survey of deep penetrating radar. / Brown R., Genello J., Lynch D., Kapfer R., Norgard J., Wicks M., Amuso V. // 2004. GPR 2004. Proceedings of the Tenth International Conference on Ground Penetrating Radar. - Delft, The Netherlands, 21-24 June 2004. - Vol. 1. - P. 179-182. ↑
- C4720.** Tripoli. Design and simulation of a GPR system for deep probing. / Tripoli, Wali B., Libya, Elkhetai S.I. // 2004. GPR 2004. Proceedings of the Tenth International Conference on Ground Penetrating Radar. 2004. - Vol. 1. - P. 203-206. ↑
- C4721.** Shi J. Estimation of soil moisture with I-band multi-polarization radar. / Shi J., Chen K.S., Kim Y., Van Zyl J.J., Sun G., O'Neill P., Jackson T., Entekhabi D. // 2004. IGARSS '04. Proceedings. 2004 IEEE International Geoscience and Remote Sensing Symposium. - Anchorage, AK, 20-24 Sept. 2004. - Vol. 2. - P. 815-818. ↑
- C4722.** Srivastava S.K. RADARSAT-1 image quality evolution to the extended mission. / Srivastava S.K., Cote S., Le Dantec P., Hawkins R.K., Murnaghan K.P. // 2004. IGARSS '04. Proceedings. 2004 IEEE International Geoscience and Remote Sensing Symposium. - Anchorage, AK, 20-24 Sept. 2004. - Vol. 2. - P. 1208-1211. ↑
- C4723.** Hajnsek I. Pol-InSAR for agricultural vegetation parameter estimation. / Hajnsek I., Cloude S.R. // 2004. IGARSS '04. Proceedings. 2004 IEEE International Geoscience and Remote Sensing Symposium. - Anchorage, AK, 20-24 Sept. 2004. - Vol. 2. - P. 1224-1227. ↑
- C4724.** Nett H. Atmospheric dynamics mission: Aeolus. / Nett H., Endemann M. // 2004. IGARSS '04. Proceedings. 2004 IEEE International Geoscience and Remote Sensing Symposium. - Anchorage, AK, 20-24 Sept. 2004. - Vol. 2. - P. 1190-1195. ↑
- C4725.** Bredin C. High resolution SAR micro-satellite based on passive reflectors. / Bredin C., Goutoule J.M., Sanchez R., Aguttes J.-P., Amiot T. // 2004. IGARSS '04. Proceedings. 2004 IEEE International Geoscience and Remote Sensing Symposium. - Anchorage, AK, 20-24 Sept. 2004. - Vol. 2. - P. 1196-1199. ↑
- C4726.** Ballester-Berman J.D. Retrieval of height and topography of corn fields by polarimetric SAR interferometry. / Ballester-Berman J.D., Lopez-Sanchez J.-M., Fortuny-Guasch J. // 2004. IGARSS '04. Proceedings. 2004 IEEE International Geoscience and Remote Sensing Symposium. - Anchorage, AK, 20-24 Sept. 2004. - Vol. 2. - P. 1228-1231. ↑
- C4727.** Fornaro G. Spaceborne 3D SAR tomography: experiments with ers data. / Fornaro G., Serafino F. // 2004. IGARSS '04. Proceedings. 2004 IEEE International Geoscience and Remote Sensing Symposium. - Anchorage, AK, 20-24 Sept. 2004. - Vol. 2. - P. 1240-1243. ↑
- C4728.** Liseno A. Parameter inversion of "reduced" SAR flight-tracks: first results over forest. / Liseno A., Papathanassiou K.P., Moreira A., Pierri R. // 2004. IGARSS '04. Proceedings. 2004 IEEE International Geoscience and Remote Sensing Symposium. - Anchorage, AK, 20-24 Sept. 2004. - Vol. 2. - P. 1244-1247. ↑
- C4729.** Tabb M. Full maximum likelihood inversion of polinsar scattering models. / Tabb M., Flynn T., Carande R. // 2004. IGARSS '04. Proceedings. 2004 IEEE International Geoscience and Remote Sensing Symposium. - Anchorage, AK, 20-24 Sept. 2004. - Vol. 2. - P. 1232-1235. ↑
- C4730.** D'Hondt O. Local orientation analysis of spatial texture from polarimetric SAR data. / D'Hondt O., Ferro-Famil L., Pottier E. // 2004. IGARSS '04. Proceedings. 2004 IEEE International Geoscience and Remote Sensing Symposium. - Anchorage, AK, 20-24 Sept. 2004. - Vol. 2. - P. 1236-1239. ↑
- C4731.** Brule L. RADARSAT-2 program update. / Brule L., Smyth J., Baeggli H. // 2004. IGARSS '04. Proceedings. 2004 IEEE International Geoscience and Remote Sensing Symposium. - Anchorage, AK, 20-24

Sept. 2004. - Vol. 2. - P. 1186-1189. ↑

C4732. Runge H. Mapping of tidal currents with SAR along track interferometry. / Runge H., Suchandt S., Breit H., Eineder M., Schulz-Stellenfleth J., Bard J., Romeiser R. // 2004. IGARSS '04. Proceedings. 2004 IEEE International Geoscience and Remote Sensing Symposium. - Anchorage, AK, 20-24 Sept. 2004. - Vol. 2. - P. 1156-1159. ↑

C4733. Farquharson G. Microwave radar remote sensing of surface currents in the nearshore region. / Farquharson G., Behn M., Perkovic D., Culcuoglu Z., Frasier S.J. // 2004. IGARSS '04. Proceedings. 2004 IEEE International Geoscience and Remote Sensing Symposium. - Anchorage, AK, 20-24 Sept. 2004. - Vol. 2. - P. 1160-1163. ↑

C4734. Wakabayashi H. Glacier flow estimation by SAR image correlation. / Wakabayashi H., Nishio F. // 2004. IGARSS '04. Proceedings. 2004 IEEE International Geoscience and Remote Sensing Symposium. - Anchorage, AK, 20-24 Sept. 2004. - Vol. 2. - P. 1136-1139. ↑

C4735. Davis C.H. Decadal mass balance of the antarctic ice sheet and its contribution to global sea level rise. / Davis C.H., Yonghong Li. // 2004. IGARSS '04. Proceedings. 2004 IEEE International Geoscience and Remote Sensing Symposium. - Anchorage, AK, 20-24 Sept. 2004. - Vol. 2. - P. 1152-1155. ↑

C4736. Teague C.C. UHF riversonde observations of cowlitz river flow velocity at Castle Rock, Washington. / Teague C.C., Barrick D.E., Lilleboe P.M. // 2004. IGARSS '04. Proceedings. 2004 IEEE International Geoscience and Remote Sensing Symposium. - Anchorage, AK, 20-24 Sept. 2004. - Vol. 2. - P. 1164-1166. ↑

C4737. Ebuchi N. Observation of the Soya warm current using HF ocean radar. / Ebuchi N., Fukamachi Y., Ohshima K.I., Shirasawa K., Ishikawa M., Takatsuka T., Daibo T., Wakatsuchi M. // 2004. IGARSS '04. Proceedings. 2004 IEEE International Geoscience and Remote Sensing Symposium. - Anchorage, AK, 20-24 Sept. 2004. - Vol. 2. - P. 1175-1178. ↑

C4738. Trujillo D.A. Accuracy of surface current velocity measurements obtained from HF radar in Corpus Christi Bay, Texas. / Trujillo D.A., Kelly F.J., Perez J.C., Riddles H.R., Bonner J.S. // 2004. IGARSS '04. Proceedings. 2004 IEEE International Geoscience and Remote Sensing Symposium. - Anchorage, AK, 20-24 Sept. 2004. - Vol. 2. - P. 1179-1182. ↑

C4739. Vesecky J.F. Using multifrequency HF radar to estimate ocean wind fields. / Vesecky J.F., Drake J.A., Laws K., Ludwig F.L., Teague C.C., Meadows L.A. // 2004. IGARSS '04. Proceedings. 2004 IEEE International Geoscience and Remote Sensing Symposium. - Anchorage, AK, 20-24 Sept. 2004. - Vol. 2. - P. 1167-1170. ↑

C4740. Cochin V. Anomaly detection in VHF radar measurements. / Cochin V., Mercier G., Garello R., Mariette V., Broche P. // 2004. IGARSS '04. Proceedings. 2004 IEEE International Geoscience and Remote Sensing Symposium. - Anchorage, AK, 20-24 Sept. 2004. - Vol. 2. - P. 1171-1174. ↑

C4741. Bazi Y. An approach to unsupervised change detection in multitemporal SAR images based on the Generalized Gaussian distribution. / Bazi Y., Bruzzone L., Melgani F. // 2004. IGARSS '04. Proceedings. 2004 IEEE International Geoscience and Remote Sensing Symposium. 20-24 Sept. 2004. - Vol. 2. - P. 1402-1405. ↑

C4742. Tian Y.F. Techniques for seismic damages assessment by using remotely sensed images. / Tian Y.F., Zhang J.F. // 2004. IGARSS '04. Proceedings. 2004 IEEE International Geoscience and Remote Sensing Symposium. 20-24 Sept. 2004. - Vol. 2. - P. 1422-1425. ↑

C4743. Del Frate F. Oil spill detection by means of neural networks algorithms: a sensitivity analysis. / Del Frate F., Salvatori L. // 2004. IGARSS '04. Proceedings. 2004 IEEE International Geoscience and Remote Sensing Symposium. 20-24 Sept. 2004. - Vol. 2. - P. 1370-1373. ↑

C4744. Wang J.R. Remote measurements of snowfalls in Wakasa Bay, Japan with Airborne Millimeter-wave Imaging Radiometer and Cloud Radar. / Wang J.R., Racette P., Liu G.S., Austin R.T., Sekelsky S.M. // 2004. IGARSS '04. Proceedings. 2004 IEEE International Geoscience and Remote Sensing Symposium. 20-24 Sept. 2004. - Vol. 2. - P. 1386-1389. ↑

C4745. Palubinskas G. Radar signatures of road vehicles. / Palubinskas G., Runge H., Reinartz P. // 2004. IGARSS '04. Proceedings. 2004 IEEE International Geoscience and Remote Sensing Symposium. 20-24 Sept. 2004. - Vol. 2. - P. 1498-1501. ↑

- C4746.** Moser G. Finite mixture models and stochastic expectation-maximization for SAR amplitude probability density function estimation based on a dictionary of parametric families. / Moser G., Zerubia J., Serpico S.B. // 2004. IGARSS '04. Proceedings. 2004 IEEE International Geoscience and Remote Sensing Symposium. 20-24 Sept. 2004. - Vol. 2. - P. 1510-1513. ↑
- C4747.** Nolte N. Next generation on-board SAR processor for compact airborne systems. / Nolte N., Simon-Klar C., Langemeyer S., Kirscht M., Pirsch P. // 2004. IGARSS '04. Proceedings. 2004 IEEE International Geoscience and Remote Sensing Symposium. 20-24 Sept. 2004. - Vol. 2. - P. 1514-1517. ↑
- C4748.** Meyer F. The feasibility of traffic monitoring with TerraSAR-X-analyses and consequences. / Meyer F., Hinz S. // 2004. IGARSS '04. Proceedings. 2004 IEEE International Geoscience and Remote Sensing Symposium. 20-24 Sept. 2004. - Vol. 2. - P. 1502-1505. ↑
- C4749.** Bon N. Airborne scan mode ISAR imagery of ships using high resolution spectral methods and particle filter. / Bon N., Khenchaf A., Garelo R. // 2004. IGARSS '04. Proceedings. 2004 IEEE International Geoscience and Remote Sensing Symposium. 20-24 Sept. 2004. - Vol. 2. - P. 1506-1509. ↑
- C4750.** Huhnerfuss H. Sea slicks and oil spills-the chemical structure and morphology determines the remote sensing signals. / Huhnerfuss H., Hoffmann F., Simon-Kutscher J., Alpers W., Gade M. // 2004. IGARSS '04. Proceedings. 2004 IEEE International Geoscience and Remote Sensing Symposium. 20-24 Sept. 2004. - Vol. 2. - P. 1366-1369. ↑
- C4751.** Dente L. On the assimilation of C-band radar data into CERES-wheat model. / Dente L., Rinaldi M., Mattia F., Satalino G. // 2004. IGARSS '04. Proceedings. 2004 IEEE International Geoscience and Remote Sensing Symposium. - Anchorage, AK, 20-24 Sept. 2004. - Vol. 2. - P. 1284-1287. ↑
- C4752.** Ringelmann N. Planting date estimation in semi-arid environments based on Ku-band radar scatterometer data. / Ringelmann N., Scipal K., Bartalis Z., Wagner W. // 2004. IGARSS '04. Proceedings. 2004 IEEE International Geoscience and Remote Sensing Symposium. - Anchorage, AK, 20-24 Sept. 2004. - Vol. 2. - P. 1288-1291. ↑
- C4753.** Zheng-Shu Zhou. 3-D broadband ground-based polarimetric SAR data processing for the monitoring of vegetation growth variations. / Zheng-Shu Zhou, Hamasaki T., Sato M., Boerner W.-M. // 2004. IGARSS '04. Proceedings. 2004 IEEE International Geoscience and Remote Sensing Symposium. - Anchorage, AK, 20-24 Sept. 2004. - Vol. 2. - P. 1248-1251. ↑
- C4754.** Brown S.T. Simultaneous retrieval of surface wind speed and rain rate using radar and radiometer measurements. / Brown S.T., Ruf C.S. // 2004. IGARSS '04. Proceedings. 2004 IEEE International Geoscience and Remote Sensing Symposium. - Anchorage, AK, 20-24 Sept. 2004. - Vol. 2. - P. 1252-1255. ↑
- C4755.** Mushkin A. Estimating subpixel surface roughness using remotely sensed stereoscopic data. / Mushkin A., Gillespie A. // 2004. IGARSS '04. Proceedings. 2004 IEEE International Geoscience and Remote Sensing Symposium. 20-24 Sept. 2004. - Vol. 2. - P. 1292-1295. ↑
- C4756.** Sobjaerg S.S. Influence from polarized galactic background noise on L-band measurements of the sea surface salinity. / Sobjaerg S.S., Skou N. // 2004. IGARSS '04. Proceedings. 2004 IEEE International Geoscience and Remote Sensing Symposium. 20-24 Sept. 2004. - Vol. 2. - P. 1354-1357. ↑
- C4757.** Yueh S.H. Microwave remote sensing modeling of ocean surface salinity and winds using an empirical sea surface spectrum. 2004. IGARSS '04. Proceedings. 2004 IEEE International Geoscience and Remote Sensing Symposium. 20-24 Sept. 2004. - Vol. 2. - P. 1358-1361. ↑
- C4758.** Nghiem S.V. Observations of Arctic environmental change. 2004. IGARSS '04. Proceedings. 2004 IEEE International Geoscience and Remote Sensing Symposium. 20-24 Sept. 2004. - Vol. 2. - P. 1322 vol.2. ↑
- C4759.** Ruofei Zhong. Performance evaluation of microwave radiometer carried by Shenzhou IV for land surface parameters retrieval. / Ruofei Zhong, Huadong Guo, Weimin Wang, Boqin Zhu. // 2004. IGARSS '04. Proceedings. 2004 IEEE International Geoscience and Remote Sensing Symposium. 20-24 Sept. 2004. - Vol. 2. - P. 1346-1349. ↑
- C4760.** Zafar B.J. SOM of space borne precipitation radar rain profiles on global scale. / Zafar B.J., Chandrasekar V. // 2004. IGARSS '04. Proceedings. 2004 IEEE International Geoscience and Remote Sensing

Symposium. 20-24 Sept. 2004. - Vol. 2. - P. 925-928. ↑

C4761. Rose C.R. Space borne GPM dual-frequency radar simulation from high resolution ground radar observations. / Rose C.R., Chandrasekar V. // 2004. IGARSS '04. Proceedings. 2004 IEEE International Geoscience and Remote Sensing Symposium. 20-24 Sept. 2004. - Vol. 2. - P. 929-932. ↑

C4762. Flaming G.M. Measurement of global precipitation. 2004. IGARSS '04. Proceedings. 2004 IEEE International Geoscience and Remote Sensing Symposium. 20-24 Sept. 2004. - Vol. 2. - P. 918-920. ↑

C4763. Bidwell S.W. Preparations for Global Precipitation Measurement (GPM) ground validation. / Bidwell S.W., Durning J.F., Everett D.F., Schwaller M.R., Smith E.A., Wolff D.B. // 2004. IGARSS '04. Proceedings. 2004 IEEE International Geoscience and Remote Sensing Symposium. 20-24 Sept. 2004. - Vol. 2. - P. 921-924. ↑

C4764. Tagawa T. Suppression of surface clutter interference with precipitation measurement from space by the Dual frequency Precipitation Radar. / Tagawa T., Okamoto K., Hanado H., Kozu T. // 2004. IGARSS '04. Proceedings. 2004 IEEE International Geoscience and Remote Sensing Symposium. 20-24 Sept. 2004. - Vol. 2. - P. 933-936. ↑

C4765. Perissin D. ERS-ENVISAT Permanent Scatterers. / Perissin D., Prati C., Rocca F., Ferretti A. // 2004. IGARSS '04. Proceedings. 2004 IEEE International Geoscience and Remote Sensing Symposium. 20-24 Sept. 2004. - Vol. 2. - P. 985-988. ↑

C4766. Wiesmann A. Combination of point and extended target based interferometric techniques. / Wiesmann A., Werner C., Strozzi T., Wegmuller U. // 2004. IGARSS '04. Proceedings. 2004 IEEE International Geoscience and Remote Sensing Symposium. 20-24 Sept. 2004. - Vol. 2. - P. 989-991. ↑

C4767. Toporkov J.V. Initial vector velocity estimates from the UMass Dual Beam Interferometer. / Toporkov J.V., Sletten M.A., Perkovic D., Farquharson G., Frasier S.J. // 2004. IGARSS '04. Proceedings. 2004 IEEE International Geoscience and Remote Sensing Symposium. 20-24 Sept. 2004. - Vol. 2. - P. 976-979. ↑

C4768. Bamler R. Split band interferometry versus absolute ranging with wideband SAR systems. / Bamler R., Eineder M. // 2004. IGARSS '04. Proceedings. 2004 IEEE International Geoscience and Remote Sensing Symposium. 20-24 Sept. 2004. - Vol. 2. - P. 980-984. ↑

C4769. Stout J. Selected analyses of TRMM instantaneous rainfall data. / Stout J., Kwiatkowski J. // 2004. IGARSS '04. Proceedings. 2004 IEEE International Geoscience and Remote Sensing Symposium. 20-24 Sept. 2004. - Vol. 2. - P. 914-917. ↑

C4770. Thoma D. Comparison of two methods for extracting surface soil moisture from C-band radar imagery. / Thoma D., Moran M., Bryant R., Collins C.H., Rahman M., Skirvin S. // 2004. IGARSS '04. Proceedings. 2004 IEEE International Geoscience and Remote Sensing Symposium. - Anchorage, AK, 20-24 Sept. 2004. - Vol. 2. - P. 827-830. ↑

C4771. Graf T. Estimation of snowfall over the sea of Japan using AMSR-E passive microwave remote sensing observation. / Graf T., Koike T., Pfaff T., Muramoto K., Aonashi K. // 2004. IGARSS '04. Proceedings. 2004 IEEE International Geoscience and Remote Sensing Symposium. - Anchorage, AK, 20-24 Sept. 2004. - Vol. 2. - P. 865-868. ↑

C4772. Paloscia S. Soil properties estimates from SAR data by using a bayesian approach combined with IEM. / Paloscia S., Santi E., Pettinato S., Angiulli M. // 2004. IGARSS '04. Proceedings. 2004 IEEE International Geoscience and Remote Sensing Symposium. - Anchorage, AK, 20-24 Sept. 2004. - Vol. 2. - P. 819-822. ↑

C4773. Allain S. Two novel surface model based inversion algorithms using multi-frequency poSAR data. / Allain S., Ferro-Famil L., Pottier E. // 2004. IGARSS '04. Proceedings. 2004 IEEE International Geoscience and Remote Sensing Symposium. - Anchorage, AK, 20-24 Sept. 2004. - Vol. 2. - P. 823-826. ↑

C4774. Shibata A. How much seawinds wind direction data improve AMSR SST. 2004. IGARSS '04. Proceedings. 2004 IEEE International Geoscience and Remote Sensing Symposium. - Anchorage, AK, 20-24 Sept. 2004. - Vol. 2. - P. 869-870. ↑

C4775. Kim M.-J. Millimeter-wave measurement of frozen hydrometeors during the 2003 Wakasa bay field experiment. / Kim M.-J., Chang D.-E., Weinman J.A., Wang J.R., Tanelli S., Roman-Nieves J.I., Sekelsky S.M. //

2004. IGARSS '04. Proceedings. 2004 IEEE International Geoscience and Remote Sensing Symposium. 20-24 Sept. 2004. - Vol. 2. - P. 906-909. ↑

C4776. Takahashi N. The characteristics of system noise of TRMM/PR and their application to the rain detection algorithm. / Takahashi N., Iguchi T. // 2004. IGARSS '04. Proceedings. 2004 IEEE International Geoscience and Remote Sensing Symposium. 20-24 Sept. 2004. - Vol. 2. - P. 910-913. ↑

C4777. Nguyen H. Simulation of SAR images of a forested area based on a 3-D full-wave model of wave scattering. / Nguyen H., Roussel H., Tabbara W. // 2004. IGARSS '04. Proceedings. 2004 IEEE International Geoscience and Remote Sensing Symposium. - Anchorage, AK, 20-24 Sept. 2004. - Vol. 2. - P. 885-887. ↑

C4778. Sun G. Combined tree growth, I-system, and radar backscatter modeling. / Sun G., Ranson K.J., Zhifeng Guo. // 2004. IGARSS '04. Proceedings. 2004 IEEE International Geoscience and Remote Sensing Symposium. - Anchorage, AK, 20-24 Sept. 2004. - Vol. 2. - P. 891-894. ↑

C4779. Matsuoka M. Building damage detection using satellite SAR intensity images for the 2003 Algeria and Iran earthquakes. / Matsuoka M., Yamazaki F. // 2004. IGARSS '04. Proceedings. 2004 IEEE International Geoscience and Remote Sensing Symposium. - Anchorage, AK, 20-24 Sept. 2004. - Vol. 2. - P. 1099-1102. ↑

C4780. Inglada J. On the real capabilities of remote sensing for disaster management-feedback from real cases. / Inglada J., Giros A. // 2004. IGARSS '04. Proceedings. 2004 IEEE International Geoscience and Remote Sensing Symposium. - Anchorage, AK, 20-24 Sept. 2004. - Vol. 2. - P. 1110-1112. ↑

C4781. Mathur A. Automated texture recognition system based on 2D minimum variance spectral estimation. / Mathur A., Younan N.H., Bruce L.M. // 2004. IGARSS '04. Proceedings. 2004 IEEE International Geoscience and Remote Sensing Symposium. 20-24 Sept. 2004. - Vol. 2. - P. 1061-1064. ↑

C4782. Fujita M. Polarimetric feature of small urban area measured with SIR-C. / Fujita M., Miho Y. // 2004. IGARSS '04. Proceedings. 2004 IEEE International Geoscience and Remote Sensing Symposium. 20-24 Sept. 2004. - Vol. 2. - P. 1069-1072. ↑

C4783. Stebler O. Swiss alpine airborne sar experiment (SASARE) part I: multi-baseline polarimetric SAR inter-ferometry studies at L- and P-band. / Stebler O., Barmettler A., Divis L., Small D., Meier E., Nuesch D., Schwerzmann A. // 2004. IGARSS '04. Proceedings. 2004 IEEE International Geoscience and Remote Sensing Symposium. - Anchorage, AK, 20-24 Sept. 2004. - Vol. 2. - P. 1116-1120. ↑

C4784. Rao Y.S. SAR interferometry for DEM generation and movemnet of Indian glaciers. / Rao Y.S., Venkataraman G., Rao K.S., Snehmani. // 2004. IGARSS '04. Proceedings. 2004 IEEE International Geoscience and Remote Sensing Symposium. - Anchorage, AK, 20-24 Sept. 2004. - Vol. 2. - P. 1128-1131. ↑

C4785. Bousquet L. Velocities field of mountain glacier obtained by synthetic aperture radar interferometry. comparison of insar and surveyed velocities. / Bousquet L., Gay M., Legresy B., Gabriel-vasile, Trouve E. // 2004. IGARSS '04. Proceedings. 2004 IEEE International Geoscience and Remote Sensing Symposium. - Anchorage, AK, 20-24 Sept. 2004. - Vol. 2. - P. 1132-1135. ↑

C4786. Barmettler A. Swiss alpine airborne sar experiment (SASARE) part II-imaging of high alpine glaciers at the VHF-band. / Barmettler A., Stebler O., Small D., Meier E., Nuesch D. // 2004. IGARSS '04. Proceedings. 2004 IEEE International Geoscience and Remote Sensing Symposium. - Anchorage, AK, 20-24 Sept. 2004. - Vol. 2. - P. 1121-1123. ↑

C4787. Storvold R. SAR firn line detection and correlation to glacial mass balance; Svartisen Glacier, northern Norway. / Storvold R., Hogda K.A., Malnes E. // 2004. IGARSS '04. Proceedings. 2004 IEEE International Geoscience and Remote Sensing Symposium. - Anchorage, AK, 20-24 Sept. 2004. - Vol. 2. - P. 1124-1127. ↑

C4788. Peng Xu. A comparison on texture classification algorithms for remote sensing data. / Peng Xu, Min Dai, Chan A.K. // 2004. IGARSS '04. Proceedings. 2004 IEEE International Geoscience and Remote Sensing Symposium. 20-24 Sept. 2004. - Vol. 2. - P. 1057-1060. ↑

C4789. Moreira A. TanDEM-X: a TerraSAR-X add-on satellite for single-pass SAR interferometry. / Moreira A., Krieger G., Hajnsek I., Hounam D., Werner M., Riegger S., Settelmeier E. // 2004. IGARSS '04. Proceedings. 2004 IEEE International Geoscience and Remote Sensing Symposium. 20-24 Sept. 2004. - Vol. 2. - P. 1000-1003. ↑

- C4790.** Franceschetti G. Interferometric coherence of SAR signals backscattered by a building. / Franceschetti G., Iodice A., Riccio D., Ruello G. // 2004. IGARSS '04. Proceedings. 2004 IEEE International Geoscience and Remote Sensing Symposium. 20-24 Sept. 2004. - Vol. 2. - P. 1004-1006. ↑
- C4791.** Prats P. Efficient detection and correction of residual motion errors in airborne SAR interferometry. / Prats P., Reigber A., Mallorqui J.J., Broquetas A. // 2004. IGARSS '04. Proceedings. 2004 IEEE International Geoscience and Remote Sensing Symposium. 20-24 Sept. 2004. - Vol. 2. - P. 992-995. ↑
- C4792.** Costantini M. Combining multitemporal SAR differential interferograms: a curvature based method. / Costantini M., Minati F., Pietranera L. // 2004. IGARSS '04. Proceedings. 2004 IEEE International Geoscience and Remote Sensing Symposium. 20-24 Sept. 2004. - Vol. 2. - P. 996-999. ↑
- C4793.** Pulliainen J. Monitoring of soil moisture and vegetation water content variations in boreal forest from C-band SAR data. / Pulliainen J., Hari P., Hallikainen M., Patrikainen N., Peramaki M., Kolari P. // 2004. IGARSS '04. Proceedings. 2004 IEEE International Geoscience and Remote Sensing Symposium. 20-24 Sept. 2004. - Vol. 2. - P. 1013-1016. ↑
- C4794.** Santoro M. Investigations on ARD monitoring in Siberian forest using spaceborne SAR. / Santoro M., Schumilius C. // 2004. IGARSS '04. Proceedings. 2004 IEEE International Geoscience and Remote Sensing Symposium. 20-24 Sept. 2004. - Vol. 2. - P. 1029-1032. ↑
- C4795.** Rosenqvist A. An overview of the JERS-1 SAR Global Boreal Forest Mapping (GBFM) project. / Rosenqvist A., Shimada M., Chapman B., McDonald K., De Grandi G., Jonsson H., Williams C., Rauste Y., Nilsson M., Sango D., Matsumoto M. // 2004. IGARSS '04. Proceedings. 2004 IEEE International Geoscience and Remote Sensing Symposium. 20-24 Sept. 2004. - Vol. 2. - P. 1033-1036. ↑
- C4796.** McNeill S.J. Biophysical parameter retrieval in production forest stands using C-band polarimetric radar. / McNeill S.J., Pairman D., North H.C. // 2004. IGARSS '04. Proceedings. 2004 IEEE International Geoscience and Remote Sensing Symposium. 20-24 Sept. 2004. - Vol. 2. - P. 1017-1020. ↑
- C4797.** Pan Liang. Backscattering simulation for nonuniform forest canopies using multilayer MIMICS. / Pan Liang, Moghaddam M., Pierce L. // 2004. IGARSS '04. Proceedings. 2004 IEEE International Geoscience and Remote Sensing Symposium. 20-24 Sept. 2004. - Vol. 2. - P. 1021-1024. ↑
- C4798.** Xiaolong Dong. Feasibility and design of the surface penetrating radar for lunar lander. / Xiaolong Dong, Bo Sun, Suyun Zhu, Huguang Liu, Jingshan Jiang. // 2004. IGARSS '04. Proceedings. 2004 IEEE International Geoscience and Remote Sensing Symposium. 20-24 Sept. 2004. - Vol. 3. - P. 1778-1780. ↑
- C4799.** Dubois-Fernandez P. Clutter statistical analysis for high resolution SAR data. / Dubois-Fernandez P., Cantalloube H., Dupuis X. // 2004. IGARSS '04. Proceedings. 2004 IEEE International Geoscience and Remote Sensing Symposium. 20-24 Sept. 2004. - Vol. 3. - P. 1781-1783. ↑
- C4800.** Boerner E. Simulation of distributed Spotlight raw data from X-SAR/SRTM Stripmap data. / Boerner E., Balss U., Eineder M. // 2004. IGARSS '04. Proceedings. 2004 IEEE International Geoscience and Remote Sensing Symposium. - Anchorage, AK, 20-24 Sept. 2004. - Vol. 3. - P. 1770-1773. ↑
- C4801.** Eldhuset K. Raw signal simulation for very high resolution SAR based on polarimetric scattering theory. 2004. IGARSS '04. Proceedings. 2004 IEEE International Geoscience and Remote Sensing Symposium. - Anchorage, AK, 20-24 Sept. 2004. - Vol. 3. - P. 1774-1777. ↑
- C4802.** Amberg V. Structure extraction from high resolution SAR data on urban areas. / Amberg V., Coulon M., Marthon P., Spigai M. // 2004. IGARSS '04. Proceedings. 2004 IEEE International Geoscience and Remote Sensing Symposium. 20-24 Sept. 2004. - Vol. 3. - P. 1784-1787. ↑
- C4803.** Vasile G. Improving coherence estimation for high-resolution polarimetric SAR interferometry. / Vasile G., Trouve E., Ciuc M., Bolon P., Buzuloiu V. // 2004. IGARSS '04. Proceedings. 2004 IEEE International Geoscience and Remote Sensing Symposium. 20-24 Sept. 2004. - Vol. 3. - P. 1796-1799. ↑
- C4804.** Liu C. Improved ship detection using polarimetric SAR data. / Liu C., Vachon P.W., Geling G.W. // 2004. IGARSS '04. Proceedings. 2004 IEEE International Geoscience and Remote Sensing Symposium. - Anchorage, AK, 20-24 Sept. 2004. - Vol. 3. - P. 1800-1803. ↑

- C4805.** Tison C. Retrieval of building shapes from shadows in high resolution SAR interferometric images. / Tison C., Tupin F., Maitre H. // 2004. IGARSS '04. Proceedings. 2004 IEEE International Geoscience and Remote Sensing Symposium. 20-24 Sept. 2004. - Vol. 3. - P. 1788-1791. ↑
- C4806.** Alberga V. Potential of coherent decompositions in SAR polarimetry and interferometry. / Alberga V., Krogager E., Chandra M., Wanielik G. // 2004. IGARSS '04. Proceedings. 2004 IEEE International Geoscience and Remote Sensing Symposium. 20-24 Sept. 2004. - Vol. 3. - P. 1792-1795. ↑
- C4807.** Franceschetti G. Efficient hybrid stripmap/spotlight SAR raw signal simulation. / Franceschetti G., Guida R., Iodice A., Riccio D., Ruello G. // 2004. IGARSS '04. Proceedings. 2004 IEEE International Geoscience and Remote Sensing Symposium. 20-24 Sept. 2004. - Vol. 3. - P. 1767-1769. ↑
- C4808.** Marquez-Martinez J. Radiometric resolution optimization for future SAR systems. / Marquez-Martinez J., Mittermayer J., Rodriguez-Cassola M. // 2004. IGARSS '04. Proceedings. 2004 IEEE International Geoscience and Remote Sensing Symposium. - Anchorage, AK, 20-24 Sept. 2004. - Vol. 3. - P. 1738-1741. ↑
- C4809.** Horie H. Near nadir scattering properties at W-band frequency for the sea surface. / Horie H., Kuroiwa H., Kumagai H. // 2004. IGARSS '04. Proceedings. 2004 IEEE International Geoscience and Remote Sensing Symposium. - Anchorage, AK, 20-24 Sept. 2004. - Vol. 3. - P. 1742-1745. ↑
- C4810.** Small D. Robust radiometric terrain correction for SAR image comparisons. / Small D., Meier E., Nuesch D. // 2004. IGARSS '04. Proceedings. 2004 IEEE International Geoscience and Remote Sensing Symposium. - Anchorage, AK, 20-24 Sept. 2004. - Vol. 3. - P. 1730-1733. ↑
- C4811.** Dall J. Azimuth phase coding for range ambiguity suppression in SAR. / Dall J., Kusk A. // 2004. IGARSS '04. Proceedings. 2004 IEEE International Geoscience and Remote Sensing Symposium. - Anchorage, AK, 20-24 Sept. 2004. - Vol. 3. - P. 1734-1737. ↑
- C4812.** Fujita M. A polarization-rotating Van Atta array reflector and its application to polarimetric radar calibration. / Fujita M., Nakamura S. // 2004. IGARSS '04. Proceedings. 2004 IEEE International Geoscience and Remote Sensing Symposium. - Anchorage, AK, 20-24 Sept. 2004. - Vol. 3. - P. 1746-1749. ↑
- C4813.** Ender J.H.G. New aspects of bistatic SAR: processing and experiments. / Ender J.H.G., Walterscheid I., Brenner A.R. // 2004. IGARSS '04. Proceedings. 2004 IEEE International Geoscience and Remote Sensing Symposium. 20-24 Sept. 2004. - Vol. 3. - P. 1758-1762. ↑
- C4814.** Krieger G. SAR signal reconstruction from non-uniform displaced phase centre sampling. / Krieger G., Gebert N., Moreira A. // 2004. IGARSS '04. Proceedings. 2004 IEEE International Geoscience and Remote Sensing Symposium. - Anchorage, AK, 20-24 Sept. 2004. - Vol. 3. - P. 1763-1766. ↑
- C4815.** Weib M. Synchronisation of bistatic radar systems. 2004. IGARSS '04. Proceedings. 2004 IEEE International Geoscience and Remote Sensing Symposium. 20-24 Sept. 2004. - Vol. 3. - P. 1750-1753. ↑
- C4816.** Fjortoft R. Impact of ambiguities in multistatic SAR: some specificities of an L-band interferometric cartwheel. / Fjortoft R., Souyris J.-C., Gaudin J.-M., Durand P., Massonnet D. // 2004. IGARSS '04. Proceedings. 2004 IEEE International Geoscience and Remote Sensing Symposium. - Anchorage, AK, 20-24 Sept. 2004. - Vol. 3. - P. 1754-1757. ↑
- C4817.** Tunaley J.K.E. Algorithms for ship detection and tracking using satellite imagery. 2004. IGARSS '04. Proceedings. 2004 IEEE International Geoscience and Remote Sensing Symposium. - Anchorage, AK, 20-24 Sept. 2004. - Vol. 3. - P. 1804-1807. ↑
- C4818.** Dankert H. Retrieval of ocean surface wave fields using marine radar-image sequences. / Dankert H., Rosenthal W. // 2004. IGARSS '04. Proceedings. 2004 IEEE International Geoscience and Remote Sensing Symposium. - Anchorage, AK, 20-24 Sept. 2004. - Vol. 3. - P. 1884-1887. ↑
- C4819.** Konig T. A new historic ERS wave mode data set for oceanographic applications. / Konig T., Lehner S., Schulz-Stellenfleth J., Schattler B. // 2004. IGARSS '04. Proceedings. 2004 IEEE International Geoscience and Remote Sensing Symposium. - Anchorage, AK, 20-24 Sept. 2004. - Vol. 3. - P. 1888-1891. ↑
- C4820.** Narayan U. A simple algorithm for spatial disaggregation of radiometer derived soil moisture using higher resolution radar observations. / Narayan U., Lakshmi V., Njoku E.G. // 2004. IGARSS '04. Proceedings.

2004 IEEE International Geoscience and Remote Sensing Symposium. - Anchorage, AK, 20-24 Sept. 2004. - Vol. 3. - P. 1877-1879. ↑

C4821. Lehner S. Extreme wave statistics from radar data sets. / Lehner S., Gunther H. // 2004. IGARSS '04. Proceedings. 2004 IEEE International Geoscience and Remote Sensing Symposium. - Anchorage, AK, 20-24 Sept. 2004. - Vol. 3. - P. 1880-1883. ↑

C4822. Schulz-Stellenfleth J. Investigation of typhoons using ERS-2 SAR wave mode data. / Schulz-Stellenfleth J., Niedermeier A., Lehner S., Horstmann J. // 2004. IGARSS '04. Proceedings. 2004 IEEE International Geoscience and Remote Sensing Symposium. - Anchorage, AK, 20-24 Sept. 2004. - Vol. 3. - P. 1892-1895. ↑

C4823. Dankert H. Ocean surface winds retrieved from marine radar-image sequences. / Dankert H., Horstmann J., Rosenthal W. // 2004. IGARSS '04. Proceedings. 2004 IEEE International Geoscience and Remote Sensing Symposium. - Anchorage, AK, 20-24 Sept. 2004. - Vol. 3. - P. 1903-1906. ↑

C4824. Anterrieu E. A strip adaptive processing approach for the SMOS space mission. / Anterrieu E., Picard B., Martin-Neira M., Waldteufel P., Suess M., Vergely J.-L., Kerr Y., Roques S. // 2004. IGARSS '04. Proceedings. 2004 IEEE International Geoscience and Remote Sensing Symposium. - Anchorage, AK, 20-24 Sept. 2004. - Vol. 3. - P. 1922-1925. ↑

C4825. Duk-Jin Kim. Observations of near-inertial internal waves in the East (Japan) Sea by Synthetic Aperture Radar. / Duk-Jin Kim, SungHyun Nam, Moon W.M., Kuh Kim. // 2004. IGARSS '04. Proceedings. 2004 IEEE International Geoscience and Remote Sensing Symposium. - Anchorage, AK, 20-24 Sept. 2004. - Vol. 3. - P. 1896-1898. ↑

C4826. Xiaofeng Li. Analysis of island wakes and katabatic winds imaged by RADARSAT-1 synthetic aperture radar. / Xiaofeng Li, Weizhong Zheng, Pichel W.G., Cheng-Zhi Zou, Clemente-Colon P., Friedman K.S. // 2004. IGARSS '04. Proceedings. 2004 IEEE International Geoscience and Remote Sensing Symposium. - Anchorage, AK, 20-24 Sept. 2004. - Vol. 3. - P. 1899-1902. ↑

C4827. Bolten J. Assimilation of remotely sensed soil moisture into a hydrologic model. / Bolten J., Lakshmi V. // 2004. IGARSS '04. Proceedings. 2004 IEEE International Geoscience and Remote Sensing Symposium. - Anchorage, AK, 20-24 Sept. 2004. - Vol. 3. - P. 1874-1876. ↑

C4828. Tadono T. Calibration and validation plans of ALOS optical sensors. / Tadono T., Shimada M., Watanabe M., Furuta R., Hashimoto T. // 2004. IGARSS '04. Proceedings. 2004 IEEE International Geoscience and Remote Sensing Symposium. - Anchorage, AK, 20-24 Sept. 2004. - Vol. 3. - P. 1831-1834. ↑

C4829. Touzi R. On the use of symmetric scatterers for calibration and validation of PALSAR polarimetric modes. / Touzi R., Shimada M. // 2004. IGARSS '04. Proceedings. 2004 IEEE International Geoscience and Remote Sensing Symposium. - Anchorage, AK, 20-24 Sept. 2004. - Vol. 3. - P. 1835-1837. ↑

C4830. Gamba P. High resolution InSAR "Builtscapes" improvement using LIDAR as ancillary data. / Gamba P., Dell'Acqua F., Cisotta F., Lisini G. // 2004. IGARSS '04. Proceedings. 2004 IEEE International Geoscience and Remote Sensing Symposium. - Anchorage, AK, 20-24 Sept. 2004. - Vol. 3. - P. 1808-1811. ↑

C4831. Ebuchi N. Comparison of ocean surface vector winds observed by SeaWinds on ADEOS-II with ocean buoy data. / Ebuchi N., Graber H.C., Caruso M.J. // 2004. IGARSS '04. Proceedings. 2004 IEEE International Geoscience and Remote Sensing Symposium. - Anchorage, AK, 20-24 Sept. 2004. - Vol. 3. - P. 1819-1822. ↑

C4832. Storvold R. Snow covered area retrieval using Envisat ASAR wide-swath in mountainous areas. / Storvold R., Malnes E. // 2004. IGARSS '04. Proceedings. 2004 IEEE International Geoscience and Remote Sensing Symposium. - Anchorage, AK, 20-24 Sept. 2004. - Vol. 3. - P. 1845-1848. ↑

C4833. Milne T. Assessment of wetland ecosystems and flooding in the Tonle Sap Basin, Cambodia, using AIRSAR. / Milne T., Tapley I.J. // 2004. IGARSS '04. Proceedings. 2004 IEEE International Geoscience and Remote Sensing Symposium. - Anchorage, AK, 20-24 Sept. 2004. - Vol. 3. - P. 1858-1861. ↑

C4834. Wdowinski S. InSAR-based hydrology of the Everglades, South Florida. / Wdowinski S., Amelung F., Miralles-Wilhelm F., Dixon T., Carande R. // 2004. IGARSS '04. Proceedings. 2004 IEEE International Geoscience and Remote Sensing Symposium. - Anchorage, AK, 20-24 Sept. 2004. - Vol. 3. - P. 1870-1873. ↑

- C4835.** Hallikainen M. Retrieval of snow characteristics from spaceborne scatterometer data. / Hallikainen M., Halme P., Lahtinen P., Pulliainen J. // 2004. IGARSS '04. Proceedings. 2004 IEEE International Geoscience and Remote Sensing Symposium. 20-24 Sept. 2004. - Vol. 3. - P. 1849-1852. ↑
- C4836.** Leshkevich G.A. Recent anomalies in Great Lakes ice cover based on statistical analysis and observation. / Leshkevich G.A., Nghiem S.V. // 2004. IGARSS '04. Proceedings. 2004 IEEE International Geoscience and Remote Sensing Symposium. - Anchorage, AK, 20-24 Sept. 2004. - Vol. 3. - P. 1857 vol.3. ↑
- C4837.** Torres S.M. Range and velocity ambiguity mitigation techniques for the WSR-88D weather radar. / Torres S.M., Zrnic D.S. // 2004. IGARSS '04. Proceedings. 2004 IEEE International Geoscience and Remote Sensing Symposium. - Anchorage, AK, 20-24 Sept. 2004. - Vol. 3. - P. 1727-1729. ↑
- C4838.** Nieto-Boree J.C. Analysis of nonlinear ocean wave features in synthetic aperture radar imagery. / Nieto-Boree J.C., Schulz-Stellenfleth J., Niedermeier A. // 2004. IGARSS '04. Proceedings. 2004 IEEE International Geoscience and Remote Sensing Symposium. 20-24 Sept. 2004. - Vol. 5. - P. 3584-3587. ↑
- C4839.** Raizer V. Passive microwave detection of bubble wakes. 2004. IGARSS '04. Proceedings. 2004 IEEE International Geoscience and Remote Sensing Symposium. 20-24 Sept. 2004. - Vol. 5. - P. 3592-3594. ↑
- C4840.** Hilliard L.M. Lightweight linear broadband antennas enabling small UAV wing systems and space flight nanosat concept. / Hilliard L.M., Mead J., Rincon R., Hildebrand P.H. // 2004. IGARSS '04. Proceedings. 2004 IEEE International Geoscience and Remote Sensing Symposium. - Anchorage, AK, 20-24 Sept. 2004. - Vol. 5. - P. 3577-3580. ↑
- C4841.** Trizna D. Marine radar imaging of nearshore bar structure: biases due to tidal and RMS wave height variations. / Trizna D., Hathaway K., McNinch J. // 2004. IGARSS '04. Proceedings. 2004 IEEE International Geoscience and Remote Sensing Symposium. - Anchorage, AK, 20-24 Sept. 2004. - Vol. 5. - P. 3581-3583. ↑
- C4842.** Rozenberg A. Laboratory study of fine structure of the short surface waves due to breaking: two-directional wave propagation. / Rozenberg A., Ritter M. // 2004. IGARSS '04. Proceedings. 2004 IEEE International Geoscience and Remote Sensing Symposium. 20-24 Sept. 2004. - Vol. 5. - P. 3595-3597. ↑
- C4843.** Souza Filho P.W.M. Environmental sensitivity mapping for oil spill in the Amazon coast using remote sensing and GIS technology. / Souza Filho P.W.M., Goncalves F.D., de Miranda F.P., Beisl C.H., de Faria Almeida E. // 2004. IGARSS '04. Proceedings. 2004 IEEE International Geoscience and Remote Sensing Symposium. - Anchorage, AK, 20-24 Sept. 2004. - Vol. 3. - P. 1565-1568. ↑
- C4844.** Winter E.M. Detection of surface mines using hyperspectral sensors. 2004. IGARSS '04. Proceedings. 2004 IEEE International Geoscience and Remote Sensing Symposium. - Anchorage, AK, 20-24 Sept. 2004. - Vol. 3. - P. 1597-1600. ↑
- C4845.** Jingsong Yang. Optimal polarization for the observation of ocean features with SAR. / Jingsong Yang, Weigen Huang, Qingmei Xiao, Bin Fu, Lu Yao. // 2004. IGARSS '04. Proceedings. 2004 IEEE International Geoscience and Remote Sensing Symposium. 20-24 Sept. 2004. - Vol. 5. - P. 3599-3601. ↑
- C4846.** Stephen H. Analysis of scatterometer observations of Saharan ergs using a simple rough facet model. / Stephen H., Long D.G. // 2004. IGARSS '04. Proceedings. 2004 IEEE International Geoscience and Remote Sensing Symposium. - Anchorage, AK, 20-24 Sept. 2004. - Vol. 3. - P. 1534-1537. ↑
- C4847.** Archer F. Introduction, overview, and status of the Microwave Autonomous Copter System (MACS). / Archer F., Shutko A.M., Coleman T.L., Haldin A., Novichikhin E., Sidorov I. // 2004. IGARSS '04. Proceedings. 2004 IEEE International Geoscience and Remote Sensing Symposium. - Anchorage, AK, 20-24 Sept. 2004. - Vol. 5. - P. 3574-3576. ↑
- C4848.** Ahmad K.A. Application of QuikSCAT radiometer rain rates to near-real-time global precipitation estimates: a global precipitation mission pathfinder. / Ahmad K.A., Jones W.L., Kasparis T. // 2004. IGARSS '04. Proceedings. 2004 IEEE International Geoscience and Remote Sensing Symposium. 20-24 Sept. 2004. - Vol. 5. - P. 3547-3550. ↑
- C4849.** Min-Jeong Kim. Parameterizations of single scattering properties of frozen hydrometeors at millimeter-wave frequencies. / Min-Jeong Kim, Weinman J.A. // 2004. IGARSS '04. Proceedings. 2004 IEEE International Geoscience and Remote Sensing Symposium. 20-24 Sept. 2004. - Vol. 5. - P. 3551-3554. ↑

- C4850.** Zhen Li. Soil moisture measurement and retrieval using Envisat ASAR imagery. / Zhen Li, Xin Ren, Ximvu Li, Lei Wang. // 2004. IGARSS '04. Proceedings. 2004 IEEE International Geoscience and Remote Sensing Symposium. 20-24 Sept. 2004. - Vol. 5. - P. 3539-3542. ↑
- C4851.** Wehn H. Prediction of locust outbreaks from RADARSAT-1 multi-angle data. / Wehn H., Rabus B., Wood D., McCardle A. // 2004. IGARSS '04. Proceedings. 2004 IEEE International Geoscience and Remote Sensing Symposium. 20-24 Sept. 2004. - Vol. 5. - P. 3543-3546. ↑
- C4852.** Min-Jeong Kim. Computation of electromagnetic characteristics of frozen hydrometeors at millimeter-wave frequencies. / Min-Jeong Kim, Weinman J.A., Sun W. // 2004. IGARSS '04. Proceedings. 2004 IEEE International Geoscience and Remote Sensing Symposium. - Anchorage, AK, 20-24 Sept. 2004. - Vol. 5. - P. 3555-3558. ↑
- C4853.** Senbokuva Y. Development of the spaceborne Dual-frequency Precipitation Radar for the Global Precipitation Measurement mission. / Senbokuva Y., Satoh S., Furukawa K., Koiima M., Hanado H., Takahashi N., Iguchi T., Nakamura K. // 2004. IGARSS '04. Proceedings. 2004 IEEE International Geoscience and Remote Sensing Symposium. - Anchorage, AK, 20-24 Sept. 2004. - Vol. 5. - P. 3566-3569. ↑
- C4854.** Zafar B.J. Classification of precipitation type from space borne precipitation radar data and 2D wavelet analysis. / Zafar B.J., Chandrasekar V. // 2004. IGARSS '04. Proceedings. 2004 IEEE International Geoscience and Remote Sensing Symposium. 20-24 Sept. 2004. - Vol. 5. - P. 3570-3573. ↑
- C4855.** Meagher J.P. Mass and mean size dual-frequency radar relations for frozen hydrometeors. / Meagher J.P., Haddad Z.S. // 2004. IGARSS '04. Proceedings. 2004 IEEE International Geoscience and Remote Sensing Symposium. - Anchorage, AK, 20-24 Sept. 2004. - Vol. 5. - P. 3559-3561. ↑
- C4856.** Mubarak K. Examination of surface cross section statistics over ocean and land. / Mubarak K., Almidfa K., Chandrasekar V. // 2004. IGARSS '04. Proceedings. 2004 IEEE International Geoscience and Remote Sensing Symposium. 20-24 Sept. 2004. - Vol. 5. - P. 3562-3565. ↑
- C4857.** Gader P. Multi-sensor and algorithm fusion with the Choquet integral: applications to landmine detection. / Gader P., Mendez-Vasquez A., Chamberlin K., Bolton J., Zare A. // 2004. IGARSS '04. Proceedings. 2004 IEEE International Geoscience and Remote Sensing Symposium. - Anchorage, AK, 20-24 Sept. 2004. - Vol. 3. - P. 1605-1608. ↑
- C4858.** Johnson J.T. Design and demonstration of an interference suppressing microwave radiometer. / Johnson J.T., Hampson G.A., Ellingson S.W. // 2004. IGARSS '04. Proceedings. 2004 IEEE International Geoscience and Remote Sensing Symposium. - Anchorage, AK, 20-24 Sept. 2004. - Vol. 3. - P. 1683-1686. ↑
- C4859.** Johnson J.T. Airborne radio frequency interference studies at C-band using a digital receiver. / Johnson J.T., Gasiewski A.J., Hampson G.A., Ellingson S.W., Krishnamachari R., Klein M. // 2004. IGARSS '04. Proceedings. 2004 IEEE International Geoscience and Remote Sensing Symposium. 20-24 Sept. 2004. - Vol. 3. - P. 1687-1690. ↑
- C4860.** Kidd R. A diurnal difference indicator for freeze-thaw monitoring from Ku band scatterometer applied within the Siberia II project. / Kidd R., Scipal K., Bartalis Z., Wagner W. // 2004. IGARSS '04. Proceedings. 2004 IEEE International Geoscience and Remote Sensing Symposium. - Anchorage, AK, 20-24 Sept. 2004. - Vol. 3. - P. 1671-1674. ↑
- C4861.** Maurer J. Simulation and measurement of 24 GHz Short Range Radar (SRR) Interference. / Maurer J., Younis M., Fortuny-Guasch J., Wiesbeck W. // 2004. IGARSS '04. Proceedings. 2004 IEEE International Geoscience and Remote Sensing Symposium. 20-24 Sept. 2004. - Vol. 3. - P. 1675-1678. ↑
- C4862.** Prati C. Requirements for a space mission for DInSAR and PS analysis based on past and present missions. / Prati C., Rocca F., Ferretti A. // 2004. IGARSS '04. Proceedings. 2004 IEEE International Geoscience and Remote Sensing Symposium. - Anchorage, AK, 20-24 Sept. 2004. - Vol. 3. - P. 1695-1698. ↑
- C4863.** Tsatsoulis C. Intelligent matchmaking for Polar Ice Sheet Data collection and delivery. / Tsatsoulis C., Sivashanmugam S., Perry S. // 2004. IGARSS '04. Proceedings. 2004 IEEE International Geoscience and Remote Sensing Symposium. - Anchorage, AK, 20-24 Sept. 2004. - Vol. 3. - P. 1711-1714. ↑
- C4864.** Randa J. Errors due to the reflectivity of calibration targets. / Randa J., Walker D.K., Cox A.E., Billinger

R.L. // 2004. IGARSS '04. Proceedings. 2004 IEEE International Geoscience and Remote Sensing Symposium. - Anchorage, AK, 20-24 Sept. 2004. - Vol. 3. - P. 1715-1718. ↑

C4865. Roth A. Scientific use of TerraSAR-X. 2004. IGARSS '04. Proceedings. 2004 IEEE International Geoscience and Remote Sensing Symposium. - Anchorage, AK, 20-24 Sept. 2004. - Vol. 3. - P. 1699-1702. ↑

C4866. Xiaolong Dong. The radar altimeter and scatterometer of China's HY-2 satellite. / Xiaolong Dong, Ke Xu, Huguang Liu, Jingshan Jiang. // 2004. IGARSS '04. Proceedings. 2004 IEEE International Geoscience and Remote Sensing Symposium. 20-24 Sept. 2004. - Vol. 3. - P. 1703-1706. ↑

C4867. Solberg R. Multi-sensor and time-series approaches for monitoring of snow parameters. / Solberg R., Amlien J., Koren H., Eikvil L., Malnes E., Stordal R. // 2004. IGARSS '04. Proceedings. 2004 IEEE International Geoscience and Remote Sensing Symposium. - Anchorage, AK, 20-24 Sept. 2004. - Vol. 3. - P. 1661-1666. ↑

C4868. Ho K.C. Improving landmine detection using frequency domain features from ground penetrating radar. / Ho K.C., Gader P.D., Wilson J.N. // 2004. IGARSS '04. Proceedings. 2004 IEEE International Geoscience and Remote Sensing Symposium. - Anchorage, AK, 20-24 Sept. 2004. - Vol. 3. - P. 1617-1620. ↑

C4869. Torriero P. Application of texture feature classification methods to landmine/clutter discrimination in off-lane GPR data. / Torriero P., Collins L. // 2004. IGARSS '04. Proceedings. 2004 IEEE International Geoscience and Remote Sensing Symposium. - Anchorage, AK, 20-24 Sept. 2004. - Vol. 3. - P. 1621-1624. ↑

C4870. Hambaryan A.K. An experimental complex for multi-frequency, short distance, coincident, microwave active-passive and in-situ combined measurements of soil and snow moistures. / Hambaryan A.K., Manukyan M.R., Hambaryan V.K., Darbinyan S.A., Arakelyan A.K. // 2004. IGARSS '04. Proceedings. 2004 IEEE International Geoscience and Remote Sensing Symposium. - Anchorage, AK, 20-24 Sept. 2004. - Vol. 3. - P. 1609-1612. ↑

C4871. Scott W.R. Combined seismic, radar, and induction sensor for landmine detection. / Scott W.R., Kangwook Kim, Larson G.D., Gurbuz A.C., McClellan J.H. // 2004. IGARSS '04. Proceedings. 2004 IEEE International Geoscience and Remote Sensing Symposium. - Anchorage, AK, 20-24 Sept. 2004. - Vol. 3. - P. 1613-1616. ↑

C4872. McNairn H. A national inventory of land management practices: estimating soil conservation practices using optical and radar imagery. / McNairn H., Smith A., Huffman E., Jarvis I., Pacheco A., Gauthier E. // 2004. IGARSS '04. Proceedings. 2004 IEEE International Geoscience and Remote Sensing Symposium. - Anchorage, AK, 20-24 Sept. 2004. - Vol. 3. - P. 1629-1632. ↑

C4873. Jiancheng Shi. Estimation of snow water equivalence with two Ku-band dual polarization radar. 2004. IGARSS '04. Proceedings. 2004 IEEE International Geoscience and Remote Sensing Symposium. - Anchorage, AK, 20-24 Sept. 2004. - Vol. 3. - P. 1649-1652. ↑

C4874. Callens M. Analysis of soil roughness measurements using a 25 m laser profiler and a 4 m wide meshboard. / Callens M., Verhoest N.E.C. // 2004. IGARSS '04. Proceedings. 2004 IEEE International Geoscience and Remote Sensing Symposium. - Anchorage, AK, 20-24 Sept. 2004. - Vol. 3. - P. 1653-1656. ↑

C4875. Abuzar M. Measuring spatial variability of crops and soils at sub-paddock scale using remote sensing technologies. / Abuzar M., Rampant P., Fisher P. // 2004. IGARSS '04. Proceedings. 2004 IEEE International Geoscience and Remote Sensing Symposium. - Anchorage, AK, 20-24 Sept. 2004. - Vol. 3. - P. 1633-1636. ↑

C4876. Derksen C. Evaluating spaceborne passive microwave snow water equivalent retrievals across the Canadian northern boreal-tundra ecotone. / Derksen C., Walker A. // 2004. IGARSS '04. Proceedings. 2004 IEEE International Geoscience and Remote Sensing Symposium. - Anchorage, AK, 20-24 Sept. 2004. - Vol. 3. - P. 1641-1644. ↑

C4877. Mineart G.M. An examination of U.S. plans for meeting operational ocean observation needs with radar altimetry. / Mineart G.M., Rau M.D., Finkelstein J.L. // OCEANS '04. MTS/IEEE TECHNO-OCEAN '04. - Kobe, 9-12 Nov. 2004. - Vol. 3. - P. 1797-1802. ↑

C4878. Tran Tuan Dung. An integrated approach of remote sensing and geophysics for investigating geological structure in the East Vietnam Sea. / Tran Tuan Dung, Trinh Hoai Thu. // OCEANS '04. MTS/IEEE TECHNO-OCEAN '04. - Kobe, 9-12 Nov. 2004. - Vol. 4. - P. 1815-1820. ↑

- C4879.** Liu A.K. Nonlinear internal wave study during ASIAEX. / Liu A.K., Zhao Y., Tang T.Y., Hsu M.K. // 2004. UT '04. 2004 International Symposium on Underwater Technology. 20-23 April 2004. - P. 231-238. ↑
- C4880.** Son N.S. Design of an operation control and remote monitoring system of small unmanned ship for close-range observations. / Son N.S., Kim S.Y., Van S.H. // OCEANS '04. MTT/IEEE TECHNO-OCEAN '04. 9-12 Nov. 2004. - Vol. 2. - P. 1093-1101. ↑
- C4881.** Kozai K. Airborne polarimetric SAR monitoring for ships and coastal seas. / Kozai K., Ishida H., Koguchi N., Wakabayashi N., Yano Y., Hayashi M. // OCEANS '04. MTT/IEEE TECHNO-OCEAN '04. - Kobe, 9-12 Nov. 2004. - Vol. 4. - P. 1821-1824. ↑
- C4882.** Aris M.A.B. Nondestructive and noncontact dielectric measurement methods for low-loss liquids using free space microwave measurement system in 8-12.5 GHz frequency range. / Aris M.A.B., Ghodgaonkar D.K., Khadri N. // 2004. RFM 2004. Proceedings RF and Microwave Conference. 5-6 Oct. 2004. - P. 182-189. ↑
- C4883.** {no data available}. 2004 4th International Conference on Microwave and Millimeter Wave Technology Proceedings (IEEE Cat. No.04EX827). Proceedings Microwave and Millimeter Wave Technology, 2004. ICMMT 4th International Conference on. 18-21 Aug. 2004. - {no data available}. ↑
- C4884.** Nishi K. Survey report of offshore wind conditions in prospect of offshore wind energy conversion systems in Japan. / Nishi K., Shiraishi S., Hamano M., Umeki Y., Kume H. // OCEANS '04. MTT/IEEE TECHNO-OCEAN '04. - Kobe, 9-12 Nov. 2004. - Vol. 4. - P. 1830-1834. ↑
- C4885.** Aris M.A.B. Nondestructive and noncontact dielectric measurement method for high-loss liquids using free space microwave measurement system in 8-12.5 GHz frequency range. / Aris M.A.B., Ghodgaonkar D.K. // 2004. RFM 2004. Proceedings RF and Microwave Conference. 5-6 Oct. 2004. - P. 169-176. ↑
- C4886.** Ashby R. Seeing beyond the perimeter: the Advanced Exterior Sensor (AES). / Ashby R., Pritchard D.A. // 2004. 38th Annual 2004 International Carnahan Conference on Security Technology. 11-14 Oct. 2004. - P. 182-188. ↑
- C4887.** Krul L. Radar development at the technical University Delft after world war II. 2004. EURAD. First European Radar Conference. - Amsterdam, The Netherlands, 11-15 Oct. 2004. - P. 1-4. ↑
- C4888.** Khlusov V. Detection of objects with non-reciprocal properties by polarization radar. / Khlusov V., Ligthart L., Sharygin G. // 2004. EURAD. First European Radar Conference. - Amsterdam, The Netherlands, 11-15 Oct. 2004. - P. 69-72. ↑
- C4889.** {no data available}. Introduction to the 1st European Radar Conference 2004. 2004. EURAD. First European Radar Conference. - Amsterdam, The Netherlands, 11-15 Oct. 2004. - P. iii. ↑
- C4890.** {no data available}. EuRAD 2004 sessions. 2004. EURAD. First European Radar Conference. - Amsterdam, The Netherlands, 11-15 Oct. 2004. - P. vii. ↑
- C4891.** Kalmykov I.A. The using SICH-1/SICH-1M side-looking radar data for ecological environment monitoring. / Kalmykov I.A., Tsymbal V.N., Yefimov V.B. // 2004. EURAD. First European Radar Conference. - Amsterdam, The Netherlands, 11-15 Oct. 2004. - P. 337-340. ↑
- C4892.** Witzgall H.E. Compression of tactical real-valued SAR imagery in the complex SAR phase history domain. / Witzgall H.E., Goldstein J.S. // 2004. Conference Record of the Thirty-Eighth Asilomar Conference on Signals, Systems and Computers. 7-10 Nov. 2004. - Vol. 2. - P. 1678-1681. ↑
- C4893.** Schofield O. The growth of the New Jersey Shelf Observing System for monitoring plumes and blooms on the Mid-Atlantic continental shelf. / Schofield O., Chant R., Kohut J., Glenn S. // OCEANS '04. MTT/IEEE TECHNO-OCEAN '04. 9-12 Nov. 2004. - Vol. 1. - P. 127-132. ↑
- C4894.** {no data available}. Conference Record of the Thirty-Eighth Asilomar Conference on Signals, Systems and Computers (IEEE Cat. No.04CH37592). 2004. Conference Record of the Thirty-Eighth Asilomar Conference on Signals, Systems and Computers. 7-10 Nov. 2004. - Vol. 1. - {no data available}. ↑
- C4895.** {no data available}. Session MA1b Radar and Remote Sensing. 2004. Conference Record of the Thirty-Eighth Asilomar Conference on Signals, Systems and Computers. 7-10 Nov. 2004. - Vol. 1. - P. 1-2. ↑

- C4896.** Zhang ZhaoHui. An automatic method of coarse registration between multi-source satellite images. / Zhang ZhaoHui, Pan ChunHong, Ma SongDe. // 2004. Proceedings of the 2004 Intelligent Sensors, Sensor Networks and Information Processing Conference. 14-17 Dec. 2004. - P. 205-209. ↑
- C4897.** Yang Jianxi. A study of signal-processing about wind and temperature profiler radars in the troposphere. / Yang Jianxi, An Jianping, Bu Xiangyuan. // 2004. Proceedings. ICSP '04. 2004 7th International Conference on Signal Processing. 31 Aug.-4 Sept. 2004. - Vol. 3. - P. 2143-2146. ↑
- C4898.** Wei Lin. Unsupervised segmentation of the POL-SAR image using similarity parameters in sequential projection pursuit model. / Wei Lin, Zheng Tian, Xian-bin Wen, Fan He. // 2004. Proceedings. ICSP '04. 2004 7th International Conference on Signal Processing. 31 Aug.-4 Sept. 2004. - Vol. 1. - P. 769-772. ↑
- C4899.** Takano T. Development of a low-power high-sensitivity cloud profiling FM-CW radar at 95 GHz. / Takano T., Akita K., Kubo H., Kawamura Y., Kumagai H., Takamura T., Nakanishi Y., Nakajima T. // 2004. Proceedings. 2004 Asia-Pacific Radio Science Conference. 24-27 Aug. 2004. - P. 325-328. ↑
- C4900.** Lianlin Li. Restore of broadband radar pulse distorted by the Martian ionosphere. / Lianlin Li, Fang Li. // 2004. Proceedings. 2004 Asia-Pacific Radio Science Conference. 24-27 Aug. 2004. - P. 363-365. ↑
- C4901.** Xia Weiping. A real-time compressing method for complex SAR images. / Xia Weiping, Wang Zhensong, Zhai Jiefu, Han Jizhong. // 2004. Proceedings. ICSP '04. 2004 7th International Conference on Signal Processing. 31 Aug.-4 Sept. 2004. - Vol. 1. - P. 816-818. ↑
- C4902.** Wen Bi-yang. DDC design by using FPGA in HF OSMAR system. / Wen Bi-yang, Ma Zhi-gang, Zhou Hao, Bai Li-yun, Lei Zhi-yong. // 2004. Proceedings. ICCEA 2004. 2004 3rd International Conference on Computational Electromagnetics and Its Applications. 1-4 Nov. 2004. - P. 500-503. ↑
- C4903.** Wu Yan. Multiresolution wavelet decomposition to merge Landsat TM and SPOT panchromatic data. / Wu Yan, Li Ming, Liao Guisheng. // 2004. Proceedings. ICCEA 2004. 2004 3rd International Conference on Computational Electromagnetics and Its Applications. 1-4 Nov. 2004. - P. 521-524. ↑
- C4904.** Ping Wen Jiang. External calibration of the CRS-1 satellite. / Ping Wen Jiang, Khang Lihong, Braun H.M., Lentz H., Kicherer S., Borisch W. // 2004. Proceedings. ICCEA 2004. 2004 3rd International Conference on Computational Electromagnetics and Its Applications. 1-4 Nov. 2004. - P. 395-398. ↑
- C4905.** Ping Wen Jiang. L-Band SAR-processor for the Chinese SAR satellite. / Ping Wen Jiang, Zhang Yongjun, Zhao Bin, Braun H.M., Fritsch B. // 2004. Proceedings. ICCEA 2004. 2004 3rd International Conference on Computational Electromagnetics and Its Applications. 1-4 Nov. 2004. - P. 399-402. ↑
- C4906.** Mingxing Gao. A method for characterizing a target in polarimetric radar remote sensing. / Mingxing Gao, Jian Yang, Yingning Peng. // 2004. Proceedings. 2004 Asia-Pacific Radio Science Conference. 24-27 Aug. 2004. - P. 316-319. ↑
- C4907.** Refaat T.F. Novel infrared phototransistors for atmospheric CO2 profiling at 2 μ m wavelength. / Refaat T.F., Nurul Abedin M., Sulima O.V., Singh U.N., Ismail S. // 2004. IEDM Technical Digest. IEEE International Electron Devices Meeting. 13-15 Dec. 2004. - P. 355-358. ↑
- C4908.** Sluzek A. A feasibility study on a novel method of visual obstacle detection. / Sluzek A., Seong T.C. // 2004. ICIP '04. 2004 International Conference on Image Processing. 24-27 Oct. 2004. - Vol. 4. - P. 2447-2450. ↑
- C4909.** Chun-Yueh Huang. Design of a portable potentiostat for electrochemical sensors. / Chun-Yueh Huang, Yu-Chien Wang, Hung-Chieh Chen, Kuo-Chuan Ho. // 2004. Proceedings of the 2004 Intelligent Sensors, Sensor Networks and Information Processing Conference. 14-17 Dec. 2004. - P. 331-336. ↑
- C4910.** {no data available}. 2004 International Conference on Image Processing (ICIP) (IEEE Cat. No.04CH37580). 2004. ICIP '04. 2004 International Conference on Image Processing. 24-27 Oct. 2004. - Vol. 1. - {no data available}. ↑
- C4911.** Danly B.G. Opportunities for NRL WARLOC radar validation and calibration of NASA Earth Observing Space Missions. / Danly B.G., Miller S.D., Manheimer W., Fliflet A.W., Linde G., Ngo M., Cheung W.J. // 2004. Conference Digest of the 2004 Joint 29th International Conference on Infrared and Millimeter Waves, 2004 and

12th International Conference on Terahertz Electronics. 27 Sept.-1 Oct. 2004. - P. 807-808. ↑

C4912. Yan Songhua. The design of frequency synthesizer for the ocean state measuring and analyzing radar. / Yan Songhua, Wu Shicai, Yang Zijie, Wen Biyang. // 2004. Proceedings. 2004 Asia-Pacific Radio Science Conference. 24-27 Aug. 2004. - P. 254-257. ↑

C4913. Yan Songhua. The effect of phase noise on the remote sensing of ocean surface currents. / Yan Songhua, Wu Shicai, Yang Zijie, Wen Biyang. // 2004. Proceedings. 2004 Asia-Pacific Radio Science Conference. 24-27 Aug. 2004. - P. 299-302. ↑

C4914. {no data available}. 2004 Asia-Pacific Radio Science Conference Proceedings (IEEE Cat. No.04EX825). 2004. Proceedings. 2004 Asia-Pacific Radio Science Conference. 24-27 Aug. 2004. - {no data available}. ↑

C4915. Ya-Qiu Jin. Polarimetric EM scattering and information retrieval in SAR remote sensing. 2004. Proceedings. 2004 Asia-Pacific Radio Science Conference. 24-27 Aug. 2004. - P. K1-K4. ↑

C4916. Salim T. FPGA implementation of a phased array DBF using polyphase filters. / Salim T., Devlin J., Whittington J. // 2004. Proceedings. 2004 IEEE International Conference on Field-Programmable Technology. 6-8 Dec. 2004. - P. 339-342. ↑

C4917. Sakamoto T. Fast imaging of a target in inhomogeneous media for pulse radar systems. / Sakamoto T., Sato T. // 2004. IGARSS '04. Proceedings. 2004 IEEE International Geoscience and Remote Sensing Symposium. - Anchorage, AK, 20-24 Sept. 2004. - Vol. 3. - P. 2070-2073. ↑

C4918. Lin Sun. Analysis on uncertainty in the MODIS retrieved land surface temperature using field measurements and high resolution images. / Lin Sun, Liang-Fu Chen, Qiang Liu, Qin-Huo Liu, Ai-Bin Song. // 2004. IGARSS '04. Proceedings. 2004 IEEE International Geoscience and Remote Sensing Symposium. - Anchorage, AK, 20-24 Sept. 2004. - Vol. 3. - P. 2083-2086. ↑

C4919. Prakash A. Space-based observations in the International Polar Year: educational opportunities to strengthen the STEM pipeline. / Prakash A., Gens R., Kelley J., Alexander V., Johnson L., Yanow G. // 2004. IGARSS '04. Proceedings. 2004 IEEE International Geoscience and Remote Sensing Symposium. 20-24 Sept. 2004. - Vol. 3. - P. 1972-1975. ↑

C4920. Izzawati I.H.W. The impact of forest heterogeneity on the height retrieval using X-band interferometry. / Izzawati I.H.W., Wallington E.D. // 2004. IGARSS '04. Proceedings. 2004 IEEE International Geoscience and Remote Sensing Symposium. - Anchorage, AK, 20-24 Sept. 2004. - Vol. 3. - P. 2042-2045. ↑

C4921. Chymitdorzhev T.N. Electromagnetic wave attenuation for propagation through a forest belt. / Chymitdorzhev T.N., Dagurov P.N., Dmitriev A.V., Mironov V.L. // 2004. IGARSS '04. Proceedings. 2004 IEEE International Geoscience and Remote Sensing Symposium. - Anchorage, AK, 20-24 Sept. 2004. - Vol. 3. - P. 2091-2094. ↑

C4922. Scheuchl B. ENVISAT ASAR AP data for operational sea ice monitoring. / Scheuchl B., Caves R., Flett D., DeAbreu R., Arkett M., Cumming I. // 2004. IGARSS '04. Proceedings. 2004 IEEE International Geoscience and Remote Sensing Symposium. 20-24 Sept. 2004. - Vol. 3. - P. 2142-2145. ↑

C4923. Mahoney A. Landfast sea ice extent and variability in the Alaskan Arctic derived from SAR imagery. / Mahoney A., Eicken H., Graves A., Shapiro L., Cotter P. // 2004. IGARSS '04. Proceedings. 2004 IEEE International Geoscience and Remote Sensing Symposium. - Anchorage, AK, 20-24 Sept. 2004. - Vol. 3. - P. 2146-2149. ↑

C4924. Deschamps A. Temporal soil moisture estimates from Radarsat-1 and Envisat ASAR for flood forecasting. / Deschamps A., Pultz TJ, Pietroniro A., Best K. // 2004. IGARSS '04. Proceedings. 2004 IEEE International Geoscience and Remote Sensing Symposium. - Anchorage, AK, 20-24 Sept. 2004. - Vol. 3. - P. 2119-2122. ↑

C4925. Makynen M. Dependence between spatial statistics and distance for C-band backscattering signatures of the Baltic Sea ice. / Makynen M., Manninen T., Simila M., Karvonen J., Hallikainen M. // 2004. IGARSS '04. Proceedings. 2004 IEEE International Geoscience and Remote Sensing Symposium. - Anchorage, AK, 20-24 Sept. 2004. - Vol. 3. - P. 2138-2141. ↑

- C4926.** Macauley M.K. Public policymaking and climate change: The essential but little known contribution of earth science remote sensing data and products. 2004. IGARSS '04. Proceedings. 2004 IEEE International Geoscience and Remote Sensing Symposium. - Anchorage, AK, 20-24 Sept. 2004. - Vol. 3. - P. 1958-1960. ↑
- C4927.** Wegmuller U. Monitoring mining induced surface deformation. / Wegmuller U., Werner C., Strozzi T., Wiesmann A. // 2004. IGARSS '04. Proceedings. 2004 IEEE International Geoscience and Remote Sensing Symposium. - Anchorage, AK, 20-24 Sept. 2004. - Vol. 3. - P. 1933-1935. ↑
- C4928.** Ranson K.J. Use of ICESat GLAS data for forest disturbance studies in central Siberia. / Ranson K.J., Sun G., Kovacs K., Kharuk V.I. // 2004. IGARSS '04. Proceedings. 2004 IEEE International Geoscience and Remote Sensing Symposium. - Anchorage, AK, 20-24 Sept. 2004. - Vol. 3. - P. 1936-1939. ↑
- C4929.** Picard B. Impact of solar radiation on sea surface salinity remote sensing by spaceborne synthetic aperture imaging radiometers. / Picard B., Reul N., Waldteufel P., Anterrieu E. // 2004. IGARSS '04. Proceedings. 2004 IEEE International Geoscience and Remote Sensing Symposium. - Anchorage, AK, 20-24 Sept. 2004. - Vol. 3. - P. 1926-1929. ↑
- C4930.** Le Vine D.M. Comparison of measured galactic background radiation at L-band with model. / Le Vine D.M., Abraham S., Kerr Y.H., Wilson W.J., Skou N., Sobjaerg S. // 2004. IGARSS '04. Proceedings. 2004 IEEE International Geoscience and Remote Sensing Symposium. 20-24 Sept. 2004. - Vol. 3. - P. 1930-1932. ↑
- C4931.** Reagan J. Spaceborne lidar aerosol retrieval approaches based on aerosol model constraints. / Reagan J., Wang X., Catrall C., Thome K. // 2004. IGARSS '04. Proceedings. 2004 IEEE International Geoscience and Remote Sensing Symposium. - Anchorage, AK, 20-24 Sept. 2004. - Vol. 3. - P. 1940-1943. ↑
- C4932.** Rall J.A.R. Spectral ratio biospheric lidar. / Rall J.A.R., Knox R.G. // 2004. IGARSS '04. Proceedings. 2004 IEEE International Geoscience and Remote Sensing Symposium. - Anchorage, AK, 20-24 Sept. 2004. - Vol. 3. - P. 1951-1954. ↑
- C4933.** Biggar S. Laser-based system for ground-based measurement of backscatter surface reflectance. / Biggar S., Thome K., Geis J., Burkhart C. // 2004. IGARSS '04. Proceedings. 2004 IEEE International Geoscience and Remote Sensing Symposium. - Anchorage, AK, 20-24 Sept. 2004. - Vol. 3. - P. 1955-1957. ↑
- C4934.** Gimmestad G.G. 1.5 microns: the future of unattended aerosol lidar?. / Gimmestad G.G., Roberts D.W. // 2004. IGARSS '04. Proceedings. 2004 IEEE International Geoscience and Remote Sensing Symposium. - Anchorage, AK, 20-24 Sept. 2004. - Vol. 3. - P. 1944-1946. ↑
- C4935.** Repasky K.S. Diode laser transmitter for water vapor DIAL measurements. / Repasky K.S., Shaw J.A., Carlsten J.L., Obland M.D., Meng L.S., Hoffman D.S. // 2004. IGARSS '04. Proceedings. 2004 IEEE International Geoscience and Remote Sensing Symposium. 20-24 Sept. 2004. - Vol. 3. - P. 1947-1950. ↑
- C4936.** Nghiem S.V. The secret of the Svalbard sea ice barrier. / Nghiem S.V., Van Woert M.L., Neumann G. // 2004. IGARSS '04. Proceedings. 2004 IEEE International Geoscience and Remote Sensing Symposium. - Anchorage, AK, 20-24 Sept. 2004. - Vol. 3. - P. 2150 vol.3. ↑
- C4937.** Kipke M.V. Application of the audio interface for ground penetrating radar data representation and interpretation. / Kipke M.V., Okhten N.A., Nikolayev V.A., Badeykin A.V. // 2004 Second International Workshop Ultrawideband and Ultrashort Impulse Signals. 19-22 Sept. 2004. - P. 220-222. ↑
- C4938.** Ksendzук A.V. Some aspects of usage of the pseudo noise sequences in the radiolocation systems. / Ksendzук A.V., Volosyuk V.K. // 2004 Second International Workshop Ultrawideband and Ultrashort Impulse Signals. 19-22 Sept. 2004. - P. 234-236. ↑
- C4939.** Blinov V.S. The analysis of the matching opportunity of the parameters of the wideband through ionosphere signals with real dispersion radio line. 2004 Second International Workshop Ultrawideband and Ultrashort Impulse Signals. 19-22 Sept. 2004. - P. 168-170. ↑
- C4940.** Samkov S.V. Signal processing in UWB radars of small distance. 2004 Second International Workshop Ultrawideband and Ultrashort Impulse Signals. 19-22 Sept. 2004. - P. 208-210. ↑
- C4941.** Ksendzук AV. Advantages of the wideband and ultra wideband signals in the remote sensing. / Ksendzук AV, Volosyuk V.K., Sologub N.S. // 2004 Second International Workshop Ultrawideband and Ultrashort

Impulse Signals. 19-22 Sept. 2004. - P. 240-242. ↑

C4942. Zaikov E.A. The eigenvector-based identification of shallow buried targets in ground penetrating radar. / Zaikov E.A., Mikhnev V.A., Maksimovitch Y.S. // 2004. CriMico 2004. 2004 14th International Crimean Conference on Microwave and Telecommunication Technology. 13-17 Sept. 2004. - P. 699-700. ↑

C4943. Salim T. FPGA implementation of digital upconversion using distributed arithmetic FIR filters. / Salim T., Devlin J., Whittington J. // 2004. Proceedings. 2004 IEEE International Conference on Field-Programmable Technology. 6-8 Dec. 2004. - P. 335-338. ↑

C4944. Golovko M.M. The automatic determination of soil permittivity using the response from a subsurface local object. 2004 Second International Workshop Ultrawideband and Ultrashort Impulse Signals. 19-22 Sept. 2004. - P. 248-250. ↑

C4945. Hasegawa Y. GPR-based adaptive sensing: GPR manipulation according to terrain configurations. / Hasegawa Y., Yokoe K., Kawai Y., Fukuda T. // 2004. (IROS 2004). Proceedings. 2004 IEEE/RSJ International Conference on Intelligent Robots and Systems. 28 Sept.-2 Oct. 2004. - Vol. 3. - P. 3021-3026. ↑

C4946. van t Klooster K. A few examples of interferometry applications in space-related active and passive remote sensing. 2004 Second International Workshop Ultrawideband and Ultrashort Impulse Signals. 19-22 Sept. 2004. - P. 55-58. ↑

C4947. Omar A.H. Aerosol optical properties derived from lidar observations using cluster analysis. / Omar A.H., Babakaeva T. // 2004. IGARSS '04. Proceedings. 2004 IEEE International Geoscience and Remote Sensing Symposium. - Anchorage, AK, 20-24 Sept. 2004. - Vol. 3. - P. 2212-2215. ↑

C4948. Jirousek M. A multi-frequency microwave aperture synthesis radiometer for high-resolution imaging. / Jirousek M., Peichl M., Voegelé A., Suess H. // 2004. IGARSS '04. Proceedings. 2004 IEEE International Geoscience and Remote Sensing Symposium. - Anchorage, AK, 20-24 Sept. 2004. - Vol. 3. - P. 2222-2225. ↑

C4949. Howell S.E.L. An evaluation of SeaWinds/QuikSCAT data for the estimation of the decay status of first-year sea ice. / Howell S.E.L., Yackel J.J., De Abreu R.A., Galdsetzer T., Breneman C. // 2004. IGARSS '04. Proceedings. 2004 IEEE International Geoscience and Remote Sensing Symposium. - Anchorage, AK, 20-24 Sept. 2004. - Vol. 3. - P. 2151-2154. ↑

C4950. Berkoff T.A. Observations of aerosols using the Micro-Pulse Lidar NETwork (MPLNET). / Berkoff T.A., Welton E.J., Campbell J.R., Valencia S., Spinhirne J.D., Tsay S.-C., Holben B.N. // 2004. IGARSS '04. Proceedings. 2004 IEEE International Geoscience and Remote Sensing Symposium. - Anchorage, AK, 20-24 Sept. 2004. - Vol. 3. - P. 2208-2211. ↑

C4951. Sunghyun Kim. Point target angular resolution in near field for Ka-band interferometric synthetic aperture radiometer with sub-Y-type array configuration. / Sunghyun Kim, Junho Choi, Hyuk Park, Hojin Lee, Yonghoon Kim, Gum-sil Kang. // 2004. IGARSS '04. Proceedings. 2004 IEEE International Geoscience and Remote Sensing Symposium. - Anchorage, AK, 20-24 Sept. 2004. - Vol. 3. - P. 2234-2236. ↑

C4952. {no data available}. 2004 Second International Workshop Ultrawideband and Ultrashort Impulse Signals (IEEE Cat. No.04EX925). 2004 Second International Workshop Ultrawideband and Ultrashort Impulse Signals. 19-22 Sept. 2004. - P. 0_1. ↑

C4953. Yanovsky F.J. Wideband radar remote sensing of the atmosphere: a data interpretation problem. / Yanovsky F.J., Kharchenko V.P., Ligthart L.P. // 2004 Second International Workshop Ultrawideband and Ultrashort Impulse Signals. 19-22 Sept. 2004. - P. 42-47. ↑

C4954. Lay-Ekuakille A. Signal deconvolution with successive filterings. / Lay-Ekuakille A., Scarano A.V., Trotta A. // 2004. Proceedings of the Lightwave Technologies in Instrumentation and Measurement Conference. 19-20 Oct. 2004. - P. 106-110. ↑

C4955. Thomas M. Discontinuous Non-Rigid Motion Analysis of Sea Ice using C-Band Synthetic Aperture Radar Satellite Imagery. / Thomas M., Geiger C., Kambhamettu C. // 2004. CVPRW 04. Conference on Computer Vision and Pattern Recognition Workshop. 27-02 June 2004. - P. 24. ↑

C4956. Jianming Wang. Retrieving soil moisture over bare soil from ERS wind scatterometer data. / Jianming

Wang, Shi J., Shengli Wu, Wei Liu. // 2004. IGARSS '04. Proceedings. 2004 IEEE International Geoscience and Remote Sensing Symposium. - Anchorage, AK, 20-24 Sept. 2004. - Vol. 5. - P. 3536-3538. ↑

C4957. Yongming Du. Estimate LAI of crops using airborne multi-angular data. / Yongming Du, Qiang Liu, Qing-Huo Liu, Liang-Fu Chen. // 2004. IGARSS '04. Proceedings. 2004 IEEE International Geoscience and Remote Sensing Symposium. - Anchorage, AK, 20-24 Sept. 2004. - Vol. 7. - P. 4477-4479. ↑

C4958. Angiulli M. L-band active-passive and L-C-X-bands passive data for soil moisture retrieval, two different approaches in comparison. / Angiulli M., Notarnicola C., Posa F., Pampaloni P. // 2004. IGARSS '04. Proceedings. 2004 IEEE International Geoscience and Remote Sensing Symposium. - Anchorage, AK, 20-24 Sept. 2004. - Vol. 7. - P. 4492-4495. ↑

C4959. Chandrasekar V. Validation of raindrop size distribution retrieval from spaceborne radar using ground polarimetric radar observations. / Chandrasekar V., Wanyu Li. // 2004. IGARSS '04. Proceedings. 2004 IEEE International Geoscience and Remote Sensing Symposium. - Anchorage, AK, 20-24 Sept. 2004. - Vol. 7. - P. 4402-4405. ↑

C4960. Dogan O. High resolution radar imaging using GPOF based data extrapolation. / Dogan O., Erer I. // 2004. IGARSS '04. Proceedings. 2004 IEEE International Geoscience and Remote Sensing Symposium. - Anchorage, AK, 20-24 Sept. 2004. - Vol. 7. - P. 4470-4473. ↑

C4961. KelIndorfer J.M. Vegetation height derivation from Shuttle Radar Topography Mission data in southeast Georgia, USA. / KelIndorfer J.M., Walker W.S., Dobson M.C., Vona M., Clutter M. // 2004. IGARSS '04. Proceedings. 2004 IEEE International Geoscience and Remote Sensing Symposium. - Anchorage, AK, 20-24 Sept. 2004. - Vol. 7. - P. 4512-4515. ↑

C4962. Marschalk U. Comparison of DEMs derived from SRTM/X- and C-band. / Marschalk U., Roth A., Eineder M., Suchandt S. // 2004. IGARSS '04. Proceedings. 2004 IEEE International Geoscience and Remote Sensing Symposium. - Anchorage, AK, 20-24 Sept. 2004. - Vol. 7. - P. 4531-4534. ↑

C4963. Schattler B. TerraSAR-L SAR parameter simulation. / Schattler B., Boerner E. // 2004. IGARSS '04. Proceedings. 2004 IEEE International Geoscience and Remote Sensing Symposium. - Anchorage, AK, 20-24 Sept. 2004. - Vol. 7. - P. 4535-4538. ↑

C4964. Torres R. The TerraSAR-L mission and system. / Torres R., Lokas S., Moller H.L., Zink M., Simpson D.M. // 2004. IGARSS '04. Proceedings. 2004 IEEE International Geoscience and Remote Sensing Symposium. - Anchorage, AK, 20-24 Sept. 2004. - Vol. 7. - P. 4519-4522. ↑

C4965. Rosenqvist A. Implementation of systematic data observation strategies for ALOS PALSAR, PRISM and AVNIR-2. / Rosenqvist A., Shimada M., Watanabe M., Tadono T., Yamauchi K. // 2004. IGARSS '04. Proceedings. 2004 IEEE International Geoscience and Remote Sensing Symposium. - Anchorage, AK, 20-24 Sept. 2004. - Vol. 7. - P. 4527-4530. ↑

C4966. Nakamura K. Study on the sea ice thickness observation in the Sea of Okhotsk by using dual-frequency and fully polarimetric airborne SAR (Pi-SAR) data. / Nakamura K., Wakabayashi H., Nakayama M., Naoki K., Toyota T., Kojima S., Nishio F., Uratsuka S. // 2004. IGARSS '04. Proceedings. 2004 IEEE International Geoscience and Remote Sensing Symposium. - Anchorage, AK, 20-24 Sept. 2004. - Vol. 7. - P. 4386-4389. ↑

C4967. Xin Xiao. An effective algorithm in radar image processing. / Xin Xiao, Rui Zhang, Yiming Pi, Jianxi Huang. // 2004. IGARSS '04. Proceedings. 2004 IEEE International Geoscience and Remote Sensing Symposium. - Anchorage, AK, 20-24 Sept. 2004. - Vol. 6. - P. 4255-4257. ↑

C4968. Kan Zeng. A simple boundary process technique for empirical mode decomposition. / Kan Zeng, Ming-Xia He. // 2004. IGARSS '04. Proceedings. 2004 IEEE International Geoscience and Remote Sensing Symposium. - Anchorage, AK, 20-24 Sept. 2004. - Vol. 6. - P. 4258-4261. ↑

C4969. Tello M. Use of the multiresolution capability of wavelets for ship detection in SAR imagery. / Tello M., Mallorqui J.J., Aguasca A., Lopez-Martinez C. // 2004. IGARSS '04. Proceedings. 2004 IEEE International Geoscience and Remote Sensing Symposium. - Anchorage, AK, 20-24 Sept. 2004. - Vol. 6. - P. 4247-4250. ↑

C4970. Wei Song. High resolution DBS imaging and the moving target trajectory forming with raw SAR/GMTI

Data. / Wei Song, Wang Hongyuan. // 2004. IGARSS '04. Proceedings. 2004 IEEE International Geoscience and Remote Sensing Symposium. - Anchorage, AK, 20-24 Sept. 2004. - Vol. 6. - P. 4251-4254. ↑

C4971. Zhu Junjie. A wavelet transform method to detect boundaries between land and water in SAR image. / Zhu Junjie, Guo Huadong, Fan Xiangtao, Shao Yun. // 2004. IGARSS '04. Proceedings. 2004 IEEE International Geoscience and Remote Sensing Symposium. - Anchorage, AK, 20-24 Sept. 2004. - Vol. 6. - P. 4262-4264. ↑

C4972. Yanfang Dong. Radar backscatter of rice fields from ASAR data and modeling. / Yanfang Dong, Yong Pang, Guoqing Sun, Zhongjun Zhang. // 2004. IGARSS '04. Proceedings. 2004 IEEE International Geoscience and Remote Sensing Symposium. - Anchorage, AK, 20-24 Sept. 2004. - Vol. 6. - P. 4332-4335. ↑

C4973. Karvonen J. Open water detection from Baltic sea ice SAR imagery. / Karvonen J., Simila M., Makynen M. // 2004. IGARSS '04. Proceedings. 2004 IEEE International Geoscience and Remote Sensing Symposium. - Anchorage, AK, 20-24 Sept. 2004. - Vol. 7. - P. 4382-4385. ↑

C4974. Tagawa T. Measurement of scattering coefficient dependence on soil moisture content and surface roughness by 35 GHz polarimetric scatterometer. / Tagawa T., Okamoto K., Higuchi A., Ushio T., Hanado H. // 2004. IGARSS '04. Proceedings. 2004 IEEE International Geoscience and Remote Sensing Symposium. - Anchorage, AK, 20-24 Sept. 2004. - Vol. 6. - P. 4295-4298. ↑

C4975. Pan Liang. Application of bistatic MIMICS to forest canopies. / Pan Liang, Pierce L. // 2004. IGARSS '04. Proceedings. 2004 IEEE International Geoscience and Remote Sensing Symposium. 20-24 Sept. 2004. - Vol. 6. - P. 4328-4331. ↑

C4976. Schattler B. The TerraSAR-L basic product tree. / Schattler B., Fritz T., Eineder M., Breit H., Zink M. // 2004. IGARSS '04. Proceedings. 2004 IEEE International Geoscience and Remote Sensing Symposium. - Anchorage, AK, 20-24 Sept. 2004. - Vol. 7. - P. 4539-4542. ↑

C4977. Friedman K.S. Eddy detection using RADARSAT-1 synthetic aperture radar. / Friedman K.S., Xiaofeng Li, Pichel W.G., Clemente-Colon P., Walker N., Veenstra T. // 2004. IGARSS '04. Proceedings. 2004 IEEE International Geoscience and Remote Sensing Symposium. - Anchorage, AK, 20-24 Sept. 2004. - Vol. 7. - P. 4707-4710. ↑

C4978. Bin Fu. Application of multi-band and full-polarization SAR in shallow sea bottom topography measurement. / Bin Fu, Jinsong Yang, Weigen Huang. // 2004. IGARSS '04. Proceedings. 2004 IEEE International Geoscience and Remote Sensing Symposium. - Anchorage, AK, 20-24 Sept. 2004. - Vol. 7. - P. 4711-4714. ↑

C4979. Yi Zhou. Applications of CBERS-2 image data in flood disaster remote sensing monitoring. / Yi Zhou, Shixin Wang, Weiqi Zhou, Pei Zhang. // 2004. IGARSS '04. Proceedings. 2004 IEEE International Geoscience and Remote Sensing Symposium. - Anchorage, AK, 20-24 Sept. 2004. - Vol. 7. - P. 4696-4699. ↑

C4980. Bertacca M. A FARIMA based analysis for wind falls and oil slicks discrimination in sea SAR imagery. / Bertacca M., Berizzi F., Dalle Mese E., Capria A. // 2004. IGARSS '04. Proceedings. 2004 IEEE International Geoscience and Remote Sensing Symposium. - Anchorage, AK, 20-24 Sept. 2004. - Vol. 7. - P. 4703-4706. ↑

C4981. Greidanus H. Applicability of the K distribution to RADARSAT maritime imagery. 2004. IGARSS '04. Proceedings. 2004 IEEE International Geoscience and Remote Sensing Symposium. - Anchorage, AK, 20-24 Sept. 2004. - Vol. 7. - P. 4715-4718. ↑

C4982. Girard-Ardhuin F. Oil slick detection by SAR imagery: algorithms comparison. / Girard-Ardhuin F., Mercier G., Collard F., Garello R. // 2004. IGARSS '04. Proceedings. 2004 IEEE International Geoscience and Remote Sensing Symposium. - Anchorage, AK, 20-24 Sept. 2004. - Vol. 7. - P. 4726-4729. ↑

C4983. Niedermeier A. SAR ocean wave measurements based on an empirical imaging model. / Niedermeier A., Schulz-Stellenfleth J., Nieto Borge J.C. // 2004. IGARSS '04. Proceedings. 2004 IEEE International Geoscience and Remote Sensing Symposium. - Anchorage, AK, 20-24 Sept. 2004. - Vol. 7. - P. 4730-4733. ↑

C4984. Weigen Huang. An improved CFAR model for ship detection in SAR imagery. / Weigen Huang, Peng Chen, Jingsong Yang, Bin Fu, Qingmei Xiao, Lu Yao, Changbao Zhou. // 2004. IGARSS '04. Proceedings. 2004 IEEE International Geoscience and Remote Sensing Symposium. - Anchorage, AK, 20-24 Sept. 2004. - Vol. 7. - P. 4719-4722. ↑

- C4985.** Yingjian Liu. Sea surface ship detection in SAR images. / Yingjian Liu, Qian Feng. // 2004. IGARSS '04. Proceedings. 2004 IEEE International Geoscience and Remote Sensing Symposium. - Anchorage, AK, 20-24 Sept. 2004. - Vol. 7. - P. 4723-4725. ↑
- C4986.** Solbo S. Mapping of flooding in the Alessandria area with ERS. / Solbo S., Pettinato S., Paloscia S., Santi E., Brusotti P., Solheim I. // 2004. IGARSS '04. Proceedings. 2004 IEEE International Geoscience and Remote Sensing Symposium. - Anchorage, AK, 20-24 Sept. 2004. - Vol. 7. - P. 4689-4692. ↑
- C4987.** Weise K. Dualband-TerraSAR simulation/campaign results for L-band configuration. / Weise K., Davidson M.W.J. // 2004. IGARSS '04. Proceedings. 2004 IEEE International Geoscience and Remote Sensing Symposium. - Anchorage, AK, 20-24 Sept. 2004. - Vol. 7. - P. 4556-4559. ↑
- C4988.** Yonezawa C. Land surface observation using multi-polarization ENVISAT ASAR data. / Yonezawa C., Tomiyama N., Yamakoshi T. // 2004. IGARSS '04. Proceedings. 2004 IEEE International Geoscience and Remote Sensing Symposium. - Anchorage, AK, 20-24 Sept. 2004. - Vol. 7. - P. 4564-4567. ↑
- C4989.** Schattler B. A description of the data-driven SAR data workflow in the TerraSAR-X Payload Ground Segment. / Schattler B., Wolfmüller M., Reissig R., Damerow H., Breit H., Diedrich E. // 2004. IGARSS '04. Proceedings. 2004 IEEE International Geoscience and Remote Sensing Symposium. - Anchorage, AK, 20-24 Sept. 2004. - Vol. 7. - P. 4543-4547. ↑
- C4990.** Takaku J. High resolution DEM generation from ALOS PRISM data-simulation and evaluation. / Takaku J., Futamura N., Iijima T., Tadono T., Shimada M., Shibasaki R. // 2004. IGARSS '04. Proceedings. 2004 IEEE International Geoscience and Remote Sensing Symposium. - Anchorage, AK, 20-24 Sept. 2004. - Vol. 7. - P. 4548-4551. ↑
- C4991.** Dabrowska-Zielinska K. Biophysical properties of wetlands vegetation retrieved from satellite images. / Dabrowska-Zielinska K., Gruszczynska M., Yesou H., Kowalik W., Hoscilo A., Malck I. // 2004. IGARSS '04. Proceedings. 2004 IEEE International Geoscience and Remote Sensing Symposium. - Anchorage, AK, 20-24 Sept. 2004. - Vol. 7. - P. 4580-4583. ↑
- C4992.** Ren-Hua Zhang. The estimation of distribution in field scale of surface aerodynamic roughness using remote sensing data. / Ren-Hua Zhang, Cai-Ying Zhu, Xiao-Min Sun, Zhi-Lin Zhu. // 2004. IGARSS '04. Proceedings. 2004 IEEE International Geoscience and Remote Sensing Symposium. - Anchorage, AK, 20-24 Sept. 2004. - Vol. 7. - P. 4666-4669. ↑
- C4993.** Posa F. Soil parameters retrieval from remotely sensed data: efficiency of neural network and Bayesian approaches. / Posa F., Notarnicola C., Angiulli M. // 2004. IGARSS '04. Proceedings. 2004 IEEE International Geoscience and Remote Sensing Symposium. - Anchorage, AK, 20-24 Sept. 2004. - Vol. 7. - P. 4682-4685. ↑
- C4994.** Hermitte J.L. Monitoring the Siberian boreal forest using ENVISAT/ASAR data: first analysis results. / Hermitte J.L., Le Toan T., Grippa M., Bouvet A. // 2004. IGARSS '04. Proceedings. 2004 IEEE International Geoscience and Remote Sensing Symposium. - Anchorage, AK, 20-24 Sept. 2004. - Vol. 7. - P. 4586-4589. ↑
- C4995.** Budkewitsch P. Temporal snow cover variation and terrain characteristics of Peary caribou habitats in the Canadian arctic using optical and InSAR data. / Budkewitsch P., Molch K., McGregor R., Maher A., Treitz P., Ferguson M.A.D. // 2004. IGARSS '04. Proceedings. 2004 IEEE International Geoscience and Remote Sensing Symposium. - Anchorage, AK, 20-24 Sept. 2004. - Vol. 7. - P. 4609 vol.7. ↑
- C4996.** Tang Zhi. Analysis on noise reduction method for interferometric SAR image. / Tang Zhi, Li Jingwen, Zhou Yingqing. // 2004. IGARSS '04. Proceedings. 2004 IEEE International Geoscience and Remote Sensing Symposium. - Anchorage, AK, 20-24 Sept. 2004. - Vol. 6. - P. 4243-4246. ↑
- C4997.** Tiaiihe Chi. Agent communication based SAR image parallel processing. / Tiaiihe Chi, Huabin Chen, Xin Zhang, Qinmin Wang, Chongcheng Chen, Yimin Lu. // 2004. IGARSS '04. Proceedings. 2004 IEEE International Geoscience and Remote Sensing Symposium. - Anchorage, AK, 20-24 Sept. 2004. - Vol. 6. - P. 3923-3925. ↑
- C4998.** Junfeng Wang. SAR automatic range-migration correction. / Junfeng Wang, Xingzhao Liu. // 2004. IGARSS '04. Proceedings. 2004 IEEE International Geoscience and Remote Sensing Symposium. - Anchorage, AK, 20-24 Sept. 2004. - Vol. 6. - P. 3926-3929. ↑

- C4999.** Belfiore S. Joint despeckling and edge detection of SAR images based on the Mumford-Shah functional. / Belfiore S., Scopigno R., Grangetto M., Magli E. // 2004. IGARSS '04. Proceedings. 2004 IEEE International Geoscience and Remote Sensing Symposium. - Anchorage, AK, 20-24 Sept. 2004. - Vol. 6. - P. 3915-3918. ↑
- C5000.** Yong Li. Geometric distortion correction in the subaperture processing for high squint airborne SAR imaging. / Yong Li, Daiyin Zhu, Zhaoda Zhu. // 2004. IGARSS '04. Proceedings. 2004 IEEE International Geoscience and Remote Sensing Symposium. - Anchorage, AK, 20-24 Sept. 2004. - Vol. 6. - P. 3919-3922. ↑
- C5001.** Kaizhi Wang. Squint-spotlight SAR imaging by subband combination and range-walk removal. / Kaizhi Wang, Xingzhao Liu. // 2004. IGARSS '04. Proceedings. 2004 IEEE International Geoscience and Remote Sensing Symposium. - Anchorage, AK, 20-24 Sept. 2004. - Vol. 6. - P. 3930-3933. ↑
- C5002.** Xin Xiao. Realization of SAR real-time processor by FPGA. / Xin Xiao, Rui Zhang, Xiaobo Yang, Gang Zhang. // 2004. IGARSS '04. Proceedings. 2004 IEEE International Geoscience and Remote Sensing Symposium. - Anchorage, AK, 20-24 Sept. 2004. - Vol. 6. - P. 3942-3944. ↑
- C5003.** Klugmann D. Calibration of portable FM-CW Doppler radar profilers with an artificial target. / Klugmann D., Stephan R. // 2004. IGARSS '04. Proceedings. 2004 IEEE International Geoscience and Remote Sensing Symposium. 20-24 Sept. 2004. - Vol. 6. - P. 3953-3955. ↑
- C5004.** Ling Wang. Study on airborne ISAR imaging of ship targets. / Ling Wang, Daiyin Zhu, Zhaoda Zhu. // 2004. IGARSS '04. Proceedings. 2004 IEEE International Geoscience and Remote Sensing Symposium. - Anchorage, AK, 20-24 Sept. 2004. - Vol. 6. - P. 3934-3937. ↑
- C5005.** Woods D. Automatic extraction of vertical obstruction information from interferometric SAR elevation data. / Woods D., Folley C., Yit-Tsi Kwan, Houshmand B. // 2004. IGARSS '04. Proceedings. 2004 IEEE International Geoscience and Remote Sensing Symposium. 20-24 Sept. 2004. - Vol. 6. - P. 3938-3941. ↑
- C5006.** Chen C.H. A novel theory of SAR image restoration and enhancement with ICA. / Chen C.H., Xianju Wang. // 2004. IGARSS '04. Proceedings. 2004 IEEE International Geoscience and Remote Sensing Symposium. - Anchorage, AK, 20-24 Sept. 2004. - Vol. 6. - P. 3911-3914. ↑
- C5007.** Kampa K. An adaptive multiscale filter for segmenting vegetation in ALSM data. / Kampa K., Slatton K.C. // 2004. IGARSS '04. Proceedings. 2004 IEEE International Geoscience and Remote Sensing Symposium. - Anchorage, AK, 20-24 Sept. 2004. - Vol. 6. - P. 3837-3840. ↑
- C5008.** Hiep Quang Luong. Automatic registration of synthetic aperture radar (SAR) images. / Hiep Quang Luong, Gautama S., Philips W. // 2004. IGARSS '04. Proceedings. 2004 IEEE International Geoscience and Remote Sensing Symposium. - Anchorage, AK, 20-24 Sept. 2004. - Vol. 6. - P. 3864-3867. ↑
- C5009.** Ghedira H. The effect of some internal neural network parameters on SAR texture classification performance. / Ghedira H., Bernier M. // 2004. IGARSS '04. Proceedings. 2004 IEEE International Geoscience and Remote Sensing Symposium. - Anchorage, AK, 20-24 Sept. 2004. - Vol. 6. - P. 3845-3848. ↑
- C5010.** Borghgraef A. Change detection in SAR images: spatial accuracy analysis. / Borghgraef A., Sidharta Gautama. // 2004. IGARSS '04. Proceedings. 2004 IEEE International Geoscience and Remote Sensing Symposium. 20-24 Sept. 2004. - Vol. 6. - P. 3857-3860. ↑
- C5011.** Mahapatra P.R. Vector reconstruction and mosaicing from multiple Doppler weather radar velocity data. / Mahapatra P.R., Makkapti V.V. // 2004. IGARSS '04. Proceedings. 2004 IEEE International Geoscience and Remote Sensing Symposium. - Anchorage, AK, 20-24 Sept. 2004. - Vol. 6. - P. 3868-3871. ↑
- C5012.** Jardini M.G.M. Use of geo-referenced images for the surveillance of transmission lines right-of-way. / Jardini M.G.M., Jardini J.A., Schmidt H.P., Magrini L.C., Quintanilha J.A., Crispino S., Campos U.S. // 2004. IGARSS '04. Proceedings. 2004 IEEE International Geoscience and Remote Sensing Symposium. 20-24 Sept. 2004. - Vol. 6. - P. 3891-3894. ↑
- C5013.** Olsen R.B. Signatures of vessels in ENVISAT AP-mode imagery. / Olsen R.B., Arnesen T.N., Eldhuset K. // 2004. IGARSS '04. Proceedings. 2004 IEEE International Geoscience and Remote Sensing Symposium. 20-24 Sept. 2004. - Vol. 6. - P. 3895-3897. ↑

- C5014.** Mercier G. SAR image change detection using distance between distributions of classes. / Mercier G., Derrode S. // 2004. IGARSS '04. Proceedings. 2004 IEEE International Geoscience and Remote Sensing Symposium. - Anchorage, AK, 20-24 Sept. 2004. - Vol. 6. - P. 3872-3875. ↑
- C5015.** Refice A. Assessment of multitemporal DInSAR stepwise processing. / Refice A., Bovenga F., Nutricato R., Chiaradia M.T. // 2004. IGARSS '04. Proceedings. 2004 IEEE International Geoscience and Remote Sensing Symposium. - Anchorage, AK, 20-24 Sept. 2004. - Vol. 6. - P. 3876-3879. ↑
- C5016.** Spinhirne J.D. Aerosol and cloud measurements at 532 and 1064 nm by the GLAS polar orbiting lidar instrument. / Spinhirne J.D., Palm S.P., Hlavka D.L., Hart W.D., Mahesh A., Welton E.J. // 2004. IGARSS '04. Proceedings. 2004 IEEE International Geoscience and Remote Sensing Symposium. - Anchorage, AK, 20-24 Sept. 2004. - Vol. 6. - P. 3956-3959. ↑
- C5017.** Greidanus H. Benchmarking operational SAR ship detection. / Greidanus H., Clayton P., Indregard M., Staples G., Suzuki N., Vachoir P., Wackerman C., Tennvassas T., Mallorqui J., Kourti N., Ringrose R., Melief H. // 2004. IGARSS '04. Proceedings. 2004 IEEE International Geoscience and Remote Sensing Symposium. - Anchorage, AK, 20-24 Sept. 2004. - Vol. 6. - P. 4215-4218. ↑
- C5018.** Gurcan R. An edge detection method using 2-D autoregressive lattice prediction filters for remotely sensed images. / Gurcan R., Erer I., Kent S. // 2004. IGARSS '04. Proceedings. 2004 IEEE International Geoscience and Remote Sensing Symposium. - Anchorage, AK, 20-24 Sept. 2004. - Vol. 6. - P. 4219-4222. ↑
- C5019.** Yongming Xu. Extraction mechanism of alteration zones using ASTER imagery. / Yongming Xu, Qizhong Lin, Yun Shao, Lu Wang. // 2004. IGARSS '04. Proceedings. 2004 IEEE International Geoscience and Remote Sensing Symposium. - Anchorage, AK, 20-24 Sept. 2004. - Vol. 6. - P. 4174-4175. ↑
- C5020.** D'Elia C. An MRF based technique for speckle reduction in SAR images. / D'Elia C., Ferraiuolo G., Pascasio V., Schirni G. // 2004. IGARSS '04. Proceedings. 2004 IEEE International Geoscience and Remote Sensing Symposium. - Anchorage, AK, 20-24 Sept. 2004. - Vol. 6. - P. 4211-4214. ↑
- C5021.** Sang-Hoon Hong. Extraction of ground control points (GCPs) from synthetic aperture radar image using DEM. / Sang-Hoon Hong, Jung H.-S., Won J.-S., Hong-Gab Kim. // 2004. IGARSS '04. Proceedings. 2004 IEEE International Geoscience and Remote Sensing Symposium. 20-24 Sept. 2004. - Vol. 6. - P. 4223-4226. ↑
- C5022.** Saevarsson B.B. Combined wavelet and curvelet denoising of SAR images. / Saevarsson B.B., Sveinsson J.R., Benediktsson J.A. // 2004. IGARSS '04. Proceedings. 2004 IEEE International Geoscience and Remote Sensing Symposium. - Anchorage, AK, 20-24 Sept. 2004. - Vol. 6. - P. 4235-4238. ↑
- C5023.** Qulin Tan. A study on rice field edge extraction in Radarsat SAR images. / Qulin Tan, Jiping Hu, Siwen Bi, Zhengjun Liu. // 2004. IGARSS '04. Proceedings. 2004 IEEE International Geoscience and Remote Sensing Symposium. - Anchorage, AK, 20-24 Sept. 2004. - Vol. 6. - P. 4239-4242. ↑
- C5024.** Huang C.M. DEM generation from stereo SAR images based on polynomial rectification and height displacement. / Huang C.M., Guo J.K., Zhao Z., Xiao Z., Qiu C.P., Pang L., Wang Z.Y. // 2004. IGARSS '04. Proceedings. 2004 IEEE International Geoscience and Remote Sensing Symposium. 20-24 Sept. 2004. - Vol. 6. - P. 4227-4230. ↑
- C5025.** Kwang-Yong Kim. Implementation of a SAR image mapping module using the OGC grid coverage. / Kwang-Yong Kim, Soo Jeong, Kyung-Ok Kim. // 2004. IGARSS '04. Proceedings. 2004 IEEE International Geoscience and Remote Sensing Symposium. - Anchorage, AK, 20-24 Sept. 2004. - Vol. 6. - P. 4231-4234. ↑
- C5026.** Yan Fuli. Determination and implications of the rock physical parameter in the Maergaichaka fault, Tibet, China, using remote sensing data. / Yan Fuli, Xu Guangwei, Song Yougui, Fan Xiangtao, Zhou Weiqi, Wang Litao. // 2004. IGARSS '04. Proceedings. 2004 IEEE International Geoscience and Remote Sensing Symposium. - Anchorage, AK, 20-24 Sept. 2004. - Vol. 6. - P. 4164-4166. ↑
- C5027.** Wenbo Xu. Synergy of multitemporal Radarsat SAR and Landsat ETM data for extracting agricultural crops structure. / Wenbo Xu, Bingfang Wu, Yichen Tian, Jianxi Huang, Yong Zhang. // 2004. IGARSS '04. Proceedings. 2004 IEEE International Geoscience and Remote Sensing Symposium. - Anchorage, AK, 20-24 Sept. 2004. - Vol. 6. - P. 4073-4076. ↑
- C5028.** Xiaoyu Song. Use of airborne hyperspectral image data to assess winter wheat yield. / Xiaoyu Song,

Jihua Wang, Liangyun Liu, Xuzhang Xue, Chunjiang Zhao. // 2004. IGARSS '04. Proceedings. 2004 IEEE International Geoscience and Remote Sensing Symposium. - Anchorage, AK, 20-24 Sept. 2004. - Vol. 6. - P. 4080-4083. ↑

C5029. Walthall C.L. Analysis of surrogate indicators for evidence of subsurface preferential flow pathways: impact of subsurface preferential flow on variability of NDVI. / Walthall C.L., Gish T.J., Chinkuyu A., Dulaney W., Kaul M., Daughtry C.S.T. // 2004. IGARSS '04. Proceedings. 2004 IEEE International Geoscience and Remote Sensing Symposium. 20-24 Sept. 2004. - Vol. 6. - P. 3992-3995. ↑

C5030. Blaes X. Bi-dimensional soil roughness measurement by photogrammetry for SAR modelling of agricultural surfaces. / Blaes X., Defourny P., Callensand M., Verhoest N.E.C. // 2004. IGARSS '04. Proceedings. 2004 IEEE International Geoscience and Remote Sensing Symposium. - Anchorage, AK, 20-24 Sept. 2004. - Vol. 6. - P. 4038-4041. ↑

C5031. Loescher K. Application of a SAR image archive to climatological analysis of coastal wind storms. / Loescher K., Youne G., Winstead N., Colle B. // 2004. IGARSS '04. Proceedings. 2004 IEEE International Geoscience and Remote Sensing Symposium. - Anchorage, AK, 20-24 Sept. 2004. - Vol. 6. - P. 4127-4130. ↑

C5032. Chow J. Penetrating radar study of the collapse features in a Nantou earth slide, Central Taiwan. / Chow J., Hua J.J., Wen-Neng Wang. // 2004. IGARSS '04. Proceedings. 2004 IEEE International Geoscience and Remote Sensing Symposium. - Anchorage, AK, 20-24 Sept. 2004. - Vol. 6. - P. 4143-4146. ↑

C5033. Rousseaux F. Detection of systematic error areas on a DTM by comparison with a high resolution LIDAR DTM. 2004. IGARSS '04. Proceedings. 2004 IEEE International Geoscience and Remote Sensing Symposium. - Anchorage, AK, 20-24 Sept. 2004. - Vol. 6. - P. 4160-4163. ↑

C5034. Almeida-Filho R. Exploration assessment in a petroleum frontier area offshore the Amazon River mouth using RADARSAT-1 images. / Almeida-Filho R., de Miranda F.P., Lorenzzetti J.A., Pedroso E.C., Beisl C.H., Landau L., Baptista M.C., Camargo E.G. // 2004. IGARSS '04. Proceedings. 2004 IEEE International Geoscience and Remote Sensing Symposium. - Anchorage, AK, 20-24 Sept. 2004. - Vol. 6. - P. 4135-4138. ↑

C5035. Beisl C.H. Use of genetic algorithm to identify the source point of seepage slick clusters interpreted from Radarsat-1 images in the Gulf of Mexico. / Beisl C.H., Pedroso E.C., Soler L.S., Evsukoff A.G., Miranda F.P., Mendoza A., Vera A., Macedo J.M. // 2004. IGARSS '04. Proceedings. 2004 IEEE International Geoscience and Remote Sensing Symposium. - Anchorage, AK, 20-24 Sept. 2004. - Vol. 6. - P. 4139-4142. ↑

C5036. Berardino P. On the extension of the SBAS algorithm for the generation of ERS/ENVISAT deformation time-series. / Berardino P., Sansosti E., Lanari R., Pepe A. // 2004. IGARSS '04. Proceedings. 2004 IEEE International Geoscience and Remote Sensing Symposium. 20-24 Sept. 2004. - Vol. 5. - P. 3318-3320. ↑

C5037. Berardino P. A quantitative analysis of the SBAS algorithm performance. / Berardino P., Casu F., Fornaro G., Lanari R., Manunta M., Manzo M., Sansosti E. // 2004. IGARSS '04. Proceedings. 2004 IEEE International Geoscience and Remote Sensing Symposium. - Anchorage, AK, 20-24 Sept. 2004. - Vol. 5. - P. 3321-3324. ↑

C5038. Lehner S. TerraSAR-X for oceanography mission overview. / Lehner S., Horstmann J., Schulz-Stellenfleth J. // 2004. IGARSS '04. Proceedings. 2004 IEEE International Geoscience and Remote Sensing Symposium. 20-24 Sept. 2004. - Vol. 5. - P. 3303-3306. ↑

C5039. Chaabane F. Combination of multiple interferograms for monitoring temporal evolution of ground deformation. / Chaabane F., Tupin F., Maitre H. // 2004. IGARSS '04. Proceedings. 2004 IEEE International Geoscience and Remote Sensing Symposium. - Anchorage, AK, 20-24 Sept. 2004. - Vol. 5. - P. 3314-3317. ↑

C5040. Perkovic D. Gulf Stream observations obtained with the UMass Dual Beam Interferometer and an infrared camera. / Perkovic D., Toporkov J.V., Sletten M.A., Farquharson G., Frasier S.J., Marmorino G.O., Judd K.P. // 2004. IGARSS '04. Proceedings. 2004 IEEE International Geoscience and Remote Sensing Symposium. 20-24 Sept. 2004. - Vol. 5. - P. 3325-3328. ↑

C5041. Lombardini F. Feasibility study of along-track SAR interferometry with the COSMO-Skymed satellite system. / Lombardini F., Bordonni F., Gini F. // 2004. IGARSS '04. Proceedings. 2004 IEEE International Geoscience and Remote Sensing Symposium. - Anchorage, AK, 20-24 Sept. 2004. - Vol. 5. - P. 3337-3340. ↑

- C5042.** Lombard F. Experiments of interferometric layover solution with the three-antenna airborne AER-II SAR system. / Lombard F., Ender J., RoBing L., Galletto M., Verrazzani L. // 2004. IGARSS '04. Proceedings. 2004 IEEE International Geoscience and Remote Sensing Symposium. - Anchorage, AK, 20-24 Sept. 2004. - Vol. 5. - P. 3341-3344. ↑
- C5043.** Fornaro G. Airborne differential interferometry: X-Band experiments. / Fornaro G., Lanari R., Sansosti E., Franceschetti G., Perna S., Gois A., Moreira J. // 2004. IGARSS '04. Proceedings. 2004 IEEE International Geoscience and Remote Sensing Symposium. 20-24 Sept. 2004. - Vol. 5. - P. 3329-3332. ↑
- C5044.** Li Tao. Monitoring city subsidence by D-InSAR in Tianjin area. / Li Tao, Liu Jingnan, Liao Mingsheng, Kuang Shaojun, Lu Xu. // 2004. IGARSS '04. Proceedings. 2004 IEEE International Geoscience and Remote Sensing Symposium. 20-24 Sept. 2004. - Vol. 5. - P. 3333-3336. ↑
- C5045.** Macfarlane D.G. AVTIS-a dual-mode imaging millimetre wave radar/radiometer for volcanological surveying. / Macfarlane D.G., Robertson D.A. // 2004. IGARSS '04. Proceedings. 2004 IEEE International Geoscience and Remote Sensing Symposium. 20-24 Sept. 2004. - Vol. 5. - P. 3299-3302. ↑
- C5046.** Von Ann J.M. The operational impact of QuikSCAT winds at the National Oceanic and Atmospheric Administration Ocean Prediction Center. / Von Ann J.M., Sienkiewicz J.M. // 2004. IGARSS '04. Proceedings. 2004 IEEE International Geoscience and Remote Sensing Symposium. - Anchorage, AK, 20-24 Sept. 2004. - Vol. 5. - P. 3180-3183. ↑
- C5047.** Yijun He. Validation of wind vector retrieval from ENVISAT ASAR images. / Yijun He, Qingping Zou. // 2004. IGARSS '04. Proceedings. 2004 IEEE International Geoscience and Remote Sensing Symposium. - Anchorage, AK, 20-24 Sept. 2004. - Vol. 5. - P. 3184-3187. ↑
- C5048.** Qian Feng. Wind retrieval over the China Seas using satellite synthetic aperture radar. / Qian Feng, Mingqiang Fang, Yingjian Liu, Laibu Wang. // 2004. IGARSS '04. Proceedings. 2004 IEEE International Geoscience and Remote Sensing Symposium. - Anchorage, AK, 20-24 Sept. 2004. - Vol. 5. - P. 3169-3171. ↑
- C5049.** Rozenberg A. Laboratory measurements of wave-turbulence interaction for scatterometry application. 2004. IGARSS '04. Proceedings. 2004 IEEE International Geoscience and Remote Sensing Symposium. - Anchorage, AK, 20-24 Sept. 2004. - Vol. 5. - P. 3176-3179. ↑
- C5050.** Bosch D. In situ soil moisture network for validation of remotely sensed data. / Bosch D., Lakshmi V., Jackson T., Jacobs J., Moran S. // 2004. IGARSS '04. Proceedings. 2004 IEEE International Geoscience and Remote Sensing Symposium. - Anchorage, AK, 20-24 Sept. 2004. - Vol. 5. - P. 3188-3190. ↑
- C5051.** Amici S. Radiometric calibration and preliminary results of airborne 2003 FASA Campaign. / Amici S., Buongiorno M.F., Di Stefano G., Marconi P., Pippi I., Pugnaghi S., Haschberger P., Tank V., Oertel D., Kick H. // 2004. IGARSS '04. Proceedings. 2004 IEEE International Geoscience and Remote Sensing Symposium. 20-24 Sept. 2004. - Vol. 5. - P. 3215-3218. ↑
- C5052.** Xiaolong Dong. Spatial averaging techniques for pulse compression of spaceborne meteorological radar. / Xiaolong Dong, Huguang Liu, Jingshan Jiang. // 2004. IGARSS '04. Proceedings. 2004 IEEE International Geoscience and Remote Sensing Symposium. 20-24 Sept. 2004. - Vol. 5. - P. 3292-3294. ↑
- C5053.** Tanelli S. Rainfall and snowfall observations by the airborne dual-frequency precipitation radar during the Wakasa Bay Experiment. / Tanelli S., Im E., Durden S.L., Meagher J.P. // 2004. IGARSS '04. Proceedings. 2004 IEEE International Geoscience and Remote Sensing Symposium. - Anchorage, AK, 20-24 Sept. 2004. - Vol. 5. - P. 3195-3198. ↑
- C5054.** Tauchi T. Assimilation of the Aqua/AMSR-E data to numerical weather predictions. / Tauchi T., Takeuchi Y., Sato Y. // 2004. IGARSS '04. Proceedings. 2004 IEEE International Geoscience and Remote Sensing Symposium. 20-24 Sept. 2004. - Vol. 5. - P. 3199-3202. ↑
- C5055.** Romeiser R. On the suitability of a TerraSAR-L Interferometric Cartwheel for ocean current measurements. 2004. IGARSS '04. Proceedings. 2004 IEEE International Geoscience and Remote Sensing Symposium. 20-24 Sept. 2004. - Vol. 5. - P. 3345-3348. ↑
- C5056.** LuoJus K. Accuracy assessment for HUT snow covered area estimation method. / LuoJus K., Pulliainen L., Hallikainen M. // 2004. IGARSS '04. Proceedings. 2004 IEEE International Geoscience and Remote Sensing

Symposium. 20-24 Sept. 2004. - Vol. 5. - P. 3511-3514. ↑

C5057. Dranpob A. Soil moisture analysis using RADARSAT satellite image in the Choke Canyon Reservoir Watershed, South Texas. / Dranpob A., Chang N.B., Beaman M., Wyatt C. // 2004. IGARSS '04. Proceedings. 2004 IEEE International Geoscience and Remote Sensing Symposium. 20-24 Sept. 2004. - Vol. 5. - P. 3515-3518. ↑

C5058. Weigen Huang. Satellite observation of the Zhejiang-Fujian coastal front in the East China Sea. / Weigen Huang, Xiulin Lou, Jingsong Yang, Aiqing Shi, Qingmei Xiao, Chuanlan Lin. // 2004. IGARSS '04. Proceedings. 2004 IEEE International Geoscience and Remote Sensing Symposium. - Anchorage, AK, 20-24 Sept. 2004. - Vol. 5. - P. 3489-3491. ↑

C5059. Alvarez J. RADARSAT based surface soil moisture retrieval on agricultural catchments of Navarre (Spain). / Alvarez J., Verhoest N.E.C., Casali J., Gonzalez-Audicana M., Lopez J.J. // 2004. IGARSS '04. Proceedings. 2004 IEEE International Geoscience and Remote Sensing Symposium. - Anchorage, AK, 20-24 Sept. 2004. - Vol. 5. - P. 3507-3510. ↑

C5060. Liu Wei. Estimation of the change of soil moisture in vegetated surface with multi-temporal AirSAR data. / Liu Wei, Jian Cheng Shi, Jian Ming Wang, Yu Qin. // 2004. IGARSS '04. Proceedings. 2004 IEEE International Geoscience and Remote Sensing Symposium. - Anchorage, AK, 20-24 Sept. 2004. - Vol. 5. - P. 3519-3521. ↑

C5061. Bignami C. Preliminary results on soil moisture mapping in Alessandria area (Northern Italy) using Envisat A-SAR. / Bignami C., Pierdicca N., Pulvirenti L., Ticconi F., Paloscia S., Pettinato S., Santi E., Solbo S. // 2004. IGARSS '04. Proceedings. 2004 IEEE International Geoscience and Remote Sensing Symposium. 20-24 Sept. 2004. - Vol. 5. - P. 3529-3531. ↑

C5062. Tabatabaeenejad A. Backscattering of electromagnetic waves from layered rough surfaces and its application in estimating deep soil moisture. / Tabatabaeenejad A., Moghaddam M. // 2004. IGARSS '04. Proceedings. 2004 IEEE International Geoscience and Remote Sensing Symposium. - Anchorage, AK, 20-24 Sept. 2004. - Vol. 5. - P. 3526-3528. ↑

C5063. Low A. Derivation of hydrological parameters from ENVISAT ASAR wide swath data. / Low A., Waske B., Ludwig R., Mauser W. // 2004. IGARSS '04. Proceedings. 2004 IEEE International Geoscience and Remote Sensing Symposium. 20-24 Sept. 2004. - Vol. 5. - P. 3522-3525. ↑

C5064. Satalino G. On the accuracy of soil moisture content retrieved at pixel, segment or field scale, from advanced-SAR data: a simulation study. / Satalino G., Pasquariello G., Mattia F., Dente L. // 2004. IGARSS '04. Proceedings. 2004 IEEE International Geoscience and Remote Sensing Symposium. 20-24 Sept. 2004. - Vol. 5. - P. 3532-3535. ↑

C5065. Fleming A.H. A comparison of satellite and cruise chlorophyll-a measurements in the Scotia Sea, Antarctica. / Fleming A.H., Korb R.E. // 2004. IGARSS '04. Proceedings. 2004 IEEE International Geoscience and Remote Sensing Symposium. 20-24 Sept. 2004. - Vol. 5. - P. 3485-3486. ↑

C5066. Tuong Thuy Vu. LIDAR-based change detection of buildings in dense urban areas. / Tuong Thuy Vu, Matsuoka M., Yamazaki F. // 2004. IGARSS '04. Proceedings. 2004 IEEE International Geoscience and Remote Sensing Symposium. 20-24 Sept. 2004. - Vol. 5. - P. 3413-3416. ↑

C5067. Jouny I.I. Scattering analysis using fractional Fourier with applications in mine detection. 2004. IGARSS '04. Proceedings. 2004 IEEE International Geoscience and Remote Sensing Symposium. - Anchorage, AK, 20-24 Sept. 2004. - Vol. 5. - P. 3460-3463. ↑

C5068. de Salvador L. IFSAR: an airborne interferometric SAR simulator. / de Salvador L., Bemad P., Fidalgo A., Ilundain G., Dominguez J.M., Ojalvo L. // 2004. IGARSS '04. Proceedings. 2004 IEEE International Geoscience and Remote Sensing Symposium. - Anchorage, AK, 20-24 Sept. 2004. - Vol. 5. - P. 3349-3352. ↑

C5069. Zhang Yanjie. InSAR coherence estimation. / Zhang Yanjie, Prinnet V. // 2004. IGARSS '04. Proceedings. 2004 IEEE International Geoscience and Remote Sensing Symposium. - Anchorage, AK, 20-24 Sept. 2004. - Vol. 5. - P. 3353-3355. ↑

C5070. Komarov S.A. Measurement and simulation of L-band emission for a larch forest stand. / Komarov

S.A., Kleshchenko V.N., Shcherbinin V.V., Mironov V.L. // 2004. IGARSS '04. Proceedings. 2004 IEEE International Geoscience and Remote Sensing Symposium. 20-24 Sept. 2004. - Vol. 5. - P. 3464-3467. ↑

C5071. Mironov V.L. Bound water spectroscopy for the soils with varying mineralogy. 2004. IGARSS '04. Proceedings. 2004 IEEE International Geoscience and Remote Sensing Symposium. 20-24 Sept. 2004. - Vol. 5. - P. 3478-3480. ↑

C5072. Camps A. Sea surface brightness temperature at L-band: impact of surface currents. / Camps A., Vall-llossera M., Miranda J., Font J. // 2004. IGARSS '04. Proceedings. 2004 IEEE International Geoscience and Remote Sensing Symposium. - Anchorage, AK, 20-24 Sept. 2004. - Vol. 5. - P. 3481-3484. ↑

C5073. Yakubov V.P. Measured spectrum and polarization of wideband radar signal from forest stand. / Yakubov V.P., Telpukhovskiy E.D., Moiseenko N.A., Mironov V.L. // 2004. IGARSS '04. Proceedings. 2004 IEEE International Geoscience and Remote Sensing Symposium. 20-24 Sept. 2004. - Vol. 5. - P. 3471-3473. ↑

C5074. Mironov V.L. Spectral dielectric properties of moist soils in the microwave band. 2004. IGARSS '04. Proceedings. 2004 IEEE International Geoscience and Remote Sensing Symposium. 20-24 Sept. 2004. - Vol. 5. - P. 3474-3477. ↑

C5075. Esteban Fernandez D. Wind fields from hurricane Isabel. / Esteban Fernandez D., Ken E., Frasier S., Carswell J., Charm P., Black P., Marks F., Zhang A. // 2004. IGARSS '04. Proceedings. 2004 IEEE International Geoscience and Remote Sensing Symposium. - Anchorage, AK, 20-24 Sept. 2004. - Vol. 5. - P. 3165-3168. ↑

C5076. Basili P. Integration of digital elevation data scanning 3D and interferometric SAR systems. / Basili P., Capom M., Bonafoni S., Mattioli V. // 2004. IGARSS '04. Proceedings. 2004 IEEE International Geoscience and Remote Sensing Symposium. 20-24 Sept. 2004. - Vol. 5. - P. 2811-2814. ↑

C5077. Hsing-Chung Chang. Validation of DEMs derived from radar interferometry, airborne laser scanning and photogrammetry by using GPS-RTK. / Hsing-Chung Chang, Linlin Ge, Rizos C., Milne T. // 2004. IGARSS '04. Proceedings. 2004 IEEE International Geoscience and Remote Sensing Symposium. 20-24 Sept. 2004. - Vol. 5. - P. 2815-2818. ↑

C5078. Schistad Solberg A. Algorithms for oil spill detection in Radarsat and ENVISAT SAR images. / Schistad Solberg A., Brekke C., Solberg R., Ove Husoy P. // 2004. IGARSS '04. Proceedings. 2004 IEEE International Geoscience and Remote Sensing Symposium. - Anchorage, AK, 20-24 Sept. 2004. - Vol. 7. - P. 4909-4912. ↑

C5079. Jilong Yang. Effect of precipitation on ocean wind scatterometry. / Jilong Yang, Xuehu Zhang, Xiuwan Chen, Yinghai Ke, Esteban D., Carswell J., Frasier S., McLaughlin D.J., Chang P., Black P., Marks F. // 2004. IGARSS '04. Proceedings. 2004 IEEE International Geoscience and Remote Sensing Symposium. - Anchorage, AK, 20-24 Sept. 2004. - Vol. 7. - P. 4913-4916. ↑

C5080. Bruniquel J. Spaceborne P-band radar for ice-sheet sounding: design and performances. / Bruniquel J., Houpeit A., Richard J., Phalippou L., Dechambre M., Guijarro J. // 2004. IGARSS '04. Proceedings. 2004 IEEE International Geoscience and Remote Sensing Symposium. 20-24 Sept. 2004. - Vol. 5. - P. 2834-2837. ↑

C5081. Xianjun Zhou. An algorithm to acquire the average height of land surface. / Xianjun Zhou, Xiulin Hu, Yunyu Zhang. // 2004. IGARSS '04. Proceedings. 2004 IEEE International Geoscience and Remote Sensing Symposium. 20-24 Sept. 2004. - Vol. 5. - P. 2889-2892. ↑

C5082. Del Frate F. Seismic source parameters from InSAR data through neural networks [through reads through]. / Del Frate F., Rossi F., Schiavon G., Stramondo S. // 2004. IGARSS '04. Proceedings. 2004 IEEE International Geoscience and Remote Sensing Symposium. 20-24 Sept. 2004. - Vol. 5. - P. 2981-2984. ↑

C5083. Lei Pang. High resolution airborne SAR triangulation application supported by sparse-GCPs. / Lei Pang, Mingbo Zhang, Jixian Zhang, Guoman Huang. // 2004. IGARSS '04. Proceedings. 2004 IEEE International Geoscience and Remote Sensing Symposium. 20-24 Sept. 2004. - Vol. 5. - P. 2838-2840. ↑

C5084. Wallace J. The effects of scale on fractal dimension of topography: a case study from Sudbury, Ontario, Canada. / Wallace J., Morris B., Howarth P. // 2004. IGARSS '04. Proceedings. 2004 IEEE International Geoscience and Remote Sensing Symposium. - Anchorage, AK, 20-24 Sept. 2004. - Vol. 5. - P. 2845-2848. ↑

C5085. Qulin Tan. Measuring lake water level using multi-source remote sensing images combined with

hydrological statistical data. / Qulin Tan, Siwen Bi, Jiping Hu, Zhengjun Liu. // 2004. IGARSS '04. Proceedings. 2004 IEEE International Geoscience and Remote Sensing Symposium. - Anchorage, AK, 20-24 Sept. 2004. - Vol. 7. - P. 4885-4888. ↑

C5086. Parikh N.C. Remote Internet-based lidar experimentation and education. / Parikh N.C., Parikh J.A., Clark M., Damon M., Mandable S., Connors M. // 2004. IGARSS '04. Proceedings. 2004 IEEE International Geoscience and Remote Sensing Symposium. - Anchorage, AK, 20-24 Sept. 2004. - Vol. 7. - P. 4779-4782. ↑

C5087. Bretar F. Solving the strip adjustment problem of 3D airborne lidar data. / Bretar F., Pierrot-Deseilligny M., Roux M. // 2004. IGARSS '04. Proceedings. 2004 IEEE International Geoscience and Remote Sensing Symposium. - Anchorage, AK, 20-24 Sept. 2004. - Vol. 7. - P. 4734-4737. ↑

C5088. Pang Yong. Effects of forest spatial structure on large footprint lidar waveform. / Pang Yong, Guoqing Sun, Li Zengyuan. // 2004. IGARSS '04. Proceedings. 2004 IEEE International Geoscience and Remote Sensing Symposium. - Anchorage, AK, 20-24 Sept. 2004. - Vol. 7. - P. 4738-4741. ↑

C5089. Gelautz M. Web-based visualization and animation of geospatial data using X3D. / Gelautz M., Brandejski M., Kilzer F., Amelung F. // 2004. IGARSS '04. Proceedings. 2004 IEEE International Geoscience and Remote Sensing Symposium. - Anchorage, AK, 20-24 Sept. 2004. - Vol. 7. - P. 4773-4775. ↑

C5090. Wiesmann A. SAR based products for the implementation of humanitarian aid and development assistance projects within the UNOSAT project. / Wiesmann A., Wegmuller U., Haeberlin Y., Retiere A., Senegas O., Strozzi T., Werner C. // 2004. IGARSS '04. Proceedings. 2004 IEEE International Geoscience and Remote Sensing Symposium. - Anchorage, AK, 20-24 Sept. 2004. - Vol. 7. - P. 4803-4806. ↑

C5091. Tsuchida M. A simulator of synthetic aperture radar images; land, ocean surface, and man-made targets. / Tsuchida M., Suwa K., Iwamoto M. // 2004. IGARSS '04. Proceedings. 2004 IEEE International Geoscience and Remote Sensing Symposium. - Anchorage, AK, 20-24 Sept. 2004. - Vol. 7. - P. 4836-4838. ↑

C5092. Drunpob A. Optimal siting of hydrological monitoring stations with respect to remote sensing-based geo-environmental patterns. / Drunpob A., Chang N.B., Beaman M., Du Q., Wyatt C. // 2004. IGARSS '04. Proceedings. 2004 IEEE International Geoscience and Remote Sensing Symposium. - Anchorage, AK, 20-24 Sept. 2004. - Vol. 7. - P. 4873-4876. ↑

C5093. Lemoine G. Near real time vessel detection using spaceborne SAR imagery in support of fisheries monitoring and control operations. / Lemoine G., Chesworth J., Schwartz-Juste G., Kourti N., Shepherd I. // 2004. IGARSS '04. Proceedings. 2004 IEEE International Geoscience and Remote Sensing Symposium. - Anchorage, AK, 20-24 Sept. 2004. - Vol. 7. - P. 4825-4828. ↑

C5094. Ling Peng. Remote sensing study based on IRSA Remote Sensing Image Processing System. / Ling Peng, Zhongming Zhao, Linli Cui, Lu Wang. // 2004. IGARSS '04. Proceedings. 2004 IEEE International Geoscience and Remote Sensing Symposium. - Anchorage, AK, 20-24 Sept. 2004. - Vol. 7. - P. 4829-4832. ↑

C5095. Sircar S. Lateral and subsidence movement estimation using InSAR. / Sircar S., Power D., Randell C., Youden Y., Gill E. // 2004. IGARSS '04. Proceedings. 2004 IEEE International Geoscience and Remote Sensing Symposium. - Anchorage, AK, 20-24 Sept. 2004. - Vol. 5. - P. 2991-2994. ↑

C5096. Lamy M. Short wave spectrum modulation by a surface current field and long waves for SAR imaging process simulation. / Lamy M., Le Caillec J.-M., Garelo R., Kenchaf A. // 2004. IGARSS '04. Proceedings. 2004 IEEE International Geoscience and Remote Sensing Symposium. - Anchorage, AK, 20-24 Sept. 2004. - Vol. 5. - P. 3100-3102. ↑

C5097. Schneiderhan T. Wind parameter analysis of two offshore windpark sites. / Schneiderhan T., Schulz-Stellenfleth J., Lehner S., Horstmann J., Konig T. // 2004. IGARSS '04. Proceedings. 2004 IEEE International Geoscience and Remote Sensing Symposium. - Anchorage, AK, 20-24 Sept. 2004. - Vol. 5. - P. 3103-3106. ↑

C5098. Feiya Zhu. Multilayer perceptron classification for ENVISAT-ASAR imagery. / Feiya Zhu, Huadong Guo, Qing Dong, Changlin Wang. // 2004. IGARSS '04. Proceedings. 2004 IEEE International Geoscience and Remote Sensing Symposium. - Anchorage, AK, 20-24 Sept. 2004. - Vol. 5. - P. 3077-3079. ↑

C5099. Greco M. Analysis of polarimetric marine scattering at different range resolutions. / Greco M., Gini F., Verrazzani L., Balleri A. // 2004. IGARSS '04. Proceedings. 2004 IEEE International Geoscience and Remote

Sensing Symposium. - Anchorage, AK, 20-24 Sept. 2004. - Vol. 5. - P. 3096-3099. ↑

C5100. Ji-Eun Kim. Enhancement of Doppler centroid for ocean surface current retrieval from ERS-1/2 raw SAR. / Ji-Eun Kim, Duk-jin Kim, Moon W.M. // 2004. IGARSS '04. Proceedings. 2004 IEEE International Geoscience and Remote Sensing Symposium. - Anchorage, AK, 20-24 Sept. 2004. - Vol. 5. - P. 3118-3120. ↑

C5101. Colin E. Comparison between simulations and interferometric polarimetric SAR P-band data on a pine-trees forest. / Colin E., Titin-Schnaider C., Thirion L., Tabbara W. // 2004. IGARSS '04. Proceedings. 2004 IEEE International Geoscience and Remote Sensing Symposium. - Anchorage, AK, 20-24 Sept. 2004. - Vol. 5. - P. 3128-3131. ↑

C5102. Matsuoka T. Influence of antenna aperture length on observations of the Kuroshio surface current by the NICT HF ocean radar. / Matsuoka T., Sato K., Kojima S., Fujii S. // 2004. IGARSS '04. Proceedings. 2004 IEEE International Geoscience and Remote Sensing Symposium. - Anchorage, AK, 20-24 Sept. 2004. - Vol. 5. - P. 3124-3127. ↑

C5103. Ivanov L.M. Mesoscale and submesoscale zoo observed with HF radar in Monterey Bay. / Ivanov L.M., Melnichenko O.V. // 2004. IGARSS '04. Proceedings. 2004 IEEE International Geoscience and Remote Sensing Symposium. - Anchorage, AK, 20-24 Sept. 2004. - Vol. 5. - P. 3121-3123. ↑

C5104. Xinwu Li. Inversion of vegetation height using SIR-C dual frequency polarimetric SAR interferometry data. / Xinwu Li, Huadong Guo, Zhen Li, Lei Wang. // 2004. IGARSS '04. Proceedings. 2004 IEEE International Geoscience and Remote Sensing Symposium. - Anchorage, AK, 20-24 Sept. 2004. - Vol. 5. - P. 3132-3135. ↑

C5105. Du G. A novel Radon transform-based method for ship wake detection. / Du G., Yeo T.S. // 2004. IGARSS '04. Proceedings. 2004 IEEE International Geoscience and Remote Sensing Symposium. - Anchorage, AK, 20-24 Sept. 2004. - Vol. 5. - P. 3069-3072. ↑

C5106. French N. Remote sensing of frozen lakes on the North Slope of Alaska. / French N., Savage S., Shuchman R., Edson R., Payne J., Josberger E. // 2004. IGARSS '04. Proceedings. 2004 IEEE International Geoscience and Remote Sensing Symposium. 20-24 Sept. 2004. - Vol. 5. - P. 3008-3011. ↑

C5107. Gerbaux M. Validation of a glacier surface mass balance model using remote sensing. / Gerbaux M., Dedieu J.-P., Etchevers P., Vincent C. // 2004. IGARSS '04. Proceedings. 2004 IEEE International Geoscience and Remote Sensing Symposium. 20-24 Sept. 2004. - Vol. 5. - P. 3005-3007. ↑

C5108. Zhang J.F. To measure the cumulate crustal deformation of important faults system on the Western China by PS InSAR technique. / Zhang J.F., Gong L.X., Chang Z.Q. // 2004. IGARSS '04. Proceedings. 2004 IEEE International Geoscience and Remote Sensing Symposium. 20-24 Sept. 2004. - Vol. 5. - P. 2998-3001. ↑

C5109. Hussein Z.A. Angular and frequency correlation for sea-ice thickness retrieval. / Hussein Z.A., Kuga Y., Ishimaru A., Jaruwatanadilok S., Kyung Pak. // 2004. IGARSS '04. Proceedings. 2004 IEEE International Geoscience and Remote Sensing Symposium. 20-24 Sept. 2004. - Vol. 5. - P. 3012-3017. ↑

C5110. Kimura H. Ice sheet motion in inland Antarctica from JERS-1 SAR interferometry. / Kimura H., Kanamori T., Wakabayashi H., Nishio F. // 2004. IGARSS '04. Proceedings. 2004 IEEE International Geoscience and Remote Sensing Symposium. - Anchorage, AK, 20-24 Sept. 2004. - Vol. 5. - P. 3018-3020. ↑

C5111. Kasapoglu N.G. Feature extraction of SAR data based on eigenvector of texture samples. / Kasapoglu N.G., Ersoy O., Yazgan B. // 2004. IGARSS '04. Proceedings. 2004 IEEE International Geoscience and Remote Sensing Symposium. 20-24 Sept. 2004. - Vol. 5. - P. 3042-3045. ↑

C5112. Qong M. Scattering mechanism identification based on the rotation and eccentric angles of polarimetric SAR data. 2004. IGARSS '04. Proceedings. 2004 IEEE International Geoscience and Remote Sensing Symposium. - Anchorage, AK, 20-24 Sept. 2004. - Vol. 5. - P. 3054-3057. ↑

C5113. Scharien R.K. Analyses of C-band microwave backscatter to wind roughened first-year sea ice melt ponds. / Scharien R.K., Yackel J.J. // 2004. IGARSS '04. Proceedings. 2004 IEEE International Geoscience and Remote Sensing Symposium. 20-24 Sept. 2004. - Vol. 5. - P. 3025-3028. ↑

C5114. Karvonen J. Comparison of SAR data and operational sea ice products to EM ice thickness measurements in the Baltic Sea. / Karvonen J., Simila M., Haapala J., Haas C., Makynen M. // 2004. IGARSS

'04. Proceedings. 2004 IEEE International Geoscience and Remote Sensing Symposium. - Anchorage, AK, 20-24 Sept. 2004. - Vol. 5. - P. 3021-3024. ↑

C5115. Le Traon P.Y. SSALTO/DUACS and operational altimetry. / Le Traon P.Y., Dibarboure G., Dorandeu J. // 2003. IGARSS '03. Proceedings. 2003 IEEE International Geoscience and Remote Sensing Symposium. 21-25 July 2003. - Vol. 2. - P. 824-826. ↑

C5116. Benveniste J. ENVISAT RA-2/MWR cross-calibration and validation final results. 2003. IGARSS '03. Proceedings. 2003 IEEE International Geoscience and Remote Sensing Symposium. 21-25 July 2003. - Vol. 2. - P. 815-817. ↑

C5117. Raggam H. Approaches to automate image geocoding and registration. / Raggam H., Fernandez M.D.V. // 2003. IGARSS '03. Proceedings. 2003 IEEE International Geoscience and Remote Sensing Symposium. 21-25 July 2003. - Vol. 2. - P. 812-814. ↑

C5118. Emery W.J. Sampling the mesoscale ocean surface currents with various satellite altimeter configurations. / Emery W.J., Baldwin D., Matthews D. // 2003. IGARSS '03. Proceedings. 2003 IEEE International Geoscience and Remote Sensing Symposium. 21-25 July 2003. - Vol. 2. - P. 821-823. ↑

C5119. Bonnefond P. Calibrating the Jason-1 measurement system. / Bonnefond P., Haines B., Born G., Exertier P., Gill S., Jan G., Jeansou E., Kubitschek D., Laurain O. // 2003. IGARSS '03. Proceedings. 2003 IEEE International Geoscience and Remote Sensing Symposium. 21-25 July 2003. - Vol. 2. - P. 818-820. ↑

C5120. Jiancheng Shi. On estimation of snow water equivalence using L-band and Ku-band radar. / Jiancheng Shi, Yueh S., Cline D. // 2003. IGARSS '03. Proceedings. 2003 IEEE International Geoscience and Remote Sensing Symposium. 21-25 July 2003. - Vol. 2. - P. 845-847. ↑

C5121. Dedieu J.-P. Radiometric and geometric correction of RADARSAT-1 images acquired in alpine regions for mapping the snow water equivalent (SWE). / Dedieu J.-P., Gauthier Y., Bernier M., Hardy S., Vincent P., Durand Y. // 2003. IGARSS '03. Proceedings. 2003 IEEE International Geoscience and Remote Sensing Symposium. 21-25 July 2003. - Vol. 2. - P. 851-853. ↑

C5122. Martini A. Polarimetric study of scattering from dry snow cover in alpine areas. / Martini A., Ferro-Famil L., Pottier E. // 2003. IGARSS '03. Proceedings. 2003 IEEE International Geoscience and Remote Sensing Symposium. 21-25 July 2003. - Vol. 2. - P. 854-856. ↑

C5123. Lefevre J.-M. Impact of using several altimeters for improving numerical wave analyses and forecasts. / Lefevre J.-M., Skandrani C., Queffeuilou P. // 2003. IGARSS '03. Proceedings. 2003 IEEE International Geoscience and Remote Sensing Symposium. 21-25 July 2003. - Vol. 2. - P. 827-829. ↑

C5124. Hallikainen M.T. Combined active and passive microwave remote sensing of snow in Finland. / Hallikainen M.T., Halme P., Takala M., Pulliainen J. // 2003. IGARSS '03. Proceedings. 2003 IEEE International Geoscience and Remote Sensing Symposium. 21-25 July 2003. - Vol. 2. - P. 830-832. ↑

C5125. Vikhamar D. A constrained spectral unmixing approach to snow-cover mapping in forests using MODIS data. / Vikhamar D., Solberg R. // 2003. IGARSS '03. Proceedings. 2003 IEEE International Geoscience and Remote Sensing Symposium. 21-25 July 2003. - Vol. 2. - P. 833-835. ↑

C5126. Krieger G. Analysis of system concepts for bi- and multi-static SAR missions. / Krieger G., Fiedler H., Houman D., Moreira A. // 2003. IGARSS '03. Proceedings. 2003 IEEE International Geoscience and Remote Sensing Symposium. 21-25 July 2003. - Vol. 2. - P. 770-772. ↑

C5127. Kamal Sarabandi. GLORIA: Geostationary/Low-Earth Orbiting Radar Image Acquisition System: a multi-static GEO/LEO synthetic aperture radar satellite constellation for Earth observation. / Kamal Sarabandi, Kellendorfer J., Pierce L. // 2003. IGARSS '03. Proceedings. 2003 IEEE International Geoscience and Remote Sensing Symposium. 21-25 July 2003. - Vol. 2. - P. 773-775. ↑

C5128. Ferrazzoli P. A further insight into the potential of bistatic SAR in monitoring the Earth surface. / Ferrazzoli P., Guerriero L., Del Monaco C.I., Solimini D. // 2003. IGARSS '03. Proceedings. 2003 IEEE International Geoscience and Remote Sensing Symposium. 21-25 July 2003. - Vol. 2. - P. 776-777. ↑

C5129. Sato M. Landmine detection by a broadband GPR system. / Sato M., Guangyou Fang, Zhaofa Zeng. //

2003. IGARSS '03. Proceedings. 2003 IEEE International Geoscience and Remote Sensing Symposium. 21-25 July 2003. - Vol. 2. - P. 758-760. ↑

C5130. Kolba M.P. Buried land mine detection using complex natural resonances on GPR data. / Kolba M.P., Jouny I.I. // 2003. IGARSS '03. Proceedings. 2003 IEEE International Geoscience and Remote Sensing Symposium. 21-25 July 2003. - Vol. 2. - P. 761-763. ↑

C5131. Bin Sai. Effective clutter removal for detecting non-metallic mines in various soil fields. / Bin Sai, Ligthart L.P. // 2003. IGARSS '03. Proceedings. 2003 IEEE International Geoscience and Remote Sensing Symposium. 21-25 July 2003. - Vol. 2. - P. 764-766. ↑

C5132. Cherniakov M. Analysis of space-surface interferometric bistatic radar. / Cherniakov M., Zeng T., Plakidis E. // 2003. IGARSS '03. Proceedings. 2003 IEEE International Geoscience and Remote Sensing Symposium. 21-25 July 2003. - Vol. 2. - P. 778-780. ↑

C5133. Nashashibi A.Y. Millimeter-wave polarimetric bistatic radar scattering from rough soil surfaces. / Nashashibi A.Y., Ulaby F.T. // 2003. IGARSS '03. Proceedings. 2003 IEEE International Geoscience and Remote Sensing Symposium. 21-25 July 2003. - Vol. 2. - P. 788-790. ↑

C5134. Lehner M. Automated image matching between geocoded Landsat-TM scenes and MOMS-2P stereo imager for DEM and orthoimage production. / Lehner M., Muller R. // 2003. IGARSS '03. Proceedings. 2003 IEEE International Geoscience and Remote Sensing Symposium. 21-25 July 2003. - Vol. 2. - P. 794-796. ↑

C5135. Hosford S. Fusion of airborne laser altimeter and RADARSAT data for DEM generation. / Hosford S., Baghdadi N., Bourguin B., Daniels P., King C. // 2003. IGARSS '03. Proceedings. 2003 IEEE International Geoscience and Remote Sensing Symposium. 21-25 July 2003. - Vol. 2. - P. 806-808. ↑

C5136. Zavorotny V. Seasonal polarimetric measurements of soil moisture using tower-based GPS bistatic radar. / Zavorotny V., Masters D., Gasiewski A., Bartram B., Katzberg S., Axelrad P., Zamora R. // 2003. IGARSS '03. Proceedings. 2003 IEEE International Geoscience and Remote Sensing Symposium. 21-25 July 2003. - Vol. 2. - P. 781-783. ↑

C5137. Cherniakov M. Galileo signal-based bistatic system for avalanche prediction. / Cherniakov M., Zeng T., Plakidis E. // 2003. IGARSS '03. Proceedings. 2003 IEEE International Geoscience and Remote Sensing Symposium. 21-25 July 2003. - Vol. 2. - P. 784-786. ↑

C5138. Terzuoli A.J. Topics in passive bistatic remote sensing. / Terzuoli A.J., Paul Gilgallon P., Howland P. // 2003. IGARSS '03. Proceedings. 2003 IEEE International Geoscience and Remote Sensing Symposium. 21-25 July 2003. - Vol. 2. - P. 787 vol.2. ↑

C5139. Engen G. New approach for snow water equivalent (SWE) estimation using repeat pass interferometric SAR. / Engen G., Guneriusen T., Overrein O. // 2003. IGARSS '03. Proceedings. 2003 IEEE International Geoscience and Remote Sensing Symposium. 21-25 July 2003. - Vol. 2. - P. 857-859. ↑

C5140. Dong Qing. Variograms: practical method to process polarimetric SAR data. / Dong Qing, Guo Huadong, Shao Yun, Li Zhen, Wang Changlin. // 2003. IGARSS '03. Proceedings. 2003 IEEE International Geoscience and Remote Sensing Symposium. 21-25 July 2003. - Vol. 2. - P. 932-934. ↑

C5141. Xiaojian Xu. Enhanced resolution in 3-D interferometric ISAR imaging using an iterative SVA procedure. / Xiaojian Xu, Narayanan R.M. // 2003. IGARSS '03. Proceedings. 2003 IEEE International Geoscience and Remote Sensing Symposium. 21-25 July 2003. - Vol. 2. - P. 935-937. ↑

C5142. Priess M. A change detection technique for repeat pass interferometric SAR. / Priess M., Gray D., Stacy N. // 2003. IGARSS '03. Proceedings. 2003 IEEE International Geoscience and Remote Sensing Symposium. 21-25 July 2003. - Vol. 2. - P. 938-940. ↑

C5143. Praks J. Examination of forest polarimetric backscattering with coherent cylinder model. / Praks J., Pulliainen J., Ahtonen P., Hallikainen M. // 2003. IGARSS '03. Proceedings. 2003 IEEE International Geoscience and Remote Sensing Symposium. 21-25 July 2003. - Vol. 2. - P. 923-925. ↑

C5144. Turner D. Visualisation of cross-polarised response patterns over short vegetation. / Turner D., Woodhouse I.H. // 2003. IGARSS '03. Proceedings. 2003 IEEE International Geoscience and Remote Sensing Symposium. 21-25 July 2003. - Vol. 2. - P. 926-928. ↑

Symposium. 21-25 July 2003. - Vol. 2. - P. 926-928. ↑

C5145. Sahyun Hong. Application of Gaussian Markov random field model to unsupervised classification in polarimetric SAR image. / Sahyun Hong, Moon W.M. // 2003. IGARSS '03. Proceedings. 2003 IEEE International Geoscience and Remote Sensing Symposium. 21-25 July 2003. - Vol. 2. - P. 929-931. ↑

C5146. Garelo R. Current maps and bathymetry from P-band SAR images: preliminary results. / Garelo R., Le Caillec J.-M., Dupuis H., Marieu V., Durand N., Dreuillet P., Titin-Schnaider C. // 2003. IGARSS '03. Proceedings. 2003 IEEE International Geoscience and Remote Sensing Symposium. 21-25 July 2003. - Vol. 2. - P. 960-962. ↑

C5147. Braun N. Sea-surface current measurements with an X band radar. / Braun N., Bezuglov A., Schymura G., Ziemer F. // 2003. IGARSS '03. Proceedings. 2003 IEEE International Geoscience and Remote Sensing Symposium. 21-25 July 2003. - Vol. 2. - P. 963-965. ↑

C5148. Lavrova O.Y. SAR observations of typical phenomena in the Black Sea shore area. / Lavrova O.Y., Bucharova T.Y., Mityagina M.I. // 2003. IGARSS '03. Proceedings. 2003 IEEE International Geoscience and Remote Sensing Symposium. 21-25 July 2003. - Vol. 2. - P. 966-968. ↑

C5149. Kampes B.M. Velocity field retrieval from long term coherent points in radar interferometric stacks. / Kampes B.M., Adam N. // 2003. IGARSS '03. Proceedings. 2003 IEEE International Geoscience and Remote Sensing Symposium. 21-25 July 2003. - Vol. 2. - P. 941-943. ↑

C5150. Marghany M. Polarised AIRSAR along track interferometry for shoreline change modeling. 2003. IGARSS '03. Proceedings. 2003 IEEE International Geoscience and Remote Sensing Symposium. 21-25 July 2003. - Vol. 2. - P. 945-947. ↑

C5151. Fornaro G. Phase difference based multiple acquisition phase unwrapping. / Fornaro G., Pauciuolo A., Sansosti E. // 2003. IGARSS '03. Proceedings. 2003 IEEE International Geoscience and Remote Sensing Symposium. 21-25 July 2003. - Vol. 2. - P. 948-950. ↑

C5152. Kerr Y.H. SMOS: analysis of perturbing effects over land surfaces. / Kerr Y.H., Secherre F., Lastenet J., Wigneron J.-P. // 2003. IGARSS '03. Proceedings. 2003 IEEE International Geoscience and Remote Sensing Symposium. 21-25 July 2003. - Vol. 2. - P. 908-910. ↑

C5153. Picon A.J. A study on cloud-top height retrieval by using MISR and MODIS data. / Picon A.J., Vasquez R. // 2003. IGARSS '03. Proceedings. 2003 IEEE International Geoscience and Remote Sensing Symposium. 21-25 July 2003. - Vol. 2. - P. 872-874. ↑

C5154. Nirala M.L. Optimal precipitation estimation using multisensor microwave datasets. 2003. IGARSS '03. Proceedings. 2003 IEEE International Geoscience and Remote Sensing Symposium. 21-25 July 2003. - Vol. 2. - P. 875-877. ↑

C5155. Tanelli S. Measuring vertical rainfall velocity through spaceborne Doppler radar: performance analysis and system requirements. / Tanelli S., Im E., Durden S.L., Facheris L. // 2003. IGARSS '03. Proceedings. 2003 IEEE International Geoscience and Remote Sensing Symposium. 21-25 July 2003. - Vol. 2. - P. 878-880. ↑

C5156. Xiong X. An overview of MODIS on-orbit calibration and instrument performance. / Xiong X., Salomonson V.V., Barnes W.L. // 2003. IGARSS '03. Proceedings. 2003 IEEE International Geoscience and Remote Sensing Symposium. 21-25 July 2003. - Vol. 2. - P. 860-862. ↑

C5157. Chu D.A. Multiyear MODIS observation of global aerosols from EOS Terra/Aqua satellites: validation, variability, and application. / Chu D.A., Kaufman Y.J., Remer L.A., Tanre D., Jeong M.J. // 2003. IGARSS '03. Proceedings. 2003 IEEE International Geoscience and Remote Sensing Symposium. 21-25 July 2003. - Vol. 2. - P. 863-865. ↑

C5158. Ryzhkov A. Development of a classification algorithm for operational polarimetric NEXRAD radar. / Ryzhkov A., Zrnich D., Doviak R., Pengfei Zhang. // 2003. IGARSS '03. Proceedings. 2003 IEEE International Geoscience and Remote Sensing Symposium. 21-25 July 2003. - Vol. 2. - P. 869-871. ↑

C5159. Wood E.F. Soil moisture retrieval over the southern Great Plains: comparisons between experimental remote sensing data and operational products. / Wood E.F., Gao H., Drusch M., Jackson T., Bindish R. // 2003.

IGARSS '03. Proceedings. 2003 IEEE International Geoscience and Remote Sensing Symposium. 21-25 July 2003. - Vol. 2. - P. 893-895. ↑

C5160. Masters D. Airborne GPS bistatic radar soil moisture measurements during SMEX02. / Masters D., Katzberg S., Axelrad P. // 2003. IGARSS '03. Proceedings. 2003 IEEE International Geoscience and Remote Sensing Symposium. 21-25 July 2003. - Vol. 2. - P. 896-898. ↑

C5161. Laymon C.A. Validation of aircraft and satellite remote sensing of brightness temperature and derived soil moisture using a hydrologic/radiobrightness model. / Laymon C.A., Crosson W.L., Limaye A. // 2003. IGARSS '03. Proceedings. 2003 IEEE International Geoscience and Remote Sensing Symposium. 21-25 July 2003. - Vol. 2. - P. 899-901. ↑

C5162. Marzano F.S. Numerical simulation of multiple effects due to convective clouds on satellite radar reflectivity at 14 and 35 GHz. / Marzano F.S., Ferrauto G., Roberti L., di Michele S., Mugnai A., Tassa A. // 2003. IGARSS '03. Proceedings. 2003 IEEE International Geoscience and Remote Sensing Symposium. 21-25 July 2003. - Vol. 2. - P. 881-883. ↑

C5163. Leon-Colon L.V. Active rain gauge concept for moderate to heavy precipitation using W-band and S-band Doppler radars. / Leon-Colon L.V., Cruz-Pol S.L., Sekelsky S.M. // 2003. IGARSS '03. Proceedings. 2003 IEEE International Geoscience and Remote Sensing Symposium. 21-25 July 2003. - Vol. 2. - P. 884-886. ↑

C5164. Berges J.C. Neural networks and tree classifiers: an application to rainfall estimation. 2003. IGARSS '03. Proceedings. 2003 IEEE International Geoscience and Remote Sensing Symposium. 21-25 July 2003. - Vol. 2. - P. 887-889. ↑

C5165. Buckner J.L. NASA Advanced Component Technology Program, investments in remote sensing technologies. 2003. IGARSS '03. Proceedings. 2003 IEEE International Geoscience and Remote Sensing Symposium. 21-25 July 2003. - Vol. 1. - P. 494-496. ↑

C5166. Yueh S.H. Compact dual-frequency microstrip antenna feed for future soil moisture and sea surface salinity missions. / Yueh S.H., Wilson W.J., Njoku E., Kona K.S., Bahadori K., Rahmat-Samii Y. // 2003. IGARSS '03. Proceedings. 2003 IEEE International Geoscience and Remote Sensing Symposium. 21-25 July 2003. - Vol. 1. - P. 497-499. ↑

C5167. Moghaddam M. Microwave Observatory of Subcanopy and Subsurface (MOSS): a low-frequency radar for global deep soil moisture measurements. / Moghaddam M., Rodriguez E., Rahmat-Samii Y., Moller D., Hoffman J., Huang J., Saatchi S. // 2003. IGARSS '03. Proceedings. 2003 IEEE International Geoscience and Remote Sensing Symposium. 21-25 July 2003. - Vol. 1. - P. 500-502. ↑

C5168. van Zyl J.J. The use of polarimetric and interferometric SAR data in floodplain mapping. / van Zyl J.J., Yunjin Kim. // 2003. IGARSS '03. Proceedings. 2003 IEEE International Geoscience and Remote Sensing Symposium. 21-25 July 2003. - Vol. 1. - P. 443-445. ↑

C5169. Beaulieu J.-M. Segmentation of textured scenes using polarimetric SARs. / Beaulieu J.-M., Touzi R. // 2003. IGARSS '03. Proceedings. 2003 IEEE International Geoscience and Remote Sensing Symposium. 21-25 July 2003. - Vol. 1. - P. 446-448. ↑

C5170. Scheuchl B. Consolidation of a pixel-based classification using neighborhood information. / Scheuchl B., Cumming I., Hajnsek I. // 2003. IGARSS '03. Proceedings. 2003 IEEE International Geoscience and Remote Sensing Symposium. 21-25 July 2003. - Vol. 1. - P. 449-451. ↑

C5171. Amzajerdian F. 2-micron coherent Doppler lidar for space-based global wind field mapping. / Amzajerdian F., Kavaya M.J., Singh U., Jirong Yu. // 2003. IGARSS '03. Proceedings. 2003 IEEE International Geoscience and Remote Sensing Symposium. 21-25 July 2003. - Vol. 1. - P. 515-517. ↑

C5172. Juneke W.N. First observations with the UMass dual-beam InSAR. / Juneke W.N., Ramanathan A., Farquharson G., Frasier S.J., Tessier R., McLaughlin D.J., Sletten M.A., Toporkov J.V. // 2003. IGARSS '03. Proceedings. 2003 IEEE International Geoscience and Remote Sensing Symposium. 21-25 July 2003. - Vol. 1. - P. 530-532. ↑

C5173. Brenner A.R. Very wideband radar imaging with the airborne SAR sensor PAMIR. / Brenner A.R., Ender J.H.G. // 2003. IGARSS '03. Proceedings. 2003 IEEE International Geoscience and Remote Sensing

Symposium. 21-25 July 2003. - Vol. 1. - P. 533-535. ↑

C5174. Tomiyasu K. Conceptual spaceborne Ka-band spotlight synthetic aperture radar with reconfigurable aperture. 2003. IGARSS '03. Proceedings. 2003 IEEE International Geoscience and Remote Sensing Symposium. 21-25 July 2003. - Vol. 1. - P. 539-541. ↑

C5175. Heer C. Investigations on a new high resolution wide swath SAR concept. / Heer C., Soualle F., Zahn R., Reber R. // 2003. IGARSS '03. Proceedings. 2003 IEEE International Geoscience and Remote Sensing Symposium. 21-25 July 2003. - Vol. 1. - P. 521-523. ↑

C5176. Blanchard A. On the concept of an all digital sensor design. / Blanchard A., Golden J., Morgan R. // 2003. IGARSS '03. Proceedings. 2003 IEEE International Geoscience and Remote Sensing Symposium. 21-25 July 2003. - Vol. 1. - P. 524-526. ↑

C5177. Krieger G. Potential of digital beamforming in bi- and multistatic SAR. / Krieger G., Moreira A. // 2003. IGARSS '03. Proceedings. 2003 IEEE International Geoscience and Remote Sensing Symposium. 21-25 July 2003. - Vol. 1. - P. 527-529. ↑

C5178. Jackson T.J. Soil moisture retrieval and AMSR-E validation using an airborne microwave radiometer in SMEX02. / Jackson T.J., Bindlish R., Klein M., Gasiewski A.J., Njoku E.G. // 2003. IGARSS '03. Proceedings. 2003 IEEE International Geoscience and Remote Sensing Symposium. 21-25 July 2003. - Vol. 1. - P. 401-403. ↑

C5179. van Zyl J.J. Quantitative analysis of SMEX'02 AIRSAR data for soil moisture inversion. / van Zyl J.J., Njoku E.G., Jackson T.J. // 2003. IGARSS '03. Proceedings. 2003 IEEE International Geoscience and Remote Sensing Symposium. 21-25 July 2003. - Vol. 1. - P. 404-406. ↑

C5180. O'Niell P.E. Soil moisture retrieval through changing corn using active/passive microwave remote sensing. / O'Niell P.E., Joseph A., De Lannoy G, Lang R., Utku C., Kim E., Houser P., Gish T. // 2003. IGARSS '03. Proceedings. 2003 IEEE International Geoscience and Remote Sensing Symposium. 2003. - Vol. 1. - P. 407-409. ↑

C5181. Schueler C. VIIRS sensor performance. / Schueler C., Clement J.E., Darnton L., DeLuccia F., Scalione T., Swenson H. // 2003. IGARSS '03. Proceedings. 2003 IEEE International Geoscience and Remote Sensing Symposium. 21-25 July 2003. - Vol. 1. - P. 369-372. ↑

C5182. Grano V. Introduction, overview, and status of the NPOESS aerosol polarimetry sensor (APS). / Grano V., Ubhayakar S., Haas J.M., Schueler C. // 2003. IGARSS '03. Proceedings. 2003 IEEE International Geoscience and Remote Sensing Symposium. 21-25 July 2003. - Vol. 1. - P. 374-376. ↑

C5183. Anderson C. Integrating SAR and optical products for crop management (Isocrop) iophysical parameter retrieval using X and L band SAR data. / Anderson C., Bryson R., Alford J., Madrigal C., Holmes G. // 2003. IGARSS '03. Proceedings. 2003 IEEE International Geoscience and Remote Sensing Symposium. 21-25 July 2003. - Vol. 1. - P. 398-400. ↑

C5184. Boerner W.-M. Need for developing multi-band single and multiple pass POLinSAR monitoring platforms in air and space. / Boerner W.-M., Moreira A., Papathanassiou K.P., Hajnsek I., Pottier E., Ferro-Famil L., Reigber A., Cloude S.R., Sato M., Yamaguchi Y., Yamada H., Lee J.S., Ainsworth T.L., Schuler D.L., Touzi R., Lukowski T. // 2003. IGARSS '03. Proceedings. 2003 IEEE International Geoscience and Remote Sensing Symposium. 21-25 July 2003. - Vol. 1. - P. 422-424. ↑

C5185. Ferro-Famil L. Analysis of anisotropic behavior using sub-aperture polarimetric SAR data. / Ferro-Famil L., Reigber A., Pottier E., Boerner W.M. // 2003. IGARSS '03. Proceedings. 2003 IEEE International Geoscience and Remote Sensing Symposium. 21-25 July 2003. - Vol. 1. - P. 434-436. ↑

C5186. Breuer A. Full polarimetry versus partial polarimetry for quantitative surface parameter estimation. / Breuer A., Hajnsek I., Ferro-Famil L., Pottier E. // 2003. IGARSS '03. Proceedings. 2003 IEEE International Geoscience and Remote Sensing Symposium. 21-25 July 2003. - Vol. 1. - P. 437-439. ↑

C5187. Allain S. Influence of resolution cell size for surface parameters retrieval from polarimetric SAR data. / Allain S., Ferro-Famil L., Pottier E., Fortuny J. // 2003. IGARSS '03. Proceedings. 2003 IEEE International Geoscience and Remote Sensing Symposium. 21-25 July 2003. - Vol. 1. - P. 440-442. ↑

- C5188.** Kimura K. Pi-SAR image analysis using polarimetric scattering parameters and total power. / Kimura K., Yamaguchi Y., Yamada H. // 2003. IGARSS '03. Proceedings. 2003 IEEE International Geoscience and Remote Sensing Symposium. 21-25 July 2003. - Vol. 1. - P. 425-427. ↑
- C5189.** Lee J.S. Polarization orientation estimation and applications: a review. / Lee J.S., Schuler D.L., Ainsworth T.L., Boerner W.-M. // 2003. IGARSS '03. Proceedings. 2003 IEEE International Geoscience and Remote Sensing Symposium. 21-25 July 2003. - Vol. 1. - P. 428-430. ↑
- C5190.** Sato M. Classification of tree types by polarimetric Pi-SAR. / Sato M., Koike T. // 2003. IGARSS '03. Proceedings. 2003 IEEE International Geoscience and Remote Sensing Symposium. 21-25 July 2003. - Vol. 1. - P. 431-433. ↑
- C5191.** Aguttes J.P. The SAR train concept: required antenna area distributed over N smaller satellites, increase of performance by N. 2003. IGARSS '03. Proceedings. 2003 IEEE International Geoscience and Remote Sensing Symposium. 21-25 July 2003. - Vol. 1. - P. 542-544. ↑
- C5192.** Morris J.T. A study of the X-band entropy of breaking ocean waves. / Morris J.T., Anderson S.J., Cloude S.R. // 2003. IGARSS '03. Proceedings. 2003 IEEE International Geoscience and Remote Sensing Symposium. 21-25 July 2003. - Vol. 2. - P. 711-713. ↑
- C5193.** Lindstrom S. WindSat SDR and EDR on orbit calibration and validation. / Lindstrom S., Ruf C. // 2003. IGARSS '03. Proceedings. 2003 IEEE International Geoscience and Remote Sensing Symposium. 21-25 July 2003. - Vol. 2. - P. 714-716. ↑
- C5194.** Johnson J.T. A study of sea emission models for WindSat. / Johnson J.T., Theunissen W.H., ellingson S.W. // 2003. IGARSS '03. Proceedings. 2003 IEEE International Geoscience and Remote Sensing Symposium. 21-25 July 2003. - Vol. 2. - P. 717-719. ↑
- C5195.** Ferro-Famil L. Scene characterization using sub-aperture polarimetric interferometric SAR data. / Ferro-Famil L., Reigber A., Pottier E. // 2003. IGARSS '03. Proceedings. 2003 IEEE International Geoscience and Remote Sensing Symposium. 21-25 July 2003. - Vol. 2. - P. 702-704. ↑
- C5196.** Lee J.S. Coherence estimation and speckle filtering based on scattering properties. / Lee J.S., Grunes M.R., Ainsworth T.L., Schuler D.L., Cloude S.R. // 2003. IGARSS '03. Proceedings. 2003 IEEE International Geoscience and Remote Sensing Symposium. 21-25 July 2003. - Vol. 2. - P. 705-707. ↑
- C5197.** Schuler D.L. Measurement of ocean wave spectra using polarimetric SAR data. / Schuler D.L., Lee J.S., Kasilingam D., Pottier E. // 2003. IGARSS '03. Proceedings. 2003 IEEE International Geoscience and Remote Sensing Symposium. 21-25 July 2003. - Vol. 2. - P. 708-710. ↑
- C5198.** Palubinska G. Radiometric normalization of optical remote sensing imagery. / Palubinska G., Muller R., Reinartz P. // 2003. IGARSS '03. Proceedings. 2003 IEEE International Geoscience and Remote Sensing Symposium. 21-25 July 2003. - Vol. 2. - P. 720-722. ↑
- C5199.** Yarovoy A.G. Multi-waveform full-polarimetric GPR for landmine detection. / Yarovoy A.G., Ligthart L.P., Schukin A.D., Kaploun I.V. // 2003. IGARSS '03. Proceedings. 2003 IEEE International Geoscience and Remote Sensing Symposium. 21-25 July 2003. - Vol. 2. - P. 749-751. ↑
- C5200.** Cooper P. Ultra wideband endfire synthetic aperture radar for landmine detection. / Cooper P., Verwey G., Purry C. // 2003. IGARSS '03. Proceedings. 2003 IEEE International Geoscience and Remote Sensing Symposium. 21-25 July 2003. - Vol. 2. - P. 752-754. ↑
- C5201.** Yarovoy A. Impact of ground clutter on buried object detection by ground penetrating radar [penetrating read penetrating]. / Yarovoy A., Kovalenko V., Fogar A. // 2003. IGARSS '03. Proceedings. 2003 IEEE International Geoscience and Remote Sensing Symposium. 21-25 July 2003. - Vol. 2. - P. 755-757. ↑
- C5202.** Velloso M.L.F. Relative radiometric correction on remotely sensed data for land cover change detection: an unsupervised clustering approach. / Velloso M.L.F., de Souza F.J., Almeida N.N. // 2003. IGARSS '03. Proceedings. 2003 IEEE International Geoscience and Remote Sensing Symposium. 21-25 July 2003. - Vol. 2. - P. 723-725. ↑
- C5203.** Zhihao Qin. A methodology for true orthorectification of large-scale urban aerial images and automatic

detection of building occlusions using digital surface model. / Zhihao Qin, Wenjuan Li, Manchun Li, Zhongxin Chen, Goqing Zhou. // 2003. IGARSS '03. Proceedings. 2003 IEEE International Geoscience and Remote Sensing Symposium. 21-25 July 2003. - Vol. 2. - P. 729-731. ↑

C5204. Tsai V.J.D. Automatic shadow detection and radiometric restoration on digital aerial images. 2003. IGARSS '03. Proceedings. 2003 IEEE International Geoscience and Remote Sensing Symposium. 21-25 July 2003. - Vol. 2. - P. 732-733. ↑

C5205. Zarco-Tajeda P.J. Detection of chlorophyll fluorescence in vegetation from airborne hyperspectral CASI imagery in the red edge spectral region. / Zarco-Tajeda P.J., Miller J.R., Haboudane D., Tremblay N., Apostol S. // 2003. IGARSS '03. Proceedings. 2003 IEEE International Geoscience and Remote Sensing Symposium. 21-25 July 2003. - Vol. 1. - P. 598-600. ↑

C5206. Chen C.W. Observational architectures for enabling earthquake forecasting. / Chen C.W., Raymond C.A., Madsen S.N. // 2003. IGARSS '03. Proceedings. 2003 IEEE International Geoscience and Remote Sensing Symposium. 21-25 July 2003. - Vol. 1. - P. 618-620. ↑

C5207. Ferraro R.R. Rainfall over land from the AMSR-E. / Ferraro R.R., McCollum J.R. // 2003. IGARSS '03. Proceedings. 2003 IEEE International Geoscience and Remote Sensing Symposium. 21-25 July 2003. - Vol. 1. - P. 669-671. ↑

C5208. Sylvander S. Geometrical performance of the VEGETATION products. / Sylvander S., Albert-Grousset I., Henry P. // 2003. IGARSS '03. Proceedings. 2003 IEEE International Geoscience and Remote Sensing Symposium. 21-25 July 2003. - Vol. 1. - P. 573-575. ↑

C5209. Moya I. Possible approaches to remote sensing of photosynthetic activity. / Moya I., Cartelat A., Cericovic Z.G., Ducruet J.-M., Evain S., Flexas J., Goulas Y., Louis J., Meyer S., Moise N., Ounis A. // 2003. IGARSS '03. Proceedings. 2003 IEEE International Geoscience and Remote Sensing Symposium. 21-25 July 2003. - Vol. 1. - P. 588-590. ↑

C5210. Cecchi G. A high spectral resolution sensor for active and passive remote sensing of vegetation fluorescence. / Cecchi G., Lognoli D., Mochi I., Palombi L., Petrini E., Raimondi V. // 2003. IGARSS '03. Proceedings. 2003 IEEE International Geoscience and Remote Sensing Symposium. 21-25 July 2003. - Vol. 1. - P. 591-593. ↑

C5211. Paloscia S. A semi-empirical algorithm for estimating soil moisture from dual-frequency microwave AMSR data. / Paloscia S., Santi E. // 2003. IGARSS '03. Proceedings. 2003 IEEE International Geoscience and Remote Sensing Symposium. 21-25 July 2003. - Vol. 1. - P. 677-679. ↑

C5212. Hajnsek I. A hybrid scattering model for surface parameter estimation using polarimetric SAR interferometry. / Hajnsek I., Papathanassiou K.P., Cloude S.R. // 2003. IGARSS '03. Proceedings. 2003 IEEE International Geoscience and Remote Sensing Symposium. 21-25 July 2003. - Vol. 2. - P. 693-695. ↑

C5213. Ainsworth T.L. Optimal image classification employing "optimal" polarimetric variables. / Ainsworth T.L., Lee J.S. // 2003. IGARSS '03. Proceedings. 2003 IEEE International Geoscience and Remote Sensing Symposium. 21-25 July 2003. - Vol. 2. - P. 696-698. ↑

C5214. Skriver H. Evaluation of the Wishart test statistics for polarimetric SAR data. / Skriver H., Nielsen A.A., Conradsen K. // 2003. IGARSS '03. Proceedings. 2003 IEEE International Geoscience and Remote Sensing Symposium. 21-25 July 2003. - Vol. 2. - P. 699-701. ↑

C5215. Chang A.T.C. Global SWE monitoring using AMSR-E data. / Chang A.T.C., Kelly R.E.J., Foster J.L., Hall D.K. // 2003. IGARSS '03. Proceedings. 2003 IEEE International Geoscience and Remote Sensing Symposium. 21-25 July 2003. - Vol. 1. - P. 680-682. ↑

C5216. Refice A. Polarimetric optimisation applied to permanent scatterers identification. / Refice A., Mattia F., de Carolis G. // 2003. IGARSS '03. Proceedings. 2003 IEEE International Geoscience and Remote Sensing Symposium. 21-25 July 2003. - Vol. 2. - P. 687-689. ↑

C5217. Mattia F. On the sensitivity of polarimetric coherence to small and large scale surface roughness. / Mattia F., le Toan T., Jong-Sen Lee, Schuler D.L. // 2003. IGARSS '03. Proceedings. 2003 IEEE International Geoscience and Remote Sensing Symposium. 21-25 July 2003. - Vol. 2. - P. 690-692. ↑

- C5218.** Kamal Sarabandi. Phenomenology of millimeter-wave signal propagation and scattering for detection of targets camouflaged under foliage. / Kamal Sarabandi, Nashashibi A.Y. // 2003. IGARSS '03. Proceedings. 2003 IEEE International Geoscience and Remote Sensing Symposium. 21-25 July 2003. - Vol. 2. - P. 1344-1346. ↑
- C5219.** Arslan A.N. Investigating relationship between correlation lengths and physical properties of wet snow. / Arslan A.N., Pulliainen J., Hallikainen M. // 2003. IGARSS '03. Proceedings. 2003 IEEE International Geoscience and Remote Sensing Symposium. 21-25 July 2003. - Vol. 2. - P. 1347-1349. ↑
- C5220.** Williams M.L. Modeling the SAR response of pine forest in Southern Finland. / Williams M.L., Manninen T., Kellomaki S., Ikonen V.-P., Sievanen R., Lehtonen M., Nikinmaa E., Vesala T. // 2003. IGARSS '03. Proceedings. 2003 IEEE International Geoscience and Remote Sensing Symposium. 21-25 July 2003. - Vol. 2. - P. 1350-1352. ↑
- C5221.** Winker D.M. The CALIPSO mission. / Winker D.M., Pelon J. // 2003. IGARSS '03. Proceedings. 2003 IEEE International Geoscience and Remote Sensing Symposium. 21-25 July 2003. - Vol. 2. - P. 1329-1331. ↑
- C5222.** Murphy R.E. Extending climate data records from the EOS era into the NPOESS era. / Murphy R.E., Henegar J., Wharton S., Guenther B., Kealy P.M. // 2003. IGARSS '03. Proceedings. 2003 IEEE International Geoscience and Remote Sensing Symposium. 21-25 July 2003. - Vol. 2. - P. 1332-1334. ↑
- C5223.** Vecchia A.D. A model study of leaf curvature effect on microwave vegetation scattering. / Vecchia A.D., Ferrazzoli P., Guerriero L. // 2003. IGARSS '03. Proceedings. 2003 IEEE International Geoscience and Remote Sensing Symposium. 21-25 July 2003. - Vol. 2. - P. 1341-1343. ↑
- C5224.** de Badereau D. Radar remote sensing of forests at low frequencies: a 3D electromagnetic scattering model. / de Badereau D., N'guyen H., Roussel H., Tabbara W. // 2003. IGARSS '03. Proceedings. 2003 IEEE International Geoscience and Remote Sensing Symposium. 21-25 July 2003. - Vol. 2. - P. 1353-1355. ↑
- C5225.** Kyrola E. GOMOS validation. / Kyrola E., Tamminen J., Sofieva V., Hassinen S., Leppelmeier G.W., Bertaux J.L., Hauchecorne A., Dalaudier F., Cot C., d'Andon O.F., Barrot G., Mangin A., Guirlet M., Theodore B., Koopman R., Fraisse R., Fussen D., Vanhellemont F. // 2003. IGARSS '03. Proceedings. 2003 IEEE International Geoscience and Remote Sensing Symposium. 21-25 July 2003. - Vol. 2. - P. 1365-1367. ↑
- C5226.** Hauchecorne A. First scientific results on GOMOS/ENVISAT. / Hauchecorne A., Bertaux J.L., Hembise O., Mangin A., Kyrola E. // 2003. IGARSS '03. Proceedings. 2003 IEEE International Geoscience and Remote Sensing Symposium. 21-25 July 2003. - Vol. 2. - P. 1368-1370. ↑
- C5227.** Bryant N. Automatic co-registration of space-based sensors for precision change detection and analysis. / Bryant N., Zobrist A., Logan T. // 2003. IGARSS '03. Proceedings. 2003 IEEE International Geoscience and Remote Sensing Symposium. 21-25 July 2003. - Vol. 2. - P. 1371-1373. ↑
- C5228.** Roth F. Host medium transformation of the early-time radar response of a buried dielectric target. / Roth F., van Genderen P., Verhaegen M. // 2003. IGARSS '03. Proceedings. 2003 IEEE International Geoscience and Remote Sensing Symposium. 21-25 July 2003. - Vol. 2. - P. 1356-1358. ↑
- C5229.** Mikhnev V. Characterization of shallow underground targets using wideband microwave reflectometry. / Mikhnev V., Maksimovitch Y., Vainikainen P. // 2003. IGARSS '03. Proceedings. 2003 IEEE International Geoscience and Remote Sensing Symposium. 21-25 July 2003. - Vol. 2. - P. 1359-1361. ↑
- C5230.** Bloemenkamp R.F. Imaging of high-frequency full-vectorial GPR data using measured footprints. / Bloemenkamp R.F., Slob E.C. // 2003. IGARSS '03. Proceedings. 2003 IEEE International Geoscience and Remote Sensing Symposium. 21-25 July 2003. - Vol. 2. - P. 1362-1364. ↑
- C5231.** Long D.G. Ultra high resolution wind retrieval for SeaWinds. / Long D.G., Luke J.B., Plant W. // 2003. IGARSS '03. Proceedings. 2003 IEEE International Geoscience and Remote Sensing Symposium. 21-25 July 2003. - Vol. 2. - P. 1264-1266. ↑
- C5232.** Arakelyan A.K. Radar methods for atmospheric stratification condition unambiguous determination by synergy data of sea surface altimetric and scatterometric observations. / Arakelyan A.K., Hambaryan A.K. // 2003. IGARSS '03. Proceedings. 2003 IEEE International Geoscience and Remote Sensing Symposium. 21-25 July 2003. - Vol. 2. - P. 1267-1269. ↑

- C5233.** Wackerman C. Operational estimation of coastal wind vectors from RADARSAT SAR imagery. / Wackerman C., Horstmann J., Koch W. // 2003. IGARSS '03. Proceedings. 2003 IEEE International Geoscience and Remote Sensing Symposium. 21-25 July 2003. - Vol. 2. - P. 1270-1272. ↑
- C5234.** Adams I.S. Combined active/passive hurricane wind retrieval algorithm for the Seawinds scatterometer. / Adams I.S., Jones W.L., Jun Dong Park, Kasparis T. // 2003. IGARSS '03. Proceedings. 2003 IEEE International Geoscience and Remote Sensing Symposium. 21-25 July 2003. - Vol. 2. - P. 1253-1256. ↑
- C5235.** Soisuvann S. Combined active and passive microwave sensing of ocean surface wind vector from TRMM. / Soisuvann S., Jones W.L., Kasparis T. // 2003. IGARSS '03. Proceedings. 2003 IEEE International Geoscience and Remote Sensing Symposium. 21-25 July 2003. - Vol. 2. - P. 1257-1260. ↑
- C5236.** Dankert H. Ocean winds retrieved from X-band radar-image sequences. / Dankert H., Horstmann J., Magnusson A.-K., Rosenthal W. // 2003. IGARSS '03. Proceedings. 2003 IEEE International Geoscience and Remote Sensing Symposium. 21-25 July 2003. - Vol. 2. - P. 1261-1263. ↑
- C5237.** Pandolfi M. Systematic tropospheric aerosol lidar measurements over Potenza in the frame of EARLINET. / Pandolfi M., Amodeo A., Mona L., Pappalardo G. // 2003. IGARSS '03. Proceedings. 2003 IEEE International Geoscience and Remote Sensing Symposium. 21-25 July 2003. - Vol. 2. - P. 1282-1284. ↑
- C5238.** Romeiser R. On the suitability of TerraSAR-X split antenna mode for current measurements by along-track interferometry. / Romeiser R., Breit H., Eineder M., Runge H., Flament P., De Jong K., Vogelzang J. // 2003. IGARSS '03. Proceedings. 2003 IEEE International Geoscience and Remote Sensing Symposium. 21-25 July 2003. - Vol. 2. - P. 1320-1322. ↑
- C5239.** Boerner E. Evaluation of TerraSAR-X Spotlight processing accuracy based on a new Spotlight raw data simulator. / Boerner E., Lord R., Mittermayer J., Bamler R. // 2003. IGARSS '03. Proceedings. 2003 IEEE International Geoscience and Remote Sensing Symposium. 21-25 July 2003. - Vol. 2. - P. 1323-1325. ↑
- C5240.** Stephens G.L. The CloudSat Mission. / Stephens G.L., Vane D.G. // 2003. IGARSS '03. Proceedings. 2003 IEEE International Geoscience and Remote Sensing Symposium. 21-25 July 2003. - Vol. 2. - P. 1326-1328. ↑
- C5241.** De Abreu R. Operational sea ice monitoring with RADARSAT-2-a glimpse into the future. / De Abreu R., Flett D., Scheuchl B., Ramsay B. // 2003. IGARSS '03. Proceedings. 2003 IEEE International Geoscience and Remote Sensing Symposium. 21-25 July 2003. - Vol. 2. - P. 1308-1310. ↑
- C5242.** Lukowski T.I. Synthetic Aperture Radar for Search and Rescue: studies at natural resources Canada-update. / Lukowski T.I., Bing Yue. // 2003. IGARSS '03. Proceedings. 2003 IEEE International Geoscience and Remote Sensing Symposium. 21-25 July 2003. - Vol. 2. - P. 1311-1313. ↑
- C5243.** Shen Chiu. Clutter effects on ground moving target velocity estimation with SAR along-track interferometry. 2003. IGARSS '03. Proceedings. 2003 IEEE International Geoscience and Remote Sensing Symposium. 21-25 July 2003. - Vol. 2. - P. 1314-1319. ↑
- C5244.** Dubois-Fernandez P. Using Pol-InSAR at X-band: preliminary observations. / Dubois-Fernandez P., Dupuis X., Garestier F., Paillou P. // 2003. IGARSS '03. Proceedings. 2003 IEEE International Geoscience and Remote Sensing Symposium. 21-25 July 2003. - Vol. 3. - P. 1435-1437. ↑
- C5245.** Ender J.H.G. Signal theoretical aspects of bistatic SAR. 2003. IGARSS '03. Proceedings. 2003 IEEE International Geoscience and Remote Sensing Symposium. 21-25 July 2003. - Vol. 3. - P. 1438-1441. ↑
- C5246.** Homer J. Non-cooperative bistatic SAR imaging system: spatial resolution analysis. / Homer J., Mojarrabi B., Palmer J., Kubik K., Donskoi E. // 2003. IGARSS '03. Proceedings. 2003 IEEE International Geoscience and Remote Sensing Symposium. 21-25 July 2003. - Vol. 3. - P. 1446-1448. ↑
- C5247.** Yamada H. Forest height feature extraction in polarimetric SAR interferometry by using rotational invariance property. / Yamada H., Yamaguchi Y., Boerner W.M. // 2003. IGARSS '03. Proceedings. 2003 IEEE International Geoscience and Remote Sensing Symposium. 21-25 July 2003. - Vol. 3. - P. 1426-1428. ↑
- C5248.** Papathanassiou K.P. The effect of temporal decorrelation on the inversion of forest parameters from Pol-InSAR data. / Papathanassiou K.P., Cloude S.R. // 2003. IGARSS '03. Proceedings. 2003 IEEE International

Geoscience and Remote Sensing Symposium. 21-25 July 2003. - Vol. 3. - P. 1429-1431. ↑

C5249. Dall J. Polarimetric SAR interferometry applied to land ice: first results. / Dall J., Papathanassiou K.P., Skriver H. // 2003. IGARSS '03. Proceedings. 2003 IEEE International Geoscience and Remote Sensing Symposium. 21-25 July 2003. - Vol. 3. - P. 1432-1434. ↑

C5250. Moccia A. Oceanographic applications of spaceborne bistatic SAR. / Moccia A., Rufino G., De Luca M. // 2003. IGARSS '03. Proceedings. 2003 IEEE International Geoscience and Remote Sensing Symposium. 21-25 July 2003. - Vol. 3. - P. 1452-1454. ↑

C5251. Lucas R.M. Remote sensing to support Australia's commitment to international agreements: a role for synthetic aperture radar. / Lucas R.M., Lee A., Milne A.K., Cronin N., Moghaddam M. // 2003. IGARSS '03. Proceedings. 2003 IEEE International Geoscience and Remote Sensing Symposium. 21-25 July 2003. - Vol. 3. - P. 1477-1479. ↑

C5252. Wessels J. Operational wetlands monitoring for the Ramsar convention: TESEO powers a breakthrough. / Wessels J., Ball D., Prieto D.F., Ahern F. // 2003. IGARSS '03. Proceedings. 2003 IEEE International Geoscience and Remote Sensing Symposium. 21-25 July 2003. - Vol. 3. - P. 1486-1489. ↑

C5253. Holecz F. Desertification-a land degradation support service. / Holecz F., Heimo C., Moreno J., Goussard J., Fernandez D., Rubio J.L., Chen Erxue, Magsar E., Lo M., Chemini A., Stoessel F., Rosenqvist A. // 2003. IGARSS '03. Proceedings. 2003 IEEE International Geoscience and Remote Sensing Symposium. 21-25 July 2003. - Vol. 3. - P. 1490-1492. ↑

C5254. Cumming I.G. Interpretations of the omega-K algorithm and comparisons with other algorithms. / Cumming I.G., Neo Y.L., Wong F.H. // 2003. IGARSS '03. Proceedings. 2003 IEEE International Geoscience and Remote Sensing Symposium. 21-25 July 2003. - Vol. 3. - P. 1455-1458. ↑

C5255. Massonnet D. Radar processing and geometric specificity of bistatic data. / Massonnet D., Souyris J., Gaudin J. // 2003. IGARSS '03. Proceedings. 2003 IEEE International Geoscience and Remote Sensing Symposium. 21-25 July 2003. - Vol. 3. - P. 1459-1461. ↑

C5256. Reigber A. Wavenumber domain SAR focusing with integrated motion compensation. / Reigber A., Potsis A., Alivizatos E., Uzunoglu N., Moreira A. // 2003. IGARSS '03. Proceedings. 2003 IEEE International Geoscience and Remote Sensing Symposium. 21-25 July 2003. - Vol. 3. - P. 1465-1467. ↑

C5257. Low A. Mesoscale soil moisture estimation from SAR data using subscale landuse information. / Low A., Ludwig R., Mauser W. // 2003. IGARSS '03. Proceedings. 2003 IEEE International Geoscience and Remote Sensing Symposium. 21-25 July 2003. - Vol. 2. - P. 1396-1398. ↑

C5258. Zribi M. Surface soil moisture estimation using active microwave ERS wind scatterometer and SAR data. / Zribi M., Le Hegarat-Masclé S., Ottele C., Kammoun B., Guerin C. // 2003. IGARSS '03. Proceedings. 2003 IEEE International Geoscience and Remote Sensing Symposium. 21-25 July 2003. - Vol. 2. - P. 1399-1401. ↑

C5259. Yunjin Kim. A soil moisture algorithm using tilted Bragg approximation. / Yunjin Kim, van Zyl J., Jiancheng Shi. // 2003. IGARSS '03. Proceedings. 2003 IEEE International Geoscience and Remote Sensing Symposium. 21-25 July 2003. - Vol. 2. - P. 1402-1404. ↑

C5260. Chibani Y. Multisource image fusion by using the redundant wavelet decomposition. 2003. IGARSS '03. Proceedings. 2003 IEEE International Geoscience and Remote Sensing Symposium. 21-25 July 2003. - Vol. 2. - P. 1383-1385. ↑

C5261. Bujor F.T. Application of log-cumulants to change detection on multi-temporal SAR images. / Bujor F.T., Nicolas J.-M., Trouve E., Rudant J.-P. // 2003. IGARSS '03. Proceedings. 2003 IEEE International Geoscience and Remote Sensing Symposium. 21-25 July 2003. - Vol. 2. - P. 1386-1388. ↑

C5262. Schneider R.Z. Entropy among a sequence of SAR images for change detection. / Schneider R.Z., Fernandes D. // 2003. IGARSS '03. Proceedings. 2003 IEEE International Geoscience and Remote Sensing Symposium. 21-25 July 2003. - Vol. 2. - P. 1389-1391. ↑

C5263. Khadhra K.B. Analysis of multi-frequency polarimetric data for assessment of bare soil roughness. /

Khadhra K.B., Singh D., Boerner T., Hounam D., Wiesbeck W. // 2003. IGARSS '03. Proceedings. 2003 IEEE International Geoscience and Remote Sensing Symposium. 21-25 July 2003. - Vol. 2. - P. 1405-1407. ↑

C5264. Allain S. Surface parameter retrieval from polarimetric and multi-frequency SAR data. / Allain S., Ferro-Famil L., Pottier E. // 2003. IGARSS '03. Proceedings. 2003 IEEE International Geoscience and Remote Sensing Symposium. 21-25 July 2003. - Vol. 2. - P. 1417-1419. ↑

C5265. Yang Hu. Temporal and spatial soil moisture change pattern detection using multi-temporal Radarsat SCANSAR images. / Yang Hu, Jiancheng Shi, Li Zhen, Huadong Guo, Zhongjun Zhang. // 2003. IGARSS '03. Proceedings. 2003 IEEE International Geoscience and Remote Sensing Symposium. 21-25 July 2003. - Vol. 2. - P. 1420-1422. ↑

C5266. Cloude S.R. A coherent EM scattering model for dual baseline POLInSAR. / Cloude S.R., Williams M.L. // 2003. IGARSS '03. Proceedings. 2003 IEEE International Geoscience and Remote Sensing Symposium. 21-25 July 2003. - Vol. 3. - P. 1423-1425. ↑

C5267. Louis J. Surface roughness characterization for SAR applications. / Louis J., Floury N., Davidson M., Attema E., Borgeaud M. // 2003. IGARSS '03. Proceedings. 2003 IEEE International Geoscience and Remote Sensing Symposium. 21-25 July 2003. - Vol. 2. - P. 1408-1410. ↑

C5268. Satalino G. Model-based methods for soil moisture estimations from SAR data. / Satalino G., Pasquariello G., Mattia F. // 2003. IGARSS '03. Proceedings. 2003 IEEE International Geoscience and Remote Sensing Symposium. 21-25 July 2003. - Vol. 2. - P. 1411-1413. ↑

C5269. Chanzy A. Influence of surface roughness frequency components of radar backscattering: consequences on roughness sampling. / Chanzy A., Molineaux B., Zribi M. // 2003. IGARSS '03. Proceedings. 2003 IEEE International Geoscience and Remote Sensing Symposium. 21-25 July 2003. - Vol. 2. - P. 1414-1416. ↑

C5270. Raney R.K. Abyss-Lite: improved bathymetry from a dedicated small satellite delay-Doppler radar altimeter. / Raney R.K., Smith W.H.F., Sandwell D.T., Jensen J.R., Porter D.L., Reynolds E. // 2003. IGARSS '03. Proceedings. 2003 IEEE International Geoscience and Remote Sensing Symposium. 21-25 July 2003. - Vol. 2. - P. 1083-1085. ↑

C5271. Phalippou L. Future radar altimeter concepts for ocean applications. / Phalippou L., Cotton D., Guijarro J., Menard Y., Vincent P. // 2003. IGARSS '03. Proceedings. 2003 IEEE International Geoscience and Remote Sensing Symposium. 21-25 July 2003. - Vol. 2. - P. 1086-1088. ↑

C5272. Caubet E. Phase B and breadboard results of the Ka-band altimeter for future microsatellite altimetry missions. / Caubet E., Steunou N., Meerman M., Thouvenot E., Vincent P. // 2003. IGARSS '03. Proceedings. 2003 IEEE International Geoscience and Remote Sensing Symposium. 21-25 July 2003. - Vol. 2. - P. 1089-1091. ↑

C5273. Martinez-Benjamin J.J. JASON-1 calibration campaign at the Ibiza island area. / Martinez-Benjamin J.J., Martinez-Garcia M., Nunez Andres A., Oritz Castellon M.A., Talaya J., Martin Davila J., Garate J., Ferrandiz J.M., Vigo-Aguiar M.I., Perez B., Alvarez E., Sevilla M., Rodriguez G. // 2003. IGARSS '03. Proceedings. 2003 IEEE International Geoscience and Remote Sensing Symposium. 21-25 July 2003. - Vol. 2. - P. 1071-1073. ↑

C5274. Tran N. Comparison of microwave radiometer brightness temperature over a hot reference area. / Tran N., Obligis E., Eymard L., Ruf C. // 2003. IGARSS '03. Proceedings. 2003 IEEE International Geoscience and Remote Sensing Symposium. 21-25 July 2003. - Vol. 2. - P. 1074-1076. ↑

C5275. Guijarro J. Innovative radar altimeter concepts. / Guijarro J., Santoleri R., Nardelli B.B., Borgarelli L., Croci R., Venturini R., Alberti G. // 2003. IGARSS '03. Proceedings. 2003 IEEE International Geoscience and Remote Sensing Symposium. 21-25 July 2003. - Vol. 2. - P. 1080-1082. ↑

C5276. Tianhe Chi. Application of GPS in airborne SAR image based disaster evaluation. / Tianhe Chi, Xin Zhang, Caiying Zhu, Yumin Tan. // 2003. IGARSS '03. Proceedings. 2003 IEEE International Geoscience and Remote Sensing Symposium. 21-25 July 2003. - Vol. 2. - P. 1092-1093. ↑

C5277. Hawkins R.K. ASAR AP mode performance and applications potential. / Hawkins R.K., Touzi R., Wolfe J., Meadows P.J., Pasquali P., Flett D. // 2003. IGARSS '03. Proceedings. 2003 IEEE International Geoscience

and Remote Sensing Symposium. 21-25 July 2003. - Vol. 2. - P. 1115-1117. ↑

C5278. Closa J. The ASAR wide swath mode products. / Closa J., Rosich B., Monti-Guarnieri A. // 2003. IGARSS '03. Proceedings. 2003 IEEE International Geoscience and Remote Sensing Symposium. 21-25 July 2003. - Vol. 2. - P. 1118-1120. ↑

C5279. Small D. Geometric performance of ENVISAT ASAR products. / Small D., Holzner J., Raggam H., Kosmann D., Schubert A. // 2003. IGARSS '03. Proceedings. 2003 IEEE International Geoscience and Remote Sensing Symposium. 21-25 July 2003. - Vol. 2. - P. 1121-1123. ↑

C5280. Mironov V.L. Soil dielectric spectroscopic parameters dependence on humus content. / Mironov V.L., Bobrov P.P. // 2003. IGARSS '03. Proceedings. 2003 IEEE International Geoscience and Remote Sensing Symposium. 21-25 July 2003. - Vol. 2. - P. 1106-1108. ↑

C5281. Rosich B. ASAR instrument performance and product quality status. / Rosich B., Zink M., Torres R., Closa J., Buck C. // 2003. IGARSS '03. Proceedings. 2003 IEEE International Geoscience and Remote Sensing Symposium. 21-25 July 2003. - Vol. 2. - P. 1109-1111. ↑

C5282. Meadows P.J. ASAR image mode product quality. / Meadows P.J., Wright P.A. // 2003. IGARSS '03. Proceedings. 2003 IEEE International Geoscience and Remote Sensing Symposium. 21-25 July 2003. - Vol. 2. - P. 1112-1114. ↑

C5283. Crout R.L. Current navy applications of satellite remotely sensed data. / Crout R.L., Kent C. // 2003. IGARSS '03. Proceedings. 2003 IEEE International Geoscience and Remote Sensing Symposium. 21-25 July 2003. - Vol. 2. - P. 1026-1028. ↑

C5284. Cooley T. Terrain categorization using a background spectral library. / Cooley T., Cipar J., Lockwood R. // 2003. IGARSS '03. Proceedings. 2003 IEEE International Geoscience and Remote Sensing Symposium. 21-25 July 2003. - Vol. 2. - P. 1029-1031. ↑

C5285. Gierull C.H. Raw data based two-aperture SAR ground moving target indication. / Gierull C.H., Sikaneta I.C. // 2003. IGARSS '03. Proceedings. 2003 IEEE International Geoscience and Remote Sensing Symposium. 21-25 July 2003. - Vol. 2. - P. 1032-1034. ↑

C5286. Ranson K.J. Multi-sensor approach for assessing the taiga-tundra boundary. / Ranson K.J., Sun G., Kharuk V.I., Kovacs K. // 2003. IGARSS '03. Proceedings. 2003 IEEE International Geoscience and Remote Sensing Symposium. 21-25 July 2003. - Vol. 2. - P. 969-971. ↑

C5287. Beaulne P.D. Preliminary design of a SAR-GMTI processing system for RADARSAT-2 MODEX data. / Beaulne P.D., Gierull C.H., Livinstone C.E., Sikaneta I.C., Chiu S., Gong S., Quinton M. // 2003. IGARSS '03. Proceedings. 2003 IEEE International Geoscience and Remote Sensing Symposium. 21-25 July 2003. - Vol. 2. - P. 1019-1021. ↑

C5288. Hornstein J. 3D global ozone proxy fields and the NPOESS OMPS assimilation experiment, for improved numerical weather predictions for military operations. / Hornstein J., Allen D., Randall C., Mango S. // 2003. IGARSS '03. Proceedings. 2003 IEEE International Geoscience and Remote Sensing Symposium. 21-25 July 2003. - Vol. 2. - P. 1022-1025. ↑

C5289. Eugenio F. Automatic structures detection and spatial registration using multisensor satellite imagery. / Eugenio F., Rovaris E., Marcello J., Marques F. // 2003. IGARSS '03. Proceedings. 2003 IEEE International Geoscience and Remote Sensing Symposium. 21-25 July 2003. - Vol. 2. - P. 1038-1040. ↑

C5290. Gao Xin. The analysis and application of spline interpolation for multisensor and multiresolution image registration. / Gao Xin, Wang Chao, Zhang Weiguo, Wu Ji, Liu Hao. // 2003. IGARSS '03. Proceedings. 2003 IEEE International Geoscience and Remote Sensing Symposium. 21-25 July 2003. - Vol. 2. - P. 1056-1058. ↑

C5291. Hinz S. A fusion strategy for extraction of urban road nets from multiple images. 2003. IGARSS '03. Proceedings. 2003 IEEE International Geoscience and Remote Sensing Symposium. 21-25 July 2003. - Vol. 2. - P. 1059-1061. ↑

C5292. Jimenez-Munoz J.C. Synergistic use of DAIS bands to retrieve land surface emissivity and temperature. / Jimenez-Munoz J.C., Sobrino J.A., El-Kharraz J., Gomez M., Romaguera M., Soria G. // 2003.

IGARSS '03. Proceedings. 2003 IEEE International Geoscience and Remote Sensing Symposium. 21-25 July 2003. - Vol. 2. - P. 1062-1064. ↑

C5293. Toutin T. Multi sensor block adjustment. / Toutin T., Chenier R., Carbonneau Y. // 2003. IGARSS '03. Proceedings. 2003 IEEE International Geoscience and Remote Sensing Symposium. 21-25 July 2003. - Vol. 2. - P. 1041-1043. ↑

C5294. Pellizzeri T.M. Multisource urban classification: joint processing of optical and SAR data for land cover mapping. / Pellizzeri T.M., Lombardo P., Gamba P., dell'Acqua F. // 2003. IGARSS '03. Proceedings. 2003 IEEE International Geoscience and Remote Sensing Symposium. 21-25 July 2003. - Vol. 2. - P. 1044-1046. ↑

C5295. Storvik G. Parameter estimation and classification of multiscale remote sensing data. / Storvik G., Fjotoft R., Solberg A.H.S. // 2003. IGARSS '03. Proceedings. 2003 IEEE International Geoscience and Remote Sensing Symposium. 21-25 July 2003. - Vol. 2. - P. 1047-1049. ↑

C5296. Holzner J. Analysis of interferometric signals based on coherence and power spectral density. 2003. IGARSS '03. Proceedings. 2003 IEEE International Geoscience and Remote Sensing Symposium. 21-25 July 2003. - Vol. 2. - P. 1196-1198. ↑

C5297. Fornaro G. Monitoring areal deformation via multipass SAR differential interferometry. / Fornaro G., Lanari R., Sansosti E., Serafino F., Usai S. // 2003. IGARSS '03. Proceedings. 2003 IEEE International Geoscience and Remote Sensing Symposium. 21-25 July 2003. - Vol. 2. - P. 1199-1201. ↑

C5298. Hanssen R. Resolving the acquisition ambiguity for atmospheric monitoring in multi-pass radar interferometry. / Hanssen R., Moiseev D., Businger S. // 2003. IGARSS '03. Proceedings. 2003 IEEE International Geoscience and Remote Sensing Symposium. 21-25 July 2003. - Vol. 2. - P. 1202-1205. ↑

C5299. Breit H. Traffic monitoring using SRTM along-track interferometry. / Breit H., Eineder M., Holzner J., Runge H., Bamler R. // 2003. IGARSS '03. Proceedings. 2003 IEEE International Geoscience and Remote Sensing Symposium. 21-25 July 2003. - Vol. 2. - P. 1187-1189. ↑

C5300. Scheiber R. A three-step phase correction approach for airborne repeat-pass interferometric SAR data. 2003. IGARSS '03. Proceedings. 2003 IEEE International Geoscience and Remote Sensing Symposium. 21-25 July 2003. - Vol. 2. - P. 1190-1192. ↑

C5301. Colesanti C. Permanent Scatterers: precision assessment and multi-platform analysis. / Colesanti C., Ferretti A., Locatelli R., Novali F., Savio G. // 2003. IGARSS '03. Proceedings. 2003 IEEE International Geoscience and Remote Sensing Symposium. 21-25 July 2003. - Vol. 2. - P. 1193-1195. ↑

C5302. Lombardini F. Differential tomography: a new framework for SAR interferometry. 2003. IGARSS '03. Proceedings. 2003 IEEE International Geoscience and Remote Sensing Symposium. 21-25 July 2003. - Vol. 2. - P. 1206-1208. ↑

C5303. Tanner A.B. Development of a high stability L-band radiometer for ocean salinity measurements. / Tanner A.B., Wilson W.J., Pellerano F.A. // 2003. IGARSS '03. Proceedings. 2003 IEEE International Geoscience and Remote Sensing Symposium. 21-25 July 2003. - Vol. 2. - P. 1238-1240. ↑

C5304. Fernandez D.E. Hurricane wind and rain measurements using a dual polarized C/Ku-band airborne radar profiler. / Fernandez D.E., Xuehu Zhang, Carswell J., McLaughlin D., Chang P., Connor L., Black P.G., Marks F.D. // 2003. IGARSS '03. Proceedings. 2003 IEEE International Geoscience and Remote Sensing Symposium. 21-25 July 2003. - Vol. 2. - P. 1247-1248. ↑

C5305. Yueh S.H. QuikSCAT wind retrievals for tropical cyclones. / Yueh S.H., Stiles B., Liu W.T. // 2003. IGARSS '03. Proceedings. 2003 IEEE International Geoscience and Remote Sensing Symposium. 21-25 July 2003. - Vol. 2. - P. 1250-1252. ↑

C5306. Skou N. Aspects of the SMOS pre-launch calibration. 2003. IGARSS '03. Proceedings. 2003 IEEE International Geoscience and Remote Sensing Symposium. 21-25 July 2003. - Vol. 2. - P. 1222-1225. ↑

C5307. Rautiainen K. Development of airborne aperture synthetic radiometer (HUT-2D). / Rautiainen K., Butora R., Auer T., Kettunen J., Kainulainen J., Mononen I., Beltrami D., Hallikainen. // 2003. IGARSS '03. Proceedings. 2003 IEEE International Geoscience and Remote Sensing Symposium. 21-25 July 2003. - Vol. 2. -

P. 1232-1234. ↑

C5308. England A.W. Performance of STAR-Light receivers during CLPX. / England A.W., Pham H., De Roo R., van Nieuwstadt L., Yam L. // 2003. IGARSS '03. Proceedings. 2003 IEEE International Geoscience and Remote Sensing Symposium. 21-25 July 2003. - Vol. 2. - P. 1235-1237. ↑

C5309. Arnaud A. ASAR ERS interferometric phase continuity. / Arnaud A., Adam N., Hanssen R., Inglada J., Duro J., Closa J., Eineder M. // 2003. IGARSS '03. Proceedings. 2003 IEEE International Geoscience and Remote Sensing Symposium. 21-25 July 2003. - Vol. 2. - P. 1133-1135. ↑

C5310. Henry J.B. ENVISAT multipolarised ASAR data for flood mapping. / Henry J.B., Chastanet P., Fellah K., Desnos Y.L. // 2003. IGARSS '03. Proceedings. 2003 IEEE International Geoscience and Remote Sensing Symposium. 21-25 July 2003. - Vol. 2. - P. 1136-1138. ↑

C5311. Rosenkranz P.W. Cloud liquid water retrievals from aqua AMSU/HSB. 2003. IGARSS '03. Proceedings. 2003 IEEE International Geoscience and Remote Sensing Symposium. 21-25 July 2003. - Vol. 2. - P. 1142-1144. ↑

C5312. Monti Guarnieri A. ENVISAT ASAR scanSAR interferometry. / Monti Guarnieri A., Caffirio C., Guccione P., Pasquali P., Desnos Y.L. // 2003. IGARSS '03. Proceedings. 2003 IEEE International Geoscience and Remote Sensing Symposium. 21-25 July 2003. - Vol. 2. - P. 1124-1126. ↑

C5313. Johnsen H. Validation of ASAR wave mode level 2 product. / Johnsen H., Engen G., Chapron B. // 2003. IGARSS '03. Proceedings. 2003 IEEE International Geoscience and Remote Sensing Symposium. 21-25 July 2003. - Vol. 2. - P. 1127-1129. ↑

C5314. Colesanti C. ERS-ENVISAT permanent scatterers interferometry. / Colesanti C., Ferretti A., Prati C., Perissin D., Rocca F. // 2003. IGARSS '03. Proceedings. 2003 IEEE International Geoscience and Remote Sensing Symposium. 21-25 July 2003. - Vol. 2. - P. 1130-1132. ↑

C5315. Weissman D.E. Calibrating the quickSCAT/SeaWinds radar for measuring rainrate over the oceans and improving wind vector estimates. / Weissman D.E., Bourassa M.A., Durden S.L. // 2003. IGARSS '03. Proceedings. 2003 IEEE International Geoscience and Remote Sensing Symposium. 21-25 July 2003. - Vol. 2. - P. 1145-1147. ↑

C5316. Vijayan L. Campaign mode observation of tropical convection using ground-based radar systems. / Vijayan L., Viswanathan G., Ranga Rao R., Jain A.R., Narayana Rao D., Anandan V.K., Rajesh Rao P., Kalyana Sundaram S., Suresh R., Thampi S.B. // 2003. IGARSS '03. Proceedings. 2003 IEEE International Geoscience and Remote Sensing Symposium. 21-25 July 2003. - Vol. 2. - P. 1157-1159. ↑

C5317. Vulpiani G. Sensitivity analysis of self-consistent polarimetric rain retrieval to C-Band radar observables. / Vulpiani G., Picciotti E., Ferrauto G., Marzano F.S. // 2003. IGARSS '03. Proceedings. 2003 IEEE International Geoscience and Remote Sensing Symposium. 21-25 July 2003. - Vol. 2. - P. 1160-1162. ↑

C5318. Berardino P. A two-scale differential SAR interferometry approach for investigating earth surface deformations. / Berardino P., Fornaro G., Lanari R., Manunta M., Manzo M., Pepe A., Sansosti E. // 2003. IGARSS '03. Proceedings. 2003 IEEE International Geoscience and Remote Sensing Symposium. 21-25 July 2003. - Vol. 2. - P. 1184-1186. ↑

C5319. Tokay A. An overview of the Keys area precipitation project (KAPP). / Tokay A., Wolff D.B., Fisher B., Jianxin Wang, Marks D., Silberstein D., Bashor P., Augustine D., Makofski D., Pippitt J., Kelley B., Shupp L. // 2003. IGARSS '03. Proceedings. 2003 IEEE International Geoscience and Remote Sensing Symposium. 21-25 July 2003. - Vol. 2. - P. 1148-1150. ↑

C5320. Marzano F.S. Multivariate probability matching of satellite infrared and microwave radiometric measurements for rainfall retrieval at the geostationary scale. / Marzano F.S., Palmacci M., Cimini D., Giuliani G., Tapiador F., Turk J.F. // 2003. IGARSS '03. Proceedings. 2003 IEEE International Geoscience and Remote Sensing Symposium. 21-25 July 2003. - Vol. 2. - P. 1151-1153. ↑

C5321. Capsoni C. Radar estimate of attenuation at K band in stratiform rain using a physical model of the melting layer. / Capsoni C., Caboni V., D'Amico M., Zanardi M. // 2003. IGARSS '03. Proceedings. 2003 IEEE International Geoscience and Remote Sensing Symposium. 21-25 July 2003. - Vol. 2. - P. 1154-1156. ↑

- C5322.** Overton J. NPOESS Field Terminal Segment. 2003. IGARSS '03. Proceedings. 2003 IEEE International Geoscience and Remote Sensing Symposium. 21-25 July 2003. - Vol. 1. - P. 363-365. ↑
- C5323.** Vadlamani A. Improving the detection capability of spatial failure modes using downward-looking sensors in terrain database integrity monitors. / Vadlamani A., de Haag M.U. // 2003. DASC '03. The 22nd Digital Avionics Systems Conference. 12-16 Oct. 2003. - Vol. 2. - P. 9.C.5-91-12. ↑
- C5324.** Boric-Lubecke O. Wireless IC Doppler radars for sensing of heart and respiration activity. / Boric-Lubecke O., Droitcour A.D., Lubecke V.M., Jenshan Lin, Kovacs G.T.A. // 2003. TELSIKS 2003. 6th International Conference on Telecommunications in Modern Satellite, Cable and Broadcasting Service. 1-3 Oct. 2003. - Vol. 1. - P. 337-344. ↑
- C5325.** Suksmono A.B. Recursive transform-based phase unwrapping. / Suksmono A.B., Hirose A. // 2003. ICIP 2003. Proceedings. 2003 International Conference on Image Processing. 14-17 Sept. 2003. - Vol. 3. - P. III-145-8. ↑
- C5326.** Shkvarko Y.V. Modeling and simulation of the fused Bayesian-regularization method for remote sensing imagery with synthetic aperture arrays. / Shkvarko Y.V., Leyva-Montiel J.L., Acosta-Salas J. // 2003. 4th International Conference on Antenna Theory and Techniques. 9-12 Sept. 2003. - Vol. 1. - P. 97-100. ↑
- C5327.** Lukin K.A. Synthetic aperture antenna for near field applications. / Lukin K.A., Natarov M.P., Skresanov V.N. // 2003. 4th International Conference on Antenna Theory and Techniques. 9-12 Sept. 2003. - Vol. 1. - P. 290-293. ↑
- C5328.** Bangolae S.L. Performance evaluation of a memory-based TCP-friendly rate adaptation algorithm for a real-time radar application. / Bangolae S.L., Jayasumana A.P., Chandrasekar V. // 2003. LCN '03. Proceedings. 28th Annual IEEE International Conference on Local Computer Networks. 20-24 Oct. 2003. - P. 319-322. ↑
- C5329.** Ruhe M. Air- and space borne remote sensing systems for traffic data collection -European contributions. / Ruhe M., Dalaff C., Kuhne R., Woessler R. // 2003. Proceedings. 2003 IEEE Intelligent Transportation Systems. 12-15 Oct. 2003. - Vol. 1. - P. 750-752. ↑
- C5330.** Barnes N.P. Role of nonlinear optics in NASA remote sensing program. 2003. LEOS 2003. The 16th Annual Meeting of the IEEE Lasers and Electro-Optics Society. 27-28 Oct. 2003. - Vol. 2. - P. 937-938. ↑
- C5331.** Goryshnya Y.V. Modelling of remote sensing characteristics of salt wet soils in decimeter wavelength range. 2003. CriMiCo 2003. 13th International Crimean Conference Microwave and Telecommunication Technology. 8-12 Sept. 2003. - P. 723-725. ↑
- C5332.** Pengwei Hao. Co-histogram and its application in remote sensing image compression evaluation. / Pengwei Hao, Qingyun Shi, Ying Chen. // 2003. ICIP 2003. Proceedings. 2003 International Conference on Image Processing. 14-17 Sept. 2003. - Vol. 3. - P. III-177-80. ↑
- C5333.** Lacoste C. Road network extraction in remote sensing by a Markov object process. / Lacoste C., Descombes X., Zerubia J. // 2003. ICIP 2003. Proceedings. 2003 International Conference on Image Processing. 14-17 Sept. 2003. - Vol. 3. - P. III-1017-20. ↑
- C5334.** Tsymbal O.V. Removal of impulse bursts in satellite images. / Tsymbal O.V., Lukin V.V., Koivisto P.T., Melnik V.P. // 2003. Proceedings of the Second IEEE International Workshop on Intelligent Data Acquisition and Advanced Computing Systems: Technology and Applications. - Lviv, 8-10 Sept. 2003. - P. 324-329. ↑
- C5335.** Yanovsky F.J. Remote sensing of troposphere for aviation safety: antenna aspect. 2003. 4th International Conference on Antenna Theory and Techniques. 9-12 Sept. 2003. - Vol. 1. - P. 71-76. ↑
- C5336.** Simpson J.J. Global three-dimensional FDTD modeling of impulsive ELF propagation about the Earth. / Simpson J.J., Taflove A. // 2003. IEEE Antennas and Propagation Society International Symposium. 22-27 June 2003. - Vol. 4. - P. 940-943. ↑
- C5337.** Mitra V. Neural network for LIDAR detection of fish. / Mitra V., Chia-Jiu Wang, Edwards G. // 2003. Proceedings of the International Joint Conference on Neural Networks. 20-24 July 2003. - Vol. 2. - P. 1001-1006. ↑

- C5338.** Xin XU. Multiscale SAR image segmentation using a double Markov random field model. / Xin XU, Deren LI, Hong Sun. // 2003. Proceedings. Seventh International Symposium on Signal Processing and Its Applications. 1-4 July 2003. - Vol. 1. - P. 349-352. ↑
- C5339.** Weydahl D.J. Comparing RADARSAT-1 and IKONOS satellite images for urban features detection. / Weydahl D.J., Bretar F., Bjerke P. // 2003. 2nd GRSS/ISPRS Joint Workshop on Remote Sensing and Data Fusion over Urban Areas. 22-23 May 2003. - P. 305-308. ↑
- C5340.** Peters L. Jr. Ground penetrating radar (GPR) studies at the ElectroScience Laboratory (ESL). 2003. IEEE Antennas and Propagation Society International Symposium. 22-27 June 2003. - Vol. 4. - P. 574-577. ↑
- C5341.** Johnson J.T. Microwave remote sensing research at the ElectroScience laboratory. 2003. IEEE Antennas and Propagation Society International Symposium. 22-27 June 2003. - Vol. 4. - P. 598-601. ↑
- C5342.** Bi Jiantao. Research on the quickly evaluation of flooding disaster based on the parallel geographic image processing system. / Bi Jiantao, Fang jinyun, Chi Tianhe, He Jianbang. // 2003. PDCAT'2003. Proceedings of the Fourth International Conference on Parallel and Distributed Computing, Applications and Technologies. 27-29 Aug. 2003. - P. 817-820. ↑
- C5343.** Morales-Mendoza L.J. Antenna-based processing of the radar data for zone detection in remote sensing imagery. / Morales-Mendoza L.J., Shkvarko Y.V., Leyva-Montiel J.L., Vazquez-Bautista R.F. // 2003. 4th International Conference on Antenna Theory and Techniques. 9-12 Sept. 2003. - Vol. 2. - P. 531-534. ↑
- C5344.** Bondarenko B.F. Remote monitoring of sea surface HFSWR. / Bondarenko B.F., Bondarchuk G.M., Dmitriyeva N.V., Zarudnev I.I., Lupan Y.O., Platonov S.Y., Tymchuk V.V. // 2003. 4th International Conference on Antenna Theory and Techniques. 9-12 Sept. 2003. - Vol. 2. - P. 644-647. ↑
- C5345.** Bobby P.E. Estimation of ocean surface currents beyond the region of overlap of dual-site HF radar. / Bobby P.E., Gill E.W. // 2003. IEEE CCECE 2003. Canadian Conference on Electrical and Computer Engineering. 4-7 May 2003. - Vol. 3. - P. 1909-1912. ↑
- C5346.** Boustani A.E. An optimal wavelet for raw SAR data compression. / Boustani A.E., Brunham K., Kinsner W. // 2003. IEEE CCECE 2003. Canadian Conference on Electrical and Computer Engineering. 4-7 May 2003. - Vol. 3. - P. 2071-2074. ↑
- C5347.** Tianhe Chi. Agent communication based SAR image parallel processing. / Tianhe Chi, Xin Zhang, Hongqiao Wu, Jinyun Fang. // 2003. PDCAT'2003. Proceedings of the Fourth International Conference on Parallel and Distributed Computing, Applications and Technologies. 27-29 Aug. 2003. - P. 532-534. ↑
- C5348.** Bychkov D.M. Vegetation and forestry study by radar remote sensing. / Bychkov D.M., Gavrilenko A.S., Yegorova L.O., Ivanov V.K., Silin O.O., Stadnyk O.M., Yatsevych S.Ye. // 2003. CriMiCo 2003. 13th International Crimean Conference Microwave and Telecommunication Technology. 8-12 Sept. 2003. - P. 750-752. ↑
- C5349.** Kobayashi T. Progress in high-spectral resolution lidars for remote sensing of the environment. 2003. CLEO/Pacific Rim 2003. The 5th Pacific Rim Conference on Lasers and Electro-Optics. 15-19 Dec. 2003. - Vol. 2. - P. 641 vol.2. ↑
- C5350.** Lagrosas N. Automatic correction of optical alignment deterioration of a continuously operated Mie lidar. / Lagrosas N., Takeuchi N., Yoshii Y., Kuze H., Naito S., Okazaki J., Sone A., Kan H. // 2003. CLEO/Pacific Rim 2003. The 5th Pacific Rim Conference on Lasers and Electro-Optics. 15-19 Dec. 2003. - Vol. 2. - P. 728 vol.2. ↑
- C5351.** Chan Bong Park. ACA lidar system for continuous monitoring of aerosols, dust and cloud in troposphere at Suwon, Korea. / Chan Bong Park, Choo Hie Lee. // 2003. CLEO/Pacific Rim 2003. The 5th Pacific Rim Conference on Lasers and Electro-Optics. 15-19 Dec. 2003. - Vol. 2. - P. 729 vol.2. ↑
- C5352.** Su Fulin. An algorithm of bridge detection in remote sensing images based on fractal. / Su Fulin, Wu Zhongmou, Lin Xiaoli. // 2003. Proceedings. 2003 6th International SYmposium on Antennas, Propagation and EM Theory. 28 Oct.-1 Nov. 2003. - P. 600-602. ↑
- C5353.** Su Fulin. An algorithm for remote sensing imaging of moving target with conventional narrow-band

radar. / Su Fulin, Wu Zhongmou, Lin Xiaoli. // 2003. Proceedings. 2003 6th International Symposium on Antennas, Propagation and EM Theory. 28 Oct.-1 Nov. 2003. - P. 603-607. ↑

C5354. Imaki M. Compact long-path absorption laser radar system for measuring greenhouse molecular concentration. / Imaki M., Tada T., Higashikawa T., Hayashi A., Kobayashi T. // 2003. CLEO/Pacific Rim 2003. The 5th Pacific Rim Conference on Lasers and Electro-Optics. 15-19 Dec. 2003. - Vol. 2. - P. 581 vol.2. ↑

C5355. Barber B.C. Ocean imaging using multichannel along track interferometry. 2003. Proceedings of the International Radar Conference. 3-5 Sept. 2003. - P. 251-256. ↑

C5356. Reid I.M. Atmospheric radar for the 0.5-110 km region. 2003. Proceedings of the International Radar Conference. 3-5 Sept. 2003. - P. 264-269. ↑

C5357. Carter D.J.Q. Low-cost realisation of space-borne synthetic aperture radar-MICROSAR (September 2003). / Carter D.J.Q., Hall C.D., Cohen M.A.B., Alderson E.A., Rutten D.C. // 2003. Proceedings of the International Radar Conference. 3-5 Sept. 2003. - P. 327-332. ↑

C5358. Chen V.C. Advanced synthetic aperture radar imaging and feature analysis. / Chen V.C., Lipps R., Bottoms M. // 2003. Proceedings of the International Radar Conference. 3-5 Sept. 2003. - P. 22-29. ↑

C5359. Colesanti C. Multi-image satellite SAR interferometry: state of the art and future trends. / Colesanti C., Ferretti A., Prati C., Rocca F. // 2003. Proceedings of the International Radar Conference. 3-5 Sept. 2003. - P. 239-244. ↑

C5360. Rombach M. Description and applications of the multipolarized dual band OrbiSAR-1 InSAR sensor. / Rombach M., Moreira J. // 2003. Proceedings of the International Radar Conference. 3-5 Sept. 2003. - P. 245-250. ↑

C5361. Su Fulin. An algorithm of road detection in remote sensing images based on B-spline wavelet. / Su Fulin, Wu Zhongmou, Lin Xiaoli. // 2003. Proceedings. 2003 6th International Symposium on Antennas, Propagation and EM Theory. 28 Oct.-1 Nov. 2003. - P. 592-595. ↑

C5362. Skou N. Microwave remote sensing: needs and requirements concerning technology. 2003. 33rd European Microwave Conference. 7-9 Oct. 2003. - Vol. 2. - P. 863-866. ↑

C5363. Gloanec M. Advance MMICs for remote sensing and radar applications. / Gloanec M., Camiade M., Serru V., Ouarch Z., Beilenhoff K. // 2003. 33rd European Microwave Conference. 7-9 Oct. 2003. - Vol. 2. - P. 871-874. ↑

C5364. Johansen T.K. Ultra-wideband MMICs for remote sensing applications. / Johansen T.K., Vidkjaer J., Krozer V. // 2003. 33rd European Microwave Conference. 7-9 Oct. 2003. - Vol. 2. - P. 879-882. ↑

C5365. Ksendzuk A.V. Optimisation transmitter-receiver location in bistatic SAR. 2003. CriMiCo 2003. 13th International Crimean Conference Microwave and Telecommunication Technology. 8-12 Sept. 2003. - P. 763-766. ↑

C5366. Poygina M.I. Research institute "Orion" has more that 40 years experience in the field of microwave and millimeter-wave technology. / Poygina M.I., Pasechnik Z.F., Tsvirko Yu.A., Karushkin N.F., Mal'tsev S.B. // 2003. CriMiCo 2003. 13th International Crimean Conference Microwave and Telecommunication Technology. 8-12 Sept. 2003. - P. 814-820. ↑

C5367. Moreira A. Spaceborne synthetic aperture radar (SAR) systems: state of the art and future developments. / Moreira A., Krieger G. // 2003. 33rd European Microwave Conference. 7-9 Oct. 2003. - Vol. 1. - P. 101-104. ↑


C5368. Gao Huotao. Optimal design of broadband loaded receiving antenna for HFSWR using simulated annealing. / Gao Huotao, Li Jie, Zheng Xia, Wei Zhongwei. // 2003. Proceedings. 2003 6th International Symposium on Antennas, Propagation and EM Theory. 28 Oct.-1 Nov. 2003. - P. 30-33. ↑


C5369. Zhang Min. Low-grazing backscattering efficiency from clustering vegetation. / Zhang Min, Bai Lu, Wu Zhensen, Song Yuexia. // 2003. Proceedings. 2003 6th International Symposium on Antennas, Propagation and EM Theory. 28 Oct.-1 Nov. 2003. - P. 468-471. ↑


- C5370.** Tateiba M. Wave scattering in random media and its application to remote sensing. 2003. Proceedings. 2003 6th International SYmposium on Antennas, Propagation and EM Theory. 28 Oct.-1 Nov. 2003. - P. 588-591. ↑
- C5371.** Yabuki M. Determination of vertical distributions of aerosol optical parameters by use of multiwavelength lidar data. / Yabuki M., Kuze H., Lagrosas N., Takeuchi N., Shiobara M. // 2003. CLEO/Pacific Rim 2003. The 5th Pacific Rim Conference on Lasers and Electro-Optics. 15-19 Dec. 2003. - Vol. 1. - P. 296 Vol.1. ↑
- C5372.** Kobayashi T. Progress in high-spectral resolution lidars for remote sensing of the environment. 2003. CLEO/Pacific Rim 2003. The 5th Pacific Rim Conference on Lasers and Electro-Optics. 15-19 Dec. 2003. - Vol. 1. - P. 339 Vol.1. ↑
- C5373.** {no data available}. ISAPE'03. 2003 6th International Symposium on Antennas, Propagation and EM Theory (IEEE. Cat. No.03EX681). 2003. Proceedings. 2003 6th International SYmposium on Antennas, Propagation and EM Theory. 28 Oct.-1 Nov. 2003. - {no data available}. ↑
- C5374.** Darwish A. Urban land-cover classification: an object based perspective. / Darwish A., Leukert K., Reinhardt W. // 2003. 2nd GRSS/ISPRS Joint Workshop on Remote Sensing and Data Fusion over Urban Areas. 22-23 May 2003. - P. 278-282. ↑
- C5375.** Bangolae S.L. Gigabit networking: digitized radar data transfer and beyond. / Bangolae S.L., Jayasumana A.P., Chandrasekar V. // 2003. ICC '03. IEEE International Conference on Communications. 11-15 May 2003. - Vol. 1. - P. 684-688. ↑
- C5376.** Schleijsen H.M.A. Landmine detection technology research programme at TNO. 2003. Proceedings of the 2nd International Workshop on Advanced Ground Penetrating Radar. 14-16 May 2003. - P. 138-143. ↑
- C5377.** Lay-Ekuakille A. Output characterization of ground-based and integrated optical sensor for retrieved aerosol error minimization. / Lay-Ekuakille A., De Tomasi F., Perrone M.R., Trotta A. // 2003. IMTC '03. Proceedings of the 20th IEEE Instrumentation and Measurement Technology Conference. 20-22 May 2003. - Vol. 2. - P. 1018-1021. ↑
- C5378.** Belmont A.R. Non-uniform sampling issues arising in shallow angle wave profiling LIDAR. / Belmont A.R., Horwood J.M.K., Thurley R.W.F. // 2003. Proceedings of the IEEE/OES Seventh Working Conference on Current Measurement Technology. 13-15 March 2003. - P. 135-139. ↑
- C5379.** Jakobsson A. On the estimation of interferometric phases for multibaseline SAR interferometry using a relaxation-based technique. / Jakobsson A., Gini F., Lombardini F. // 2003. Proceedings. (ICASSP '03). 2003 IEEE International Conference on Acoustics, Speech, and Signal Processing. 6-10 April 2003. - Vol. 5. - P. V-277-80. ↑
- C5380.** Rodriguez P. High frequency radar astronomy with HAARP. / Rodriguez P., Kennedy E., Kossey P. // 2003. Proceedings of the 2003 IEEE Radar Conference. 5-8 May 2003. - P. 154-159. ↑
- C5381.** Woolard D.L. Terahertz-frequency remote-sensing of biological warfare agents. / Woolard D.L., Brown E.R., Samuels A.C., Jensen J.O., Globus T., Gelmont B., Wolski M. // 2003 IEEE MTT-S International Microwave Symposium Digest. 8-13 June 2003. - Vol. 2. - P. 763-766. ↑
- C5382.** Yang J. Generalized optimization of polarimetric contrast enhancement. / Yang J., Guiwei Dong, Yingning Peng, Yamaguchi Y., Yamada H. // 2003. IEEE Antennas and Propagation Society International Symposium. 22-27 June 2003. - Vol. 1. - P. 198-201. ↑
- C5383.** Zheng-Shu Zhou. Ground-based polarimetric SAR systems for environment studies. / Zheng-Shu Zhou, Motoyuki Sato. // 2003. IEEE Antennas and Propagation Society International Symposium. 22-27 June 2003. - Vol. 1. - P. 202-205. ↑
- C5384.** Yaqing Tu. A new method of high-accuracy level-measure based on combining radar frequency-modulation and phase-discrimination. / Yaqing Tu, Kaichun Ren, Du Zhang. // 2003. IMTC '03. Proceedings of the 20th IEEE Instrumentation and Measurement Technology Conference. 20-22 May 2003. - Vol. 2. - P. 1057-1060. ↑


- C5385.** Droitcour A.D. Range correlation effect on ISM band I/Q CMOS radar for non-contact vital signs sensing. / Droitcour A.D., Boric-Lubecke O., Lubecke V.M., Lin J., Kovacs G.T.A. // 2003 IEEE MTT-S International Microwave Symposium Digest. 8-13 June 2003. - Vol. 3. - P. 1945-1948. ↑
- C5386.** Huawu Deng. Advanced Gaussian MRF rotation-invariant texture features for classification of remote sensing imagery. / Huawu Deng, Clausi D.A. // 2003. Proceedings. 2003 IEEE Computer Society Conference on Computer Vision and Pattern Recognition. 18-20 June 2003. - Vol. 2. - P. II-685-90. ↑
- C5387.** Haus B.K. Refraction and shoaling of surface waves by currents and topography as observed by HF radars. / Haus B.K., Graber H.C., Ramos R. // 2003. Proceedings of the IEEE/OES Seventh Working Conference on Current Measurement Technology. 13-15 March 2003. - P. 115-118. ↑
- C5388.** Kelly F.J. A comparison of near-surface current measurements by ADCP and HF-Radar on the west Florida shelf. / Kelly F.J., Bonner J.S., Perez J.C., Trujillo D., Weisberg R.H., Luther M.E., He R. // 2003. Proceedings of the IEEE/OES Seventh Working Conference on Current Measurement Technology. 13-15 March 2003. - P. 70-74. ↑
- C5389.** Roarty H. Intercomparison of an ADCP, ADP, standard and long-range HF radar: influence of horizontal and vertical shear. / Roarty H., Kohut J., Glenn S. // 2003. Proceedings of the IEEE/OES Seventh Working Conference on Current Measurement Technology. 13-15 March 2003. - P. 75-78. ↑
- C5390.** Vesecky J. Constructing surface current maps from HF radars with different operating frequencies. / Vesecky J., Drake J., Laws K., Teague C., Fernandez D., Paduan J. // 2003. Proceedings of the IEEE/OES Seventh Working Conference on Current Measurement Technology. 13-15 March 2003. - P. 79-82. ↑
- C5391.** Cumming I. Compression of RADARSAT data with block adaptive wavelets. / Cumming I., Jing Wang. // 2003. Proceedings. DCC 2003 Data Compression Conference. 25-27 March 2003. - P. 419. ↑
- C5392.** Teague C.C. Initial river test of a monostatic RiverSonde streamflow measurement system. / Teague C.C., Barrick D.E., Lilleboe P.M., Cheng T.T. // 2003. Proceedings of the IEEE/OES Seventh Working Conference on Current Measurement Technology. 13-15 March 2003. - P. 46-50. ↑
- C5393.** Barrick D. Profiling river surface velocities and volume flow estimation with bistatic UHF RiverSonde radar. / Barrick D., Teague C., Lilleboe P., Cheng R., Gartner J. // 2003. Proceedings of the IEEE/OES Seventh Working Conference on Current Measurement Technology. 13-15 March 2003. - P. 55-59. ↑
- C5394.** Aguilar H. Jr. Fitting normal modes to HF radial and total surface current vector data over enclosed bays and estuaries. / Aguilar H. Jr., Fitzgerald R., Barrick D., Bonner J., Perez J. // 2003. Proceedings of the IEEE/OES Seventh Working Conference on Current Measurement Technology. 13-15 March 2003. - P. 101-104. ↑
- C5395.** Barrick D. Marrying quantitative and graphic tidal analysis tools with HF radar current map outputs. / Barrick D., James D., Isaacson J. // 2003. Proceedings of the IEEE/OES Seventh Working Conference on Current Measurement Technology. 13-15 March 2003. - P. 105-110. ↑
- C5396.** Fitzgerald R. Simplified calculation of constituent tidal currents and height from HF radar profiles across the mouth of bays and sounds. / Fitzgerald R., Barrick D., Sewell G. // 2003. Proceedings of the IEEE/OES Seventh Working Conference on Current Measurement Technology. 13-15 March 2003. - P. 111-114. ↑
- C5397.** Meadows L.A. High frequency radar measurements of friction velocity in the marine boundary layer. / Meadows L.A., Jacobs S.J., Vesecky J.F. // 2003. Proceedings of the IEEE/OES Seventh Working Conference on Current Measurement Technology. 13-15 March 2003. - P. 83-87. ↑
- C5398.** Drake J. Vector wind field measurements using multifrequency HF radar. / Drake J., Vesecky J., Laws K., Teague C., Ludwig F., Paduan J. // 2003. Proceedings of the IEEE/OES Seventh Working Conference on Current Measurement Technology. 13-15 March 2003. - P. 88-91. ↑
- C5399.** Lipa B. Uncertainties in SeaSonde current velocities. 2003. Proceedings of the IEEE/OES Seventh Working Conference on Current Measurement Technology. 13-15 March 2003. - P. 95-100. ↑
- C5400.** Qiu X.H. An efficient compensation approach for nonuniform sampling of rotating angle in ISAR imaging. / Qiu X.H., Zhao Y., Cao Y., Udupa S. // 2003. IEEE Antennas and Propagation Society International





Symposium. 22-27 June 2003. - Vol. 3. - P. 203-206. 


C5401. Quartulli M. Information extraction from high resolution SAR data for urban scene understanding. / Quartulli M., Datcu M. // 2003. 2nd GRSS/ISPRS Joint Workshop on Remote Sensing and Data Fusion over Urban Areas. 22-23 May 2003. - P. 115-119. 


C5402. Soergel U. Visibility analysis of man-made objects in SAR images. / Soergel U., Thoennessen U., Stilla U. // 2003. 2nd GRSS/ISPRS Joint Workshop on Remote Sensing and Data Fusion over Urban Areas. 22-23 May 2003. - P. 120-124. 


C5403. Dell'Acqua F. Simulation and analysis of fine resolution SAR images in urban areas. / Dell'Acqua F., Gamba P., Iodice A., Lisini G., Riccio D., Ruello G. // 2003. 2nd GRSS/ISPRS Joint Workshop on Remote Sensing and Data Fusion over Urban Areas. 22-23 May 2003. - P. 133-136. 


C5404. Huber M. Fusion of LIDAR data and aerial imagery for automatic reconstruction of building surfaces. / Huber M., Schickler W., Hinz S., Baumgartner A. // 2003. 2nd GRSS/ISPRS Joint Workshop on Remote Sensing and Data Fusion over Urban Areas. 22-23 May 2003. - P. 82-86. 


C5405. Latry C. SPOT5 THX: a 2.5m fused product. / Latry C., Vadon H., Lefevre M.J., De Boissezon H. // 2003. 2nd GRSS/ISPRS Joint Workshop on Remote Sensing and Data Fusion over Urban Areas. 22-23 May 2003. - P. 87-89. 


C5406. Tison C. Classification of X-band high resolution SAR images over urban areas: Markovian segmentation using Mellin transform. / Tison C., Nicolas J.-M., Tupin F. // 2003. 2nd GRSS/ISPRS Joint Workshop on Remote Sensing and Data Fusion over Urban Areas. 22-23 May 2003. - P. 110-114. 


C5407. Quartulli M. Information extraction from high resolution SAR data for urban scene understanding. / Quartulli M., Datcu M. // 2003. 2nd GRSS/ISPRS Joint Workshop on Remote Sensing and Data Fusion over Urban Areas. 22-23 May 2003. - P. 253-257. 


C5408. Dekker R.J. Texture analysis and classification of SAR images of urban areas. 2003. 2nd GRSS/ISPRS Joint Workshop on Remote Sensing and Data Fusion over Urban Areas. 22-23 May 2003. - P. 258-262. 


C5409. Karjalainen M. Urban change detection in the Helsinki metropolitan region using Radarsat-1 fine beam SAR images. / Karjalainen M., Hyypä J., Devillairs Y. // 2003. 2nd GRSS/ISPRS Joint Workshop on Remote Sensing and Data Fusion over Urban Areas. 22-23 May 2003. - P. 273-277. 


C5410. Pellizzeri T.M. Flood monitoring in urban areas: statistical vs. neurofuzzy approach. / Pellizzeri T.M., Gamba P., Lombardo P., Dell'Acqua F., Tortora A. // 2003. 2nd GRSS/ISPRS Joint Workshop on Remote Sensing and Data Fusion over Urban Areas. 22-23 May 2003. - P. 211-215. 

C5411. Bennett A.J. Infrastructure analysis from high resolution SAR and InSAR imagery. / Bennett A.J., Blacknell D. // 2003. 2nd GRSS/ISPRS Joint Workshop on Remote Sensing and Data Fusion over Urban Areas. 22-23 May 2003. - P. 230-235. 

C5412. Nakagawa M. Integrating high resolution air-borne linear CCD (TLS) imagery and LIDAR data. / Nakagawa M., Shibasaki R. // 2003. 2nd GRSS/ISPRS Joint Workshop on Remote Sensing and Data Fusion over Urban Areas. 22-23 May 2003. - P. 236-240. 

C5413. Guillaso S. Urban area analysis based on ESPRIT/MUSIC methods using polarimetric interferometric SAR. / Guillaso S., Ferro-Famil L., Reigber A., Pottier E. // 2003. 2nd GRSS/ISPRS Joint Workshop on Remote Sensing and Data Fusion over Urban Areas. 22-23 May 2003. - P. 77-81. 

C5414. Roth A. TerraSAR-X: a new perspective for scientific use of high resolution spaceborne SAR data. 2003. 2nd GRSS/ISPRS Joint Workshop on Remote Sensing and Data Fusion over Urban Areas. 22-23 May 2003. - P. 4-7. 

C5415. Csatho B. Spectral interpretation based on multisensor fusion for urban mapping. / Csatho B., Schenk T., Suyoung Seo. // 2003. 2nd GRSS/ISPRS Joint Workshop on Remote Sensing and Data Fusion over Urban Areas. 22-23 May 2003. - P. 8-12. 

C5416. Franceschetti G. Information content in SAR images of urban areas. / Franceschetti G., Iodice A.,

Riccio D., Ruello G. // 2003. 2nd GRSS/ISPRS Joint Workshop on Remote Sensing and Data Fusion over Urban Areas. 22-23 May 2003. - P. 43-46. ↑

C5417. Lyzenga D.R. Estimation of ocean wave spectra from microwave backscatter and emissivity measurements. 2003. IEEE Antennas and Propagation Society International Symposium. 22-27 June 2003. - Vol. 3. - P. 396-399. ↑

C5418. Azadegan R. Analytical formulation of the scattering by a slightly rough dielectric boundary, covered with a homogenous dielectric layer. / Azadegan R., Sarabandi K. // 2003. IEEE Antennas and Propagation Society International Symposium. 22-27 June 2003. - Vol. 3. - P. 420-423. ↑

C5419. {no data available}. 2nd GRSS/ISPRS Joint Workshop on Remote Sensing and Data Fusion over Urban Areas. URBAN 2003 (Cat. No.03EX646). 2003. 2nd GRSS/ISPRS Joint Workshop on Remote Sensing and Data Fusion over Urban Areas. 22-23 May 2003. - {no data available}. ↑

C5420. Aiazzi B. Land cover classification of urban and sub-urban areas via fuzzy nearest-mean reclustering of SAR features. / Aiazzi B., Alparone L., Baronti S. // 2003. 2nd GRSS/ISPRS Joint Workshop on Remote Sensing and Data Fusion over Urban Areas. 22-23 May 2003. - P. 62-66. ↑

C5421. Sithole G. Automatic structure detection in a point-cloud of an urban landscape. / Sithole G., Vosselman G. // 2003. 2nd GRSS/ISPRS Joint Workshop on Remote Sensing and Data Fusion over Urban Areas. 22-23 May 2003. - P. 67-71. ↑

C5422. Tupin F. Extraction of 3D information using overlay detection on SAR images. 2003. 2nd GRSS/ISPRS Joint Workshop on Remote Sensing and Data Fusion over Urban Areas. 22-23 May 2003. - P. 72-76. ↑

C5423. Pellizzeri T.M. Model-based processing of multifrequency polarimetric SAR images of urban areas. / Pellizzeri T.M., Lombardo P., Meloni M. // 2003. 2nd GRSS/ISPRS Joint Workshop on Remote Sensing and Data Fusion over Urban Areas. 22-23 May 2003. - P. 47-51. ↑

C5424. Colesanti C. Multi-platform permanent scatterers analysis: first results. / Colesanti C., Ferretti A., Locatelli R., Savio G. // 2003. 2nd GRSS/ISPRS Joint Workshop on Remote Sensing and Data Fusion over Urban Areas. 22-23 May 2003. - P. 52-56. ↑

C5425. Lanari R. A differential SAR interferometry approach for monitoring urban deformation phenomena. / Lanari R., Mora O., Manunta M., Mallorqui J.J., Berardino P., Guarino S., Zeni G., Pepe A., Sansosti E. // 2003. 2nd GRSS/ISPRS Joint Workshop on Remote Sensing and Data Fusion over Urban Areas. 22-23 May 2003. - P. 57-61. ↑

C5426. Norman R.J. Backscatter ionogram inversion. 2003. Proceedings of the International Radar Conference. 3-5 Sept. 2003. - P. 368-374. ↑

C5427. Weydahl D.J. Analysis of X-SAR SRTM elevation data to estimate surface cover heights over land areas. / Weydahl D.J., Sagstuen J., Dick O., Ronning H., Hansen L. // 2003. IGARSS '03. Proceedings. 2003 IEEE International Geoscience and Remote Sensing Symposium. 21-25 July 2003. - Vol. 1. - P. 112-114. ↑

C5428. Yarovoy A.G. Monte Carlo simulations of surface clutter in GPR scenarios. 2003. IGARSS '03. Proceedings. 2003 IEEE International Geoscience and Remote Sensing Symposium. 21-25 July 2003. - Vol. 1. - P. 130-132. ↑

C5429. Baudier C. Scattering by rough surfaces: comparison between simulations and experimental radar data. / Baudier C., Dusseaux R. // 2003. IGARSS '03. Proceedings. 2003 IEEE International Geoscience and Remote Sensing Symposium. 21-25 July 2003. - Vol. 1. - P. 133-135. ↑

C5430. Srivastava S.K. RADARSAT-1 image quality maintained in extended mission. / Srivastava S.K., Le Dantec P., Gray R., Hawkins R.K., Murnaghan K.P. // 2003. IGARSS '03. Proceedings. 2003 IEEE International Geoscience and Remote Sensing Symposium. 21-25 July 2003. - Vol. 1. - P. 103-105. ↑

C5431. Singhroy V. Terrain interpretation from SAR techniques. / Singhroy V., Assouad P., Barnett P., Molch K. // 2003. IGARSS '03. Proceedings. 2003 IEEE International Geoscience and Remote Sensing Symposium. 21-25 July 2003. - Vol. 1. - P. 106-108. ↑

- C5432.** Strozzi T. Validation of the X-SAR SRTM DEM for ERS and JERS SAR geocoding and 2-pass differential interferometry in alpine regions. / Strozzi T., Wegmuller U., Wiesmann A., Werner C. // 2003. IGARSS '03. Proceedings. 2003 IEEE International Geoscience and Remote Sensing Symposium. 21-25 July 2003. - Vol. 1. - P. 109-111. ↑
- C5433.** Wegmuller U. Radargrammetry and space triangulation for DEM generation and image ortho-rectification. / Wegmuller U., Werner C., Wiesmann A., Strozzi T. // 2003. IGARSS '03. Proceedings. 2003 IEEE International Geoscience and Remote Sensing Symposium. 21-25 July 2003. - Vol. 1. - P. 179-181. ↑
- C5434.** Hoonyol Lee. Radargrammetry of opposite-side stereo Magellan synthetic aperture radar on Venus. / Hoonyol Lee, Morgan J.V., Warner M.R. // 2003. IGARSS '03. Proceedings. 2003 IEEE International Geoscience and Remote Sensing Symposium. 21-25 July 2003. - Vol. 1. - P. 182-184. ↑
- C5435.** Cantalloube H.-M.J. Airborne X-band SAR imaging with 10 cm resolution-technical challenge and preliminary results. / Cantalloube H.-M.J., Dubois-Fernandez P. // 2003. IGARSS '03. Proceedings. 2003 IEEE International Geoscience and Remote Sensing Symposium. 21-25 July 2003. - Vol. 1. - P. 185-187. ↑
- C5436.** Dabrowska-Zielinska K. Examination of crop characteristics using microwave data. / Dabrowska-Zielinska K., Inoue Y., Kowalik W., Gruszczynska M. // 2003. IGARSS '03. Proceedings. 2003 IEEE International Geoscience and Remote Sensing Symposium. 21-25 July 2003. - Vol. 1. - P. 158-160. ↑
- C5437.** Zhang Hong. A new image registration method for multi-frequency airborne high-resolution SAR images. / Zhang Hong, Wang Chao, Tang Yixian, Liu Zhi. // 2003. IGARSS '03. Proceedings. 2003 IEEE International Geoscience and Remote Sensing Symposium. 21-25 July 2003. - Vol. 1. - P. 167-169. ↑
- C5438.** Sidharta Gautama. Using graph matching to compare VHR satellite images with GIS data. / Sidharta Gautama, Borghgraef A. // 2003. IGARSS '03. Proceedings. 2003 IEEE International Geoscience and Remote Sensing Symposium. 21-25 July 2003. - Vol. 1. - P. 173-175. ↑
- C5439.** Alexandrov V.Y. A comparative analysis of data on multiyear sea ice distribution in the Arctic as retrieved from satellite passive microwave radiometer and radar images. / Alexandrov V.Y., Johannessen O.M., Samsonov I.V., Bobylev L.P., Kloster K. // 2003. IGARSS '03. Proceedings. 2003 IEEE International Geoscience and Remote Sensing Symposium. 21-25 July 2003. - Vol. 1. - P. 77-79. ↑
- C5440.** McCandles S.W. Jr. The origin, evolution and legacy of SEASAT. 2003. IGARSS '03. Proceedings. 2003 IEEE International Geoscience and Remote Sensing Symposium. 21-25 July 2003. - Vol. 1. - P. 32-34. ↑
- C5441.** Alpers W. Ocean surface wave imaging from Seasat to Envisat. 2003. IGARSS '03. Proceedings. 2003 IEEE International Geoscience and Remote Sensing Symposium. 21-25 July 2003. - Vol. 1. - P. 35-37. ↑
- C5442.** Monaldo F. SEASAT sees the winds with SAR. 2003. IGARSS '03. Proceedings. 2003 IEEE International Geoscience and Remote Sensing Symposium. 21-25 July 2003. - Vol. 1. - P. 38-40. ↑
- C5443.** Shimoda H. Present status of GCOM mission. 2003. IGARSS '03. Proceedings. 2003 IEEE International Geoscience and Remote Sensing Symposium. 21-25 July 2003. - Vol. 1. - P. 22-24. ↑
- C5444.** Lifermann A. POLDER on ADEOS-2. / Lifermann A., Proy C. // 2003. IGARSS '03. Proceedings. 2003 IEEE International Geoscience and Remote Sensing Symposium. 21-25 July 2003. - Vol. 1. - P. 25 vol.1. ↑
- C5445.** Igarashi T. ADEOS-II calibration and validation plan. / Igarashi T., Matsuura N. // 2003. IGARSS '03. Proceedings. 2003 IEEE International Geoscience and Remote Sensing Symposium. 21-25 July 2003. - Vol. 1. - P. 29-31. ↑
- C5446.** Dokken S.T. Geophysical interpretation of ScanSAR data in relation to SSM/I data and numerical models of Arctic sea ice. 2003. IGARSS '03. Proceedings. 2003 IEEE International Geoscience and Remote Sensing Symposium. 21-25 July 2003. - Vol. 1. - P. 68-70. ↑
- C5447.** Anderson H.S. Polar sea ice mapping using SeaWinds data. / Anderson H.S., Long D.G. // 2003. IGARSS '03. Proceedings. 2003 IEEE International Geoscience and Remote Sensing Symposium. 21-25 July 2003. - Vol. 1. - P. 71-73. ↑
- C5448.** Karvonen J. Ice thickness estimation using SAR data and ice thickness history. / Karvonen J., Simila

M., Heiler I. // 2003. IGARSS '03. Proceedings. 2003 IEEE International Geoscience and Remote Sensing Symposium. 21-25 July 2003. - Vol. 1. - P. 74-76. ↑

C5449. Wei Lu. Spatial decision support system for sediment related disaster prevention planning. / Wei Lu, Doihara T., Ogawa K., Matsuda M. // 2003. IGARSS '03. Proceedings. 2003 IEEE International Geoscience and Remote Sensing Symposium. 21-25 July 2003. - Vol. 1. - P. 41-43. ↑

C5450. Ge Chen. A new approach for tracking the trajectory of oceanic warm pool. / Ge Chen, Lixing Fang, Chaoyang Fang. // 2003. IGARSS '03. Proceedings. 2003 IEEE International Geoscience and Remote Sensing Symposium. 21-25 July 2003. - Vol. 1. - P. 50-52. ↑

C5451. Mohammed Shokr. Evaluation of ice concentration algorithms using data fusion of SSM/I and Radarsat. / Mohammed Shokr, Markus T. // 2003. IGARSS '03. Proceedings. 2003 IEEE International Geoscience and Remote Sensing Symposium. 21-25 July 2003. - Vol. 1. - P. 65-67. ↑

C5452. Corr D.G. Classification of urban SAR imagery using object oriented techniques. / Corr D.G., Walker A., Benz U., Lingenfelder I., Rodrigues A. // 2003. IGARSS '03. Proceedings. 2003 IEEE International Geoscience and Remote Sensing Symposium. 21-25 July 2003. - Vol. 1. - P. 188-190. ↑

C5453. Plant W.J. Comparison of wind vectors and air-sea temperature differences measured during SHOWEX. / Plant W.J., Foster R., Graber H., Drennan W.M., Mahrt L., Irisov V., Long D.G. // 2003. IGARSS '03. Proceedings. 2003 IEEE International Geoscience and Remote Sensing Symposium. 21-25 July 2003. - Vol. 1. - P. 242-244. ↑

C5454. Liu W.T. Air-sea interaction with multiple sensors-Seasat legacy. / Liu W.T., Wenqing Tang. // 2003. IGARSS '03. Proceedings. 2003 IEEE International Geoscience and Remote Sensing Symposium. 21-25 July 2003. - Vol. 1. - P. 248-250. ↑

C5455. Moghaddam M. Mapping wetlands of the North American boreal zone from satellite radar imagery. / Moghaddam M., McDonald K., Cihlar J., Wenjun Chen. // 2003. IGARSS '03. Proceedings. 2003 IEEE International Geoscience and Remote Sensing Symposium. 21-25 July 2003. - Vol. 1. - P. 261-263. ↑

C5456. Monaldo F. Combining SAR and scatterometer data to improve high resolution wind speed retrievals. / Monaldo F., Thompson D., Winstead N. // 2003. IGARSS '03. Proceedings. 2003 IEEE International Geoscience and Remote Sensing Symposium. 21-25 July 2003. - Vol. 1. - P. 233-235. ↑

C5457. Askari F. RADARSAT mapping of BORA/SIROCCO winds in the Adriatic Sea. / Askari F., Signell R.P., Chiggiato J., Doyle J. // 2003. IGARSS '03. Proceedings. 2003 IEEE International Geoscience and Remote Sensing Symposium. 21-25 July 2003. - Vol. 1. - P. 236-238. ↑

C5458. Bourassa M.A. The development and application of a sea surface stress model function for the QuickSCAT and ADEOS-II sea winds scatterometers. / Bourassa M.A., Weissman D.E. // 2003. IGARSS '03. Proceedings. 2003 IEEE International Geoscience and Remote Sensing Symposium. 21-25 July 2003. - Vol. 1. - P. 239-241. ↑

C5459. Palmer J. Improving on the monostatic radar cross section of targets by employing sea clutter to emulate a bistatic radar. / Palmer J., Homer J., Mojarrabi B. // 2003. IGARSS '03. Proceedings. 2003 IEEE International Geoscience and Remote Sensing Symposium. 21-25 July 2003. - Vol. 1. - P. 324-326. ↑

C5460. Ramnath V.K. Estimation of soil moisture using Radarsat repeat-passes. / Ramnath V.K., King R.L., Younan N.H. // 2003. IGARSS '03. Proceedings. 2003 IEEE International Geoscience and Remote Sensing Symposium. 21-25 July 2003. - Vol. 1. - P. 327-329. ↑

C5461. Cunningham J.D. The National Polar-orbiting Operational Environmental Satellite System future US operational Earth observation system. / Cunningham J.D., Ricker F.L., Nelson C.S. // 2003. IGARSS '03. Proceedings. 2003 IEEE International Geoscience and Remote Sensing Symposium. 21-25 July 2003. - Vol. 1. - P. 351-356. ↑

C5462. Ezraty R. New-ice detection using microwave sensors. 2003. IGARSS '03. Proceedings. 2003 IEEE International Geoscience and Remote Sensing Symposium. 21-25 July 2003. - Vol. 1. - P. 270-272. ↑

C5463. Bouillon A. SPOT5 geometric image quality. / Bouillon A., Breton E., De Lussy F., Gachet R. // 2003.

IGARSS '03. Proceedings. 2003 IEEE International Geoscience and Remote Sensing Symposium. 21-25 July 2003. - Vol. 1. - P. 303-305. ↑

C5464. Kubik P. Pushing the limits of SPOT HRV resolution with steered viewing modes. / Kubik P., Duchon P., Sebbag I. // 2003. IGARSS '03. Proceedings. 2003 IEEE International Geoscience and Remote Sensing Symposium. 21-25 July 2003. - Vol. 1. - P. 312-314. ↑

C5465. Horstmann J. SAR measurements of ocean wind and wave fields in hurricanes. / Horstmann J., Vachon P., Lehner S., Hoja D. // 2003. IGARSS '03. Proceedings. 2003 IEEE International Geoscience and Remote Sensing Symposium. 21-25 July 2003. - Vol. 1. - P. 230-232. ↑

C5466. Aiazzi B. Coherence estimation from multilook detected SAR images. / Aiazzi B., Alparone L., Baronti S., Garzelli A. // 2003. IGARSS '03. Proceedings. 2003 IEEE International Geoscience and Remote Sensing Symposium. 21-25 July 2003. - Vol. 1. - P. 200-202. ↑

C5467. Yahia M. Unsupervised classification of polarimetric SAR images using neural networks. / Yahia M., Belhadj Z. // 2003. IGARSS '03. Proceedings. 2003 IEEE International Geoscience and Remote Sensing Symposium. 21-25 July 2003. - Vol. 1. - P. 203-205. ↑

C5468. Zhang Q. Novel registration technique of InSAR and InSAR. / Zhang Q., Yeo T.S. // 2003. IGARSS '03. Proceedings. 2003 IEEE International Geoscience and Remote Sensing Symposium. 21-25 July 2003. - Vol. 1. - P. 206-208. ↑

C5469. Tunaley J.K.E. The estimation of ship velocity from SAR imagery. 2003. IGARSS '03. Proceedings. 2003 IEEE International Geoscience and Remote Sensing Symposium. 21-25 July 2003. - Vol. 1. - P. 191-193. ↑

C5470. Touzi R. The SSCM for ship characterization using polarimetric SAR. / Touzi R., Charbonneau F. // 2003. IGARSS '03. Proceedings. 2003 IEEE International Geoscience and Remote Sensing Symposium. 21-25 July 2003. - Vol. 1. - P. 194-196. ↑

C5471. Foucher S. Multiscale classification and filtering of SAR images using Dempster-Shafer theory. / Foucher S., Boucher J.-M., Benie G.B. // 2003. IGARSS '03. Proceedings. 2003 IEEE International Geoscience and Remote Sensing Symposium. 21-25 July 2003. - Vol. 1. - P. 197-199. ↑

C5472. Antonello G. A ground-based interferometer for the safety monitoring of landslides and structural deformations. / Antonello G., Casagli N., Farina P., Fortuny J., Leva D., Nico G., Sieber A.J., Tarchi D. // 2003. IGARSS '03. Proceedings. 2003 IEEE International Geoscience and Remote Sensing Symposium. 21-25 July 2003. - Vol. 1. - P. 218-220. ↑

C5473. Pathier E. Contributions of InSAR to study active tectonics of Taiwan. / Pathier E., Angelier J., Fruneau B., Deffontaines B. // 2003. IGARSS '03. Proceedings. 2003 IEEE International Geoscience and Remote Sensing Symposium. 21-25 July 2003. - Vol. 1. - P. 221-223. ↑

C5474. Engen G. Curvature effects in ocean surface scattering. / Engen G., Johnsen H., Chapron B. // 2003. IGARSS '03. Proceedings. 2003 IEEE International Geoscience and Remote Sensing Symposium. 21-25 July 2003. - Vol. 1. - P. 224-226. ↑

C5475. Kircher M. Remote sensing observation of mining induced subsidence by means of differential SAR-interferometry. / Kircher M., Roth A., Adam N., Kampes B., Neugebauer H.J. // 2003. IGARSS '03. Proceedings. 2003 IEEE International Geoscience and Remote Sensing Symposium. 21-25 July 2003. - Vol. 1. - P. 209-211. ↑

C5476. Strozzi T. Land subsidence monitoring service in the Lagoon of Venice. / Strozzi T., Tosi L., Wegmuller U., Werner C., Teatini P., Carbognin L. // 2003. IGARSS '03. Proceedings. 2003 IEEE International Geoscience and Remote Sensing Symposium. 21-25 July 2003. - Vol. 1. - P. 212-214. ↑

C5477. Allievi J. Monitoring slow mass movements with the Permanent Scatterers technique. / Allievi J., Ambrosi C., Ceriani M., Colesanti C., Crosta G.B., Ferretti A., Fossati D. // 2003. IGARSS '03. Proceedings. 2003 IEEE International Geoscience and Remote Sensing Symposium. 21-25 July 2003. - Vol. 1. - P. 215-217. ↑

C5478. Lang R.H. Measurement of the dielectric constant of seawater at L-band. / Lang R.H., Utku C., Le Vine

DM. // 2003. IGARSS '03. Proceedings. 2003 IEEE International Geoscience and Remote Sensing Symposium. 21-25 July 2003. - Vol. 1. - P. 19-21. ↑

C5479. Weissman D.E. Satellite measurements of backscatter from rain-induced roughness on the sea surface using QuickSCAT and TRMM. / Weissman D.E., Bourassa M.E. // OCEANS 2003. Proceedings. - San Diego, CA, USA, 2003. - Vol. 1. - P. 537 Vol.1. ↑

C5480. {no data available}. Oceans 2003. Celebrating the Past .. Teaming Toward the Future (IEEE Cat. No.03CH37492). OCEANS 2003. Proceedings. 22-26 Sept. 2003. - Vol. 3. - {no data available}. ↑

C5481. Jacobs G.A. Operational oceanographic applications for the Wide Swath Ocean Altimeter. OCEANS 2003. Proceedings. 22-26 Sept. 2003. - Vol. 3. - P. 1312 Vol.3. ↑

C5482. Craeye C. A relationship between atmospheric rain reflectivity and elevation variance due to drop impact on the sea surface. / Craeye C., Sobieski P., Bliven L.F. // OCEANS 2003. Proceedings. - San Diego, CA, USA, 2003. - Vol. 1. - P. 528-531. ↑

C5483. Hilburn K.A. Rain effects on SeaWinds data. / Hilburn K.A., Wentz F.J. // OCEANS 2003. Proceedings. - San Diego, CA, USA, 2003. - Vol. 1. - P. 532-535. ↑

C5484. Stiles B.W. Rain, wind, and backscatter: modeling rain effects on Ku-band ocean wind scatterometers. / Stiles B.W., Yueh S. // OCEANS 2003. Proceedings. - San Diego, CA, USA, 2003. - Vol. 1. - P. 536 Vol.1. ↑

C5485. Arakelyan Artashes. Radar method for atmospheric stratification condition unambiguous determination by synergy data of sea surface altimetric and scatterometric observations. / Arakelyan Artashes, Astghik H. // OCEANS 2003. Proceedings. 22-26 Sept. 2003. - Vol. 3. - P. 1322 Vol.3. ↑

C5486. Romeiser R. Towards an operational spaceborne system for high-resolution current measurements in coastal areas. / Romeiser R., Runge H., Breit H., Eineder M., Flament P. // OCEANS 2003. Proceedings. 22-26 Sept. 2003. - Vol. 3. - P. 1524-1530. ↑

C5487. Atlas R. Impact of seawinds scatterometer data on ocean surface analysis and weather prediction. / Atlas R., Bloom S.C., Ardizzone J., Brin E., Terry J. // OCEANS 2003. Proceedings. 22-26 Sept. 2003. - Vol. 3. - P. 1598-1601. ↑

C5488. Raney R.K. The delay-Doppler radar altimeter: robust and improved measurement capabilities. / Raney R.K., Jensen J.R., Porter D.L. // OCEANS 2003. Proceedings. 22-26 Sept. 2003. - Vol. 3. - P. 1313-1316. ↑

C5489. Porter D.L. Ocean observations with a space-based delay-Doppler altimeter constellation. / Porter D.L., Raney R.K., Jensen J.R. // OCEANS 2003. Proceedings. 22-26 Sept. 2003. - Vol. 3. - P. 1317-1320. ↑

C5490. Finkelstein J.L. GEOSAT follow-on GFO radar altimeter satellite performance. / Finkelstein J.L., Rau M., McMillan J. // OCEANS 2003. Proceedings. 22-26 Sept. 2003. - Vol. 3. - P. 1321 Vol.3. ↑

C5491. Contreras R.F. Modeling rain effects on microwave backscatter from the ocean. / Contreras R.F., Plant W.J. // OCEANS 2003. Proceedings. - San Diego, CA, USA, 2003. - Vol. 1. - P. 524-527. ↑

C5492. Jiao Pei-nan. Probing of the artificial hole in the ionosphere with the HF skywave radar. / Jiao Pei-nan, Ma Tie-han, Xu Guo-liang, Li Zong-qiang, Zhang Xin-sheng, Xu Fei. // 2003. Proceedings of the International Radar Conference. 3-5 Sept. 2003. - P. 588-592. ↑

C5493. Yunhan Dong. L-band VV clutter analysis for natural land. 2003. Proceedings of the International Radar Conference. 3-5 Sept. 2003. - P. 625-630. ↑

C5494. Gurgel K.-W. HF surface wave radar for oceanography-a review of activities in Germany. / Gurgel K.-W., Essen H.-H., Schlick T. // 2003. Proceedings of the International Radar Conference. 3-5 Sept. 2003. - P. 700-705. ↑

C5495. Sciotti M. Subsurface sounding of Mars: multi-pulse detection of water-related interfaces. / Sciotti M., Lombardo P., Pastina D., Pellizzeri A.M. // 2003. Proceedings of the International Radar Conference. 3-5 Sept. 2003. - P. 400-405. ↑

C5496. Anderson S. Limits to the extraction of information from multi-hop skywave radar signals. 2003.

Proceedings of the International Radar Conference. 3-5 Sept. 2003. - P. 497-503. ↑

C5497. Picardi G. Mars Advanced Radar for Subsurface and Ionosphere Sounding (MARSIS): subsurface performances evaluation. / Picardi G., Biccari D., Bazzoni A., Fois F., Iorio M., Seu R., Melacci P., Federico C., Frigeri A., Minelli G., Marinangeli L., Orosei R., Calabrese D., Zampolini E., Johnson W.T.K., Jordan R.L., Plaut J., Safaenili A. // 2003. Proceedings of the International Radar Conference. 3-5 Sept. 2003. - P. 515-521. ↑

C5498. Cunningham J.D. The National Polar-orbiting Operational Environment Satellite System capabilities for operational ocean remote sensing. / Cunningham J.D., Nelson C.S. // OCEANS 2003. Proceedings. - San Diego, CA, USA, 2003. - Vol. 1. - P. 203-207. ↑

C5499. Radoi E. Statistical analysis of real sea clutter data measured by a high resolution radar at low grazing angles. / Radoi E., Quinquis A., Saulais P. // OCEANS 2003. Proceedings. - San Diego, CA, USA, 2003. - Vol. 1. - P. 445 Vol.1. ↑

C5500. Bliven L.F. Ring-wave measurements form natural rain. OCEANS 2003. Proceedings. - San Diego, CA, USA, 2003. - Vol. 1. - P. 521-523. ↑

C5501. Anderson S.J. Investigations with SECAR-a bistatic HF surface wave radar. / Anderson S.J., Edwards P.J., Marrone P., Abramovich Y.I. // 2003. Proceedings of the International Radar Conference. 3-5 Sept. 2003. - P. 717-722. ↑

C5502. Koshevaya S. Scattering of ultrashort electromagnetic pulses by nonlinearly reflecting targets. / Koshevaya S., Grimalsky V., Moreno E., Gutierrez E. // 2003. CEEM 2003. Proceedings. Asia-Pacific Conference on Environmental Electromagnetics. 4-7 Nov. 2003. - P. 509-513. ↑

C5503. Girard-Ardhuin F. Oil slick detection by SAR imagery: potential and limitation. / Girard-Ardhuin F., Mercier G., Garello R. // OCEANS 2003. Proceedings. - San Diego, CA, USA, 2003. - Vol. 1. - P. 164-169. ↑

C5504. Gangopadhyaya A. A modified velocity projection method for estimating the subsurface velocity structure of the Chesapeake Bay outflow plume. / Gangopadhyaya A., Mied R.P., Shen C.Y., Evans T.E., Marmorino G.O. // OCEANS 2003. Proceedings. 22-26 Sept. 2003. - Vol. 3. - P. 1738 Vol.3. ↑

C5505. Zavala-Hidalgo J. A new temporal interpolation method for high-frequency vector wind fields. / Zavala-Hidalgo J., Bourassa M.A., Morey S.L., O'Brien J.J., Yu P. // OCEANS 2003. Proceedings. 22-26 Sept. 2003. - Vol. 2. - P. 1050-1053. ↑

C5506. Zou Kun. A new method for calibration of SAR image. / Zou Kun, Fang Xueli, Dong Zhen. // 2003. Proceedings. 2003 IEEE International Conference on Robotics, Intelligent Systems and Signal Processing. 8-13 Oct. 2003. - Vol. 2. - P. 1174-1178. ↑

C5507. Zou Xing Liang. Feature-based multi-resolution SAR and TM images auto-registration. / Zou Xing Liang, Ma Hong Bing, Ge Cheng Hui. // 2003. Proceedings. 2003 IEEE International Conference on Robotics, Intelligent Systems and Signal Processing. 8-13 Oct. 2003. - Vol. 2. - P. 1278-1282. ↑

C5508. Sandwell D.T. Improved global marine gravity by retracking altimeter waveforms. OCEANS 2003. Proceedings. 22-26 Sept. 2003. - Vol. 2. - P. 756 Vol.2. ↑

C5509. Parker B. Integrating bathymetry, topography, and shoreline, and the importance of vertical datums. / Parker B., Milbert D., Hess K., Gill S. // OCEANS 2003. Proceedings. 22-26 Sept. 2003. - Vol. 2. - P. 758-764. ↑

C5510. Bourassa M.A. Fine resolution satellite-based winds for episodic events. / Bourassa M.A., O'Brien J.J. // OCEANS 2003. Proceedings. 22-26 Sept. 2003. - Vol. 2. - P. 1046-1049. ↑

C5511. Font J. The determination of surface salinity with SMOS-recent results and main issues. / Font J., Lagerloef G., Le Vine D., Camps A., Zanife O.Z. // 2003. IGARSS '03. Proceedings. 2003 IEEE International Geoscience and Remote Sensing Symposium. 21-25 July 2003. - Vol. 1. - P. 7-9. ↑

C5512. Boutin J. Uncertainties on salinity retrieved from SMOS measurements over global ocean. / Boutin J., Waldteufel P., Martin N., Kerr Y., Caudal G., Dinnat E., Etcheto J. // 2003. IGARSS '03. Proceedings. 2003 IEEE International Geoscience and Remote Sensing Symposium. 21-25 July 2003. - Vol. 1. - P. 10-12. ↑

- C5513.** Waldteufel P. A cardioid model for multi-angular radiometric observations. / Waldteufel P., Vergely J.L., Cot C. // 2003. IGARSS '03. Proceedings. 2003 IEEE International Geoscience and Remote Sensing Symposium. 21-25 July 2003. - Vol. 1. - P. 16-18. ↑
- C5514.** Majurec N. Triple-frequency radar for cloud and precipitation microphysics research. / Majurec N., Sekelsky S.M., Schaubert D.H., Hong Y., Rutledge S.A., Stephens G.L., Heymsfield A. // 2003. ICECom 2003. 17th International Conference on Applied Electromagnetics and Communications. 1-3 Oct. 2003. - P. 18-21. ↑
- C5515.** {no data available}. IGARSS 2003. 2003 IEEE International Geoscience and Remote Sensing Symposium. Proceedings (IEEE Cat. No.03CH37477). 2003. IGARSS '03. Proceedings. 2003 IEEE International Geoscience and Remote Sensing Symposium. 21-25 July 2003. - Vol. 1. - {no data available}. ↑
- C5516.** Kerr Y.H. The Soil Moisture and Ocean Salinity mission. / Kerr Y.H., Waldteufel P., Wigneron J.-P., Font J., Berger M. // 2003. IGARSS '03. Proceedings. 2003 IEEE International Geoscience and Remote Sensing Symposium. 21-25 July 2003. - Vol. 1. - P. 1-3. ↑
- C5517.** Glenn S.M. NEOS: the North East Ocean Observing System by: Scott Glenn & NEOS partners. OCEANS 2003. Proceedings. 22-26 Sept. 2003. - Vol. 2. - P. 712 Vol.2. ↑
- C5518.** Heron M.L. Performance of a VHF ocean surface radar in the surf zone. / Heron M.L., Prytz A. // OCEANS 2003. Proceedings. 22-26 Sept. 2003. - Vol. 4. - P. 2037-2042. ↑
- C5519.** Lipphardt B.L. Jr. Surface transport and mixing in Monterey Bay. I: Objective surface current maps. / Lipphardt B.L. Jr., Kirwan A.D. Jr., Grosch C.E., Paduan J.D., Wiggins S., Small D., Ide K. // OCEANS 2003. Proceedings. 22-26 Sept. 2003. - Vol. 4. - P. 2043 Vol.4. ↑
- C5520.** Astghik H. A complex of polarimetric, combined active-passive sensors of L-, C-, and X-band of frequencies for vessel and airborne application. / Astghik H., Artashes A. // OCEANS 2003. Proceedings. 22-26 Sept. 2003. - Vol. 4. - P. 2262 Vol.4. ↑
- C5521.** Ermakov S.A. Bound waves and radar backscattering from the sea surface. / Ermakov S.A., Sergievskaya I.A., Shchegolkov Y.B. // OCEANS 2003. Proceedings. 22-26 Sept. 2003. - Vol. 4. - P. 1824 Vol.4. ↑
- C5522.** Schuler D. Ocean environment sensing using polarimetric and interferometric SAR. / Schuler D., Sletten M., Ainsworth T., Lee J.S., Frasier S., Holt B. // OCEANS 2003. Proceedings. 22-26 Sept. 2003. - Vol. 4. - P. 1829-1834. ↑
- C5523.** Gerstoft P. Posteriori estimation of low altitude propagation loss from radar sea clutter data. / Gerstoft P., Rogers L.T., Hodgkiss W.S. // OCEANS 2003. Proceedings. 22-26 Sept. 2003. - Vol. 4. - P. 2032-2036. ↑
- C5524.** Dugan J.P. Detection of small targets in ocean wave clutter using panchromatic time series imagery. / Dugan J.P., Piotrowski C.C., Campion D.C. // OCEANS 2003. Proceedings. 22-26 Sept. 2003. - Vol. 5. - P. 2560-2565. ↑
- C5525.** Kassem M.J.B. Bistatic mapping radar BISAR. / Kassem M.J.B., Khenchaf A. // OCEANS 2003. Proceedings. 22-26 Sept. 2003. - Vol. 5. - P. P2754-P2760. ↑
- C5526.** Lamy M. A new ocean SAR imaging process simulator. / Lamy M., Le Caillec J.-M., Garelo R., Khenchaf A. // OCEANS 2003. Proceedings. 22-26 Sept. 2003. - Vol. 5. - P. SP2845-SP2850. ↑
- C5527.** Trizna D.B. Multi-frequency HF radar for mapping current shear and vector winds. / Trizna D.B., Xu L. // OCEANS 2003. Proceedings. 22-26 Sept. 2003. - Vol. 4. - P. 2332-2334. ↑
- C5528.** Kohut J.T. Recent results from a nested multi-static HF radar network for the NorthEast Observing System (NEOS). / Kohut J.T., Glenn S.M., Roarty H.J. // OCEANS 2003. Proceedings. 22-26 Sept. 2003. - Vol. 4. - P. 2335 Vol.4. ↑
- C5529.** Gill E. An alternate analysis for the second-order high frequency bistatic radar cross section of the ocean surface-patch scatter and its inversion. / Gill E., Weimin Huang, Jianjun Zhang. // OCEANS 2003. Proceedings. 22-26 Sept. 2003. - Vol. 4. - P. 2336-2340. ↑
- C5530.** Paillou P. The SAHARASAR project: potential support to water prospecting in arid Africa by SAR. /

Paillou P., Rosenqvist A. // 2003. IGARSS '03. Proceedings. 2003 IEEE International Geoscience and Remote Sensing Symposium. 21-25 July 2003. - Vol. 3. - P. 1493-1495. ↑

C5531. Ji Huibo. A modified apodization method in SAR/ISAR processing. / Ji Huibo, Wang Yiding, Wu Yirong, Hong Jan. // 2003. IGARSS '03. Proceedings. 2003 IEEE International Geoscience and Remote Sensing Symposium. 21-25 July 2003. - Vol. 6. - P. 3991-3994. ↑

C5532. Low A. Generation of geometrically and radiometrically terrain corrected ScanSAR images. / Low A., Mauser W. // 2003. IGARSS '03. Proceedings. 2003 IEEE International Geoscience and Remote Sensing Symposium. 21-25 July 2003. - Vol. 6. - P. 3995-3997. ↑

C5533. Malladi R.K. Speckle filtering of SAR images using Hülder regularity analysis of the sparse code. / Malladi R.K., Kasilingam D., Costa A.H. // 2003. IGARSS '03. Proceedings. 2003 IEEE International Geoscience and Remote Sensing Symposium. 21-25 July 2003. - Vol. 6. - P. 3998-4000. ↑

C5534. Xinwu Li. Extraction of vegetation parameters based on simulated annealing algorithm using polarimetric SAR interferometry data. / Xinwu Li, Huadong Guo, Jingjuan Liao, Zhen Li, Changlin Wang. // 2003. IGARSS '03. Proceedings. 2003 IEEE International Geoscience and Remote Sensing Symposium. 21-25 July 2003. - Vol. 6. - P. 3982-3984. ↑

C5535. Aresu E. Impact of ScanSAR images' radiometric calibration on vessels and identification. / Aresu E., Schwartz G. // 2003. IGARSS '03. Proceedings. 2003 IEEE International Geoscience and Remote Sensing Symposium. 21-25 July 2003. - Vol. 6. - P. 3985-3987. ↑

C5536. Fukuda S. Simulation study of stochastic dark line features in in correlated K-distributed images. / Fukuda S., Nakaichi Y., Hirose H. // 2003. IGARSS '03. Proceedings. 2003 IEEE International Geoscience and Remote Sensing Symposium. 21-25 July 2003. - Vol. 6. - P. 3988-3990. ↑

C5537. Morales-Mendoza L.J. Enhanced zone detection in radar images via fusing the maximum entropy and variational analysis methods. / Morales-Mendoza L.J., Shkvarko Y.V., Vazquez-Bautista R.F. // 2003. IGARSS '03. Proceedings. 2003 IEEE International Geoscience and Remote Sensing Symposium. 21-25 July 2003. - Vol. 6. - P. 4001-4003. ↑

C5538. Sakamoto T. An estimation method of target location and scattered waveforms for UWB pulse radar systems. / Sakamoto T., Sato T. // 2003. IGARSS '03. Proceedings. 2003 IEEE International Geoscience and Remote Sensing Symposium. 21-25 July 2003. - Vol. 6. - P. 4013-4015. ↑

C5539. Steckler C. Using radarsat to detect and monitor stationary fishing gear and aquaculture gear on the eastern Gulf of Thailand. / Steckler C., Niemann K.O., Flaherty M.S. // 2003. IGARSS '03. Proceedings. 2003 IEEE International Geoscience and Remote Sensing Symposium. 21-25 July 2003. - Vol. 6. - P. 4016-4018. ↑

C5540. Qulin Tan. All direction auto-adaptive dynamic window filter for noise suppression in SLC SAR image. / Qulin Tan, Yun Shao, Songlin Yang, Qingzhao Wei. // 2003. IGARSS '03. Proceedings. 2003 IEEE International Geoscience and Remote Sensing Symposium. 21-25 July 2003. - Vol. 6. - P. 4019-4021. ↑

C5541. Oller G. Edge detection and extraction for SAR images. / Oller G., Marthon P., Rognant L. // 2003. IGARSS '03. Proceedings. 2003 IEEE International Geoscience and Remote Sensing Symposium. 21-25 July 2003. - Vol. 6. - P. 4004-4006. ↑

C5542. Yiming Pi. Airport detection and runway recognition in SAR images. / Yiming Pi, Luhong Fan, Xiaobo Yang. // 2003. IGARSS '03. Proceedings. 2003 IEEE International Geoscience and Remote Sensing Symposium. 21-25 July 2003. - Vol. 6. - P. 4007-4009. ↑

C5543. Pierce L. Texture estimation in SAR images of forests. / Pierce L., Pan Liang, Dobson M.C. // 2003. IGARSS '03. Proceedings. 2003 IEEE International Geoscience and Remote Sensing Symposium. 21-25 July 2003. - Vol. 6. - P. 4010-4012. ↑

C5544. Colin E. A new parameter for IFPOL coherence optimization methods. / Colin E., Titin-Schnaider C., Tabbara W. // 2003. IGARSS '03. Proceedings. 2003 IEEE International Geoscience and Remote Sensing Symposium. 21-25 July 2003. - Vol. 6. - P. 3979-3981. ↑

C5545. Sadjadi F.A. A philosophical discussion of the physical limits of radar. 2003. IGARSS '03. Proceedings.

2003 IEEE International Geoscience and Remote Sensing Symposium. 21-25 July 2003. - Vol. 6. - P. 3857-3859. ↑

C5546. Yanjuan Yao. Leaf area index inversion using multiangular and multispectral data sets. / Yanjuan Yao, Guangjian Yan, Jindi Wang, Peijuan Wang, Yonghua Qu, Kaiguang Zhao. // 2003. IGARSS '03. Proceedings. 2003 IEEE International Geoscience and Remote Sensing Symposium. 21-25 July 2003. - Vol. 6. - P. 3869-3871. ↑

C5547. Baronti S. Spectral and radiometric distortion evaluation of pan-sharpened XS imagery obtained from compressed XS and pan data. / Baronti S., Aiazzi B., Alparone L., Santurri L., Selva M. // 2003. IGARSS '03. Proceedings. 2003 IEEE International Geoscience and Remote Sensing Symposium. 21-25 July 2003. - Vol. 6. - P. 3890-3892. ↑

C5548. Ferraiuolo G. Unsupervised Bayesian reconstruction of microwave images from real data. / Ferraiuolo G., Pascasio V., Ronza V. // 2003. IGARSS '03. Proceedings. 2003 IEEE International Geoscience and Remote Sensing Symposium. 21-25 July 2003. - Vol. 6. - P. 3842-3844. ↑

C5549. Liseno A. Linear distribution-based retrieval of underground voids. / Liseno A., Colella N., Pierri R., Soldovieri F. // 2003. IGARSS '03. Proceedings. 2003 IEEE International Geoscience and Remote Sensing Symposium. 21-25 July 2003. - Vol. 6. - P. 3848-3850. ↑

C5550. Migliaccio M. TSVD spatial resolution enhancement of microwave radiometer data: a sensitivity study. / Migliaccio M., Gambardella A. // 2003. IGARSS '03. Proceedings. 2003 IEEE International Geoscience and Remote Sensing Symposium. 21-25 July 2003. - Vol. 6. - P. 3854-3856. ↑

C5551. Wu Fan. Fusion of airborne synthetic aperture radiometer and Landsat ETM+ images. / Wu Fan, Wang Chao, Zhang Weiguo, Zhang Hong, Wu Ji, Liu Hao. // 2003. IGARSS '03. Proceedings. 2003 IEEE International Geoscience and Remote Sensing Symposium. 21-25 July 2003. - Vol. 6. - P. 3899-3901. ↑

C5552. Zhang Zhaohui. Water body extraction from multi-source satellite images. / Zhang Zhaohui, Prinett V., Ma Songde. // 2003. IGARSS '03. Proceedings. 2003 IEEE International Geoscience and Remote Sensing Symposium. 21-25 July 2003. - Vol. 6. - P. 3970-3972. ↑

C5553. Liu Xiuqing. Improvement research on texture-detection in full-polarization SAR image filter. / Liu Xiuqing, Yang Zhen, Yang Ruliang. // 2003. IGARSS '03. Proceedings. 2003 IEEE International Geoscience and Remote Sensing Symposium. 21-25 July 2003. - Vol. 6. - P. 3973-3975. ↑

C5554. Pellizzeri T.M. Polarimetric SAR image processing: Wishart vs. "H/A/alpha" segmentation and classification schemes. / Pellizzeri T.M., Lombardo P.L., Ferriero P. // 2003. IGARSS '03. Proceedings. 2003 IEEE International Geoscience and Remote Sensing Symposium. 21-25 July 2003. - Vol. 6. - P. 3976-3978. ↑

C5555. Chambenoit Y. Performance assessment of multitemporal SAR images' visual interpretation. / Chambenoit Y., Classeau N., Trouve E., Rudant J.-P. // 2003. IGARSS '03. Proceedings. 2003 IEEE International Geoscience and Remote Sensing Symposium. 21-25 July 2003. - Vol. 6. - P. 3911-3913. ↑

C5556. Maire C. SAR DEM filtering by mean of Bayesian and multi-scale, nonstationary methods. / Maire C., Datcu M., Audenino P. // 2003. IGARSS '03. Proceedings. 2003 IEEE International Geoscience and Remote Sensing Symposium. 21-25 July 2003. - Vol. 6. - P. 3916-3918. ↑

C5557. Jing Tang. Extraction of momentum flux of monochromatic gravity waves using spectroscopic imaging. / Jing Tang, Kamalabadi F., Liu A.Z., Swenson G.R. // 2003. IGARSS '03. Proceedings. 2003 IEEE International Geoscience and Remote Sensing Symposium. 21-25 July 2003. - Vol. 6. - P. 3961-3963. ↑

C5558. Ulfarsson M.O. Wavelet footprints for speckle reduction of SAR images. / Ulfarsson M.O., Sveinsson J.R., Benediktsson J.A. // 2003. IGARSS '03. Proceedings. 2003 IEEE International Geoscience and Remote Sensing Symposium. 21-25 July 2003. - Vol. 6. - P. 4092-4094. ↑

C5559. Zheng Mingjie. A novel multi-channel SAR moving targets detection and image method. / Zheng Mingjie, Yang Ruliang. // 2003. IGARSS '03. Proceedings. 2003 IEEE International Geoscience and Remote Sensing Symposium. 21-25 July 2003. - Vol. 6. - P. 4095-4097. ↑

C5560. Daiyin Zhu. Operation and processing for scan mode patch-mapping SAR. / Daiyin Zhu, Zhaoda Zhu,

Shaohua Ye, Kunhui Zhang. // 2003. IGARSS '03. Proceedings. 2003 IEEE International Geoscience and Remote Sensing Symposium. 21-25 July 2003. - Vol. 6. - P. 4098-4100. ↑

C5561. Saevarsson B.B. Speckle reduction of SAR images using adaptive curvelet domain. / Saevarsson B.B., Sveinsson J.R., Benediktsson J.A. // 2003. IGARSS '03. Proceedings. 2003 IEEE International Geoscience and Remote Sensing Symposium. 21-25 July 2003. - Vol. 6. - P. 4083-4085. ↑

C5562. Sanz J. Platform and mode independent SAR data processor based on the extended chirp scaling algorithm. / Sanz J., Prats P., Mallorqui J.J. // 2003. IGARSS '03. Proceedings. 2003 IEEE International Geoscience and Remote Sensing Symposium. 21-25 July 2003. - Vol. 6. - P. 4086-4088. ↑

C5563. Subiza B. An approach to SAR imaging by means of non-uniform FFTs. / Subiza B., Gimeno-Nieves E., Lopez-Sanchez J.M., Fortuny-Guasch J. // 2003. IGARSS '03. Proceedings. 2003 IEEE International Geoscience and Remote Sensing Symposium. 21-25 July 2003. - Vol. 6. - P. 4089-4091. ↑

C5564. Inglada J. Change detection on SAR images by using a parametric estimation of the Kullback-Leibler divergence. 2003. IGARSS '03. Proceedings. 2003 IEEE International Geoscience and Remote Sensing Symposium. 21-25 July 2003. - Vol. 6. - P. 4104-4106. ↑

C5565. Kodera N. A source estimation method to locate anomalous electromagnetic source in ELF band with global noise separation by ICA. / Kodera N., Takumi I., Hata M., Yasukawa H. // 2003. IGARSS '03. Proceedings. 2003 IEEE International Geoscience and Remote Sensing Symposium. 21-25 July 2003. - Vol. 7. - P. 4129-4131. ↑

C5566. Murakami S. Study on analysis of EM radiation source based on eigenvector. / Murakami S., Takumi I., Hata M., Yasukawa H. // 2003. IGARSS '03. Proceedings. 2003 IEEE International Geoscience and Remote Sensing Symposium. 21-25 July 2003. - Vol. 7. - P. 4132-4134. ↑

C5567. Saito M. Study on locating simulation of EM radiation source and transfer characteristic in ELF electromagnetic field. / Saito M., Yasukawa H. // 2003. IGARSS '03. Proceedings. 2003 IEEE International Geoscience and Remote Sensing Symposium. 21-25 July 2003. - Vol. 7. - P. 4135-4137. ↑

C5568. Karszenbaum H. A SAR time series analysis toolbox for extracting fire affected areas in wetlands. / Karszenbaum H., Tiffenberg J., Grings F., Martinez J.M., Kandus P., Pratolongo P. // 2003. IGARSS '03. Proceedings. 2003 IEEE International Geoscience and Remote Sensing Symposium. 21-25 July 2003. - Vol. 6. - P. 4107-4109. ↑

C5569. Kidd R.A. The development of a processing environment for time-series analysis of SeaWinds scatterometer data. / Kidd R.A., Trommler M., Wagner W. // 2003. IGARSS '03. Proceedings. 2003 IEEE International Geoscience and Remote Sensing Symposium. 21-25 July 2003. - Vol. 6. - P. 4110-4112. ↑

C5570. Lindenbergh R. Eolian deformation detection and modeling using airborne laser altimetry. / Lindenbergh R., Hanssen R. // 2003. IGARSS '03. Proceedings. 2003 IEEE International Geoscience and Remote Sensing Symposium. 21-25 July 2003. - Vol. 6. - P. 4113-4116. ↑

C5571. Quartulli M. Stochastic modelling for structure reconstruction from high-resolution SAR data. / Quartulli M., Datcu M. // 2003. IGARSS '03. Proceedings. 2003 IEEE International Geoscience and Remote Sensing Symposium. 21-25 July 2003. - Vol. 6. - P. 4080-4082. ↑

C5572. Becker J.-M. Linear structures' detection on SAR multi-temporal sets using the Polar Transform. / Becker J.-M., Coltuc D. // 2003. IGARSS '03. Proceedings. 2003 IEEE International Geoscience and Remote Sensing Symposium. 21-25 July 2003. - Vol. 6. - P. 4050-4052. ↑

C5573. Berens P. Extended range migration algorithm for squinted spotlight SAR. 2003. IGARSS '03. Proceedings. 2003 IEEE International Geoscience and Remote Sensing Symposium. 21-25 July 2003. - Vol. 6. - P. 4053-4055. ↑

C5574. Coltuc Daniela. A solution for linking the sparse aligned pixels in multi-temporal SAR sets. / Coltuc Daniela., Becker J.-M. // 2003. IGARSS '03. Proceedings. 2003 IEEE International Geoscience and Remote Sensing Symposium. 21-25 July 2003. - Vol. 6. - P. 4056-4058. ↑

C5575. Vidal-Pantaleoni A. Quality evaluation for efficient ScanSAR data processing algorithms. / Vidal-

Pantaleoni A., Ferrando M. // 2003. IGARSS '03. Proceedings. 2003 IEEE International Geoscience and Remote Sensing Symposium. 21-25 July 2003. - Vol. 6. - P. 4022-4024. ↑

C5576. Wessel B. The role of context for road extraction from SAR imagery. / Wessel B., Wiedemann C., Ebner H. // 2003. IGARSS '03. Proceedings. 2003 IEEE International Geoscience and Remote Sensing Symposium. 21-25 July 2003. - Vol. 6. - P. 4025-4027. ↑

C5577. Hua Xie. Mutual information based registration of SAR images. / Hua Xie, Pierce L.E., Ulaby F.T. // 2003. IGARSS '03. Proceedings. 2003 IEEE International Geoscience and Remote Sensing Symposium. 21-25 July 2003. - Vol. 6. - P. 4028-4031. ↑

C5578. Crespo J.C. Real time phase preserving SAR processor based on COTS architecture. / Crespo J.C., Gutierrez-Rios J. // 2003. IGARSS '03. Proceedings. 2003 IEEE International Geoscience and Remote Sensing Symposium. 21-25 July 2003. - Vol. 6. - P. 4059-4061. ↑

C5579. Hao Liu. Applying fractional Fourier transform to radar imaging of moving targets. / Hao Liu, Minhui Zhu. // 2003. IGARSS '03. Proceedings. 2003 IEEE International Geoscience and Remote Sensing Symposium. 21-25 July 2003. - Vol. 6. - P. 4071-4073. ↑

C5580. Meta A. High resolution airborne FM-CW SAR: digital signal processing aspects. / Meta A., Hoogeboom P. // 2003. IGARSS '03. Proceedings. 2003 IEEE International Geoscience and Remote Sensing Symposium. 21-25 July 2003. - Vol. 6. - P. 4074-4076. ↑

C5581. Mittermayer J. Analysis of range ambiguity suppression in SAR by up and down chirp modulation for point and distributed targets. / Mittermayer J., Martinez J.M. // 2003. IGARSS '03. Proceedings. 2003 IEEE International Geoscience and Remote Sensing Symposium. 21-25 July 2003. - Vol. 6. - P. 4077-4079. ↑

C5582. De Stefano M. Robust Doppler Centroid estimate for ERS and ENVISAT. / De Stefano M., Guarnieri A.M. // 2003. IGARSS '03. Proceedings. 2003 IEEE International Geoscience and Remote Sensing Symposium. 21-25 July 2003. - Vol. 6. - P. 4062-4064. ↑

C5583. Erbas C. SAR raw data aspects and focusing via high precision algorithms. 2003. IGARSS '03. Proceedings. 2003 IEEE International Geoscience and Remote Sensing Symposium. 21-25 July 2003. - Vol. 6. - P. 4065-4067. ↑

C5584. Fornaro G. Phase accuracy of motion compensated airborne SAR images. / Fornaro G., Sansosti E., Franceschetti G., Perna S. // 2003. IGARSS '03. Proceedings. 2003 IEEE International Geoscience and Remote Sensing Symposium. 21-25 July 2003. - Vol. 6. - P. 4068-4070. ↑

C5585. Rouveure R. A multi-layer feed-forward perceptron for microwave signals processing. / Rouveure R., Faure P., Monod M.-O. // 2003. IGARSS '03. Proceedings. 2003 IEEE International Geoscience and Remote Sensing Symposium. 21-25 July 2003. - Vol. 6. - P. 3519-3521. ↑

C5586. Stilla U. Perceptual grouping of regular structures for automatic detection of man-made objects. / Stilla U., Michaelsen E., Soergel U., Schulz K. // 2003. IGARSS '03. Proceedings. 2003 IEEE International Geoscience and Remote Sensing Symposium. 21-25 July 2003. - Vol. 6. - P. 3525-3527. ↑

C5587. Disney M.I. Modelling the radiometric response of a dynamic, 3D structural model of Scots pine in the optical and microwave domains. / Disney M.I., Saich P., Lewis P. // 2003. IGARSS '03. Proceedings. 2003 IEEE International Geoscience and Remote Sensing Symposium. 21-25 July 2003. - Vol. 6. - P. 3537-3539. ↑

C5588. Kasapoglu N.G. Hierarchical decision tree classification of SAR data with feature extraction method based on spatial variations. / Kasapoglu N.G., Yazgan B., Akleman F. // 2003. IGARSS '03. Proceedings. 2003 IEEE International Geoscience and Remote Sensing Symposium. 21-25 July 2003. - Vol. 6. - P. 3453-3455. ↑

C5589. Kelldorfer J.M. Forest biomass inversion from SAR using object oriented image analysis techniques. / Kelldorfer J.M., Ulaby F.T. // 2003. IGARSS '03. Proceedings. 2003 IEEE International Geoscience and Remote Sensing Symposium. 21-25 July 2003. - Vol. 6. - P. 3465-3467. ↑

C5590. Mercier G. Multiscale oil slick segmentation with Markov chain model. / Mercier G., Derrode S., Pieczynski W., Le Caillec J.-M., Garelo R. // 2003. IGARSS '03. Proceedings. 2003 IEEE International Geoscience and Remote Sensing Symposium. 21-25 July 2003. - Vol. 6. - P. 3501-3503. ↑

C5591. Gade M. Two-dimensional sea surface current fields derived from multi-sensor satellite data. / Gade M., Fiedler G., Dreschler-Fischer L. // 2003. IGARSS '03. Proceedings. 2003 IEEE International Geoscience and Remote Sensing Symposium. 21-25 July 2003. - Vol. 6. - P. 3540-3542. ↑

C5592. Hubbert J.C. Range-velocity mitigation via SZ phase coding for NEXRAD WSR-88D radars. / Hubbert J.C., Meymaris G., Keeler R.J. // 2003. IGARSS '03. Proceedings. 2003 IEEE International Geoscience and Remote Sensing Symposium. 21-25 July 2003. - Vol. 6. - P. 3610-3612. ↑

C5593. Nies H. Orbit estimation of the interferometric cartwheel using an extended linearized Kalman filter. / Nies H., Loffeld O., Gebhardt U., Peters V. // 2003. IGARSS '03. Proceedings. 2003 IEEE International Geoscience and Remote Sensing Symposium. 21-25 July 2003. - Vol. 6. - P. 3616-3619. ↑

C5594. Bogdanov A.V. Multiple classifier system based on attractor dynamics. / Bogdanov A.V., Schoner G., Steinhage A., Sandven S. // 2003. IGARSS '03. Proceedings. 2003 IEEE International Geoscience and Remote Sensing Symposium. 21-25 July 2003. - Vol. 6. - P. 3635-3637. ↑

C5595. Lewis P. Modelling the radiometric response of a dynamic, 3D structural model of wheat in the optical and microwave domains. / Lewis P., Saich P., Disney M., Andrieu B., Fournier C., Ljutovac S. // 2003. IGARSS '03. Proceedings. 2003 IEEE International Geoscience and Remote Sensing Symposium. 21-25 July 2003. - Vol. 6. - P. 3543-3545. ↑

C5596. Saich P. Biophysical parameter retrieval from forest and crop canopies in the optical and microwave domains using 3D models of canopy structure. / Saich P., Lewis P., Disney M.I. // 2003. IGARSS '03. Proceedings. 2003 IEEE International Geoscience and Remote Sensing Symposium. 21-25 July 2003. - Vol. 6. - P. 3546-3548. ↑

C5597. Zakharova L. Classification of surface covers by combining optical and microwave data for Baikal Lake region. / Zakharova L., Zakharov A., Darizhapov D., Schmullius C. // 2003. IGARSS '03. Proceedings. 2003 IEEE International Geoscience and Remote Sensing Symposium. 21-25 July 2003. - Vol. 6. - P. 3549-3551. ↑

C5598. Karvonen J. Feature detection from preprocessed sea ice SAR data based on higher-order statistics. 2003. IGARSS '03. Proceedings. 2003 IEEE International Geoscience and Remote Sensing Symposium. 21-25 July 2003. - Vol. 6. - P. 3450-3452. ↑

C5599. Beisl C.H. Assessment of environmental sensitivity index of flooding areas in western Amazonia using fuzzy logic in the dual season GRFM JERS-1 SAR image mosaics. / Beisl C.H., de Miranda F.P., Evsukoff A.G., Pedroso E.C. // 2003. IGARSS '03. Proceedings. 2003 IEEE International Geoscience and Remote Sensing Symposium. 2003. - Vol. 5. - P. 3228-3230. ↑

C5600. Csaplovics E. Environmental monitoring of tropical wetlands in semi-arid Sub-Saharan Africa-what about remote sensing?. 2003. IGARSS '03. Proceedings. 2003 IEEE International Geoscience and Remote Sensing Symposium. 2003. - Vol. 5. - P. 3231-3233. ↑

C5601. de Carvalho O.A. Jr. Spectral mixture analysis of ASTER image in Brazilian Savanna. / de Carvalho O.A. Jr., Bloise C.P.L., de Carvalho A.P.F., Guimaraes R.F., de Souza Martins E. // 2003. IGARSS '03. Proceedings. 2003 IEEE International Geoscience and Remote Sensing Symposium. 2003. - Vol. 5. - P. 3234-3236. ↑

C5602. Schwartz A. Mesoscale modeling investigation using PENNSYLVANIA/NCAR MM5 model and remote sensing technology for weather simulation and prediction. / Schwartz A., Vatti M., Remata Reddy S. // 2003. IGARSS '03. Proceedings. 2003 IEEE International Geoscience and Remote Sensing Symposium. 2003. - Vol. 5. - P. 3187-3189. ↑

C5603. Chaabane F. Correction of local and global tropospheric effects on differential SAR interferograms for the study of earthquake phenomena. / Chaabane F., Avallone A., Tupin F., Briole P., Maitre H. // 2003. IGARSS '03. Proceedings. 2003 IEEE International Geoscience and Remote Sensing Symposium. 2003. - Vol. 5. - P. 3199-3201. ↑

C5604. Hirata Y. The extraction of canopy-understory vegetation-topography structure using helicopter-borne LIDAR measurement between a plantation and a broad-leaved forest. / Hirata Y., Sato K., Sakai A., Kuramoto S., Akiyama Y. // 2003. IGARSS '03. Proceedings. 2003 IEEE International Geoscience and Remote Sensing Symposium. 2003. - Vol. 5. - P. 3222-3224. ↑

- C5605.** Zhifeng Guo. A three-dimensional radar backscatter model for larch forest using L-system. / Zhifeng Guo, Guoqing Sun, Zhongjun Zhang. // 2003. IGARSS '03. Proceedings. 2003 IEEE International Geoscience and Remote Sensing Symposium. 2003. - Vol. 5. - P. 3245-3247. ↑
- C5606.** Yan Fuli. Determination of the displacements along the Maergaichaka fault, using remote sensing data, Tibet, China. / Yan Fuli, Lu Huaifu, Yang Hu, Li Zhen, Fan Xiangtao, Shao Yun, Li Xinwu. // 2003. IGARSS '03. Proceedings. 2003 IEEE International Geoscience and Remote Sensing Symposium. 2003. - Vol. 5. - P. 3332-3334. ↑
- C5607.** Shutko A. Examples of data collected from "PRIRODA-MIR" Space Station by microwave radiometers, optical and infrared sensors over the territory of Africa. / Shutko A., Marechek S., Nazarov L., Tishchenko Y., Sidorenko A., Kutuza B., Chukhlantsev A., Golovachev S., Novichikhin E., Haldin A., Coleman T.L., Archer F. // 2003. IGARSS '03. Proceedings. 2003 IEEE International Geoscience and Remote Sensing Symposium. 2003. - Vol. 5. - P. 3368-3370. ↑
- C5608.** Escalante-Ramirez B. SAR-image classification with a directional-oriented discrete Hermite transform and Markov random fields. / Escalante-Ramirez B., Lopez-Quiroz P., Silvan-Cardenas J.L. // 2003. IGARSS '03. Proceedings. 2003 IEEE International Geoscience and Remote Sensing Symposium. 21-25 July 2003. - Vol. 6. - P. 3423-3425. ↑
- C5609.** Morrison K. Towards a quantitative understanding of the effects of wind motion on airborne and satellite SAR imagery of vegetation. 2003. IGARSS '03. Proceedings. 2003 IEEE International Geoscience and Remote Sensing Symposium. 2003. - Vol. 5. - P. 3281-3283. ↑
- C5610.** Abouma-Simba S. Combination of SAR, SPOT, and geophysical data for geological mapping: the Nyanga Basin (SW Gabon) example. / Abouma-Simba S., Deroin J.P., Regnault J.M. // 2003. IGARSS '03. Proceedings. 2003 IEEE International Geoscience and Remote Sensing Symposium. 2003. - Vol. 5. - P. 3314-3316. ↑
- C5611.** Catani F. The contribution of spaceborne SAR interferometry to geomorphological analyses. / Catani F., Farina P., Moretti S., Nico G. // 2003. IGARSS '03. Proceedings. 2003 IEEE International Geoscience and Remote Sensing Symposium. 2003. - Vol. 5. - P. 3323-3325. ↑
- C5612.** Huot E. Landslide tracking with a curve evolution model driven by interferometric data. / Huot E., Yahia H., Herlin I. // 2003. IGARSS '03. Proceedings. 2003 IEEE International Geoscience and Remote Sensing Symposium. 21-25 July 2003. - Vol. 6. - P. 3802-3804. ↑
- C5613.** Knedlik S. Sensitivity of DEMs generated from interferometric cartwheel configurations. / Knedlik S., Loffeld O., Nies H. // 2003. IGARSS '03. Proceedings. 2003 IEEE International Geoscience and Remote Sensing Symposium. 21-25 July 2003. - Vol. 6. - P. 3805-3807. ↑
- C5614.** Kohlhasse A.O. Estimating orbital trajectories from fringe gradients in SAR interferograms for measuring crustal strain. / Kohlhasse A.O., Feigl K.L., Massonnet D., Ferretti A. // 2003. IGARSS '03. Proceedings. 2003 IEEE International Geoscience and Remote Sensing Symposium. 21-25 July 2003. - Vol. 6. - P. 3808-3810. ↑
- C5615.** Kouame J.L. Evaluation of the potential of radar ENVISAT data for the updating of numerical thematic maps on the coastal fringe of French Guyana. / Kouame J.L., Classeau N., Rudant J.-P., Trebossen H. // 2003. IGARSS '03. Proceedings. 2003 IEEE International Geoscience and Remote Sensing Symposium. 21-25 July 2003. - Vol. 6. - P. 3718-3720. ↑
- C5616.** Guoqing Zhou. US National Large-scale City orthoimage standard initiative. / Guoqing Zhou, Changqing Song, Susan Benjamin, Schickler W. // 2003. IGARSS '03. Proceedings. 2003 IEEE International Geoscience and Remote Sensing Symposium. 21-25 July 2003. - Vol. 6. - P. 3739-3741. ↑
- C5617.** Abdelfattah R. InSAR coherence optimisation using second kind statistics. / Abdelfattah R., Nicolas J.M. // 2003. IGARSS '03. Proceedings. 2003 IEEE International Geoscience and Remote Sensing Symposium. 21-25 July 2003. - Vol. 6. - P. 3799-3801. ↑
- C5618.** Moisseev D. Influence of hydrometeors on InSAR observations. / Moisseev D., Hanssen R. // 2003. IGARSS '03. Proceedings. 2003 IEEE International Geoscience and Remote Sensing Symposium. 21-25 July 2003. - Vol. 6. - P. 3811-3814. ↑

- C5619.** Kun Ren. Simulation of interferogram image for spaceborne SAR system. / Kun Ren, Prinnet V., Xiangquan Shi, Gang Wu. // 2003. IGARSS '03. Proceedings. 2003 IEEE International Geoscience and Remote Sensing Symposium. 21-25 July 2003. - Vol. 6. - P. 3824-3826. ↑
- C5620.** Jing-Fa Zhang. The research of difference interferometric SAR technique. / Jing-Fa Zhang, Qiming Qin. // 2003. IGARSS '03. Proceedings. 2003 IEEE International Geoscience and Remote Sensing Symposium. 21-25 July 2003. - Vol. 6. - P. 3827-3829. ↑
- C5621.** Bennaceur L. Retrieval of multi-scale roughness parameters and soil moisture by numerical inversion. / Bennaceur L., Boussema M.R., Belhadj Z. // 2003. IGARSS '03. Proceedings. 2003 IEEE International Geoscience and Remote Sensing Symposium. 21-25 July 2003. - Vol. 6. - P. 3836-3838. ↑
- C5622.** Pascazio V. Performance assessment of multi-frequency SAR interferometry based on statistical estimation. / Pascazio V., Schirinzi G. // 2003. IGARSS '03. Proceedings. 2003 IEEE International Geoscience and Remote Sensing Symposium. 21-25 July 2003. - Vol. 6. - P. 3815-3817. ↑
- C5623.** Peng Hailiang. Comparative study of InSAR topography reconstruction algorithms based on look vector's orthogonal decomposition. / Peng Hailiang, Wang Yanping. // 2003. IGARSS '03. Proceedings. 2003 IEEE International Geoscience and Remote Sensing Symposium. 21-25 July 2003. - Vol. 6. - P. 3818-3820. ↑
- C5624.** Kun Ren. Comparison of satellite baseline estimation methods for interferometry applications. / Kun Ren, Prinnet V., Xiangquan Shi, Feng Wang. // 2003. IGARSS '03. Proceedings. 2003 IEEE International Geoscience and Remote Sensing Symposium. 21-25 July 2003. - Vol. 6. - P. 3821-3823. ↑
- C5625.** Min-Sil Yang. Decision level fusion of multi-frequency polarimetric SAR and optical data with Dempster-Shafer evidence theory. / Min-Sil Yang, Moon W.M. // 2003. IGARSS '03. Proceedings. 2003 IEEE International Geoscience and Remote Sensing Symposium. 21-25 July 2003. - Vol. 6. - P. 3668-3670. ↑
- C5626.** Richards J. Information and understanding: analysis of remotely sensed data. 2003 IEEE Workshop on Advances in Techniques for Analysis of Remotely Sensed Data. 27-28 Oct. 2003. - P. 1-9. ↑
- C5627.** Xue Liu. Combining MISR, ETM+ and SAR data to improve land cover and land use classification for carbon cycle research. / Xue Liu, Kafatos M., Gomez R.B., Goetz S.J. // 2003 IEEE Workshop on Advances in Techniques for Analysis of Remotely Sensed Data. 27-28 Oct. 2003. - P. 80-85. ↑
- C5628.** Chiarella M. Multisensor image fusion and mining: from neural systems to COTS software with application to remote sensing AFE. / Chiarella M., Fay D.A., Waxman A.M., Ivey R.T., Bomberger N. // 2003 IEEE Workshop on Advances in Techniques for Analysis of Remotely Sensed Data. 27-28 Oct. 2003. - P. 100-107. ↑
- C5629.** Farah I.R. Multispectral satellite image analysis based on the method of blind separation and fusion of sources. / Farah I.R., Ahmed M.B., Boussema M.R. // 2003. IGARSS '03. Proceedings. 2003 IEEE International Geoscience and Remote Sensing Symposium. 21-25 July 2003. - Vol. 6. - P. 3638-3640. ↑
- C5630.** Onana V.P. Change detection in urban context with multitemporal ERS-SAR images by using data fusion approach. / Onana V.P., Trouve E., Mauris G., Rudant J.P., Frison P.L. // 2003. IGARSS '03. Proceedings. 2003 IEEE International Geoscience and Remote Sensing Symposium. 21-25 July 2003. - Vol. 6. - P. 3650-3652. ↑
- C5631.** Flora P. RADARSAT-1 and LANDSAT7 ETM+ integration for kimberlite exploration in the Buffalo Head Hills area, northern central Alberta. 2003. IGARSS '03. Proceedings. 2003 IEEE International Geoscience and Remote Sensing Symposium. 21-25 July 2003. - Vol. 6. - P. 3653-3655. ↑
- C5632.** Kersten P.R. Classification of polarimetric synthetic aperture radar images using fuzzy clustering. / Kersten P.R., Lee J.S., Ainsworth T.L., Grunes M.R. // 2003 IEEE Workshop on Advances in Techniques for Analysis of Remotely Sensed Data. 27-28 Oct. 2003. - P. 150-156. ↑
- C5633.** Boehm C. Analysis of high resolution polarimetric SAR in urban areas. / Boehm C., Schenkel R. // 2003 IEEE Workshop on Advances in Techniques for Analysis of Remotely Sensed Data. 27-28 Oct. 2003. - P. 315-319. ↑
- C5634.** Rokhmatuloh. Study on the spectral quality preservation derived from multisensor image fusion

techniques between JERS-1 SAR and Landsat TM data. / Rokhmatuloh, Tateishi R., Wikantika K., Munadi K., Aslam M. // 2003. IGARSS '03. Proceedings. 2003 IEEE International Geoscience and Remote Sensing Symposium. 21-25 July 2003. - Vol. 6. - P. 3656-3658. ↑

C5635. Soergel U. Determination of optimal SAR illumination aspects in build-up areas. / Soergel U., Schulz K., Thoennessen U., Stilla U. // 2003. IGARSS '03. Proceedings. 2003 IEEE International Geoscience and Remote Sensing Symposium. 21-25 July 2003. - Vol. 6. - P. 3662-3664. ↑

C5636. Lampropoulos G.A. Automatic registration of electro-optical and SAR images. / Lampropoulos G.A., Chan J., Secker J., Li Y., Jouan A. // 2003 IEEE Workshop on Advances in Techniques for Analysis of Remotely Sensed Data. 27-28 Oct. 2003. - P. 219-226. ↑

C5637. Sanghun Lim. Hydrometeor classification system using dual-polarization radar measurements. / Sanghun Lim, Chandrasekar V. // 2003 IEEE Workshop on Advances in Techniques for Analysis of Remotely Sensed Data. 27-28 Oct. 2003. - P. 227-236. ↑

C5638. Dell'Acqua F. Discriminating urban environments using multi-scale texture and multiple SAR images. / Dell'Acqua F., Gamba P. // 2003 IEEE Workshop on Advances in Techniques for Analysis of Remotely Sensed Data. 27-28 Oct. 2003. - P. 308-314. ↑

C5639. Garrison J.L. Anisotropy in reflected GPS measurements of ocean winds. 2003. IGARSS '03. Proceedings. 2003 IEEE International Geoscience and Remote Sensing Symposium. 21-25 July 2003. - Vol. 7. - P. 4480-4482. ↑

C5640. Fujita M. Experimental study of a polarization-rotating Van Atta array with reduced co-polarized radar cross-section. / Fujita M., Murakami C. // 2003. IGARSS '03. Proceedings. 2003 IEEE International Geoscience and Remote Sensing Symposium. 21-25 July 2003. - Vol. 7. - P. 4503-4505. ↑

C5641. Fujita M. Reflection characteristics of a retrodirective PARC. / Fujita M., Nakamura S., Murakami C. // 2003. IGARSS '03. Proceedings. 2003 IEEE International Geoscience and Remote Sensing Symposium. 21-25 July 2003. - Vol. 7. - P. 4506-4508. ↑

C5642. Muhtar Qong. An unsupervised classification method for polarimetric SAR images with a projection approach. 2003. IGARSS '03. Proceedings. 2003 IEEE International Geoscience and Remote Sensing Symposium. 21-25 July 2003. - Vol. 7. - P. 4471-4473. ↑

C5643. Stacy N.J.S. The DSTO Ingara airborne X-Band SAR polarimetric upgrade: first results. / Stacy N.J.S., Badger D.P., Goh A.S., Preiss M., Williams M.L. // 2003. IGARSS '03. Proceedings. 2003 IEEE International Geoscience and Remote Sensing Symposium. 21-25 July 2003. - Vol. 7. - P. 4474-4476. ↑

C5644. Zhang Xiaoling. The analysis of interferometric SAR imaging precision in the distributed micro-satellite system. / Zhang Xiaoling, Zeng Bin, Huang Shunji. // 2003. IGARSS '03. Proceedings. 2003 IEEE International Geoscience and Remote Sensing Symposium. 21-25 July 2003. - Vol. 7. - P. 4477-4479. ↑

C5645. Schwerdt M. Calibration concept for the TerraSAR-X instrument. / Schwerdt M., Hounam D., Stangl M. // 2003. IGARSS '03. Proceedings. 2003 IEEE International Geoscience and Remote Sensing Symposium. 21-25 July 2003. - Vol. 7. - P. 4509-4511. ↑

C5646. Robinson D.Q. CALIPSO and CloudSat missions offer student opportunities in atmospheric research, remote sensing, and data comparisons globally. / Robinson D.Q., Krumm D., Kozusko F., Maggi B.H. // 2003. IGARSS '03. Proceedings. 2003 IEEE International Geoscience and Remote Sensing Symposium. 21-25 July 2003. - Vol. 7. - P. 4531-4533. ↑

C5647. Rommen B. Earth observation instrument frequencies: a valuable resource to protect. 2003. IGARSS '03. Proceedings. 2003 IEEE International Geoscience and Remote Sensing Symposium. 21-25 July 2003. - Vol. 7. - P. 4543-4545. ↑

C5648. Braaten D. Outreach activities of the Polar Radar for Ice Sheet Measurement (PRISM) project. / Braaten D., Holvoet J., Bowen C., Koeppe M., Gogineni S. // 2003. IGARSS '03. Proceedings. 2003 IEEE International Geoscience and Remote Sensing Symposium. 21-25 July 2003. - Vol. 7. - P. 4585-4586. ↑

C5649. Wang Yanping. Locating calibrators in airborne InSAR calibration. / Wang Yanping, Peng Hailiang. //

2003. IGARSS '03. Proceedings. 2003 IEEE International Geoscience and Remote Sensing Symposium. 21-25 July 2003. - Vol. 7. - P. 4515-4517. ↑

C5650. Zakharov A.I. On the stability of large antennas as calibration targets. / Zakharov A.I., Zherdev P.A., Borisov M.M., Sokolov A.B., van't Klooster C.G.M. // 2003. IGARSS '03. Proceedings. 2003 IEEE International Geoscience and Remote Sensing Symposium. 21-25 July 2003. - Vol. 7. - P. 4518-4520. ↑

C5651. Xiaojian Xu. Impact of different correlation receiving techniques on the imaging performance of UWB random noise radar. / Xiaojian Xu, Narayanan R.M. // 2003. IGARSS '03. Proceedings. 2003 IEEE International Geoscience and Remote Sensing Symposium. 21-25 July 2003. - Vol. 7. - P. 4525-4527. ↑

C5652. Pairman D. Improved polarimetric SAR classification by application of terrain azimuth slope corrections. / Pairman D., McNeill S.J. // 2003. IGARSS '03. Proceedings. 2003 IEEE International Geoscience and Remote Sensing Symposium. 21-25 July 2003. - Vol. 7. - P. 4468-4470. ↑

C5653. Zakharov A.I. Comparison of multipolarization SAR systems depending on the way of the full scattering matrix measurements. 2003. IGARSS '03. Proceedings. 2003 IEEE International Geoscience and Remote Sensing Symposium. 21-25 July 2003. - Vol. 7. - P. 4419-4421. ↑

C5654. Chopping M. Validation of bidirectional reflectance models using the first scene acquired by the CHRIS sensor over the Jornada Experimental Range. / Chopping M., Lihong Su, Schmugge T., Rango A. // 2003. IGARSS '03. Proceedings. 2003 IEEE International Geoscience and Remote Sensing Symposium. 21-25 July 2003. - Vol. 7. - P. 4425-4427. ↑

C5655. Dangel S. Combined field and laboratory goniometer system-FIGOS and LAGOS. / Dangel S., Kneubuhler M., Kohler R., Schaepman M., Schopfer J., Schaepman-Strub G., Itten K. // 2003. IGARSS '03. Proceedings. 2003 IEEE International Geoscience and Remote Sensing Symposium. 21-25 July 2003. - Vol. 7. - P. 4428-4430. ↑

C5656. Thuy Vu T. Wavelet-based system for classification of airborne laser scanner data. / Thuy Vu T., Yokoyama R., Yamazaki F., Tokunaga M. // 2003. IGARSS '03. Proceedings. 2003 IEEE International Geoscience and Remote Sensing Symposium. 21-25 July 2003. - Vol. 7. - P. 4404-4406. ↑

C5657. Wang X. Cabannes versus Rayleigh scattering and terrestrial backscatter ratio revisited in LITE in support of CALIPSO. / Wang X., Reagan J.A., Dobler J., Rubio M. // 2003. IGARSS '03. Proceedings. 2003 IEEE International Geoscience and Remote Sensing Symposium. 21-25 July 2003. - Vol. 7. - P. 4407-4409. ↑

C5658. Shibayama M. Polarization characteristics of a mixed seeding pasture and its application for predicting the ratio of legumes. 2003. IGARSS '03. Proceedings. 2003 IEEE International Geoscience and Remote Sensing Symposium. 21-25 July 2003. - Vol. 7. - P. 4413-4415. ↑

C5659. Cerutti-Maori D.J.E. An approach to multistatic spaceborne SAR/MTI processing and performance analysis. / Cerutti-Maori D.J.E., Ender J.H.G. // 2003. IGARSS '03. Proceedings. 2003 IEEE International Geoscience and Remote Sensing Symposium. 21-25 July 2003. - Vol. 7. - P. 4446-4449. ↑

C5660. Margarit G. Orbital SAR simulator of fishing vessel polarimetric signatures based on high frequency electromagnetic calculations. / Margarit G., Blanco P., Sanz J., Mallorqui J.J. // 2003. IGARSS '03. Proceedings. 2003 IEEE International Geoscience and Remote Sensing Symposium. 21-25 July 2003. - Vol. 7. - P. 4459-4461. ↑

C5661. Nakagawa K. Development of a new C-band polarimetric Doppler weather radar in Japan. / Nakagawa K., Hanado H., Satoh S., Takahashi N., Iguchi T., Fukutani K. // 2003. IGARSS '03. Proceedings. 2003 IEEE International Geoscience and Remote Sensing Symposium. 21-25 July 2003. - Vol. 7. - P. 4462-4464. ↑

C5662. Ouchi K. Fully polarimetric classification accuracy. / Ouchi K., Davidson G., Saito G., Ishitsuka N., Mohri K., Uratsuka S. // 2003. IGARSS '03. Proceedings. 2003 IEEE International Geoscience and Remote Sensing Symposium. 21-25 July 2003. - Vol. 7. - P. 4465-4467. ↑

C5663. Rombach M. Newest technology of mapping by using airborne interferometric synthetic aperture radar systems. / Rombach M., Fernandes A.C., Luebeck D., Moreira J. // 2003. IGARSS '03. Proceedings. 2003 IEEE International Geoscience and Remote Sensing Symposium. 21-25 July 2003. - Vol. 7. - P. 4450-4452. ↑

- C5664.** Dong Qing. Targets classification of semi-arid region using polarimetric SAR data \$an example in Xinjiang, China. / Dong Qing, Guo Huadong, Li Zhen, Wang Changlin. // 2003. IGARSS '03. Proceedings. 2003 IEEE International Geoscience and Remote Sensing Symposium. 21-25 July 2003. - Vol. 7. - P. 4453-4455. ↑
- C5665.** Hubbert J.C. Utilization of the radar polarimetric covariance matrix for polarization error and precipitation canting angle estimation. / Hubbert J.C., Bringi V.N. // 2003. IGARSS '03. Proceedings. 2003 IEEE International Geoscience and Remote Sensing Symposium. 21-25 July 2003. - Vol. 7. - P. 4456-4458. ↑
- C5666.** Bibby D.J. A RF model of an active array antenna for a spaceborne SAR. / Bibby D.J., Knight A.J. // 2003. (ICAP 2003). Twelfth International Conference on (Conf. Publ. No. 491) Antennas and Propagation. 31 March-3 April 2003. - Vol. 2. - P. 703-706. ↑
- C5667.** Sengupta N. Humidity gradients derived from wind profiler radar and RASS in presence of elevated ducts. / Sengupta N., Lehmann V., Goersdorf U. // 2003. (ICAP 2003). Twelfth International Conference on (Conf. Publ. No. 491) Antennas and Propagation. 31 March-3 April 2003. - Vol. 2. - P. 670-673. ↑
- C5668.** Roullier-Callaghan A. A topological feature extraction system from lidar data with the application of radiowave propagation modelling. / Roullier-Callaghan A., Al-Nuaimi M., Kidner D. // 2003. (ICAP 2003). Twelfth International Conference on (Conf. Publ. No. 491) Antennas and Propagation. 31 March-3 April 2003. - Vol. 2. - P. 522-525. ↑
- C5669.** Aydemir M.E. A novel approach for synthetic aperture radar image processing based on Genetic Algorithm. / Aydemir M.E., Gunel T., Erer I., Kurnaz S. // 2003. RAST '03. International Conference on. Proceedings of Recent Advances in Space Technologies. 20-22 Nov. 2003. - P. 365-368. ↑
- C5670.** Yildirim I. A comparison of non-parametric spectral estimators for SAR imaging. / Yildirim I., Tezel N.S., Erer I., Yazgan B. // 2003. RAST '03. International Conference on. Proceedings of Recent Advances in Space Technologies. 20-22 Nov. 2003. - P. 369-374. ↑
- C5671.** Turk A.S. EMI and atmospheric noise measurements for determining HF bandwidth occupancy profile of East-Mediterranean Sea. / Turk A.S., Tasdelen I., Pelitci N., Bahadirlar Y. // 2003. EMC '03. 2003 IEEE International Symposium on Electromagnetic Compatibility. 11-16 May 2003. - Vol. 1. - P. 621-624. ↑
- C5672.** Thurai M. Melting layer model evaluation in Singapore. / Thurai M., Iguchi T., Goddard J., Ong J.T., Awaka J. // 2003. (ICAP 2003). Twelfth International Conference on (Conf. Publ. No. 491) Antennas and Propagation. 31 March-3 April 2003. - Vol. 1. - P. 357-360. ↑
- C5673.** Martirosyan A.E. Method for remote sensing of the atmosphere by using laser generated flashes. 2003. CLEO/Europe. 2003 Conference on Lasers and Electro-Optics Europe. 22-27 June 2003. - P. 501. ↑
- C5674.** Weibring P. Remote analysis of gas mixtures using an optical parametric oscillator based lidar system. / Weibring P., Abrahamsson C., Sjolholm M., Smith J.N., Edner H., Svanberg S. // 2003. CLEO/Europe. 2003 Conference on Lasers and Electro-Optics Europe. 22-27 June 2003. - P. 472. ↑
- C5675.** Singh U.N. Laser technology maturation and risk reduction for space-based remote sensing. / Singh U.N., Heaps W.S. // 2003. CLEO/Europe. 2003 Conference on Lasers and Electro-Optics Europe. 22-27 June 2003. - P. 67. ↑
- C5676.** Pogutsa C. Studying of the modeling optimum methods of random processes and fields. 2003. SIBCON 2003. The IEEE-Siberian Conference on Control and Communications. 1-2 Oct. 2003. - P. 84-86. ↑
- C5677.** Muramoto K. Z-R relationship for individual snowfall and its evaluation. / Muramoto K., Ebisu S., Servomaa H., Kubo M., Shiina T. // SICE 2003 Annual Conference. - Fukui, Japan, 4-6 Aug. 2003. - Vol. 2. - P. 1715-1718. ↑
- C5678.** Boric-Lubecke O. Wireless LAN PC card sensing of vital signs. / Boric-Lubecke O., Awater G., Lubecke V.M. // 2003. IEEE Topical Conference on Wireless Communication Technology. 15-17 Oct. 2003. - P. 206-207. ↑
- C5679.** Papila I. Hidden Gauss Markov model for multiscale remotely sensed image segmentation. / Papila I., Yazgan B. // 2003. RAST '03. International Conference on. Proceedings of Recent Advances in Space Technologies. 20-22 Nov. 2003. - P. 349-354. ↑

- C5680.** Kidd R.A. Monitoring freeze-thaw events in Siberia using the seawinds Ku-band scatterometer: first results. / Kidd R.A., Trommler M., Wagner W. // 2003. IGARSS '03. Proceedings. 2003 IEEE International Geoscience and Remote Sensing Symposium. 21-25 July 2003. - Vol. 7. - P. 4608-4610. ↑
- C5681.** Abshire J.B. Geoscience laser altimeter system (GLAS) for the ICESat mission-pre-launch performance. / Abshire J.B., Xiaoli Sun, Riris H., Sirota M., Palm S., Ketchum E.A. // 2003. CLEO '03. Conference on Lasers and Electro-Optics. 1-6 June 2003. - P. 3. ↑
- C5682.** Geiser P. 3-dimensional mid-infrared remote sensing of gas concentrations in combustions. / Geiser P., Willer U., Schade W. // 2003. CLEO '03. Conference on Lasers and Electro-Optics. 1-6 June 2003. - P. 882-883. ↑
- C5683.** Gloanec M. Advanced MMICs for Remote Sensing and Radar Applications. / Gloanec M., Camiade M., Serru V., Ouarch Z., Beilenhoff K. // 2003. 33rd European Microwave Conference. - Munich, Germany, Oct. 2003. - P. 871-874. ↑
- C5684.** Skou Niels. Microwave Remote Sensing: Needs and Requirements Concerning Technology. 2003. 33rd European Microwave Conference. - Munich, Germany, Oct. 2003. - P. 863-866. ↑
- C5685.** Nicoll J. Development and application of a SAR training processor. / Nicoll J., Gens R. // 2003. IGARSS '03. Proceedings. 2003 IEEE International Geoscience and Remote Sensing Symposium. 21-25 July 2003. - Vol. 7. - P. 4593-4595. ↑
- C5686.** {no data available}. Proceedings of International Conference on Recent Advances in Space Technologies (IEEE Cat. No.03EX743). 2003. RAST '03. International Conference on. Proceedings of Recent Advances in Space Technologies. 20-22 Nov. 2003. - {no data available}. ↑
- C5687.** Sandau R. Potentials for high-resolution imaging with small satellites. 2003. RAST '03. International Conference on. Proceedings of Recent Advances in Space Technologies. 20-22 Nov. 2003. - P. 112-118. ↑
- C5688.** Kent S. Synthetic aperture radar image processing using cellular neural networks. / Kent S., Ucan O.N., Ensari T. // 2003. RAST '03. International Conference on. Proceedings of Recent Advances in Space Technologies. 20-22 Nov. 2003. - P. 308-310. ↑
- C5689.** Heremans R. Automatic detection of flooded areas on ENVISAT/ASAR images using an object-oriented classification technique and an active contour algorithm. / Heremans R., Willekens A., Borghys D., Verbeeck B., Valckenborgh J., Acheroy M., Perneel C. // 2003. RAST '03. International Conference on. Proceedings of Recent Advances in Space Technologies. 20-22 Nov. 2003. - P. 311-316. ↑
- C5690.** Mamen R. Applying space technologies for human benefit; the Canadian experience and global trends. 2003. RAST '03. International Conference on. Proceedings of Recent Advances in Space Technologies. 20-22 Nov. 2003. - P. 1-8. ↑
- C5691.** Munder J. TerraSAR-X, German X-band remote sensing system. / Munder J., Miller D. // 2003. RAST '03. International Conference on. Proceedings of Recent Advances in Space Technologies. 20-22 Nov. 2003. - P. 14-18. ↑
- C5692.** Hacihaliloglu I. DCT and wavelet based image compression in satellite images. / Hacihaliloglu I., Kartal M. // 2003. RAST '03. International Conference on. Proceedings of Recent Advances in Space Technologies. 20-22 Nov. 2003. - P. 79-84. ↑
- C5693.** Fernandez D.E. The Imaging Wind and Rain Airborne Profiler-a dual frequency dual polarized conically scanning airborne profiling radar. / Fernandez D.E., Xuehu Zhang, Castells A., McLaughlin D., Carswell J., Paul Chang, Connor L., Black P., Marks F. // 2003. IGARSS '03. Proceedings. 2003 IEEE International Geoscience and Remote Sensing Symposium. 21-25 July 2003. - Vol. 7. - P. 4246-4248. ↑
- C5694.** Hussein Z.A. Design and development of a dual-frequency (Ku/Ka), dual-polarization, wide-angle scanning airborne rain radar antenna system. / Hussein Z.A., Durden S.L., Im E. // 2003. IGARSS '03. Proceedings. 2003 IEEE International Geoscience and Remote Sensing Symposium. 21-25 July 2003. - Vol. 7. - P. 4249-4251. ↑
- C5695.** Coatanhay A. Regularization of Laplace transform inversion for subsurface conductivity and permittivity

profile estimation using GPR signals. 2003. IGARSS '03. Proceedings. 2003 IEEE International Geoscience and Remote Sensing Symposium. 21-25 July 2003. - Vol. 7. - P. 4258 vol.7. ↑

C5696. Axelsson S.R.J. Noise radar using random phase and frequency modulation. 2003. IGARSS '03. Proceedings. 2003 IEEE International Geoscience and Remote Sensing Symposium. 21-25 July 2003. - Vol. 7. - P. 4226-4231. ↑

C5697. Sato T. An adaptive clutter rejection scheme for atmospheric radars. / Sato T., Kamio K. // 2003. IGARSS '03. Proceedings. 2003 IEEE International Geoscience and Remote Sensing Symposium. 21-25 July 2003. - Vol. 7. - P. 4235-4237. ↑

C5698. Axelsson S. SAR/MTI from helicopters. / Axelsson S., Nelander A. // 2003. IGARSS '03. Proceedings. 2003 IEEE International Geoscience and Remote Sensing Symposium. 21-25 July 2003. - Vol. 7. - P. 4242-4245. ↑

C5699. Cope M.K. Assessment of a digital quadrature demodulator for a stepped frequency radar. / Cope M.K., Langman A., Inggs M.R. // 2003. IGARSS '03. Proceedings. 2003 IEEE International Geoscience and Remote Sensing Symposium. 21-25 July 2003. - Vol. 7. - P. 4259-4261. ↑

C5700. Fernandez D.M. Calibration of HF radar systems with ships of opportunity. / Fernandez D.M., Vesecky J., Teague C. // 2003. IGARSS '03. Proceedings. 2003 IEEE International Geoscience and Remote Sensing Symposium. 21-25 July 2003. - Vol. 7. - P. 4271-4273. ↑

C5701. Forget P. Radar sea echo in UHF in coastal zone: experimental observations and theory. / Forget P., Barbin Y., Currier P., Saillard M. // 2003. IGARSS '03. Proceedings. 2003 IEEE International Geoscience and Remote Sensing Symposium. 21-25 July 2003. - Vol. 7. - P. 4274-4276. ↑

C5702. Laws K. Merging surface current data from HF radars operating at different frequencies. / Laws K., Drake J., Fernandez D., Teague C., Paduan J. // 2003. IGARSS '03. Proceedings. 2003 IEEE International Geoscience and Remote Sensing Symposium. 21-25 July 2003. - Vol. 7. - P. 4277-4279. ↑

C5703. Dreuillet P. P band data collection and investigations utilizing the RAMSES SAR facility. / Dreuillet P., Paillou P., Cantalloube H., Titin-Schnaider C., Pastore L., Dupuis H., Lafon V., Garelo R., Le Caillec J.-M., Champion I., Dechambre M., Chapoulie R., Martinaud M., Coulombeix C., Dubois-Fernandez P., Duplessis O. // 2003. IGARSS '03. Proceedings. 2003 IEEE International Geoscience and Remote Sensing Symposium. 21-25 July 2003. - Vol. 7. - P. 4262-4264. ↑

C5704. Telpukhovskiy E.D. Wideband radar phenomenology of forest stands. / Telpukhovskiy E.D., Yakubov V.P., Mironov V.L., Sarabandi K., Tsepelev G.M. // 2003. IGARSS '03. Proceedings. 2003 IEEE International Geoscience and Remote Sensing Symposium. 21-25 July 2003. - Vol. 7. - P. 4265-4267. ↑

C5705. Ulander L.M.H. Development of the ultra-wideband LORA SAR operating in the VHF/UHF-band. / Ulander L.M.H., Blom M., Flood B., Follo P., Frolind P.-O., Gustavsson A., Jonsson T., Larsson B., Murdin D., Pettersson M., Raaf U., Stenstrom G. // 2003. IGARSS '03. Proceedings. 2003 IEEE International Geoscience and Remote Sensing Symposium. 21-25 July 2003. - Vol. 7. - P. 4268-4270. ↑

C5706. Quartly G.D. Weathering the storm: developments in the acoustic sensing of wind and rain. / Quartly G.D., Jones C.E., Guymer T.H., Birch K.G., Campbell J.M., Waddington I.N. // 2003. IGARSS '03. Proceedings. 2003 IEEE International Geoscience and Remote Sensing Symposium. 21-25 July 2003. - Vol. 7. - P. 4223-4225. ↑

C5707. Hislop G. A new diffraction tomography algorithm for ground penetrating radar. / Hislop G., Tee Tang. // 2003. IGARSS '03. Proceedings. 2003 IEEE International Geoscience and Remote Sensing Symposium. 21-25 July 2003. - Vol. 7. - P. 4151-4153. ↑

C5708. Liseno A. GPR-based shape reconstruction of metallic objects. / Liseno A., Tartaglione F., Pierri R., Soldovieri F. // 2003. IGARSS '03. Proceedings. 2003 IEEE International Geoscience and Remote Sensing Symposium. 21-25 July 2003. - Vol. 7. - P. 4154-4156. ↑

C5709. O'Neill K. Combining GPR and EMI data for discrimination of multiple subsurface metallic objects. / O'Neill K., Sun K., Chen C.C., Shubitidze F., Paulsen K.D. // 2003. IGARSS '03. Proceedings. 2003 IEEE International Geoscience and Remote Sensing Symposium. 21-25 July 2003. - Vol. 7. - P. 4157-4159. ↑

- C5710.** Axelsson S.R.J. Estimation of target position and velocity using data from multiple radar stations. 2003. IGARSS '03. Proceedings. 2003 IEEE International Geoscience and Remote Sensing Symposium. 21-25 July 2003. - Vol. 7. - P. 4140-4143. ↑
- C5711.** Ceraldi E. On the use of the specular direction copolarised ratio for the retrieval of soil dielectric constant. / Ceraldi E., Franceschetti G., Iodice A., Riccio D., Ruello G. // 2003. IGARSS '03. Proceedings. 2003 IEEE International Geoscience and Remote Sensing Symposium. 21-25 July 2003. - Vol. 7. - P. 4144-4146. ↑
- C5712.** Soriano G. A two-scale model for the ocean surface bistatic scattering. / Soriano G., Saillard M. // 2003. IGARSS '03. Proceedings. 2003 IEEE International Geoscience and Remote Sensing Symposium. 21-25 July 2003. - Vol. 7. - P. 4147-4149. ↑
- C5713.** Shubitidze F. Analysis of GPR scattering by multiple subsurface metallic objects to improve UXO discrimination. / Shubitidze F., O'Neill K., Shamatava I., Sun K., Paulsen K.D. // 2003. IGARSS '03. Proceedings. 2003 IEEE International Geoscience and Remote Sensing Symposium. 21-25 July 2003. - Vol. 7. - P. 4163-4165. ↑
- C5714.** Radoi E. Analysis and simulation of sea clutter at high range resolution and low grazing angles. / Radoi E., Quinquis A., Saulais P. // 2003. IGARSS '03. Proceedings. 2003 IEEE International Geoscience and Remote Sensing Symposium. 21-25 July 2003. - Vol. 7. - P. 4192-4194. ↑
- C5715.** Koudogbo F. Surface and volume scattering from natural and manmade rough surfaces in the process of setting up data base coefficients. / Koudogbo F., Mametsa H.J., Combes P.F. // 2003. IGARSS '03. Proceedings. 2003 IEEE International Geoscience and Remote Sensing Symposium. 21-25 July 2003. - Vol. 7. - P. 4211-4213. ↑
- C5716.** Thirion L. Study of the backscattering coefficient and the interferometric coherence of mangrove forests. / Thirion L., Chenierie I., Galy C. // 2003. IGARSS '03. Proceedings. 2003 IEEE International Geoscience and Remote Sensing Symposium. 21-25 July 2003. - Vol. 7. - P. 4217-4219. ↑
- C5717.** Mironov V.L. Frozen soil dielectric model using unfrozen water spectroscopic parameters. / Mironov V.L., Kaupp V.H., Komarov S.A., Kleshchenko V.N. // 2003. IGARSS '03. Proceedings. 2003 IEEE International Geoscience and Remote Sensing Symposium. 21-25 July 2003. - Vol. 7. - P. 4172-4174. ↑
- C5718.** Tianhe Chi. Research on parallel computation based remote sensing image processing for natural disaster monitoring and assessment. / Tianhe Chi, Huabin Chen, Xin Zhang, Hongqiao Wu. // 2003. IGARSS '03. Proceedings. 2003 IEEE International Geoscience and Remote Sensing Symposium. 21-25 July 2003. - Vol. 7. - P. 4180-4182. ↑
- C5719.** Melief H.W. Modeling radar backscatter from breaking waves on the surface. / Melief H.W., Greidanus H., Hoogeboom P., van Genderen P. // 2003. IGARSS '03. Proceedings. 2003 IEEE International Geoscience and Remote Sensing Symposium. 21-25 July 2003. - Vol. 7. - P. 4189-4191. ↑
- C5720.** Werner C. Interferometric Point Target Analysis with JERS-1 L-band SAR data. / Werner C., Wegmuller U., Wiesmann A., Strozzi T. // 2003. IGARSS '03. Proceedings. 2003 IEEE International Geoscience and Remote Sensing Symposium. 21-25 July 2003. - Vol. 7. - P. 4359-4361. ↑
- C5721.** Werner C. Interferometric point target analysis for deformation mapping. / Werner C., Wegmuller U., Strozzi T., Wiesmann A. // 2003. IGARSS '03. Proceedings. 2003 IEEE International Geoscience and Remote Sensing Symposium. 21-25 July 2003. - Vol. 7. - P. 4362-4364. ↑
- C5722.** Yonezawa C. Perturbation caused by cloud in ERS SAR interferogram. / Yonezawa C., Takeuchi S. // 2003. IGARSS '03. Proceedings. 2003 IEEE International Geoscience and Remote Sensing Symposium. 21-25 July 2003. - Vol. 7. - P. 4365-4367. ↑
- C5723.** Meyer F. Multi-temporal repeat-pass interferometry for an improved analysis of Arctic glaciers. 2003. IGARSS '03. Proceedings. 2003 IEEE International Geoscience and Remote Sensing Symposium. 21-25 July 2003. - Vol. 7. - P. 4347-4349. ↑
- C5724.** Prats P. Calibration of interferometric airborne SAR images using a multisquint processing approach. / Prats P., Mallorqui J.J., Broquetas A. // 2003. IGARSS '03. Proceedings. 2003 IEEE International Geoscience and Remote Sensing Symposium. 21-25 July 2003. - Vol. 7. - P. 4353-4355. ↑

- C5725.** Reigber A. Options for high-precision motion compensation for airborne differential SAR interferometry. / Reigber A., Prats P., Scheiber R., Mallorqui J.J. // 2003. IGARSS '03. Proceedings. 2003 IEEE International Geoscience and Remote Sensing Symposium. 21-25 July 2003. - Vol. 7. - P. 4356-4358. ↑
- C5726.** Suchandt S. Experiences with SRTM/X-SAR phase unwrapping using the minimum cost flow method. / Suchandt S., Eineder M. // 2003. IGARSS '03. Proceedings. 2003 IEEE International Geoscience and Remote Sensing Symposium. 21-25 July 2003. - Vol. 7. - P. 4380-4382. ↑
- C5727.** Raney R.K. LaRA-2002: results of the airborne laser and radar altimeter campaign over Greenland, Svalbard, and Arctic sea ice. / Raney R.K., Leuschen C.J., Chapman R.D., Jensen J.R., Gotwols B.L. // 2003. IGARSS '03. Proceedings. 2003 IEEE International Geoscience and Remote Sensing Symposium. 21-25 July 2003. - Vol. 7. - P. 4392-4394. ↑
- C5728.** Berkoff T.A. Investigation of overlap correction techniques for the Micro-Pulse Lidar NETWORK (MPLNET). / Berkoff T.A., Welton E.J., Campbell J.R., Scott V.S., Spinhirne J.D. // 2003. IGARSS '03. Proceedings. 2003 IEEE International Geoscience and Remote Sensing Symposium. 21-25 July 2003. - Vol. 7. - P. 4395-4397. ↑
- C5729.** Howard A.Q. Jr. Estimation of aerosol concentration from elastic scattering LIDAR data. / Howard A.Q. Jr., Lemire G.W., Marshall M.S. // 2003. IGARSS '03. Proceedings. 2003 IEEE International Geoscience and Remote Sensing Symposium. 21-25 July 2003. - Vol. 7. - P. 4398-4403. ↑
- C5730.** Wang Chao. The vector digital TV filtering and phase unwrapping. / Wang Chao, Gao Xin, Zhang Hong. // 2003. IGARSS '03. Proceedings. 2003 IEEE International Geoscience and Remote Sensing Symposium. 21-25 July 2003. - Vol. 7. - P. 4383-4385. ↑
- C5731.** Wang Feng. Phase unwrapping based on active contour model. / Wang Feng, Wu Gang, Prinnet V., Ren Kun. // 2003. IGARSS '03. Proceedings. 2003 IEEE International Geoscience and Remote Sensing Symposium. 21-25 July 2003. - Vol. 7. - P. 4386-4388. ↑
- C5732.** Davenport I.J. Derivation of soil surface properties from airborne laser altimetry. / Davenport I.J., Holden N., Pentreath R.J. // 2003. IGARSS '03. Proceedings. 2003 IEEE International Geoscience and Remote Sensing Symposium. 21-25 July 2003. - Vol. 7. - P. 4389-4391. ↑
- C5733.** Mallorqui J.J. Phase statistics and quality evaluation of deformation maps with multiple-image differential interferometry. / Mallorqui J.J., Blanco P., Broquetas A., Mora O. // 2003. IGARSS '03. Proceedings. 2003 IEEE International Geoscience and Remote Sensing Symposium. 21-25 July 2003. - Vol. 7. - P. 4344-4346. ↑
- C5734.** D'Amico M. The MANTISSA project: first results from the Italian field experiments. / D'Amico M., Pinotti M., Capsoni C. // 2003. IGARSS '03. Proceedings. 2003 IEEE International Geoscience and Remote Sensing Symposium. 21-25 July 2003. - Vol. 7. - P. 4314-4316. ↑
- C5735.** de Wit J.J.M. High resolution FM-CW SAR performance analysis. / de Wit J.J.M., Hoogeboom P. // 2003. IGARSS '03. Proceedings. 2003 IEEE International Geoscience and Remote Sensing Symposium. 21-25 July 2003. - Vol. 7. - P. a4317-a4319. ↑
- C5736.** Jordan J.E. Data-linking for integration of remote sensing and in-situ measurements for airborne atmospheric experiments. / Jordan J.E., Strapp J.W. // 2003. IGARSS '03. Proceedings. 2003 IEEE International Geoscience and Remote Sensing Symposium. 21-25 July 2003. - Vol. 7. - P. 4320-4322. ↑
- C5737.** Matsuoka T. HF ocean radar observation of surface currents induced by a typhoon in the East China Sea. / Matsuoka T., Sato K., Kojima S., Fujii S. // 2003. IGARSS '03. Proceedings. 2003 IEEE International Geoscience and Remote Sensing Symposium. 21-25 July 2003. - Vol. 7. - P. 4280-4282. ↑
- C5738.** Sakai S. Short-time observation of coastal currents with DBF radar. / Sakai S., Hirakuchi H., Matsuyama M., Tsubono T., Mori N. // 2003. IGARSS '03. Proceedings. 2003 IEEE International Geoscience and Remote Sensing Symposium. 21-25 July 2003. - Vol. 7. - P. 4283-4285. ↑
- C5739.** Teague C.C. Geometries for streamflow measurement using a UHF RiverSonde. / Teague C.C., Barrick D.E., Lilleboe P.M. // 2003. IGARSS '03. Proceedings. 2003 IEEE International Geoscience and Remote Sensing Symposium. 21-25 July 2003. - Vol. 7. - P. 4286-4288. ↑

- C5740.** Karaev V.Yu. A Doppler knife-beam radar altimeter concept for novel sea state parameters. / Karaev V.Yu., Kanevsky M.B., Balandina G.N., Gommenginger C.P., Challenor P.G., Srokosz M.A. // 2003. IGARSS '03. Proceedings. 2003 IEEE International Geoscience and Remote Sensing Symposium. 21-25 July 2003. - Vol. 7. - P. 4323-4325. ↑
- C5741.** Weiss M. EBiRa: Experimental Bistatic Radar for air surveillance. 2003. IGARSS '03. Proceedings. 2003 IEEE International Geoscience and Remote Sensing Symposium. 21-25 July 2003. - Vol. 7. - P. 4335-4337. ↑
- C5742.** Antonello G. Assessment of local topographic maps obtained by ground-based SAR interferometry. / Antonello G., Fortuny J., Leva D., Nico G., Tarchi D. // 2003. IGARSS '03. Proceedings. 2003 IEEE International Geoscience and Remote Sensing Symposium. 21-25 July 2003. - Vol. 7. - P. 4338-4340. ↑
- C5743.** Zeng Bin. The study of the parameters to interferometric SAR height-measurement and velocity-measurement precision in the Cluster Micro-Satellite system. / Zeng Bin, Zhang Xiaoling, Huang Shunji. // 2003. IGARSS '03. Proceedings. 2003 IEEE International Geoscience and Remote Sensing Symposium. 21-25 July 2003. - Vol. 7. - P. 4341-4343. ↑
- C5744.** Johansen Tom K. Ultra-wideband MMICs for remote sensing applications. / Johansen Tom K., Vidkjaer Jens, Krozer Viktor. // 2003. 33rd European Microwave Conference. - Munich, Germany, Oct. 2003. - P. 879-882. ↑
- C5745.** Pieraccini M. A ground based remote sensing radar technique for dynamic testing of large structures. / Pieraccini M., Luzi G., Mecatti D., Atzeni C. // 2003. IGARSS '03. Proceedings. 2003 IEEE International Geoscience and Remote Sensing Symposium. 21-25 July 2003. - Vol. 7. - P. 4326-4328. ↑
- C5746.** Suwa K. A bandwidth extrapolation technique of polarimetric radar data and a recursive method of polarimetric linear prediction coefficient estimation. / Suwa K., Iwamoto M. // 2003. IGARSS '03. Proceedings. 2003 IEEE International Geoscience and Remote Sensing Symposium. 21-25 July 2003. - Vol. 7. - P. 4329-4331. ↑
- C5747.** Storvik B. Joint distributions for correlated radar images. / Storvik B., Storvik G., Fjortoft R. // 2003. IGARSS '03. Proceedings. 2003 IEEE International Geoscience and Remote Sensing Symposium. 21-25 July 2003. - Vol. 3. - P. 2011-2013. ↑
- C5748.** Lombardini F. Adaptive spectral estimation for multibaseline SAR tomography with airborne L-band data. / Lombardini F., Reigber A. // 2003. IGARSS '03. Proceedings. 2003 IEEE International Geoscience and Remote Sensing Symposium. 21-25 July 2003. - Vol. 3. - P. 2014-2016. ↑
- C5749.** Luiza M. Texture classification approach using conditional local variance model. / Luiza M., Velloso F., de Souza F.J., Almeida N.N. // 2003. IGARSS '03. Proceedings. 2003 IEEE International Geoscience and Remote Sensing Symposium. 21-25 July 2003. - Vol. 3. - P. 2048-2050. ↑
- C5750.** Schiavon G. High resolution multi-spectral analysis of urban areas with quickbird imagery and synergy with ERS data. / Schiavon G., Del Frate F., Solimini C. // 2003. IGARSS '03. Proceedings. 2003 IEEE International Geoscience and Remote Sensing Symposium. 21-25 July 2003. - Vol. 3. - P. 1972-1974. ↑
- C5751.** Henry C. Target detection and analysis based on spectral analysis of a SAR image: a simulation approach. / Henry C., Souyris J., Marthon P. // 2003. IGARSS '03. Proceedings. 2003 IEEE International Geoscience and Remote Sensing Symposium. 21-25 July 2003. - Vol. 3. - P. 2005-2007. ↑
- C5752.** Vazquez-Bautista R.F. Aggregating the statistical estimation and variational analysis methods in radar imagery. / Vazquez-Bautista R.F., Shkvarko Y.V., Morales-Mendoza L.J. // 2003. IGARSS '03. Proceedings. 2003 IEEE International Geoscience and Remote Sensing Symposium. 21-25 July 2003. - Vol. 3. - P. 2008-2010. ↑
- C5753.** Sang-Wan Kim. Measurement of sea level by L-band SAR. / Sang-Wan Kim, Joong-Sun Won. // 2003. IGARSS '03. Proceedings. 2003 IEEE International Geoscience and Remote Sensing Symposium. 21-25 July 2003. - Vol. 3. - P. 2106-2108. ↑
- C5754.** Costa M. Estimate of net primary production of aquatic vegetation of the amazon floodplain using SAR satellite data. / Costa M., Niemann O. // 2003. IGARSS '03. Proceedings. 2003 IEEE International Geoscience

and Remote Sensing Symposium. 21-25 July 2003. - Vol. 3. - P. 2131-2133. ↑

C5755. Ludwig M. Impact of new technologies on future space-borne radar design. / Ludwig M., Buck C.H., Mangenot C., Suess M. // 2003. IGARSS '03. Proceedings. 2003 IEEE International Geoscience and Remote Sensing Symposium. 21-25 July 2003. - Vol. 3. - P. 2137-2139. ↑

C5756. Mittermayer J. Conceptual studies for exploiting the TerraSAR-X dual receive antenna. / Mittermayer J., Runge H. // 2003. IGARSS '03. Proceedings. 2003 IEEE International Geoscience and Remote Sensing Symposium. 21-25 July 2003. - Vol. 3. - P. 2140-2142. ↑

C5757. Costanzo S. Microstrip permanent scatterers for SAR interferometry applications. / Costanzo S., Venneri F., Di Massa G., Angiulli G. // 2003. IGARSS '03. Proceedings. 2003 IEEE International Geoscience and Remote Sensing Symposium. 21-25 July 2003. - Vol. 3. - P. 2109-2111. ↑

C5758. Sabater J.M. Physical analysis of atmospheric delay signal observed in stacked radar interferometric data. / Sabater J.M., Hanssen R., Kampes B.M., Fusco A., Adam N. // 2003. IGARSS '03. Proceedings. 2003 IEEE International Geoscience and Remote Sensing Symposium. 21-25 July 2003. - Vol. 3. - P. 2112-2115. ↑

C5759. Joong-Sun Won. Tidal flat DEM generation by satellite remote sensing. / Joong-Sun Won, Young-Ho Na, Sang-Wan Kim. // 2003. IGARSS '03. Proceedings. 2003 IEEE International Geoscience and Remote Sensing Symposium. 21-25 July 2003. - Vol. 3. - P. 2116-2118. ↑

C5760. Amitai E. Challenges and proposed solutions for validation of spaceborne rain rate estimates. / Amitai E., Liao L., Wolff D.B., Marks D.A., Silberstein D.S. // 2003. IGARSS '03. Proceedings. 2003 IEEE International Geoscience and Remote Sensing Symposium. 21-25 July 2003. - Vol. 3. - P. 1966-1968. ↑

C5761. Anderson C. Observations and modelling of the response of along-track SAR interferometry to mesoscale ocean features. / Anderson C., Macklin T., Wolf J., Srokosz M. // 2003. IGARSS '03. Proceedings. 2003 IEEE International Geoscience and Remote Sensing Symposium. 21-25 July 2003. - Vol. 3. - P. 1927-1929. ↑

C5762. Pierce L. Regrowth biomass estimation in the amazon using JERS-1/RADARSAT SAR composites. / Pierce L., Pan Liang, Dobson M.C., Kelndorfer J., Barros O., dos Santos J.R., Soares J.V. // 2003. IGARSS '03. Proceedings. 2003 IEEE International Geoscience and Remote Sensing Symposium. 21-25 July 2003. - Vol. 3. - P. 1933-1935. ↑

C5763. Engdahl M.E. Combined land-cover classification and stem volume estimation using multitemporal ERS tandem INSAR data. / Engdahl M.E., Pulliainen J., Hallikainen M. // 2003. IGARSS '03. Proceedings. 2003 IEEE International Geoscience and Remote Sensing Symposium. 21-25 July 2003. - Vol. 3. - P. 1936-1938. ↑

C5764. Dankert H. Investigation of ocean wave groups using radar-image sequences. / Dankert H., Nieto-Borge J., Rosenthal W. // 2003. IGARSS '03. Proceedings. 2003 IEEE International Geoscience and Remote Sensing Symposium. 21-25 July 2003. - Vol. 3. - P. 1918-1920. ↑

C5765. Hoja D. A new wind sea /swell classification method for complex ENVISAT ASAR wave mode data. / Hoja D., Schulz-Stellenfleth J., Lehner S. // 2003. IGARSS '03. Proceedings. 2003 IEEE International Geoscience and Remote Sensing Symposium. 21-25 July 2003. - Vol. 3. - P. 1921-1923. ↑

C5766. Queffeulou P. Mediterranean sea wind and wave characteristics from satellite, buoy and numerical model data. / Queffeulou P., Bentamy A., Laverne T., Lefevre J.-M., Skandrani C. // 2003. IGARSS '03. Proceedings. 2003 IEEE International Geoscience and Remote Sensing Symposium. 21-25 July 2003. - Vol. 3. - P. 1924-1926. ↑

C5767. Eriksson L.E.B. The potential of ALOS single polarization INSAR for estimation of growing stock volume in Boreal forest. / Eriksson L.E.B., Santoro M., Schmullius C., Wiesmann A. // 2003. IGARSS '03. Proceedings. 2003 IEEE International Geoscience and Remote Sensing Symposium. 21-25 July 2003. - Vol. 3. - P. 1939-1941. ↑

C5768. Mardiana R. Dual-frequency rain profiling method without the use of surface reference technique. / Mardiana R., Iguchi T., Takahashi N., Hanado H. // 2003. IGARSS '03. Proceedings. 2003 IEEE International Geoscience and Remote Sensing Symposium. 21-25 July 2003. - Vol. 3. - P. 1954-1956. ↑

- C5769.** Takahashi N. Utilization of range profile data of surface echo from TRMM/PR. / Takahashi N., Hanado H., Iguchi T. // 2003. IGARSS '03. Proceedings. 2003 IEEE International Geoscience and Remote Sensing Symposium. 21-25 July 2003. - Vol. 3. - P. 1957-1959. ↑
- C5770.** Liang Liao. Evaluation of TRMM PR attenuation by radar mirror image. / Liang Liao, Meneghini R. // 2003. IGARSS '03. Proceedings. 2003 IEEE International Geoscience and Remote Sensing Symposium. 21-25 July 2003. - Vol. 3. - P. 1963-1965. ↑
- C5771.** Mette T. Height-biomass allometry in temperate forests performance accuracy of height-biomass allometry. / Mette T., Hajnsek I., Papathanassiou K. // 2003. IGARSS '03. Proceedings. 2003 IEEE International Geoscience and Remote Sensing Symposium. 21-25 July 2003. - Vol. 3. - P. 1942-1944. ↑
- C5772.** Balzter H. Potential of polarimetric SAR interferometry for forest carbon accounting. / Balzter H., Rowland C., Milne R., Stebler O., Patenaude G., Dawson T., Saich P. // 2003. IGARSS '03. Proceedings. 2003 IEEE International Geoscience and Remote Sensing Symposium. 21-25 July 2003. - Vol. 3. - P. 1945-1947. ↑
- C5773.** Gorgucci E. Ground validation during EGPM: possible concepts for an Italian distributed site. / Gorgucci E., Baldini L., Mugnai A., Siccardi F., Chandrasekar V. // 2003. IGARSS '03. Proceedings. 2003 IEEE International Geoscience and Remote Sensing Symposium. 21-25 July 2003. - Vol. 3. - P. 1951-1953. ↑
- C5774.** Trabal del Valle J.M. Puerto Rico deployable radar network design; site survey. / Trabal del Valle J.M., Colom-Ustariz J.G., Cruz-Pol S.L., Sekelsky S.M. // 2003. IGARSS '03. Proceedings. 2003 IEEE International Geoscience and Remote Sensing Symposium. 21-25 July 2003. - Vol. 4. - P. 2353-2355. ↑
- C5775.** Zrnic D.S. Polarimetric properties of chaff. / Zrnic D.S., Ryzhkov A.V. // 2003. IGARSS '03. Proceedings. 2003 IEEE International Geoscience and Remote Sensing Symposium. 21-25 July 2003. - Vol. 4. - P. 2359-2361. ↑
- C5776.** Tianhe Chi. Research on information system for natural disaster monitoring and assessment. / Tianhe Chi, Xin Zhang, Huabin Chen, Yumin Tan. // 2003. IGARSS '03. Proceedings. 2003 IEEE International Geoscience and Remote Sensing Symposium. 21-25 July 2003. - Vol. 4. - P. 2404-2406. ↑
- C5777.** Keeler J. NEXRAD data quality by spectral processing. Spectral processing on NCAR's S-Pol radar. / Keeler J., Hubbert J., Lutz J. // 2003. IGARSS '03. Proceedings. 2003 IEEE International Geoscience and Remote Sensing Symposium. 21-25 July 2003. - Vol. 4. - P. 2341-2343. ↑
- C5778.** Li W. Investigations in radar rainfall estimation using neural networks. / Li W., Chandrasekar V., Xu G. // 2003. IGARSS '03. Proceedings. 2003 IEEE International Geoscience and Remote Sensing Symposium. 21-25 July 2003. - Vol. 4. - P. 2347-2349. ↑
- C5779.** Ryzhkov A.V. Effective shape of raindrops. Polarimetric radar perspective. / Ryzhkov A.V., Schuur T.J. // 2003. IGARSS '03. Proceedings. 2003 IEEE International Geoscience and Remote Sensing Symposium. 21-25 July 2003. - Vol. 4. - P. 2350-2352. ↑
- C5780.** Ito Y. A degree estimation model of earthquake damage using temporal coherence ratio. / Ito Y., Hosokawa M., Matsuoka M. // 2003. IGARSS '03. Proceedings. 2003 IEEE International Geoscience and Remote Sensing Symposium. 21-25 July 2003. - Vol. 4. - P. 2410-2412. ↑
- C5781.** Usai S. MINERVA: an INSAR monitoring system for volcanic hazard. / Usai S., Sansosti E., Tampellini L., Borgstrom S., Ricciardi G., Spaans J., Pepe A., Guarino S., Maddalena V., van Persie M., Berardino P., Lanari R., Fornaro G., Seifert F.M. // 2003. IGARSS '03. Proceedings. 2003 IEEE International Geoscience and Remote Sensing Symposium. 21-25 July 2003. - Vol. 4. - P. 2433-2435. ↑
- C5782.** Zakharov A.I. Monitoring of the forests state in the Chernobyl area using remote sensing data. / Zakharov A.I., Zakharova L., Sinilo V.P., Sorochinsky M.V. // 2003. IGARSS '03. Proceedings. 2003 IEEE International Geoscience and Remote Sensing Symposium. 21-25 July 2003. - Vol. 4. - P. 2474-2476. ↑
- C5783.** Zakharova L. On the use of ERS INSAR data in the ecological monitoring of the Baikal region. / Zakharova L., Zakharov A., Darizhapov D., Schmullius C. // 2003. IGARSS '03. Proceedings. 2003 IEEE International Geoscience and Remote Sensing Symposium. 21-25 July 2003. - Vol. 4. - P. 2477-2479. ↑
- C5784.** Lehner S. Analysis of two dimensional sea surface elevation fields using spaceborne SAR. / Lehner S.,

Niedermeier A., Nieto Borge J.C., Schulz-Stellenfleth J., Dankert H., Horstmann J., Rosenthal W. // 2003. IGARSS '03. Proceedings. 2003 IEEE International Geoscience and Remote Sensing Symposium. 21-25 July 2003. - Vol. 4. - P. 2419-2421. ↑

C5785. Paganini M. SLAM, the development of an EO service to support the legal obligations of Swiss and Italian Geological Risk Services in landslide risk forecasting and prevention. / Paganini M., Palazzo F., Arino O., Manunta P., Ferretti A., Gontier E., Wunderle S., Pasquali P., Strozzi T., Zilger J., van Westen C. // 2003. IGARSS '03. Proceedings. 2003 IEEE International Geoscience and Remote Sensing Symposium. 21-25 July 2003. - Vol. 4. - P. 2422-2424. ↑

C5786. Schiavon G. Landslide identification by SAR interferometry: the Sarno case. / Schiavon G., Del Frate F., D'Ottavio D., Stramondo S. // 2003. IGARSS '03. Proceedings. 2003 IEEE International Geoscience and Remote Sensing Symposium. 21-25 July 2003. - Vol. 4. - P. 2428-2429. ↑

C5787. Belchansky G.I. Estimating multiyear sea-ice concentration using passive microwave data and MLP neural networks. / Belchansky G.I., Alpatsky I.V., Ereemeev V.A., Mordvintsev I.N., Platonov N.G., Douglas D.C. // 2003. IGARSS '03. Proceedings. 2003 IEEE International Geoscience and Remote Sensing Symposium. 21-25 July 2003. - Vol. 4. - P. 2332-2334. ↑

C5788. Del Frate F. On the potential of multi-polarization and multi-temporal C-band SAR data in classifying crops. / Del Frate F., Schiavon G., Solimini D., Borgeaud M., Hoekman D.H., Vissers M.A.M. // 2003. IGARSS '03. Proceedings. 2003 IEEE International Geoscience and Remote Sensing Symposium. 21-25 July 2003. - Vol. 4. - P. 2195-2196. ↑

C5789. Riedel T. Impact of interception on the thematic analyses of SAR data in agricultural areas. / Riedel T., Schumliuss C.C. // 2003. IGARSS '03. Proceedings. 2003 IEEE International Geoscience and Remote Sensing Symposium. 21-25 July 2003. - Vol. 4. - P. 2218-2220. ↑

C5790. Braun N. Field studies on the action of rain on the radar backscattering from wind-roughened water surfaces. / Braun N., Gade M. // 2003. IGARSS '03. Proceedings. 2003 IEEE International Geoscience and Remote Sensing Symposium. 21-25 July 2003. - Vol. 4. - P. 2248-2250. ↑

C5791. Hounam D. Techniques for reducing SAR antenna size. / Hounam D., Mittermayer J. // 2003. IGARSS '03. Proceedings. 2003 IEEE International Geoscience and Remote Sensing Symposium. 21-25 July 2003. - Vol. 3. - P. 2143-2145. ↑

C5792. Im E. Instrument concept of NEXRAD in space (NIS)-a geostationary radar for hurricane studies. / Im E., Smith E.A., Durden S.L., Tanelli S., Huang J., Rahmat-Samii Y., Lou M. // 2003. IGARSS '03. Proceedings. 2003 IEEE International Geoscience and Remote Sensing Symposium. 21-25 July 2003. - Vol. 3. - P. 2146-2148. ↑

C5793. Toledano C. Aerosol Arctic Campaign at ALOMAR (69N, 16E, Norway) in June-July 2002. / Toledano C., Cachorro V.E., De Frutos A.M., Vergaz R., Mar Sorribas M. // 2003. IGARSS '03. Proceedings. 2003 IEEE International Geoscience and Remote Sensing Symposium. 21-25 July 2003. - Vol. 4. - P. 2185-2187. ↑

C5794. Essen H. Propagation within boundary layers over sea at millimeterwaves and infrared wavelengths. / Essen H., Fuchs H.-H., Stein K. // 2003. IGARSS '03. Proceedings. 2003 IEEE International Geoscience and Remote Sensing Symposium. 21-25 July 2003. - Vol. 4. - P. 2251-2253. ↑

C5795. Le Hegarat-Masclé S. Use of ERS/SAR measurements for soil geometric and aerodynamic roughness estimation in semi-arid and arid areas. / Le Hegarat-Masclé S., Zribi M., Marticorena B., Bergametti G., Kardous M., Callot Y., Chazette P., Rajot J.-L. // 2003. IGARSS '03. Proceedings. 2003 IEEE International Geoscience and Remote Sensing Symposium. 21-25 July 2003. - Vol. 4. - P. 2272-2274. ↑

C5796. Randriambelo T. Lidar measurements of tropospheric ozone over Reunion Island: influence of the synoptic situations. / Randriambelo T., Baray J.-L., Baldy S., Thompson A.M., Oltmans S., Keckhut P. // 2003. IGARSS '03. Proceedings. 2003 IEEE International Geoscience and Remote Sensing Symposium. 21-25 July 2003. - Vol. 4. - P. 2311-2313. ↑

C5797. Mora O. Development of a multiple adjustment processor for generation of DEMs over large areas using SAR data. / Mora O., Perez F., Pala V., Arbiol R. // 2003. IGARSS '03. Proceedings. 2003 IEEE International Geoscience and Remote Sensing Symposium. 21-25 July 2003. - Vol. 4. - P. 2326-2328. ↑

- C5798.** Mityagina M.I. Two polarization radar imagery of sea surface: the dependence on atmospheric stability. / Mityagina M.I., Lavrova O., Bocharova T., Pungin V. // 2003. IGARSS '03. Proceedings. 2003 IEEE International Geoscience and Remote Sensing Symposium. 21-25 July 2003. - Vol. 4. - P. 2260-2262. ↑
- C5799.** Lefort A. Interferometric coherence for change detection in the Nasca region of Peru. / Lefort A., Grippa M., Walker N., Stewart L.J., Woodhouse I.H. // 2003. IGARSS '03. Proceedings. 2003 IEEE International Geoscience and Remote Sensing Symposium. 21-25 July 2003. - Vol. 4. - P. 2263-2265. ↑
- C5800.** Sciotti M. GPR for archaeological investigations: real performance assessment for different surface and subsurface conditions. / Sciotti M., Colone F., Pastina D., Bucciarelli T. // 2003. IGARSS '03. Proceedings. 2003 IEEE International Geoscience and Remote Sensing Symposium. 21-25 July 2003. - Vol. 4. - P. 2266-2268. ↑
- C5801.** Gogineni S. Polar radar for ice sheet measurements. / Gogineni S., Prescott G., Braaten D., Allen C. // 2003. IGARSS '03. Proceedings. 2003 IEEE International Geoscience and Remote Sensing Symposium. 21-25 July 2003. - Vol. 3. - P. 1607-1609. ↑
- C5802.** Ashcraft I.S. Relating micro ave backscatter azimuth modulation to surface properties of the greenland ice sheet. / Ashcraft I.S., Long D.G. // 2003. IGARSS '03. Proceedings. 2003 IEEE International Geoscience and Remote Sensing Symposium. 21-25 July 2003. - Vol. 3. - P. 1610-1612. ↑
- C5803.** Moghaddam M. Quantifying the biomass of australian subtropical woodlands using SAR inversion models. / Moghaddam M., Lucas R.M. // 2003. IGARSS '03. Proceedings. 2003 IEEE International Geoscience and Remote Sensing Symposium. 21-25 July 2003. - Vol. 3. - P. 1619-1621. ↑
- C5804.** Zine S. Comparison between SAR and wind scatterometers data for surface parameters monitoring over a sahelian agropastoral area. / Zine S., Frison P., Rudant J., Jarlan L., Mougin E., Hiernaux P., Gerard B. // 2003. IGARSS '03. Proceedings. 2003 IEEE International Geoscience and Remote Sensing Symposium. 21-25 July 2003. - Vol. 3. - P. 1582-1584. ↑
- C5805.** Khvorostovsky K.S. Greenland ice sheet elevation change from 1992 to 1999 derived from ERS-1 and ERS-2 satellite altimeter measurements. / Khvorostovsky K.S., Bobylev L.P., Johannessen O.M. // 2003. IGARSS '03. Proceedings. 2003 IEEE International Geoscience and Remote Sensing Symposium. 21-25 July 2003. - Vol. 3. - P. 1601-1603. ↑
- C5806.** Ashcraft I.S. Increasing temporal resolution in greenland ablation estimation using passive and active microwave data. / Ashcraft I.S., Long D.G. // 2003. IGARSS '03. Proceedings. 2003 IEEE International Geoscience and Remote Sensing Symposium. 21-25 July 2003. - Vol. 3. - P. 1604-1606. ↑
- C5807.** De Grandi G. The GBFM radar mosaic of the Eurasian Taiga: a groundwork for the bio-physical characterization of an ecosystem with relevance to global change studies. / De Grandi G., Achard F., Mollicone D., Rauste Y. // 2003. IGARSS '03. Proceedings. 2003 IEEE International Geoscience and Remote Sensing Symposium. 21-25 July 2003. - Vol. 3. - P. 1625-1627. ↑
- C5808.** Lopez-Martinez C. Model based PolSAR and PolInSAR speckle noise reduction. / Lopez-Martinez C., Fabregas X. // 2003. IGARSS '03. Proceedings. 2003 IEEE International Geoscience and Remote Sensing Symposium. 21-25 July 2003. - Vol. 3. - P. 1645-1647. ↑
- C5809.** Nomula M. Estimating vegetation bias in polarimetric SAR interferometry. / Nomula M., Kasilingam D., Cloude S. // 2003. IGARSS '03. Proceedings. 2003 IEEE International Geoscience and Remote Sensing Symposium. 21-25 July 2003. - Vol. 3. - P. 1648-1650. ↑
- C5810.** Malhotra S. The dependence of polarimetric coherence on surface roughness for very rough surfaces. / Malhotra S., Kasilingam D., Schuler D. // 2003. IGARSS '03. Proceedings. 2003 IEEE International Geoscience and Remote Sensing Symposium. 21-25 July 2003. - Vol. 3. - P. 1654-1656. ↑
- C5811.** Del Frate F. On the retrieval of forest biomass from SAR data by neural networks. / Del Frate F., Solimini D. // 2003. IGARSS '03. Proceedings. 2003 IEEE International Geoscience and Remote Sensing Symposium. 21-25 July 2003. - Vol. 3. - P. 1637-1638. ↑
- C5812.** Hallberg B. Individual tree detection using CARABAS-II. / Hallberg B., Lars G.S., Ulander M.H., Frolind P. // 2003. IGARSS '03. Proceedings. 2003 IEEE International Geoscience and Remote Sensing Symposium. 21-25 July 2003. - Vol. 3. - P. 1639-1641. ↑

- C5813.** Satake M. Characteristics of radar reflectivity of rain forests measured by space-borne Ku-band radar. / Satake M., Hanado H. // 2003. IGARSS '03. Proceedings. 2003 IEEE International Geoscience and Remote Sensing Symposium. 21-25 July 2003. - Vol. 3. - P. 1642-1644. ↑
- C5814.** Hommels A. Preliminary ASTER and INSAR imagery combination for mud volcano dynamics, Azerbaijan. / Hommels A., Scholte K.H., Munoz-Sabater J., Hanssen R.F., Van der Meer F.D., Kroonenberg S.B., Aliyeva E., Huseynov D., Guliev I. // 2003. IGARSS '03. Proceedings. 2003 IEEE International Geoscience and Remote Sensing Symposium. 21-25 July 2003. - Vol. 3. - P. 1573-1575. ↑
- C5815.** Young S.A. Adaptive algorithms for the fully-automated retrieval of cloud and aerosol extinction profiles from CALIPSO lidar data. / Young S.A., Vaughan M.A., Winker D.M. // 2003. IGARSS '03. Proceedings. 2003 IEEE International Geoscience and Remote Sensing Symposium. 21-25 July 2003. - Vol. 3. - P. 1517-1519. ↑
- C5816.** Chomette O. Retrieval of cloud emissivity and particle size frame of the CALIPSO mission. / Chomette O., Garnier A., Pelon J., Lifermann A., Bret-Dibat T., Ackerman S., Chepfer H., Dubuisson P., Giraud V., Hu Y., Kratz D., Noel V., Platt C.M.R., Sirou F., Stubenrauch C. // 2003. IGARSS '03. Proceedings. 2003 IEEE International Geoscience and Remote Sensing Symposium. 21-25 July 2003. - Vol. 3. - P. 1520-1522. ↑
- C5817.** Noel V. Synergies of CALIOP with aqua-train instruments. / Noel V., Yongxaing Hu, Chiriaco M. // 2003. IGARSS '03. Proceedings. 2003 IEEE International Geoscience and Remote Sensing Symposium. 21-25 July 2003. - Vol. 3. - P. 1523-1525. ↑
- C5818.** Schumilius C. SIBERIA-II: sensor systems and data products for greenhouse gas accounting. / Schumilius C., Hese S. // 2003. IGARSS '03. Proceedings. 2003 IEEE International Geoscience and Remote Sensing Symposium. 21-25 July 2003. - Vol. 3. - P. 1499-1501. ↑
- C5819.** Bianco L. Combining microwave radiometer and wind profiler radar measurements to improve accuracy and resolution of atmospheric humidity profiling. / Bianco L., Cimini D., Marzano F., Ware R. // 2003. IGARSS '03. Proceedings. 2003 IEEE International Geoscience and Remote Sensing Symposium. 21-25 July 2003. - Vol. 3. - P. 1505-1507. ↑
- C5820.** Winker D.M. Cloud-Aerosol Lidar with Orthogonal Polarization (CALIOP). / Winker D.M., Hostetler C.A., Hunt W.H. // 2003. IGARSS '03. Proceedings. 2003 IEEE International Geoscience and Remote Sensing Symposium. 21-25 July 2003. - Vol. 3. - P. 1514-1516. ↑
- C5821.** Omar A.H. Selection algorithm for the CALIPSO lidar aerosol extinction-to-backscatter ratio. / Omar A.H., Winker D.M., Jae-Gwang Won, Vaughan M.A., Hostetler C.A., Reagan J.A. // 2003. IGARSS '03. Proceedings. 2003 IEEE International Geoscience and Remote Sensing Symposium. 21-25 July 2003. - Vol. 3. - P. 1526-1530. ↑
- C5822.** Sart F. The two emergencies of "El Salvador" in the frame of the international charter "space and major disasters". / Sart F., Inglada J., Bessis J.L. // 2003. IGARSS '03. Proceedings. 2003 IEEE International Geoscience and Remote Sensing Symposium. 21-25 July 2003. - Vol. 3. - P. 1543-1545. ↑
- C5823.** Wiesmann A. Subsidence monitoring over oil fields with L-band SAR interferometry. / Wiesmann A., Wegmuller U., Werner C., Strozzi T. // 2003. IGARSS '03. Proceedings. 2003 IEEE International Geoscience and Remote Sensing Symposium. 21-25 July 2003. - Vol. 3. - P. 1546-1548. ↑
- C5824.** Stephen H. Surface statistics of the saharan ergs observed in the yo azimuth modulation. / Stephen H., Long D.G. // 2003. IGARSS '03. Proceedings. 2003 IEEE International Geoscience and Remote Sensing Symposium. 21-25 July 2003. - Vol. 3. - P. 1549-1551. ↑
- C5825.** Reagan J.A. LITE aerosol retrievals at 1064 nm with improved aerosol retrieval approaches in support of CALIPSO. / Reagan J.A., Wang X. // 2003. IGARSS '03. Proceedings. 2003 IEEE International Geoscience and Remote Sensing Symposium. 21-25 July 2003. - Vol. 3. - P. 1531-1533. ↑
- C5826.** Abshire J.B. Geoscience laser altimeter system (GLAS) on the ICESat mission: pre-launch and on-orbit measurement performance. / Abshire J.B., Xiaoli Sun, Riris H., Sirota M., McGarry J., Palm S., Ketchum E.A., Follas R.B. // 2003. IGARSS '03. Proceedings. 2003 IEEE International Geoscience and Remote Sensing Symposium. 21-25 July 2003. - Vol. 3. - P. 1534-1536. ↑
- C5827.** Spinhirne J. Atmospheric measurements by the geoscience laser altimeter system: initial results. /

Spinhirne J., Welton E., Palm S., Hlavka D., Hart W., Mahesh A. // 2003. IGARSS '03. Proceedings. 2003 IEEE International Geoscience and Remote Sensing Symposium. 21-25 July 2003. - Vol. 3. - P. 1537-1539. ↑

C5828. Iwata T. Precision geolocation determination and pointing management for the advanced land observing satellite (ALOS). 2003. IGARSS '03. Proceedings. 2003 IEEE International Geoscience and Remote Sensing Symposium. 21-25 July 2003. - Vol. 3. - P. 1845-1848. ↑

C5829. Shimada M. Calibration and validation of palsar (II) use of polarimetric active radar calibrator and the Amazon rainforest data. / Shimada M., Tanaka H., Tadono T., Watanabe M. // 2003. IGARSS '03. Proceedings. 2003 IEEE International Geoscience and Remote Sensing Symposium. 21-25 July 2003. - Vol. 3. - P. 1849-1851. ↑

C5830. Strozzi T. Detection and monitoring of unstable high-mountain slopes with L-band SAR interferometry. / Strozzi T., Kaab A., Frauenfelder R., Wegmuller U. // 2003. IGARSS '03. Proceedings. 2003 IEEE International Geoscience and Remote Sensing Symposium. 21-25 July 2003. - Vol. 3. - P. 1852-1854. ↑

C5831. Xingsong Hou. Wavelet packet remote-sensing images coding algorithm based on quadtree classification and UTCQ. / Xingsong Hou, Guizhong Liu, YiYang Zou. // 2003. IGARSS '03. Proceedings. 2003 IEEE International Geoscience and Remote Sensing Symposium. 21-25 July 2003. - Vol. 3. - P. 1826-1829. ↑

C5832. Benazza-Benyahia A. Adapted vector-lifting schemes for multiband textured image coding. / Benazza-Benyahia A., Pesquet J.-C., Gharbia M.H. // 2003. IGARSS '03. Proceedings. 2003 IEEE International Geoscience and Remote Sensing Symposium. 21-25 July 2003. - Vol. 3. - P. 1833-1835. ↑

C5833. Suzuki S. Level 1 data processing algorithm for ALOS PRISM and AVNIR-2. 2003. IGARSS '03. Proceedings. 2003 IEEE International Geoscience and Remote Sensing Symposium. 21-25 July 2003. - Vol. 3. - P. 1842-1844. ↑

C5834. Deroin J.P. Retrieval of land surface parameters in the zone of Chotts, Tunisia, from SIR-C/X-SAR data. / Deroin J.P., Bec V., Zorilla M., Burollet P.F., Simonin A. // 2003. IGARSS '03. Proceedings. 2003 IEEE International Geoscience and Remote Sensing Symposium. 21-25 July 2003. - Vol. 3. - P. 1867-1869. ↑

C5835. Zecchetto S. Wavenumber spectra of the Mediterranean Sea winds derived from the NASA QuikSCAT data. / Zecchetto S., De Biasio F. // 2003. IGARSS '03. Proceedings. 2003 IEEE International Geoscience and Remote Sensing Symposium. 21-25 July 2003. - Vol. 3. - P. 1907-1909. ↑

C5836. Hauser D. Ocean wave spectrum and radar cross-section analysis from coincident ENVISAT ASAR observations and airborne polarimetric radar measurements performed during the VALPARESO experiment. / Hauser D., Mouche A., Chapron B., Johnsen H., Daloze J.-F., Guerin C., Caudal G., Lefevre J.-M. // 2003. IGARSS '03. Proceedings. 2003 IEEE International Geoscience and Remote Sensing Symposium. 21-25 July 2003. - Vol. 3. - P. 1910-1914. ↑

C5837. Schneiderhan T. Use of SAR cross spectra for wind retrieval from envisat ASAR wave mode data. / Schneiderhan T., Schulz-Stellenfleth J., Lehner S., Horstmann J., Hoja D. // 2003. IGARSS '03. Proceedings. 2003 IEEE International Geoscience and Remote Sensing Symposium. 21-25 July 2003. - Vol. 3. - P. 1915-1917. ↑

C5838. Paillou P. A JERS-1 radar mosaic for subsurface geology mapping in East Sahara. / Paillou P., Rosenqvist A. // 2003. IGARSS '03. Proceedings. 2003 IEEE International Geoscience and Remote Sensing Symposium. 21-25 July 2003. - Vol. 3. - P. 1870-1872. ↑

C5839. Im E. Development status of the cloud profiling radar for the cloudsat mission. / Im E., Durden S.L., Chialin Wu. // 2003. IGARSS '03. Proceedings. 2003 IEEE International Geoscience and Remote Sensing Symposium. 21-25 July 2003. - Vol. 3. - P. 1898-1900. ↑

C5840. Nieto Borge J.C. Comparison of spatial and spectral sea state parameters measured by space borne SAR, nautical radar and in situ sensors. / Nieto Borge J.C., Danker H., Hessner K., Lehner S. // 2003. IGARSS '03. Proceedings. 2003 IEEE International Geoscience and Remote Sensing Symposium. 21-25 July 2003. - Vol. 3. - P. 1904-1906. ↑

C5841. El-Boustani A. Investigation of wavelets for raw SAR data compression. / El-Boustani A., Brunham K., Kinsner W. // 2003. IGARSS '03. Proceedings. 2003 IEEE International Geoscience and Remote Sensing

Symposium. 21-25 July 2003. - Vol. 3. - P. 1814-1816. ↑

C5842. Iguchi T. The dual-frequency precipitation radar for the GPM core satellite. / Iguchi T., Hanado H., Takahashi N., Kobayashi S., Satoh S. // 2003. IGARSS '03. Proceedings. 2003 IEEE International Geoscience and Remote Sensing Symposium. 21-25 July 2003. - Vol. 3. - P. 1698-1700. ↑

C5843. Stocker E.F. Precipitation processing system for the global precipitation measurement mission. 2003. IGARSS '03. Proceedings. 2003 IEEE International Geoscience and Remote Sensing Symposium. 21-25 July 2003. - Vol. 3. - P. 1704-1706. ↑

C5844. Meneghini R. On the use of the log-normal particle size distribution to characterize global rain. / Meneghini R., Rincon R., Liang Liao. // 2003. IGARSS '03. Proceedings. 2003 IEEE International Geoscience and Remote Sensing Symposium. 21-25 July 2003. - Vol. 3. - P. 1707-1709. ↑

C5845. Langemeyer S. A compact and flexible multi-DSP system for real-time SAR applications. / Langemeyer S., Kloos H., Simon-Klar C., Friebe L., Hinrichs W., Lieske H., Pirsch P. // 2003. IGARSS '03. Proceedings. 2003 IEEE International Geoscience and Remote Sensing Symposium. 21-25 July 2003. - Vol. 3. - P. 1657-1659. ↑

C5846. Gens R. Issues and challenges for standardizing level zero format for SAR data. / Gens R., LaBelle-Hamer N. // 2003. IGARSS '03. Proceedings. 2003 IEEE International Geoscience and Remote Sensing Symposium. 21-25 July 2003. - Vol. 3. - P. 1660-1662. ↑

C5847. Nakamura K. Japan's progress for the global precipitation measurement (GPM). / Nakamura K., Iguchi T., Oki R. // 2003. IGARSS '03. Proceedings. 2003 IEEE International Geoscience and Remote Sensing Symposium. 21-25 July 2003. - Vol. 3. - P. 1695-1697. ↑

C5848. Chandrasekar V. Estimation of raindrop size distribution from TRMM precipitation radar observations. / Chandrasekar V., Mubarak K., Lim S. // 2003. IGARSS '03. Proceedings. 2003 IEEE International Geoscience and Remote Sensing Symposium. 21-25 July 2003. - Vol. 3. - P. 1712-1714. ↑

C5849. Gimmestad G.G. NEXLASER-an unattended tropospheric aerosol and ozone lidar-first results. / Gimmestad G.G., Roberts D.W., Stewart J.M., West L.L., Wood J.W. // 2003. IGARSS '03. Proceedings. 2003 IEEE International Geoscience and Remote Sensing Symposium. 21-25 July 2003. - Vol. 3. - P. 1754-1756. ↑

C5850. Whiteman D. Use of Raman lidar for validation of aqua retrievals and the study of air radiances. / Whiteman D., Demoz B., Zhien Wang, Barnet C., Hoff R., McMillan W., Veselovskii I., McCann K., Russo F., Gambacorta A., Lightner K., Maddy E., Comer J., Kolb N., DeSlover D., Jedlovec G., Cadirola M. // 2003. IGARSS '03. Proceedings. 2003 IEEE International Geoscience and Remote Sensing Symposium. 21-25 July 2003. - Vol. 3. - P. 1757-1759. ↑

C5851. Pappalardo G. Lidar observations of etna volcanic aerosol. / Pappalardo G., Amodeo A., Mona L., Pandolfi M. // 2003. IGARSS '03. Proceedings. 2003 IEEE International Geoscience and Remote Sensing Symposium. 21-25 July 2003. - Vol. 3. - P. 1760-1762. ↑

C5852. Guillaso S. Analysis of built-up areas from polarimetric interferometric SAR images. / Guillaso S., Ferro-Famil L., Reigber A., Pottier E. // 2003. IGARSS '03. Proceedings. 2003 IEEE International Geoscience and Remote Sensing Symposium. 21-25 July 2003. - Vol. 3. - P. 1727-1729. ↑

C5853. Gasiewski A.J. Estimation of coupling between mobile vehicular radars and satellite radiometers. / Gasiewski A.J., Zavorotny V.U. // 2003. IGARSS '03. Proceedings. 2003 IEEE International Geoscience and Remote Sensing Symposium. 21-25 July 2003. - Vol. 3. - P. 1748-1750. ↑

C5854. Ellingson S.W. Design of an L-band microwave radiometer with active mitigation of interference. / Ellingson S.W., Hampson G.A., Johnson J.T. // 2003. IGARSS '03. Proceedings. 2003 IEEE International Geoscience and Remote Sensing Symposium. 21-25 July 2003. - Vol. 3. - P. 1751-1753. ↑

C5855. Sang-Wan Kim. DInSAR measurements of reclaimed costal land. / Sang-Wan Kim, Joong-Sun Won, Kyo-Young Song. // 2003. IGARSS '03. Proceedings. 2003 IEEE International Geoscience and Remote Sensing Symposium. 21-25 July 2003. - Vol. 4. - P. 2930-2932. ↑

C5856. Zhen Li. Frozen ground deformation monitoring using SAR interferometry. / Zhen Li, Xinwu Li, Xin Ren,

Qin Dong. // 2003. IGARSS '03. Proceedings. 2003 IEEE International Geoscience and Remote Sensing Symposium. 21-25 July 2003. - Vol. 4. - P. 2933-2935. ↑

C5857. Petrat L. Simulation of abandoned mining induced surface movements for estimating DInSAR detection limits. / Petrat L., Wegmuller U. // 2003. IGARSS '03. Proceedings. 2003 IEEE International Geoscience and Remote Sensing Symposium. 21-25 July 2003. - Vol. 4. - P. 2936-2938. ↑

C5858. Shrestha S.M. High resolution image reconstruction by GPR using MUSIC and SAR processing method for landmine detection. / Shrestha S.M., Arai I. // 2003. IGARSS '03. Proceedings. 2003 IEEE International Geoscience and Remote Sensing Symposium. 21-25 July 2003. - Vol. 4. - P. 2921-2923. ↑

C5859. Casagli N. Ground-based SAR interferometry as a tool for landslide monitoring during emergencies. / Casagli N., Farina P., Leva D., Nico G., Tarchi D. // 2003. IGARSS '03. Proceedings. 2003 IEEE International Geoscience and Remote Sensing Symposium. 21-25 July 2003. - Vol. 4. - P. 2924-2926. ↑

C5860. Colombo D. Land subsidence in the Firenze-Prato-Pistoia basin measured by means of spaceborne SAR interferometry. / Colombo D., Farina P., Moretti S., Nico G., Prati C. // 2003. IGARSS '03. Proceedings. 2003 IEEE International Geoscience and Remote Sensing Symposium. 21-25 July 2003. - Vol. 4. - P. 2927-2929. ↑

C5861. Raucoules D. Comparison between InSAR and leveling. / Raucoules D., Carnec C., Le Mouelic S., King C., Maisons C. // 2003. IGARSS '03. Proceedings. 2003 IEEE International Geoscience and Remote Sensing Symposium. 21-25 July 2003. - Vol. 4. - P. 2939-2941. ↑

C5862. Rey L. Sital the radar altimeter for the cryosat mission, pre-launch performances. / Rey L., de Chateau-Thierry P., Phalippou L., Mavrocordatos C. // 2003. IGARSS '03. Proceedings. 2003 IEEE International Geoscience and Remote Sensing Symposium. 2003. - Vol. 5. - P. 2974-2976. ↑

C5863. Moisseev D. Towards an atmosphere free interferogram; first comparison between ENVISAT's ASAR and MERIS water vapor observations. / Moisseev D., Hanssen R., Sabater J. // 2003. IGARSS '03. Proceedings. 2003 IEEE International Geoscience and Remote Sensing Symposium. 2003. - Vol. 5. - P. 2977-2980. ↑

C5864. Quartly G.D. Rain-flagging of the Envisat altimeter. / Quartly G.D., Srokosz M.A. // 2003. IGARSS '03. Proceedings. 2003 IEEE International Geoscience and Remote Sensing Symposium. 2003. - Vol. 5. - P. 2984-2986. ↑

C5865. Bengier S.N. Remotely sensed determination of flood surface gradients for hydrological modelling of semi-arid floodplains. 2003. IGARSS '03. Proceedings. 2003 IEEE International Geoscience and Remote Sensing Symposium. 21-25 July 2003. - Vol. 4. - P. 2950-2952. ↑

C5866. Mlisa A. Preliminary assessment of SRTM X band DEMs of Southern Africa for hydrogeological studies. / Mlisa A., Hartnady C., Inggs M.R. // 2003. IGARSS '03. Proceedings. 2003 IEEE International Geoscience and Remote Sensing Symposium. 21-25 July 2003. - Vol. 4. - P. 2953-2955. ↑

C5867. Hilburn K. Rain effects on SeaWinds data. / Hilburn K., Wentz F., Mears C. // 2003. IGARSS '03. Proceedings. 2003 IEEE International Geoscience and Remote Sensing Symposium. 2003. - Vol. 5. - P. 2971-2976. ↑

C5868. Luzi G. Joint-Time Frequency Analysis for investigating layered structures by surface penetrating radar. / Luzi G., Mecatti D., Noferini L., Pieraccini M., Atzeni C. // 2003. IGARSS '03. Proceedings. 2003 IEEE International Geoscience and Remote Sensing Symposium. 21-25 July 2003. - Vol. 4. - P. 2918-2920. ↑

C5869. Fortuny-Guasch J. Experimental validation of an electromagnetic model for rice crops using a wide-band polarimetric radar. / Fortuny-Guasch J., Martinez-Vazquez A., Riccio D., Lopez-Sanchez J.M., Ballester J.D. // 2003. IGARSS '03. Proceedings. 2003 IEEE International Geoscience and Remote Sensing Symposium. 21-25 July 2003. - Vol. 4. - P. 2866-2868. ↑

C5870. Kotz B. Multi-resolution imaging spectroscopy resolving the structure of heterogeneous canopies for forest fire fuel properties mapping. / Kotz B., Schaepman M., Morsdorf F., Itten K., Allgower B., Bowyer P. // 2003. IGARSS '03. Proceedings. 2003 IEEE International Geoscience and Remote Sensing Symposium. 21-25 July 2003. - Vol. 4. - P. 2869-2871. ↑

- C5871.** Kuplich T.M. Relating SAR image texture and backscatter to tropical forest biomass. / Kuplich T.M., Curran P.J., Atkinson P.M. // 2003. IGARSS '03. Proceedings. 2003 IEEE International Geoscience and Remote Sensing Symposium. 21-25 July 2003. - Vol. 4. - P. 2872-2874. ↑
- C5872.** Kelly R.E.J. The effect of sub-pixel areal distribution of snow on the estimation of snow depth from spaceborne passive microwave instruments. / Kelly R.E.J., Chang A.T.C., Foster J.L., Hall D.K. // 2003. IGARSS '03. Proceedings. 2003 IEEE International Geoscience and Remote Sensing Symposium. 21-25 July 2003. - Vol. 4. - P. 2834 vol.4. ↑
- C5873.** Brown C.G. Estimation of red pine tree height using Shuttle Radar Topography Mission and ancillary data. / Brown C.G., Sarabandi K. // 2003. IGARSS '03. Proceedings. 2003 IEEE International Geoscience and Remote Sensing Symposium. 21-25 July 2003. - Vol. 4. - P. 2850-2852. ↑
- C5874.** Del Frate F. Investigating the performance of radar configurations in crop monitoring. / Del Frate F., Ferrazzoli P., Guerriero L., Strozzi T., Wegmuller U., Cookmartin G., Quegan S. // 2003. IGARSS '03. Proceedings. 2003 IEEE International Geoscience and Remote Sensing Symposium. 21-25 July 2003. - Vol. 4. - P. 2860-2862. ↑
- C5875.** Prevot L. Estimating vegetation biophysical properties from high resolution images: a comparison between radar and optical data. / Prevot L., Dubois-Fernandez P., Chanzy A., Dechambre M., Zribi M., Baghdadi N. // 2003. IGARSS '03. Proceedings. 2003 IEEE International Geoscience and Remote Sensing Symposium. 21-25 July 2003. - Vol. 4. - P. 2884 vol.4. ↑
- C5876.** Ciarletti V. Experimental validation of a GPR dedicated to the Martian subsurface exploration (Pyla sand dune). / Ciarletti V., Berthelie J.J., Ney R., Bonaime S., Dolon F., Reinex A., Bauche G., Nevejans D., Hegg E. // 2003. IGARSS '03. Proceedings. 2003 IEEE International Geoscience and Remote Sensing Symposium. 21-25 July 2003. - Vol. 4. - P. 2906-2908. ↑
- C5877.** Cull J. Complex impedance mapping using GPR survey methods. / Cull J., Massie D., Roberts J. // 2003. IGARSS '03. Proceedings. 2003 IEEE International Geoscience and Remote Sensing Symposium. 21-25 July 2003. - Vol. 4. - P. 2909-2911. ↑
- C5878.** Kutuza B. Some estimations of water lenses position based on experimental data obtained by SAR operating at P and VHF bands. / Kutuza B., Kalinkevich A., Shishkova O., Plushev V., Manakov V. // 2003. IGARSS '03. Proceedings. 2003 IEEE International Geoscience and Remote Sensing Symposium. 21-25 July 2003. - Vol. 4. - P. 2915-2917. ↑
- C5879.** Prevot L. Surface soil moisture estimation from SAR data over wheat fields during the ADAM project. / Prevot L., Poenaru V., Voicu P., Vintila R., DeBoissezon H., Pourthie N. // 2003. IGARSS '03. Proceedings. 2003 IEEE International Geoscience and Remote Sensing Symposium. 21-25 July 2003. - Vol. 4. - P. 2885-2887. ↑
- C5880.** Ciarletti V. Influence of the soil tillage and degradation due to rain upon the radar scattered signal. / Ciarletti V., Baudier C., Taconet O., Dusseaux R., Dibi T., Boissard P., Bresson L.M. // 2003. IGARSS '03. Proceedings. 2003 IEEE International Geoscience and Remote Sensing Symposium. 21-25 July 2003. - Vol. 4. - P. 2894-2896. ↑
- C5881.** Paillou P. A phase signature for detecting subsurface moisture using polarimetric L-band SAR: example of the Pyla dune-France. / Paillou P., August T., Lasne Y., Grandjean G., Ruffie G. // 2003. IGARSS '03. Proceedings. 2003 IEEE International Geoscience and Remote Sensing Symposium. 21-25 July 2003. - Vol. 4. - P. 2897-2899. ↑
- C5882.** Ahmad K. Precipitation measurements using the QuikSCAT Radiometer. / Ahmad K., Jones W.L., Kasparis T. // 2003. IGARSS '03. Proceedings. 2003 IEEE International Geoscience and Remote Sensing Symposium. 2003. - Vol. 5. - P. 3132-3135. ↑
- C5883.** Bidwell S.W. Validation and error characterization for the Global Precipitation Measurement. / Bidwell S.W., Adams W.J., Bibyk I.K., Everett D.F., Smith E.A., Yuter S.E. // 2003. IGARSS '03. Proceedings. 2003 IEEE International Geoscience and Remote Sensing Symposium. 2003. - Vol. 5. - P. 3136-3138. ↑
- C5884.** Di Michele S. The Bayesian Algorithm for Microwave Precipitation Retrieval (BAMPR): potential and application to TRMM data. / Di Michele S., Tassa A., Mugnai A., Marzano F.S. // 2003. IGARSS '03. Proceedings. 2003 IEEE International Geoscience and Remote Sensing Symposium. 2003. - Vol. 5. - P. 3142-

3144. ↑

C5885. Schulz-Stellenfleth J. Global ocean wave measurements from ENVISAT ASAR data using a parametric inversion scheme. / Schulz-Stellenfleth J., Hoja D., Lehner S. // 2003. IGARSS '03. Proceedings. 2003 IEEE International Geoscience and Remote Sensing Symposium. 2003. - Vol. 5. - P. 3111-3113. ↑

C5886. Wiesmann A. ASAR multi-swath techniques. / Wiesmann A., Wegmuller U., Werner C., Strozzi T. // 2003. IGARSS '03. Proceedings. 2003 IEEE International Geoscience and Remote Sensing Symposium. 2003. - Vol. 5. - P. 3114-3116. ↑

C5887. Guirlet M. Validation of GOMOS O3 vertical profiles. / Guirlet M., Theodore B., Hembise O., Mangin A. // 2003. IGARSS '03. Proceedings. 2003 IEEE International Geoscience and Remote Sensing Symposium. 2003. - Vol. 5. - P. 3117-3119. ↑

C5888. Iida Y. Sampling simulation of five sun synchronous orbit satellites' group and TRMM rainfall estimation using radar-AmeDAS composites. / Iida Y., Okamoto K. // 2003. IGARSS '03. Proceedings. 2003 IEEE International Geoscience and Remote Sensing Symposium. 2003. - Vol. 5. - P. 3148-3150. ↑

C5889. Tagawa T. Calculations of surface clutter interference with precipitation measurement from space by 35.5 GHz radar for Global Precipitation Measurement Mission. / Tagawa T., Okamoto K. // 2003. IGARSS '03. Proceedings. 2003 IEEE International Geoscience and Remote Sensing Symposium. 2003. - Vol. 5. - P. 3172-3174. ↑

C5890. Zafar B. Evaluation of precipitation type determination from TRMM observations. / Zafar B., Mubarak K., Chandrasekar V. // 2003. IGARSS '03. Proceedings. 2003 IEEE International Geoscience and Remote Sensing Symposium. 2003. - Vol. 5. - P. 3175-3177. ↑

C5891. Aouf L. Impact of ASAR ENVISAT directional wave spectra on wave forecast. / Aouf L., Lefevre J.-M., Hauser D., Chapron B. // 2003. IGARSS '03. Proceedings. 2003 IEEE International Geoscience and Remote Sensing Symposium. 2003. - Vol. 5. - P. 3178-3180. ↑

C5892. Inoue T. Deep convection observed from split window of GOES and PR/TRMM, LIS/TRMM. 2003. IGARSS '03. Proceedings. 2003 IEEE International Geoscience and Remote Sensing Symposium. 2003. - Vol. 5. - P. 3151-3153. ↑

C5893. Min-Jeong Kim. Spaceborne passive microwave measurement of snowfall over land. / Min-Jeong Kim, Skofronick-Jackson G., Weinman J.A., Dong-Eon Chang. // 2003. IGARSS '03. Proceedings. 2003 IEEE International Geoscience and Remote Sensing Symposium. 2003. - Vol. 5. - P. 3163-3165. ↑

C5894. Shin D.-B. Precipitation retrievals using radiometric and spatial information of passive microwave radiometers. / Shin D.-B., Chiu L.S. // 2003. IGARSS '03. Proceedings. 2003 IEEE International Geoscience and Remote Sensing Symposium. 2003. - Vol. 5. - P. 3169-3171. ↑

C5895. Olsen R.B. The ship detection capability of ENVISAT's ASAR. / Olsen R.B., Wahl T. // 2003. IGARSS '03. Proceedings. 2003 IEEE International Geoscience and Remote Sensing Symposium. 2003. - Vol. 5. - P. 3108-3110. ↑

C5896. Krainak M.A. Tunable solid-etalon filter for the ICESat/GLAS 532 nm channel lidar receiver. / Krainak M.A., Stephen M.A., Martino A.J., Lancaster R.S., Allan G.R., Lunt D.L. // 2003. IGARSS '03. Proceedings. 2003 IEEE International Geoscience and Remote Sensing Symposium. 2003. - Vol. 5. - P. 3020-3022. ↑

C5897. Fan Jinlong. Using multitemporal RADARSAT-1 data to extract paddy rice structure in southern China. / Fan Jinlong, Wu Bingfang, Huang Huiping. // 2003. IGARSS '03. Proceedings. 2003 IEEE International Geoscience and Remote Sensing Symposium. 2003. - Vol. 5. - P. 3046-3048. ↑

C5898. Yiming Pi. Design and analysis of multi-mode cluster SAR. / Yiming Pi, Xin Xiao, Jianyu Yang. // 2003. IGARSS '03. Proceedings. 2003 IEEE International Geoscience and Remote Sensing Symposium. 2003. - Vol. 5. - P. 3049-3051. ↑

C5899. Wegmuller U. ENVISAT ASAR for land cover information. / Wegmuller U., Strozzi T., Wiesmann A., Werner C. // 2003. IGARSS '03. Proceedings. 2003 IEEE International Geoscience and Remote Sensing Symposium. 2003. - Vol. 5. - P. 2996-2998. ↑

- C5900.** Klein U. Microwave instruments development in ESA's Earth Observation Future Programmes. / Klein U., Guijarro J., Rommen B., Vogel P., de Maagt P., Lin C.C. // 2003. IGARSS '03. Proceedings. 2003 IEEE International Geoscience and Remote Sensing Symposium. 2003. - Vol. 5. - P. 3008-3010. ↑
- C5901.** Rodriguez E. Centimetric sea surface height accuracy using the Wide-Swath Ocean altimeter. / Rodriguez E., Pollard B. // 2003. IGARSS '03. Proceedings. 2003 IEEE International Geoscience and Remote Sensing Symposium. 2003. - Vol. 5. - P. 3011-3013. ↑
- C5902.** Anterrieu E. Self characterization of modelling parameters for synthetic aperture imaging radiometers. / Anterrieu E., Gratton S., Picard B. // 2003. IGARSS '03. Proceedings. 2003 IEEE International Geoscience and Remote Sensing Symposium. 2003. - Vol. 5. - P. 3052-3054. ↑
- C5903.** Fouques S. A numerical study of the nonlinear ocean-SAR spectral transform. / Fouques S., Krogstad H.E. // 2003. IGARSS '03. Proceedings. 2003 IEEE International Geoscience and Remote Sensing Symposium. 2003. - Vol. 5. - P. 3099-3101. ↑
- C5904.** Horstmann J. Ocean wind field retrieval using ENVISAT ASAR data. / Horstmann J., Koch W. // 2003. IGARSS '03. Proceedings. 2003 IEEE International Geoscience and Remote Sensing Symposium. 2003. - Vol. 5. - P. 3102-3104. ↑
- C5905.** Guarnieri A.M. Wide-angle azimuth antenna pattern estimation in SAR images. / Guarnieri A.M., D'Aria D. // 2003. IGARSS '03. Proceedings. 2003 IEEE International Geoscience and Remote Sensing Symposium. 2003. - Vol. 5. - P. 3105-3107. ↑
- C5906.** Audenino P. Qualification of SRTM DEM. A first approach toward an application dependant qualification framework. / Audenino P., Rognant L., Chassery J.M. // 2003. IGARSS '03. Proceedings. 2003 IEEE International Geoscience and Remote Sensing Symposium. 2003. - Vol. 5. - P. 3082-3084. ↑
- C5907.** Romeiser R. Validation of SRTM-derived surface currents off the Dutch coast by numerical circulation model results. / Romeiser R., Breit H., Eineder M., Runge H., Flament P., de Jong K., Vogelzang J. // 2003. IGARSS '03. Proceedings. 2003 IEEE International Geoscience and Remote Sensing Symposium. 2003. - Vol. 5. - P. 3085-3087. ↑
- C5908.** Buckreuss S. The terraSAR-X satellite project. / Buckreuss S., Balzer W., Muhlbauer P., Werninghaus R., Pitz W. // 2003. IGARSS '03. Proceedings. 2003 IEEE International Geoscience and Remote Sensing Symposium. 2003. - Vol. 5. - P. 3096-3098. ↑
- C5909.** Olsen R.B. Rapid Environmental Assessment at high latitudes. / Olsen R.B., Jensen J.K., Torsas M., Hackett B., Engedahl H. // 2003. IGARSS '03. Proceedings. 2003 IEEE International Geoscience and Remote Sensing Symposium. 21-25 July 2003. - Vol. 4. - P. 2653-2655. ↑
- C5910.** Yingjian Liu. An Automatic Ship Detection system using ERS SAR images. / Yingjian Liu, Mingqiang Fang, Qian Feng, Laibu Wang. // 2003. IGARSS '03. Proceedings. 2003 IEEE International Geoscience and Remote Sensing Symposium. 21-25 July 2003. - Vol. 4. - P. 2656-2658. ↑
- C5911.** Bentz C.M. Multi-sensor synergetic analysis of mesoscale oceanic features: Campos Basin, southeastern Brazil. / Bentz C.M., Lorenzetti J., Kampel M. // 2003. IGARSS '03. Proceedings. 2003 IEEE International Geoscience and Remote Sensing Symposium. 21-25 July 2003. - Vol. 4. - P. 2662-2664. ↑
- C5912.** Nepomuceno A.M. P-band radar data classification by neural network for Amazonian land cover assessment. / Nepomuceno A.M., Freitas C.C., Valeriano D.M., dos Santos J.R., Dutra L.V., da Silva N.C., de CSanta Rosa A.N. // 2003. IGARSS '03. Proceedings. 2003 IEEE International Geoscience and Remote Sensing Symposium. 21-25 July 2003. - Vol. 4. - P. 2620-2622. ↑
- C5913.** Torma M. The effect of seasonal and weather conditions to land cover class separability in ERS radar data. / Torma M., Engdahl M. // 2003. IGARSS '03. Proceedings. 2003 IEEE International Geoscience and Remote Sensing Symposium. 21-25 July 2003. - Vol. 4. - P. 2635-2637. ↑
- C5914.** Diani M. Dim target detection in IR maritime surveillance systems. / Diani M., Acito N., Corsini G. // 2003. IGARSS '03. Proceedings. 2003 IEEE International Geoscience and Remote Sensing Symposium. 21-25 July 2003. - Vol. 4. - P. 2650-2652. ↑

- C5915.** Berizzi F. Fractal mapping for sea surface anomalies recognition. / Berizzi F., Bertini G., Condello R., Dell'Acqua F., Holt B., Gamba P., Garzelli A., Martorella M. // 2003. IGARSS '03. Proceedings. 2003 IEEE International Geoscience and Remote Sensing Symposium. 21-25 July 2003. - Vol. 4. - P. 2665-2667. ↑
- C5916.** Ivanov L.M. HF radar detects submesoscale spiral eddies in Monterey Bay. / Ivanov L.M., Melnichenko O.V. // 2003. IGARSS '03. Proceedings. 2003 IEEE International Geoscience and Remote Sensing Symposium. 21-25 July 2003. - Vol. 4. - P. 2682-2684. ↑
- C5917.** Marghany M. Utilization of Hopfield neural network and quasi-linear model for longshore current pattern simulation from RADARSAT. 2003. IGARSS '03. Proceedings. 2003 IEEE International Geoscience and Remote Sensing Symposium. 21-25 July 2003. - Vol. 4. - P. 2688-2690. ↑
- C5918.** Martorella M. Use of synoptic real data for relating the sea surface roughness to the backscattering signal fractal dimension. / Martorella M., Berizzi F., Zecchetto S., De Biasio F. // 2003. IGARSS '03. Proceedings. 2003 IEEE International Geoscience and Remote Sensing Symposium. 21-25 July 2003. - Vol. 4. - P. 2691-2693. ↑
- C5919.** Bulatov M.G. Microwave radiation and backscatter of the sea surface perturbed by underwater gas bubble flow. / Bulatov M.G., Kravtsov Yu.A., Pungin V.G., Raev M.D., Skvortsov E.I. // 2003. IGARSS '03. Proceedings. 2003 IEEE International Geoscience and Remote Sensing Symposium. 21-25 July 2003. - Vol. 4. - P. 2668-2670. ↑
- C5920.** Dankert H. Retrieval of surface-current fields and bathymetries using radar-image sequences. 2003. IGARSS '03. Proceedings. 2003 IEEE International Geoscience and Remote Sensing Symposium. 21-25 July 2003. - Vol. 4. - P. 2671-2673. ↑
- C5921.** Dong Qing. The internal wave extraction from composing sea surface using SAR image. / Dong Qing, Guo Huadong, Han Chunming. // 2003. IGARSS '03. Proceedings. 2003 IEEE International Geoscience and Remote Sensing Symposium. 21-25 July 2003. - Vol. 4. - P. 2674-2676. ↑
- C5922.** Dedieu J.-P. Glacier mass balance determination by remote sensing in the French Alps: progress and limitation for time series monitoring. / Dedieu J.-P., Rabatel A., Vincent C., Valla F., Thibert E., Arnaud Y. // 2003. IGARSS '03. Proceedings. 2003 IEEE International Geoscience and Remote Sensing Symposium. 21-25 July 2003. - Vol. 4. - P. 2602-2604. ↑
- C5923.** Yamada Y. Relation between ground features and mathematical morphology using JERS-1/SAR data during flooding time in paddy areas. 2003. IGARSS '03. Proceedings. 2003 IEEE International Geoscience and Remote Sensing Symposium. 21-25 July 2003. - Vol. 4. - P. 2526-2528. ↑
- C5924.** Wallington E.D. Assessing L-band SAR modes for commercial forest management. / Wallington E.D., Turner D., Woodhouse I.H., Malthus T.J., Suarez-Minguez C. // 2003. IGARSS '03. Proceedings. 2003 IEEE International Geoscience and Remote Sensing Symposium. 21-25 July 2003. - Vol. 4. - P. 2541-2543. ↑
- C5925.** Walter F. A production line for forest stem volume measurements from VHF SAR data. / Walter F., Fransson J.E.S., Gustavsson A., Larsson B., Smith G., Ulander L.M.H., Ostman I. // 2003. IGARSS '03. Proceedings. 2003 IEEE International Geoscience and Remote Sensing Symposium. 21-25 July 2003. - Vol. 4. - P. 2544-2546. ↑
- C5926.** Gimeno M. Fire scar detection in Central Portugal using RADARSAT-1 and ERS-2 SAR data. / Gimeno M., San-Miguel-Ayanz J., Liberta G. // 2003. IGARSS '03. Proceedings. 2003 IEEE International Geoscience and Remote Sensing Symposium. 21-25 July 2003. - Vol. 4. - P. 2491-2493. ↑
- C5927.** Solbo S. Mapping surface-water with Radarsat at arbitrary incidence angles. / Solbo S., Malnes E., Guneriusen T., Solheim I., Eltoft T. // 2003. IGARSS '03. Proceedings. 2003 IEEE International Geoscience and Remote Sensing Symposium. 21-25 July 2003. - Vol. 4. - P. 2517-2519. ↑
- C5928.** Vatti M. Simulations of "The historic Southeast Louisiana and Southern Mississippi flood activity during May 8-10th, 1995" to build a prototype GIS/RS based ERAISA (Environmental Risk Assessment Integrative Systems Approach) for Gulf Coastal states of the United States. / Vatti M., Remata S.R., Chigbu P. // 2003. IGARSS '03. Proceedings. 2003 IEEE International Geoscience and Remote Sensing Symposium. 21-25 July 2003. - Vol. 4. - P. 2520-2522. ↑

- C5929.** Dechambre M. Polarimetric analysis of P-BAND SAR data acquired over a forested area: "the PYLA 2001 experiment". / Dechambre M., Le Hegarat S., Dreuillet P., Champion I. // 2003. IGARSS '03. Proceedings. 2003 IEEE International Geoscience and Remote Sensing Symposium. 21-25 July 2003. - Vol. 4. - P. 2550-2552. ↑
- C5930.** Rowland C.S. Biomass estimation of Thetford forest from L-band SAR data: potential and limitations. / Rowland C.S., Balzter H., Dawson T.P., Luckman A., Skinner L., Patenaude G. // 2003. IGARSS '03. Proceedings. 2003 IEEE International Geoscience and Remote Sensing Symposium. 21-25 July 2003. - Vol. 4. - P. 2577-2579. ↑
- C5931.** Pang Yong. Comparison of tree height estimations from C and L-band InSAR data. / Pang Yong, Li Zengyuan, Guoqing Sun, Chen Erxue, Che Xuejian. // 2003. IGARSS '03. Proceedings. 2003 IEEE International Geoscience and Remote Sensing Symposium. 21-25 July 2003. - Vol. 4. - P. 2586-2588. ↑
- C5932.** Xiao Cheng. Blue-ice domain discrimination using interferometric coherence in Antarctic Grove Mountains. / Xiao Cheng, Yanmei Zhang, Zhen Li, Yun Shao. // 2003. IGARSS '03. Proceedings. 2003 IEEE International Geoscience and Remote Sensing Symposium. 21-25 July 2003. - Vol. 4. - P. 2599-2601. ↑
- C5933.** Folkesson K. Stem volume retrieval at stand level using multiple low-frequency SAR images. / Folkesson K., Smith G., Ulander L.M.H. // 2003. IGARSS '03. Proceedings. 2003 IEEE International Geoscience and Remote Sensing Symposium. 21-25 July 2003. - Vol. 4. - P. 2556-2558. ↑
- C5934.** Im S.T. Radarsat data for Siberian plain ecosystems classification. / Im S.T., Gorodzankina S.M., Kharuk V.I., Ranson K.J. // 2003. IGARSS '03. Proceedings. 2003 IEEE International Geoscience and Remote Sensing Symposium. 21-25 July 2003. - Vol. 4. - P. 2562-2564. ↑
- C5935.** Neeff T. Tropical forest biomass measurement by backscatter and DEM information as derived from airborne SAR. / Neeff T., Dutra L.V., dos Santos J.R., da Costa Freitas C., Araujo L.S. // 2003. IGARSS '03. Proceedings. 2003 IEEE International Geoscience and Remote Sensing Symposium. 21-25 July 2003. - Vol. 4. - P. 2571-2573. ↑
- C5936.** Yun Shao. Effect of dielectric properties of moist salinized soils on backscattering coefficients extracted from RADARSAT image. / Yun Shao, Huadong Guo, Qingrong Hu, Yuan Lu, Qing Dong, Chunming Han. // 2003. IGARSS '03. Proceedings. 2003 IEEE International Geoscience and Remote Sensing Symposium. 21-25 July 2003. - Vol. 4. - P. 2789-2791. ↑
- C5937.** Wilson W.J. Precision ocean salinity measurements using the Passive Active L/S-band aircraft instrument. / Wilson W.J., Yueh S.H., Dinardo S., Yi Chao, Fuk Li. // 2003. IGARSS '03. Proceedings. 2003 IEEE International Geoscience and Remote Sensing Symposium. 21-25 July 2003. - Vol. 4. - P. 2792-2794. ↑
- C5938.** Yueh S.H. Aquarius instrument design for sea surface salinity measurements. / Yueh S.H., Wilson W.J., Edelstein W., Farra D., Johnson M., Pellerano F., LeVine D., Hilderbrand P. // 2003. IGARSS '03. Proceedings. 2003 IEEE International Geoscience and Remote Sensing Symposium. 21-25 July 2003. - Vol. 4. - P. 2795-2797. ↑
- C5939.** Herique A. Calibration of the CONSERT/ROSETTA radar. / Herique A., Kofman W. // 2003. IGARSS '03. Proceedings. 2003 IEEE International Geoscience and Remote Sensing Symposium. 21-25 July 2003. - Vol. 4. - P. 2753-2755. ↑
- C5940.** Nouvel J.-F. Marsis radar signal simulation. / Nouvel J.-F., Herique A., Kofman W., Safaeinili A. // 2003. IGARSS '03. Proceedings. 2003 IEEE International Geoscience and Remote Sensing Symposium. 21-25 July 2003. - Vol. 4. - P. 2756-2758. ↑
- C5941.** Abdel-Razak Mohamed Z. Potentiality of RADARSAT-1 images in the detection of salt affected soils in the arid zone: Wadi El-Natron, Egypt. / Abdel-Razak Mohamed Z., Bonn F., Giugni L.P., Mahmood A. // 2003. IGARSS '03. Proceedings. 2003 IEEE International Geoscience and Remote Sensing Symposium. 21-25 July 2003. - Vol. 4. - P. 2777-2779. ↑
- C5942.** Alexandrov V.Y. Iceberg identification in the Eurasian Arctic using SAR images. / Alexandrov V.Y., Sandven S., Kloster K. // 2003. IGARSS '03. Proceedings. 2003 IEEE International Geoscience and Remote Sensing Symposium. 21-25 July 2003. - Vol. 4. - P. 2798-2801. ↑

- C5943.** Ramasami V. A low frequency wideband depth sounder for sea ice. / Ramasami V., Gogineni S., Holt B., Kanagaratnam P., Gurumoorthy K., Namburi S.K., Henslee J., Braaten D., Mahoney A., Lytle V. // 2003. IGARSS '03. Proceedings. 2003 IEEE International Geoscience and Remote Sensing Symposium. 21-25 July 2003. - Vol. 4. - P. 2811-2813. ↑
- C5944.** Cordisco E. Sensitivity of satellite observations to snow characteristics. / Cordisco E., Prigent C., Aires F. // 2003. IGARSS '03. Proceedings. 2003 IEEE International Geoscience and Remote Sensing Symposium. 21-25 July 2003. - Vol. 4. - P. 2817-2819. ↑
- C5945.** Derksen C. Development of a cross-platform (SMMR and SSM/I) passive microwave derived snow water equivalent dataset for climatological applications. / Derksen C., Walker A., Ledrew E. // 2003. IGARSS '03. Proceedings. 2003 IEEE International Geoscience and Remote Sensing Symposium. 21-25 July 2003. - Vol. 4. - P. 2820-2822. ↑
- C5946.** Gogineni S. An ultra-wideband radar for measurements of snow thickness over sea ice. / Gogineni S., Wong K., Krishnan S., Kanagaratnam P., Markus T., Lytle V. // 2003. IGARSS '03. Proceedings. 2003 IEEE International Geoscience and Remote Sensing Symposium. 21-25 July 2003. - Vol. 4. - P. 2802-2804. ↑
- C5947.** Gutierrez S. Optical flow and scale-space theory applied to sea-ice motion estimation in Antarctica. / Gutierrez S., Long D.G. // 2003. IGARSS '03. Proceedings. 2003 IEEE International Geoscience and Remote Sensing Symposium. 21-25 July 2003. - Vol. 4. - P. 2805-2807. ↑
- C5948.** Kouraev A.V. Variations of sea ice extent in the Caspian and Aral seas derived from combination of active and passive satellite microwave data. / Kouraev A.V., Papa F., Mognard N.M., Buharizin P.I., Cazenave A., Cretaux J.-F., Dozortseva J., Remy F. // 2003. IGARSS '03. Proceedings. 2003 IEEE International Geoscience and Remote Sensing Symposium. 21-25 July 2003. - Vol. 4. - P. 2808-2810. ↑
- C5949.** Kanaa T.F.N. Detection of oil slick signatures in SAR images by fusion of hysteresis thresholding responses. / Kanaa T.F.N., Tonye E., Mercier G., Onana V.P., Ngono J.M., Frison P.L., Rudant J.P., Garello R. // 2003. IGARSS '03. Proceedings. 2003 IEEE International Geoscience and Remote Sensing Symposium. 21-25 July 2003. - Vol. 4. - P. 2750-2752. ↑
- C5950.** Duk-Jin Kim. Evaluation of ENVISAT ASAR data for measurement of surface wind field over the Korean east coast. / Duk-Jin Kim, Moon W.M., SungHyun Nam. // 2003. IGARSS '03. Proceedings. 2003 IEEE International Geoscience and Remote Sensing Symposium. 21-25 July 2003. - Vol. 4. - P. 2712-2714. ↑
- C5951.** Kojima S. Estimation of directional wave spectra from SAR image. / Kojima S., Hashimoto N. // 2003. IGARSS '03. Proceedings. 2003 IEEE International Geoscience and Remote Sensing Symposium. 21-25 July 2003. - Vol. 4. - P. 2715-2717. ↑
- C5952.** Moore R.K. Correcting scatterometer ocean measurements for rain effects using radiometer data: application to SeaWinds on ADEOS-2. / Moore R.K., Braaten D., Natarajakumar B., Kurisunkal V.J. // 2003. IGARSS '03. Proceedings. 2003 IEEE International Geoscience and Remote Sensing Symposium. 21-25 July 2003. - Vol. 4. - P. 2724-2726. ↑
- C5953.** Hasager C.B. Offshore wind maps from ERS-2 SAR and wind resource modelling. / Hasager C.B., Nielsen M., Rathman O., Furevik B.R., Hamre T. // 2003. IGARSS '03. Proceedings. 2003 IEEE International Geoscience and Remote Sensing Symposium. 21-25 July 2003. - Vol. 4. - P. 2709-2711. ↑
- C5954.** Choisnard J. RADARSAT-1 SAR scenes for wind power mapping in coastal area: Gulf of St-Lawrence case. / Choisnard J., Bernier M., Lafrance G. // 2003. IGARSS '03. Proceedings. 2003 IEEE International Geoscience and Remote Sensing Symposium. 21-25 July 2003. - Vol. 4. - P. 2700-2702. ↑
- C5955.** Fichaux N. Evaluating the offshore wind potential. A combined approach using remote sensing and statistical methods. / Fichaux N., Ranchin T. // 2003. IGARSS '03. Proceedings. 2003 IEEE International Geoscience and Remote Sensing Symposium. 21-25 July 2003. - Vol. 4. - P. 2703-2705. ↑
- C5956.** Gommenginger C.P. An empirical model to retrieving ocean wave period from nadir altimeter data. / Gommenginger C.P., Srokosz M.A., Challenor P.G., Cotton P.D. // 2003. IGARSS '03. Proceedings. 2003 IEEE International Geoscience and Remote Sensing Symposium. 21-25 July 2003. - Vol. 4. - P. 2706-2708. ↑
- C5957.** Sobaerg S.S. An airborne campaign measuring wind signatures from the sea surface using an L-band

polarimetric radiometer. / Sobjaerg S.S., Skou N. // 2003. IGARSS '03. Proceedings. 2003 IEEE International Geoscience and Remote Sensing Symposium. 21-25 July 2003. - Vol. 4. - P. 2738-2740. ↑

C5958. Quintero-Marmol A.M. Operational applications of RADARSAT-1 for the monitoring of natural oil seeps in the South Gulf of Mexico. / Quintero-Marmol A.M., Pedroso E.C., Beisl C.H., Caceres R.G., de Miranda F.P., Bannerman K., Welgan P., Castillo O.L. // 2003. IGARSS '03. Proceedings. 2003 IEEE International Geoscience and Remote Sensing Symposium. 21-25 July 2003. - Vol. 4. - P. 2744-2746. ↑

C5959. Solberg A.H.S. Automatic detection of oil spills in ENVISAT, Radarsat and ERS SAR images. / Solberg A.H.S., Dokken S.T., Solberg R. // 2003. IGARSS '03. Proceedings. 2003 IEEE International Geoscience and Remote Sensing Symposium. 21-25 July 2003. - Vol. 4. - P. 2747-2749. ↑

C5960. Pons J. Passive polarimetric remote sensing of the ocean surface during the Rough Evaporation Duct experiment (RED 2001). / Pons J., Reising S.C., Padmanabhan S., Camps A., Duffo N. // 2003. IGARSS '03. Proceedings. 2003 IEEE International Geoscience and Remote Sensing Symposium. 21-25 July 2003. - Vol. 4. - P. 2732-2734. ↑

C5961. Niedermeier A. Spatial domain techniques to derive sea state parameters from ERS and ENVISAT SAR imageries. / Niedermeier A., Schulz-Stellenfleth J., Borge J.C.N., Lehner S. // 2003. IGARSS '03. Proceedings. 2003 IEEE International Geoscience and Remote Sensing Symposium. 21-25 July 2003. - Vol. 4. - P. 2729-2731. ↑

C5962. Sarti M. A scatterometer inversion procedure for the Mediterranean Sea. / Sarti M., Migliaccio M. // 2003. IGARSS '03. Proceedings. 2003 IEEE International Geoscience and Remote Sensing Symposium. 21-25 July 2003. - Vol. 4. - P. 2735-2737. ↑

© В.И. Карнышев, 2011

Тематический реферативный сборник сгенерирован в автоматическом режиме
с использованием специализированного программного модуля (ПИО ТУСУР)